

**PREPARATION AND CHARACTERIZATION OF
RESORBABLE CALCIUM PHOSPHATE
BASED BIOCERAMICS**

**A Thesis Submitted to
the Graduate School of Engineering and Sciences of
Izmir Institute of Technology
in Partial Fulfillment of the Requirements for the Degree of**

DOCTOR OF PHILOSOPHY

in Chemical Engineering

**by
Ali Emrah ÇETİN**

**March 2010
İZMİR**

We approve the thesis of **Ali Emrah ÇETİN**

Prof. Dr. Muhsin ÇİFTÇİOĞLU
Supervisor

Prof. Dr. Funda TIHMINLIOĞLU
Committee Member

Assoc. Prof. Dr. Oğuz BAYRAKTAR
Committee Member

Assoc. Prof. Dr. Yekta GÖKSUNGUR
Committee Member

Prof. Dr. Mustafa DEMİRCİOĞLU
Committee Member

01 March 2010

Prof. Dr. Mehmet POLAT
Head of the Department of Chemical
Engineering

Assoc. Prof. Dr. Talat YALÇIN
Dean of the Graduate School of
Engineering and Sciences

ACKNOWLEDGEMENTS

I would like to thank my advisor, Professor Dr. Muhsin Çiftçiođlu, for his supervision, encouragement, patience and confidence during my research. I am heartily grateful to him for his invaluable advices, suggestions, kindness, encouragement and support not only during my thesis but also in my life. He is indeed more than advisor to me.

I would also like to express my gratefulness to Assoc. Prof. Dr. Ođuz Bayraktar for his advices, support, encouragement and help during my study. I am grateful to him and Professor Dr. Semra Ülkü for the facilities in Biochemical Engineering Research Laboratory.

I owe my deepest gratitude to Professor Dr. Mustafa Demirciođlu for his invaluable contributions and critique on the chemical analysis fundamentals and experimental analysis. I would like to thank Professor Dr. Funda Tihminliođlu and Assoc. Prof. Dr. Yekta Göksungur for their contribution and suggestions.

I would like to thank Dr. Gerard L. Vogel from American Dental Association Foundation, Paffenbarger Research Center, National Institute of Standards and Technology for sending me his articles and analysis protocols. I also thank him for his suggestions.

I want express my thankfulness to my friend Deniz ŐimŐek for his help in powder preparation and in the use of cold isostatic press. I also thank him for his invaluable friendship and support. I also thank to Rukiye Çiftçiođlu for her kindness, support and encouragement during my study. I am grateful to my friends Dilek Yalçın, Özlem Çađlar Duvarcı, Zelal Polat, Hüsnü Arda Yurtsever, Ali Bora Balta, Alihan Karakaya, Filiz Özmihçı and İlker Erdem for their help, support and encouragement. I owe my thanks to Nesrin Tatlıdil for BET surface area measurements and Nesrin Gaffarođlu for her help in ICP analysis. I also thank to my friends, Evrim Yakut, Gökhan Erdođan, Duygu Ođuz Kılıç and Mine Bahçeci for XRD, SEM and TGA analyses at Materials Research Center in İzmir Institute of Technology.

Finally I am grateful to my mother Nazmiye Çetin, my sister Eylem and her husband Hulusi Demirciođlu for their endless support, encouragement and love.

This thesis was partially supported by Scientific Research Project BAP 2008IYTE01.

ABSTRACT

PREPARATION AND CHARACTERIZATION OF RESORBABLE CALCIUM PHOSPHATE BASED BIOCERAMICS

The main objective of this study was to determine the behavior of hydroxyapatite powders in solutions containing major ions found in human blood plasma. Research efforts however were focused on two different fields, chemical analysis and dissolution testing of hydroxyapatite. Arsenazo III-calcium analysis method was selected and modified for the low level calcium analysis whereas malachite green phosphate assay was used for phosphate determinations. Arsenazo III reagents with different dye concentrations and pH values were tested for the analysis of low levels of calcium. The effects of ions at their blood plasma concentration levels on the modified calcium analysis method were further evaluated. Effects of these ions on the accuracy of phosphate analysis by malachite green assay were also investigated.

Dissolution behavior of synthesized and commercial hydroxyapatite was investigated by immersing pellets in several solutions. Calcium and phosphate release kinetics in ultrapure water, sodium chloride and sodium bicarbonate solutions were investigated. Commercial hydroxyapatite pellets were also immersed separately in magnesium chloride, and sodium chloride/bicarbonate solutions. Calcium concentrations in solutions were found to decrease in the following order: sodium chloride > ultrapure water > bicarbonate. Phosphate concentrations in solutions were found to follow an order of sodium bicarbonate > sodium chloride > ultrapure water. Bicarbonate-phosphate ion exchange was observed in bicarbonate ion containing solutions. Magnesium-calcium ion exchange and adsorption of phosphates on hydroxyapatite surfaces were found to be effective in magnesium ion containing solution.

ÖZET

ÖZÜMLENEBİLEN KALSİYUM FOSFAT BAZLI BİYOSERAMİKLERİN HAZIRLANMASI VE KARAKTERİZASYONU

Bu çalışmanın temel amacı hidroksiapatit tozlarının kan plazmasındaki temel iyonları içeren çözeltilerdeki çözünürlük davranışının belirlenmesidir. Çalışmada uygulanan deneysel yaklaşımlar kimyasal analizler ve hidroksiapatitin çözünürlük davranışının sınanması alanlarında odaklanmıştır. Bu çalışmada Arsenazo III kalsiyum analizi düşük derişimlerdeki kalsiyumun belirlenmesi için seçilmiş ve modifiye edilmiştir. Fosfat analizi içinse malahit yeşili temelli fosfat analiz metodu kullanılmıştır. Farklı boya derişimlerine ve pH değerlerine sahip Arsenazo III belirteçleri düşük derişimlerdeki kalsiyumun belirlenmesi için araştırılmıştır. Ayrıca iyonların kan plazmasındaki konsantrasyonlarının kalsiyum analizi üzerine etkileri belirlenmiştir. Bu iyonların malahit yeşili bazlı fosfat tayini üzerine etkileri de araştırılmıştır.

Ticari hidroksiapatit ve bu çalışmada sentezlenen hidroksiapatit tozlarının çözünürlük davranışları, bu tozlardan elde edilen pelletlerin çeşitli çözeltiler içerisinde tutulmasıyla araştırılmıştır. Saf su, sodyum klorür ve sodyum bikarbonat çözeltileri içerisindeki kalsiyum ve fosfat salınım kinetiği araştırılmıştır. Ayrıca ticari hidroksiapatit tozundan elde edilen pelletlerin magnesium klorür çözeltisi ve sodyum klorür ve sodyum bikarbonat karışımı içeren çözeltideki çözünürlük davranışları da incelenmiştir. En yüksek kalsiyum derişimi sodyum klorür çözeltisi içinde gözlenirken, sırası ile saf su ve sodyum bikarbonat çözeltilerinde daha düşük olarak bulunmuştur. En yüksek fosfat derişimi ise sodyum bikarbonat çözeltisinde gözlenirken, sırasıyla sodyum klorür çözeltisi ve saf suda daha düşük olarak belirlenmiştir. Bikarbonat içeren çözeltilerde, bikarbonat-fosfat iyon deęişimi gözlenmiştir. Magnezyum içeren çözeltide ise magnezyum-kalsiyum iyon deęişimi ile fosfat iyonlarının hidroksiapatit yüzeyine adsorpsiyonun etkin olduęu görülmüştür.

TABLE OF CONTENTS

LIST OF FIGURES	x
LIST OF TABLES	xxi
ABBREVIATIONS	xxiv
CHAPTER 1. INTRODUCTION	1
CHAPTER 2. BIOCERAMICS BONE AND CALCIUM PHOPHATES	3
2.1. Bioceramics	3
2.2. Bone	8
2.3. Calcium Phosphate Based Ceramics.....	13
2.3.1. Calcium Orthophosphates.....	13
2.3.2. Calcium Phosphate Bone Cements	24
CHAPTER 3. PHOSPHATE AND CALCIUM ANALYSES	28
3.1. Phosphate Analysis	28
3.2. Calcium Analysis	31
CHAPTER 4. SOLUBILITY AND DISSOLUTION OF CALCIUM PHOSPHATES	37
4.1. Solubility of Calcium Phosphates.....	37
4.2. Dissolution of Calcium Phosphates	49
CHAPTER 5. MATERIALS AND METHODS	59
5.1. Materials	59
5.2. Methods	59
5.2.1. Chemical Analyses	61
5.2.1.1. Optimization of Microplate Based Arsenazo III Calcium Analysis	61
5.2.1.1.1. Preparation of Calcium Standard Solutions.....	63

5.2.1.1.2. Analysis	64
5.2.1.1.3. Data Analysis.....	64
5.2.1.2. Calcium Determination in Different Electrolyte Solutions by Microplate Based Arsenazo III-Calcium Analysis	65
5.2.1.2.1. Preparation of Calcium Standard Solutions.....	65
5.2.1.2.2. Analysis	66
5.2.1.3. Microplate Based Malachite Green Phosphate Assay	67
5.2.1.3.1. Preparation of Reagents	68
5.2.1.3.2. Preparation of Phosphate Standard Solutions.....	69
5.2.1.3.3. Analysis	73
5.2.2. Powder Synthesis and Characterization.....	74
5.2.2.1. Synthesis of Nano-Sized Hydroxyapatite Powder.....	74
5.2.2.2. Characterization of Powders.....	75
5.2.2.2.1. X-Ray Diffraction Analysis	75
5.2.2.2.2. Thermogravimetric Analysis	75
5.2.2.2.3. BET Surface Area.....	76
5.2.2.2.4. Scanning Electron Microscopy	76
5.2.2.2.5. Fourier Transform Infrared Radiation (FTIR) Analysis	76
5.2.2.2.6. Determination of Calcium/Phosphate Molar Ratios	76
5.2.3. Dissolution of Cold Isostatically Pressed Hydroxyapatite Pellets.....	77
 CHAPTER 6. RESULTS AND DISCUSSION.....	79
6.1. Chemical Analyses	79
6.1.1. Optimization of Microplate Based Arsenazo III Calcium Analysis.....	79
6.1.1.1. Arsenazo III in Acetate Buffer.....	79
6.1.1.2. Arsenazo III in Formate Buffer	101
6.1.1.3. Arsenazo III in Imidazole-Cl Buffer.....	112

6.1.2. Calcium Determination in Different Electrolyte Solutions by Microplate Based Arsenazo III-Calcium Analysis	142
6.1.3. Microplate Based Malachite Green Phosphate Assay	164
6.2. Characterization of Powders	175
6.2.1. XRD Analysis of Powders	175
6.2.2. Thermogravimetric Analyses.....	176
6.2.3. BET Surface Area.....	177
6.2.4. Scanning Electron Microscopy	179
6.2.5. FTIR Analysis.....	181
6.2.6. Calcium/Phosphate Molar Ratios	187
6.3. Dissolution of Cold Isostatically Pressed Hydroxyapatite pellets	187
CHAPTER 7. CONCLUSION	213
REFERENCES	216
APPENDICES	
APPENDIX A. CALCIUM REMOVAL FROM ARSENAZO III DYE SOLUTIONS	229
APPENDIX B. DETERMINATION OF ARSENAZO III CONCENTRATION IN PURIFIED SOLUTIONS	232
APPENDIX C. PREPARATION OF ARSENAZO III REAGENTS TO BE USED IN CALCIUM ANALYSIS	235
APPENDIX D. RESULTS OF CALCIUM REMOVAL FROM ARSENAZO III SOLUTIONS.....	241
APPENDIX E. ARSENAZO III CONCENTRATION IN PURIFIED SOLUTIONS	243
APPENDIX F. ABSORBANCE VALUES MEASURED AT 600 nm IN THE OPTIMIZATION OF MICROPLATE BASED ARSENAZO III-CALCIUM ANALYSIS.....	245

APPENDIX G. CALCIUM DETERMINATION IN DIFFERENT ELECTROLYTE SOLUTIONS BY MICROPLATE BASED ARSENAZO III-CALCIUM ANALYSIS	257
APPENDIX H. SPECTRA AND CALIBRATION CURVES FOR MALACHITE GREEN PHOSPHATE ASSAY	271

LIST OF FIGURES

<u>Figure</u>	<u>Page</u>
Figure 2.1. SEM image of plate-like cancellous bone with columnar structure	11
Figure 2.2. Hierarchical structure of bone from micro to nano-assembly	12
Figure 2.3. Optical image of transverse cross section of compact lamellar human femoral bone	13
Figure 2.4. Fractions of phosphate species of phosphoric acid ionization with respect to pH.....	18
Figure 2.5. Solubilities of calcium phosphate compounds as total calcium concentration in the solution with respect to solution pH	19
Figure 3.1. Contracted (A) and extended conformations (B) of Arsenazo III	33
Figure 3.2. Postulated structures found with bivalent and trivalent cations forming 1:1 complexes and trivalent ions forming 1:1 complexes (A), with tetravalent cations forming 1:1 complexes (B)	33
Figure 4.1. Solubility diagram.....	38
Figure 4.2. Dual-constant composition titration system	56
Figure 6.1. Spectra of calcium standard solutions (0.25-1.75 ppm) -60 μ M AIII in 100 mM acetate buffer pH 5.4 (150 μ L standard- 150 μ L dye reagent).....	81
Figure 6.2. Spectra of calcium standard solutions (0.25-1.75 ppm) - 60 μ M AIII in 100 mM acetate buffer pH 5.4 (150 μ L standard- 150 μ L dye reagent) obtained by subtracting blank values	81
Figure 6.3. Spectra of calcium standard solutions (10-70 ppm) - 60 μ M AIII in 100 mM acetate buffer pH 5.4 (150 μ L standard- 150 μ L dye reagent)	82
Figure 6.4. Spectra of calcium standard solutions (10-70 ppm) - 60 μ M AIII in 100 mM acetate buffer pH 5.4 (150 μ L standard- 150 μ L dye reagent) obtained by subtracting blank values.....	82

Figure 6.5. Absorbance values of calcium standards (0.25-2 ppm) - 60 μ M AIII in 100 mM acetate buffer pH 5.4 (150 μ L standard-150 μ L dye reagent) at 650 nm a. without subtracting blank values, b. with subtracting blank values.....	84
Figure 6.6. Absorbance values of calcium standards (1-8 ppm) - 60 μ M AIII in 100 mM acetate buffer pH 5.4 (150 μ L standard-150 μ L dye reagent) at 650 nm a. without subtracting blank values, b. with subtracting blank values.....	85
Figure 6.7. Absorbance values of calcium standards (10-80 ppm) - 60 μ M AIII in 100 mM acetate buffer pH 5.4 (150 μ L standard-150 μ L dye reagent) at 650 nm a. without subtracting blank values, b. with subtracting blank values.....	86
Figure 6.8. Spectra of calcium standards (0.25-2 ppm) - $\frac{1}{2}$ (60 μ M AIII in 100 mM acetate buffer pH 5.4) (150 μ L standard-150 μ L dye reagent)	88
Figure 6.9. Spectra of calcium standards (0.25-2 ppm) - $\frac{1}{2}$ (60 μ M AIII in 100 mM acetate buffer pH 5.4) (150 μ L standard-150 μ L dye reagent) obtained by subtracting blank values.....	88
Figure 6.10. Absorbance values of calcium standards (0.25-2 ppm) – $\frac{1}{2}$ (60 μ M AIII in 100 mM acetate buffer pH 5.4) (150 μ L standard-150 μ L dye reagent) at 650 nm a. without subtracting blank values, b. with subtracting blank values	89
Figure 6.11. Absorbance values of calcium standards (1-8 ppm) – $\frac{1}{2}$ (60 μ M AIII in 100 mM acetate buffer pH 5.4) (150 μ L standard-150 μ L dye reagent) at 650 nm a. without subtracting blank values, b. with subtracting blank values	90
Figure 6.12. Absorbance values of calcium standards (10-80 ppm) – $\frac{1}{2}$ (60 μ M AIII in 100 mM acetate buffer pH 5.4) (150 μ L standard-150 μ L dye reagent) at 650 nm a. without subtracting blank values, b. with subtracting blank values	90
Figure 6.13. Plot of $\alpha/(1-\alpha)$ vs. $[Ca]_t - \alpha[Ar]_t$ Dye reagent: 60 μ M Arsenazo III in 100 mM acetate buffer pH 5.4 Calcium concentration of standard solutions: 0.25-2 ppm and 1-8 ppm (Reagent to standard volume ratio of 150 μ L/150 μ L)	95

Figure 6.14. Plot of $\alpha/(1-\alpha)$ vs. $[Ca]_t - \alpha[Ar]_t$ Dye reagent: $\frac{1}{2}$ (60 μ M Arsenazo III in 100 mM acetate buffer pH 5.4) Calcium concentration of standard solutions: 0.25-2 ppm and 1-8 ppm (Reagent to standard volume ratio of 150 μ L/150 μ L)	96
Figure 6.15. Spectra of blank and 1 ppm calcium standard solutions Dye: 120 μ M AIII in 100 mM acetate buffer pH 5.4 (150 μ L standard - 150 μ L dye reagent)	99
Figure 6.16. Spectra of calcium standard solutions (2-8 ppm) – 120 μ M AIII in 100 mM acetate buffer pH 5.4 (150 μ L standard – 150 μ L dye reagent)	99
Figure 6.17. Spectra of calcium standard solutions (1-8 ppm) – 120 μ M AIII in 100 mM acetate buffer pH 5.4 (150 μ L standard- 150 μ L dye reagent) obtained by subtracting blank values	100
Figure 6.18. Absorbance values of calcium standards (1-8 ppm) - 120 μ M AIII in 100 mM acetate buffer pH 5.4 (150 μ L standard- 150 μ L dye reagent) at 650 nm a. without subtracting blank values, b. with subtracting blank values	100
Figure 6.19. Spectra of calcium standard solutions (0.25-1.75 ppm) - 60 μ M AIII in formate buffer pH 3.8 (150 μ L standard- 150 μ L dye reagent)	102
Figure 6.20. Spectra of calcium standard solutions (1-7 ppm) - 60 μ M AIII in formate buffer pH 3.8 (150 μ L standard- 150 μ L dye reagent)	103
Figure 6.21. Spectra of calcium standard solutions (1-7 ppm) - 60 μ M AIII in formate buffer pH 3.8 (150 μ L standard- 150 μ L dye reagent) obtained by subtracting blank values.....	104
Figure 6.22. Spectra of calcium standard solutions (10-70 ppm) - 60 μ M AIII in formate buffer pH 3.8 (150 μ L standard- 150 μ L dye reagent)	104
Figure 6.23. Spectra of calcium standard solutions (10-70 ppm) - 60 μ M AIII in formate buffer pH 3.8 (150 μ L standard- 150 μ L dye reagent) obtained by subtracting blank values.....	105

Figure 6.24. Absorbance values of calcium standards (0.25-2 ppm) -60 μ M AIII in formate buffer pH 3.8 (150 μ L standard-150 μ L dye reagent) at 650 nm a. without subtracting blank values, b. with subtracting blank values.....	106
Figure 6.25. Absorbance values of calcium standards (1-8 ppm) - 60 μ M AIII in formate buffer pH 3.8 (150 μ L standard-150 μ L dye reagent) at 650 nm a. without subtracting blank values, b. with subtracting blank values.....	107
Figure 6.26. Absorbance values of calcium standards (10-80 ppm) - 60 μ M AIII in formate buffer pH 3.8 (150 μ L standard-150 μ L dye reagent) at 650 nm a. without subtracting blank values, b. with subtracting blank values.....	107
Figure 6.27. Absorbance values of calcium standards (0.25-2 ppm) – $\frac{1}{2}$ (60 μ M AIII in formate buffer pH 3.8) (150 μ L standard-150 μ L dye reagent) at 650 nm a. without subtracting blank values, b. with subtracting blank values	108
Figure 6.28. Plot of $\alpha/(1-\alpha)$ vs. $[Ca]_t - \alpha[Ar]_t$ Dye reagent: 60 μ M Arsenazo III in formate buffer pH 3.8 Calcium concentration of standard reagents: 0.25-2 ppm and 1-8 ppm (Reagent to standard volume ratio of 150 μ L/150 μ L).....	109
Figure 6.29. Spectra of calcium standard solutions (10-70 ppm) - 120 μ M AIII in formate buffer pH 3.8 (150 μ L standard- 150 μ L dye reagent)	110
Figure 6.30. Spectra of calcium standard solutions (10-70 ppm) - 120 μ M AIII in formate buffer pH 3.8 (150 μ L standard- 150 μ L dye reagent) obtained by subtracting blank values.....	111
Figure 6.31. Absorbance values of calcium standards (10-80 ppm) - 120 μ M AIII in formate buffer pH 3.8 (150 μ L standard-150 μ L dye reagent) at 650 nm a. without subtracting blank values, b. with subtracting blank values	111
Figure 6.32. Spectra of calcium standard solutions (0.25-1.75 ppm) - 60 μ M AIII in 100 mM imidazole-Cl pH 6.5 (150 μ L standard-150 μ L dye reagent).....	114

Figure 6.33. Spectra of calcium standard solutions (0.25-1.75 ppm) - 60 μM AIII in 100 mM imidazole-Cl pH 6.5 (150 μL standard- 150 μL dye reagent) obtained by subtracting blank values	114
Figure 6.34. Spectra of calcium standard solutions (10-70 ppm)-60 μM AIII in 100 mM imidazole-Cl pH 6.5 (150 μL standard- 150 μL dye reagent).....	116
Figure 6.35. Spectra of calcium standard solutions (10-70 ppm)-60 μM AIII in 100 mM imidazole-Cl pH 6.5 (150 μL standard- 150 μL dye reagent) obtained by subtracting blank values	116
Figure 6.36. Absorbance values of calcium standards (0.25-2 ppm) – 60 μM AIII in 100 mM Imidazole-Cl buffer pH 6.5 (150 μL standard-150 μL dye reagent) at 650 nm a. without subtracting blank values, b. with subtracting blank values	117
Figure 6.37. Absorbance values of calcium standards (1-8 ppm) – 60 μM AIII in 100 mM Imidazole-Cl buffer pH 6.5 (150 μL standard-150 μL dye reagent) at 650 nm a. without subtracting blank values, b. with subtracting blank values	117
Figure 6.38. Absorbance values of calcium standards (10-80 ppm) – 60 μM AIII in 100 mM Imidazole-Cl buffer pH 6.5 (150 μL standard-150 μL dye reagent) at 650 nm a. without subtracting blank values, b. with subtracting blank values	118
Figure 6.39. Absorbance values of calcium standards (0.25-2 ppm) – $\frac{1}{2}$ (60 μM AIII in 100 mM Imidazole-Cl buffer pH 6.5) (150 μL standard-150 μL dye reagent) at 650 nm a. without subtracting blank values, b. with subtracting blank values	118
Figure 6.40. Absorbance values of calcium standards (1-8 ppm) - $\frac{1}{2}$ (60 μM AIII in 100 mM Imidazole-Cl buffer pH 6.5) (150 μL standard-150 μL dye reagent) at 650 nm a. without subtracting blank values, b. with subtracting blank values.....	119
Figure 6.41. Plot of $\alpha/(1-\alpha)$ vs. $[\text{Ca}]_t - \alpha[\text{Ar}]_t$ Dye reagent: 60 μM Arsenazo III in 100 mM imidazole-Cl pH 6.5 Calcium concentration of standard solutions: 0.25-2 ppm and 1-8 ppm (Reagent to standard volume ratio of 150 $\mu\text{L}/150 \mu\text{L}$)	121

Figure 6.42. Spectra of calcium standard solutions (0.25-1.75 ppm)-60 μ M AIII in 200 mM imidazole-Cl pH 6.5 (150 μ L standard- 150 μ L dye reagent).....	122
Figure 6.43. Spectra of calcium standard solutions (1-7 ppm)-60 μ M AIII in 200 mM imidazole-Cl pH 6.5 (150 μ L standard- 150 μ L dye reagent).....	122
Figure 6.44. Spectra of calcium standard solutions (1-7 ppm) -60 μ M AIII in 200 mM imidazole-Cl pH 6.5 (150 μ L standard- 150 μ L dye reagent) obtained by subtracting blank values	124
Figure 6.45. Spectra of calcium standard solutions (10-70 ppm) -60 μ M AIII in 200 mM imidazole-Cl pH 6.5 (150 μ L standard- 150 μ L dye reagent).....	124
Figure 6.46. Spectra of calcium standard solutions (10-70 ppm) -60 μ M AIII in 200 mM imidazole-Cl pH 6.5 (150 μ L standard- 150 μ L dye reagent) obtained by subtracting blank values	125
Figure 6.47. Absorbance values of calcium standards (0.25-2 ppm) -60 μ M AIII in 200 mM Imidazole-Cl buffer pH 6.5 (150 μ L standard- 150 μ L dye reagent) at 650 nm a. without subtracting blank values, b. with subtracting blank values	125
Figure 6.48. Absorbance values of calcium standards (1-8 ppm) -60 μ M AIII in 200 mM Imidazole-Cl buffer pH 6.5 (150 μ L standard- 150 μ L dye reagent) at 650 nm a. without subtracting blank values, b. with subtracting blank values	126
Figure 6.49. Absorbance values of calcium standards (10-80 ppm) - 60 μ M AIII in 200 mM Imidazole-Cl buffer pH 6.5 (150 μ L standard- 150 μ L dye reagent) at 650 nm a. without subtracting blank values, b. with subtracting blank values	127
Figure 6.50. Plot of $\alpha/(1-\alpha)$ vs. $[Ca]_t-\alpha[Ar]_t$ Dye reagent: 60 μ M Arsenazo III in 200 mM imidazole-Cl pH 6.5 Calcium concentration of standard solutions: 0.25-2 ppm and 1-8 ppm (Reagent to standard volume ratio of 150 μ l/150 μ l).....	128
Figure 6.51. Spectra of calcium standard solutions (1-7 ppm)-200 μ M AIII in 200 mM imidazole-Cl pH 6.5 (150 μ L standard- 150 μ L dye reagent).....	130

Figure 6.52. Spectra of calcium standard solutions (1-7 ppm)-200 μ M AIII in 200 mM imidazole-Cl pH 6.5 (150 μ L standard-150 μ L dye reagent) obtained by subtracting blank values	130
Figure 6.53. Spectra of calcium standard solutions (10-70 ppm)-200 μ M AIII in 200 mM imidazole-Cl pH 6.5 (150 μ L standard-150 μ L dye reagent)	131
Figure 6.54. Spectra of calcium standard solutions (10-70 ppm)-200 μ M AIII in 200 mM imidazole-Cl pH 6.5 (150 μ L standard-150 μ L dye reagent) obtained by subtracting blank values	131
Figure 6.55. Absorbance values of calcium standards (1-8 ppm)-200 μ M AIII in 200 mM Imidazole-Cl buffer pH 6.5 (150 μ L standard-150 μ L dye reagent) at 650 nm a. without subtracting blank values, b. with subtracting blank values	132
Figure 6.56. Absorbance values of calcium standards (10-80 ppm) - 200 μ M AIII in 200 mM Imidazole-Cl buffer pH 6.5 (150 μ L standard-150 μ L dye reagent) at 650 nm a. without subtracting blank values, b. with subtracting blank values	133
Figure 6.57. Plot of $\alpha/(1-\alpha)$ vs. $[Ca]_t - \alpha[Ar]_t$ Dye reagent: 200 μ M Arsenazo III in 200 mM imidazole-Cl pH 6.5 Calcium concentration of standard solutions : 1-8 ppm (Reagent to standard volume ratio of 150 μ L/150 μ L)	134
Figure 6.58. Absorbance values of calcium standards (10-80 ppm) – 500 μ M AIII in 200 mM Imidazole-Cl buffer pH 6.5 (150 μ L standard-150 μ L dye reagent) at 650 nm a. without subtracting blank values, b. with subtracting blank values.....	135
Figure 6.59. Spectra of calcium standard solutions prepared in ultrapure water.....	145
Figure 6.60. Spectra of calcium standard solutions prepared in ultrapure water obtained by subtracting blank value	145
Figure 6.61. Calibration curve obtained by measuring absorbances of calcium standards prepared in ultrapure water at 650 nm	146
Figure 6.62. Calibration curve obtained by measuring absorbances of calcium standards prepared in ultrapure water at 600 nm	147

Figure 6.63. Calibration curve obtained by measuring absorbances of calcium standards prepared in ultrapure water at 655 nm	148
Figure 6.64. Calibration curve obtained by measuring absorbances of calcium standards prepared in ultrapure water at 500 nm	149
Figure 6.65. XRD profiles of DHA and HA powders.....	175
Figure 6.66. TG analysis profile of the sample HA	176
Figure 6.67. TG analysis profile of the sample DHA	177
Figure 6.68. Adsorption and desorption of N ₂ on HA powder	178
Figure 6.69. Adsorption and desorption of N ₂ on DHA powder.....	178
Figure 6.70. SEM micrographs of HA powder	179
Figure 6.71. SEM micrographs of DHA powder	180
Figure 6.72. FTIR spectrum of DHA powder	181
Figure 6.73. FTIR spectra of HA powder	184
Figure 6.74. Time dependent pH changes during dissolution of HA pellets in ultrapure water, 142 mM NaCl and 27 mM NaHCO ₃	193
Figure 6.75. Time dependent pH changes during dissolution of HA and DHA pellets in CO ₂ free ultrapure water, CO ₂ free 142 mM NaCl and 27 mM NaHCO ₃	194
Figure 6.76. Time dependent pH changes during dissolution of DHA pellets in 27 mM NaHCO ₃ and HA pellets in 115 mM NaCl and 27 mM NaHCO ₃ containing solution	195
Figure 6.77. Conductivities of the solutions during HA dissolution in ultrapure water	195
Figure 6.78. Conductivities of the solutions during HA dissolution in 142 mM NaCl and 27 mM NaHCO ₃	196
Figure 6.79. Conductivities of the solutions during HA and DHA dissolution in CO ₂ free ultrapure water	196
Figure 6.80. Conductivities of solutions during dissolution of HA and DHA pellets in CO ₂ free 142 mM NaCl and 27 mM NaHCO ₃ solutions.....	197
Figure 6.81. Conductivities of solutions during dissolution of HA in CO ₂ free 1.5 mM MgCl ₂	198
Figure 6.82. Calcium release profile upon dissolution of HA pellets in ultrapure water in which dissolved carbon dioxide	

was not removed	198
Figure 6.83. Calcium release profile upon dissolution of HA pellets in carbon dioxide free ultrapure water	199
Figure 6.84. Calcium release profile upon dissolution of DHA pellets in carbon dioxide free ultrapure water	200
Figure 6.85. Phosphate concentrations in solutions upon dissolution of HA pellets in ultrapure water in which dissolved carbon dioxide was not removed	201
Figure 6.86. Phosphate concentrations in solutions upon dissolution of HA pellets in CO ₂ free ultrapure water	201
Figure 6.87. Phosphate concentrations in solutions upon dissolution of DHA pellets in CO ₂ free ultrapure water	202
Figure 6.88. Calcium release from HA pellets in 142 mM NaCl in which dissolved carbon dioxide was not removed	203
Figure 6.89. Calcium release from HA pellets in CO ₂ free 142 mM NaCl	204
Figure 6.90. Calcium release from DHA pellets in CO ₂ free 142 mM NaCl	205
Figure 6.91. Phosphate release from HA pellets in 142 mM NaCl in which dissolved carbon dioxide was not removed	205
Figure 6.92. Phosphate release from HA pellets in CO ₂ free 142 mM NaCl	206
Figure 6.93. Phosphate release from DHA pellets in CO ₂ free 142 mM NaCl	206
Figure 6.94. Calcium release from HA pellets in 27 mM NaHCO ₃	208
Figure 6.95. Calcium release from DHA pellets in 27 mM NaHCO ₃	208
Figure 6.96. Phosphate release from HA pellets in 27 mM NaHCO ₃	209
Figure 6.97. Phosphate release from DHA pellets in 27 mM NaHCO ₃	209
Figure 6.98. Calcium release from HA pellets in 115 mM NaCl and 27 mM NaHCO ₃ containing solution.....	210
Figure 6.99. Phosphate release from HA pellets in 115 mM NaCl and 27 mM NaHCO ₃ containing solution.....	211
Figure 6.100. Calcium release from HA pellets in CO ₂ free 1.5 mM MgCl ₂	212
Figure 6.101. Phosphate release from HA pellets in CO ₂ free 1.5 mM MgCl ₂	212

LIST OF TABLES

<u>Table</u>	<u>Page</u>
Table 2.1. Medical applications of bioceramics	5
Table 2.2. Types of Implant-Tissue Response	6
Table 2.3. Types of Bioceramic Tissue Attachment and Bioceramic Classification	6
Table 2.4. Composition of bone.....	8
Table 2.5. Composition and physical properties of inorganic phases of adult dentine, enamel and bone	10
Table 2.6. Calcium phosphate compounds	16
Table 2.7. Crystallographic properties of several calcium phosphates.....	17
Table 2.8. Possible substituted calcium phosphate apatite phases.....	23
Table 2.9. Commercially available calcium phosphate cements, their compositions and manufacturers	26
Table 3.1. Commercial arsenazo III-calcium determination kits.....	35
Table 4.1. Solubility product constants reported for hydroxyapatite	47
Table 4.2. Solubility product constants for calcium phosphate phases other than hydroxyapatite	48
Table 4.3. Composition of simulated body fluids.....	51
Table 4.4. Reagents used to prepare simulated body fluids.....	52
Table 5.1. Materials used and their specifications	60
Table 5.2. Arsenazo III dye reagents and the range of calcium concentrations used in this study	62
Table 5.3. Electrolyte solutions used to prepare phosphate standards.....	69
Table 5.4. Number of replicates used in malachite green phosphate assay	70
Table 5.5. Reagents used to prepare SBFA and SBFB solutions	72
Table 5.6. Ionic compositions of SBFA and SBFB solutions.....	72
Table 5.7. Electrolyte solutions used in dissolution of hydroxyapatite powder	77
Table 6.1. Molar absorptivities of free arsenazo III and calcium- arsenazo III complexes	136

Table 6.2.	The nature of absorbance versus concentration curves obtained in calcium analysis by arsenazo III reagents	139
Table 6.3.	Linear calibration responses obtained in arsenazo III-calcium analysis.....	140
Table 6.4.	Absorbance values of blank reagent and absorbance ranges of standards in arsenazo III-calcium analysis.....	141
Table 6.5.	Electrolyte solutions used to prepare calcium standards	143
Table 6.6.	Calculated F_0 values and confidence limits for rejection of null hypothesis in two-sided F -test for Arsenazo III-calcium analysis	154
Table 6.7.	Results of F -test for the validation of the assumption of the equality of variances by two-sided F -test for Arsenazo III-calcium analysis	155
Table 6.8.	Calculated t_0 values and t values for the rejection of null hypothesis in two-sided t -tests for Arsenazo III-calcium analysis.....	156
Table 6.9.	Results of t -tests for the validation of the equality of the means and interferences for Arsenazo III-calcium analysis	157
Table 6.10.	Calibration equations for calcium standards prepared in different electrolytes constructed by absorbance values at 650 nm in Arsenazo III-calcium analysis	162
Table 6.11.	Calibration equations for calcium standards prepared in different electrolytes constructed at ΔA values at 650 nm in Arsenazo III-calcium analysis	163
Table 6.12.	Calibration equations obtained by using absorbances in malachite green phosphate assay	166
Table 6.13.	Calibration equations obtained by using ΔA values in malachite green phosphate assay	168
Table 6.14.	Calculated F_0 values and confidence limits for rejection of null hypothesis in two-sided F -test for malachite green phosphate assay.....	171
Table 6.15.	Results of F -test for the validation of the assumption of the equality of variances by two-sided F -test for malachite green phosphate assay	172

Table 6.16. Calculated t_0 values and t values for the rejection of null hypothesis in two-sided t -tests for malachite green phosphate assay.....	173
Table 6.17. Results of t -tests for the validation of the equality of the means and interferences for malachite green phosphate assay.....	174
Table 6.18. FTIR peaks of hydroxyapatite powders and their assignments	186
Table 6.19. Properties of HA pellets obtained by cold isostatic pressing.....	189
Table 6.20. Properties of DHA pellets obtained by cold isostatic pressing.....	191

ABBREVIATIONS

<i>a</i>	Activity
<i>A</i>	Absorbance
A_{\max}	Maximum absorbance
A_{\min}	Minimum absorbance
ACP	Amorphous calcium phosphate
AIII	Arsenazo III
ATR	Attenuated total reflectance
BET	Brunauer Emmet Teller
<i>c</i>	Concentration
CaAIII	Calcium arsenazo III complex
CPC	Calcium phosphate cement
CDHA	Calcium deficient hydroxyapatite
CIP	Cold isostatic press
DCPA	Dicalcium phosphate anhydrous
DCPD	Dicalcium phosphate dihydrate
HA	Hydroxyapatite
HD-PE	High density polyethylene
<i>I</i>	Ionic strength
<i>F</i>	<i>F</i> -statistic
FA	Fluorapatite
FTIR	Fourier transform infrared radiation
<i>G</i>	Gibbs free energy
MCPA	Monocalcium phosphate monohydrate
MCPD	Monocalcium phosphate dihydrate
<i>n</i>	Sample size
<i>K</i>	Ionization constant
K_{app}	Apparent binding constant
K_{D}	Dissociation constant
K_{c}	Concentration solubility product
K_{sp}	Activity solubility product

OCP	Octacalcium phosphate
OXA	Oxyapatite
P	Power
PHA	Precipitated hydroxyapatite
pK	Negative logarithm of ionization, binding, dissociation or solubility product
PVA	Polyvinyl alcohol
ppm	Parts per million
R	Ideal gas constant
s	Undersaturation ratio
S	Sample standard deviation
S^2	Sample variance
S_p	Estimate of $\sigma_1^2 = \sigma_2^2 = \sigma^2$
SEM	Scanning electron microscopy
t	t -statistics
T	Temperature
TCP	Tricalcium phosphate
TEM	Transmission electron microscopy
TG	Thermogravimetric
TTCP	Tetracalcium phosphate
\bar{x}	Sample mean
XRD	X-ray diffraction
ν	Degrees of freedom
z	Charge of ion
α	Confidence interval in t - and F - statistics
α	Alpha
α_i	Effective diameter of hydrated ion
β	Beta
γ	Activity coefficient
Δ	Delta
ϵ	Molar absorptivity
ζ	Zeta

λ	Wavelength
μ	Population mean
σ	Population standard deviation
σ^2	Population variance

CHAPTER 1

INTRODUCTION

Calcium phosphate materials are generally used as bone substitute materials in non-load bearing applications. They are also used as dental implants. Among all calcium phosphate phases, synthetic hydroxyapatite has received special interest in the studies of bone substitute materials due to its similarity with inorganic phase of the bone (apatite). Resorption of bone by osteoclasts and bone formation by osteoblasts, bonding of materials to the bone, dissolution of bone substitutes in time and replacement with newly formed bone are all directly related to the solubilities and dissolution behavior of bone and materials. Saturation level of the solutions with respect to calcium phosphate phases is the most important factor in the determination of behavior of hydroxyapatite in solution. Undersaturation, saturation and supersaturation degrees of solutions with respect to several calcium phosphates determine whether sample will dissolve or precipitation will occur.

Solubility studies of calcium phosphate compounds are generally based on the determination of equilibrium calcium and phosphate concentrations and calculation of solubility product constants. However, immersion of several calcium phosphate compounds into simulated body fluids or several electrolytes and monitoring of calcium or phosphate release or both are also called as solubility testing. These studies are in fact batch dissolution studies and irrelevant to the determinations of thermodynamic solubility constant. Dissolution studies have been performed by batch dissolution experiments or constant composition dissolution kinetics tests. Batch dissolution experiments are based on immersion of powder into electrolytical solutions and monitoring of calcium and phosphate concentrations in the solutions. Hydroxyapatite dissolution studies by batch dissolution experiments are generally focused on the dissolution testing of powder in acidic solutions in order to predict osteoclastic resorption behaviors or in solutions buffered to physiological pH value.

The main disadvantage of batch dissolution experiments is the change of solution composition which changes the undersaturation level resulting in a variable thermodynamic driving force. This can be overcome by conducting experiments in a

constant composition dissolution kinetics methodology. Titrating dissolution medium with two titrant solutions (one containing all background ions and calcium and another containing all background ions and phosphate) is used to keep the composition of the dissolution medium constant by diluting the dissolution media. Volumes of the titrants used are plotted against time and dissolution rates are then calculated. Constant composition dissolution kinetics studies are valuable for the determination of dissolution and crystallization mechanisms because change of Gibb's free energy is held constant during dissolution or crystallization.

Although solution compositions are not held constant in batch experiments and this is considered as their main disadvantage, changes in solution compositions are required in some cases. Calcium phosphate bone cement is the most common example. In bone cements, two or more calcium phosphate compounds are used. Phases are mixed with a solution in which calcium phosphate phases dissolve and hydroxyapatite precipitates. In these systems time dependent calcium and phosphate release from samples is important and results in cement setting.

The major objective of this study was to determine the dissolution behavior of hydroxyapatite powders in solutions containing major ions found in human blood plasma. However because of the problems associated with low levels of calcium and phosphate analysis in the presence of higher amount of background matrices, experiments were also performed on the chemical analyses methods. A calcium analysis method was modified for the low levels of calcium in the solutions. The effects of the presence of several electrolytical solutions on calcium analysis were determined. Similarly, interferences resulting from background ions on phosphate analysis were evaluated. By using calibration curves obtained in the presence of electrolytes, dissolution of hydroxyapatite powders in several electrolytical solutions were determined.

CHAPTER 2

BIOCERAMICS BONE AND CALCIUM PHOSPHATES

2.1. Bioceramics

A biomaterial was defined as “any substance (other than a drug) or combination of substances, synthetic or natural in origin, which can be used for any period of time, as a whole or as a part of a system which treats, augments or replaces any tissue, organ, or function of the body” by The National Institute of Health Consensus Development Conference (Dee et al., 2002). Several metallic, polymeric and ceramic materials or combinations of these have been used as biomaterials. Metals and their alloys are preferred for the load-bearing implant applications whereas polymers are used for the replacement and augmentation of soft tissues and in drug delivery systems and tissue engineering applications (Dee et al., 2002). Ceramic materials used in the repair, reconstruction and replacement of diseased or damaged parts are called bioceramics (Hench, 1998). Bioceramics are generally used in the orthopedic applications alone or as coatings for metallic implants and composites with polymeric materials.

Stainless steel 316L, alloys cobalt-chromium-molibdenum, titanium and Ti6Al4V are the most widely used metallic implant materials (Dee et al., 2002). Polyethylene, poly(vinyl chloride), silicone rubber, poly(ethylene terephthalate), poly(lactic acid), polytetrafluoroethylene, poly(methyl methacrylate), poly(lactide-co-glycolide) and poly(glycolic acid) are the examples of polymers used in the biomedical applications (Dee et al., 2002). Although metallic implants are commonly used for load bearing applications, they are actually not the perfect biomaterials due to their lack of biocompatibility, insufficient corrosion resistance and mechanical properties which do not match with those of surrounding tissues (Dee et al., 2002). Dense fibrous tissue formation and encapsulation of metallic implant material, resulting with the improper stress distribution and loosening of the implants, are observed for almost all metallic implants (Suchanek and Yoshimura, 1998). Biological degradation of several polymers resulting in non-toxic products is advantageous, since new tissue is formed and it replaced the polymers as they are assisting in healing.

In the case of bioceramics, several ceramic materials such as alumina (Al_2O_3), zirconia (ZrO_2), bioactive glasses, hydroxyapatite (HA), tricalcium phosphate (TCP) (Dee et al., 2002; Hench, 1998), pyrolytic carbon (Dee et al., 2002), bioactive glass-ceramics, calcium sulfate and calcium phosphate salts (Hench, 1998) are widely used. Bioceramic materials are mostly used in the orthopedic applications for the treatment of bone disease or injury. Table 2.1 summarizes the clinical applications of different bioceramics.

When any material is implanted into the bone, generally fibrous tissue is formed to encapsulate and isolate the material from the surrounding tissues (Kokubo, 1998). However, Hench (1998) has defined four types of implant and tissue responses (Table 2.2). When material implanted is toxic, it results with the death of the surrounding tissue. In the case of non-toxic but inert materials, fibrous tissue is formed. If non-toxic and bioactive material is used, interfacial bonding occurs between the biomaterial and the surrounding tissue. Non-toxic materials, which could dissolve, lead to the replacement of biomaterial with the surrounding tissue.

Hench (1998) has also classified the bioceramics according to types of bioceramic-tissue attachments considering these implant-tissue responses. Table 2.3 summarizes the types of bioceramic-tissue attachment and examples of bioceramics.

Table 2.1. Medical applications of bioceramics
(Source: Hench, 1998)

Applications	Materials
Orthopedic	Al ₂ O ₃ Stabilized ZrO ₂ HA powders Bioactive glass powders
Coatings for bioactive bonding	HA Bioactive glass ceramics
Bone space fillers	Tricalcium phosphate Calcium phosphate salts
Dental implants	Al ₂ O ₃ HA Bioactive glasses
Artificial tendon and ligament	Polylactic acid-carbon-fiber composite
Periodontal pocket obliteration	HA HA-polylactic composite Tricalcium phosphate Calcium phosphate salts Bioactive glasses
Alveolar ridge augmentation	HA HA-autogeneous bone composite Bioactive glasses
Maxillofacial reconstruction	Al ₂ O ₃ HA Polyethylene-HA composite Bioactive glasses
Spinal surgery	Bioactive-glass ceramic HA
Therapeutic treatment of tumors	Rare-earth-doped aluminosilicate glasses
Artificial heart valves	Pyrolytic carbon coating
Otolaryngological	Al ₂ O ₃ HA Bioactive glasses Bioactive-glass ceramic Polyethylene-HA composite

Table 2.2. Types of Implant-Tissue Response
(Source: Hench, 1998)

Types of Implant	Tissue Response
Toxic	Death of surrounding tissue
Nontoxic and biologically inactive (almost inert)	Formation of fibrous tissue with variable thickness
Nontoxic and biologically active (bioactive)	Formation of an interfacial bond
Nontoxic and dissolves	Replacement of material with surrounding tissue

Table 2.3. Types of Bioceramic Tissue Attachment and Bioceramic Classification
(Source: Hench, 1998)

Type of attachment	Type of bioceramic
Dense, nonporous, almost inert ceramics attach by bone growth into surface regularities by cementing the device into the tissue, or by press-fitting into a defect (morphological fixation)	Al ₂ O ₃ ZrO ₂
For porous implants, bone ingrowth occurs, which mechanically attaches the bone to the material (biological fixation)	Porous hydroxyapatite Hydroxyapatite-coated porous metals
Surface-reactive ceramics, glasses, and glass-ceramics attach directly by chemical bonding with the bone (bioactive fixation)	Bioactive glasses Bioactive glass-ceramics Dense hydroxyapatite
Resorbable ceramics and glasses in bulk or powder form designed to be slowly replaced by bone	Calcium sulfate (plaster of Paris) Tricalcium phosphate Calcium phosphate salts Bioactive glasses

Among bioceramics, alumina has been widely used in total hip prostheses, knee prostheses, bone screws, alveolar ridge and maxillofacial reconstructions, ossicular bone substitutes, keratoprotheses, segmental bone replacements and dental implants whereas zirconia has been used in total joint and hip prostheses (Hench, 1998). Excellent corrosion resistance, good biocompatibility, low friction, high wear resistance and high strength of alumina and high fracture toughness and tensile strength of zirconia make them suitable materials for the medical applications (Hench, 1998).

When a material is implanted into the body, fixation of implant is required. Formation of a fibrous tissue surrounding the biomaterial may result with failure. It is therefore required that the material should resist to the movements. This can be overcome by the use of porous biomaterials. Bone ingrowth into the pores increases the strength of the biomaterial to resist the movement. The limitation for the porous implants is that the pores should be higher than 100-150 μm . Pore size smaller than 100 μm does not stimulate the formation of vascular tissue. Surrounding tissue could only be healthy and viable if the pore size is over 100-150 μm (Hench, 1998). In order to biologically fix several metallic implants into the tissues, porous hydroxyapatite coatings can be used to promote bone ingrowth. Bioactive ceramics and glasses which have the ability to form mechanically strong bond to bone are able to induce surface time dependent modifications after implantation and subsequently form a biologically active bone-like hydroxycarbonate apatite layer (Hench, 1998). The formation of bone-like apatite layer on the surfaces can be the essential prerequisite for the bonding of bone to the implant material (Kokubo, 1998).

Resorbable bioceramics are based on the principle that the living tissues can repair themselves by the continuous cellular proliferation in time (Hench, 1998). They degrade over time and newly formed tissue replaces. Calcium phosphate based materials such as TCP are able to dissolve in the living tissue. Due to the brittleness of the ceramic materials, their use is restricted to the non-load bearing applications. Maintenance of strength and stability of the interface is the main complications. The other restriction in the use of resorbable bioceramics is that the dissolution rate of a resorbable bioceramic should be almost equal to the repair rate of living tissue. Among these restrictions, calcium phosphate based biomaterials and composites are the best candidates for bone repair since bone mineral itself is a calcium phosphate based mineral.

2.2. Bone

Bone has several functions. It supports body, moves muscles, protects vital organs, generates blood and retains the reserves of calcium, phosphate and the other ions (Sikavitsas et al., 2001; Asai et al., 2003). Bone itself is a natural inorganic/organic composite (Asai et al., 2003). It has 69 % mineral, 20 % organic matrix and 9 % water in weight (Suchanek and Yoshimura, 1998). Compositions of organic and inorganic phases of bone are shown in Table 2.4. Small quantities of proteins, polysaccharides as well as lipids are also present in the bone (Suchanek and Yoshimura, 1998). Compositions and physical properties of inorganic phases of enamel, dentine and bone are given in Table 2.5.

Table 2.4. Composition of bone
(Source: Murugan and Ramakrishna, 2005)

Inorganic wt. %		Organic	wt. %
Hydroxyapatite	~60	Collagen	~20
Carbonate	~4	Water	~9
Citrate	~0.9	Non-collagenous proteins (osteocalcin, osteonectin, osteopontin, thrombospondin, morphogenic proteins, sialoprotein, serum proteins)	~3
Sodium	~0.7		
Magnesium	~0.5		
Other traces: Cl ⁻ , F ⁻ , K ⁺ , Pb ²⁺ , Zn ²⁺ , Cu ²⁺ , Fe ²⁺		Other traces: Polysaccharides, lipids, cytokines Primary bone cells: osteoblasts, osteoclasts	

Organic matrix of the bone is mainly composed of Type I collagen and responsible for the bone tensile strength (Mickiewicz, 2001). Structural framework of collagen acts as a template for the calcium apatite growth (Song et al., 2005). Combination of hard inorganic material with an elastic collagen is responsible for the unique properties of the bone, such as low stiffness, resistance to tensile and

compressive forces and high fracture toughness (Song et al., 2005). Bone mineral has nano-sized, needle like calcium phosphate crystals (5-20 nm in width and 60 nm in length) (Ferraz et al., 2004). Bone apatite is non-stoichiometric and poorly crystallized (Ferraz et al., 2004) and contains CO_3^{2-} , Na^+ , F^- (Mickiewicz, 2001; Ferraz et al., 2004; Tampieri et al., 2005), Cl^- , K^+ (Mickiewicz, 2001), Mg^{2+} (Mickiewicz, 2001; Tampieri et al., 2005) and HPO_4^{2-} (Tampieri et al., 2005). Apatite in the bone is highly oriented with resulted chemical stability and physical strength (Asai et al., 2003). It is found as its c-plane oriented parallel to the axis of collagen (Asai et al., 2003). Presence of HPO_4^{2-} and CO_3^{2-} anions and Mg^{2+} and Na^+ cations does not alter the structure, but decreases crystallinity and increases bioresorbability (Tampieri et al., 2005; Babini and Tampieri, 2004).

Carbonate is found in bone in 4-8% and its amount changes with the age (Babini and Tampieri, 2004; Tampieri et al., 2005). Two types of carbonate substitutions are observed and called A and B site carbonate substitution. A-type substitution (found in old bone) corresponds to the carbonate substitution in OH sites of apatite while B-type substitution (found in young human beings) is referred to the substitution in the PO_4 sites (Babini and Tampieri, 2004; Tampieri et al., 2005). Among the substitute cations in bone, Mg^{2+} is the most important one. Magnesium substitution results with low crystallinity, and improved solubility and resorbability, because magnesium acts as an accelerator of nucleation kinetics of hydroxyapatite and an inhibitor of crystallization (Tampieri et al., 2005). By optimizing over the most favorable stoichiometries and having the most likely composition of the bone, two formulas for the cation and anion substitutions were given by Tampieri et al. (2005):

Cationic substitution: $\text{Ca}_{10-x}\text{M}_x(\text{PO}_4)_6(\text{OH})_2$

Anionic substitution: $\text{Ca}_{10-x/2-z/2}[(\text{HPO}_4)_z(\text{PO}_4)_{6-x-z}(\text{CO}_3)_x][(\text{OH})_{2-2y}(\text{CO}_3)_y]$.

Table 2.5. Composition and physical properties of inorganic phases of adult dentine, enamel and bone (Source: Suchanek and Yoshimura, 1998)

	Enamel	Dentine	Bone
<u>Composition^a</u>			
Calcium, Ca ²⁺ ^b	36.5	35.1	34.8
Phosphorus, as P (Ca/P) molar ^b	17.7 1.63	16.9 1.61	15.2 1.71
Sodium, Na ⁺	0.5	0.6	0.9
Magnesium, Mg ²⁺ ^b	0.44	1.23	0.72
Potassium, K ⁺ ^b	0.08	0.05	0.03
Carbonate, as CO ₃ ²⁻ ^c	3.5	5.6	7.4
Fluoride, F ⁻ ^b	0.01	0.06	0.03
Chloride, Cl ⁻ ^b	0.30	0.01	0.13
Pyrophosphate, P ₂ O ₇ ⁴⁻	0.022	0.10	0.07
Total inorganic (mineral)	97.0	70.0	65.0
Total organic ^d	1.5	20.0	25.0
Adsorbed H ₂ O	1.5	10.0	10.0
Trace elements: Sr ²⁺ , Pb ²⁺ , Zn ²⁺ , Cu ²⁺ , Fe ³⁺ , etc.			
<u>Crystallographic properties</u>			
Lattice parameters (±0.003 Å)			
<i>a</i> -axis	9.441	9.42	9.41
<i>c</i> -axis	6.880	6.88	6.89
Crystallinity index ^e	70-75	33-37	33-37
Crystallite size (aver.), Å	1,300 x 3	200 x 40	250 x 30
Ignition products (800 °C)	β - TCP+HA	β TCP+HA	- HA+CaO

^a Wt. %, ^b Ashed sample, ^c Unashed sample, IR method, ^d Principle organic component: enamel, noncollageneous; dentine and bone, collageneous, ^e Calculated from ratio of coherent/incoherent scattering, mineral, Hap = 100.

Mature bone includes two main types, compact and cancellous bone. Adult skeleton has cortical (or compact) bone in 80 % and cancellous bone (or trabecular) bone in 20 % (Skavitsas et al., 2001). Proportions differ at various locations in the skeleton. Compact bone has 10 % porosity and it includes spaces only for osteocytes, canaliculi and blood vessels (Skavitsas et al., 2001). Compact bone is highly porous (50-90%) and high porosity makes modulus of elasticity and ultimate compressive strength almost 10 times less than that of cortical bone (Skavitsas et al., 2001). Cancellous bone exhibits sponge-like morphology with a honeycomb of branching bars, plates and rods with various sizes called trabeculae (Fig. 2.1) (Suchanek and Yoshimura, 1998).

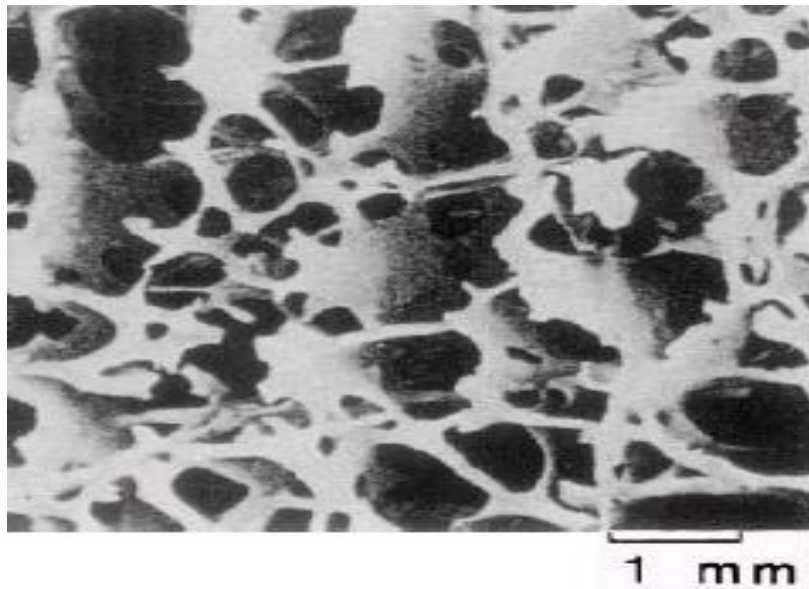


Figure 2.1. SEM image of plate-like cancellous bone with columnar structure (Source: Suchanek and Yoshimura, 1998).

Macro, micro, ultra and molecular hierarchical levels of structural organization of bone make the analysis difficult. Figure 2.2 shows the hierarchical levels and structural organization of a human bone.

At the molecular level, 20-40 nm crystals of hydroxyapatite are oriented along the collagen fibers. These mineralized collagen fibers are arranged into the lamellar sheets with a thickness of 3-7 μm . 4-20 lamellae build a concentric ring around the Haversian canal and form osteon.

When cross-section of the compact bone is determined, cylindrical osteons (Haversian system) with blood vessels running along Haversian canals, (in the center of each osteon) are observed (Fig.2.3). Canaliculi, lacunae and Volkmann's canals are connected with marrow cavity and their intercommunicating system allows the transportation of metabolic substances. Several interconnecting systems are filled with the body fluids and their volume can be up to 19 % (Suchanek and Yoshimura, 1998). Canaliculi is a canal extending outward from the central canal (Haversian canal) and Volkmann's canals run perpendicular to the central canal and connect them to the periosteal surface (Skavitsas et al., 2001).

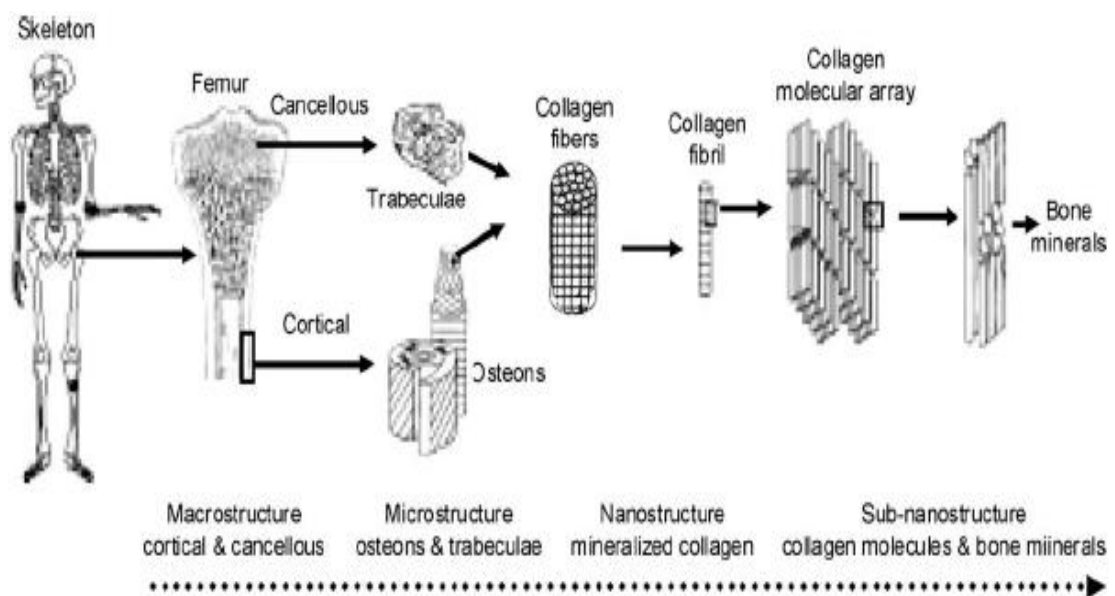


Figure 2.2. Hierarchical structure of bone, from micro to nano-assembly (Source: Murugan and Ramakrishna, 2005).

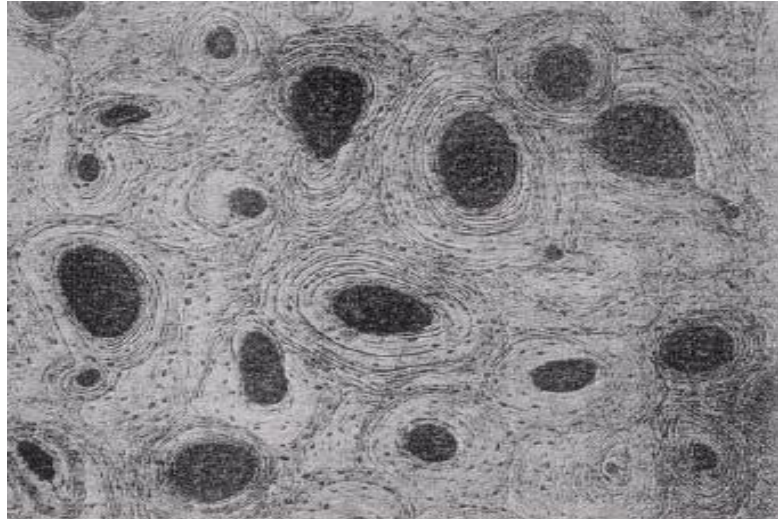


Figure 2.3. Optical image of transverse cross section of compact lamellar human femoral bone (Source: Suchanek and Yoshimura, 1998).

2.3. Calcium Phosphate Based Ceramics

Calcium phosphate compounds include calcium orthophosphates, calcium metaphosphates, calcium pyrophosphates and calcium polyphosphates. This main classification is indeed based on the nature of phosphate found in the compound. Phosphate in a compound may exist in the following forms; ortho (PO_4^{3-}), meta (PO_3^-), pyro ($\text{P}_2\text{O}_7^{4-}$), and poly (PO_3)_nⁿ⁻ and the compound is named as calcium orthophosphate, calcium metaphosphate, calcium pyrophosphate and calcium polyphosphate, respectively (Dorozhkin, 2007; Wang and Nancollas, 2008). Calcium phosphates will be used to refer calcium orthophosphates in this thesis since the focus of this thesis is one of the important members of the calcium orthophosphates, namely hydroxyapatite.

2.3.1 Calcium Orthophosphates

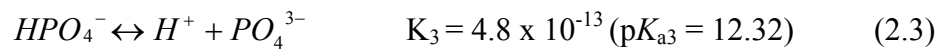
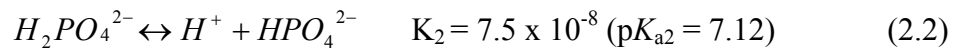
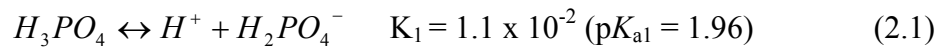
Calcium phosphates have been the subject of special interest in the scientific literature due the following reasons:

- 1) Natural calcium phosphate minerals are used to produce phosphoric acid, phosphorous containing chemicals and agricultural fertilizers (Dorozhkin and Epple, 2002; Dorozhkin, 2007).

- 2) Hydroxyapatite is the inorganic component of bone and teeth.
- 3) Some members (octacalcium phosphate and amorphous calcium phosphate) are also involved in biomineralization processes together with hydroxyapatite (Nancollas, 1992).
- 4) Calcium phosphates are also important in the pathological mineralizations (cellular microcalcifications in vascular dementia, Alzheimer's and Parkinson's diseases, astroglomas and post-traumatic epilepsy, dystrophic calcifications like seen in the calcifications of medical devices and bioprosthetic heart valves, renal calculi formation, atherosclerosis, pseudogout, gallstone formations, salivary and dental calculi formations) (Königsberger and Königsberger, 2007).
- 5) Synthetic hydroxyapatite in dense, powder, granular or porous forms and biphasic calcium phosphates (especially hydroxyapatite and TCP) have been used as bone substitute materials.
- 6) Members such as monocalcium phosphate monohydrate, dicalcium phosphate dehydrate, dicalcium phosphate anhydrous, β -TCP, amorphous calcium phosphates are used in the food industry as a food additive (Dorozhkin, 2007).
- 7) Calcium phosphates are used as filling material or intermediate for remineralization in dentistry and toothpaste ingredients as polishing and caries protecting agents (Dorozhkin, 2007).
- 8) Calcium phosphates are coated on dental and orthopaedic implants in order to improve their bone bonding abilities (Vallet-Regi and Gonzales-Calbet, 2004).
- 9) Hydroxyapatite is used for the separation of proteins and other biomolecules in the liquid chromatography (Dorozhkin, 2007).
- 10) Due to its sparingly soluble nature of hydroxyapatite, it is used to isolate and store radioactive materials.
- 11) Several calcium phosphates (monocalcium phosphate monohydrate, dicalcium phosphate dihydrate, dicalcium phosphate anhydrous, amorphous calcium phosphate, hydroxyapatite, α -tricalcium phosphate, β - tricalcium phosphate, and tetracalcium phosphate) are used in the calcium phosphate based bone cements (Bohner et al., 2005).

A general ternary system describing a compound AX in an aqueous solution, $A(OH)_n-H_nX-H_2O$, where $A(OH)_n$ is a base and H_nX is a weak acid is defined as $Ca(OH)_2-H_3PO_4-H_2O$ (Martin and Brown, 1997; Fernandez et al., 1999) or as $CaO-P_2O_5-H_2O$ (Elmore and Farr, 1940; Martin and Brown, 1997) for the calcium phosphate compounds. By considering the low and high temperature phases and grouping the all substituted compounds in a general phase (e.g. apatites), there are eleven different calcium phosphate phases in this ternary system (Dorozhkin, 2007). Besides their crystallographic properties, the most important parameter describing these calcium phosphate phases is their calcium to phosphate molar ratios (Ca/P). These phases together with their Ca/P ratios, acronyms, specific mineral names and their pH stability ranges are given in Table 2.6. Additionally crystallographic properties and densities of several calcium phosphate compounds are shown in Table 2.7.

The diversity of calcium phosphates is directly related to the presence phosphate species in the system (Lynn and Bonfield, 2005; Dorozhkin, 2007). Phosphoric acid is a polyprotic acid with three ionization constants (Christian, 1994).



When fractions of each phosphate species in the phosphoric acid ionization in the pH range of 0-14 were calculated using above stated ionization constant, one can obtain species distribution with respect to pH (Figure 2.4) (Christian, 1994).

According to Figure 2.4, only a single component is found at pH values of 1 and 14 and the pH ranges of 4-5 and 9-10. Even fractions of other components seem to equal zero, but they are not zero at all, indeed negligibly small. At other pH values, two different phosphate species always exist. Therefore when calcium and phosphate species are found in an aqueous solution, pH, solution calcium and phosphate concentrations as well as solubilities of calcium phosphates determine the phases to be formed.

Table 2.6. Calcium phosphate compounds
(Source: Bohner, 2000; Dorozhkin, 2007; and Dorozhkin, 2009)

Ca/P Ratio	Compound	Acronym/ Mineral Name	Chemical Formula	pH stability ranges at 25 °C
0.5	Monocalcium phosphate monohydrate	MCPM	$\text{Ca}(\text{H}_2\text{PO}_4)_2 \cdot \text{H}_2\text{O}$	0.0-2.0
0.5	Monocalcium phosphate anhydrous	MCPA	$\text{Ca}(\text{H}_2\text{PO}_4)_2$	stable above 100 °C
1.0	Dicalcium phosphate dihydrate	DCPD/ brushite	$\text{CaHPO}_4 \cdot 2\text{H}_2\text{O}$	2.0-6.0
1.0	Dicalcium phosphate anhydrous	DCPA (DCP)/ monetite	CaHPO_4	stable above 100 °C
1.33	Octacalcium phosphate	OCP	$\text{Ca}_8(\text{HPO}_4)_2(\text{PO}_4)_4 \cdot 5\text{H}_2\text{O}$	5.5-7.0
1.5	α -Tricalcium phosphate	α -TCP	$\alpha\text{-Ca}_3(\text{PO}_4)_2$	can not be precipitated
1.5	β -Tricalcium phosphate	β -TCP	$\beta\text{-Ca}_3(\text{PO}_4)_2$	can not be precipitated
1.2-2.2	Amorphous calcium phosphate	ACP	$\text{Ca}_x\text{H}_y(\text{PO}_4)_z \cdot n\text{H}_2\text{O}$ $n:3-4.5, 15-20 \% \text{H}_2\text{O}$	~ 5-12 always metastable
1.5-1.67	Calcium-deficient hydroxyapatite or precipitated hydroxyapatite	CDHA or PHA	$\text{Ca}_{10-x}(\text{HPO}_4)_x(\text{PO}_4)_{6-x}(\text{OH})_{2-x}$ ($0 < x < 1$)	6.5-9.5
1.67	Hydroxyapatite	HA	$\text{Ca}_{10}(\text{PO}_4)_6(\text{OH})_2$	9.5-12
1.67	Fluorapatite	FA	$\text{Ca}_{10}(\text{PO}_4)_6(\text{F})_2$	7-12
1.67	Oxyapatite	OXA	$\text{Ca}_{10}(\text{PO}_4)_6\text{O}$	-
2.0	Tetracalcium phosphate	TTCP	$\text{Ca}_4(\text{PO}_4)_2\text{O}$	can not be precipitated

Table 2.7. Crystallographic properties of several calcium phosphates
(Source: Dorozhkin and Epple, 2002; Dorozhkin, 2007)

Calcium Phosphate Compound	Unit Cell Parameters	Space Group	Number of Formula Units per Unit Cell	Density (g/cm ³)
MCPM	a = 5.6251(5) Å, b = 11.889(2) Å, c = 6.4731(8) Å $\alpha = 98.633(6)^\circ$, $\beta = 118.262(6)^\circ$, $\gamma = 83.344(6)^\circ$	triclinic <i>P1</i>	2	2.23
MCPA	a = 7.5577(5) Å, b = 8.2531(6) Å, c = 5.5504(3) Å $\alpha = 109.87(1)^\circ$, $\beta = 93.68(1)^\circ$, $\gamma = 109.15(1)^\circ$	triclinic <i>P1</i>	2	2.58
DCPD	a = 5.812(2) Å, b = 15.180(3) Å, c = 6.239(2) Å $\beta = 116.42(3)^\circ$	monoclinic <i>Ia</i>	4	2.32
D CPA	a = 6.910(1) Å, b = 6.627(2) Å, c = 6.998(2) Å $\alpha = 96.34(2)^\circ$, $\beta = 103.82(2)^\circ$, $\gamma = 88.33(2)^\circ$	triclinic <i>P1</i>	4	2.89
OCP	a = 19.692 (4) Å, b = 9.523(2) Å, c = 6.835(2) Å $\alpha = 90.15(2)^\circ$, $\beta = 92.54(2)^\circ$, $\gamma = 108.65(1)^\circ$	triclinic <i>P1</i>	1	2.61
α -TCP	a = 12.887(2) Å, b = 27.280(4) Å, c = 15.219(2) Å $\beta = 126.20(1)^\circ$	monoclinic <i>P2₁/a</i>	24	2.86
β - TCP	a = b = 10.439(1) Å, c = 37.375(6) Å, $\gamma = 120^\circ$	rhombohedral <i>R3cH</i>	21 (per hexagonal unit cell)	3.07
HA	a = 9.84214(8) Å, b = 2a, c = 6.8814(7) Å, $\gamma = 120^\circ$ (monoclinic)	monoclinic <i>P2₁/b</i>	4	3.16
	a = b = 9.4302(5) Å, c = 6.8911(2) Å, $\gamma = 120^\circ$ (hexagonal)	hexagonal <i>P6₃/m</i>	2	
FA	a = b = 9.367 Å, c = 6.884 Å, $\gamma = 120^\circ$	hexagonal <i>P6₃/m</i>	2	3.20
TTCP	a = 7.023(1) Å, b = 11.986(4) Å, c = 9.473(2) Å $\beta = 90.90(1)^\circ$	monoclinic <i>P2₁</i>	4	3.05

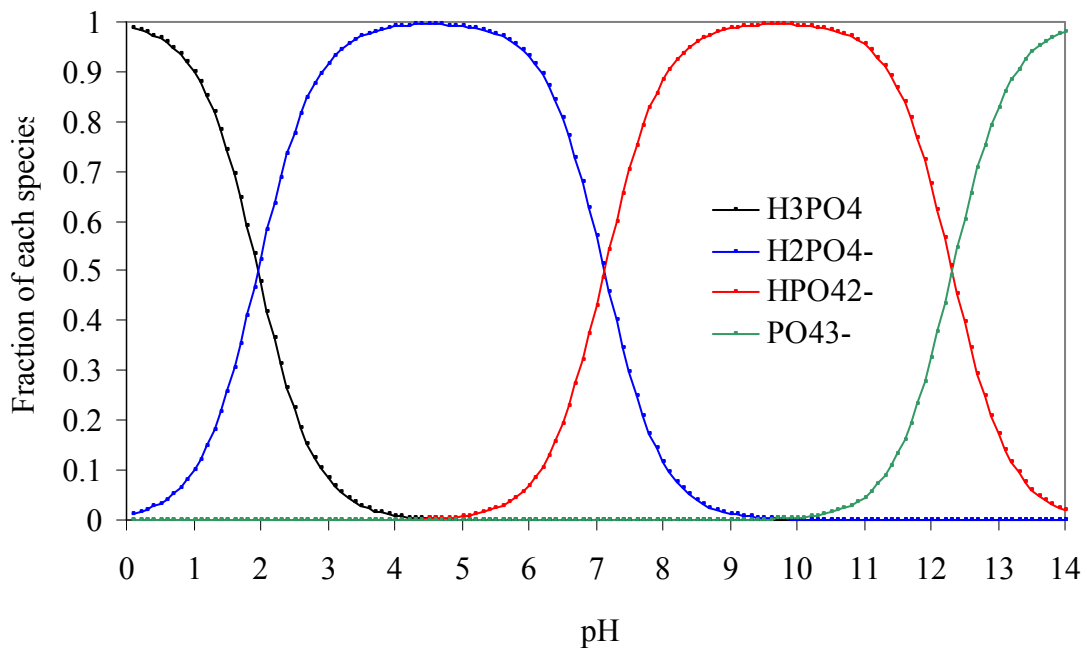


Figure 2.4. Fractions of phosphate species of phosphoric acid ionization with respect to pH.

Among the eleven different calcium phosphates, only MCPM, DCPA, DCPD, OCP, ACP and CDHA are precipitated in aqueous solutions at room temperatures, whereas MCPA, α -TCP, β -TCP, sintered HA and OXA are the products of thermal processing (Bohner, 2000).

Monocalcium phosphate monohydrate is the most acidic calcium phosphate compound and precipitates in highly acidic conditions during fertilizer production (Dorozhkin and Epple, 2002; Dorozhkin, 2007) since it is the most stable phase at the strong acidic pH values, $\text{pH} < 2$ (Table 2.6) (Dorozhkin, 2009). MCPM is also the most water-soluble calcium phosphate compound (Dorozhkin and Epple, 2002; Bohner, 2000; Dorozhkin, 2007). Figure 2.5 show solubilities of calcium phosphate compounds with respect to pH values where the solubility is given as the total calcium concentration in the solution. It can be seen from Figure 2.5 that MCPM is the most soluble calcium phosphate compound at all pH values (Bohner, 2000). Because of its high solubility and acidity, single use of MCPM as bone substitution is restricted; however it is used as bone cement together with other phases (Bohner, 2000; Dorozhkin and Epple, 2002; Dorozhkin, 2007).

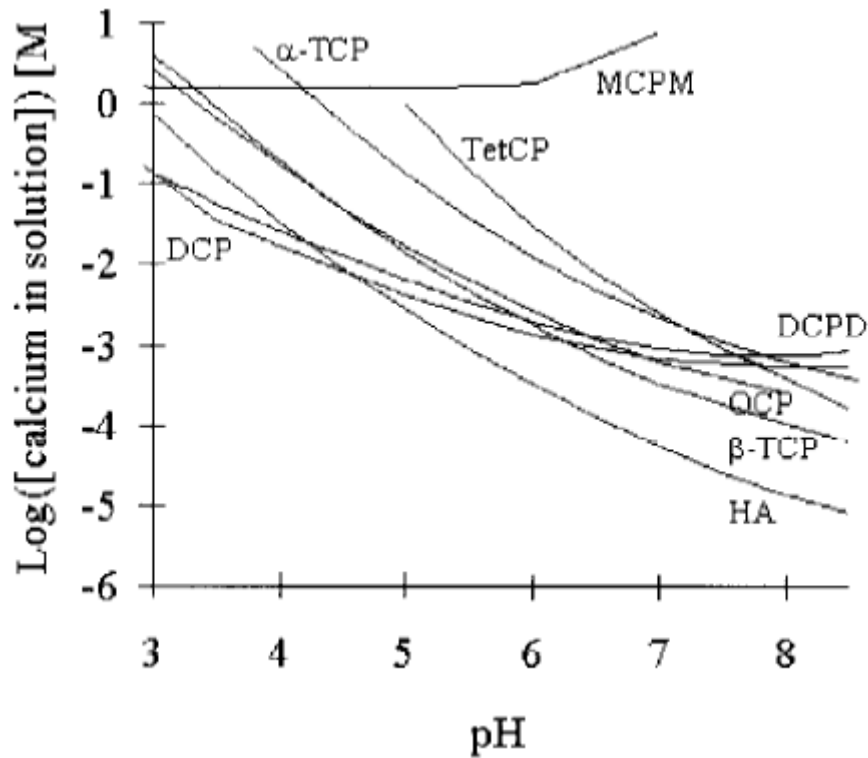


Figure 2.5. Solubilities of calcium phosphate compounds as total calcium concentration in the solution with respect to solution pH (Source: Bohner, 2000).

Monocalcium phosphate anhydrous as its name suggests is the dehydrated form of MCPM obtained by removal of water from MCPM. Crystallization of MCPMA occurs at the similar conditions where MCPM crystallizes but temperature should be over 100 °C in order to exclude water from the crystal structure (Dorozhkin and Epple, 2002; Dorozhkin, 2007). Its highly acidic and hygroscopic nature restricts its biological and commercial applications (Dorozhkin, 2007).

Dicalcium phosphate dihydrate is one of the most easily precipitated calcium phosphate compounds from aqueous solutions (Bohner, 2000; Dorozhkin and Epple, 2002; Dorozhkin, 2007). Its crystal structure is built up of parallelly arranged CaPO_4 chains having interlayered water molecules (Wang and Nancollas, 2008). DCPD is found in pathological calcifications such as urinary stones, dental calculi, pseudogout (Dorozhkin, 2007; Königsberger and Königsberger, 2007). It was also proposed as an intermediate phase in bone formation and its absence was related to the technical difficulties in detection methods (Wang and Nancollas, 2008). However, the presence of an acid phosphate containing species which is different than DCPD and OCP phases

were determined in the newly formed bone mineral (Boskey, 1998). Behavior of DCPD in an aqueous solution is pH dependent. It is reported as stable below pH 6.5 (Wang and Nancollas, 2008). However, it is converted to anhydrous form below pH 6 (Bohner, 2000). Metastable nature of DCPD makes it transform into octacalcium phosphate when pH was between 6 and 7 and into precipitated hydroxyapatite over pH 7 (Bohner, 2000). Although DCPD is biodegradable *in vivo* and converted into PHA, release of phosphoric acid upon conversion into PHA causes undesirable inflammatory reactions (Bohner, 2000).

DCPA, anhydrous dicalcium phosphate dehydrate, can be obtained by dehydration of DCPD over 80°C or precipitation in the similar conditions where DCPD precipitates but at temperatures above 100 °C (Dorozhkin, 2007). Infact, hydrolysis of DCPD results in transformation of DCPD into DCPA by dehydration when temperature is between 60 and 100 (Ito and Onuma, 2003). It is generally used in the preparation of bone cements (Bohner, 2000, Dorozhkin, 2007) and production of tetracalcium phosphate together with calcium carbonate by solid state reactions (Neira et al., 2009; Gbureck et al., 2004).

Octacalcium phosphate is a calcium phosphate phase showing structural similarities to hydroxyapatite. It consists of apatitic layers which are separated by hydrated layers (Johnsson and Nancollas, 1992; Dorozhkin and Epple 2002; Dorozhkin 2007) containing lattice water and calcium and phosphate ions (Johnsson and Nancollas, 1992). OCP is considered as a precursor phase in teeth and bone mineralization (Bohner, 2000; Dorozhkin, 2007) and an intermediate in the precipitation of hydroxyapatite and calcium deficient hydroxyapatite (PHA or CDHA) (Dorozhkin, 2007).

Tricalcium phosphate is a calcium phosphate that can only be obtained by thermal processing. It has three different crystallographic forms, high temperature forms α -TCP and super α -TCP and low temperature form β -TCP (Ito and Onuma, 2003). TCP phases can not be obtained by precipitation due to their unstable nature in aqueous solutions. However, when divalent ions such as magnesium smaller enough to fit into calcium vacancies in β -TCP are present in the solution, stabilized β -TCP, whitlockite (β -(Ca, Mg)₃(PO₄)₂), can be obtained in aqueous solutions (Johnsson and Nancollas, 1992). Although it was reported that β -TCP can not be obtained by precipitation in aqueous solutions (Dorozhkin, 2007) precipitation of amorphous calcium phosphate phase and conversion into β -TCP in methanol at room temperature was reported (Bow

et al., 2004). β -TCP is generally obtained by thermal treatment of CDHA over 800 °C (Bohner, 2000; Dorozhkin, 2007) or calcinations of mixtures containing equal moles of DCPD and CDHA with Ca/P molar ratio 1.67 (Bohner, 2000). β -TCP transforms into α -form at high temperature. This transition temperature is 1125 °C where α - to super α -transition occurs at 1430°C (Ito and Onuma, 2003). Quenching prevents α to β transformation or absence of water vapor and excess calcium oxide retards this phase transformation until cooling down to 840 °C (Eisenberger, 1940). However, transformation of super α - form can not be prevented by quenching (Ito and Onuma, 2003).

Amorphous calcium phosphate is the first phase which precipitates in highly supersaturated solutions of calcium and phosphate at neutral pH and especially at high pH values (Johnsson and Nancollas, 1992; Ito and Onuma, 2003). Generally Ca/P ratio of amorphous calcium phosphate is considered as 1.5 (Ito and Onuma, 2003). However this ratio depends on the solution composition and pH and it might be between 1.18 and 2.50 (Dorozhkin 2007; Wang and Nancollas, 2008). ACP is believed to be a precursor phase in calcium phosphate formation *in vivo* (Nancollas, 1992). ACP is highly metastable and in aqueous solutions it transforms to HA (Wang and Nancollas, 2008).

Tetracalcium phosphate is a high temperature phase. Since it can not be precipitated from aqueous solutions, solid state reactions are used to synthesize TTCP. Generally calcium carbonate and DCPA are used (Neira et al., 2009; Gbureck et al., 2004). The presence of water vapor in the heating environment, however, results in the HA formation on TTCP particles (Dorozhkin 2007). Common methods to avoid HA formation are to supply dry air or nitrogen gas into furnaces or to quench the TTCP from high temperature to room temperature (Dorozhkin, 2007).

Calcium deficient hydroxyapatite, hydroxyapatite, oxyapatite and fluorapatite all belong to apatite family. A general formula of $A_5(XO_4)_3Z$ defines the members of apatite family where A can be barium, calcium, cerium, potassium, sodium, lead, strontium and yttrium, X can be arsenic, phosphorous, silicon and vanadium and Z can be fluoride, chloride, oxygen and hydroxyl ion (Magalhães and Williams, 2007). A wide range of minerals other than calcium phosphate apatites such as lead phosphates, calcium arsenates, lead arsenates and etc. are all classified as apatite since they have similar structure (Magalhães and Williams, 2007).

Due to the presence of various cations and anions, ionic substitutions also occur in apatite lattice. Geologically, calcium phosphate apatites are generally in the form of

fluorapatite, $\text{Ca}_{10}(\text{PO}_4)_6\text{F}_2$. Partial substitutions of calcium by Sr, Ba, Mg, Mn, K, Na, Fe, phosphate by AsO_4^{3-} , CO_3^{2-} and VO_4^{3-} and fluoride by OH^- , Cl^- , Br^- , CO_3^{2-} and O^{2-} in natural apatite occurs in the nature (Dorozhkin, 2007) However, substitutions in biological apatites are restricted to only ions found in the human body, F^- , Cl^- , Na^+ , K^+ , Fe^{2+} , Zn^{2+} , Sr^{2+} , Mg^{2+} , CO_3^{2-} and citrate (Wopenka and Pasteris, 2005).

Substitutions in the apatite are governed by the rule of maintaining charge neutrality, and the presence of the exchangeable sites in the crystal lattice and by the geometrical fitting between exchanging ions (Wopenka and Pasteris, 2005). If an ion substitutes into lattice, either oppositely charged ion is incorporated or vacancies are formed to provide charge balance. Possible phases of substituted calcium phosphate apatites together with four end members (fluorapatite, chlorapatite, carbonated apatite and hydroxyapatite) are shown in Table 2.8. It should be noted that Table 2.8 excludes the phases formed by cationic incorporations upon anionic substitutions.

Hydroxyapatite, $\text{Ca}_{10}(\text{PO}_4)_6(\text{OH})_2$, is an unsubstituted pure apatite and so its Ca/P molar ratio is equal to 1.67. Two forms of hydroxyapatite exist, hexagonal and more stable monoclinic form (Wang and Nancollas, 2008). At room temperature, presence of hexagonal form is only possible by incorporation of substituting ions into the lattice thereby deviating Ca/P ratio from the stoichiometric value of 1.67 (Wang and Nancollas, 2008; Dorozhkin, 2007). Stoichiometric apatite is generally produced by high temperature calcinations of precipitated apatite which is obtained by precipitation in carbon dioxide freebasic conditions from solutions having stoichiometric amounts of calcium and phosphate and ageing in the precipitation medium (Dorozhkin, 2007). Solid state synthesis, hydrothermal and sol gel methods are also used to obtain stoichiometric hydroxyapatite (Dorozhkin, 2007). Because high temperatures are employed in the synthesis, Ca/P ratio determines the phases obtained (Huang and Best, 2007). If the ratio is higher than 1.67, β -TCP and other calcium phosphates will also be obtained together with HA, whereas at lower Ca/P ratios calcium oxide and hydroxyapatite will be formed (Huang and Best, 2007). Even the powder has the stoichiometric Ca/P ratio, the presence of water vapor in the system and temperature affect the phases formed. In dry environments oxyapatite formation from hydroxyapatite occurs when the temperature is above 900 °C (Bohner, 2000; Dorozhkin, 2007). Whether water vapor is present or not, tetracalcium phosphate and α -TCP are formed at temperatures higher than 1300 °C by decomposition of hydroxyapatite (Bohner, 2000). Because stoichiometric HA is obtained by high temperature processing, it is highly crystalline.

Table 2.8. Possible substituted calcium phosphate apatite phases
(Source: Wopenka and Pasteris, 2005)

Compound	Ca/P Molar Ratio
$\text{Ca}_{10}(\text{PO}_4)_6(\text{OH})_2$ hydroxyapatite, end-member	1.67
$\text{Ca}_{10}(\text{PO}_4)_6\text{F}_2$ fluorapatite, end-member	1.67
$\text{Ca}_{10}(\text{PO}_4)_6(\text{OH},\text{F})_2$ mixed hydroxyl-fluorapatite	1.67
$\text{Ca}_{10}(\text{PO}_4)_6(\text{Cl})_2$ chlorapatite, end-member	1.67
$\text{Ca}_{10}(\text{PO}_4)_6(\text{Cl},\text{F})_2$ mixed chlor-fluorapatite	1.67
$\text{Ca}_{10}(\text{PO}_4)_6\text{CO}_3$ A-type carbonated apatite unhydroxylated, end member	1.67
$\text{Ca}_{10-x}[(\text{PO}_4)_{6-2x}(\text{CO}_3)_{2x}]\text{F}_2$ B-type carbonated fluorapatite, end member, francolite*	≥ 1.67
$\text{Ca}_{10-x}[(\text{PO}_4)_{6-2x}(\text{CO}_3)_{2x}](\text{OH})_2$ B-type carbonated hydroxyapatite, end member, dahllite*	≥ 1.67
$\text{Ca}_{10-x}[(\text{PO}_4)_{6-2x}(\text{CO}_3)_{2x}]\text{CO}_3$ mixed A-type and B-type carbonated apatite	≥ 1.67
$\text{Ca}_{10-x}[(\text{PO}_4)_{6-x}(\text{CO}_3)_x]\text{OH}_{2-x}$ Ca- and OH- deficient B-type carbonated apatite	1.67
$\text{Ca}_{10-x}[(\text{PO}_4)_{6-x}(\text{HPO}_4)_x]\text{OH}_{2-x}$ HPO ₄ ⁻ containing apatite	≤ 1.67

* mineral name

Its high crystallinity makes it the second most stable calcium phosphate phase in aqueous solutions after fluorapatite. Since all biological apatites, dentine, enamel and bone are carbonated apatites containing Na, Mg, K, F and Cl (Suchanek and Yoshimura, 1998), stoichiometric hydroxyapatite is not found in biological systems (Dorozhkin, 2007).

Calcium deficient hydroxyapatite, $\text{Ca}_{10-x}(\text{HPO}_4)_x(\text{PO}_4)_{6-x}(\text{OH})_{2-x}$ $0 < x < 1$, is obtained by substitution of HPO_4^{2-} ions into the lattice and generation of vacancies in calcium and hydroxide sites upon substitution (Dorozhkin, 2007). Calcium to phosphorous molar ratio of CDHA is lower than 1.67 since the calcium vacancies are generated by substitution of HPO_4^{2-} ions. Maximum level of substitution is the incorporation of 1 mol HPO_4^{2-} ions (when x equals to 1). At this level, Ca/P becomes 9/6, which is equal to 1.5. Calcium to phosphorus ratio of CDHA therefore ranges between 1.5 and 1.67 (Bohner, 2000; Dorozhkin 2007). CDHA is poorly crystalline having broad X-ray diffraction peaks. CDHA is easily precipitated from calcium and phosphate solutions where carbon dioxide is expelled by boiling, but counter ions in the solutions possibly incorporate into the apatite structure (Dorozhkin, 2007). In fact this is the reason why CDHA is not found in biological systems and bone and teeth also contains sodium, potassium, magnesium, strontium, fluoride and chloride (Dorozhkin, 2007). In solutions containing dissolved carbon dioxide or in human body due to the presence of bicarbonate in blood plasma, carbonate is also present in the CDHA. Ion substituted CDHA is much more similar to biological apatites than stoichiometric apatite.

Fluorapatite, $\text{Ca}_{10}(\text{PO}_4)_6\text{F}_2$ where hydroxyl ions in hydroxyapatite were exchanged with fluoride ions, is a calcium phosphate compound characterized with its highest stability and lowest solubility (Dorozhkin, 2007).

2.3.2 Calcium Phosphate Bone Cements

In bone grafting applications, only two calcium phosphate phases HA and TCP had been widely used in orthopedic applications in powder, dense, granular and porous forms, as coatings (only HA) or as biphasic combinations until the discovery of calcium phosphate bone cements (CPC). Development of CPCs made other calcium phosphate compounds as important as HA and TCP.

Calcium phosphate bone cement is based on a hardening reaction of a mixture of solid phase containing one or more calcium phosphate compounds and aqueous solution. Mixture obtained upon mixing is either injectable or putty like material which can be molded into a desired shape. The most unique property of calcium phosphate bone cement is the setting (hardening reaction) of the mixture in a defined time interval. In orthopedic surgery, CPC cement is used during the surgical operation environment. Surgeon mixes two phases and applies into the bone defect by injection or by molding with the aid of spatula. As soon as mixing the solid and liquid parts, hardening of the cement starts. Therefore, setting time should neither be too short or too long. It should be long enough to be mixed and injected into the defect. It should harden in a short period of time after the application into the bone defect.

There are at least twenty three different commercially available calcium phosphate cements manufactured by at least thirteen companies in the orthopedic materials market (Table 2.9). Commercial names, compositions, final setting products and manufacturers of these cements are shown in Table 2.9. Calcium phosphate compounds used in these cement formulations are MCPM, DCPD, DCPA, ACP, β - and α -TCP, ACP, PHA and HA. In addition to calcium phosphate compounds CaCO_3 , $\text{Mg}_3(\text{PO}_4)_2$, SrCO_3 and CaSO_4 are used.

Table 2.9. Commercially available calcium phosphate cements, their compositions and manufacturers
(Source: Bohner et al., 2005; Ishikawa, 2008)

Commercial Cement Name	Composition of Powder	Composition of Solution	Setting Product	Manufacturer
α -BSM Embare Biobone	ACP (50%), DCPD (50 %)	H ₂ O (unbuffered saline)	Apatite	ETEX
BoneSource	TTCP (73%), DCPA (27%)	H ₂ O, mixture of Na ₂ HPO ₄ and NaH ₂ PO ₄	Apatite	Stryker-Leibinger Corp
Cementek [®]	TTCP, α -TCP mixture (87 %) Sodium glycerophosphate (13 %)	H ₃ PO ₄ (13.8 %), Ca(OH) ₂ (3.4 %), H ₂ O (82.8 %)	Apatite	Teknimed
Cementek [®] LV	TTCP, α -TCP mixture (87 %) Sodium glycerophosphate (12 %) Polydimethylsiloxane (1 %)	H ₃ PO ₄ (13.8 %), Ca(OH) ₂ (3.4 %), H ₂ O (82.8 %)	Apatite	Teknimed
Calcibon [®] (Biocement D)	α -TCP (58 %), PHA (8.5 %), DCPA (25 %), CaCO ₃ (8.5 %)	H ₂ O, Na ₂ HPO ₄ (1 %)	Apatite	Biomet
Mimix [™]	TTCP, α -TCP, C ₆ H ₅ O ₇ Na ₃ ·2H ₂ O	H ₂ O, citric acid	Apatite	Biomet
QuickSet Mimix [™]	-	-	Apatite	Biomet
Biopex [®]	α -TCP (75%), TTCP (20 or 18 %), DCPD (5%), HA (0 or 2 %)	H ₂ O, sodium succinate (12 or 13 %), sodium chondritin sulphate (5 or 5.4 %)	Apatite	Mitsubishi Materials
Biopex [®] -R	α -TCP, TTCP, DCPD, HA Mg ₃ (PO ₄) ₂	H ₂ O, sodium succinate, sodium chondritin sulphate, NaHSO ₃	Apatite	Mitsubishi Materials
KyphOs [™]	α -TCP (77%), Mg ₃ (PO ₄) ₂ (14 %), MgHPO ₄ (4.8 %), SrCO ₃ (3.6 %)	H ₂ O, (NH ₄) ₂ HPO ₄ (3.5 M)	Apatite	Kyphon

(Cont. on next page)

Table 2.9. (cont.)

Commercial Cement Name	Composition of Powder	Composition of Solution	Setting Product	Manufacturer
Callos™	-	-	Apatite	Skeletal Kinetics
Rebone	TTCP, DCPA	H ₂ O	Apatite	Shangai Rebone Biomaterials Co., Ltd.
Norian® SRS	α-TCP (85%), CaCO ₃ (12 %), MCPM (3 %)	H ₂ O, Na ₂ HPO ₄	Apatite	Synthes-Norian
Norian® CRS	α-TCP (85%), CaCO ₃ (12 %), MCPM (3 %)	H ₂ O, Na ₂ HPO ₄	Apatite	Synthes-Norian
Norian® SRS Fast Set Putty	-	-	Apatite	Synthes-Norian
Norian® CRS Fast Set Putty	-	-	Apatite	Synthes-Norian
Primafix®	TTCP, DCPA	Sodium hydrogen sulfite	Apatite	NGK Spark Plug Co.
Cerapaste®	TTCP, DCPA	Sodium dextran sulfate sulfur 5	Apatite	NGK Spark Plug Co.
ChronOS™ Inject	β-TCP (73%), MCPM (21 %), MgHPO ₄ ·3H ₂ O (5%), MgSO ₄ (<1%), Na ₂ H ₂ P ₂ O ₇ (<1 %)	H ₂ O, sodium hyaluronate (0.5 %)	Brushite	Synthes-Norian
Eurobone®	β-TCP (98%), Na ₄ P ₂ O ₇ (2 %)	H ₂ O, H ₃ PO ₄ (3.0 M), H ₂ SO ₄ (0.1 M)	Brushite	Kasios
VitalOs	Component 1: β-TCP (1.34g), Na ₂ H ₂ P ₂ O ₇ (0.025g), H ₂ O, salts (0.05 M pH 7.4 PBS solution) Component 2: MCPM (0.78g), CaSO ₄ ·H ₂ O (0.39g), H ₂ O, H ₃ PO ₄ (0.05M)		Brushite	CalciphOs

CHAPTER 3

PHOSPHATE AND CALCIUM ANALYSES

3. 1. Phosphate Analysis

Colorimetric phosphorous analysis methods are generally based on the formation of phosphomolybdate complex when molybdate is added to dilute orthophosphate solutions under acidic conditions (Cogan et al., 1999). If this reaction is performed in the presence of vanadium, yellow vanadomolybdophosphoric acid is produced and color is proportional to the orthophosphate concentration (Eaton et al., 1995). When the reaction is performed in the absence of vanadium, colorless phosphomolybdate complex is turned into molybdenum blue by the reduction of phosphomolybdate complex by the use of several reducing agents such as sulfite and aminonaphtholsulfonic acid mixture, stannous chloride, ascorbic acid and ascorbate in the presence bismuth or antimony (Cogan et al., 1999).

Among these methods, three of them (vanadomolybdate phosphoric acid, stannous chloride and ascorbic acid methods) were given in Standard Methods for the Examination of Water and Waste Water published by American Public Health Association (Eaton et al., 1995). In these methods, phosphorous is converted into dissolved orthophosphate and dissolved orthophosphate is then analyzed colorimetrically. Due to the form of phosphorous in the samples, acid hydrolysis or digestion can be applied. Phosphorous analyzed without hydrolysis and oxidative digestion is the reactive phosphorous which is a measure of orthophosphate. Particulate or dissolved condensed phosphates can be converted into dissolved orthophosphates by acid hydrolysis. Oxidative digestion of organic matters is used to convert organically bound phosphorous to orthophosphate. The vanadomolybdate phosphoric acid, stannous chloride and ascorbic acid methods are selected depending on the concentration of phosphorous in the samples. For routine analysis within the range of phosphorous concentrations between 1 to 20 mg/L (corresponding to 3 to 60 mg/L), vanadomolybdate phosphoric acid method is used. However, stannous chloride and ascorbic acid method are used for the range of 0.01 to 6 mg/L (0.03 to 18 mg PO_4^{3-} /L).

Minimum detectable concentrations are 0.2 ppm, 0.003 ppm, and 0.01 ppm phosphorous (corresponding to 0.6, 0.009 and 0.03 mg $\text{PO}_4^{3-}/\text{L}$) for vanadomolybdatephosphoric acid, stannous chloride and ascorbic acid methods, respectively.

The sensitivities of the colorimetric methods can be increased by the addition of cationic dyes (such as malachite green, crystal violet and quinaldine red) into the system (Cogan et al., 1999). Changes in the color of these dyes when added into the phosphomolybdic acid containing solutions are the basis of these assays. Malachite green dye is yellow colored in the 0.45 M H_2SO_4 concentration (corresponding to nearly pH 0.5) in the assay conditions and blue-green colored above pH 2. Addition of phosphate into the system results with the phosphomolybdate complex and it consequently turns the color of the solution into blue-green due to the electrostatic binding between blue-green form of dye and phosphomolybdate complex. Final acidity, molybdate and malachite green concentrations and necessity of stabilizers in order to avoid reduction of the color complex are the main parameters in malachite green based system.

Van Veldhoven and Mannaerts (1987) tested the effects of final acidity and different color stabilizers on the complex formation between malachite green dye and phosphomolybdate complex. They found that 0.9 N (0.45 M) H_2SO_4 as an optimum final acidity and poly vinyl alcohol with a final concentration of 0.05 (w/v) % as an optimum stabilizer. Cogan et al. (1999) reported the optimum final concentrations of malachite green and heptamolybdate as 6 mM and 120 μM , respectively in a microplate adapted malachite green assay which was automated by robotics system. They tested other cationic dyes; crystal violet and quinaldine red together with ascorbate reduction and antimonyl-modified ascorbate method in a microplate adapted format in automated system. The highest sensitivity was observed in malachite green assay. They also found that malachite green assay was suitable for the analysis of compounds containing organic phosphates or polyphosphates.

Interferences are one of the main obstacles which restrict the applicability of the assays. Microplate based malachite green assay were tested for its suitability for the analysis of phosphorous in water and soil (D'Angelo et al., 2001). Interferences rising from CaCl_2 , KCl , HCl and NaOH with concentrations 0.1, 0.2, 0.3, 0.4 0.5 and 1 M on aqueous samples containing 0.5 mg P/L were tested. Concentrations lower than or equal to 0.1 M had no effect on the absorbances. NaOH concentration of 0.4 M and HCl

concentration of 0.2 M inhibited the absorbance whereas CaCl_2 concentration greater than 0.1 M increased the absorbance. No interference was observed in the case of 1M KCl. These results show that malachite green method can be applicable for the complex solutions containing CaCl_2 , KCl, HCl and NaOH with higher concentrations when compared with the concentration range of phosphorous analysed. Phosphate dissolved in several acidic solutions was tested by Attin et al., (2005b) who used the modification of malachite green method in microplate based assay. They used HCl instead of sulfuric acid and no color stabilizer like PVA were used in their study. HCl, perchloric acid (HClO_4), oxalic acid, maleic acid, tartaric acid, citric acid, lactic acid and acetic acid was used to adjust pH of 2 in the phosphate solution. Malachite green method was found to be suitable for phosphate analysis in all acid solutions except citric acid.

Microplate readers have been in use for the microscale colorimetric analyses, for example for the analysis of inorganic N, urea, enzyme activity, C source utilization and in the immunoassays (D'Angelo et al., 2001). A microprocessor has a multichannel optical system which enables measuring absorbance of solutions at the defined wavelength (D'Angelo et al., 2001). The microplate system used in this study is a microprocessor controlled photometer system which makes possible to read and print the results of 96 well in a short time. Advantages of microplate based methods are high sensitivity, reduction in time required for the measurement of absorbance, accuracy, precision, high throughput, and low waste production (D'Angelo et al., 2001).

Microplate based malachite green assay have been widely used for phosphorous analyses in standard solutions (Cogan et al., 1999), in acidic solutions (Attin et al., 2005a), soil extracts (D'Angelo et al., 2001), phospholipids (Cogan et al., 1999), soil microbial biomass (Jeannotte et al., 2004), and beverages either modified by addition of calcium or calcium plus phosphate plus fluoride during testing of the enamel erosion by acidic soft drinks (Attin et al., 2005b).

Apatite dissolution or solubility testing requires the analysis of calcium and phosphate ions released into the aqueous solutions. Wide ranges of temperatures and pH values can be used to study apatite solubility and dissolution. Different aqueous electrolyte solutions having several ions and buffers can also be used to measure solubility or dissolution rate of to determine *in vitro* dissolution behavior. For these reasons, a phosphorous analysis method should give accurate results within the wide range of pH values and electrolyte contents. Since the interfering concentrations are high when compared to phosphate concentrations and method is suitable for the wide

range of acidic solutions, malachite green phosphate analysis can be used to analyze phosphate ions during apatite dissolution.

By the advantages of microplate based system, quick and accurate determination of phosphate ions during the apatite dissolution in several electrolyte solutions may be possible. We therefore preferred the microplate based malachite green phosphate assay in this study.

3.2. Calcium Analysis

Calcium analysis in solutions can be performed by inductively coupled plasma, atomic absorption spectroscopy, ion chromatography or spectrophotometric methods. Selection of the method depends on the availability of instrumentation, cost, sensitivity of the method, lowest limit of quantization, interferences and ease of use. The solution composition is generally important for the selection of the method. Interferences arising from the solution composition lead to inappropriate results. Among the above mentioned methods, the spectrophotometric assays are generally preferred due to the ease of application, low cost and availability.

One of the spectrophotometric methods for the calcium analysis was reported by Michaylova and Ilkova (1971). Their method based on the blue complex formation between calcium and Arsenazo III dye. The method was highly sensitive at pH 9.0 with maximum absorbance however better selectivity was reported at pH 5-6. By their methods concentration range of 0.25-1.25 ppm Ca could be analyzed. They also showed that calcium can be analyzed even in the presence of 100 folds magnesium and manganese.

Arsenazo III based calcium method has also been used for the calcium determination in the serum and plasma with some modifications (Lamkin and Williams, 1965; Gawoski and Walsh, 1989; Leary et al., 1992a; Leary et al., 1992b). Attin et al. (2005a) determined the suitability of microplate based Arsenazo-III method to analyze calcium dissolved in different acidic solutions. Wide range of acidic solutions (hydrochloric phosphoric, maleic, oxalic, lactic, tartaric, acetic, and citric acid) were used in their study. This method was not found suitable for tartaric acid, oxalic acid and citric due to their chelating abilities with calcium. Calcium with 0.25 ppm to 2 ppm levels could be analyzed with all other acidic solutions.

Arsenazo III - calcium determination was used to analyze calcium in the dissolution testing of hydroxyapatite (Bloebaum et al., 1998). They tested dissolution of particulate hydroxyapatite in solutions at three different pH levels (cacodylate buffer pH of 5.0, 6.0, and 7.1). Total calcium concentrations were analyzed by bichromatic end point methodology by Arsenazo III dye. Another application of Arsenazo III for the determination of calcium release was reported (Hannig et al., 2005). They determined calcium release from bovine enamel samples incubated in acetic, malic, tartaric, phosphoric, hydrochloric and lactic acid. These studies show that Arsenazo-III method can be used for the calcium determination in the solutions in which any calcium phosphate solubility is of interest.

Hydroxyapatite has a low solubility at and above physiological pH levels. This will lead to release of low levels of calcium into the solutions. Since Arsenazo III method enables the determination of calcium at ppm level, it can be used for the determination of calcium released from hydroxyapatite. The aim of this study is to determine hydroxyapatite solubility in solutions having ions found in human blood plasma at the same concentration levels, it is necessary to use a method which correctly determine calcium levels within the presence of other ions. Arsenazo-III method can also be used for this purpose because it has been used for the determination of serum or plasma calcium levels.

Arsenazo III is a synthetic organic molecule which have chromotropic nucleus with two analytical o'-arsono-o'-oxyazo groups (Alimarin and Savvin, 1966). Two different conformations (extended and contracted) of Arsenazo III are shown in Figure 3.1. Eight different ionizable groups are present on the Arsenazo III molecule and their pK values are $pK_1 = -2.5$, $pK_2 = 0$, $pK_3 = 2.5$, $pK_4 = 2.5$, $pK_5 = 5.3$, $pK_6 = 5.3$, $pK_7 = 7.5$ and $pK_8 = 12.4$ (Rowatt and Williams, 1989). A site in extended form and B site in contracted form are reported as the sites where large and small cations bind, respectively (Rowatt and Williams, 1989).

Double and triply charged cations form 1:1 complexes with Arsenazo III (Basargin et al., 2000). Possible structures found in the metal-Arsenazo III complexes suggested by Alimarin and Savvin (1966) are shown in Figure 3.2. Figure 3.2.A shows the possible structure which can be found with bivalent and trivalent metals which forms Arsenazo III complexes by 1:1 complexation and with tetravalent metals forming 1:2 (MeR_2) complexes. The structure found with tetravalent cations forming 1:1 complexes is shown in Figure 3.2.B. Alimarin and Savvin (1966) also suggested that

these structures can not be generalized to all elements and whole pH ranges. They also note that several studies contradict the direct involvement of oxy group of naphthelene nucleus in the metal binding (Alimarin and Savvin, 1966).

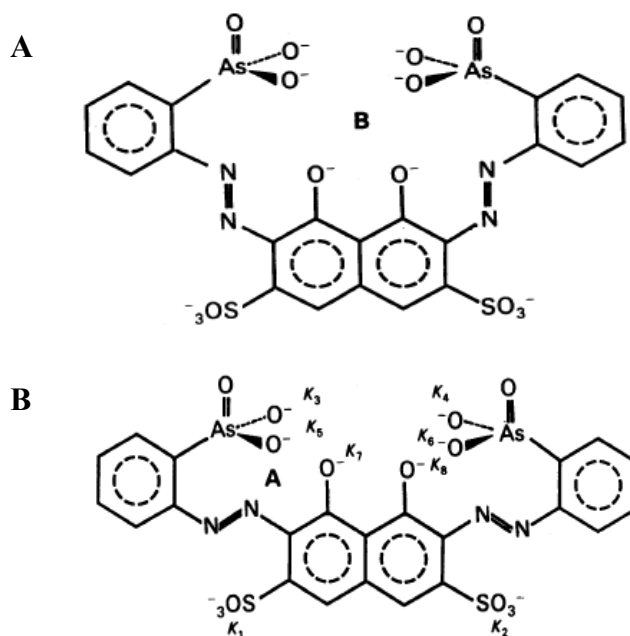


Figure 3.1. Contracted (A) and extended conformations (B) of Arsenazo III (Source: Rowatt and Williams, 1989).

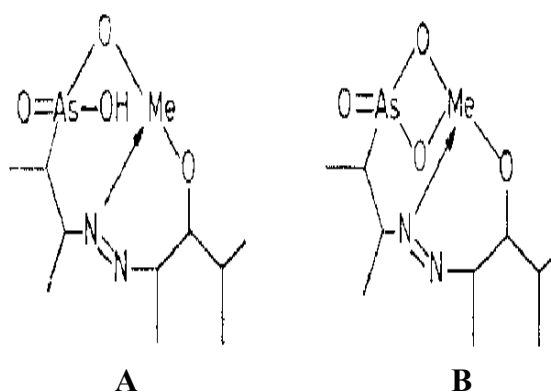


Figure 3.2. Postulated structures found with bivalent and trivalent cations forming 1:1 complexes and trivalent ions forming 1:1 complexes (A), with tetravalent cations forming 1:1 complexes (B).

Spectral characteristics and interaction of Arsenazo III with cations have received special attention (Kendrick et al., 1977; Bauer, 1981; Rowatt and Williams, 1989; Kratochvil and He, 1990; Hosten and Rohwer, 1997; Rohwer et al., 1997). Free Arsenazo III shows absorption maxima at 520-530 nm however metal Arsenazo III complexes show maximum absorption at 655-665 nm (Marczenko and Balcerzak, 2000; Rowatt and Williams, 1989). Rowatt and Williams (1989) reported that absorption of Arsenazo III at 540 nm is constant between pH 1 and 7.4 but shifts to higher wavelengths above pH 7.4. Changes in spectra were attributed to the ionization of phenolate groups at and above pH 8. Absorption of metal-dye complex is also dependent on pH (Mikhaylova and Ilkova, 1971). The presence of the second peak at 610 nm seen upon complex formation is attributed to the symmetry breakdown of the Arsenazo III molecule upon involvement of only one analytical group with complexation (Basargin et al., 2000).

Calcium and Arsenazo III binding stoichiometries have also been studied in detail (Bauer 1981; Brown and Rydqvist, 1981; Ahmed et al., 1980; Chiu and Haynes, 1980). Bauer (1981), Ahmed et al. (1980) and Chiu and Haynes (1980) showed that 1:1 complexation occurs between calcium and Arsenazo III in contrast to studies suggesting 1:2 complexation. However, Brown and Rydqvist (1981) showed 1:2 and 1:1 complexation depending on the method. Calcium binding was also suggested to occur with atom fitting between phenol hydroxyl and the arsono groups (Rowatt and Williams, 1989).

Arsenazo III-calcium complexation has also been used in many commercial calcium analyses kits (Table 3.1). These analyses kit includes Arsenazo III reagents in which Arsenazo III concentration ranges between 120 and 200 μM . Buffers are generally imidazole, MES and good's buffer with concentrations between 50 and 100 mM. pH values of the reagents are 6.5 or 6.8. Standard solutions are mixed with dye reagents generally in 10:1000 (solution to reagent ratio) volumetric ratio. Since calcium concentration in standard solutions is almost 100 mg/L and solutions are 1:100 diluted after mixing, total calcium concentration in the mixture is 1 mg/L. If solution have 1 mg/L calcium before analysis, it seems impossible to determine calcium concentrations. Therefore a method is needed to determine lower levels of calcium in the solutions.

Table 3.1. Commercial Arsenazo III-calcium determination kits

Company	C _{AsIII} (μM)	Buffer type & pH	C _{Buffer} (mM)	Standard Conc. (mg/L)	Reagent Volume (μL)	Sample (Standard) Volume (μL)	Wavelength (nm)	Linearity (mg/L)	Detection Limit (mg/L)	Reference
Diagnosticum Rt. ^a	200	MES 6.5	100	100	1000	10	650 (600)*	160	NS	Department of Biochemistry Faculty of Medicine University of Szeged, 2010
Chema Diagnostica ^b	200	Good's buffer 6.8	50	100	2000	20	660 (650)*	200	1	Chema Diagnostica, 2010
BioLabo SA France ^c	>180	Imidazol 6.8	>90	100	1000	20	650 (640-660)*	150	2.1	BioLabo, 2010
Infinity™ Thermo Fisher Inc. USA ^d	136	NS	NS	NS	300 or 350	5	Primary 600-660 Secondary 700	Between 60-150	NS	Thermo Scientific, 2010
Pointe Scientific, USA ^e	>150	NS	NS	100	1000	10	650	150	NS	Pointe Scientific, 2010
National Biochemicals Corp. USA ^e	>150	NS	NS	100	3000	30	650	150	NS	National Biochemicals, 2010
AMS Diagnostics ^d	200	Imidazole 6.75	100	NS	1000	20	650	10 to 150	10	AMS Diagnostic, 2010

Table 3.1. (cont.)

Company	C _{AIII} (μ M)	Buffer type & pH	C _{Buffer} (mM)	Standard Conc. (mg/L)	Reagent Volume (μ L)	Sample (Standard) Volume (μ L)	Wavelength (nm)	Linearity (mg/L)	Detection Limit (mg/L)	Reference
Fluitest Analyticon ^f	120	Imidazol 6.5	100	100	1000	10	650 (640- 660)*	2 to 300 ^g	2	Analyticon Diagnostics, 2010
Bt products ^h	200	Imidazol 6.75	100	NS	1000	20	650 (600- 660)*	1 to 150	NS	BT Products, 2010
Mindray ⁱ	120	Phosphate buffer NS	50	NS	1000	10	650	4 to 150	4	Mindray Medical, 2010
mti-diagnostics GmbH	120	Good's buffer 6.5	100	100	1000	10	650 (640- 660)*	2 to 300 ^g	2	mti diagnostics, 2010
CIMA Scientific ^k	150	NS	NS	100	1000	10	650	5 to 150	NS	CIMA Scientific, 2010

*optional wavelength, NS not stated, ^a 600 nm is not suggested when absorbance of working reagent greater than 1.5, ^b Bichromatic reading at 660/700 nm is also suggested, reagent contains stabilizer, ^c For bichromatic readings 700 nm was suggested as second wavelength, sensitivity was reported as 1 mg/L, color was reported to be stable for 1 hour away from light, ^d Reagent contains surfactant and 0.05 % sodium azide, ^e Reagent contains surfactant and 5.0 mM 8-hydroxyquinoline sulfonate, color was reported to be stable for 1 hour, ^f Reagent contains detergent, ^g Stated as measuring range, ^h Reagent contains surfactant, color was reported to be stable for 1 hour, ⁱ Reagent contains 8-hydroxyquinoline 5-sulfonic acid, ^k Reagent contains 5.0 mM 8-hydroxyquinoline sulfonate and stabilizer, color was reported to be stable for 1 hour.

CHAPTER 4

SOLUBILITY AND DISSOLUTION OF CALCIUM PHOSPHATES

Solubility and dissolution are two different phenomena which are important in the behavior of calcium phosphates in aqueous solutions. Solubility is directly related to equilibrium conditions (Lorimer and Cohen-Adad, 2003) whereas dissolution is generally considered as a removal of ions or molecules from the sample and transfer into the solution (Dorozhkin, 1999).

Solubilities of calcium phosphates particularly that of hydroxyapatite are of great importance because bone and teeth formation, fracture repair, caries formation and pathological mineralizations are all directly related to the solubilities of calcium phosphates. Dissolution however is important in caries formation, disease associated with bone loss, osteoclastic resorption of bone during bone turnover.

4.1. Solubility of Calcium Phosphates

Solubility of a soluble or highly soluble solid is generally expressed as the maximum amount of the solute dissolved in a given amount of the solvent. The brief definition of solubility is indeed the composition of the homogeneous mixture (solution) which is saturated (at equilibrium) with respect to one of its components (Lorimer and Cohen-Adad, 2003). Composition at the equilibrium as mass or moles of solute per mass of solvent or solution, or mass or moles of solute per volume of solvent or solution is generally used to express solubility (Mullin, 1993).

When equilibrium concentrations determined at various temperatures at constant pressure are plotted against temperature, typical solubility diagram is obtained (Figure 4.1). Three regions are present in solubility diagram, stable, metastable and labile regions (Mullin, 1993). Solid line in Figure 4.1 represent the solubility line where solid and liquid are at equilibrium. At the solubility line solution is saturated with respect to solute. However, solution is supersaturated above this line. The region under the solubility line is called stable region. At this region solution is undersaturated with

respect to solute meaning that crystallization is impossible. When equilibrium attained between solid and solvent, solvent in fact dissolves slightly more solid. This is called super solubility (Mullin, 1993) and represented as dashed line in Figure 4.1. The region between solubility and super solubility line is therefore called metastable region. At the metastable region, solution is stable until any disturbance in the solution occurs. Disturbances e.g addition of a seed results in the initiation of crystallization (Mullin, 1993; Lorimer and Cohen-Adad, 2003). Third region in solubility diagram is the region over the super solubility line (labile region) where spontaneous crystallization is possible.

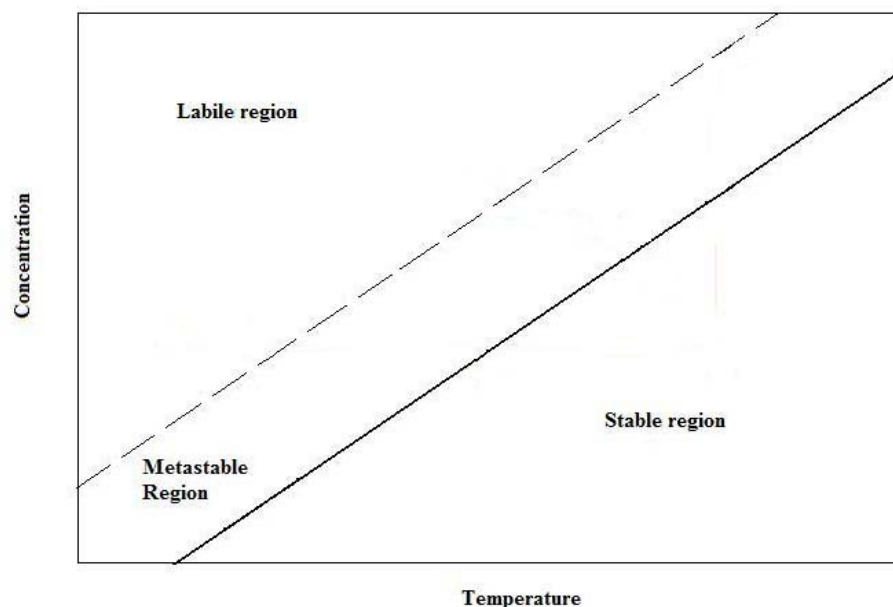


Figure 4.1 Solubility diagram
(Source: Mullin, 1993)

When a sparingly soluble substance is of interest, solubility is expressed as solubility product rather than mass or moles of the compound with respect to mass or moles of solvent. Solubility product can either be concentration solubility product or activity solubility product (Mullin, 1993). When the saturation concentrations are lower than 10^{-3} mol/L concentration solubility product is used since activity coefficients become equal to 1 at infinite dilutions (Mullin, 1993). Activity solubility product constant is used for more concentrated solutions. Dissociation of a simple sparingly soluble compound and solubility product constants are shown below (Mullin, 1993):



$$K_c = (c_+)^x (c_-)^y \quad (4.2)$$

$$K_a = (a_+)^x (a_-)^y = (c_+ \gamma_+)^x (c_- \gamma_-)^y \quad (4.3)$$

$$a = \gamma * c \quad (4.4)$$

where z^+ and z^- are valencies of the ions, c_+ and c_- are concentrations of ions, γ_+ and γ_- are activity coefficients and a_+ and a_- are ionic activities for a saturated solution. K_c and K_a are concentration and activity solubility products, respectively.

For example, thermodynamic solubility product constant of stoichiometric hydroxyapatite based on the activities of ions are as follows

$$K_a = (c_{Ca^{2+}} \gamma_{Ca^{2+}})^5 (c_{PO_4^{3-}} \gamma_{PO_4^{3-}})^3 (c_{OH^-} \gamma_{OH^-})^2 \quad (4.5)$$

or

$$K_a = (c_{Ca^{2+}} \gamma_{Ca^{2+}})^{10} (c_{PO_4^{3-}} \gamma_{PO_4^{3-}})^6 (c_{OH^-} \gamma_{OH^-})^2 \quad (4.6)$$

As shown in Equations 4.5 and 4.6, solubility product constant for hydroxyapatite can be calculated by two different expressions. Chemical composition of hydroxyapatite molecule is $Ca_5(PO_4)_3OH$. However, chemical formula of $Ca_{10}(PO_4)_6(OH)_2$ is frequently used in order to show that the unit cell of hydroxyapatite contains two hydroxyapatite molecules (Dorozhkin, 2007). Thermodynamic solubility product constant can be calculated by using different equations depending on the chemical formula used to describe hydroxyapatite.

If activity solubility product is to be calculated, prediction of activity coefficients is needed. In order to calculate activity coefficients, ionic strength of the solution are calculated first. Ionic strength of a solution is the total electrolyte concentration and calculated as follows (Christian, 1994);

$$I = \frac{1}{2} \sum c_i z_i^2 \quad (4.7)$$

where I is the ionic strength, c_i and z_i are the concentration and charge of the i^{th} ion.

Activity coefficients are calculated using theoretical expression derived by Debye-Hückel (Christian, 1994);

$$-\log \gamma_i = \frac{0.51z_i^2\sqrt{I}}{1 + 0.33\alpha_i\sqrt{I}} \quad (4.8)$$

where α_i is the effective diameter of the hydrated ion.

This equation can be used for ionic strength up to 0.2. A simplified form of Debye-Hückel equation however can be used for ionic strengths less than 0.01 (Christian, 1994).

$$-\log \gamma_i = \frac{0.51z_i^2\sqrt{I}}{1 + \sqrt{I}} \quad (4.9)$$

There are several equations developed for the higher ionic strengths such as Davies modification of the Debye-Hückel equation. Davies modification is used for ionic strength up to 0.6 (Christian, 1994).

$$-\log \gamma_i = \frac{0.51z_i^2\sqrt{I}}{1 + 0.33\alpha_i\sqrt{I}} - 0.10z_i^2I \quad (4.10)$$

Solubilities of bone mineral have received great attention in order to reveal the chemistry of bone resorption and formation in healthy state and bone loss in several pathological cases. In early reports, different strategies were used for the solubility determinations of bone and calcium phosphate phases. Holt et al. (1925) for example titrated H_3PO_4 solution with $\text{Ca}(\text{OH})_2$ and calculated the solubility products of CaHPO_4 and $\text{Ca}_3(\text{PO}_4)_2$ by using activity coefficients. According to the analysis of the precipitates, they assumed that precipitates were $\text{CaHPO}_4 \cdot 2\text{H}_2\text{O}$ and $\text{Ca}_3(\text{PO}_4)_2$. Logan and Taylor (1937) also studied the solubility products of the precipitates obtained by direct precipitation or by adding precipitates and powdered bone into the supersaturated solutions at pH 7.0-8.0. Like Holt et al. (1925) they assumed the chemical formula of the precipitates as $\text{Ca}_3(\text{PO}_4)_2$. Greenwald (1942) however used the composition of $\text{Ca}(\text{CaHPO}_4)$ to avoid inconsistencies obtained in the solubilities when the composition

of $\text{Ca}_3(\text{PO}_4)_2$ is assumed. The use of compositions of $\text{Ca}_3(\text{PO}_4)_2$ and $\text{Ca}(\text{CaHPO}_4)$ has possibly let erroneous solubility product constants since many different calcium phosphate species may exist in aqueous solutions depending on the pH and it is now well known that $\text{Ca}(\text{H}_2\text{PO}_4)_2 \cdot \text{H}_2\text{O}$, $\text{CaHPO}_4 \cdot 2\text{H}_2\text{O}$, $\text{Ca}_8(\text{HPO}_4)_2(\text{PO}_4)_4 \cdot 2\text{H}_2\text{O}$, amorphous calcium phosphate, hydroxyapatite and calcium deficient hydroxyapatite can be precipitated in solutions at physiological temperatures (Dorozhkin, 2007). Additionally, dissolution of the calcium phosphate compounds and precipitation of a new calcium phosphate compounds as well as formation of different calcium phosphate phases and hydrolysis of several calcium phosphates in aqueous solutions are also known. For example, hydroxyapatite formation from incongruent dissolution of CaHPO_4 or $\text{CaHPO}_4 \cdot 2\text{H}_2\text{O}$ in aqueous solutions was reported in the study of Brown (1992).

In contrast to early studies, Levinkas and Neuman (1955) used pure stoichiometric hydroxyapatite in order to represent bone mineral. They equilibrated the hydroxyapatite powder in saline solutions for the solubility determination. Solubility was represented as calcium and phosphate concentrations rather than solubility product constant. Contradictory to early studies in which equilibrations for 19 months were required, end point in the equilibrations was reached and remained stable from 1 to 77 days. The most important finding in their study was that the solubility was varied depending on the amount of powder used. Solution calcium to phosphate ratios were found to be higher than that of the solid phase indicating an incongruent solubility. Strates et al. (1957) also studied the solubility of bone mineral. They used supersaturated solutions at nearly neutral solutions and only determined the precipitate formation. They did not use bone powder sample in their study. Precipitation from supersaturated solutions was found to occur when the ion activity product of the solutions were above the solubility product of $\text{CaHPO}_4 \cdot 2\text{H}_2\text{O}$. Determination of calcium and phosphate contents of the precipitates showed that Ca/P ratios of the precipitates were equal to unity immediately after mixing and then increased to higher values at alkaline pH values. They suggested that precipitates hydrolyzed to hydroxyapatite and precipitation at alkaline regions were governed by the solubility of hydroxyapatite.

Rootare et al. (1962) studied the changes in the solubility products of hydroxyapatite powders with the change in solid to solution ratios. The solubility activity product was found to be dependent on solid to solution ratio and solubility was found to be lower when higher amounts of powder were dissolved. Apparent solubility of the hydroxyapatite was postulated to be governed by the hydrolysis of terminal

phosphate groups, release of ions according to hydrolysis reaction and the formation of surface complex of $\text{Ca}_2(\text{HPO}_4)(\text{OH})_2$. Incongruent dissolution behavior was not only observed by Rootare et al. (1962), Smith et al. (1974) also showed congruent dissolution (solution Ca/P ratio was 1.67) for the solid to solution ratios lower than 8 g/l upon equilibration of the powders 0.1 M KCl solution with pH 4.5 adjusted by hydrochloric acid. For the higher solid to solution ratios, dissolution was incongruent as Ca/P ratio of the solutions being higher than 1.67. Incongruent dissolutions was attributed to the variations in the surface layers of the unit cells associated with the preparation of the powder especially acetone washing of the powder.

Moreno et al. (1968) suggested that the variations of the solubility products of hydroxyapatite in some extent was due to the use of impure powders or very finely divided powders without stoichiometric Ca/P ratio. The presence of more acidic calcium phosphate compounds especially octacalcium phosphate and its decomposition products were regarded as the one of the major problems in the solubility determinations. For this reason they prepared hydroxyapatite powders by avoiding octacalcium phosphate precipitation. In order to obtain highly crystalline samples and to avoid contaminations of carbonate and acidic calcium phosphates, powders were subjected to heat treatment at 1000 °C in air and steam and washed with dilute phosphoric acid solution. Solubility studies were performed by equilibrating the powders in phosphoric acid solutions at 25 °C. During the calculations of the solubility products for hydroxyapatite powders, association constants for the ion-pairs of $[\text{CaHPO}_4]^\circ$ and $[\text{CaH}_2\text{PO}_4]^+$ was taken into account. Solubility products were calculated as 3.73×10^{-58} and 2.51×10^{-55} for the steam and air heated hydroxyapatite powders, respectively by using the formula of $\text{Ca}_5(\text{PO}_4)_6\text{OH}$. Together with heat treated hydroxyapatite powders, Moreno et al. (1968) also used precipitated hydroxyapatite powder without heat treatment. However, they could not calculate K_{sp} values for as prepared powder. Large variations in the solubility product values of as prepared powder were attributed to the presence of acidic calcium phosphate compounds and to the presence of foreign ions such as CO_3^{2-} in the sample.

Moreno et al. (1968) also discussed the previous studies on the solubility product of hydroxyapatite. Inability to obtain reliable solubility products for hydroxyapatite powders was attributed to the inhomogeneity of the powders used in previous studies. They also criticized the surface complex postulated by Rootare et al. (1962). They suggested that although stoichiometry of the surface of the powder was different than

that of bulk it is not reasonable to assume any specific composition for the surface complex. They also stated that if any surface complex was present it should be considered as another solid phase in the solubility calculations. Potential plots ($-\log(\text{Ca}^{2+})(\text{OH}^-)^2$ vs. $-\log(\text{H}^+)^3(\text{PO}_4^{3-})$) were used to determine the reciprocal of Ca/P ratio in the solid phases. They found Ca/P ratios of 1.69 and 1.68 for air and steam heated powders. They also used the values reported by Rootare et al. (1962) and plotted in potential plot. According to the slopes obtained in potential plots, data from Rootare et al. (1962) did not yield Ca/P ratio of surface complex of $\text{Ca}_2(\text{HPO}_4)(\text{OH})_2$.

Solubility of precipitated hydroxyapatite which did not exposed to heat treatment was determined at 5, 15, 25, and 37 °C by equilibrating the powder in phosphoric acid solutions by McDowell et al. (1977). Solubility products of hydroxyapatite at 5, 15, 25, and 37 °C were found to be 2.92×10^{-59} , 3.23×10^{-59} , 3.04×10^{-59} and 2.35×10^{-59} , respectively. They suggested 4.7×10^{-59} as the best solubility product constant at 25°C. Temperature dependence of the solubility product was represented by the following equation.

$$\log K_{sp} = -8219.41/T - 1.6657 - 0.098215T \quad (4.11)$$

Carbonate substitution is one of the most frequently observed ionic substitutions in hydroxyapatite. Bone mineral itself is a magnesium, sodium and carbonate substituted apatite. Because carbonate substitution in hydroxyapatite results in the change of crystal dimensions and decrease in the crystallinity of hydroxyapatite, solubility and dissolution behavior of hydroxyapatite is enhanced by the carbonate substitution (Baig et al., 1999). Because of the dependence of the solubility of hydroxyapatite on carbonate substitutions, solubility behaviors of carbonated apatite have also received special attention. Solubility properties of B- type (PO_4 carbonated) and A, B –type carbonated apatites (PO_4 and OH carbonated) were studied by Kurata et al. (2006). They showed that solubility product values were dependent on the degree of the carbonate substitution. Incongruent dissolution of the powder and precipitation of projections on the original powder were observed when B-type carbonated apatite was equilibrated in the solutions. However, central core dissolution was characteristic for A-type carbonated apatite.

In contrast to lower crystallinities of carbonate apatites where phosphate ions were replaced by carbonate ions, OH-carbonated apatites are highly crystalline. Since increase in solubility of carbonate apatites due to lattice defect formation are not valid for OH carbonated apatites, solubilities of OH carbonated apatites ($\text{Ca}_{10}(\text{PO}_4)_6(\text{CO}_3)_x(\text{OH})_{2-2x}$) were studied by Ito et al. (1997). The solubilities of OH carbonated apatites were determined in 0.1 M acetic acid sodium acetate buffers instead of phosphoric acid solutions. pH range used was 4.0-5.8 and constant CO_2 partial pressure of $10^{-3.52}$ was used throughout solubility determinations. Increase in solubility of hydroxyapatite upon carbonate substitution in OH^- sites were observed. In order to avoid sorption of ions from solution onto powder during the solubility measurements, measurements performed at isoelectric point were used as solubility constants whereas other K_{sp} were considered as apparent solubility constants. pK_{sp} values obtained at isoelectric point were expressed as

$$pK_{sp} = 118.65 - 0.47316 \times (\text{CO}_2 \text{ wt. \%})^{2.4176} \quad (4.12)$$

State of a solution for the precipitation of any phase is determined by undersaturation, saturation and supersaturation levels of the solutions with respect to that phase. Ion activity product of a solution is calculated by using solution activities of ions which compose the solid phase. For a solid phase of M_xA_y dissolved in aqueous solution, ion activity product of the solution for M_xA_y is given as follows;

$$I_{\text{M}_x\text{A}_y} = (a_+)^x (a_-)^y = (c_+ \gamma_+)^x (c_- \gamma_-)^y \quad (4.13)$$

For example, ion activity product of solutions for hydroxyapatite is calculated by equations given as follows:

$$I_{HA} = (c_{\text{Ca}^{2+}} \gamma_{\text{Ca}^{2+}})^5 (c_{\text{PO}_4^{3-}} \gamma_{\text{PO}_4^{3-}})^3 (c_{\text{OH}^-} \gamma_{\text{OH}^-}) \quad (4.14)$$

or

$$I_{HA} = (c_{\text{Ca}^{2+}} \gamma_{\text{Ca}^{2+}})^{10} (c_{\text{PO}_4^{3-}} \gamma_{\text{PO}_4^{3-}})^6 (c_{\text{OH}^-} \gamma_{\text{OH}^-})^2 \quad (4.15)$$

For the calculation of ion activities, all chemical equilibrium reactions in the solutions are taken into account. Equations for activity coefficients, equilibrium reactions, species balances, equation for charge neutrality together with equation used to calculate ionic strength are written and solved simultaneously to find activities of all ions found in the solution. Ion activity of the solution with respect to phase of interest is then calculated. Undersaturation ratio (s) or relative undersaturation (σ) is used to describe solution undersaturation, saturation and supersaturation level. Undersaturation ratio is calculated by the following formula;

$$s = \left(\frac{I}{K_{sp}} \right)^{\frac{1}{n}} \quad (4.16)$$

in which I and K_{sp} are ion activity of the solution and thermodynamic solubility product, respectively and n is number of ions in a unit formula of dissolving phase. n equals to 18 or 9 depending on the formula of hydroxyapatite used to calculate I and K_{sp} . If s is lower than unity, solution is undersaturated with respect to phase of interest and precipitation of that phase is improbable. If s is higher than unity, solution is supersaturated and precipitation occurs in the solution. When s equals to unity, ionic activity of the solution and thermodynamic solubility product constant are equal to each other. Solution in this case is saturated with respect to phase of interest. Solution is stable unless any disturbance in the system occurs. If any disturbance in the system is provided, precipitation is observed. Relative undersaturation (Equation 4.17) is also used to describe the saturation level of the solutions.

$$\sigma = 1 - s \quad (4.17)$$

As far as undersaturation ratio is known, thermodynamic driving force for the precipitation which is the change in the Gibbs free energy can be calculated as follows;

$$\Delta G = -RT \ln s \quad (4.18)$$

where ΔG is change in Gibbs free energy (J/mol), R is the universal gas constant (J/mol*K), T is absolute temperature (K) and s is undersaturation ratio (Lu and Leng, 2005).

Because of the variable solubility product constants found for carbonated apatites in weak acid solutions, metastable equilibrium solubility concept was used to describe solubility behavior of carbonated apatites (Chhetry et al. 1999). It is suggested that in acetate buffered systems, carbonate apatites show initial rapid dissolution and system reaches metastable equilibrium where dissolution is almost stopped and no nucleation or crystal growth is observed (Chhetry et al. 1999). This metastable equilibrium solubility behavior together with surface complexes was found to govern solubility behavior of carbonated apatites (Chhetry et al. 1999; Baig et al., 1999; Heslop et al, 2005). Chhetry et al. (1999) equilibrated carbonated apatite in acetate buffers with various Ca/P ratios the pH range of 4.5-6.5. Solution ion activity products were calculated by assuming CaHPO_4 , $\text{Ca}_8(\text{PO}_4)_6(\text{H})_2$, $\text{Ca}_3(\text{PO}_4)_2$, $\text{Ca}_{10}(\text{PO}_4)_6(\text{OH})_2$, $\text{Na}_x\text{Ca}_{10-x}(\text{PO}_4)_{6-x}(\text{CO}_3)_x(\text{OH})_2$ (x was taken as 0.30, 0.49, 0.91 depending on the carbonate contents of the powders), $\text{Ca}_4(\text{PO}_4)_2(\text{OH})_2$ as the surface complexes. When the solution ion activity products calculated were plotted against fraction of carbonated apatite dissolved, surface complex with a stoichiometry of $\text{Ca}_{10}(\text{PO}_4)_6(\text{OH})_2$ was shown to govern solubility behavior of carbonated apatites.

Metastable equilibrium solubility study of carbonated apatites and human dental enamel was also performed to determine increase in solubilities due to changes in crystallinities upon carbonate substitution (Baig et al., 1999). The decrease of crystallite size and increase of microstrain which are both responsible of decrease of crystallinity were refined and their effect on the solubility of carbonated apatites and human dental enamel was elucidated. They found that microstrain rather than crystallite size was the dominant factor controlling solubilities of carbonated apatites. Metastable equilibrium solubility behaviors and surface complexes of carbonated apatites with high and low crystallinities were also determined by using pH and solution strontium as the independent variables (Heslop et al., 2005). Surface complexes of $\text{Ca}_6\text{Sr}_4(\text{PO}_4)_6(\text{OH})_2$ and $\text{Ca}_6\text{Sr}_4(\text{PO}_4)_6(\text{OH})_2$ were found to govern solubility behavior of carbonated apatites with high and low crystallinities, respectively in the solutions with higher Sr/Ca ratios. When the strontium to calcium ratios in the solutions were lower (strontium content of the solution was equal and lower 40 % of calcium), surface complexes of $\text{Ca}_{10}(\text{PO}_4)_6(\text{OH})_2$ and $\text{Ca}_9(\text{HPO}_4)(\text{PO}_4)_5(\text{OH})$ were found to control solubility of highly crystalline carbonated apatite and carbonate apatite with low crystallinity, respectively.

Not the solubility of hydroxyapatite but the solubilities of other calcium phosphate phases also are important. pH stabilities and solubilities of calcium phosphates are important in the precipitation of calcium phosphates from aqueous solutions. Hydrolysis, dissolution and reprecipitation reactions are observed when calcium phosphates are immersed in aqueous solutions. All reactions of calcium phosphates in aqueous solutions are governed by the solubilities of the calcium phosphates. Solubility product constants reported for hydroxyapatite is given Table 4.1 whereas solubility product constants of other calcium phosphate compounds are shown in Table 4.2. These solubility constants are used to construct solubility diagrams which show solution calcium or phosphate compositions as a function of pH values (Fernández et al. 1999; Chow, 2009).

Table 4.1. Solubility product constants reported for hydroxyapatite

Sample	$-\log K_{sp}$	Reference
HA* 1000 °C heat treated in air	54.60 (25 °C)	Moreno et al., (1968)
HA* 1000 °C heat treated in steam	57.43 (25 °C)	Moreno et al., (1968)
HA* (precipitated)	58.53 (5 °C) 58.49 (15 °C) 58.52 (25 °C) 58.63 (37 °C)	McDowell et al., (1977)
HA* (precipitated)	58.69 (37 °C)	Markovic et al., (2004)
HA	114 (37 °C)	Gupta et al., (1987)
Nano-HA (9.1 wt. % carbon)	93.48 (21 °C)	Chow et al., (2004)
Crystalline HA	117 (21 °C)	Chow et al., (2004)
Fully OH carbonated apatite $\text{Ca}_{10}(\text{PO}_4)_6(\text{CO}_3)_2$	102.8 (25 °C)	Ito et al., (1997)

* Formula of $\text{Ca}_5(\text{PO}_4)_3(\text{OH})$ was used to calculate K_{sp} .

Table 4.2. Solubility product constants for calcium phosphate phases other than hydroxyapatite

Sample	$-\log K_{sp}$	Reference
MCPM	1.14	Dorozhkin, (2007)
MCPA	1.14	Dorozhkin, (2007)
DCPD	6.59 (25 °C) 6.63 (37 °C)	Dorozhkin, (2007)
DCPA	6.71 (5 °C) 6.79 (15 °C) 6.90 (25 °C) 7.04 (37 °C)	Sutter et al., (1971)
OCP	48.3 (4 °C) 48.3 (4.8 °C) 48.2 (6 °C) 48.3 (18 °C) 48.4 (23.5 °C) 48.7 (37 °C)	Tung et al., (1988)
OCP	49.6 (25 °C) 49.8 (45 °C)	Heughebaert and Nancollas, (1985)
α - TCP	25.5 (25 °C) 25.5 (37 °C)	Dorozhkin, (2007)
β - TCP	28.9 (25 °C) 29.5 (37 °C)	Dorozhkin, (2007)
ACP	25.7 (25 °C)	Combes and Rey, (2010)
CDHA	85.1 (25 °C) 85.1 (37 °C)	Dorozhkin, (2007)
FA	120.0 (25 °C) 119.2 (37 °C)	Dorozhkin, (2007)
TTCP	38-44 (25 °C) 37-42 (37 °C)	Dorozhkin, (2007)

4.2. Dissolution of Calcium Phosphates

Dissolution of calcium phosphate compounds is the removal of ions from the calcium phosphate compounds and transfer into the aqueous solutions. Since currently there is no method to follow the detachment of a single ion or a molecule from the material and its transfer into solution (Dorozhkin, 1999), dissolution studies are restricted to experimentation techniques available. Batch dissolution studies in which calcium phosphates are immersed into different aqueous solutions (Ducheyne et al., 1993; Valsami-Jones et al., 1998; Hankermeyer et al., 2002; Fulmer, 2002), and constant composition dissolution studies (Chin and Nancollas, 1991; Zhang and Nancollas, 1992; Tang et al., 2001; Tang et al., 2003a; Tang et al., 2003b) have been used to determine dissolution behavior of calcium phosphate compounds.

Batch dissolution studies of calcium phosphate compounds are based on the incubation calcium phosphate compounds in different aqueous solution at a defined temperature. For example, Ducheyne et al. (1993) used calcium and phosphate free Tris buffer solution with a pH of 7.4 for the determination of several calcium phosphates and their biphasic mixtures at 37 °C. The dissolution rates of calcium phosphates were found to decrease in the order of tetracalcium phosphate, α -tricalcium phosphate, β -tricalcium phosphate, oxyhydroxyapatite, calcium deficient hydroxyapatite, stoichiometric hydroxyapatite.

Valsami-Jones et al. (1998) determined the dissolution behavior of natural fluorapatite and synthetic hydroxyapatite in aqueous solutions in the pH range of 2-7 at 25 °C in the absence and presence of lead and cadmium in the solutions. Dissolution media used were 0.1 M NaNO₃, 1 % HNO₃ (NaOH was used to adjust pH) and HCl/KCl buffer. Natural fluorapatite was found to have higher dissolution rate than synthetic hydroxyapatite although it had a higher solubility. In the presence of lead in the solution, they observed that lead substituted hydroxyapatite precipitation occurred upon dissolution of synthetic hydroxyapatite. When cadmium was present in the solutions, calcium-cadmium phosphate precipitation was observed.

Fulmer et al. (2002) studied the dissolution rates of three different apatite samples were tested in Tris buffer solutions at pH of 7.3 at 37 °C. Among the hydroxyapatite samples, two of them were the apatite samples obtained by calcium phosphate cements; BoneSource ($\text{Ca}_{9.970}(\text{HPO}_4)_{0.080}(\text{PO}_4)_{5.892}(\text{CO}_3)_{0.080}(\text{OH})_{1.944}$ and

NorianCRS ($\text{Ca}_{8.8}(\text{HPO}_4)_{0.7}(\text{PO}_4)_{4.5}(\text{CO}_3)_{0.7}(\text{OH})_{1.3}$). They compared the dissolution behavior of these powders together with sintered hydroxyapatite (calcitite, $\text{Ca}_{10}(\text{PO}_4)_6(\text{OH})_2$). Initial dissolution rates together with their solubility product constants were measured. Initial dissolution rates after 10 min were found to be 0.0465, 0.1589 and 0 mg/min whereas solubility product constants were calculated as 1.19×10^{-35} , 1.49×10^{-35} and 2.92×10^{-42} for BoneSource, NorianCRS and calcitite samples, respectively.

In order to predict osteoclastic degradation of calcium phosphate samples in the body, acidic solutions simulating the osteoclastic degradation environment have also been used to determine dissolution or degradation of calcium phosphates. Koerten et al. (1999) used 0.1 M sodium acetate buffers at pH values of 4.0, 4.8 and 5.6 for the determination of degradation hydroxyapatite, β -tricalcium phosphate and fluorapatite whereas Bloebaum et al. (1998) studied the dissolution behavior of hydroxyapatite samples in 0.4 cacodylate buffers at cytoplasmic (pH 7.1), phagosomal (pH 6.0) and lysosomal (pH 5.0) pH levels. Similarly dissolution behavior of calcium deficient hydroxyapatite ($\text{Ca}_{8.8}(\text{HPO}_4)_{0.7}(\text{PO}_4)_{4.5}(\text{CO}_3)_{0.7}(\text{OH})_{1.3}$) obtained from NorianSRS cement was tested in closed and open systems using hydrochloric acid solutions (Hankermeyer et al., 2002).

In contrast to dissolution determinations in buffered solutions with various pH values, simulated body fluid is sometimes used for the solubility or dissolution behaviors of the calcium phosphates (Monteiro et al. 2003; Porter et al., 2004; Sprio et al. 2008). In fact, immersion of the samples into simulated body fluids are generally used to predict in vitro bioactivities (bone bonding abilities) of the materials (Kokubo and Takadama, 2006). Simulated body fluid is first developed by Kokubo and co-workers (Kokubo et al., 1990). Simulated body fluid is an artificial solution which contains ions found in blood plasma (Kokubo et al., 1990; Oyane et al. 2003a). This solution does not contain cells, proteins or organic compounds such as glucose present in blood. pH values of the solutions are adjusted to 7.4 by either using Tris or Hepes buffers (Oyane et al. 2003a). Several modified forms of simulated body fluids have been developed since its first use in biomaterials field (Oyane et al. 2003a; Lu and Leng, 2005). Compositions of different simulated body fluids are given in Table 4.3.

Table 4.3. Composition of simulated body fluids
(Source: Tas, 2000; Oyane et al., 2003a)

Ion	Concentration (mM)					
	Blood plasma	c-SBF	r-SBF	i-SBF	m-SBF	Tas' SBF
Na ⁺	142.0	142.0	142.0	142.0	142	142.0
K ⁺	5.0	5.0	5.0	5.0	5.0	5.0
Mg ²⁺	1.5	1.5	1.5	1.0	1.5	1.5
Ca ²⁺	2.5	2.5	2.5	1.6	2.5	2.5
Cl ⁻	103.0	147.8	103.0	103.0	103.0	125
HCO ₃ ⁻	27.0	4.2	27.0	27.0	10	27.0
HPO ₄ ²⁻	1.0	1.0	1.0	1.0	1.0	1.0
SO ₄ ²⁻	0.5	0.5	0.5	0.5	0.5	0.5
Buffer	-	Tris	Hepes	Hepes	Hepes	Tris

The first simulated body fluid developed is conventional simulated body fluid (c-SBF) (Kokubo et al., 1990). Its chloride ion concentration is higher than that in plasma whereas bicarbonate ion content is lower than that of blood plasma. Only revised simulated body fluid (r-SBF) includes ions in concentrations equal to their concentrations in blood plasma. The concentrations of all ions except bicarbonate in modified simulated body fluid (m-SBF) are equal to concentrations in blood plasma. Bicarbonate concentration was reduced from 27 mM to 10 mM in m-SBF. Ionized simulated body fluid (i-SBF) was developed to simulate free ion concentrations in blood plasma (Oyane et al., 2003). Since 0.5 mM Mg⁺ of total magnesium concentration are bound to proteins and 0.9 mM and 0.3 mM Ca²⁺ are bound to proteins and inorganic ions (such as phosphate and carbonate), magnesium and calcium concentrations was reduced 1.0 and 1.6 mM, respectively by subtracting concentrations of protien bound forms from their total concentrations in plasma (Oyane et al., 2003a). Another type of simulated body fluid was developed by Tas (2000). With his formulation, concentration of bicarbonate in c-SBF was increased from 4.2 mM to 27 mM while decreasing Cl⁻ concentration from 147.8 mM to 125 mM, closer to that of blood plasma.

pH values of the all simulated body fluids are adjusted to 7.4 at 37 °C with either Tris or Hepes (Tas, 2000, Oyane et al., 2003a, Kokubo and Takadama, 2006). When Tris was used as a buffer, pH adjustment was performed with 1 M HCl solution. In the case of Hepes, NaOH solution was used. Table 4.4 shows the amounts of reagents used to prepare 1 liter of simulated body fluids.

Table 4.4. Reagents used to prepare simulated body fluids
(Source : Tas, 2000; Oyane et al., 2003a)

Reagent ^a	Amount (g)					
	Purity (%)	c-SBF ^b	r-SBF ^c	i-SBF ^c	m-SBF ^c	Tas' SBF ^d
NaCl	> 99.5	8.036	5.403	5.585	5.403	6.547
NaHCO ₃	> 99.5	0.352	0.740	0.965	0.504	2.268
Na ₂ CO ₃	> 99.5	-	2.046	1.765	0.426	-
KCl	> 99.5	0.225	0.225	0.225	0.225	0.373 ^g
K ₂ HPO ₄ ·3H ₂ O	> 99.0	0.230	0.230	0.230	0.230	-
Na ₂ HPO ₄ ·3H ₂ O	> 99.5	-	-	-	-	0.178
MgCl ₂ ·6H ₂ O	> 98.0	0.311	0.311	0.217	0.311	0.305 ^g
1.0 M HCl	-	40 mL	-	-	-	15 mL
0.2 M NaOH	-	-	-	-	100 mL	-
Hepes	> 99.9	-	11.928	11.928 ^e	17.892 ^f	-
CaCl ₂	> 95.0	0.293	0.293	0.191	0.293	-
CaCl ₂ ·2 H ₂ O	> 99.0	-	-	-	-	0.368
Na ₂ SO ₄	> 99.0	0.072	0.072	0.072	0.072	0.071 ^g
Tris	> 99.9	6.063	-	-	-	6.057 ^g
1.0 M HCl	-	≈ 0.2 mL	-	-	-	25 mL
1.0 M NaOH	-	-	≈ 0.8 mL	≈ 0.8 mL	≈ 15 mL	-

^a Reagents are dissolved in the given order

^b Solution is buffered to pH 7.4 at 36.5 °C with Tris and 1 M HCl

^c Solutions are buffered to pH 7.4 at 36.5 °C with Hepes and 1 M NaOH

^d Solution is buffered to pH 7.4 at 37 °C with Tris and 1 M HCl

^e Hepes was added as dissolved in 100 mL

^f Hepes was added as dissolved in 100 mL of 0.2 M NaOH

^g Purities were 99.0 % for KCl and MgCl₂·6H₂O and 99.5 % for Na₂SO₄ and Tris.

Details of the preparation of simulated body fluids are briefly described in the articles of Tas (2000), Oyane et al. (2003a) and Kokubo and Takadama (2006). Concentrations of ions shown in Table 4.3 are given in Tas (2000) and Oyane et al. (2003a). However when concentrations of Cl^- and Na^+ added as HCl and NaOH solutions, respectively for the pH adjustments are taken into consideration, Cl^- concentration in c-SBF and Tas' SBF are found as 187.8 and 165.0 mM, respectively while Na^+ concentration in m-SBF is 157.0 mM (Lu and Leng, 2005). Among the all SBF solution, r-SBF is the most similar solution to blood plasma with respect to its total concentration of each ion.

Preparation of simulated body fluids should be performed carefully. The addition of reagents should be followed in the order given in Table 4.4 (Tas, 2000, Oyane et al., 2003a). For the preparation of c-SBF, prior to addition of calcium chloride, solution is acidified by adding 40 mL of 1 M HCl in order to avoid calcite precipitation. Reduction of pH results in the loss of bicarbonate by volatilization of carbon dioxide from the solution (Takadama et al. 2004). Oyane et al. (2003a) found that bicarbonate ion concentration in c-SBF was lower than nominal concentration. This was attributed to the loss of bicarbonate ion as carbondioxide gas because of the reduction of pH to 2 after addition of 1 M HCl. A new methodology was recently suggested for the preparation of SBF solution with the composition of c-SBF in which loss of bicarbonate ion was avoided (Takadama et al., 2004). Two SBF solutions (np-SBF and nl-SBF) were prepared. np-SBF solution was prepared by sequential powder dissolving methodology. In contrast to c-SBF, Hepes and 1 M NaOH were first dissolved to adjust pH to 7.4 at 36.5 °C and NaHCO_3 was dissolved just before the final pH adjustment. nl-SBF was however prepared by mixing two solutions. Calcium solution which contained all ions other than phosphate and bicarbonate was prepared. In this calcium solution concentrations of ions were equal to concentrations in c-SBF but calcium concentration was doubled. Similarly phosphate solution which contains all ions except calcium was prepared. This phosphate solution contained ions in concentrations found in c-SBF but phosphate and bicarbonate concentrations was doubled. pH values of these two solutions were adjusted to 7.4 at 36.5 °C with Hepes and 1 M NaOH. By mixing of calcium and phosphate solutions in equal volumes, nl-SBF solution was prepared.

Because simulated body fluids contain bicarbonate, calcium and phosphate ions, saturation levels of simulated body fluids with respect to calcite and hydroxyapatite were reported by Oyane et al. (2003a). With respect to calcite, r-SBF and i-SBF solutions are supersaturated, m-SBF solution is saturated and c-SBF solution is undersaturated whereas all are supersaturated with respect to hydroxyapatite. Because of the saturation and supersaturation levels of these metastable solutions, calcite or apatite nucleation occurs upon changes in the solution properties. Calcite and hydroxyapatite nucleation in the solutions or on the surfaces of the materials are likely to occur upon immersion in m-SBF, i-SBF and r-SBF. In the case of c-SBF only hydroxyapatite nucleation is possible. Oyane et al. (2003b) showed that calcium phosphate clusters with initial hydrodynamic diameter of 1 nm were formed in c-SBF and m-SBF whereas in addition to calcium phosphate clusters, calcium carbonate clusters with initial hydrodynamic diameter of 10-30 nm were formed in r-SBF and i-SBF. They suggested m-SBF for the bioactivity testing of the materials and bone-like apatite formation on the samples because of its long term stability and similarity to blood plasma.

Thorough study of the nucleation driving forces and nucleation rates of calcium phosphate phases in SBF solutions was performed by Lu and Leng (2005) using classical crystallization theories of thermodynamics and kinetics. Thermodynamic driving force (ΔG , change in Gibbs free energy) for the hydroxyapatite was found to be higher than those of OCP and DCPD. Although hydroxyapatite was found to be thermodynamically stable in SBF solutions, nucleation rate of OCP was calculated to be higher than nucleation rate of HA indicating that OCP nucleation is kinetically favored. According to its thermodynamic driving force for nucleation, DCPD nucleation was found to be improbable unless the increase in concentrations of calcium and phosphate. If calcium and phosphate concentrations in SBF is increased, DCPD precipitation in SBF is probable since the thermodynamic driving force for DCPD precipitation becomes the most greatest among those of other calcium phosphate phases. Authors also found that thermodynamic driving force for carbonate apatite precipitation was equal to that of stoichiometric hydroxyapatite precipitation whereas thermodynamic driving force for calcium deficient hydroxyapatite was calculated to be lower than that for stoichiometric apatite precipitation. However precipitation of both carbonate apatite and calcium deficient apatite were found to be more kinetically favored than stoichiometric apatite.

In order to elucidate the mechanism of dissolution of calcium phosphate compounds, constant composition (Chin and Nancollas, 1991; Zhang and Nancollas, 1992; Tang et al., 2001; Tang et al., 2003a) or dual constant composition kinetics studies (Wu et al., 2001; Tang et al., 2003b; Chow et al., 2003) have been used. The most important feature of these studies is that the thermodynamic driving for dissolution is kept constant. Since thermodynamic driving force for dissolution is the function of solution composition, it is kept constant by keeping the solution composition constant throughout the dissolution. Undersaturated solutions at constant ionic strength and pH value are prepared in double walled Pyrex glass vessels thermostated at 37 °C. Dissolution is started introducing known amounts of seeds into the system and system is continuously stirred. Titrant solutions are added into the system by stepper-motor driven burettes in order to keep the solution composition constant. A potentiometer or pH-stat system employing a pH electrode is used to control the titrant addition into the system. Once the volume of titrants added into the system, titrant volume can be plotted vs. recorded time, this gives overall dissolution rate. When two constant composition devices are incorporated into the system employing two different electrodes (pH and calcium electrode), system is called as dual constant composition kinetics study. This system is very useful when the dissolution of mixed phases is of interest (Tang et al., 2003b; Chow et al., 2003).

Ebrahimpour and colleagues was the first who introduced the use of dual constant composition system (Chow et al., 2003). A modified method of dual constant composition has been described by Chow et al. (2003). The principle behind this technique is that when the calcium phosphate phase is dissolving, its dissolution can be considered as dissolving its corresponding amount of base, acid and water thus $\text{Ca}(\text{OH})_2$, H_3PO_4 and water. Only $\text{Ca}(\text{OH})_2$ and H_3PO_4 solutions are added into the reaction vessel throughout the dissolution, however since dissolution is performed under water based system and liberated water upon dissolution is comparatively very small. Ca and P titrants having the same concentrations in the dissolution medium are added into the system by the help of calcium and pH electrode used in conjunction with reference electrode of pH electrode. In contrast to their names Ca titrant has no $\text{Ca}(\text{OH})_2$ but have other components at the same concentrations in demineralizing solution. Similarly P titrant has no H_3PO_4 but have others. Ca titrant addition is achieved by Ca ion electrode where P titrant is added via the response of pH electrode. Without the knowledge of the stoichiometry of the solution, one can use the dual constant

composition dissolution kinetic study to maintain constant composition of the dissolution media. Data obtained by titration can be used to calculate the dissolution rate as well as stoichiometry of the dissolving phase. System used by Chow et al. (2003) is shown in Figure 4.2. These authors used 40 mL dissolution medium in the experiments but kept the volume constant at 60 mL by the removal of dissolution medium.

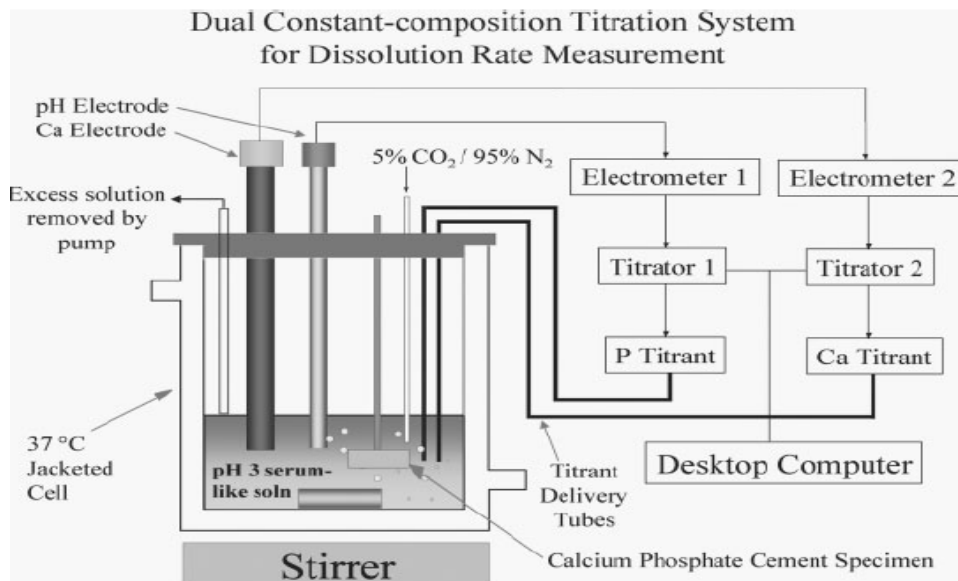


Figure 4.2. Dual-constant composition titration system
(Source: Chow et al., 2003).

Constant composition dissolution kinetics system was used to investigate the dissolution behavior of fluorapatite (Chin and Nancollas, 1991), octacalcium phosphate (Zhang and Nancollas, 1991), β -tricalcium phosphate (Tang et al., 2001), carbonated apatite (Tang et al. 2003a), brushite, β -tricalcium phosphate, octacalcium phosphate, hydroxyapatite and carbonated apatite in the absence and presence of citric acid (Tang et al., 2003b) whereas dual constant composition dissolution kinetics system was used to determine dissolution behavior of mixtures of octacalcium phosphate and tricalcium phosphate (Wu et al. 2001; Tang et al. 2003b) and hydroxyapatite, dicalcium phosphate dihydrate and calcium phosphate cements prepared by mixing powder equimolar tetracalcium phosphate and dicalcium phosphate anhydrous with water (Chow et al., 2003). All these studies provided data for the elucidation of mechanisms controlling dissolution of calcium phosphate compounds.

Because of the importance of surface properties and surface complexes in the behavior of calcium phosphate phases in aqueous solutions, recent studies have been focused on the determination of surface properties (surface composition and surface complexation) together with solubility or dissolution determinations (Skartsila and Spanos, 2007; Chairat et al., 2007; Bengtsson et al., 2009). Skartsila and Spanos (2007) determined the point zero charge of hydroxyapatite in contact with aqueous solutions containing KNO_3 by potentiometric titration, ζ -potential measurements and surface complex modelling. They found the point zero charge value of hydroxyapatite as 6.5 ± 0.2 which was lower than the values found before. They stated that considerable fraction of solution H^+ is consumed by the species coming from the dissolution because of the increase in the dissolution with the decrease in pH. They therefore suggested that these H^+ ions should be taken into consideration for the calculations of true value of point zero charge and surface charges at different pH values.

Surface characterization and dissolution of non-stoichiometric hydroxyapatite with a composition of $\text{Ca}_{8.4}(\text{HPO}_4)_{1.6}(\text{PO}_4)_{4.4}(\text{OH})_{0.4}$ was studied using potentiometric titrations, zeta potential measurements, batch dissolution studies together with Attenuated Total Reflectance Fourier Transform Infrared spectroscopy (ATR-FTIR) and X-ray Photoelectron spectroscopy by Bengtsson et al. (2009). They studied the dissolution and surface complexation of this apatite sample in 0.1 M NaCl solutions in a pH range of 3.5-10.5 at 25 °C. Within the pH range studied, three different regions were determined. Below pH 4.5, dissolution was dominant. Solution Ca/P ratio was similar to that of surface of hydroxyapatite. Dissolution and surface complexation were observed between pH 4.5 and 8.2. At low pH values, solution Ca/P ratio was found to reach to that of surface of the hydroxyapatite whereas Ca/P at neutral pH was ≈ 25 . This very high Ca/P ratio was attributed to the readsorption of phosphate ions onto hydroxyapatite surface. Surface complexation was however dominant above pH 8.2.

Similarly surface properties of fluorapatite in aqueous solution were also investigated by potentiometric titrations, batch dissolution experiments, zeta potential measurements and ATR-FTIR analysis (Chairat et al., 2007). Exchange reactions between H^+ and Ca^{2+} and OH^- and F^- ions and formation of a Ca or F depleted but P enriched layer at the surface of fluorapatite were observed. They suggested that this layer was in composition of CaHPO_4 and controlled the apparent solubility of fluorapatite.

Whether batch dissolution tests or constant composition dissolution kinetics methodology is used, dissolution data together with data obtained from potentiometric titrations, zeta potential measurements and surface characterization methods such as X-ray photoelectron electron spectroscopy and atomic force microscopy provide useful information on the behavior of hydroxyapatite in different aqueous solutions especially in the presence of physiologically important ions. The behavior of hydroxyapatite in such solutions will therefore be useful for the understanding of the mechanism of bone formation and resorption, caries formation and hydroxyapatite dissolution and crystallization phenomena.

CHAPTER 5

MATERIALS AND METHODS

5.1. Materials

Ultrapure water with a resistivity of 18.2 M Ω ·cm at 25 °C was used in this study. All the materials used and their specifications are given in Table 5.1.

NaH₂PO₄, NaCl, KCl and Na₂SO₄ were dried for 24 h at 105 °C at reduced pressure of approximately -0.9 bar in a vacuum oven (Selecta, Vaciotem-T) before use. All other materials were used as received.

5.2. Methods

Methods used in this study are divided into two groups;

- a) Chemical analyses
- b) Powder synthesis, characterization and dissolution testing of the powders

In the section of chemical analysis, low level calcium and phosphate analyses methods were used. Calcium analysis method was modified and tested for the analysis of different calcium levels. Suitability of the method for the analysis of calcium in different electrolytes containing relatively higher concentrations of several ions was further evaluated. Phosphate analysis method was tested for the suitability of phosphate determination when background ions were present in the system.

In the second section hydroxyapatite powder was synthesized and characterized together with commercial powder. Finally dissolution of the powders in different electrolytes was determined by calcium and phosphate analyses methods.

Table 5.1. Materials used and their specifications

No	Materials	Producer and Code	Specifications
1	Dowex 50WX4-100	Sigma Aldrich 428663	
2	Arsenazo III	Fluka 11090	
3	HCl	Merck 1.00314	37 %, extra pure
4	Imidazole	Sigma Aldrich I 2399	≥ 99 %
5	Sodium acetate	AppliChem A1522	Min 99 %, anhydrous
6	Acetic acid	Merck 1.00056	100 %, glacial
7	Formic acid	Merck 1.00263	
8	Potassium hydroxide	Panreac 141515.12.11	85 %, purissimum
9	CaCl ₂ ·2H ₂ O	Merck 1.02382	99.8- 103.3 %
10	Sulfuric acid	Merck 1.00713	95-98 %, extra pure
11	Filter papers	Filtrak Grade 288	80 g/m ² , d=110 mm
12	NaCl	Merck 1.06404	≥ 99.5 %
13	NaHCO ₃	Merck 1.06329	99.7-100.3 %
14	KCl	Merck 1.04936	Min 99.5 %
15	Na ₂ SO ₄	Merck 1.06637	Min 99 %
16	NaH ₂ PO ₄	Merck 1.06370	99.99 %
17	MgCl ₂ ·6H ₂ O	Merck 1.05833	99.0-102.0 %
18	Ammonium molybdate tetrahydrate	Sigma A7302	
19	Malachite green oxalate	Merck 1.01398	C. I. 42 000
20	Poly(vinyl alcohol) (PVA)	Aldrich 36,062-7	80 % hydrolyzed Average MW 9,000-10,000
21	Microplates, 96-well plate	Thermo Scientific	Cliniplate, Sterile, with lid
22	Hydroxyapatite	Sigma C5267	34.0-40.0 % calcium

5.2.1. Chemical Analyses

In order to determine low levels of calcium, Arsenazo III calcium assay was modified and tested for the calcium determination in 0.25-1 ppm, 1-8 ppm and 10-80 ppm calcium containing solutions.

5.2.1.1. Optimization of Microplate Based Arsenazo III Calcium Analysis

Arsenazo III calcium analysis method was selected and applied to microplate reader. First of all calcium initially present in the dye was removed using cation exchange column chromatography method suggested by Vogel et al. (1983). Details of the calcium removal from the dye are given in Appendix A. Determination of Arsenazo III concentration in the purified dye solution was performed according to Minganti et al. (1983) and described in Appendix B. Arsenazo III concentration was found to be 800 μM . Arsenazo III dye reagents were prepared by using this stock Arsenazo III solution.

Arsenazo III dye reagents prepared at three different pH values were tested for the analysis of three different ranges of calcium concentrations (0.25-2 ppm, 1-8 ppm and 10-80 ppm calcium). pH values of 3.8, 5.4 and 6.5 were selected. For the preparation of dye reagents at pH 3.8, 5.4 and 6.5, acetate, formate and imidazole buffers were used, respectively. Dye reagents with different Arsenazo III concentrations were prepared at these pH levels. Preparation methods for these reagents are given in Appendix C. Table 5.2 summarizes Arsenazo III solutions used for the analysis of different calcium concentration ranges.

Table 5.2. Arsenazo III dye reagents and the range of calcium concentrations used in this study

No	Arsenazo III Reagent				Reagent Volume (μL)	Concentration range of Ca^{2+} standards (ppm)	Volume of Standards (μL)
	$C_{\text{Arsenazo III}}$ (μM)	Buffer	C_{Buffer}	pH			
1	60	acetate	100	5.4	150	0.25-2	150
2	60	acetate	100	5.4	150	1-8	150
3	60	acetate	100	5.4	150	10-80	150
4*	60	acetate	100	5.4	150	0.25-2	150
5*	60	acetate	100	5.4	150	1-8	150
6*	60	acetate	100	5.4	150	10-80	150
7	120	acetate	100	5.4	150	1-8	150
8	60	formate	220	3.8	150	0.25-2	150
9	60	formate	220	3.8	150	1-8	150
10	60	formate	220	3.8	150	10-80	150
11*	60	formate	220	3.8	150	0.25-2	150
12	120	formate	220	3.8	150	10-80	150
13	60	imidazole	100	6.5	150	0.25-2	150
14	60	imidazole	100	6.5	150	1-8	150
15	60	imidazole	100	6.5	150	10-80	150
16*	60	imidazole	100	6.5	150	0.25-2	150
17*	60	imidazole	100	6.5	150	1-8	150
18	60	imidazole	200	6.5	150	0.25-2	150
19	60	imidazole	200	6.5	150	1-8	150
20	60	imidazole	200	6.5	150	10-80	150
21	200	imidazole	200	6.5	150	1-8	150
22	200	imidazole	200	6.5	150	10-80	150
23	500	imidazole	200	6.5	150	10-80	150

* Solutions were prepared by diluting the dye reagent with ultrapure water in 1:1 (volumetric) ratio.

5.2.1.1.1. Preparation of Calcium Standard Solutions

Three sets of calcium standards were prepared in this study;

- a) 0.25, 0.5, 0.75, 1, 1.25, 1.5, 2 ppm
- b) 1, 2, 3, 4, 5, 6, 7, 8 ppm
- c) 10, 20, 30, 40, 50, 60, 70, 80 ppm

Main calcium stock solution with a concentration of 2500 mg/L was prepared by dissolving 0.2293 g $\text{CaCl}_2 \cdot 2\text{H}_2\text{O}$ in ultrapure water and adjusting the volume to 25 mL in a glass volumetric flask by ultrapure water. This solution was transferred into high density-polyethylene bottle.

Intermediate standard solutions of 25 ppm and 100 ppm were prepared for the preparation of standards of sets a, and b, respectively. In order to prepare 25 ppm calcium standard solution, 250 μL from 2500 mg/L standard solution was transferred into 25 mL capacity glass volumetric flask. Solution volume was adjusted to 25 mL by ultrapure water. Solution was finally mixed well and transferred into high density-polyethylene bottle. For the preparation of 100 ppm calcium standard, 1 mL 2500 mg/L calcium solution was added into a 25 mL capacity glass volumetric flask. Ultrapure water was then added into the volumetric flask and volume was brought to 25 mL. Solution was then mixed thoroughly and taken into plastic sample bottle.

For the preparation of 0.25, 0.5, 0.75, 1, 1.25, 1.5, 1.75 and 2 ppm standards, 250, 500, 750, 1000, 1250, 1500, 1750, and 2000 microliters of 25 ppm solution were transferred into 25 mL glass volumetric flasks, respectively. Volumes of the solutions were brought to 25 mL by ultrapure water. All solutions were mixed thoroughly and transferred into plastic sample bottles.

Calcium standards, 1-8 ppm (set b), were prepared by taking 250, 500, 750, 1000, 1250, 1500, 1750, and 2000 microliters from 100 ppm solution into 25 mL glass volumetric flask for 1, 2, 3, 4, 5, 6, 7 and 8 ppm, respectively. Volumes of the solutions were adjusted to 25 mL by ultrapure water. Solutions were finally mixed well and transferred into high density-polyethylene bottles.

Calcium standards with concentrations 10-80 ppm were directly prepared by taking 100, 200, 300, 400, 500, 600, 700 and 800 microliters from 2500 mg/L solution for 10, 20, 30, 40, 50, 60, 70, and 80 ppm, respectively. Volumes were brought to 25 mL and solutions were mixed well. Solutions were taken into plastic sample bottles.

All standard solutions were kept frozen at -18 °C when they are not in use. When they were to be used, they were first thawed and left to stand in order to reach room temperature.

5.2.1.1.2. Analysis

Calcium analysis was performed in 96 well plates in a plate reader Multiskan® Spectrum (Thermo Electron Corporation, Finland). Ultrapure water treated in similar way used in the calcium solutions was used as a blank.

One hundred fifty microliters of desired solution were transferred into the wells of a 96 well microplate in 5 replicates. After adding the solutions, 150 µL of dye solutions to be tested was added into each well. The microplate was then incubated for 5 min at 25 °C in Multiskan® Spectrum plate reader. After incubating the plates in the microplate reader, absorbances were measured at 650 and 600 nm with a bandwidth of 2 nm at 25 °C. Spectra of the solutions were recorded between 400 and 700 nm with a step size of 5 nm and bandwidth of 2 nm.

5.2.1.1.3. Data Analysis

Five replicates were used for each concentration in absorbance measurements. Therefore, average values and standard deviations of absorbances for each concentration of calcium were calculated and standard deviations were reported in the figures as error bars. For spectrum scanning, spectrum of only one replicate for each calcium standard was reported.

Since wells containing blanks are specified by the user and instrument averages these values and subtracts from the absorbances of the solutions in calculations, only absorbance values were saved and blank subtraction was performed by mathematical calculations. Standard deviations in this case was calculated by Equation 5.1 and reported in the figures as error bars.

$$s = \sqrt{(s^2 + s_{blank}^2)} \quad (5.1)$$

5.2.1.2. Calcium Determination in Different Electrolyte Solutions by Microplate Based Arsenazo III-Calcium Analysis

Interferences of the several ions on the calcium determination by Arsenazo III method were tested by the preparation of calcium standard solutions in different electrolyte solutions. 200 μM Arsenazo III & 200 mM Imidazole-Cl pH 6.5 solution was used for the construction of calibration curves by using calcium standards prepared in several electrolyte solutions. Electrolytes tested were 142 mM NaCl, 27 mM NaHCO_3 , 115 mM NaCl and 27 mM NaHCO_3 containing solution, 1.5 mM $\text{MgCl}_2 \cdot 6\text{H}_2\text{O}$, 5 mM KCl, 0.5 mM Na_2SO_4 , 1 mM H_3PO_4 , 10 mM H_3PO_4 .

5.2.1.2.1. Preparation of Calcium Standard Solutions

Main standard solution (2500 mg/L calcium) and intermediate standard solution (100 mg/L calcium) were used to prepare working standard solutions. For the preparation of main standard solution, 0.2293 g calcium chloride dihydrate was dissolved in ultrapure water and solution was transferred into 25 mL capacity glass volumetric flask. Volume was adjusted to 25 mL by ultrapure water and solution mixed well. Finally solution was transferred in HD-PE plastic bottle.

Intermediate standard solution was prepared by transferring 1 mL of main standard solution into 25 mL glass volumetric flask. Volume was adjusted with ultrapure water. Solution was thoroughly mixed and then transferred into plastic sample bottle.

Working standard solutions were prepared by transferring 250, 500, 750, 1000, 1250, 1500 and 1750 μL intermediate standard solutions into 25 mL glass volumetric flasks. Volumes were adjusted to 25 mL with ultrapure water. After mixing the solutions, they were transferred into plastic sample bottles.

Preparation of standard solutions in the presence of 142 mM NaCl, 1.5 mM $\text{MgCl}_2 \cdot 6\text{H}_2\text{O}$, 5 mM KCl and 0.5 mM Na_2SO_4 were similar to the preparation of standard solutions in ultrapure water. Instead of ultrapure water, corresponding electrolyte was used as solvent.

In the case of 27 mM NaHCO₃ and 115 mM NaCl and 27 mM NaHCO₃ solutions, due to the risk of precipitation of calcium carbonate main and intermediate standard solutions were prepared in ultrapure water. Working standards in 27 mM NaHCO₃ were prepared by adding required volumes of intermediate standard solution and 3 mL of 225 mM NaHCO₃ and adjusting the volumes of the solutions to 25 mL. In the case of 115 mM NaCl and 27 mM NaHCO₃, 5 mL of 575 mM NaCl and 3 mL of 225 mM NaHCO₃ were transferred into 25 mL volumetric flasks. After the addition of ultrapure water into the volumetric flasks, required volumes of intermediate standard solutions were added, and volumes were brought to 25 mL.

Because of the possibility of precipitation of calcium phosphate phases in solutions with high concentrations of calcium and phosphate, only working standards were prepared in H₃PO₄ solutions. Main and intermediate solutions were prepared in ultrapure water. Working calcium standard solutions in 1 mM H₃PO₄ were prepared as follows: 1 mL of 25 mM H₃PO₄ solution was transferred into 25 mL capacity glass volumetric flasks. Ultrapure water was added into flasks. For the standard solutions with calcium concentrations 1, 2, 3, 4, 5, 6 and 7 mg/L, 250, 500, 750, 1000, 1250, 1500 and 1750 µL from intermediate standard solution was added into flasks, respectively. Solutions were brought to 25 mL with ultrapure water and mixed thoroughly. Working standard solutions in 10 mM H₃PO₄ was prepared by the same way used in the preparation of working standard solutions in 1 mM H₃PO₄. However, 100 mM H₃PO₄ solution was used instead of 25 mM H₃PO₄ and 2.5 mL from 100 mM H₃PO₄ solution were transferred into each flask.

5.2.1.2.2. Analysis

Calcium analysis was performed in 96 well microplates. Electrolytical solutions used to prepare calcium standards were used as blank solutions in the analysis.

One hundred fifty microliters of each solution was added into wells of a microplate. For each set of calcium concentration, five replicates were used. After addition of the solutions into wells of a microplate, 150 µL of 200 µM Arsenazo III & 200 mM imidazole-Cl pH 6.5 solution was added into each well. Solutions were mixed by circular movement of a pipette tip in the wells (a pipette tip for the each set of concentrations). After mixing the solutions, microplate was shaken for 30 seconds at

300 spm (shakes per minute) in a linear shaking mode with linear shaking amplitude (width) of 10 mm in Multiskan® Spectrum plate reader. Microplate was then incubated for 5 minutes at 150 rpm and 25 °C in an incubator (MaxQ⁴⁰⁰⁰ Barnstead, UK) with their lids closed. After the incubation, microplate was finally shaken for 30 seconds at 300 spm (shakes per minute) in a linear shaking mode with linear shaking amplitude (width) of 10 mm in Multiskan® Spectrum plate reader. After shaking, absorbances of the solutions in the wells of microplates were analyzed in Multiskan® Spectrum plate reader at wavelengths of 500, 600, 650 and 655 nm with a bandwidth of 2 nm. Spectra of the solutions were scanned between 400 and 700 nm with a stepsize of 5 nm and bandwidth of 2 nm.

Data analysis was performed as described in Section 5.2.1.1.3.

5.2.1.3. Microplate Based Malachite Green Phosphate Assay

Malachite green phosphate assay proposed by Van Veldhoven and Mannaerts (1987) with modifications of Cogan et al. (1999) was used in this study. MG assay of inorganic phosphate is based on the reaction between malachite green dye and phosphomolybdate complex formed when ammonium molybdate reacts with phosphate in acidic solutions.

According to Cogan et al. (1999), optimum final heptamolybdate and malachite green concentrations have been found as 6 mM and 120 µM, respectively. Final H₂SO₄ and PVA concentrations were suggested as 0.45 M and 0.05 (w/v) %, respectively (Van Veldhoven and Mannaerts, 1987).

Microplate reader based assay used in this study made us to measure absorbance of 96 wells in very short time. This microscale phosphate assay avoids the use of large amounts of samples and solutions. Final volume of the solution and reagents were 300 µL. According to the above mentioned optimum properties, reagent solutions with calculated concentrations were prepared.

5.2.1.3.1. Preparation of Reagents

Two reagent solutions (ammonium molybdate in sulfuric acid and malachite green and PVA containing solution) are used in the phosphate determination by malachite green based method. Preparation of reagent solutions is as follows;

Reagent A (36 mM Ammonium heptamolybdate in 2.7 M H₂SO₄):

4.4561 g ammonium heptamolybdate tetrahydrate were dissolved in approximately 60 mL ultrapure water. Solution was mixed on a magnetic stirrer. Fourteen point nine milliliters of concentrated H₂SO₄ were then added into solution. This solution was mixed thoroughly on a magnetic stirrer and left to cool down while stirring. After solution had been cooled, it was transferred to 100 mL glass volumetric flask and volume was adjusted to 100 mL with ultrapure water. Solution was then filtered through a Filtrak Grade 288 filter paper into 250 mL capacity screw capped glass bottle. In order to avoid possible light-induced changes in the solution, bottles were wrapped with aluminum foil. Reagent was stored at room temperature in the dark.

Reagent B (0.72 mM Malachite Green & 0.3 (w/v) % PVA containing solution):

0.3 g polyvinyl alcohol (PVA) was dissolved in approximately 60 mL of ultrapure water in a 100 mL capacity screw capped glass bottle. In order to facilitate the dissolution of PVA, solution was incubated in a thermostated water bath for approximately 30 minutes at 80 °C and 150 rpm. Solution was then taken and mixed by a magnetic stirrer. Solution was left to cool down to room temperature while stirring. After cooling, 0.0742 g malachite green oxalate in a beaker was dissolved in this PVA solution. Solution was then mixed thoroughly on a magnetic stirrer. This malachite green and PVA containing solution was transferred into 100 mL glass volumetric flask. Solution volume was adjusted to 100 mL by ultrapure water and solution was mixed thoroughly. Solution was then filtered through a Filtrak grade 288 filter paper into a 100 mL capacity polypropylene bottle. This blue-green reagent was protected from the light-induced changes by wrapping aluminum foil around the bottle. Solution was kept at room temperature in dark.

5.2.1.3.2. Preparation of Phosphate Standard Solutions

Phosphate (PO_4^{3-}) standard solutions with concentrations of 0.25, 0.5, 0.75, 1, 1.25, 1.5, and 1.75 ppm were used in the malachite green based phosphate assay. This range of phosphate standard solutions was prepared in ultrapure water and calibration curve was constructed. Phosphate standards in different electrolyte solutions having several ions found in human plasma were also prepared. These electrolyte solutions were used in concentrations equal to their concentrations in human plasma. Possible interferences arising from these electrolytes were tested in malachite green based phosphate analysis. Whole phosphate concentration range was used for all electrolytes tested. Besides the determination of interferences arising from the electrolytes, testing of all standard concentrations made it possible to construct calibration curves when electrolytes exist as a matrix in the solutions. Table 5.3 shows the electrolytes present as a matrix in the standard solutions.

All main, intermediate and working standard solutions were prepared freshly. Number of replicates of solution preparations and replicates of measurements are given in Table 5.4.

Table 5.3. Electrolyte solutions used to prepare phosphate standards

No	Compound	Cation	Anion
1	142 mM NaCl	142 mM Na^+	142 mM Cl^-
2	27 mM NaHCO_3	27 mM Na^+	27 mM HCO_3^-
3	115 mM NaCl / 27 mM NaHCO_3	142 mM Na^+	115 mM Cl^- / 27 mM HCO_3^-
4	2.5 mM $\text{CaCl}_2 \cdot 2\text{H}_2\text{O}$	2.5 mM Ca^{2+}	5 mM Cl^-
5	1.5 mM $\text{MgCl}_2 \cdot 6\text{H}_2\text{O}$	1.5 mM Mg^{2+}	3 mM Cl^-
6	5 mM KCl	5 mM K^+	5 mM Cl^-
7	0.5 mM Na_2SO_4	1 mM Na^+	2 mM SO_4^{2-}
8	SBFA	See Tables 5.5 and 5.6	
9	SBFB	See Tables 5.5 and 5.6	

Table 5.4. Number of replicates used in malachite green phosphate assay

No	Background electrolyte	Replicates of Solution Preparation	Replicates of Measurements for Each Phosphate Concentration Level	Total Replicates of Measurements for Each Phosphate Concentration Level
1	Ultrapure water	4	5	20
2	142 mM NaCl	4	5	20
3	27 mM NaHCO ₃	3	5	15
4	115 mM NaCl / 27 mM NaHCO ₃	3	5	15
5	2.5 mM CaCl ₂ ·2H ₂ O	3	5	15
6	1.5 mM MgCl ₂ ·6H ₂ O	3	5	15
7	5 mM KCl	3	5	15
8	0.5 mM Na ₂ SO ₄	3	5	15
9	SBFA	2	5	10
10	SBFB	1	5	5

Main phosphate stock solution containing 2500 mg/L PO₄³⁻ solution was prepared by dissolving 0.3158 g NaH₂PO₄ in ultrapure water and diluting to 100 mL in a glass volumetric flask by ultrapure water. Main stock solution was then mixed well and transferred into a high density polyethylene bottle. For the preparation of working standard solutions, an intermediate PO₄³⁻ standard solution with a concentration of 25 mg/L was prepared. For this reason, 250 µL of main standard solution was transferred into 25 mL capacity glass volumetric flask. Ultrapure water was then added into the volumetric flask and volume was adjusted to 25 mL with ultrapure water. Solution was mixed thoroughly and transferred into a HD-PE bottle.

Working standard solutions were prepared by transferring 250, 500, 750, 1000, 1250, 1500 and 1750 µL of 25 mg/L intermediate standard solution into 25 mL capacity glass volumetric flasks for 0.25, 0.5, 0.75, 1, 1.25, 1.5 and 1.75 ppm PO₄³⁻ standard solutions, respectively. Ultrapure water was added into the flasks. Volumes were adjusted to 25 mL with ultrapure water and solutions were mixed thoroughly. All working standard solutions were transferred in plastic sample bottles.

Main, intermediate and working standard solutions in 142 mM NaCl, 2.5 mM CaCl₂, 1.5 mM MgCl₂, 5 mM KCl and 0.5 mM Na₂SO₄ were prepared by the same way used to prepare phosphate standards in ultrapure water. However, instead of ultrapure water 142 mM NaCl, 2.5 mM CaCl₂, 1.5 mM MgCl₂, 5 mM KCl and 0.5 mM Na₂SO₄ solutions were used as solvents.

Preparation of phosphate standards in 27 mM NaHCO₃, 115 mM NaHCO₃ and 27 mM NaHCO₃ containing solution, SBFA and SBFB solutions was different. In the case of 27 mM NaHCO₃, main phosphate standard solution (2500 mg/L) was prepared by dissolving 0.2268 g NaHCO₃ and 0.3158 g NaH₂PO₄ in ultrapure water separately. Solutions were then combined and volume was brought to 100 ml with ultrapure water. Main standard solution containing 115 mM NaCl and 27 mM NaHCO₃ was prepared by dissolving 0.6732 g NaCl, 0.3158 grams of NaH₂PO₄ and 0.2268 grams NaHCO₃ individually in ultrapure water. They were then combined and volume was brought to 100 mL with ultrapure water. Intermediate and working standard solutions were prepared in a similar way used in the preparation of phosphate standard solutions in ultrapure water. However 27 mM NaHCO₃ was used as solvent for the preparation of intermediate and working standards in 27 mM NaHCO₃ whereas 115 mM NaCl and 27 mM NaHCO₃ containing solution was used for the preparation of intermediate and working standards in 115 mM NaCl and 27 mM NaHCO₃ containing solution.

Solutions having ion concentrations similar to simulated body fluid, but excluding phosphate ions (SBFA and SBFB) were also used to prepare phosphate standards. Table 5.5 shows amounts of reagents used to prepare SBFA and SBFB solutions whereas ionic compositions of these solutions are given in Table 5.6

For the preparation of SBFA solution, two hundreds milliliters of ultrapure water was added into a glass beaker. Each reagent was dissolved completely in ultrapure water and added into the beaker. Sequence of reagent addition was followed in the order shown in Table 5.5. During the preparation, solution in the beaker continuously stirred by a magnetic stirrer and pH of the solution was monitored. After the addition of the final reagent, solution was transferred into 500 mL capacity glass volumetric flask and volume was adjusted to 500 mL by ultrapure water. Solution was finally mixed thoroughly.

SBFB was prepared in a similar way used in the preparation of SBFA. When compared to SBFA solution, SBFB contains calcium ions (Table 5.6). During the preparation, after the addition of the calcium chloride into the solution results with the

precipitation, probably calcium carbonate precipitates. In order to avoid precipitation, before addition of calcium chloride, 15 mL 1 M HCl was added into the solution. After the addition of final reagent, solution was transferred into the 500 mL glass volumetric flask and volume was adjusted to 500 mL with ultrapure water. Solution was finally thoroughly mixed.

Main standards solutions were prepared in ultrapure water but intermediate and working standard solutions were prepared by using SBFA and SBFB solutions as solvents.

Table 5.5. Reagents used to prepare SBFA and SBFB solutions

No	Reagent	Amount (g)	
		SBFA	SBFB
1	NaCl	3.3480	3.3480
2	NaHCO ₃	1.1341	1.1341
3	KCl	0.1874	0.1874
4	MgCl ₂ 6H ₂ O	0.1525	0.1525
5	1 M HCl	-	15 mL
6	CaCl ₂ 2H ₂ O	-	0.1838
7	Na ₂ SO ₄	0.0359	0.0359

Table 5.6. Ionic compositions of SBFA and SBFB solutions

No	Ion	Concentration (mM)	
		SBFA	SBFB
1	Na ⁺	142.0	142.0
2	Cl ⁻	122.0	142.0
3	HCO ₃ ⁻	27.0	27.0
4	K ⁺	5.0	5.0
5	Mg ²⁺	1.5	1.5
6	Ca ²⁺	-	2.5
7	SO ₄ ²⁻	0.5	0.5

5.2.1.3.3. Analysis

Malachite green based phosphate analysis was performed in 96 well plates in a plate reader Multiskan® Spectrum (Thermo Electron Corporation, Finland). Ultrapure water treated in the similar way used in the phosphate solutions was used as a blank.

Two hundred microliters from the desired solution were added into the wells of a 96 well microplate in 5 replicates. After the addition of the solutions, 50 µL of 36 mM ammonium molybdate in 2.7 M H₂SO₄ were added into the wells. Microplate was then shaken for 30 seconds at 300 spm (shakes per minute) in a linear shaking mode with linear shaking amplitude (width) of 10 mm in Multiskan® Spectrum plate reader. After shaking, microplate was incubated for 10 minutes at 150 rpm and 25 °C in a shaking incubator (Ivymen, Spain or MaxQ⁴⁰⁰⁰, Barnstead, UK). Fifty microliters of reagent B (0.72 mM Malachite Green & 0.3 (w/v) % PVA containing solution) were added into each well. At this step, care should be taken to avoid bubble formation in the wells since the solution contained a surfactant (PVA). For this reason, reagent B was added into a well by careful pipetting. Attention was also paid to add reagent B into the solution in order to ensure mixing of reagent B with the mixture of sample and reagent B in the wells. For each well by using a new pipette tip, reagent B was added into the solutions not onto the solutions. After addition of the reagent B, a pipette tip for the each set of concentrations, was used to mix the solutions by circular movement of the tip in the wells. At this step, mixing of the solution by a pipette tip did not cause any significant loss from the solutions. At the end of the addition of the reagent B into the wells, microplate was again shaken for 30 seconds at 300 spm (shakes per minute) in a linear shaking mode with linear shaking amplitude (width) of 10 mm in Multiskan® Spectrum plate reader. Microplate was then incubated for 30 minutes at 150 rpm and 25 °C in a shaking incubator. Microplate was finally shaken for 30 seconds at 300 spm (shakes per minute) in a linear shaking mode with linear shaking amplitude (width) of 10 mm in Multiskan® Spectrum plate reader. After shaking, solutions in the wells of microplates were analyzed in Multiskan® Spectrum plate reader at 25°C at 650, 640, 630, 620, 610 nm with a bandwidth of 2 nm. Spectra of the solutions were measured between 400 and 700 nm with a step size of 5 nm and bandwidth of 2 nm.

Above protocol was modified for the phosphate standards prepared in solutions containing HCO_3^- ions. Addition of acid reagent results in the formation of carbon dioxide bubbles and these bubbles stick on the walls and at the bottom of the wells. For this reason, 2 mL from each standard solution were transferred into 15 mL capacity centrifuge tubes. Five hundred microliters of 36 mM ammonium molybdate in 2.7 M H_2SO_4 was added into each tube. Solutions were then vortexed in order to mix solutions well and remove carbon dioxide bubbles generated. After vortexing, 250 microliters from each solution were transferred into the wells of the microplate in five replicates. Analysis was then continued as stated above.

The lids of the microplates were removed during the transfer of standards and reagents into the wells, shaking in the Multiskan® Spectrum plate reader and during the analysis. However, during the incubations at 25°C in a thermoshake incubator, plates were incubated by their lids closed.

Data analysis was performed as described in Section 5.2.1.1.3.

5.2.2. Powder Synthesis and Characterization

Nano-sized hydroxyapatite was prepared by precipitation and resultant powder was characterized by several characterization methods.

5.2.2.1. Synthesis of Nano-Sized Hydroxyapatite Powder

Calcium nitrate tetrahydrate and diammonium hydrogen phosphate were used to prepare hydroxyapatite powder. Carbondioxide from deionized water was removed by vacuuming and deionized water was heated to 37 °C. Two hundred milliliters 0.813 M $\text{Ca}(\text{NO}_3)_2 \cdot 4\text{H}_2\text{O}$ and 200 mL of 0.484 M $(\text{NH}_4)_2\text{HPO}_4$ solutions were prepared. While solutions were kept at 37 °C, their pH values were adjusted to 10 by the addition of concentrated NH_4OH solution. $\text{Ca}(\text{NO}_3)_2 \cdot 4\text{H}_2\text{O}$ solution was added into $(\text{NH}_4)_2\text{HPO}_4$ by peristaltic pump with a rate of 10 mL/min. Solution was continuously stirred and reaction was carried out at 37 °C. Throughout the reaction, pH was continuously measured. During precipitation reaction, hydroxyapatite formation consumes OH^- ions in the solution hence pH drops. Whenever pH dropped slightly below 10, it was adjusted to 10 by the addition of concentrated $(\text{NH}_4)_2\text{HPO}_4$. Care was taken during pH

adjustments so that pH never exceeded 11. After the addition of all calcium nitrate solution, solution was aged for 24 hours at ambient temperature by continuous stirring.

After ageing, precipitate was removed from the solution by centrifugation. Precipitate was washed twice by using deionized water with a pH of 10 which was adjusted by the addition of concentrated NH_4OH . Further washings were performed only with deionized water. Washing was continued until the conductivity of supernatant was $< 15 \mu\text{S/cm}$. During washing steps in deionized water, ultrasonic treatment was used to increase the efficiency of washing. Precipitate was dried at 37°C after washing. During drying, precipitate was frequently mixed in order to provide homogenous drying and to avoid formation of a xerogel. Precipitate was finally ground in an agate mortar.

5.2.2.2. Characterization of Powders

Crystalline structures, particle size and morphology, specific surface areas, thermal behaviors, calcium and phosphate contents as well as functional groups in the crystal lattice were determined by using X-ray diffraction analysis, scanning electron microscopy, nitrogen adsorption-desorption analysis, thermogravimetric analyses, calcium and phosphate analysis and FTIR analysis, respectively.

5.2.2.2.1. X-Ray Diffraction Analysis

Crystallographic structures and properties of commercial hydroxyapatite and β -tricalcium phosphate powders were determined by Phillips X'Pert Pro X-ray diffractometer. X-ray profiles of the powders were evaluated at 2θ values between 5 to 80° . Detector employed was Phillips Panalytical X'celerator detector. X-ray scans were performed at 45 kV and 40 mA with $\text{CuK}\alpha$ radiation at $\lambda = 1.540$.

5.2.2.2.2. Thermogravimetric Analysis

Thermogravimetric analyses of the powders were performed by heating the powders up to 1100°C with a heating rate of $10^\circ\text{C}/\text{min}$ under $20 \text{ mL}/\text{min}$ nitrogen flow in Perkin Elmer TGA/DT analyzer.

5.2.2.2.3. BET Surface Area

BET surface areas and of the powders were evaluated by nitrogen adsorption-desorption analysis at 77.44 K in Micromeritics ASAP 2010 pore size analyzer.

5.2.2.2.4. Scanning Electron Microscopy

Samples for the SEM analysis were prepared by ultrasonical dispersion of the powders in 2 ml absolute ethanol. Dispersed particles were then spread over aluminum stubs. Crystal morphologies were determined in scanning electron microscope Phillips XL-30S FEG.

5.2.2.2.5. Fourier Transform Infrared Radiation (FTIR) Analysis

Fourier transform infrared radiation (FTIR) analysis of the powders was performed by KBr pellet method. KBr pellets containing 2 wt.% powders were prepared by mixing 3 mg powders with 150 mg KBr and pressing into the pellet forms. Analysis was performed in Shimadzu FTIR 8400 S after three point baseline and zero baseline corrections. Absorbance data was recorded in a scan range of 4000-400 cm^{-1} . Number of scans and resolution were 40 and 4.0, respectively.

5.2.2.2.6. Determination of Calcium/Phosphate Molar Ratios

Calcium and phosphate contents of the commercial and synthesized hydroxyapatite powders were determined by dissolving powders in HCl solutions. As a reference, calcium and phosphate contents of the commercial CaHPO_4 powder was also evaluated. Powders (approximately 0.1 g) were dissolved in a mixture of 5 mL 1 M HCl and 20 mL ultrapure water. After complete dissolution, solutions were transferred into 100 mL capacity glass volumetric flasks. Volumes were brought to 100 mL with ultrapure water and solutions were mixed thoroughly. These were used as main solutions in the calcium and phosphate determinations.

In order to obtain calcium concentrations within the calibration range, main solutions were diluted with ultrapure water in volumetric flasks. After dilutions, final HCl concentration in the solutions was 0.5 mM. Calcium in the final solutions were determined by Arsenazo III method.

For the phosphate analysis, successive dilutions of main solutions were made. By this way final HCl concentration in solutions did not exceed 0.1 M. Phosphate concentrations of the final concentrations were determined by malachite green phosphate assay.

Calcium and phosphate concentrations of the main solutions were calculated by taking dilution factors into consideration. Calcium and phosphate contents of the powders and Ca/P molar ratios were then calculated.

5.2.3. Dissolution of Cold Isostatically Pressed Hydroxyapatite Pellets

Loosely pressed hydroxyapatite pellets were obtained by pressing 0.250 g powder in a 10 mm dye at 57 MPa. These pellets were then pressed in a cold isostatic press (CIP) at 2000 bar for approximately 20 minutes.

Equilibrations of pellets obtained from both commercial hydroxyapatite and hydroxyapatite synthesized in this thesis were performed in different electrolytes. The list of electrolyte solution used in dissolution tests is given in Table 5.7.

Table 5.7. Electrolyte solutions used in dissolution of hydroxyapatite powders

Commercial hydroxyapatite (HA)	Synthesized hydroxyapatite (DHA)
<ul style="list-style-type: none"> • Ultrapure water • 142 mM NaCl • CO₂ free ultrapure water • CO₂ free 142 mM NaCl • CO₂ free 1.5 mM MgCl₂ • 27 mM NaHCO₃ • 115 mM NaCl and 27 mM NaHCO₃ containing electrolyte solution 	<ul style="list-style-type: none"> • CO₂ free ultrapure water • CO₂ free 142 mM NaCl • 27 mM NaHCO₃

Pellets were equilibrated in the electrolyte solutions for either 2 weeks or one month. A single pellet was immersed in 50 mL corresponding equilibration media in 100 mL capacity polypropylene bottles. Equilibrations were followed either for 1, 2, 3, 8, 24, 48, 96, 192 and 336 hours or 1, 2, 4, 8, 24, 48, 96, 96, 192, 360 and 720 hours. Therefore 9 or 10 pellets were used for each equilibration experiment. Pellets were removed from the solution. Solutions were kept at 4 °C until pH, conductance, calcium and phosphate analysis. Solutions left on the pellets were removed by wiping with tissue paper. Washing the pellets by ultrapure water was avoided since it may alter the surface changes occurred during equilibrations.

Calcium and phosphate analysis in the solutions were performed by diluting the samples in respective blank solutions if the dilution was necessary. Calcium and phosphate concentrations in the solutions were then analyzed by Arsenazo III-calcium and malachite green phosphate assays. Absorbance values measured at 650 nm were used to calculate ΔA values. ΔA values obtained by subtracting average of the absorbance values of the blank reagents from the average value of absorbances of the solutions were used to find concentrations in the solutions. Calibration curves constructed using ΔA values obtained from the absorbances measured at 650 nm were therefore used.

CHAPTER 6

RESULTS AND DISCUSSION

6.1. Chemical Analyses

For the determination of calcium in the dissolution media, first of all calcium analysis method was modified and tested for the determination of low levels of calcium. Interferences due to the presence of several ions on the calcium and phosphate analyses were determined.

6.1.1. Optimization of Microplate Based Arsenazo III Calcium Analysis

Optimum Arsenazo III concentration, buffer strength and pH were determined for the low level calcium analysis in the solutions. The effects of the presence of several ions on the calcium determination were also verified. Arsenazo III dye reagents buffered to pH of 5.4, 3.8 and 6.5 with acetate, formate and imidazole buffers, respectively were tested for the analysis of calcium in the standard solutions with three different calcium concentration ranges (0.25-2, 1-8 and 10-80 ppm).

6.1.1.1. Arsenazo III in Acetate Buffer

Spectrophotometric method for the analysis of calcium in ppm level by Arsenazo III in acetate buffer (pH 5.5) was reported by Michaylova and Ilkova (1971). They were able to analyze calcium in 0.030 - 1.5 ppm range by using Arsenazo III dye. They performed their analysis by combining calcium solutions with 10 mL 0.073 mM Arsenazo III in acetate buffer (pH 5.5) and diluting the solution to 25 mL. Absorbances of the solutions were measured at 600 nm. Final concentration of Arsenazo III in the solution was 29.2 μ M. Two different Arsenazo III reagents were therefore tested for the calcium analysis in this study (60 μ M Arsenazo III & 100 mM acetate buffer pH 5.4 and 120 μ M Arsenazo III & 100 mM acetate buffer pH 5.4).

60 μ M Arsenazo III & 100 mM Acetate Buffer pH 5.4:

60 μ M Arsenazo III was selected in order to obtain the same final concentration of the dye used by Michaylova and Ilkova (1971) when calcium solutions were mixed in equal amounts for the calcium analysis.

60 μ M Arsenazo III in 100 mM acetate buffer pH 5.4 was tested for the construction of the calibration curves for the 0.25-2 ppm, 1-8 ppm, and 10-80 ppm calcium ranges. Absorption spectra between 400-700 nm were scanned for these three calcium ranges in order to determine possible alterations. Figure 6.1 gives the light absorption spectra of calcium standard solutions (0.25-1.75 ppm range) analysed using 60 μ M Arsenazo III in 100 mM acetate buffer pH 5.4. According to Figure 6.1, dye itself gives a maximum absorption peak at 540 nm; however a new peak at 650 nm appears with increasing in its intensity with increasing calcium concentration. Absorption maximum of free dye shifts through higher wavelengths upon reaction of dye with calcium. This shift was found to be 15 nm when 1.75 ppm calcium was present in the system. When the values of absorbances in the range of 400-700 nm were plotted by subtracting the values of blank solution (Figure 6.2), two peaks located at 600 nm and 650 nm are observed. This shows that calcium-Arsenazo III complexation at pH 5.4 results in light absorption at these two wavelengths. Figures 6.3 and 6.4 give the absorption spectra of the complex when calcium concentration is higher. Absorption peak at 595 nm clearly becomes visible at higher calcium concentrations when spectra obtained without blanking. When calcium concentration in the standard solution was higher than 10 ppm, absorption peak of the dye shifts to 565 nm. This shift was approximately 25 nm. Intensities at 650 nm were also found be increased as expected when compared to absorption of the dye-calcium complex obtained at low levels of calcium. When the blank values are subtracted from the absorption data (Figure 6.4), maximum absorbances can also be observed at 600 and 650 nm.

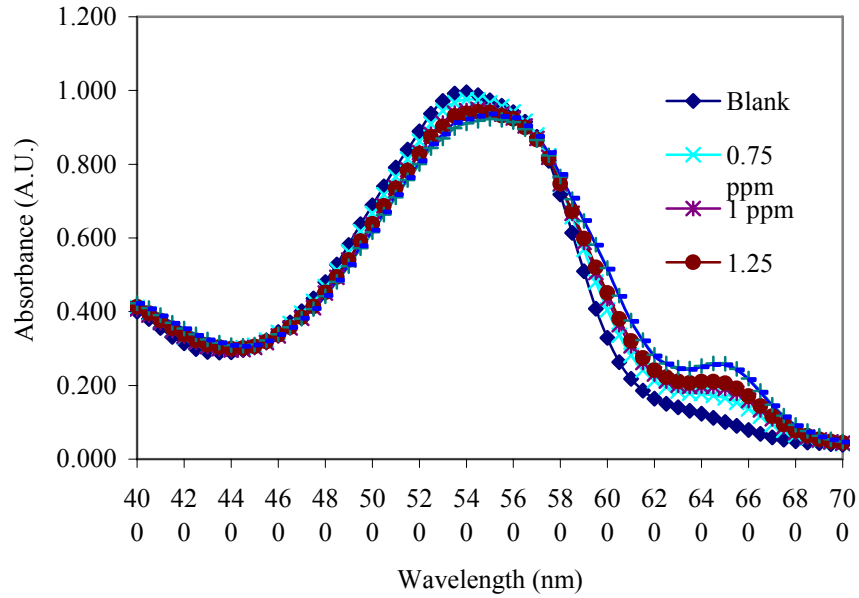


Figure 6.1. Spectra of calcium standard solutions (0.25-1.75 ppm) - 60 μ M AIII in 100 mM acetate buffer pH 5.4 (150 μ L standard- 150 μ L dye reagent).

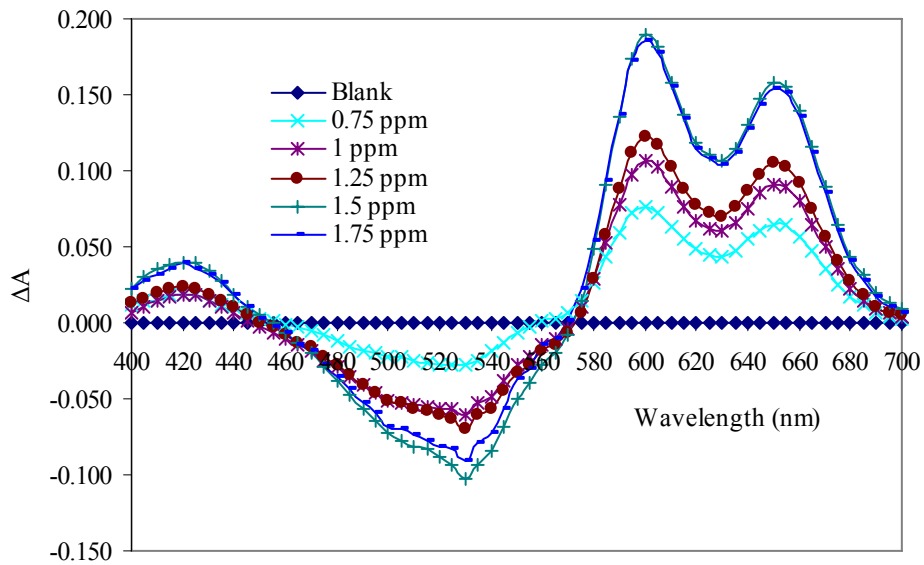


Figure 6.2. Spectra of calcium standard solutions (0.25-1.75 ppm) - 60 μ M AIII in 100 mM acetate buffer pH 5.4 (150 μ L standard- 150 μ L dye reagent) obtained by subtracting blank values.

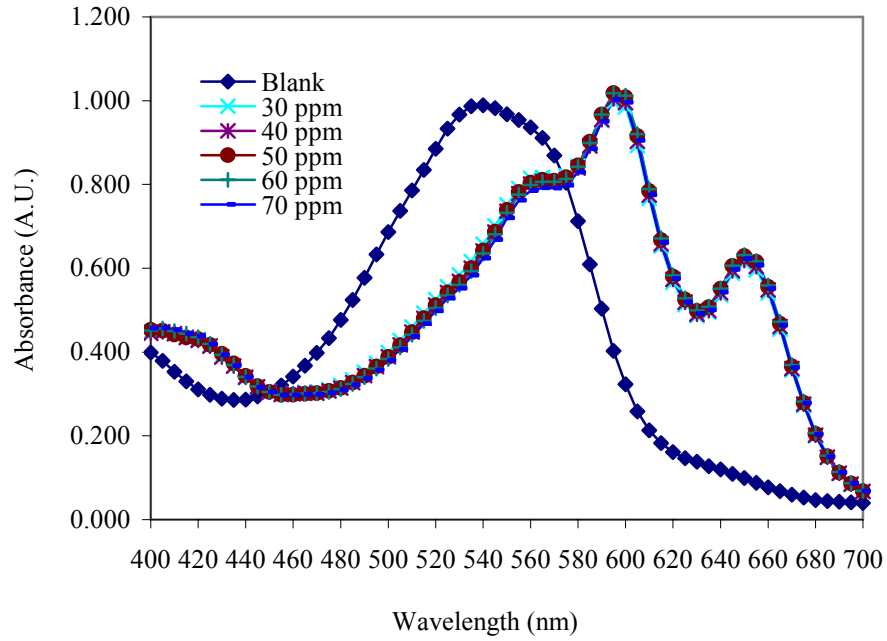


Figure 6.3. Spectra of calcium standard solutions (10-70 ppm) - 60 μ M AIII in 100 mM acetate buffer pH 5.4 (150 μ L standard- 150 μ L dye reagent).

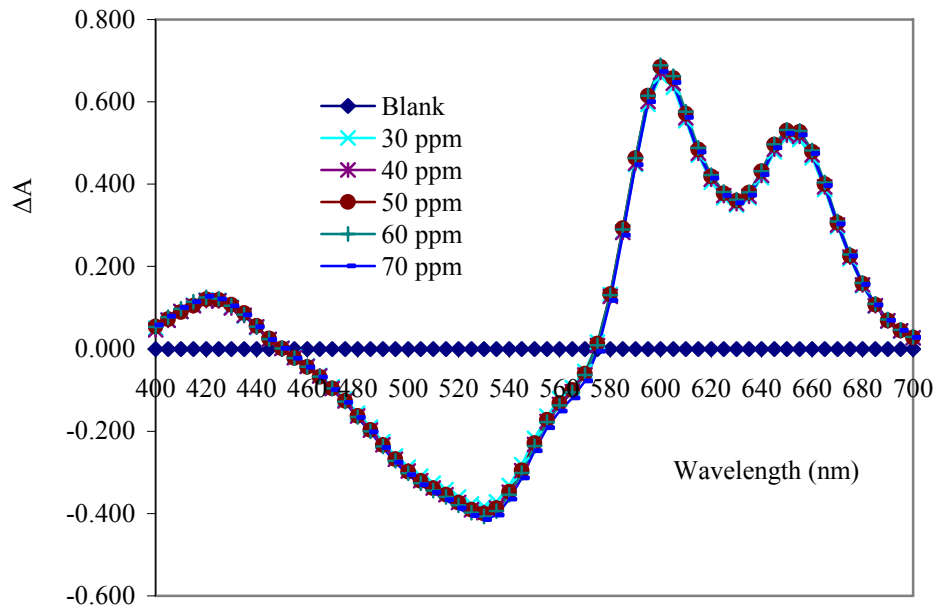


Figure 6.4. Spectra of calcium standard solutions (10-70 ppm) - 60 μ M AIII in 100 mM acetate buffer pH 5.4 (150 μ L standard- 150 μ L dye reagent), obtained by subtracting blank values.

Binding of bivalent and trivalent cations which form 1:1 complexes with Arsenazo III is suggested to occur by binding of metal ions to oxy groups of arson group and naphthelene nucleus (Alimarin and Savvin, 1966) (Figure 3.2.A). It was also suggested that this type complexation can not be generalized to all cations and pH ranges of the complex formations (Alimarin and Savvin, 1966). In some cases, naphthelene nucleus does not contribute directly to the complex formation (Alimarin and Savvin, 1966).

It is well known that two peaks are observed upon reaction of Arsenazo III with metal cations at approximately 610 and 655 nm (Alimarin and Savvin, 1966, Rowatt and Williams, 1989, Basargin et al., 2000). The peak found at 610 was attributed to the breakdown of the symmetry of the dye molecule after binding to metal cations (Basargin et al., 2000). Metal ion binding to one analytical group reduces its ionic state and this reduction affects the ionic state of the conjugated system (Basargin et al., 2000). In this study, the peak found at 650 nm was attributed to the absorption of calcium and dye complex whereas the peak obtained at 600 nm was suggested to be the result of the asymmetry of the dye molecules after complexation with calcium.

Due to the observation that calcium-Arsenazo III complex gives two absorption maxima, calcium analysis in this study was performed at two different wavelengths (600 and 650 nm). However calibrations curves obtained by absorbances measured at 600 nm are given in Appendix F for the simplicity.

For the analysis of different calcium concentration ranges first of all 0.25-2 ppm calcium standard solutions were used. Figure 6.5 shows the calibration curve obtained by measuring the absorbance values at 650 nm. Calibration obtained by subtracting the values of the blank solution from the absorbance values of the calcium standards were also presented in the same graphic. Linear calibration curve with a correlation coefficient of 0.9950 (Figure 6.5.a) was obtained with the values of absorbances measured at 650 nm. When the calibration curve was constructed by subtracting the average blank value from the average values of the solutions, correlation coefficient was slightly reduced to 0.9943. Figure 6.5 shows that it is possible to analyze 0.25-2 ppm calcium in the solution by Arsenazo III prepared in acetate buffer at 650 nm. However, absorbance response to the calcium standards used was in a narrow range (0.121 - 0.280 for 0.25 - 2 ppm, blank was 0.097).

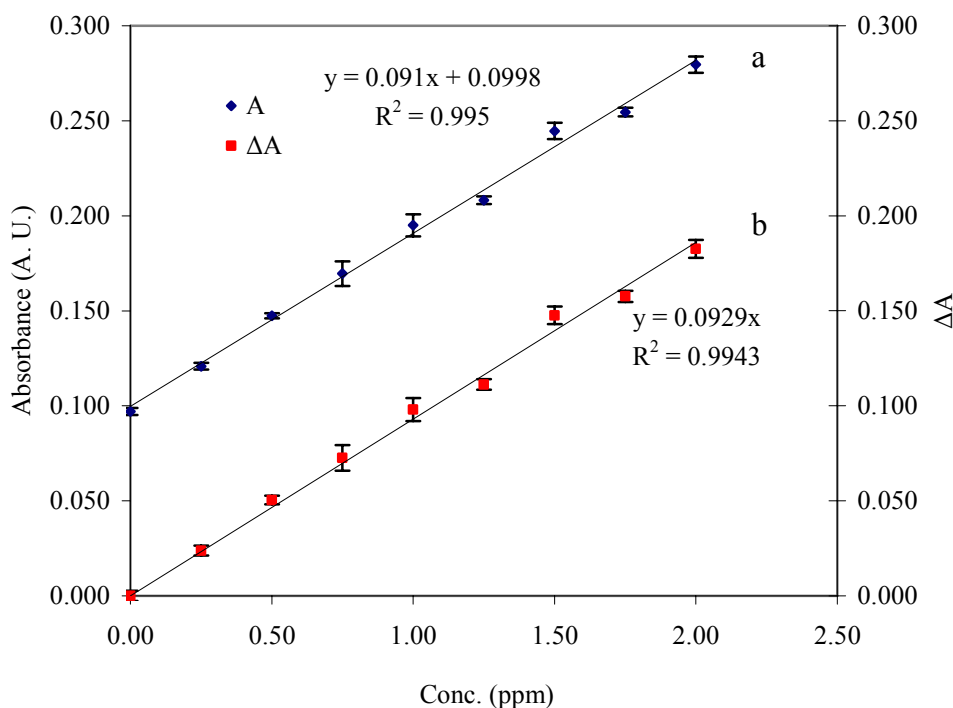


Figure 6.5. Absorbance values of calcium standards (0.25-2 ppm) - 60 μ M AIII in 100 mM acetate buffer pH 5.4 (150 μ L standard-150 μ L dye reagent) at 650 nm a. without subtracting blank values, b. with subtracting blank values.

Similar behavior was observed for the absorbance values obtained at 600 nm (Figure F.1). Correlation coefficients for the calibration curves obtained at 600 nm were smaller than those obtained at 650 nm. Additionally, for each of the solution absorbance values was higher than those obtained at 650 nm. When the blank values obtained at both wavelengths were compared, average blank value obtained at 650 nm (0.097) was considerably smaller than the average blank value obtained at 600 nm (0.329). Absorption at 650 nm is due to the absorption of the calcium-dye complex whereas absorption at 600 nm is the result of the change in the ionic state of the Arsenazo III due to the symmetry breakdown. Higher absorbance values at 600 nm may be due the effect of pH on the ionic state of the molecule and due to the reduction of symmetry of the dye molecule because of the calcium and dye complexation. Figure 3.1.B shows the ionizable groups found on the Arsenazo III. pK values of these ionizable groups are as follows: $pK_1 = -2.5$, $pK_2 = 0$, $pK_3 = 2.5$, $pK_4 = 2.5$, $pK_5 = 5.3$, $pK_6 = 5.3$, $pK_7 = 7.5$ and $pK_8 = 12.4$ (Rowatt and Williams, 1989). Repulsion forces exerted due the presence of ionized groups at pH 5.5 and calcium complexation may result in symmetry breakdown of the molecule and absorption at 600 nm occurs.

Because of the lower absorbances of the calcium-Arsenazo III complexes, higher ppm level of calcium standards was therefore prepared and analyzed by Arsenazo III dye in acetate buffer. Figure 6.6 shows the results of the analysis of 1 to 8 ppm calcium solutions with 60 μM Arsenazo III. Absorbance of calcium-Arsenazo complex reached to an equilibrium by the increase in calcium content. This was possibly due to the insufficient amount of the dye available to bound excess calcium. Since the complexation of calcium with Arsenazo III molecule is governed by the dissociation constant of Arsenazo III, a fraction of Arsenazo III bound to calcium is constant at defined dye concentration and pH regardless of the calcium concentration. This could be clearly observed when the calcium amounts in the solutions were further increased to 10-80 ppm range (Figure 6.7). By holding the concentration of Arsenazo III in the solution constant but increasing the calcium concentration, absorbances of the calcium dye complexes reached equilibrium at pH 5.4.

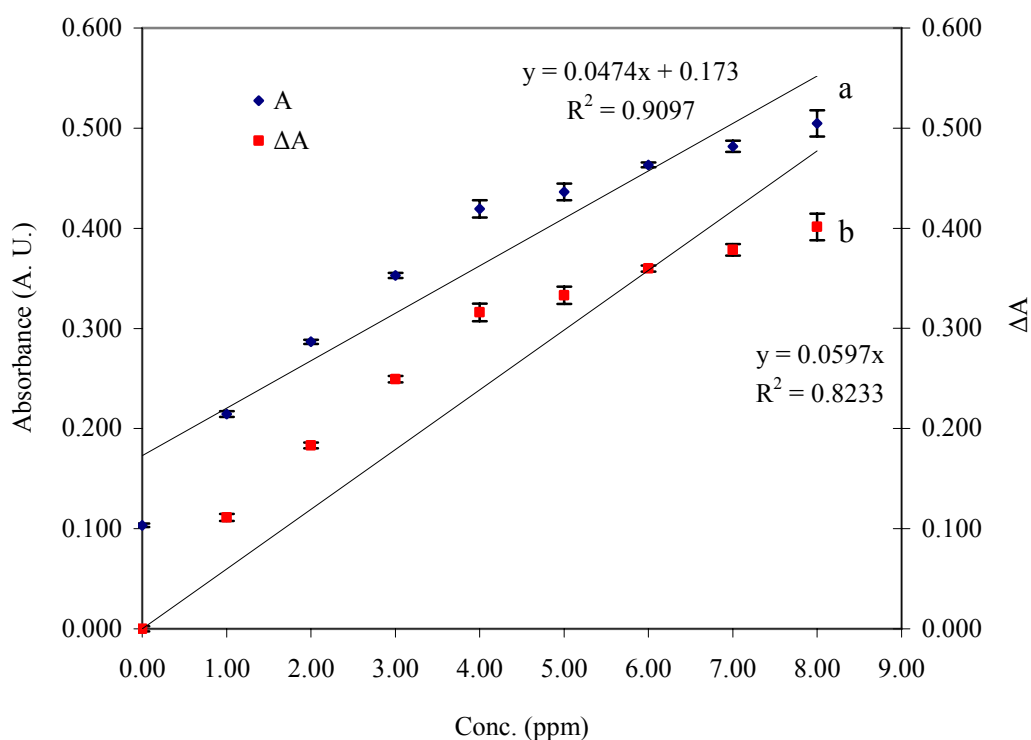


Figure 6.6. Absorbance values of calcium standards (1-8 ppm) - 60 μM AIII in 100 mM acetate buffer pH 5.4 (150 μL standard-150 μL dye reagent) at 650 nm a. without subtracting blank values, b. with subtracting blank values.

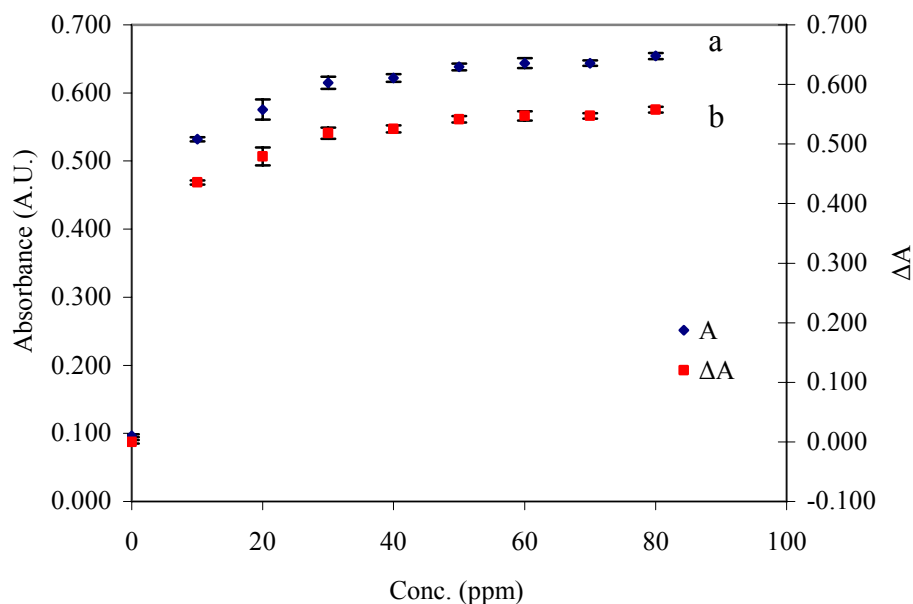
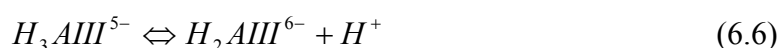
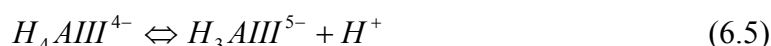
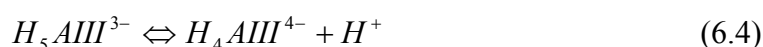
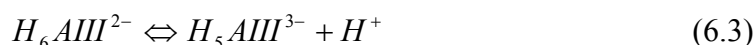
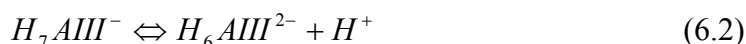


Figure 6.7. Absorbance values of calcium standards (10-80 ppm) - 60 μ M AIII in 100 mM acetate buffer pH 5.4 (150 μ L standard-150 μ L dye reagent) at 650 nm a. without subtracting blank values, b. with subtracting blank values.

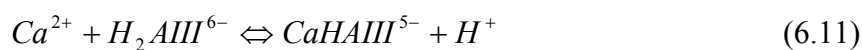
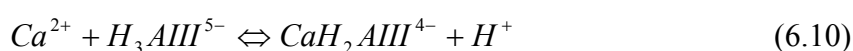
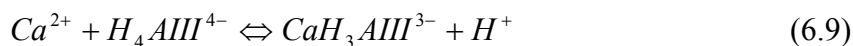
Not only Arsenazo III concentration and pH, but also buffer used is important in the calcium analysis by Arsenazo III dye. Buffers may have small calcium binding ability (Bauer, 1981). Especially, increase in negative logarithm of apparent dissociation constant (pK_{Ca}) of Arsenazo III was observed with a decrease in buffer concentration (Bauer, 1981). The reason for this was related to the increase of ionic strength due to the increase of the buffer concentration.

According to ionizable groups present on the dye molecule, Arsenazo III dye shows multiple protonation equilibria (Chiu and Haynes, 1980). Protonation reactions depending on pH can be written as follows;





Chiu and Haynes (1966) reported that H_3AIII^{5-} and H_4AIII^{4-} are dominant forms between pH 5.4 and 7.0. When calcium is present in the system at these pH values the possible equilibria can be shown as follows:



Binding affinities for the calcium was reported to decrease in the order of H_2AIII^{6-} , H_3AIII^{5-} and H_4AIII^{4-} (Chiu and Haynes, 1966). In buffered systems, equilibrium reaction of the buffer is as follows:



Protonation reactions of Arsenazo III and buffer competes with hydrogen binding. When the buffer strength increases, more buffer molecules competes with hydrogen binding, this affects the fraction of ionized species of Arsenazo III (H_2AIII^{6-} , H_3AIII^{5-} and H_4AIII^{4-}). The decrease of dissociation constant of Arsenazo III with the decrease of buffer concentration may likely be due to the above stated possible protonation and complexation equilibria of Arsenazo III.

Because of the effect of buffer strength on dissociation constant of Arsenazo III (Bauer, 1981), a dye reagent was prepared by diluting 60 μ M Arsenazo III in 100 mM acetate buffer with ultrapure water in 1:1 (v/v) ratio. This reagent had 30 μ M Arsenazo III and 50 mM acetate buffer. After mixing with calcium standards (150 μ L of standard and 150 μ L of $\frac{1}{2}$ diluted reagent), total Arsenazo III and total buffer concentrations were 15 μ M and 25 mM in the mixture, respectively. This $\frac{1}{2}$ diluted reagent was used for the all calcium concentration ranges. Absorption spectra of the calcium-arsenazo III complexes are shown in Figure 6.8. Dye reagent itself exhibit maximum absorption at

540 nm. This absorption band shifts 15 nm through longer wavelengths upon complexation of the dye with calcium. Calcium-Arsenazo III complex shows maximum absorption at around 645 nm. Difference of the spectra of the calcium containing solutions from the spectra of the blank solution shows that two absorption bands are the result of complexation at 600 and 650 nm (Figure 6.9).

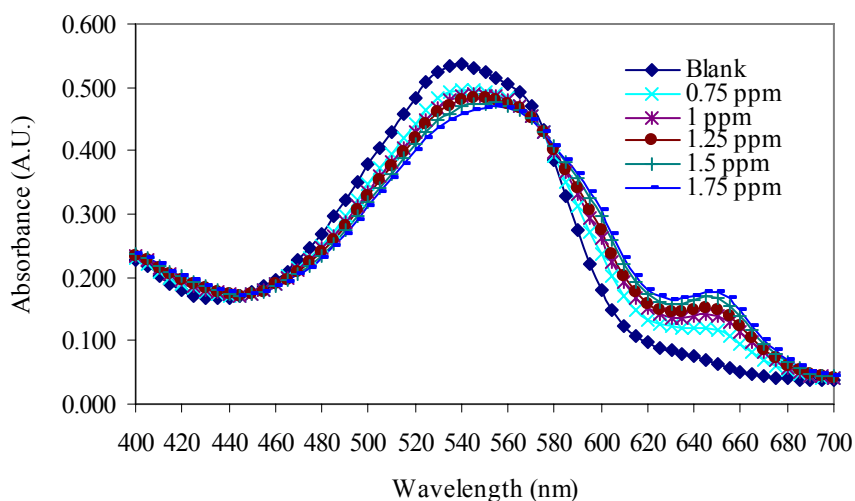


Figure 6.8. Spectra of calcium standards (0.25-2 ppm) - $\frac{1}{2}$ (60 μ M AIII in 100 mM acetate buffer pH 5.4) (150 μ L standard-150 μ L dye reagent).

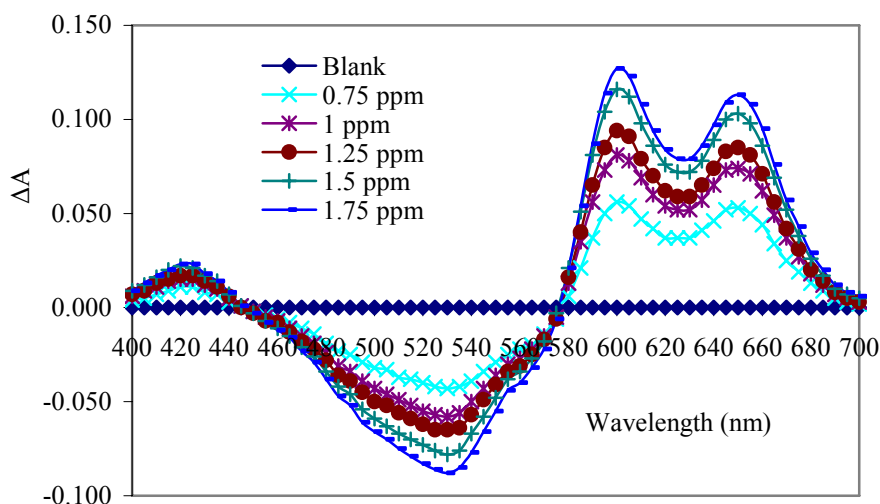


Figure 6.9. Spectra of calcium standards (0.25-2 ppm) - $\frac{1}{2}$ (60 μ M AIII in 100 mM acetate buffer pH 5.4) (150 μ L standard-150 μ L dye reagent) obtained by subtracting blank values.

Calibration curve obtained at 650 nm was found to be linear when the calcium concentration range was 0.25-2 ppm (Figure 6.10). However correlation coefficients obtained were smaller than those obtained with 60 μM Arsenazo III.

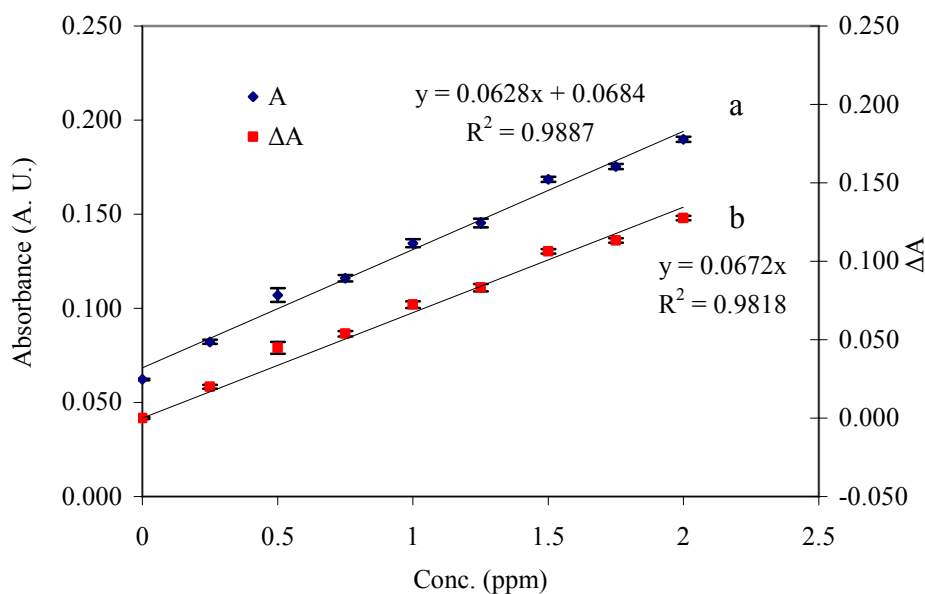


Figure 6.10. Absorbance values of calcium standards (0.25-2 ppm) - $\frac{1}{2}$ (60 μM AIII in 100 mM acetate buffer pH 5.4) (150 μL standard-150 μL dye reagent) at 650 nm a. without subtracting blank values, b. with subtracting blank values.

When calcium standard solutions within the range of 1-8 ppm and $\frac{1}{2}$ diluted were used, solution started to become saturated over 4 ppm standard solution concentration (Figure 6.11) like observed when 60 μM Arsenazo III in 100 mM acetate buffer was used.

Saturation of Arsenazo III could easily be observed when the standard solutions with 10-80 ppm calcium concentration range were used. $\frac{1}{2}$ diluted reagent turned out to be fully saturated when standard solution having 30 ppm or higher concentration of calcium (Figure 6.12). Total calcium concentration in the mixture was equal to 15 ppm when 30 ppm standard solution was combined with $\frac{1}{2}$ diluted Arsenazo III solution (150 μL dye-150 μL standard). Total final Arsenazo III and buffer concentrations were 15 μM and 25 mM, respectively.

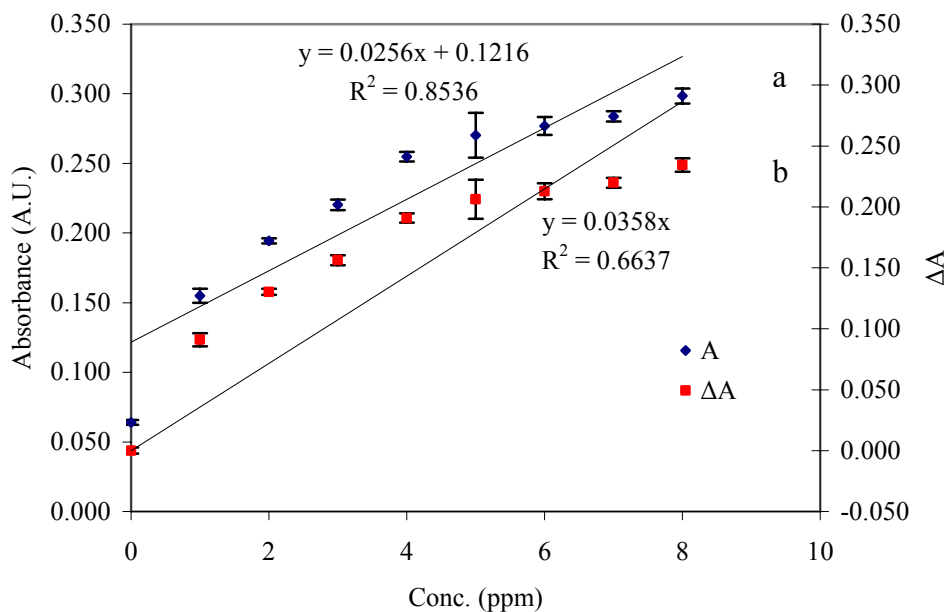


Figure 6.11. Absorbance values of calcium standards (1-8 ppm) - $\frac{1}{2}$ (60 μ M AIII in 100 mM acetate buffer pH 5.4) (150 μ L standard-150 μ L dye reagent) at 650 nm a. without subtracting blank values, b. with subtracting blank values.

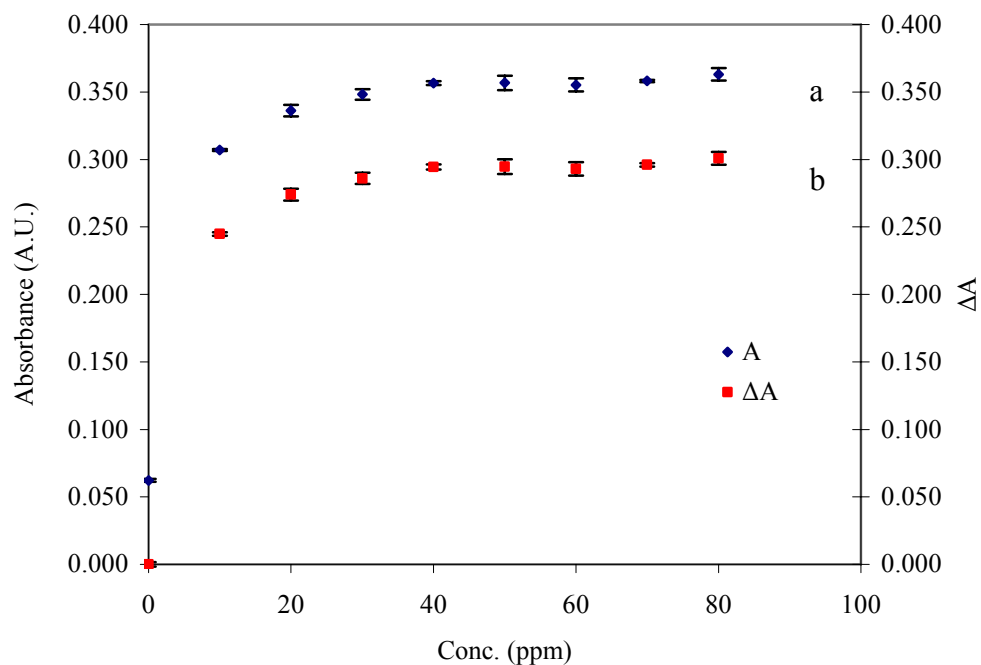


Figure 6.12. Absorbance values of calcium standards (10-80 ppm) - $\frac{1}{2}$ (60 μ M AIII in 100 mM acetate buffer pH 5.4) (150 μ L standard-150 μ L dye reagent) at 650 nm a. without subtracting blank values, b. with subtracting blank values.

Calcium-Arsenazo III dissociation constants can be obtained by measuring absorbances of the solutions, dye alone and dye saturated with calcium. Following methodology was adapted from the studies of Bauer (1981) and Ahmed et al. (1980). Calculations are as follows;

When 1:1 complex formation between calcium and Arsenazo III is assumed dissociation constant of calcium-Arsenazo III complex can be written as follows:

$$K_D = \frac{[Ca^{2+}][AIII]}{[CaAIII]} \quad (6.13)$$

Total Arsenazo III concentration in the system are the sum of concentration of free Arsenazo III and concentration of Arsenazo III in the complex. Likewise, total calcium concentration equals to free calcium concentration and calcium concentration in the complex.

$$[Ca]_t = [Ca]_f + [CaAIII] \quad (6.14)$$

$$[AIII]_t = [AIII]_f + [CaAIII] \quad (6.15)$$

It is reported that Arsenazo III shows slight absorption at 650 nm (Kendrick et al., 1977). Absorption spectra of Arsenazo III obtained in different concentrations at three pH values, 3.8, 5.4 and 6.5 in this thesis confirmed this finding.

Absorbance of the solution at 650 nm can be written as the sum of the absorbances of the complex and free dye.

$$A = \epsilon_{AIII}l[AIII]_f + \epsilon_{CaAIII}l[CaAIII] \quad (6.16)$$

When there is no calcium present in the system, the absorbance of the solution is the absorbance of the dye itself. It can be calculated as follows;

$$A_{\min} = \epsilon_{AIII}l[AIII]_t \quad (6.17)$$

If the dye is saturated with calcium, all dye molecules are complexed with calcium. Absorbance measured is equal to molar absorptivity of the complex multiplied with its concentration and pathlength.

$$A_{\max} = \varepsilon_{CaAIII} l [CaAIII] \quad (6.18)$$

Since all dye molecules are in the complex when dye is saturated with calcium, maximum absorption can also be expressed with respect to total dye present in the solution.

$$A_{\max} = \varepsilon_{CaAIII} l [AIII]_t \quad (6.19)$$

Molar absorptivities of dye and dye-calcium complex defined in Equations 6.17 and 6.18 can be inserted to the Equation 6.16 to obtain following relation.

$$A = \frac{A_{\min}}{[AIII]_t} [AIII]_f + \frac{A_{\max}}{[AIII]_t} [CaAIII] \quad (6.20)$$

Concentration of calcium dye complex can be expressed as $[AIII]_t - [AIII]_f$. If this is inserted in place of the concentration of the complex in Equation 6.20, following equations are found.

$$A = \frac{A_{\min}}{[AIII]_t} [AIII]_f + \frac{A_{\max}}{[AIII]_t} ([AIII]_t - [AIII]_f) \quad (6.21)$$

$$A = \frac{A_{\min}}{[AIII]_t} [AIII]_f + \frac{A_{\max}}{[AIII]_t} [AIII]_t - \frac{A_{\max}}{[AIII]_t} [AIII]_f \quad (6.22)$$

By rearranging the Equation 6.22, one can obtain an equation relating the free dye concentration to total dye concentration.

$$\frac{A_{\max} - A_{\min}}{A_{\max} - A} = \frac{[AIII]_t}{[AIII]_f} \quad (6.23)$$

By measuring the absorbances of the dye solution without calcium and in the saturating calcium concentrations and absorbance of dye and calcium mixture at any calcium level, free dye concentration can easily be found.

Ratio of calcium dye complex to total dye concentration defined as α can be converted into ratio of the complex to the free dye concentration as follows;

$$\alpha = \frac{[CaAIII]}{[AIII]_t} \quad (6.24)$$

$$1 - \alpha = 1 - \frac{[CaAIII]}{[AIII]_t} = \frac{[AIII]_t - [CaAIII]}{[AIII]_t} \quad (6.25)$$

$$\frac{\alpha}{1 - \alpha} = \frac{[CaAIII]}{[AIII]_t - [CaAIII]} = \frac{[CaAIII]}{[AIII]_f} \quad (6.26)$$

When both sides of the equation Equation 6.26 are multiplied with dissociation constant of the calcium dye complex, relationship between free calcium concentration and dissociation constant is obtained.

$$\frac{\alpha}{1 - \alpha} K_D = \frac{[CaAIII]}{[AIII]_f} K_D \quad (6.27)$$

$$\frac{\alpha}{1 - \alpha} K_D = [Ca]_f \quad (6.28)$$

$$\frac{\alpha}{1 - \alpha} K_D = [Ca]_t - [CaAIII] \quad (6.29)$$

According to Equation 6.24, $[CaAIII]$ is equal to $\alpha[AIII]_t$. If $[CaAIII]$ in Equation 6.29 is replaced with $\alpha[AIII]_t$, following equation is found;

$$\frac{\alpha}{1 - \alpha} = \frac{1}{K_D} ([Ca]_t - \alpha[AIII]_t) \quad (6.30)$$

By using Equations 6.14, 6.15, 6.23 and 6.24, α can be easily calculated from absorbance data measured at 650 nm. After the calculation of α , if $\alpha/(1-\alpha)$ is plotted versus $[Ca]_t - \alpha[AIII]_t$, (Equation 6.30), dissociation constant of calcium and Arsenazo III complex can be found from the slope.

Calculation of apparent dissociation constant of calcium-Arsenazo III complex were performed for both 60 μ M Arsenazo III in 100 mM acetate buffer pH 5.4 reagent and $\frac{1}{2}$ (60 μ M Arsenazo III in 100 mM acetate buffer pH 5.4) reagent by using absorbance values recorded at 650 nm. These solutions were used for three different concentration ranges of calcium; 0.25-2 ppm, 1-8 ppm and 10-80 ppm. Absorbances found for 10-80 ppm calcium range reached the constant values (Figures 6.7 and 6.12). Constant absorbances showed that Arsenazo III was saturated with calcium. By using above stated methodology, $\alpha/(1-\alpha)$ values were calculated and plotted versus $[Ca]_t - \alpha[Ar]_t$.

Figure 6.13 shows the graphs of $\alpha/(1-\alpha)$ vs. $[Ca]_t - \alpha[Ar]_t$ for 60 μ M Arsenazo III in 100 mM acetate buffer pH 5.4 dye reagent for 0.25-2 ppm and 1-8 ppm. For both calcium ranges, straight lines were observed. Dissociation constants are calculated from the slopes of the straight lines. Dissociation constants were therefore found as 30.8 and 29.8 μ M for 0.25-2 ppm and 1-8 ppm calcium ranges, respectively. Negative logarithms of dissociation constants give pK_D values. pK_D values were calculated as 4.51 and 4.53, respectively.

Graphs of $\alpha/(1-\alpha)$ vs. $[Ca]_t - \alpha[Ar]_t$ for $\frac{1}{2}$ (60 μ M Arsenazo III in 100 mM acetate buffer pH 5.4) dye reagent for 0.25-2 ppm and 1-8 ppm calcium containing standard solutions are shown in Figure 6.14. Straight lines were also observed for the 1:1 diluted reagent for both calcium ranges. Apparent dissociation constants were calculated and found as 25.4 and 26.0 μ M when calcium standards with 0.25 to 2 ppm and 1 to 8 ppm concentration ranges were mixed with dye reagent, respectively. Resultant pK_{Ca} values were 4.60 and 4.58.

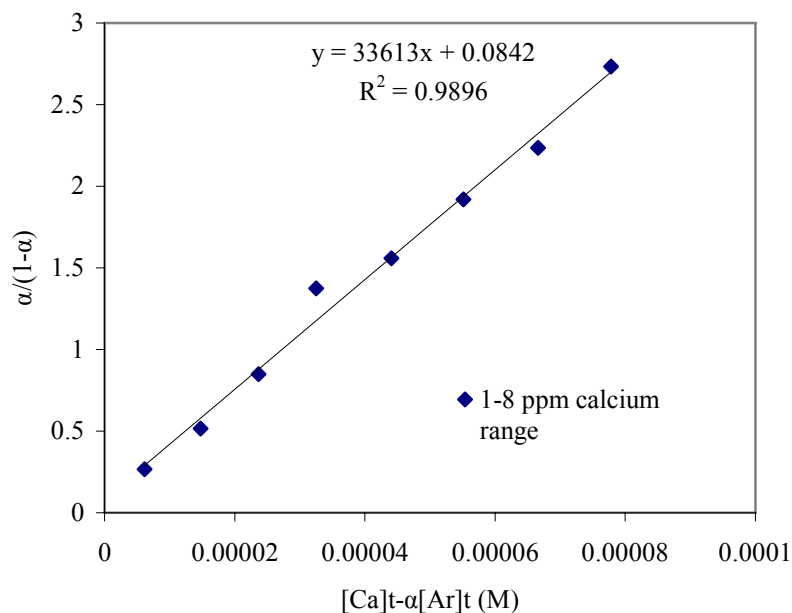
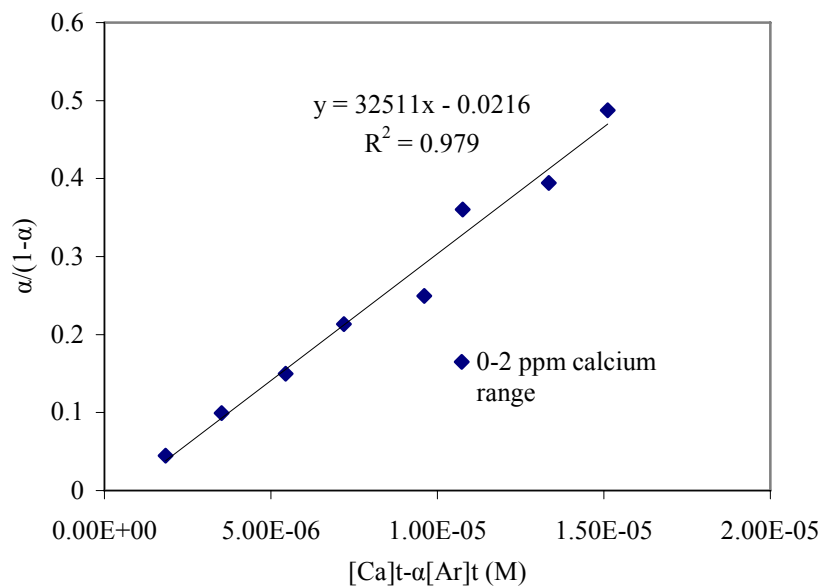


Figure 6.13. Plot of $\alpha/(1-\alpha)$ vs. $[Ca]_t - \alpha[Ar]_t$ Dye reagent: 60 μ M Arsenazo III in 100 mM acetate buffer pH 5.4 Calcium concentration of standard solutions: 0.25-2 ppm and 1-8 ppm (Reagent to standard volume ratio of 150 μ L/150 μ L).

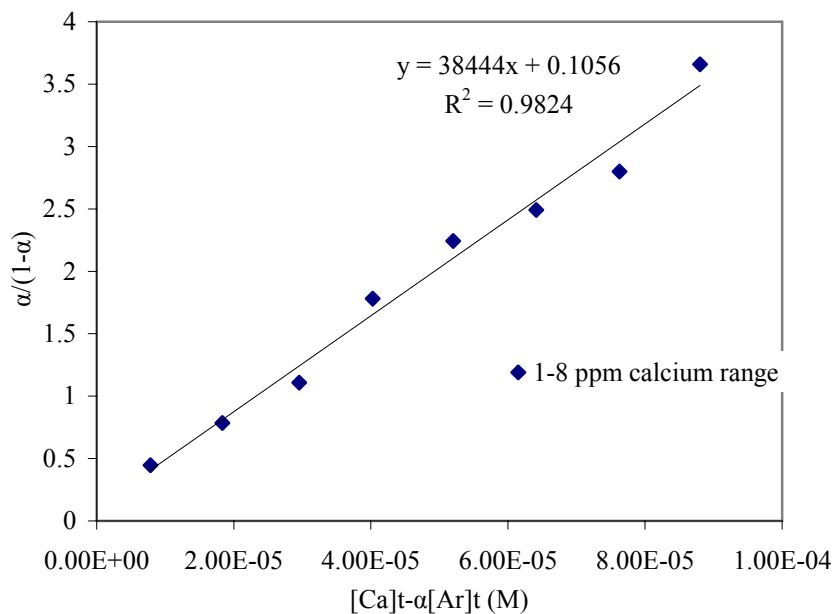
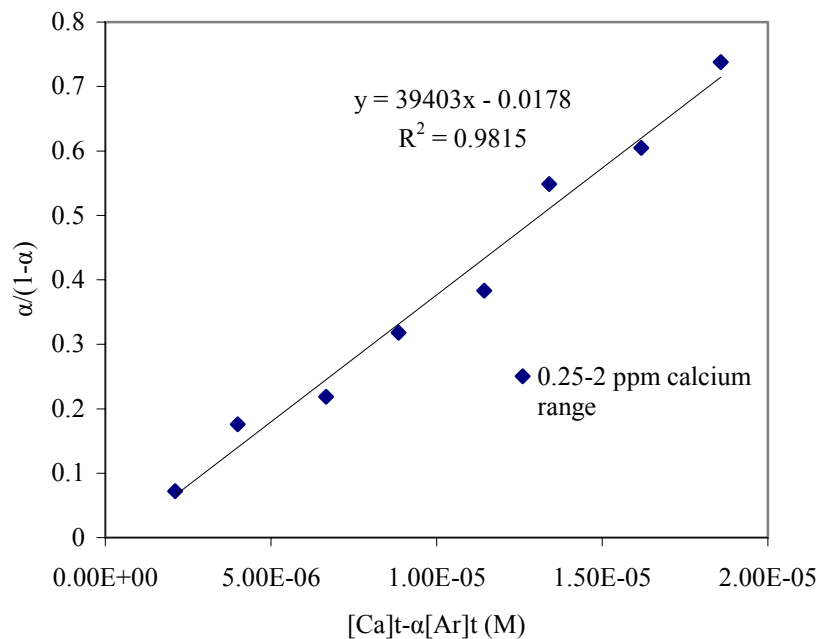


Figure 6.14. Plot of $\alpha/(1-\alpha)$ vs. $[Ca]_t - \alpha[Ar]_t$. Dye reagent: $\frac{1}{2}$ (60 μ M Arsenazo III in 100 mM acetate buffer pH 5.4) Calcium concentration of standard solutions: 0.25-2 ppm and 1-8 ppm (Reagent to standard volume ratio of 150 μ L/150 μ L).

Dissociation constant generally does not depend on the initial concentrations of the species. However, Brown and Rørdqvist (1981) reported the variation of K_D with Arsenazo III concentration and ionic strength. They showed that increase in Arsenazo III concentration from 100 μM to 316 μM decreased K_D from 389 μM to 102 μM at pH 5.0. The same increase in concentration of Arsenazo III decreased K_D from 137 to 41 μM at pH 6.0 (Brown and Rørdqvist, 1981). Dissociation constants found for 60 μM Arsenazo III in 100 mM acetate buffer pH 5.4 reagent were slightly different than those found for $\frac{1}{2}$ (60 μM Arsenazo III in 100 mM acetate buffer pH 5.4) reagent. Slight decrease in dissociation constant was observed upon 50 % reduction in Arsenazo III concentration. This was contrary to the findings of Brown and Rørdqvist (1981). However, increase of apparent pK_{Ca} values hence decrease of dissociation constants with the decrease in buffer concentration was reported by Bauer (1981). Although buffer concentration was 50 % reduced slight decrease was observed in dissociation constants in this study. This was probably due to combined effect of Arsenazo III and buffer concentration on the dissociation constant. Buffer concentration was more effective than Arsenazo III concentration at pH 5.4.

120 μM Arsenazo III & 100 mM Acetate Buffer pH 5.4:

Three different concentration ranges of calcium standard solutions were used to determine the suitability of 60 μM Arsenazo III in acetate buffer at pH 5.4 for the calcium analysis. Calcium standards with 1-8 ppm or 10-80 ppm range did not show linear absorbance response within each concentration range. Similar results were also obtained when dye reagent was diluted with ultrapure water 1:1 (v/v) ratio. A linear calibration curve was obtained with only 0.25-2 ppm calcium standard solutions when both 60 μM Arsenazo III in acetate buffer or $\frac{1}{2}$ diluted 60 μM Arsenazo III in acetate buffer were used. Absorbance values obtained for 0.25-2 ppm was in a narrow range. Practically, absorbance response to solution of interest should follow the Beer's law and absorbance values should not be higher than 1 (Marczenko and Balcerzak, 2000). Absorbance value higher than unity means that solution transmits less than 10 % of the the power of incident beam. When absorbance values are greater than one, method is subjected to large errors.

Sensitivity is defined as the minimum amount or the minimum difference of the concentration of a compound which can be determined by the method of concern (Marczenko and Balcerzak, 2000). When the absorbance responses measured in the method are in a narrow range for the calibration, sensitivity will be lower than the sensitivity of the method when absorbances range between 0 and 1. Narrow range of absorbance response obtained with 60 μM Arsenazo III forced us to search for a calcium analysis system in which the absorption range of the solution changes between 0 and 1. Therefore Arsenazo III concentration in the reagent was increased to 120 μM and tested for 1-8 ppm calcium concentration range.

Spectra of calcium standard solutions (1-7 ppm) mixed with 120 μM Arsenazo III in 100 mM acetate buffer pH 5.4 were scanned for the alterations in wavelengths where calcium-Arsenazo III complexes show maximum absorption. Figure 6.15 and 6.16 show absorption spectra of calcium standards and 120 μM Arsenazo in 100 mM acetate buffer pH 5.4 (150 μL standard-150 μL dye) mixtures. Increase in the concentration of Arsenazo III from 60 μM to 120 μM did not cause any changes in the absorption spectra. Dye itself again gave maximum absorption at 540 nm. When calcium standard solution with a concentration of 1 ppm is mixed with dye reagent, maximum absorption was still observed at 540 nm (Figure 6.15). When standard solutions containing calcium in concentrations higher than 1 ppm were mixed with dye reagent, peak of maxima of the blank solution shifted through longer wavelengths (Figure 6.16). Approximately 20 nm shift in the λ_{max} of the blank solution was observed. Calcium-Arsenazo III complex gave absorbances at 650 nm. Additionally a new peak at around 595 and 600 nm (especially at 595 nm) became apparent at high calcium concentrations (Figure 6.16). When the absorption spectra obtained by subtracting blank values from absorbances of standard solution-dye complex (Figure 6.17) was determined, a peak at 600 nm is observed together with a peak at 650-655 nm.

Calcium standard solutions in the range of 1-8 ppm were analyzed with 120 μM Arsenazo III containing reagent for the construction of a calibration curve. Figure 6.18 shows the calibration curve obtained at 650 nm. Absorbance values of standard solutions mixed with 120 μM Arsenazo in 100 mM acetate buffer at pH 5.4 obtained at 650 nm did not give a linear calibration curve when plotted vs. concentrations of standard solutions. Especially, deviation from Beer's law was started at 5 ppm or higher concentrations of standard solutions.

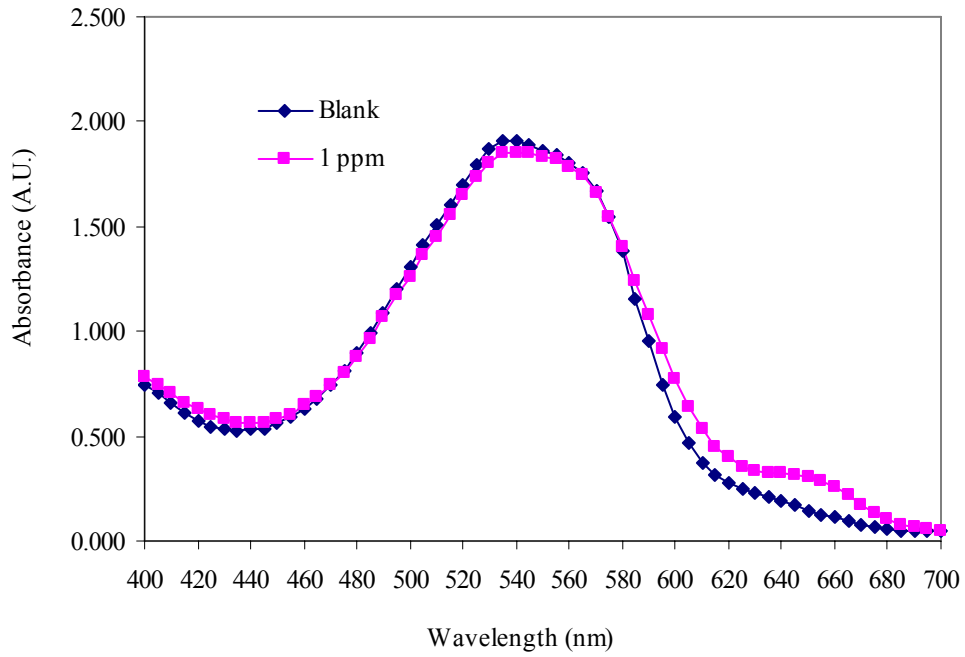


Figure 6.15. Spectra of blank and 1 ppm calcium standard solutions Dye: 120 μ M AIII in 100 mM acetate buffer pH 5.4 (150 μ L standard- 150 μ L dye reagent).

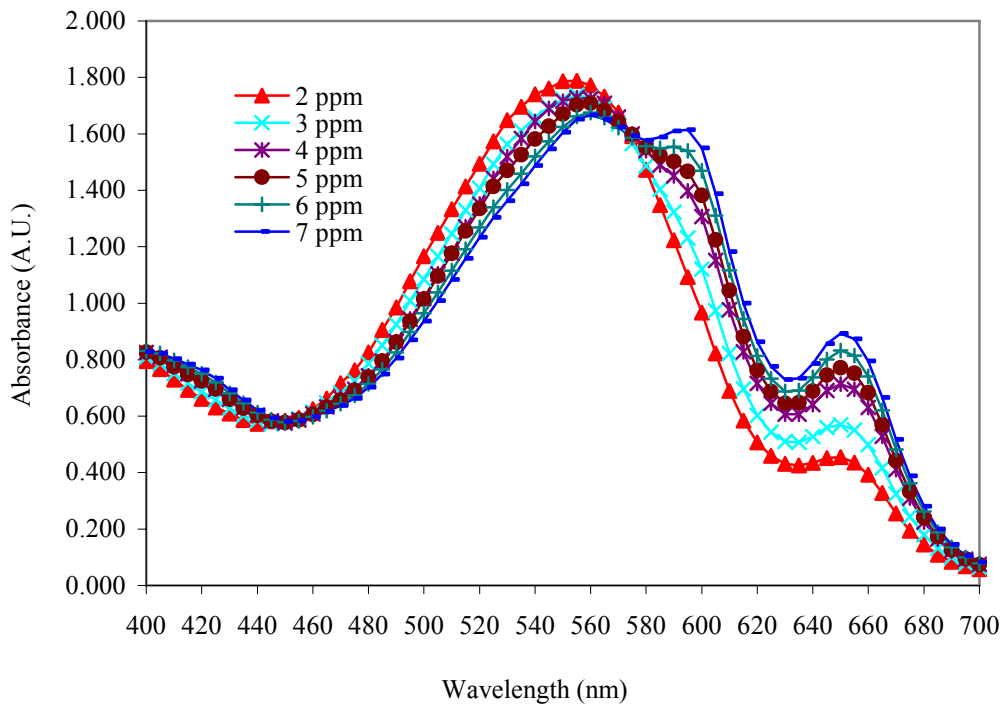


Figure 6.16. Spectra of calcium standard solutions (2-7 ppm)-120 μ M AIII in 100 mM acetate buffer pH 5.4 (150 μ L standard- 150 μ L dye reagent).

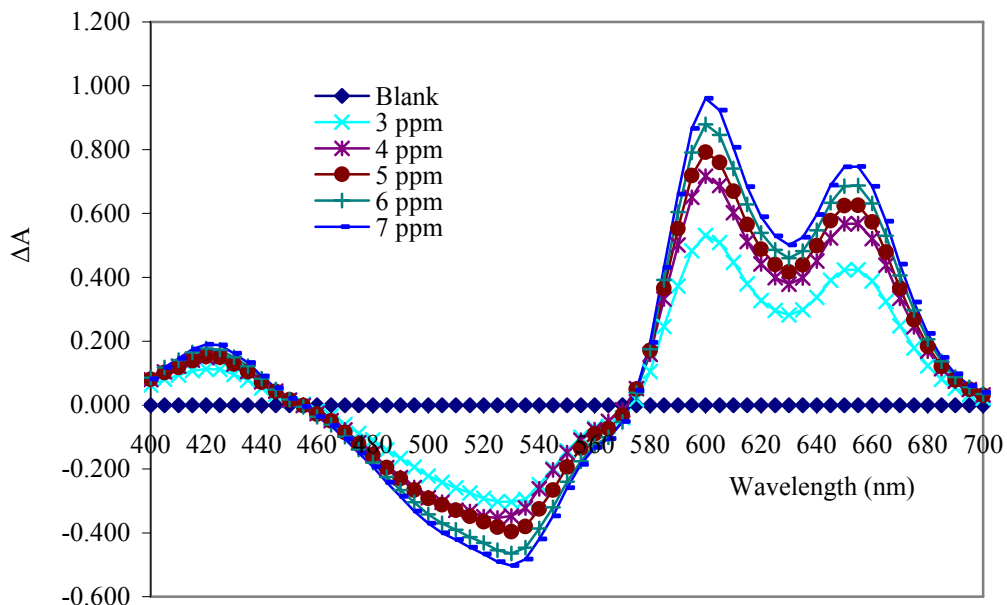


Figure 6.17. Spectra of calcium standard solutions (1-8 ppm) - 120 μ M AIII in 100 mM acetate buffer pH 5.4 (150 μ L standard - 150 μ L dye reagent) obtained by subtracting blank values.

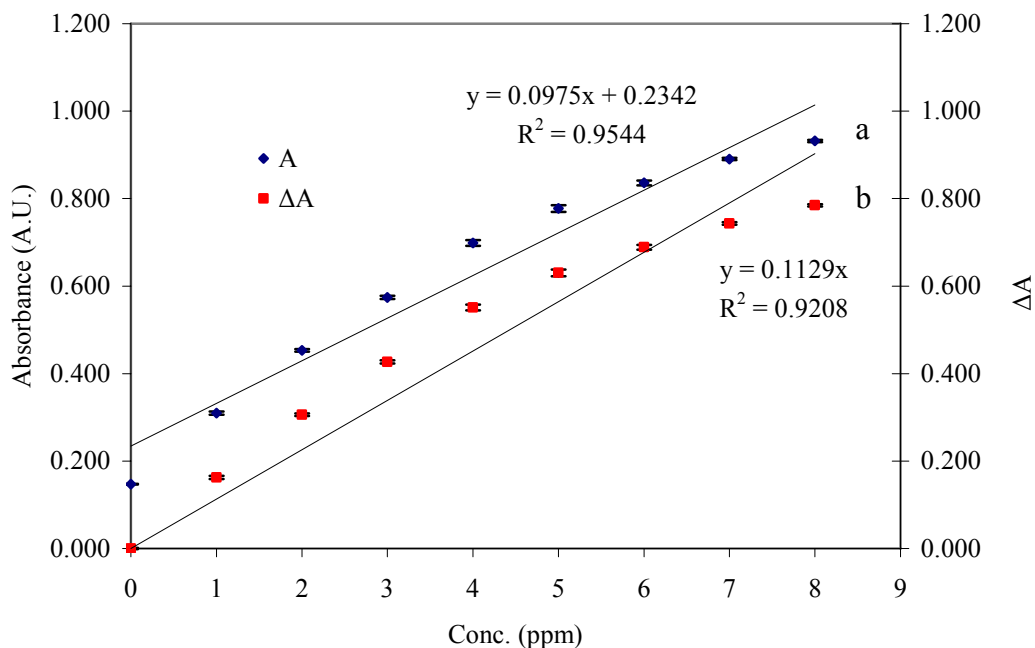


Figure 6.18. Absorbance values of calcium standards (1-7 ppm) - 120 μ M AIII in 100 mM acetate buffer pH 5.4 (150 μ L standard - 150 μ L dye reagent) at 650 nm a. without subtracting blank values, b. with subtracting blank values.

The method based on Arsenazo III in acetate buffer pH 5.5 was developed by Michaylova and Ilkova (1971). Absorbances within the range of calcium concentration of 0.030-1.5 ppm were found to follow Beer's law. They also concluded that calcium could be successfully analyzed in the presence of 100 fold higher concentrations of magnesium and manganese (II) when calcium concentration did not exceed 25 ppm. Unfortunately, it was not possible to analyze calcium below 0.125 ppm (final total concentration of calcium in the dye-standard mixture) with different Arsenazo III in acetate buffer reagents used in this study. Final total concentrations of Arsenazo III in the calcium and dye mixtures used in the study of Michaylova and Ilkova (1971) were 29.2 μM . First of all in this study, 60 μM Arsenazo III in 100 mM acetate buffer reagent was used for 0.25-2 ppm, 1-8 ppm, and 10-80 ppm. Linear calibration response was obtained for only 0.25-2 ppm level. When standard solutions were mixed with dye reagent in 1:1 (v/v) ratio, total concentration of Arsenazo III in the mixture was 30 μM . Total concentration of calcium in the mixture for the lowest calcium standard solution was 0.125 ppm. Reagent was also diluted with 1:1 ratio in order to avoid calcium binding which may arise due to binding of acetate to calcium, only 0.25-2 ppm calcium standard solutions exhibited linear calibration curve in this case. When dye concentration was increased to 120 μM to analyze 1-8 ppm calcium range, it was not possible to obtain linear calibration curve within 1 to 8 ppm calcium level.

6.1.1.2. Arsenazo III in Formate Buffer

Absorbance of Arsenazo III-calcium complex is dependent on the pH (Michaylova and Ilkova, 1971; Bauer, 1981). At pH 3-4 complexation of calcium and Arsenazo III starts and maximum absorption occurs at pH 9.0 (Michaylova and Ilkova, 1971). Complexation of divalent cations with Arsenazo III is suggested to occur by binding of the cation to oxy group of arson group and oxy group of naphthalene nucleus of the dye (Figure 3.2.A) (Alimarin and Savvin, 1966). At pH 9.0, the most of the functional groups on Arsenazo III are ionized (Figure 3.1). Two protonated forms of Arsenazo III, H_3A^{5-} and H_2A^{6-} exist at pH 9 (Němcová and Metal, 1986). Increase in binding affinity for calcium was reported in the order of $\text{H}_4\text{AIII}^{4-}$, $\text{H}_3\text{AIII}^{5-}$ and $\text{H}_2\text{AIII}^{6-}$ (Chiu and Haynes, 1966). When compared to other protonated forms found at lower pH values (H_6A^{2-} , H_5A^{3-} and H_4A^{4-}), these two forms have higher binding affinities for

calcium. Fraction of calcium bound Arsenazo III becomes higher at high pH values. This may explain why maximum absorption of calcium-Arsenazo III complex was observed at pH 9.0. In this study pH of 3.8 was also used besides pH of 5.4. pH of 3.8 was selected according to Arsenazo III calcium analysis protocol in which the reagent was buffered at pH 3.8 with formic acid and potassium hydroxide. This protocol was kindly provided by Dr. G.L. Vogel from National Institute of Standards and Technology, Maryland, USA (personal communication). Therefore Arsenazo III solutions with pH values of 3.8 were tested for different calcium concentration ranges. Formate buffer and potassium hydroxide were used to adjust pH to 3.8.

60 μ M Arsenazo III & Formate Buffer pH 3.8:

Sixty micromolar Arsenazo III in formate buffer were tested for all three calcium ranges. The spectra of 0.25-1.75 ppm standard solutions mixed with 60 μ M Arsenazo III in formate buffer is shown in Figure 6.19. Figure 6.19 shows that dye shows maximum absorption around 535-540 nm. However, absorption maxima of calcium-dye complex found at 650 nm did not appear at this calcium concentration level at pH 3.8. Spectra obtained by using 1-7 ppm calcium standard solutions were therefore used to determine the absorption spectra (Figures 6.20 and 6.21).

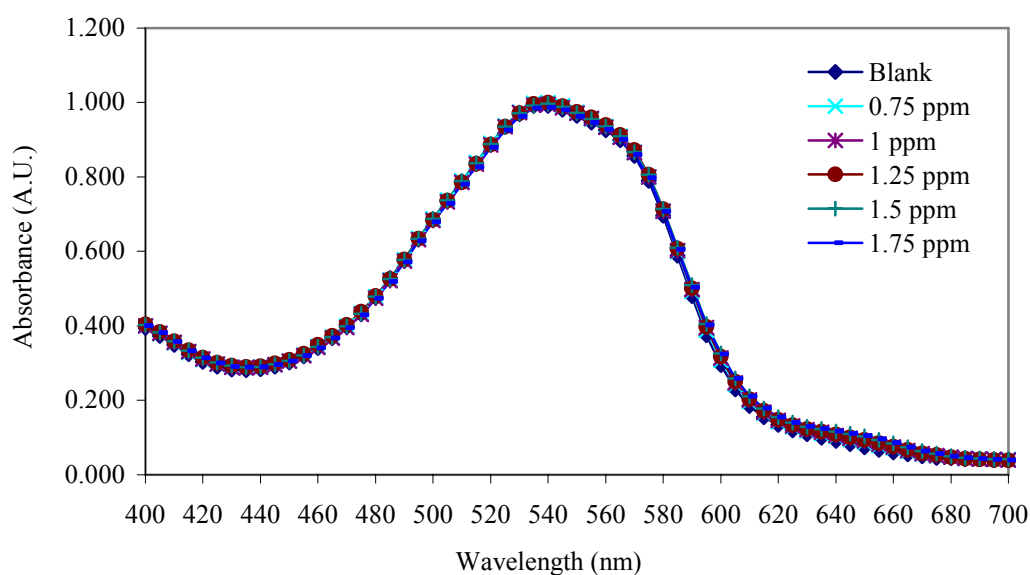


Figure 6.19. Spectra of calcium standard solutions (0.25-1.75 ppm)-60 μ M AIII in formate buffer pH 3.8 (150 μ L standard- 150 μ L dye reagent).

Dye itself has a peak of maxima around 535-540 nm. Calcium-Arsenazo III solution showed a peak around 645-650 nm (Figure 6.20) which was not observed when calcium standards in 0.25 to 2 ppm concentration range were used. In order to determine only the spectra of calcium-dye complex, absorbance values of the spectra of blank solution were subtracted from absorbances of spectra of calcium-dye complex (Figure 6.21). Spectra of calcium-Arsenazo III in formate buffer complex gave two peaks of maxima at 600 nm and 650 nm wavelengths.

Spectra of the calcium-Arsenazo III complexes also determined when higher amount of calcium containing solutions were used. Figure 6.22 shows absorption spectra of calcium-Arsenazo III complex between 400-700 nm. Absorption spectra vs. blank reagent were also graphically plotted in Figure 6.23 by subtracting blank values from absorbance values of the calcium-Arsenazo III complex.

Dye solution exhibited maximum absorption at 540 nm whereas the complex of calcium-Arsenazo III had two maximum absorptions at 595 nm and 650 nm (Figure 6.22). The peak observed at 540 nm was shifted through 560 nm when the calcium-Arsenazo III complexes were formed. Peak at 650 nm was clearly visible when 10 ppm calcium standard were mixed with dye reagent. Peak at 595 nm was however become visible only at higher concentrations.

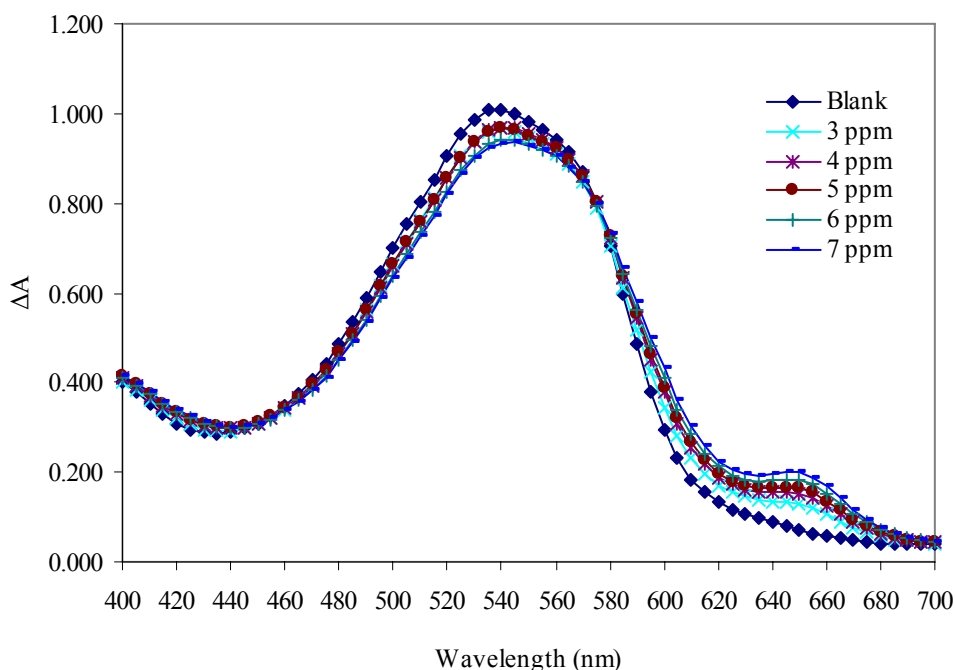


Figure 6.20. Spectra of calcium standard solutions (1-7 ppm)-60 μ M AIII in formate buffer pH 3.8 (150 μ L standard- 150 μ L dye reagent).

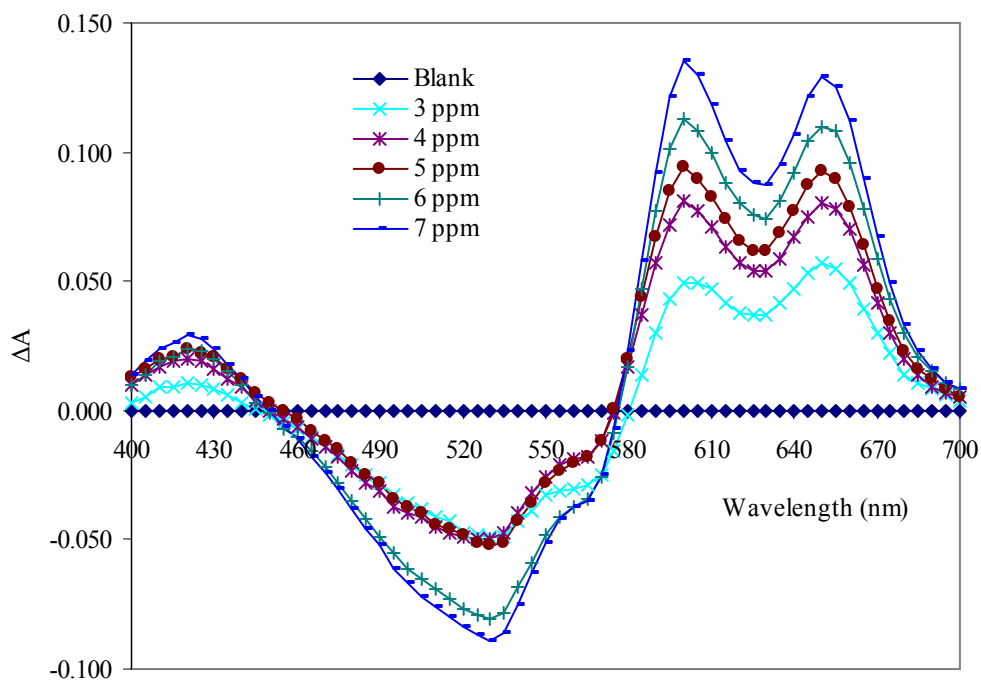


Figure 6.21. Spectra of calcium standard solutions (1-7 ppm) - 60 μM AIII in formate buffer pH 3.8 (150 μL standard- 150 μL dye reagent) obtained by subtracting blank values.

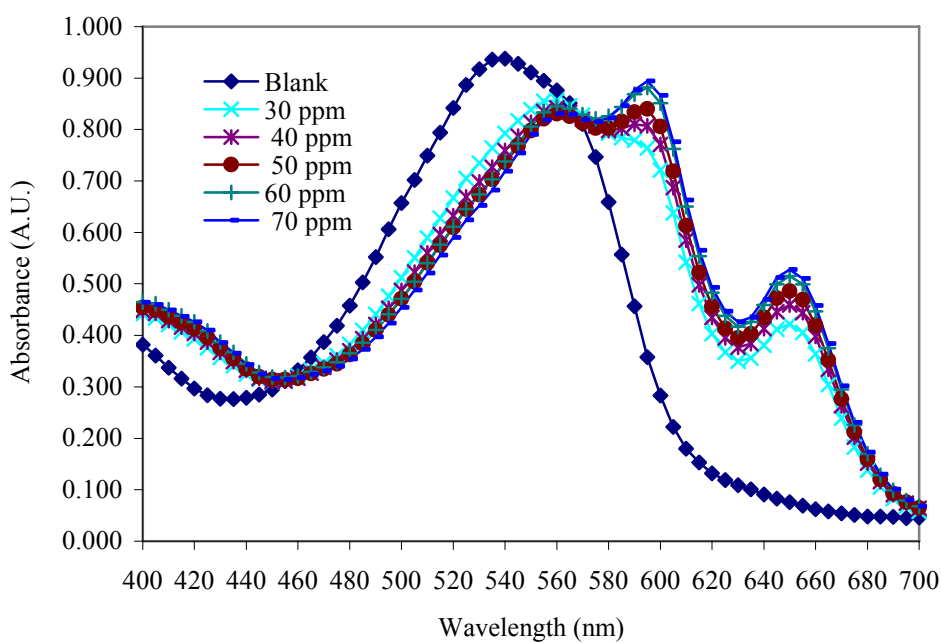


Figure 6.22. Spectra of calcium standard solutions (10-70 ppm)-60 μM AIII in formate buffer pH 3.8 (150 μL standard- 150 μL dye reagent).

Spectra of the complex vs. blank reagent (Figure 6.23) showed that maximum light absorption was observed at both 600 and 650 nm when blank values were subtracted from values of the calcium-Arsenazo III complex.

Calibration curve obtained by reacting 0.25-2 ppm calcium containing standard solution with 60 μM Arsenazo in formate buffer pH 3.8 are shown in Figure 6.24.

Figure 6.24 showed that absorbances of the calcium-Arsenazo III complex were linear for standard solutions containing 0.25-2 ppm calcium. At 650 nm, average absorbance value for the blank was 0.072. Absorbances for 0.25 and 2 ppm were found as 0.077 and 0.112. Correlation coefficient for calibration curve was found to be 0.9907. Although linear relation between the absorbance values of complex and concentrations of standard solutions was obtained, absorbance response was in very narrow range.

When calcium concentration in the standard solutions was increased to 1-8 ppm level, absorbances of the calcium-Arsenazo III complex were found to be linearly correlated with initial calcium concentration in the standard solutions (Figure 6.25). Absorbance values of the calcium-Arsenazo III complexes were in the range of 0.101-0.217 at 650 nm. Correlation coefficient was found as 0.9944.

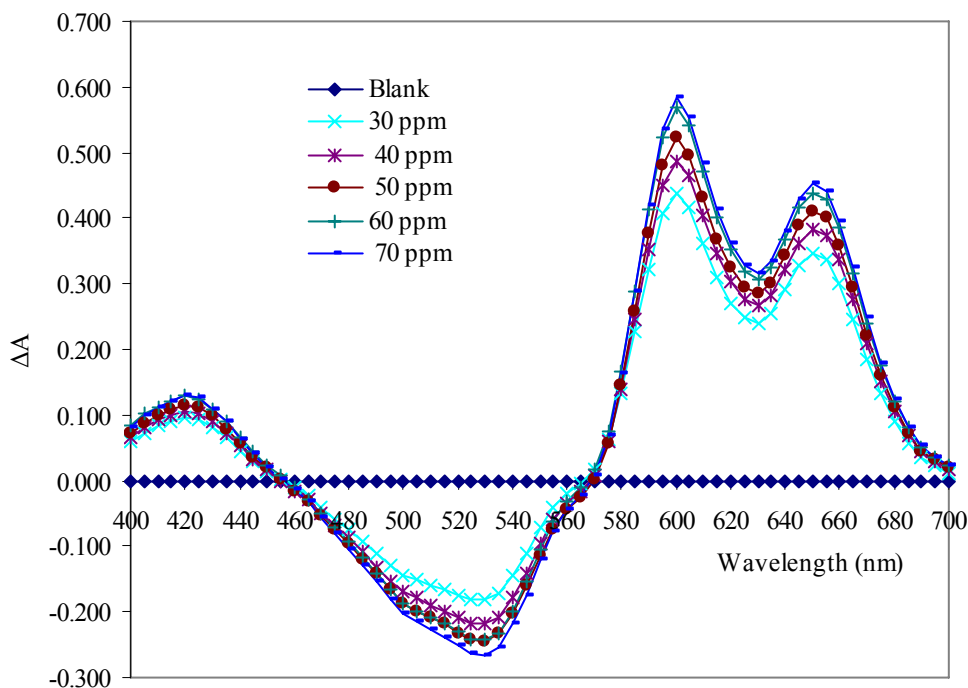


Figure 6.23. Spectra of calcium standard solutions (10-70 ppm) - 60 μM AIII in formate buffer pH 3.8 (150 μL standard- 150 μL dye reagent) obtained by subtracting blank values.

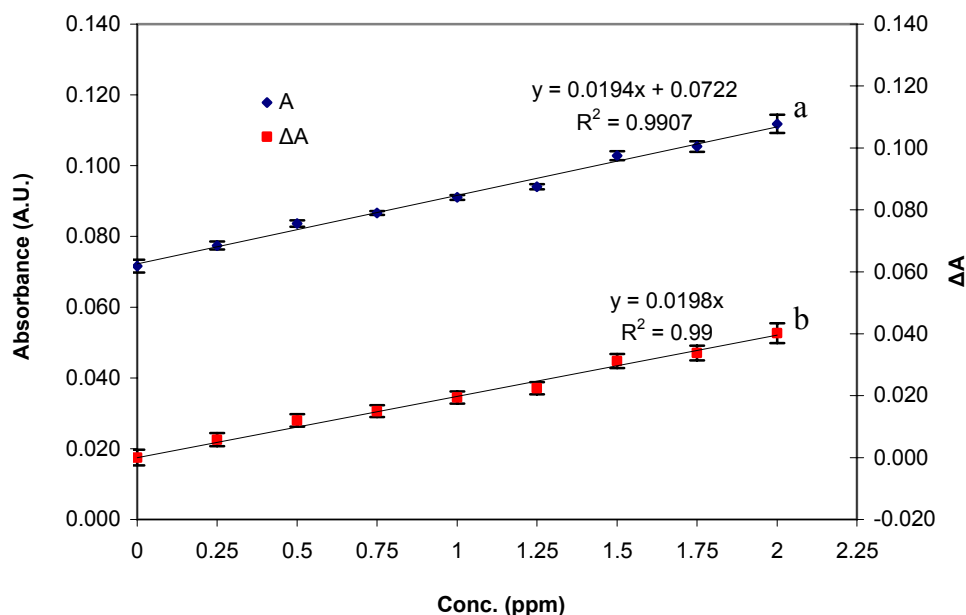


Figure 6.24. Absorbance values of calcium standards (0.25-2 ppm) - 60 μM AIII in formate buffer pH 3.8 (150 μL standard-150 μL dye reagent) at 650 nm a. without subtracting blank values, b. with subtracting blank values.

Calcium standard solutions in 10-80 ppm range did not give linear absorbance responses at 650 nm. Absorbances measured at 650 nm showed that Arsenazo III solution became saturated when higher levels of calcium were mixed with dye solution (Figures 6.26).

In order to determine the relation between absorbance of calcium-Arsenazo III complexes and calcium concentrations in standard solutions, 60 μM Arsenazo III in formate buffer pH 3.8 was diluted with ultrapure water in 1:1 (v/v) ratio and 150 μL standard solution was mixed with 150 μL $\frac{1}{2}$ diluted dye reagent. Figure 6.27 shows the absorbance values obtained at 650 nm. Narrow range of absorbances of the complex (0.062 and 0.078 for 0.25 ppm and 2 ppm, respectively) showed that $\frac{1}{2}$ diluted reagent was not useful for the analysis of calcium.

The methodology for finding the dissociation constant of calcium-Arsenazo III complex used in the Section 6.1.1.1 was employed to find dissociation constant of the complex at pH 3.8. Dye reagent used was 60 μM Arsenazo III in formate buffer pH 3.8. Absorbances measured at 650 nm were used in calculations. Saturation of the Arsenazo III was obtained when 10-80 ppm calcium range was used. Maximum absorbance obtained at the saturation and absorbance of the blank solution was used in the calculations.

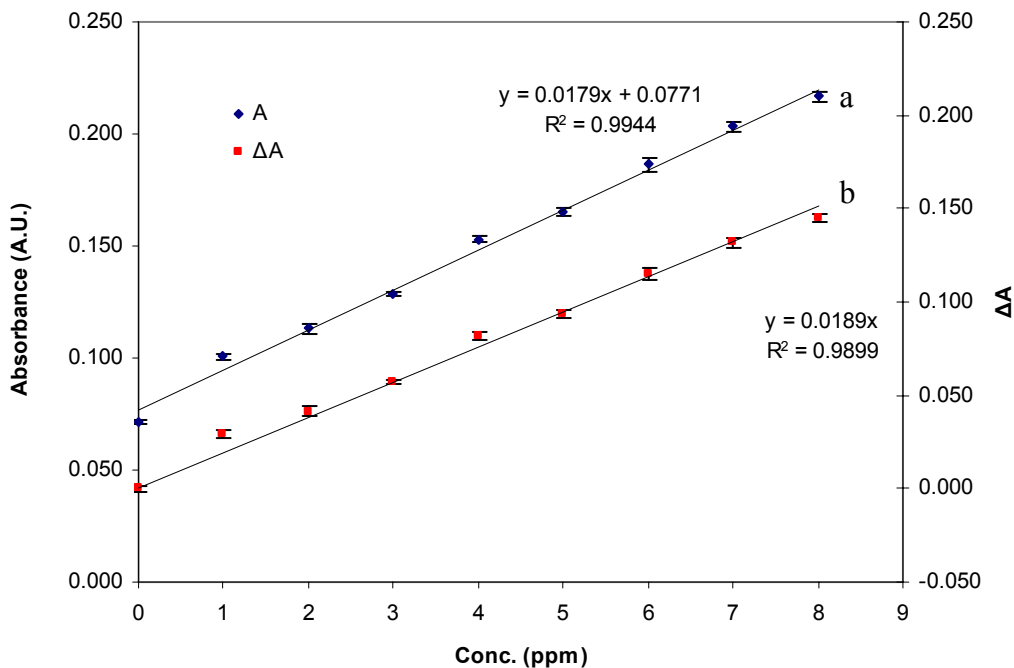


Figure 6.25. Absorbance values of calcium standards (1-8 ppm) - 60 μ M AIII in formate buffer pH 3.8 (150 μ L standard-150 μ L dye reagent) at 650 nm a. without subtracting blank values, b. with subtracting blank values.

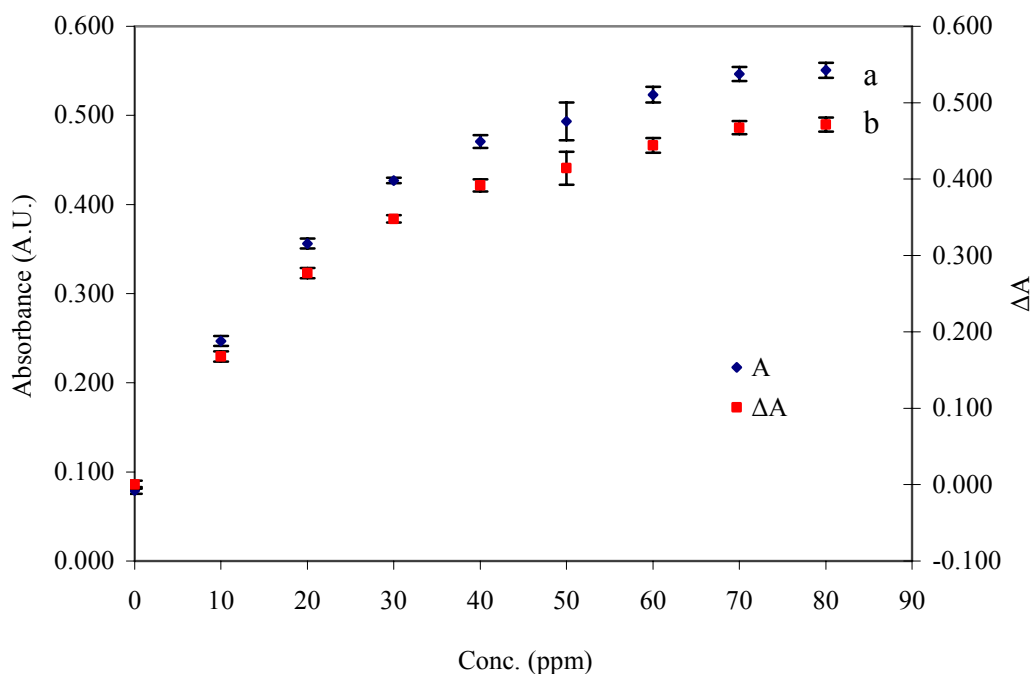


Figure 6.26. Absorbance values of calcium standards (10-80 ppm) - 60 μ M AIII in formate buffer pH 3.8 (150 μ L standard-150 μ L dye reagent) at 650 nm a. without subtracting blank values, b. with subtracting blank values.

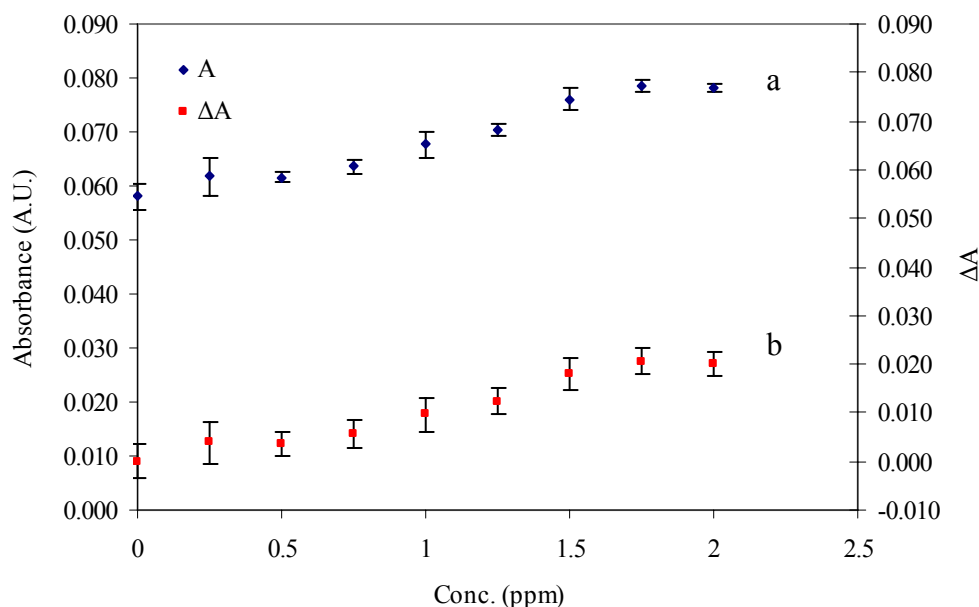


Figure 6.27. Absorbance values of calcium standards (0.25-2 ppm) - $\frac{1}{2}$ (60 μ M AIII in formate buffer pH 3.8) (150 μ L standard-150 μ L dye reagent) at 650 nm a. without subtracting blank values, b. with subtracting blank values.

Plots of $\alpha/(1-\alpha)$ vs. $[Ca]_t - \alpha[Ar]_t$ are shown in Figure 6.28. In both calcium ranges (0.25-2 ppm and 1-8 ppm), linear relationship between $\alpha/(1-\alpha)$ and $[Ca]_t - \alpha[Ar]_t$ was found. The slopes of the linear regression lines were used to calculate apparent dissociation constant of calcium-Arsenazo III complex. Apparent dissociation constant was calculated as 256 μ M when 0.25-2 ppm calcium containing standard solutions were used. Apparent dissociation constant was calculated as 209 μ M in the case of 1-8 ppm calcium concentrations. When compared to those found in pH 5.5, apparent dissociation constant was appreciably higher. Increase of dissociation constant with decrease of pH was reported by Brown and Rydqvist (1981). They found that apparent dissociation constant as 389 μ M for 100 μ M Arsenazo III at pH of 3.0, 4.0, 5.0. However dissociation constant was reported as 137 μ M at pH 6.0. According to species distribution diagram where fraction of protonated species were plotted against pH only H_5A^{3-} and H_4A^{4-} forms of Arsenazo III are found in the solutions at pH 4.0 (Němcova et al., 1986). Concentration of H_5A^{3-} is considerably higher than that of H_4A^{4-} . However when pH is raised to 5.4 fraction of H_4A^{4-} is greater than H_5A^{3-} . Lower dissociation constants found at pH 5.4 states that binding affinity of H_4A^{4-} for calcium is greater than that of H_5A^{3-} .

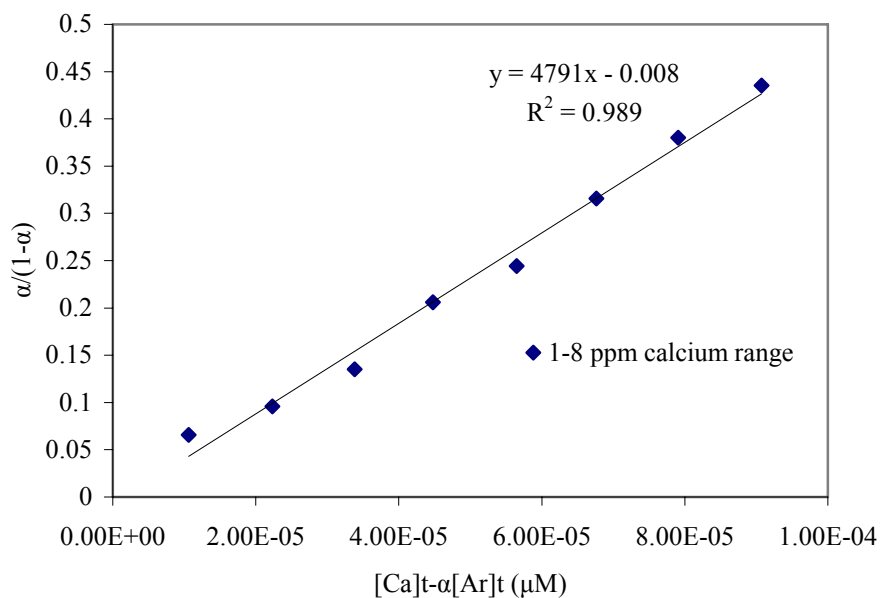
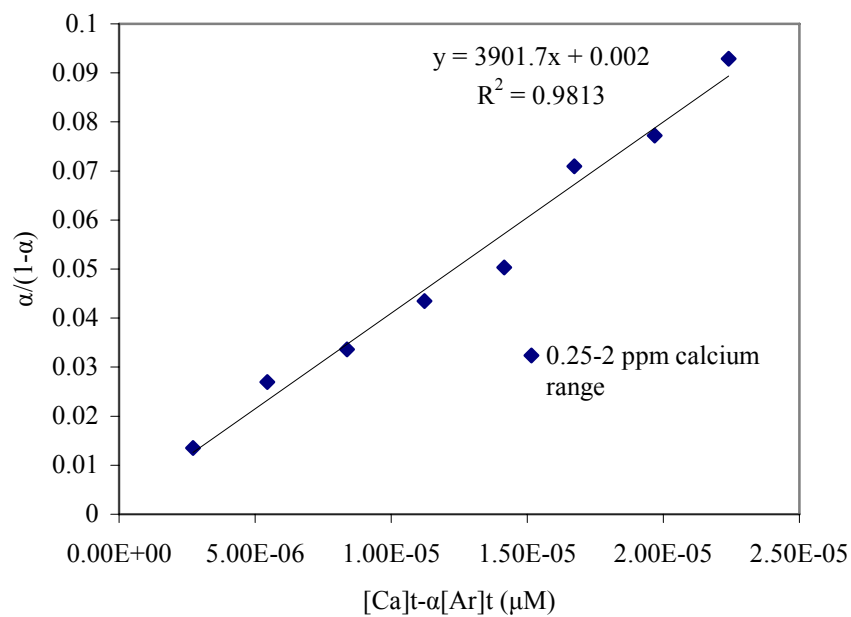


Figure 6.28. Plot of $\alpha/(1-\alpha)$ vs. $[Ca]_t - \alpha[Ar]_t$ Dye reagent: 60 μM Arsenazo III in formate buffer pH 3.8 Calcium concentration of standard reagents :0.25-2 ppm and 1-8 ppm (Reagent to standard volume ratio of 150 $\mu\text{L}/150 \mu\text{L}$).

120 μM Arsenazo III & Formate Buffer pH 3.8:

The use of 60 μM Arsenazo III in formate buffer pH 3.8 showed that dye reagent became saturated with calcium when 10-80 ppm standard solutions were used. For this reason, for the analysis of 10-80 ppm level, Arsenazo III concentration was doubled in the reagent. First of all, spectra of the calcium-Arsenazo III complex were determined (Figure 6.29).

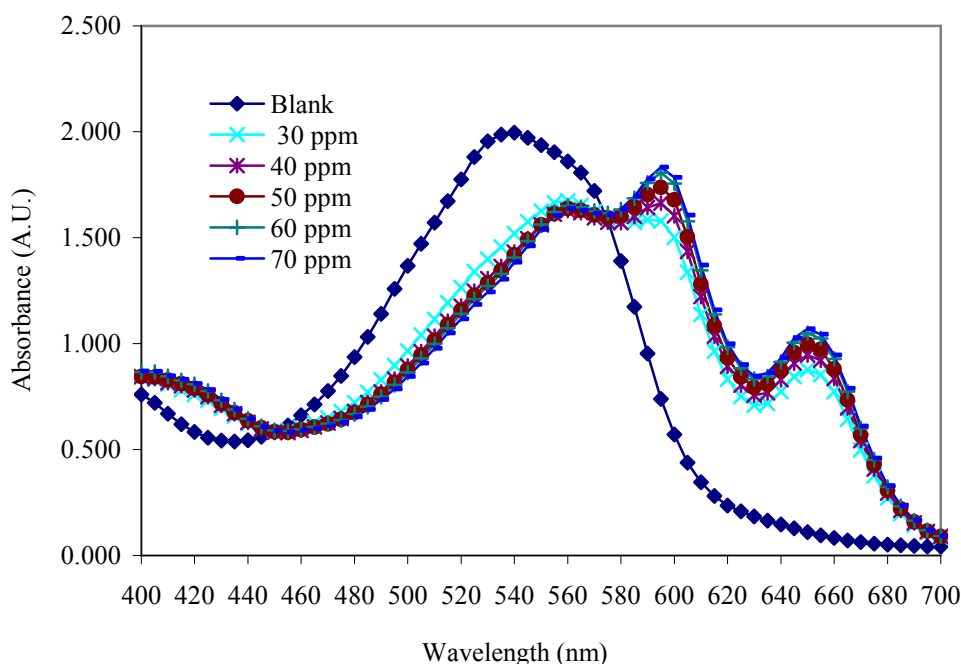


Figure 6.29. Spectra of calcium standard solutions (10-70 ppm) - 120 μM AIII in formate buffer pH 3.8 (150 μL standard- 150 μL dye reagent).

When 120 μM Arsenazo III in formate buffer at pH 3.8 was used. Blank solution exhibited maximum absorption at 540 nm. By increasing the concentration of calcium in the solutions, absorption at 540 nm was reduced and the peak shifted through 560 nm. Peak at 650 nm was clearly visible for the calcium-dye complexes. Another absorption peak at 595 nm became clearly visible at higher calcium concentrations. Spectra of the complexes obtained by subtracting absorbances of the blank showed that calcium-Arsenazo III complex exhibited two absorption maxima at 600 nm and 650 nm like in previous cases (Figure 6.30).

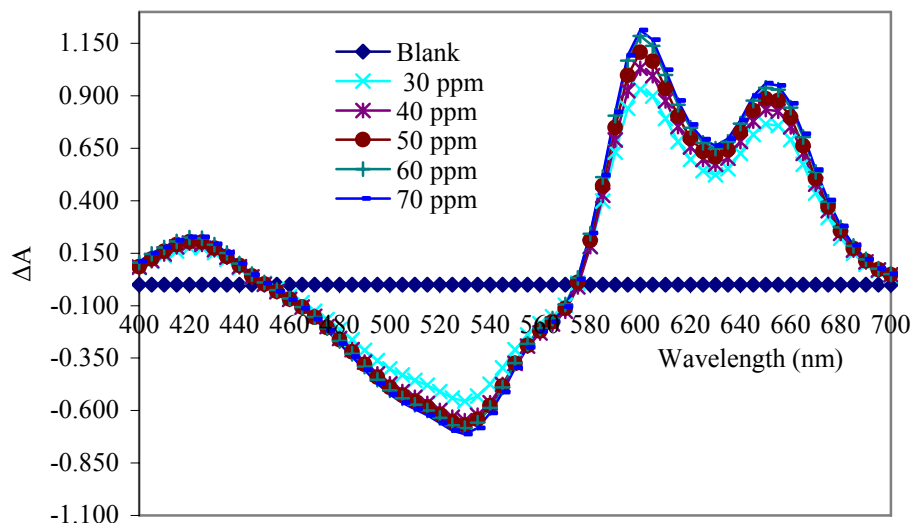


Figure 6.30. Spectra of calcium standard solutions (10-70 ppm) - 120 μM AIII in formate buffer pH 3.8 (150 μL standard- 150 μL dye reagent) obtained by subtracting blank values.

When calcium standard solutions in 10-80 ppm calcium range were combined with 120 μM Arsenazo in formate buffer pH 3.8, it was observed that Arsenazo III solution started to become saturated. Absorbances of the complexes deviate from linearity at or above 30 ppm calcium concentration of standard solutions. This can easily be observed from Figure 6.31.

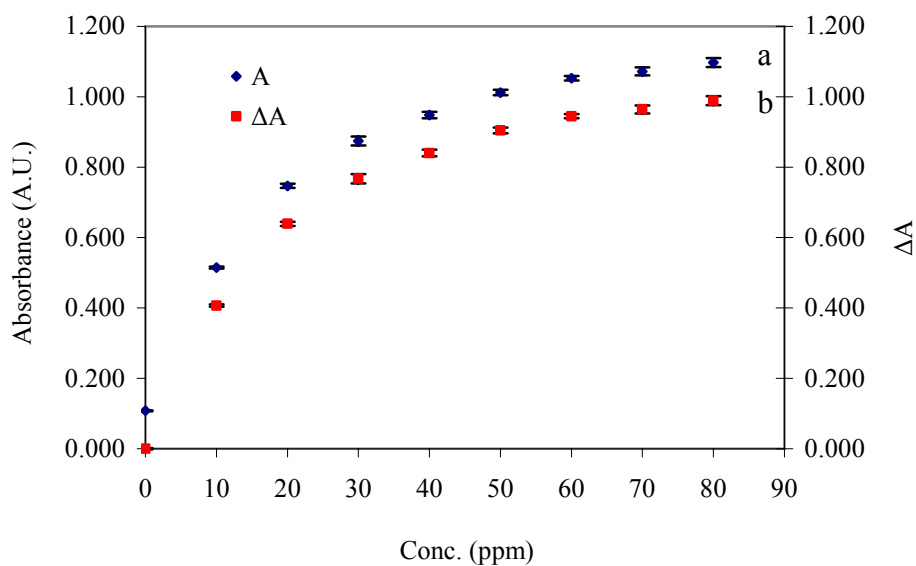


Figure 6.31. Absorbance values of calcium standards (10-80 ppm) - 120 μM AIII in formate buffer pH 3.8 (150 μL standard-150 μL dye reagent) at 650 nm a. without subtracting blank values, b. with subtracting blank values.

Two different Arsenazo III concentrations were used for the three different calcium concentration ranges. Sixty micromolar Arsenazo III solution at pH 3.8 exhibited linear absorbance response for 0.25-2 ppm and 1- 8 ppm calcium containing standard solutions. However, absorbances ranged between 0.077 and 0.112 for 0.25-2 ppm calcium concentration and between 0.101 and 0.217 for 1-8 ppm calcium range at 650 nm. Dye reagent became saturated and relation between absorbance and standard concentration deviated from Beer's law when the calcium concentrations in the standard solutions were in the range of 10 to 80 ppm. When the reagent was used after 1:1 diluted with ultrapure water absorbances almost stayed constant even calcium concentration range was 0.25 to 2 ppm. Increase of the concentration of Arsenazo III to 120 μ M resulted in the saturation of the dye and deviation from Beer's law was observed at 30 ppm calcium concentration. Low absorbances and saturation of the dye at pH 3.8 was possibly the result of the higher apparent dissociation constant of Arsenazo III.

6.1.1.3. Arsenazo III in Imidazole-Cl Buffer

Calcium analysis by Arsenazo III dye depends on the pH used. Two pH values 5.4 and 3.8 were used for the construction of calibration curves to be used in the calcium analysis for three different calcium ranges. Analysis employed at those pH values did not give calibration curves with proper absorbance ranges with respect to calcium concentration in the standard solution. Absorption of the calcium-Arsenazo III complex was found to be dependent on pH and maximum absorption was found at pH 9.0 (Michaylova and Ilkova, 1971). Since the aim of this study was to determine calcium and phosphate release from hydroxyapatite in electrolytes solutions and solubility of hydroxyapatite is very low in neutral and basic solutions, low level calcium analysis method was needed. The selection of pH 9.0 in Arsenazo III method was avoided due to the possibility of calcium phosphate or calcium carbonate precipitation in the samples. Therefore pH of 6.5 was selected for the Arsenazo III method. For this reason several Arsenazo III dye reagents were prepared in imidazole buffer. Two different buffer strengths and different Arsenazo III concentrations were selected. Selection of the buffer and Arsenazo III concentration as imidazole buffer was based on the commercial calcium analysis kits (Table 3.1). Samples and dye reagent are generally

mixed in 1:100 volumetric ratio in these analysis kit. Buffer concentration of 50 to 100 mM and Arsenazo III concentration of 120 to 200 μM are generally used. Since sample and dye are mixed in 1:100 ratio, buffer and Arsenazo III concentrations are not affected by the dilution due to the mixing of dye reagent and sample. Because the absorbance of calcium-Arsenazo III complex depends on the pH strong buffering is needed. For these reasons 100 mM and 200 mM imidazol concentrations were selected.

Reagent solutions containing Arsenazo III with concentrations of 60, 200, and 500 μM were used to obtain linear calibration curves for 0.25-2, 1-8 and 10-80 ppm calcium containing solutions in this study. When the dye reagents were mixed with standard solutions in 1:1 volumetric ratio total Arsenazo III concentrations in the mixtures was the half of the dye concentration in the reagents. Arsenazo III concentration of 30 μM was used by Michaylova and Ilkova (1971). Dye concentration of 60 μM was selected on the basis of the study of Michaylova and Ilkova (1971) whereas selection of the dye concentration of 200 μM was based on commercial kits (Table 3.1). Arsenazo III concentration of 500 μM was however used depending on the results obtained with the dye reagents having 60 μM and 200 μM Arsenazo III.

60 μM Arsenazo III & 100 mM Imidazole-Cl pH 6.5:

Sixty micromolars Arsenazo III in imidazole-Cl pH 6.5 was used for the analysis of 0.25-2 ppm, 1-8 ppm and 10-80 ppm calcium concentration ranges. Figure 6.32 shows the absorption spectra of calcium-Arsenazo III complexes obtained by reacting 60 μM Arsenazo III & 100 mM Imidazole-Cl pH 6.5 with 0.25-1.75 ppm containing standard solutions.

Blank reagent exhibited maximum absorption at 545 nm. This peak shifted to 555 nm when the calcium concentration in standard solution was increased to 1.75 ppm. Complex had a maximum absorption at 650 nm. This peak was visible only for higher calcium concentrations. When the values of blank reagent were subtracted from the values of the calcium-dye complexes, two peaks were observed at around 600 nm and 650-655 nm (Figure 6.33).

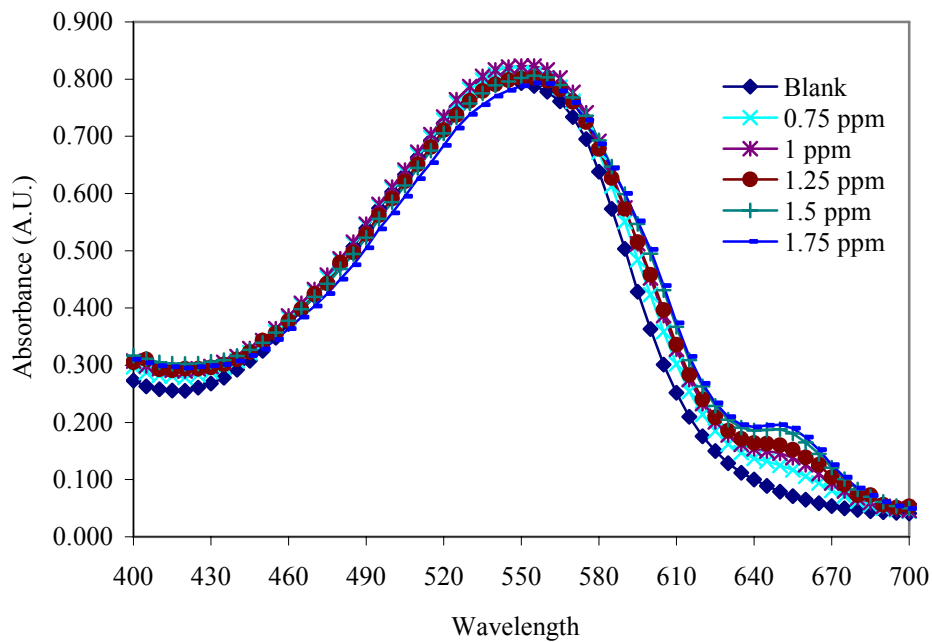


Figure 6.32. Spectra of calcium standard solutions (0.25-1.75 ppm)-60 μ M AIII in 100 mM imidazole-Cl pH 6.5 (150 μ L standard- 150 μ L dye reagent).

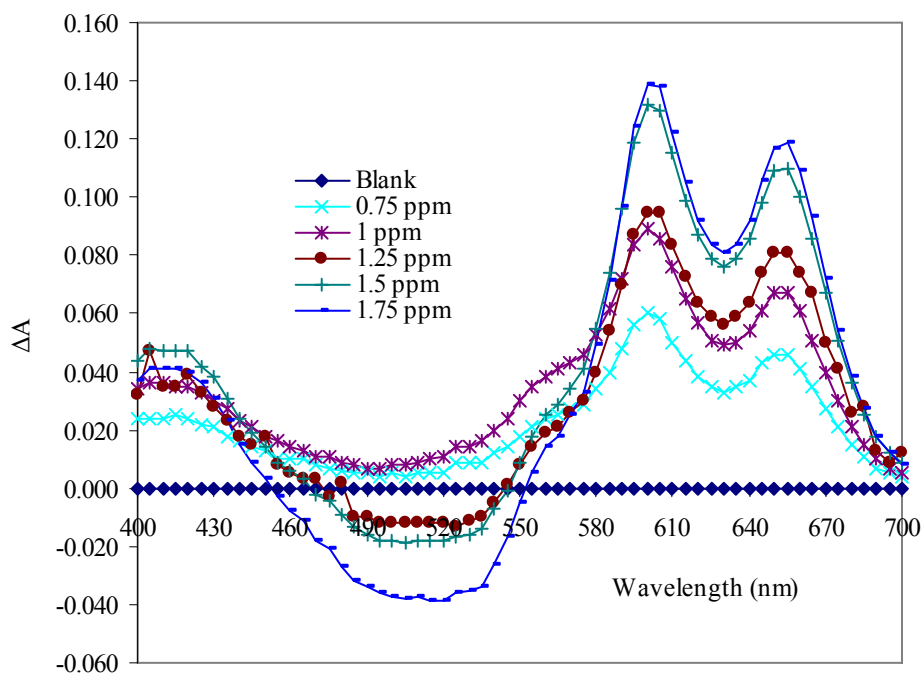


Figure 6.33. Spectra of calcium standard solutions (0.25-1.75 ppm)-60 μ M AIII in 100 mM imidazole-Cl pH 6.5 (150 μ L standard- 150 μ L dye reagent) obtained by subtracting blank values.

Peaks with maximum absorptions could easily be observed in the spectra of calcium-Arsenazo III complexes when calcium concentrations in the standard solutions were in the range of 10-70 ppm. Figure 6.34 shows the absorption spectra of the complexes. Dye itself gave a maximum absorption at 545 nm. Complexes of calcium and Arsenazo III solutions exhibited two absorption peaks at 600 nm and 655 nm. Additionally spectra of the complexes were constructed by subtracting the values of blank solution from the values of calcium-Arsenazo III complexes and this is shown in Figure 6.35.

Figure 6.35 showed that the calcium-Arsenazo III complexes exhibited two absorption maxima when the blank values were subtracted from the absorbances of complexes. A peak with higher intensity can easily be observed at 600 nm. Another peak at 655 nm was also observed.

For the calcium range of 0.25-2 ppm, linear calibration range was obtained by using 60 μ M AIII in 100 mM imidazole-Cl pH 6.5 dye solution. At 650 nm (Figure 6.36), blank solution had an absorbance value of 0.079, whereas absorbances of the calcium-Arsenazo III complex varied between 0.093-0.215 for 0.25-2 ppm calcium standard solutions. Regression coefficient of linear calibration curve was found as 0.9953.

When the calcium concentrations in the standard solutions were between 1 and 8 ppm, non-linear relation between absorbance values and calcium concentrations of standard solutions were obtained (Figure 6.37). In fact calibration curve was linear up to 4 ppm standard solution concentration; however solution starts to become saturated over 4 ppm.

Saturation of 60 μ M Arsenazo III in 100 mM imidazole-Cl pH 6.5 could be well observed when standard solutions were in 10-80 ppm calcium level. Solution was fully saturated when the standard solution with a concentration greater than 40 ppm was used (Figures 6.38).

Dye solution was also diluted with ultrapure water in 1:1 volumetric ratio for the analysis of calcium standard solutions. Diluted reagent was mixed with calcium standard solutions. Linear relation between the absorbances of calcium complexes and standard calcium concentration was obtained (Figure 6.39). Absorbance values found and regression coefficients for calibration curves were lower than those found by using 60 μ M Arsenazo III in imidazole buffer.

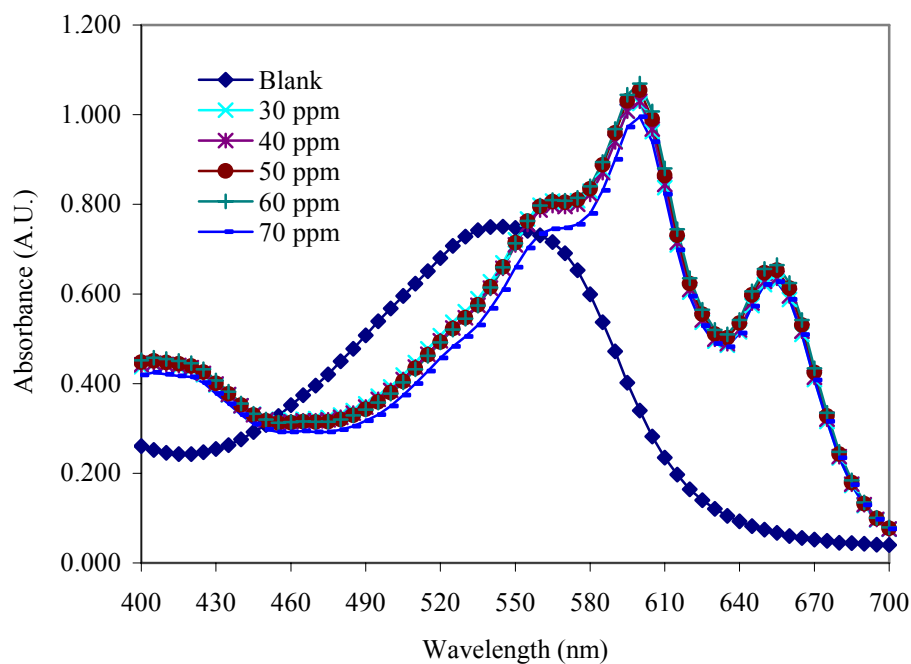


Figure 6.34. Spectra of calcium standard solutions (10-70 ppm)-60 μ M AIII in 100 mM imidazole-Cl pH 6.5 (150 μ L standard- 150 μ L dye reagent).

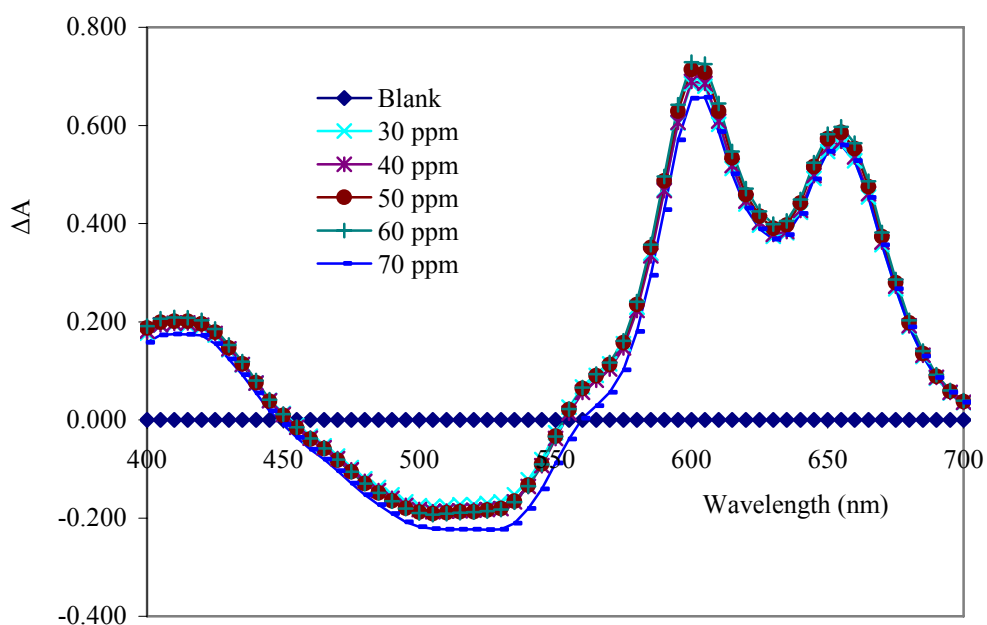


Figure 6.35. Spectra of calcium standard solutions (10-70 ppm)-60 μ M AIII in 100 mM imidazole-Cl pH 6.5 (150 μ L standard- 150 μ L dye reagent) obtained by subtracting blank values.

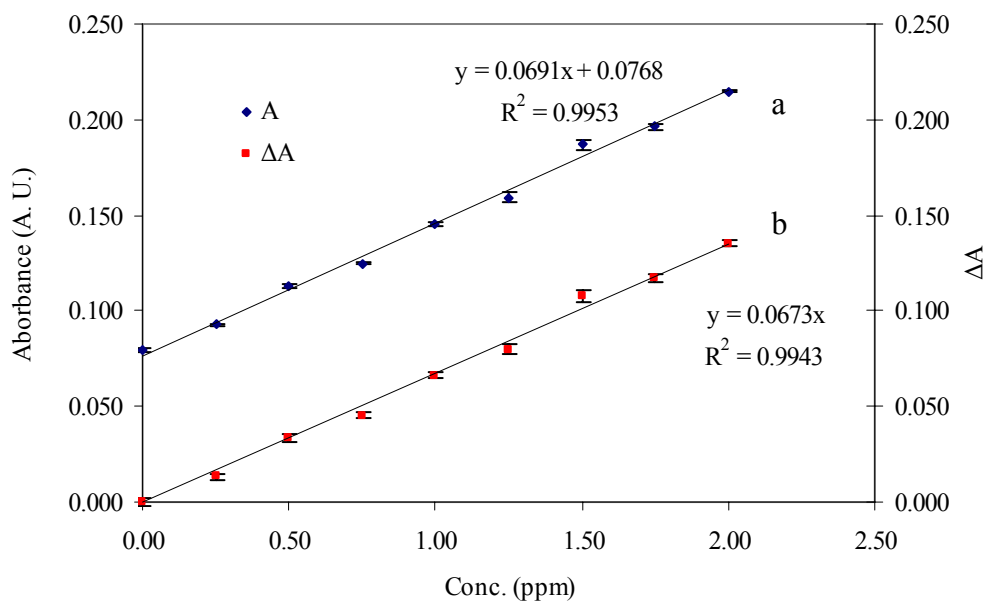


Figure 6.36. Absorbance values of calcium standards (0.25-2 ppm) - 60 μ M AIII in 100 mM Imidazole-Cl buffer pH 6.5 (150 μ L standard-150 μ L dye reagent) at 650 nm a. without subtracting blank values, b. with subtracting blank values.

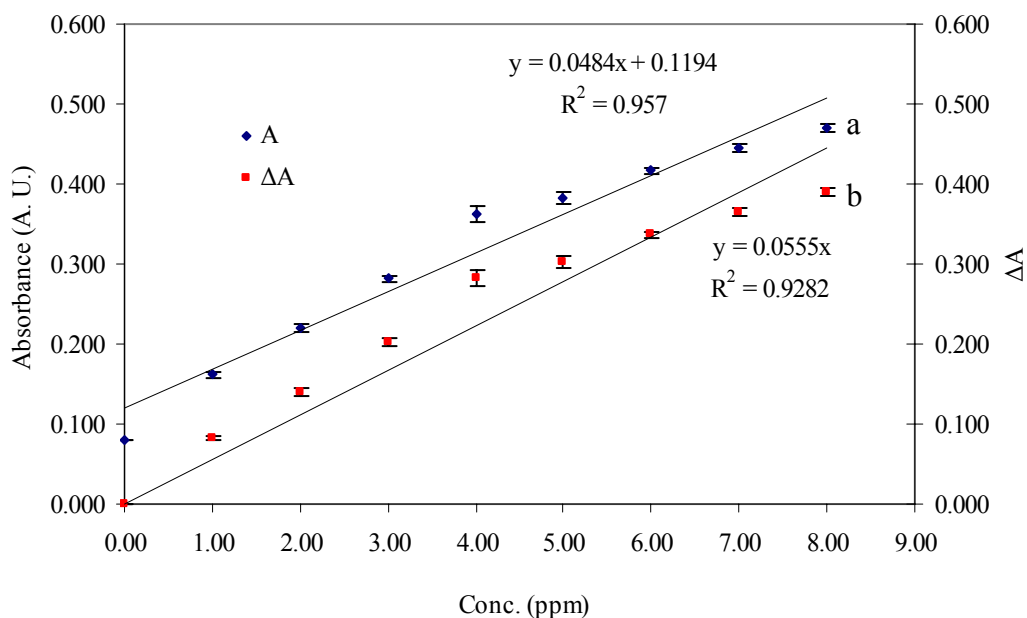


Figure 6.37. Absorbance values of calcium standards (1-8 ppm) - 60 μ M AIII in 100 mM Imidazole-Cl buffer pH 6.5 (150 μ L standard-150 μ L dye reagent) at 650 nm a. without subtracting blank values, b. with subtracting blank values.

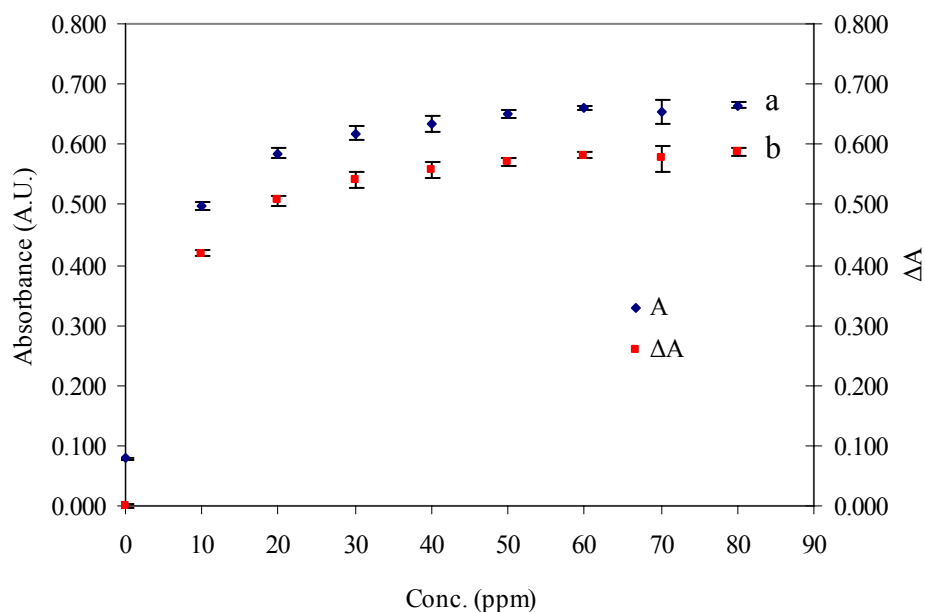


Figure 6.38. Absorbance values of calcium standards (10-80 ppm) - 60 μ M AIII in 100 mM Imidazole-Cl buffer pH 6.5 (150 μ L standard-150 μ L dye reagent) at 650 nm a. without subtracting blank values, b. with subtracting blank values.

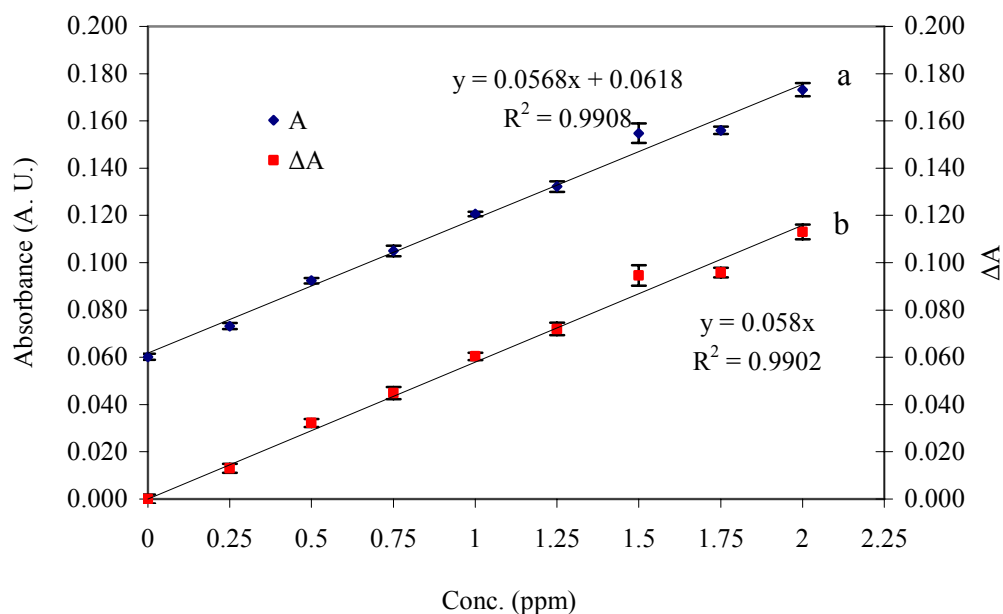


Figure 6.39. Absorbance values of calcium standards (0.25-2 ppm) - $\frac{1}{2}$ (60 μ M AIII in 100 mM Imidazole-Cl buffer pH 6.5) (150 μ L standard-150 μ L dye reagent) at 650 nm a. without subtracting blank values, b. with subtracting blank values.

Since almost a linear response was found using 60 μM Arsenazo III in imidazole buffer when calcium concentration in the standard solutions were between 1 and 8 ppm, $\frac{1}{2}$ diluted dye reagent was also tested for 1-8 ppm level. Figure 6.40 shows the relation between absorbance values measured at 650 nm and calcium concentrations in standard solutions. Solution starts to become saturated over 4 ppm standard calcium concentration.

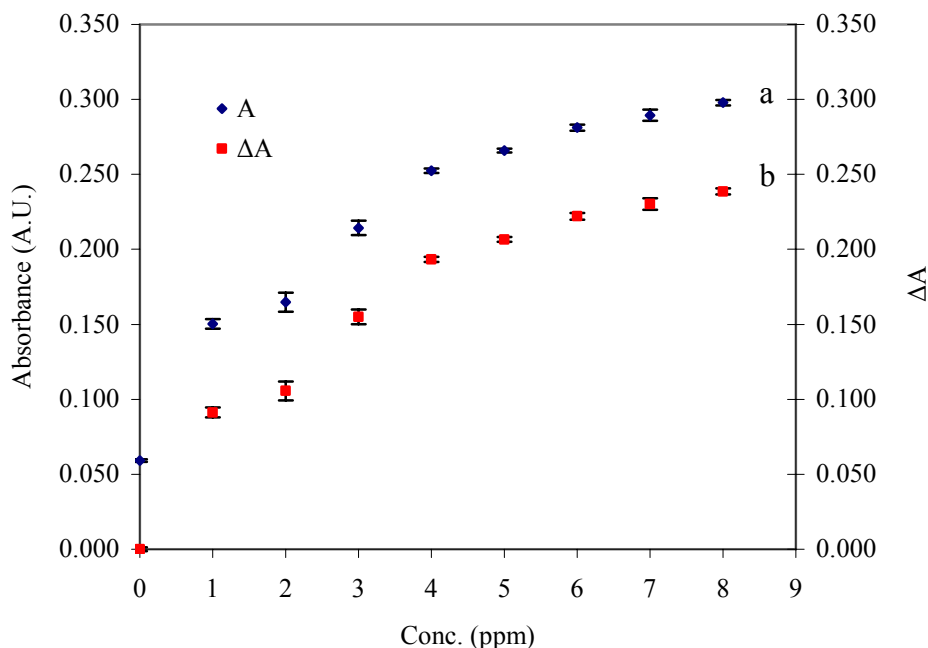


Figure 6.40. Absorbance values of calcium standards (1-8 ppm) - $\frac{1}{2}$ (60 μM AIII in 100 mM Imidazole-Cl buffer pH 6.5) (150 μL standard-150 μL dye reagent) at 650 nm a. without subtracting blank values, b. with subtracting blank values.

Dissociation constant of calcium-Arsenazo III complex at the pH 6.5 was calculated by using absorbance data obtained at 650 nm using 60 μM Arsenazo III & 100 mM Imidazole-Cl pH 6.5 reagent and 0.25-2, 1-8, 10-80 ppm calcium containing standard solutions. Figure 6.41 shows $\alpha/(1-\alpha)$ values plotted vs. $[\text{Ca}]_t - \alpha[\text{Ar}]_t$ calculated for 60 μM Arsenazo III & 100 mM Imidazole-Cl pH 6.5 reagent and 0.25-1 and 1-8 ppm calcium containing standard solutions. For both calcium concentration ranges, $\alpha/(1-\alpha)$ values were found to be linearly correlated to $[\text{Ca}]_t - \alpha[\text{Ar}]_t$ values. Dissociation constant calculated from the slopes were 55.1 and 37.5 μM for 0.25-2 and 1-8 ppm standard calcium concentrations, respectively. Negative logarithms of dissociation

constants were also calculated and found as 4.26 and 4.43 when calcium concentration range of standard solutions were 0.25-1 ppm and 1-8 ppm, respectively.

Apparent binding constant of Arsenazo III for calcium was reported as $(4.12 \pm 0.77) \times 10^4 \text{ M}^{-1}$ at pH 6.5 (Chiu and Haynes, 1980). Apparent dissociation constant can be converted into apparent binding constant by the following equation:

$$K_D = \frac{1}{K_{app}} \quad (6.31)$$

Apparent binding constant reported by Chiu and Haynes (1980) was converted into apparent dissociation constant and found as 24.3 μM . The dissociation constant found by using apparent binding constant of Arsenazo III was lower than that found in this study.

Since absorbance of calcium-Arsenazo III complex is highly dependent on pH (Michaylova and Ilkova, 1971), buffer strength is important in Arsenazo III calcium assay. After mixing the dye reagent and calcium standard solutions, complex should have the same pH value. This can be achieved by adjusting the buffer strength. For the calcium analysis of the samples, sample pH is also important. When the low levels of calcium will be determined in highly acidic or alkaline solutions, care should be taken because of the pH dependence of absorbance of calcium-Arsenazo III complex. For these reasons, dye reagents containing 200 mM imidazole were then used for the calcium determination.

60 μM Arsenazo III & 200 mM Imidazole-Cl pH 6.5:

Sixty micromolar Arsenazo III in 200 mM imidazole-Cl buffer was used for all three ranges of calcium concentrations. First of all, spectra of the complexes were determined. Spectra of standard solutions with calcium concentration range of 0.25-1.75 ppm are shown in Figure 6.42. According to Figure 6.42, dye itself showed an absorption peak at 540 nm, this peak shifts to 550 nm when calcium concentration in standard is 1.75 ppm. The peak of the complex begins to appear at around 650 nm. Spectra of standard solutions with calcium concentration range of 1-7 ppm also shown in Figure 6.43.

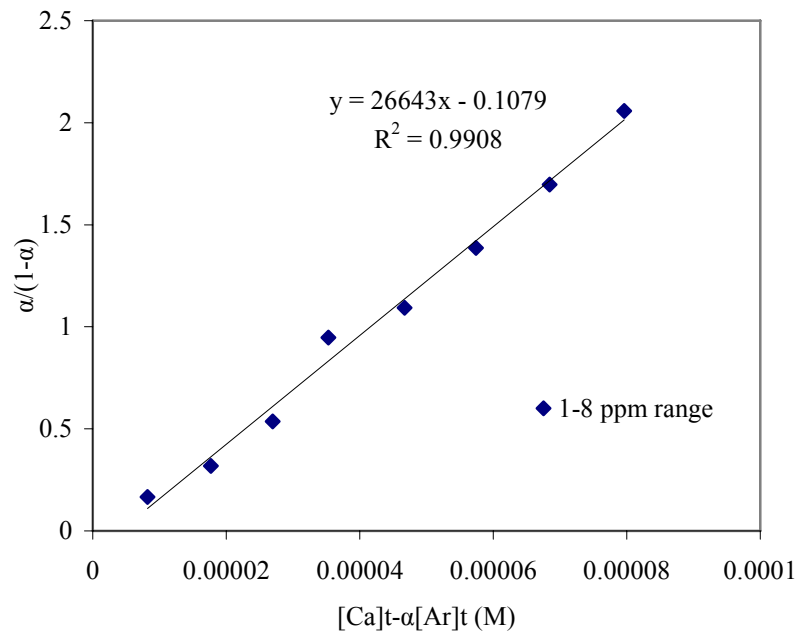
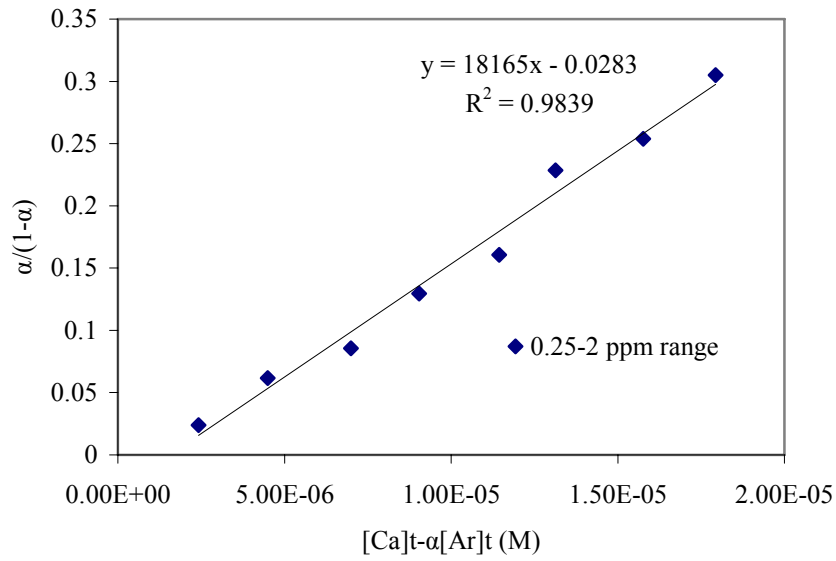


Figure 6.41. Plot of $\alpha/(1-\alpha)$ vs. $[Ca]_t - \alpha[Ar]_t$ Dye reagent: 60 μM Arsenazo III in 100 mM imidazole-Cl pH 6.5 Calcium concentration of standard solutions: 0.25-2 ppm and 1-8 ppm (Reagent to standard volume ratio of 150 $\mu\text{L}/150 \mu\text{L}$).

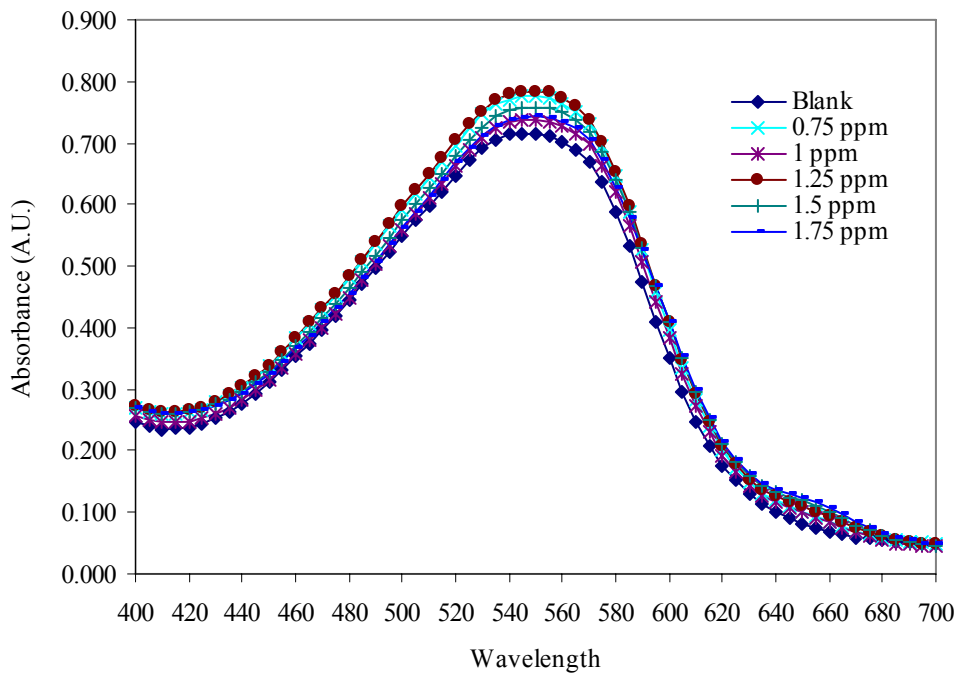


Figure 6.42. Spectra of calcium standard solutions (0.25-1.75 ppm)-60 μ M AIII in 200 mM imidazole-Cl pH 6.5 (150 μ L standard- 150 μ L dye reagent).

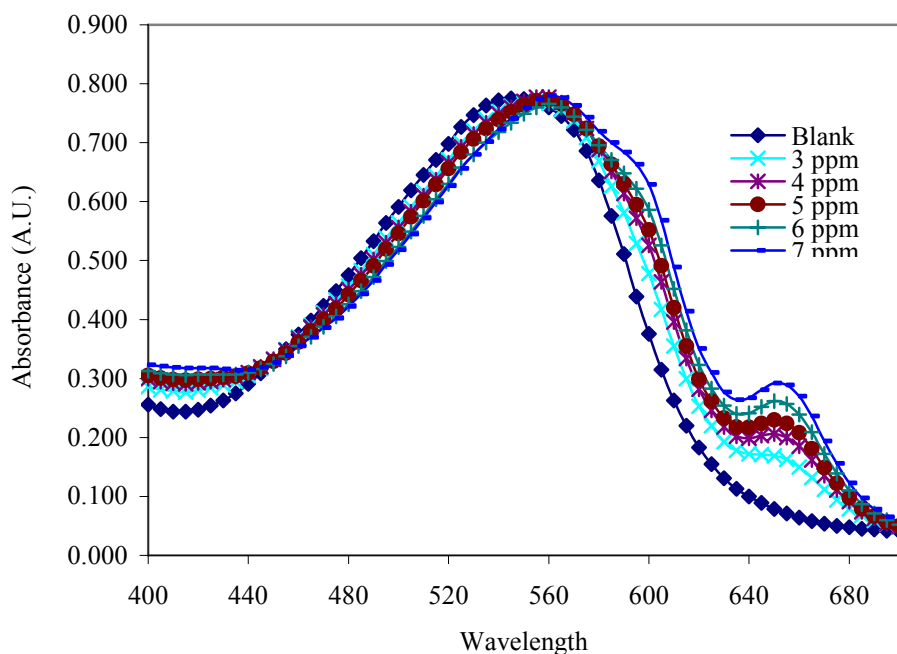


Figure 6.43. Spectra of calcium standard solutions (1-7 ppm)-60 μ M AIII in 200 mM imidazole-Cl pH 6.5 (150 μ L standard- 150 μ L dye reagent).

The nature of the spectra of calcium-Arsenazo III complexes obtained by mixing calcium standard solutions with Arsenazo III in 200 mM imidazole buffer can easily be observed when the calcium content of the standard solutions are increased to 1-7 ppm. Figure 6.43 shows the spectra of the complexes.

Figure 6.43 shows that the maximum absorption of the dye solution was observed at 540 nm. This wavelength shifts to 560 nm by increasing the concentrations of the standard solutions. Appearance of the peak of the calcium-Arsenazo III complex at 650 nm could be observed clearly when calcium concentration in the standard solutions was over 3 ppm.

When the spectra of the calcium-Arsenazo III complexes were graphically illustrated by subtraction of absorbance values of blank from the values of the complexes, two peaks, one is around 600-605 and the other is at 655 nm were observed (Figure 6.44).

The effects of the use of standard solutions with high calcium concentrations on the light absorption spectra were determined by using 10-70 ppm calcium containing standard solutions. Figure 6.45 shows that the dye solution absorbs the light at 540 nm and the complex formation gives two peaks at 600 nm and 655 nm. Distinctive shift in the absorption maximum of the blank solution was clearly observed upon complexation with calcium. The band found at 540 nm shifts through 565 nm after calcium-Arsenazo III complex formation. When the spectra of the complexes were constructed by subtraction of absorbance values of blank solutions from the absorbances of the complexes (Figure 6.46), 605 nm and 655 nm were found to be two peaks that the maximum light absorption occurs.

The use of 60 μ M Arsenazo III in 200 mM imidazole buffer pH 6.5 gave a linear calibration curve for 0.25-2 ppm calcium containing solutions when absorbances were measured at 650 nm (Figure 6.47). Average absorbance value for the blank solutions was found as 0.079. Absorbances changed between 0.084 and 0.132 for 0.25 and 2 ppm calcium concentrations, respectively. Calibration equation, $y=0.0268x+0.0768$, was obtained with a correlation coefficient of 0.9921. When ΔA values were used to construct a calibration curve, calibration equation of $y=0.0252x$ was found. In this case correlation coefficient was 0.9874.

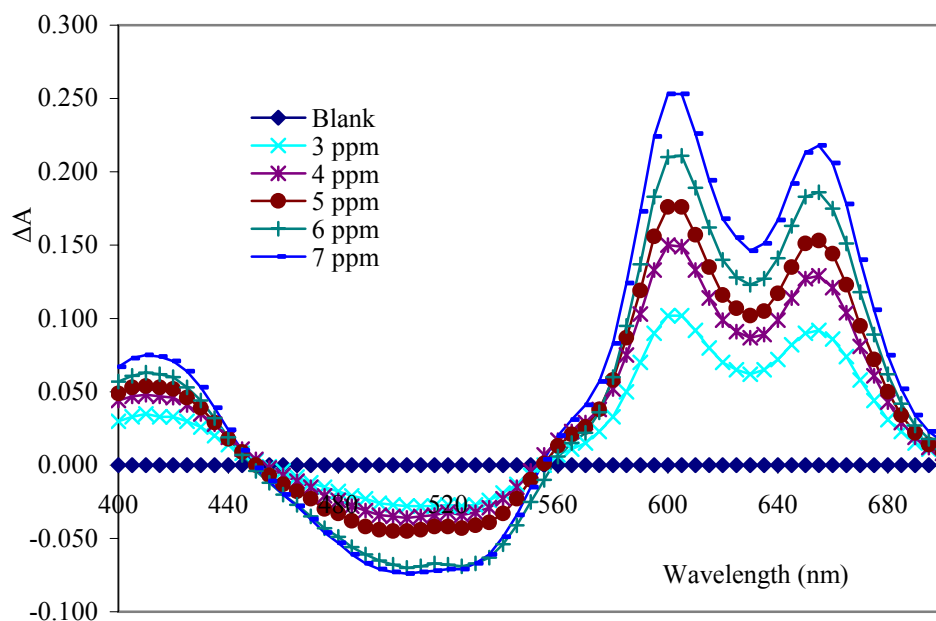


Figure 6.44. Spectra of calcium standard solutions (1-7 ppm) - 60 μ M AIII in 200 mM imidazole-Cl pH 6.5 (150 μ L standard- 150 μ L dye reagent) obtained by subtracting blank values.

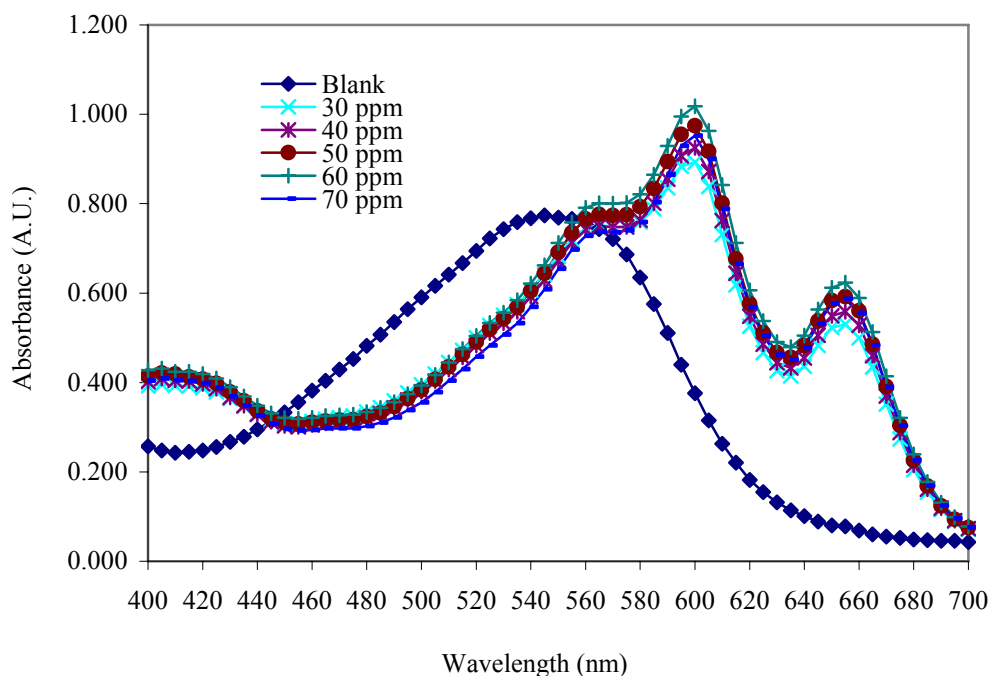


Figure 6.45. Spectra of calcium standard solutions (10-70 ppm) - 60 μ M AIII in 200 mM imidazole-Cl pH 6.5 (150 μ L standard- 150 μ L dye reagent).

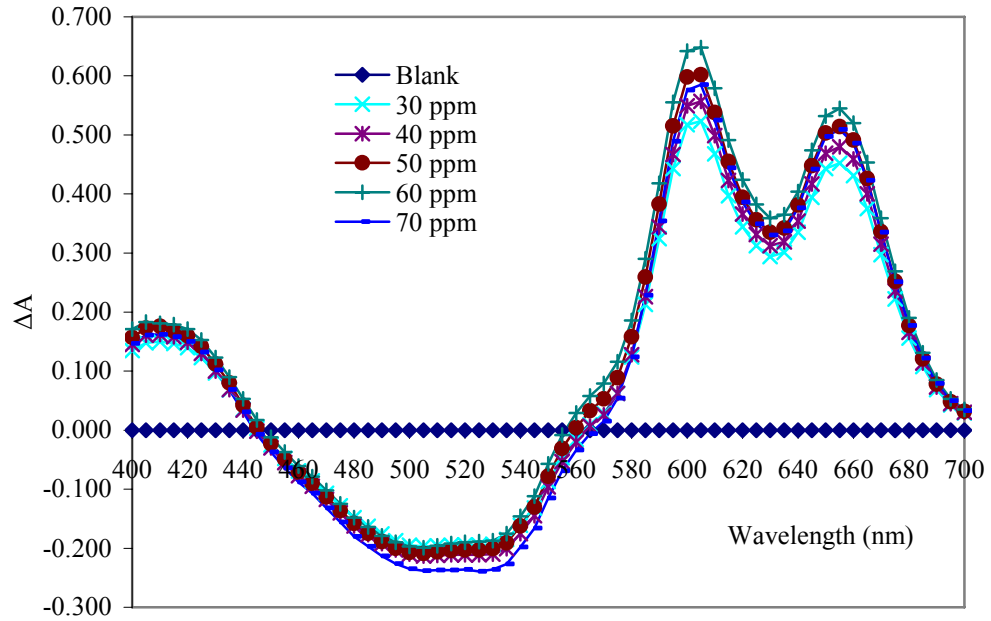


Figure 6.46. Spectra of calcium standard solutions (10-70 ppm) – 60 μ M AIII in 200 mM imidazole-Cl pH 6.5 (150 μ L standard- 150 μ L dye reagent) obtained by subtracting blank values.

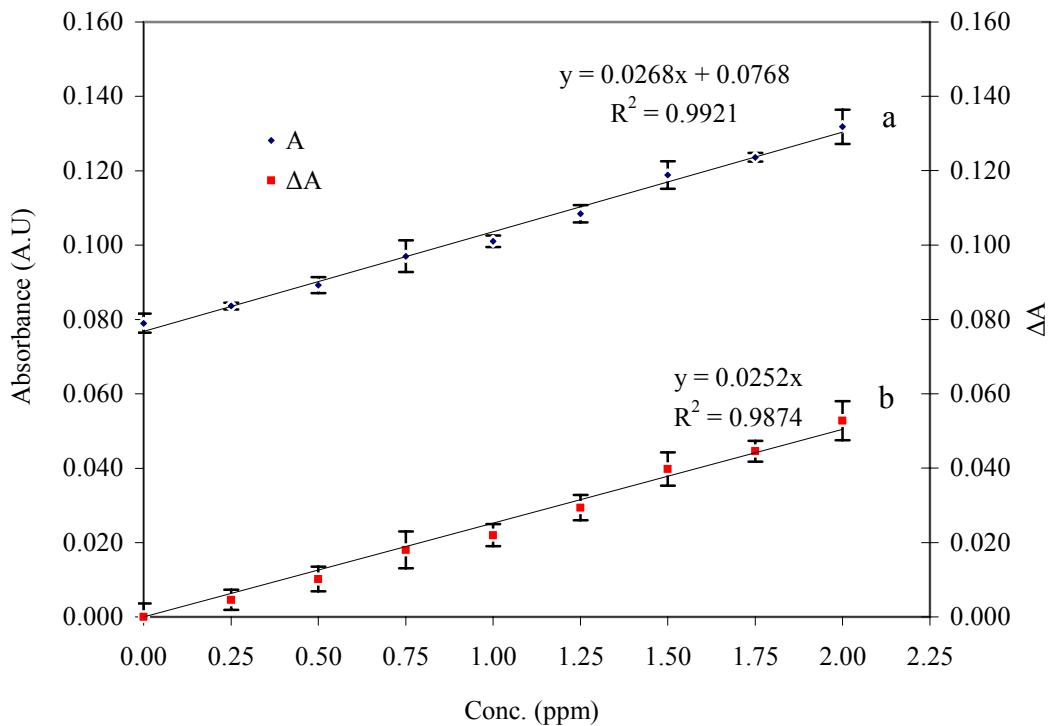


Figure 6.47. Absorbance values of calcium standards (0.25-2 ppm) - 60 μ M AIII in 200 mM Imidazole-Cl buffer pH 6.5 (150 μ L standard-150 μ L dye reagent) at 650 nm a. without subtracting blank values, b. with subtracting blank values.

Suitability of the dye reagent, 60 μM Arsenazo III in 200 mM imidazole-Cl pH 6.5, for the analysis of 1-8 ppm calcium containing solutions was also tested. Figure 6.48 shows the relation between the absorbance values and calcium concentration of the standard solutions. At 650 nm, calibration curve with an equation of $y=0.0305x+0.0783$ ($R^2=0.9983$) was obtained (Figure 6.48). Average blank value was found as 0.081. Absorbances of the complexes were ranged between 0.105 and 0.318.

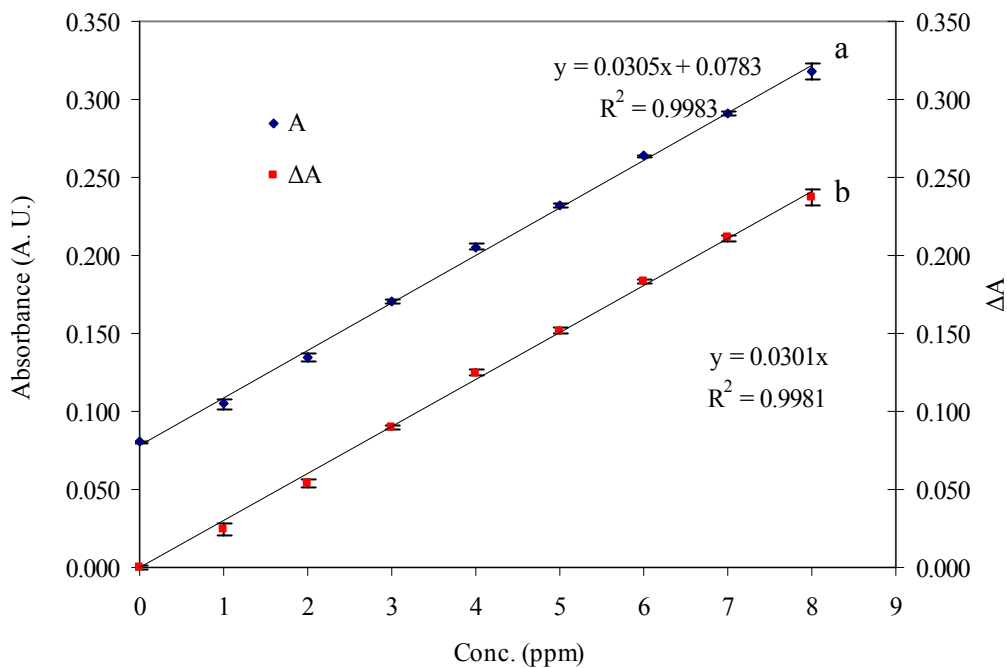


Figure 6.48. Absorbance values of calcium standards (1-8 ppm) - 60 μM AIII in 200 mM Imidazole-Cl buffer pH 6.5 (150 μL standard-150 μL dye reagent) at 650 nm a. without subtracting blank values, b. with subtracting blank values.

Saturation of the Arsenazo III dye with respect to calcium is obvious when the concentration of calcium in the standard solutions were between 10 and 80 ppm. At this concentration range, final total calcium concentrations were 5 to 40 ppm since the standard solutions and the dye reagent were mixed in 1:1 volumetric ratio. Absorbances of the complex formed became constant when the calcium concentration in the standard solution was 60 ppm (final calcium concentration of 30 ppm) (Figures 6.49).

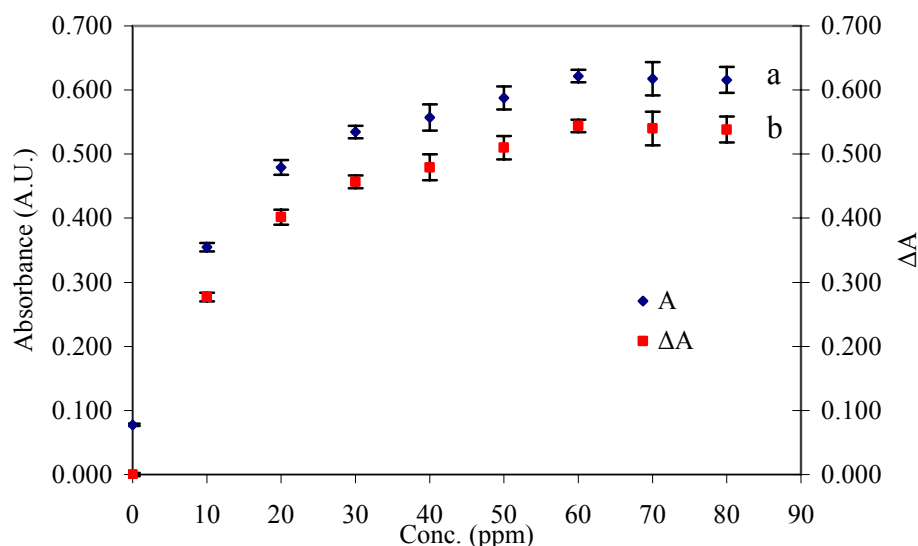


Figure 6.49. Absorbance values of calcium standards (10-80 ppm) - 60 μM AIII in 200 mM Imidazole-Cl buffer pH 6.5 (150 μL standard-150 μL dye reagent) at 650 nm a. without subtracting blank values, b. with subtracting blank values.

Apparent dissociation constant of calcium-ArsenazoIII complex was also evaluated by absorbance data obtained when 150 μL the dye reagent (60 μM Arsenazo III in 200 mM imidazole-Cl buffer pH 6.5) was mixed with 150 μL of standard solutions. Plots of $\alpha/(1-\alpha)$ vs. $[\text{Ca}]_t - \alpha[\text{Ar}]_t$ are shown in Figure 6.50. Dissociation constants calculated from the slopes of the linear regression lines were found as 1.90×10^{-4} and 1.01×10^{-4} M when 0.25-1 ppm and 1-8 ppm calcium containing standard solutions were mixed with the dye reagent, respectively. Negative logarithms of these dissociation constants were calculated as 3.72 and 3.99, respectively.

When 150 μL of 60 μM Arsenazo III in 200 mM imidazole-Cl buffer pH 6.5 was mixed with 150 μL calcium standard solution, dye reagent and standard solution became $\frac{1}{2}$ diluted. In the reaction mixture total Arsenazo III concentration was 30 μM whereas total buffer strength was 100 mM. Apparent pK_D values were found as 3.72 and 3.99. However when the dye reagent was 60 μM Arsenazo III in 100 mM imidazole-Cl buffer pH 6.5 total buffer concentration was 50 mM. By comparing the pK_D values obtained by both dye reagents, effects of buffer concentration on apparent pK_D can be evaluated. Doubling of buffer concentration decreased pK_D from 4.26 to 3.72. Bauer (1981) reported that increase of buffer concentration always decrease apparent pK_D . In his study increase of buffer concentration from 50 to 100 mM resulted in decrease of pK_D from 4.64 to 4.36 at pH 7.5.

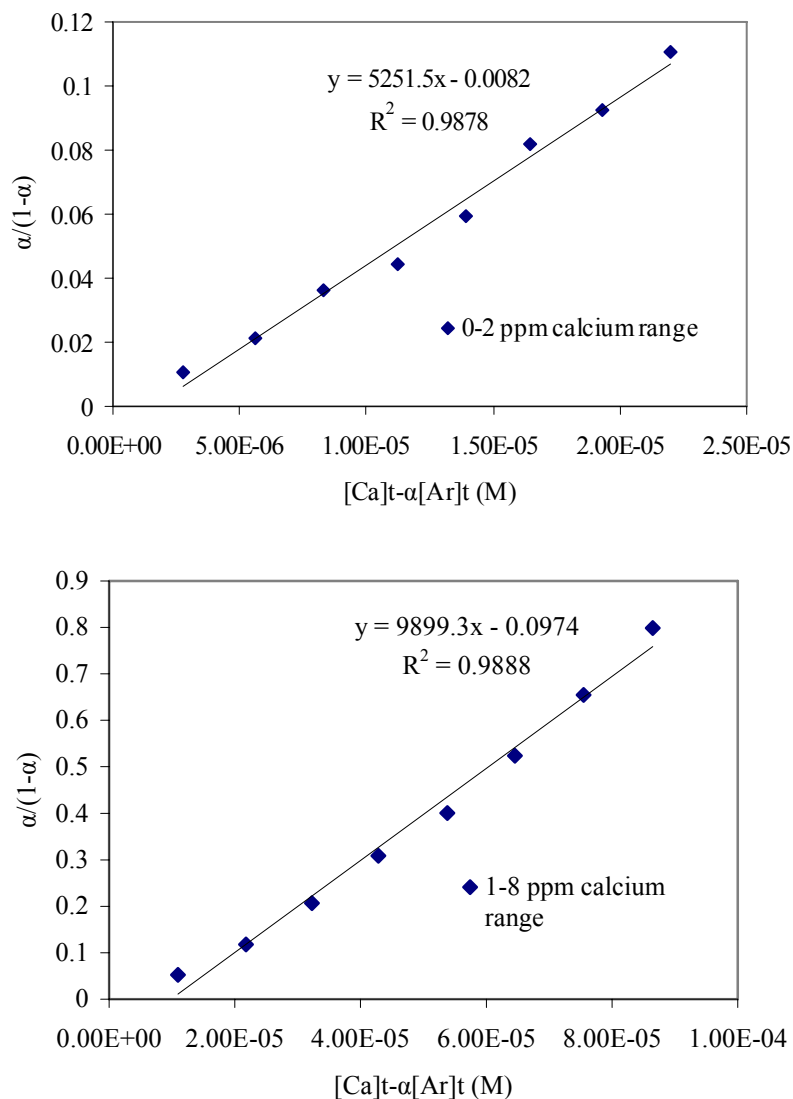


Figure 6.50. Plot of $\alpha/(1-\alpha)$ vs. $[Ca]_t - \alpha[Ar]_t$ Dye reagent: 60 μM Arsenazo III in 200 mM imidazole-Cl pH 6.5 Calcium concentration of standard solutions: 0.25-2 ppm and 1-8 ppm (Reagent to standard volume ratio of 150 μL /150 μL).

200 μM Arsenazo III & 200 mM Imidazole-Cl pH 6.5:

Absorbance of the complex of calcium and Arsenazo III is strongly dependent on the pH. Large pH range of calcium containing solutions to be analyzed may change the final pH of the complex even the dye reagent is buffered. Since standard solutions and the dye reagent are mixed in 1:1 volumetric ratio, final buffer strength was adjusted to 100 mM by using the dye reagent having 200 mM imidazole buffer.

The use of 60 μM Arsenazo III buffer resulted with the maximum absorbance of 0.655 for 8 ppm calcium containing solution. For an attempt to increase the absorbance of the complex formed by reacting equal volumes of the dye and standard solution having 8 ppm calcium close to 1, two hundreds micromolar Arsenazo III solution in 200 mM imidazole-Cl buffer with a pH 6.5 was prepared. This reagent was then used for the construction of calibration curves for 1-8 ppm and 10-80 ppm calcium standard solutions. At first absorption maxima was determined by scanning the absorbance values of the complex between 400 and 700 nm for both two concentration ranges of calcium standards. Figure 6.51 shows the spectra of the complexes formed by mixing 1-7 ppm calcium containing solutions and 200 μM AIII in 200 mM imidazole-Cl pH 6.5. Maximum absorption for the blank solution was observed at 545 nm. However, maximum absorption peak shifts through 560 nm with the increase in the calcium concentration. A second peak at 595 nm became apparent when the calcium concentration in the standard solution was 7 ppm.

When the spectra of the calcium-Arsenazo III complex were obtained by the subtraction of the blank value from those of calcium-Arsenazo III complexes (Figure 6.52), standard solutions with calcium concentration up to 7 ppm showed a peak of maxima at 600 nm. For 7 ppm calcium containing standard solution, maximum peak was found to be shifted to 605 nm. Second peak for all the solutions was observed at 650 nm for all standard solutions.

This dye reagent was also used for 10-80 ppm calcium containing standard solutions. Figure 6.53 shows the spectra of the blank and complexes formed by mixing 150 μL dye reagent and 150 μL standard solutions. Blank solution gave an absorption maximum at 550 nm. This peak shifts to 560-570 nm when calcium and dye complexes are formed. Two peaks of calcium and dye complexes were clearly visible when the calcium concentrations in the standard solutions were in the range of 10-80 ppm. For 10 ppm standard solution, the maximum absorption peak was observed at 595. This peak shifted to 600 nm when calcium in the standard solutions was equal or higher than 10 ppm. Second peak was observed at 655 nm for the all standard solution.

When spectra were constructed by subtracting the absorbance value of the blank from the absorbances of the complexes (Figure 6.54), 605 and 655 nm were two wavelengths at which maximum absorptions were observed.

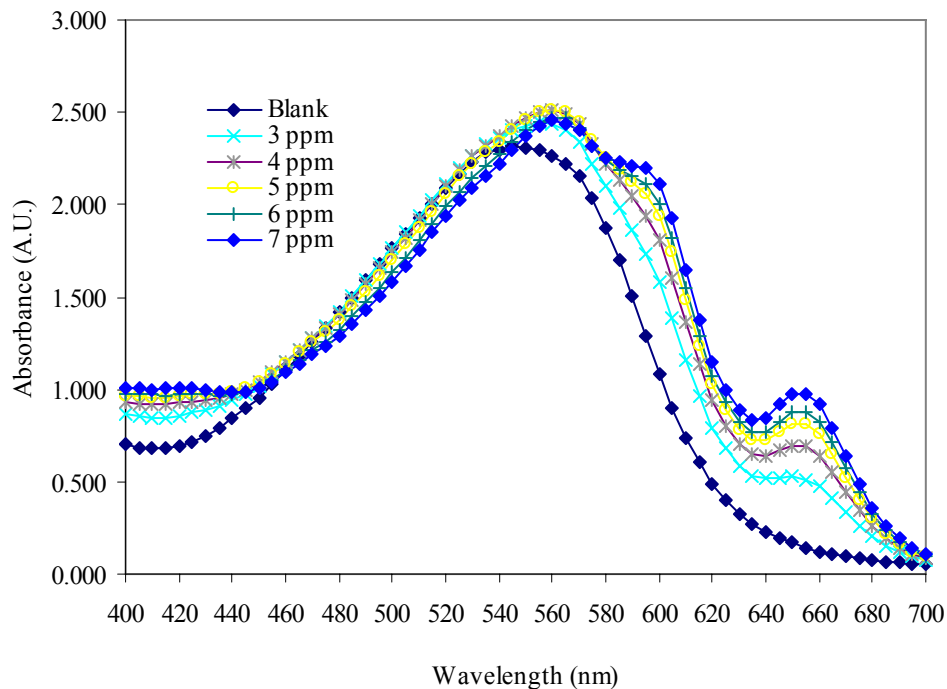


Figure 6.51. Spectra of calcium standard solutions (1-7 ppm) - 200 μ M AIII in 200 mM imidazole-Cl pH 6.5 (150 μ L standard- 150 μ L dye reagent).

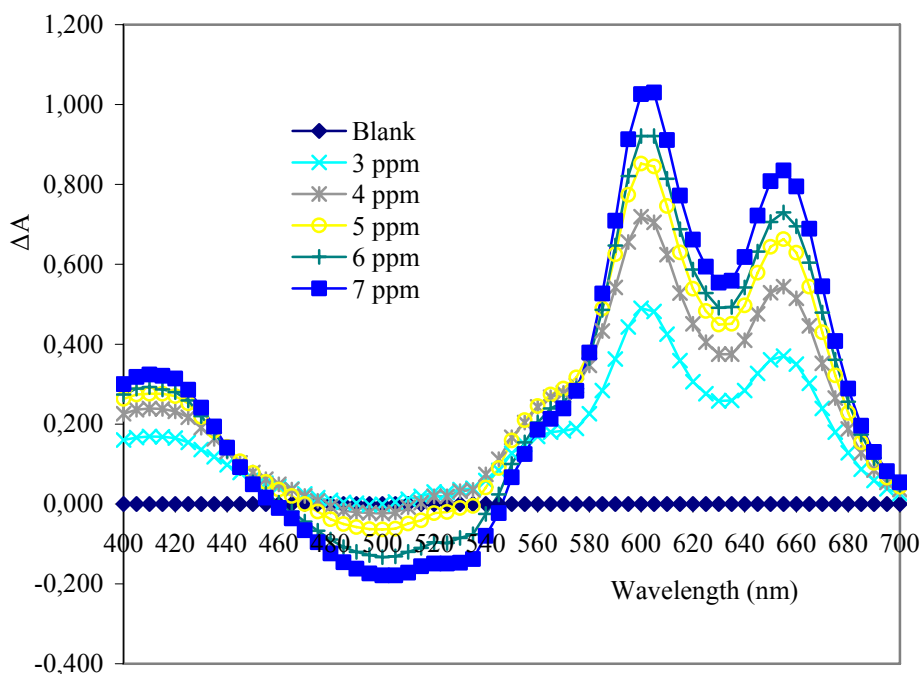


Figure 6.52. Spectra of calcium standard solutions (1-7 ppm) - 200 μ M AIII in 200 mM imidazole-Cl pH 6.5 (150 μ L standard-150 μ L dye reagent) obtained by subtracting blank values.

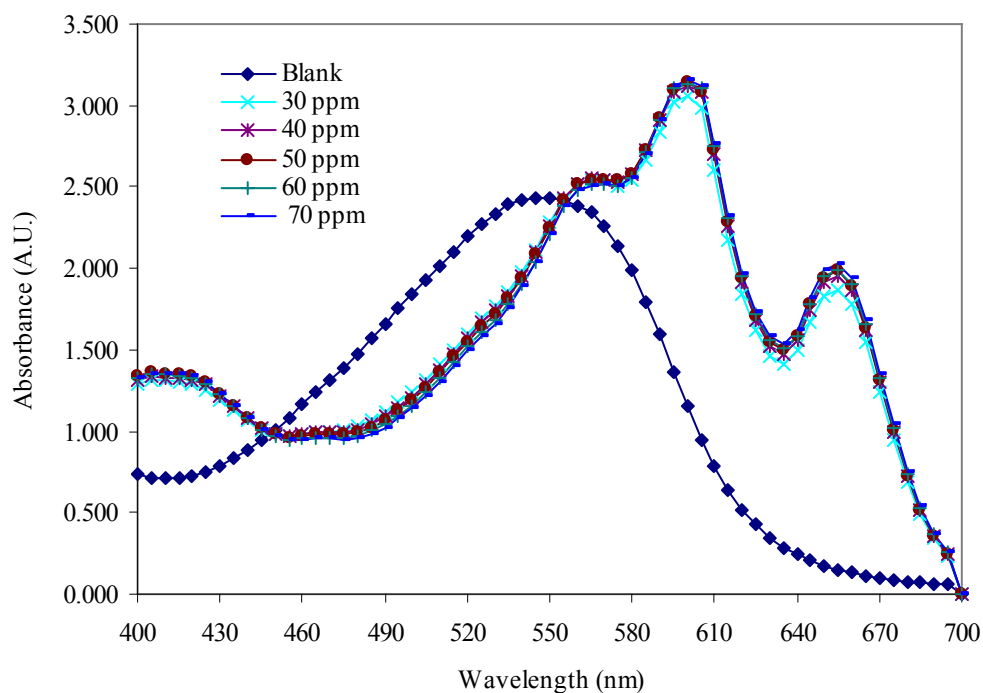


Figure 6.53. Spectra of calcium standard solutions (10-70 ppm) - 200 μ M AIII in 200 mM imidazole-Cl pH 6.5 (150 μ L standard-150 μ L dye reagent).

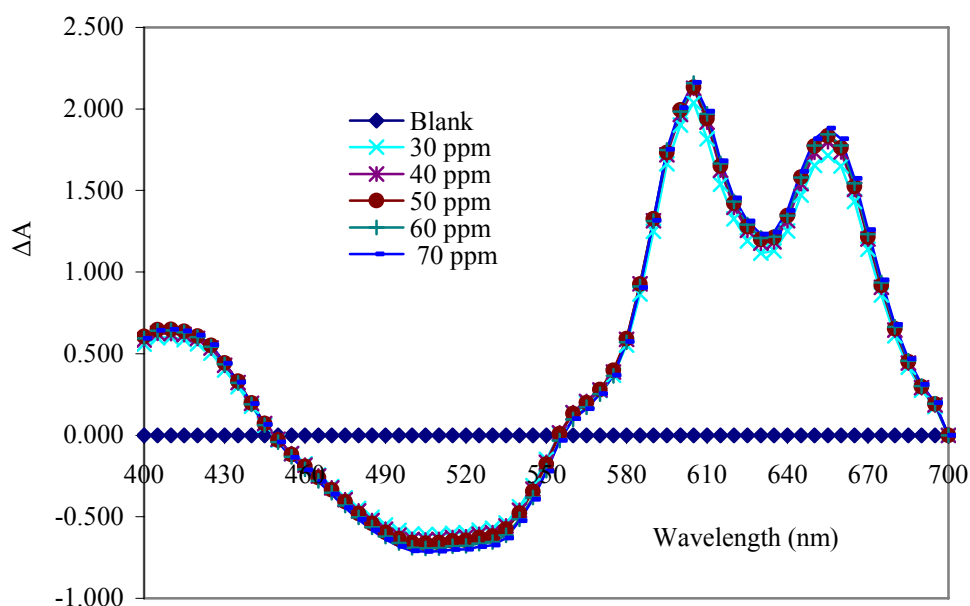


Figure 6.54. Spectra of calcium standard solutions (10-70 ppm) - 200 μ M AIII in 200 mM imidazole-Cl pH 6.5 (150 μ L standard-150 μ L dye reagent) obtained by subtracting blank values.

The dye reagent, 200 μM AIII in 200 mM Imidazole-Cl buffer pH 6.5, was found suitable for the construction of calibration curve for the calcium standards solutions having 1-8 ppm calcium. Linear calibration curve with a correlation function of $y=0.1144x+0.1872$ ($R^2=0.9954$) was obtained at 650 nm (Figure 6.55). Average absorbance of the blank solution was found as 0.175 ± 0.006 . For a spectrophotometric analysis method, absorbance value should not increase 1 and absorbances should follow the Beer's Law within the concentration range used in the analysis (Marczenko and Balcerzak, 2000). The lowest and the highest concentrations of standard solution used were 1 and 8 ppm, respectively. Average value for the complex obtained by reacting 1 ppm calcium standard and the dye reagent was 0.283 ± 0.002 . When 8 ppm calcium containing solution was used, absorbance of the complex was 1.071. These showed that 200 μM AIII in 200 mM Imidazole-Cl buffer pH 6.5 is a useful reagent for the accurate and precise analysis of calcium when the concentrations of calcium in the sample were in the range 1 to 8 ppm.

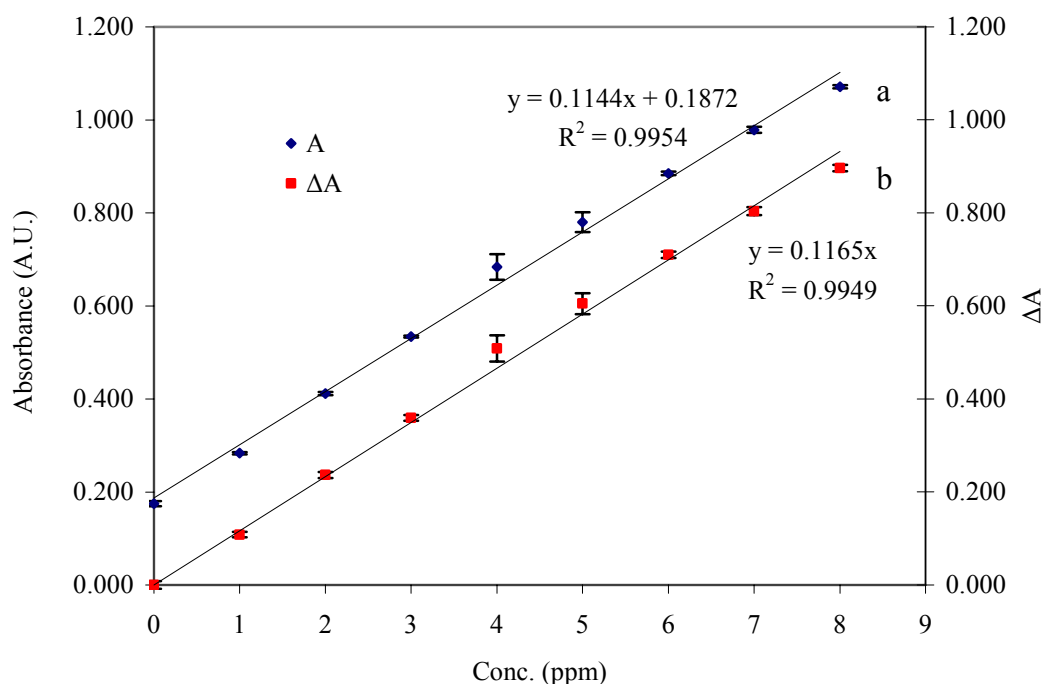


Figure 6.55. Absorbance values of calcium standards (1-8 ppm) - 200 μM AIII in 200 mM Imidazole-Cl buffer pH 6.5 (150 μL standard-150 μL dye reagent) at 650 nm a. without subtracting blank values, b. with subtracting blank values.

At 600 nm average absorbance value for the blank solution was 1.131 ± 0.024 . For 1 and 8 ppm solutions, absorbances were 1.282 ± 0.011 and 2.253 ± 0.007 , respectively. Since absorbance is defined as the logarithm of the ratio of power of the incident beam (P_0) to the power of emergent beam (P) (Equation 6.32), absorbance values of 1 and 2 means 10 and 1 % of the power of the incident beam is transmitted by the sample, respectively. Because absorbance measurements are subjected to larger error at these conditions, absorbances measured at 600 nm should not be used.

$$A = \log\left(\frac{P_0}{P}\right) \quad (6.32)$$

The suitability of the 200 μM Arsenazo in 200 mM imidazole buffer was also tested for 10 to 80 ppm calcium containing solutions. Figure 6.56 shows absorbances of the complex vs. calcium concentration in the standard solutions at 650 nm. Constant absorbances over 40 ppm standard calcium concentration showed that Arsenazo III becomes saturated with respect to calcium.

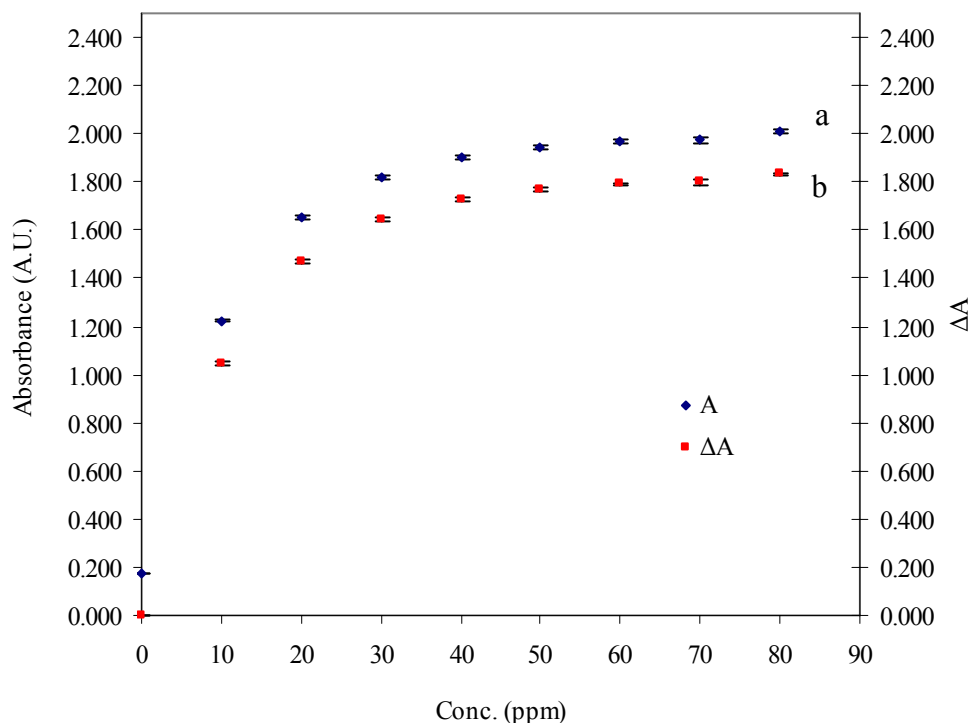


Figure 6.56. Absorbance values of calcium standards (10-80 ppm) - 200 μM AIII in 200 mM Imidazole-Cl buffer pH 6.5 (150 μL standard-150 μL dye reagent) at 650 nm a. without subtracting blank values, b. with subtracting blank values.

Dissociation constant of Arsenazo III were also calculated from the absorbance values obtained by mixing 200 μM AIII in 200 mM Imidazole-Cl buffer pH 6.5 dye reagent with standard solution sets of 1 to 8 ppm and 10 to 80 ppm. Values of $\alpha/(1-\alpha)$ was found to be linearly correlated with $[\text{Ca}]_t - \alpha[\text{Ar}]_t$ (Figure 6.57). Dissociation constant was calculated from the slope as 49 μM . pK_D value was then found as 4.31.

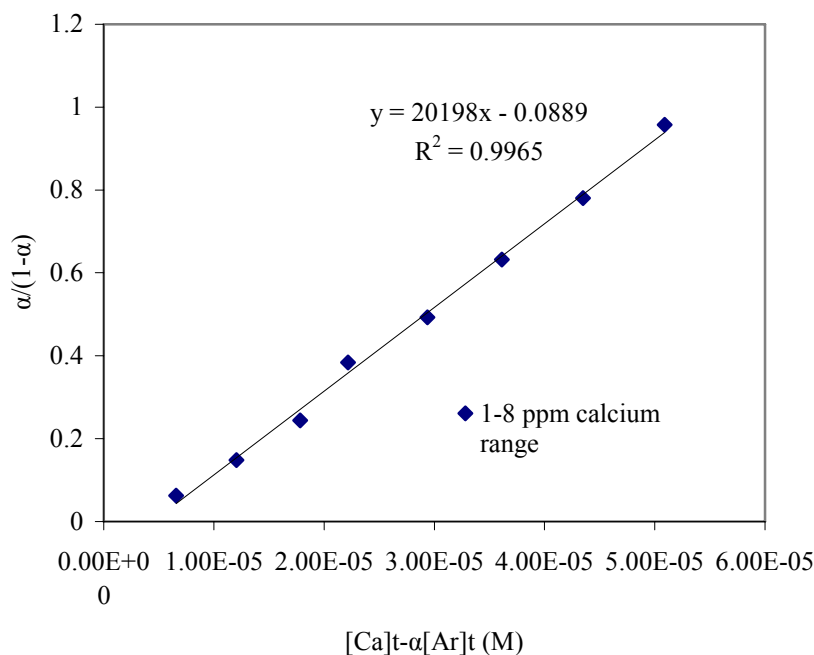


Figure 6.57. Plot of $\alpha/(1-\alpha)$ vs. $[\text{Ca}]_t - \alpha[\text{Ar}]_t$ Dye reagent: 200 μM Arsenazo III in 200 mM imidazole-Cl pH 6.5 Calcium concentration of standard solutions: 1-8 ppm (Reagent to standard volume ratio of 150 μL /150 μL).

500 μM AIII in 200 mM Imidazole-Cl buffer pH 6.5:

Upon the observation that 200 μM Arsenazo III became saturated when the standard calcium concentration was over 40 ppm, Arsenazo III concentration was raised to 500 μM . Therefore, 500 μM Arsenazo III in 200 mM imidazole-Cl pH 6.5 dye reagent was prepared and tested for the 10-80 ppm calcium containing solutions at 150 μL standard/ 150 μL dye reagent ratio). Figure 6.58 showed that absorbances become constant when the calcium in the standard solutions was over 10 ppm when absorbances were measured at 650 nm.

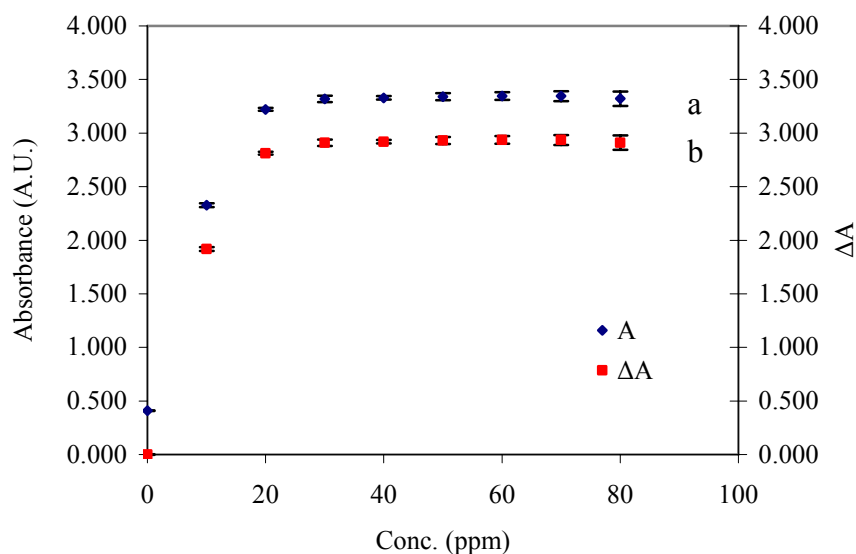


Figure 6.58. Absorbance values of calcium standards (10-80 ppm) - 500 μM AIII in 200 mM Imidazole-Cl buffer pH 6.5 (150 μL standard-150 μL dye reagent) at 650 nm a. without subtracting blank values, b. with subtracting blank values.

Using absorbances of blank values and absorbances obtained in the saturation of all Arsenazo III dye at 650 nm, $\epsilon \cdot l$ values for free Arsenazo III and calcium-Arsenazo III complexes were calculated, respectively by Equations 6.17 and 6.19. Since microplate reader is used in the calcium analysis, pathlength was smaller than 1 cm but it was same in all analyses. Therefore $\epsilon \cdot l$ values were calculated instead of ϵ . Table 6.1 summarizes the $\epsilon \cdot l$ values for free Arsenazo III and calcium-Arsenazo III complexes. Molar absorptivity of free Arsenazo III was found to be greater at pH 5.4. The lowest molar absorptivity of the dye was found at pH 3.8 with an exception for 100 μM Arsenazo III and 100 mM imidazole concentrations in the mixture. Increase of Arsenazo III concentration from 30 μM to 100 μM caused considerable reduction in molar absorptivity of free dye. Molar absorptivity of the calcium-Arsenazo III complex at pH 3.8 was found to be lowest. This explains the lower absorbance responses obtained when Arsenazo III formate buffer pH 3.8 reagents were used for calcium analysis. Molar absorptivities of calcium-dye complex were dependent buffer concentration. One fold reduction of buffer concentration at pH 6.5 resulted in 10 % increase in molar absorptivity of the complex. Buffer concentration was more effective on molar absorptivity of calcium-Arsenazo III complex than Arsenazo III concentration.

Although molar absorptivities of the complexes were found to be greater at pH 5.4, total 100 μM Arsenazo III and 100 mM imidazole concentrations in the mixtures was suitable for reliable calcium analysis. This could be related to the lower molar absorptivity of the dye at 650 nm in this condition. Since Arsenazo III and calcium complexation is governed by equilibrium association constant, the presence of higher amounts of the dye results in the higher concentration of the complexes when calcium is in sufficient amount and if the saturation of the dye is not reached.

In order to find a reliable calcium analysis, three different pH values (pH 3.8, 5.4 and 6.5) were tested for three different calcium concentration ranges (0.25-2 ppm, 1-8 ppm and 10-80 ppm). Formate, acetate and imidazole-Cl buffers were used for pHs of 3.8, 5.4 and 6.5, respectively. At each pH level, different Arsenazo III concentrations were tested for those three calcium ranges. At pH 6.5, two buffer strengths were used whereas for pH 3.8 and 5.4, only one buffer concentration at each pH was used. Non-linear or linear responses between absorbance values and concentration of standard solutions were observed. Summary of the nature of the calibration curves obtained in this study is shown in Table 6.2. Linear calibration curves obtained are highlighted in Table 6.2.

Table 6.1. Molar absorptivities of free arsenazo III and calcium-arsenazo III complexes

pH	Total dye and buffer concentrations in the mixtures	$\epsilon_{AIII}^{650} * l$	$\epsilon_{CaAIII}^{650} * l$
6.5	30 μM AIII 50 mM Imidazole	2633	22167
	30 μM AIII 100 mM Imidazole	2600	20733
	100 μM AIII 100 mM Imidazole	1750	20080
5.4	15 μM AIII 25 mM acetate	4133	24200
	30 μM AIII 50 mM acetate	3233	21800
3.8	30 μM AIII 110 mM formate	2367	18366

Regression coefficients of the calibration equations and correlation coefficients obtained at both 600 and 650 nm are shown in Table 6.3 for the cases where linear calibration curves are obtained. Absorbance of the blank values, absorbances of the standard solutions with the lowest and the highest calcium concentrations for both wavelengths are also tabulated in Table 6.4. Among the all dyes tested, 60 μM Arsenazo III in 200 mM imidazole-Cl pH 6.5, 200 μM Arsenazo III in 200 mM imidazole-Cl pH 6.5 and 60 μM Arsenazo III in 100 mM acetate buffer pH 5.4 gave considerably better results when the absorbance range for the lowest and the highest calcium concentration of standards and regression coefficients for the calibration curves are taken into consideration.

Sixty micromolar Arsenazo III in 100 mM acetate buffer pH 5.4 gave linear calibration curves for 0.25-2 ppm calcium concentration of standard solutions when the dye and standard solutions were mixed in 150 μL / 150 μL ratio. At 650 nm, calibration curve with an equation of $y=0.091x+0.0998$ ($R^2=0.995$) was obtained (Table 6.3). Absorbance of the blank value was found as 0.097 ± 0.002 . The range of absorbances for 0.25 ppm and 2 ppm calcium concentrations in standard solutions was found as 0.121 ± 0.002 and 0.280 ± 0.004 (Table 6.4). Only 60 μM Arsenazo III in 100 mM acetate buffer pH 5.4 was found useful for the analysis of 0.25-2 ppm calcium in the solutions. Although the narrow response range of absorbances was found, small standard deviations showed that this reagent could be useful for 0.25-2 ppm calcium range in the solutions.

Two reagents were found to be useful when the calcium concentration in the standard solutions were in the range of 1 to 8 ppm. When 60 μM Arsenazo III in 200 mM imidazole-Cl pH 6.5 was used, the calibration curve with a function of $y=0.0305x+0.0783$ ($R^2=0.9983$) was obtained (Table 6.3). Absorbance of the blank was 0.081 ± 0.001 whereas absorbances for 1 ppm and 8 ppm solutions were 0.105 ± 0.003 and 0.318 ± 0.006 , respectively (Table 6.4). A calibration function of $y=0.0358x+0.3728$ with a regression coefficient of 0.995 was found at 600 nm (Table 6.3). Blank value found at 600 nm was 0.379 ± 0.002 . Absorbance range was found as 0.397 ± 0.019 - 0.655 ± 0.014 (Table 6.4).

In an attempt to find accurate and precise calcium analysis in the range of 1-8 ppm resulted with a calibration function of $y=0.1144x+0.1872$ ($R^2=0.9954$) when Arsenazo III concentration was raised to 200 μM (Table 6.3). Absorbance of the blank solution was found as 0.175 ± 0.006 . Absorbances for the standard solutions with the

lowest and the highest calcium concentrations were 0.283 ± 0.002 and 1.071 ± 0.003 , respectively (Table 6.4). The large range of absorbances (0.283-1.071) with respect to calcium concentration of standard solutions makes this reagent superior for the calcium analysis. Additionally, 60 μM Arsenazo III in 100 mM acetate buffer pH 5.4 can be useful for the 0.25-2 ppm calcium containing solutions even the absorbance range is narrow.

Table 6.2. The nature of absorbance vs. concentration curves obtained in calcium analysis by Arsenazo III reagents

No	Arsenazo III Reagent				Reagent Volume (μL)	Concentration range of Ca ²⁺ standards (ppm)	Volume of standards (μL)	650 nm	600 nm
	C _{Arsenazo III} (μM)	Buffer	C _{buffer} (mM)	pH					
1	60	acetate	100	5.4	150	0.25-2	150	Linear	Linear
2	60	acetate	100	5.4	150	1-8	150	Non-linear	Non-linear
3	60	acetate	100	5.4	150	10-80	150	Non-linear	Non-linear
4*	60	acetate	100	5.4	150	0.25-2	150	Linear	Linear
5*	60	acetate	100	5.4	150	1-8	150	Non-linear	Non-linear
6*	60	acetate	100	5.4	150	10-80	150	Non-linear	Non-linear
7	120	acetate	100	5.4	150	1-8	150	Non-linear	Non-linear
8	60	formate	220	3.8	150	0.25-2	150	Linear	Linear
9	60	formate	220	3.8	150	1-8	150	Linear	Linear
10	60	formate	220	3.8	150	10-80	150	Non-linear	Non-linear
11*	60	formate	220	3.8	150	0.25-2	150	Non-linear	Non-linear
12	120	formate	220	3.8	150	10-80	150	Non-linear	Non-linear
13	60	imidazole	100	6.5	150	0.25-2	150	Linear	Linear
14	60	imidazole	100	6.5	150	1-8	150	Non-linear	Non-linear
15	60	imidazole	100	6.5	150	10-80	150	Non-linear	Non-linear
16*	60	imidazole	100	6.5	150	0.25-2	150	Linear	Linear
17*	60	imidazole	100	6.5	150	1-8	150	Non-linear	Non-linear
18	60	imidazole	200	6.5	150	0.25-2	150	Linear	Linear
19	60	imidazole	200	6.5	150	1-8	150	Linear	Linear
20	60	imidazole	200	6.5	150	10-80	150	Non-linear	Non-linear
21	200	imidazole	200	6.5	150	1-8	150	Linear	Linear
22	200	imidazole	200	6.5	150	10-80	150	Non-linear	Non-linear
23	500	imidazole	200	6.5	150	10-80	150	Non-linear	Non-linear

* denotes where ½ diluted dye reagent was used.

Table 6.3. Linear calibration responses obtained in Arsenazo III-calcium analysis

No	Arsenazo III Reagent				Reagent (μL) / Standard (μL)	$[\text{Ca}^{2+}]$ range (ppm)	650 nm			600 nm		
	$C_{\text{Arsenazo III}}$	Buffer	C_{Buffer}	pH			Regression equation $y=mx+n$		R^2	Regression equation $y=mx+n$		R^2
							m	n		m	n	
1	60	acetate	100	5.4	150/150	0.25-2	0.0910	0.0998	0.9950	0.1093	0.3292	0.9935
2*	60	acetate	100	5.4	150/150	0.25-2	0.0628	0.0684	0.9887	0.0739	0.1817	0.9924
3	60	formate	220	3.8	150/150	0.25-2	0.0194	0.0722	0.9907	0.0209	0.2982	0.9629
4	60	formate	220	3.8	150/150	1-8	0.0179	0.0771	0.9944	0.02	0.2982	0.9909
5	60	imidazole	100	6.5	150/150	0.25-2	0.0691	0.0768	0.9953	0.0805	0.3637	0.9897
6*	60	imidazole	100	6.5	150/150	0.25-2	0.0568	0.0616	0.9908	0.0604	0.2034	0.9646
7	60	imidazole	200	6.5	150/150	0.25-2	0.0268	0.0768	0.9921	0.0315	0.3620	0.9767
9	60	imidazole	200	6.5	150/150	1-8	0.0305	0.0783	0.9983	0.0358	0.3728	0.995
10	200	imidazole	200	6.5	150/150	1-8	0.1144	0.1872	0.9954	0.1412	1.1592	0.9937

* denotes where $\frac{1}{2}$ diluted dye reagent was used.

Table 6.4. Absorbance values of blank reagent and absorbance ranges of standards in Arsenazo III-calcium analysis

No	Arsenazo III Reagent				Reagent (μL) / Standard (μL)	[Ca ²⁺] Range (ppm)	650 nm		600 nm	
	C _{Arsenazo III}	Buffer	C _{Buffer}	pH			Absorbance of Blank	Absorbance Range of Standards	Absorbance of Blank	Absorbance Range of Standards
1	60	acetate	100	5.4	150/150	0.25-2	0.097 \pm 0.002	0.121 \pm 0.002 - 0.280 \pm 0.004	0.329 \pm 0.001	0.354 \pm 0.003 - 0.547 \pm 0.006
2*	60	acetate	100	5.4	150/150	0.25-2	0.062 \pm 0.000	0.082 \pm 0.001 - 0.190 \pm 0.001	0.178 \pm 0.003	0.198 \pm 0.002 - 0.327 \pm 0.002
3	60	formate	220	3.8	150/150	0.25-2	0.072 \pm 0.002	0.077 \pm 0.001 - 0.112 \pm 0.003	0.297 \pm 0.002	0.303 \pm 0.002 - 0.342 \pm 0.003
4	60	formate	220	3.8	150/150	1-8	0.071 \pm 0.001	0.101 \pm 0.002 - 0.217 \pm 0.002	0.299 \pm 0.003	0.322 \pm 0.008 - 0.458 \pm 0.010
5	60	imidazole	100	6.5	150/150	0.25-2	0.079 \pm 0.001	0.093 \pm 0.001 - 0.215 \pm 0.001	0.369 \pm 0.005	0.381 \pm 0.003 - 0.524 \pm 0.002
6*	60	imidazole	100	6.5	150/150	0.25-2	0.060 \pm 0.001	0.073 \pm 0.001 - 0.173 \pm 0.003	0.202 \pm 0.003	0.212 \pm 0.005 - 0.325 \pm 0.0313
7	60	imidazole	200	6.5	150/150	0.25-2	0.079 \pm 0.003	0.084 \pm 0.001 - 0.132 \pm 0.005	0.359 \pm 0.008	0.375 \pm 0.003 - 0.427 \pm 0.006
9	60	imidazole	200	6.5	150/150	1-8	0.081 \pm 0.001	0.105 \pm 0.003 - 0.318 \pm 0.006	0.379 \pm 0.002	0.397 \pm 0.019 - 0.655 \pm 0.014
10	200	imidazole	200	6.5	150/150	1-8	0.175 \pm 0.006	0.283 \pm 0.002 - 1.071 \pm 0.003	1.131 \pm 0.024	1.282 \pm 0.011 - 2.253 \pm 0.007

* denotes where ½ diluted dye reagent was used.

6.1.2. Calcium Determination in Different Electrolyte Solutions by Microplate Based Arsenazo III-Calcium Analysis

The presence of substances other than the compound of interest may cause interferences during the analysis of the compound. In UV-Visible spectroscopic analysis where several indicator molecules were used, competition of the other substances with the analyte for dye binding, pH changes, reduction of the molar extinction coefficient of the dye-analyte complex may yield erroneous results.

Arsenazo III calcium analysis method used in this thesis is based on the complexation of Arsenazo III dye with calcium. This analysis is also prone to possible interferences. The presence of other divalent cations may cause interferences during the analysis of calcium. Michaylova and Ilkova (1971) found that magnesium forms a complex with Arsenazo III dye when the solution pH was basic. Reduction of pH to 5.5 was used to avoid interferences coming from other divalent cations. The selection of pH 5.5 made it possible to analyze low levels of calcium even magnesium and manganese were present in amounts 100 fold higher than calcium. Although they chose pH 5.5, Zn^{2+} , Cd^{2+} , Al^{2+} and Fe^{2+} were found to cause approximately 20 nm shift in the wavelength where maximum absorption of the dye was observed. The presence of Fe^{2+} in the system was resulted with the formation of a dark-brown colored precipitate. Arsenazo III was also reported to have an affinity for Sr^{2+} and Ba^{2+} which is smaller than that for Ca^{2+} and higher than that for Mg^{2+} (Bauer, 1981).

Not only the presence of divalent cations but other cations and anions cause interferences during the analysis of calcium. Both NaCl and KCl were found to reduce pK_{Ca} , negative logarithm of dissociation constant of Arsenazo III for calcium (Bauer, 1981). The effect of KCl on the reduction of pK_{Ca} was not only due to the potassium binding to Arsenazo III but also mainly due the effect of KCl on the ionic strength of the solution (Bauer, 1981). Interferences from the presence of phosphate anions were demonstrated in a study on the determination of Mn^{2+} and Co^{2+} by Arsenazo III dye Zyryanov and Baykov, 2002). Addition of phosphate into the solutions of metal dye complexes reduced the absorbances of the complexes due to the metal phosphate complex formation.

In this study, it was shown that calcium in the range of 1 to 7 mg/L concentrations could be analyzed with dye reagent containing 200 μ M Arsenazo III and

200 mM imidazole chloride buffer at pH 6.5. However, reductions of molar absorption coefficient of the Arsenazo III-calcium complex by the presence of background ions, binding affinities of cations to Arsenazo III and changes in the absorbances of the calcium-dye complex by varying ionic strength or by the formation of calcium and anion pairs let us to check interferences when calcium analysis is performed in the presence of background electrolytes. All calcium standard solutions were prepared in the presence of different electrolytes and Arsenazo III analysis was performed. Spectra of calcium standard solutions were measured to determine wavelengths of the maximum absorption. Correlations between the absorbances of solutions with increasing calcium concentrations were determined whether Beer's law was obeyed or not. The list of electrolytes solutions in which calcium standard solutions were prepared is shown in Table 6.5. The number of replicates is also shown in Table 6.5.

Table 6.5. Electrolyte solutions used to prepare calcium standards

No	Electrolyte	Number of Replicates for Solution Preparation	Number of Replicates for Absorbance Measurements for Each Concentration Level	Total Replicates of Absorbance Measurements for Each Concentration Level
1	Ultrapure water	4	5	20
2	142 mM NaCl	2	5	10
3	27 mM NaHCO ₃	2	5	10
4	115 mM NaCl & 27 mM NaHOC ₃	2	5	10
5	1.5 mM MgCl ₂	2	5	10
6	1 mM Na ₂ HPO ₄	1	5	5
7	1 mM H ₃ PO ₄	1	5	5
8	10 mM H ₃ PO ₄	1	5	5
9	0.5 mM Na ₂ SO ₄	1	5	5
10	5 mM KCl	1	5	5

Calcium standards in ultrapure water

Spectra of calcium-Arsenazo III complexes in ultrapure water between 400 and 700 nm is given in Figure 6.59. Blank solution exhibited a maximum absorption at 545 nm. This absorption peak shifts to 560 nm when calcium concentration in the standard solutions is 7 ppm. It should be noted that total calcium concentration in the mixture is 3.5 ppm since dye reagent and standard solutions were mixed in 1:1 volume ratios. When compared to blank solution, calcium-Arsenazo III complex showed a peak of maxima at approximately 650 nm.

Difference between spectra of calcium-Arsenazo complexes and spectrum of blank solution was shown in Figure 6.60. This figure shows that calcium-Arsenazo III complexes exhibit two maximum absorption peaks at 605 and 655 nm. In addition to these, absorbances between 460 and 545 nm decreases with increasing calcium concentration.

Four different wavelengths (650, 600, 655 and 500 nm) were therefore used to measure absorbances of the calcium-Arsenazo III complexes. Both average absolute absorbances and absorbances obtained after subtraction of absorbances of blank solution from that of standard solutions were used to construct calibration curves. Absorbances of the complexes were found to be linearly correlated within the calcium concentration ranges when absorbances were measured at 650 nm (Figure 6.61). This shows that Beer's law is obeyed within the calcium concentration range of 1-7 ppm. Correlation coefficients were over 0.99 in whether absorbances or absorbances of solutions from which average of blank absorbances were used.

When absorbances were measured at 600 nm, absorbance of the blank solution was found as 1.150 (Figure 6.62). Calcium-Arsenazo III complexes showed higher absorbances. Absorbances of the solutions were again linearly correlated even absorbances were greater than unity. When ΔA values obtained by subtracting absorbance of the blank value from that of calcium standard solutions were used, ΔA values ranged between 0 and 1 (Figure 6.62). At 600 nm, absorbances and ΔA values were linearly correlated with correlation coefficients greater than 0.99. This suggests that absorbances and ΔA values obey Beer's law with the concentration ranges at 600 nm.

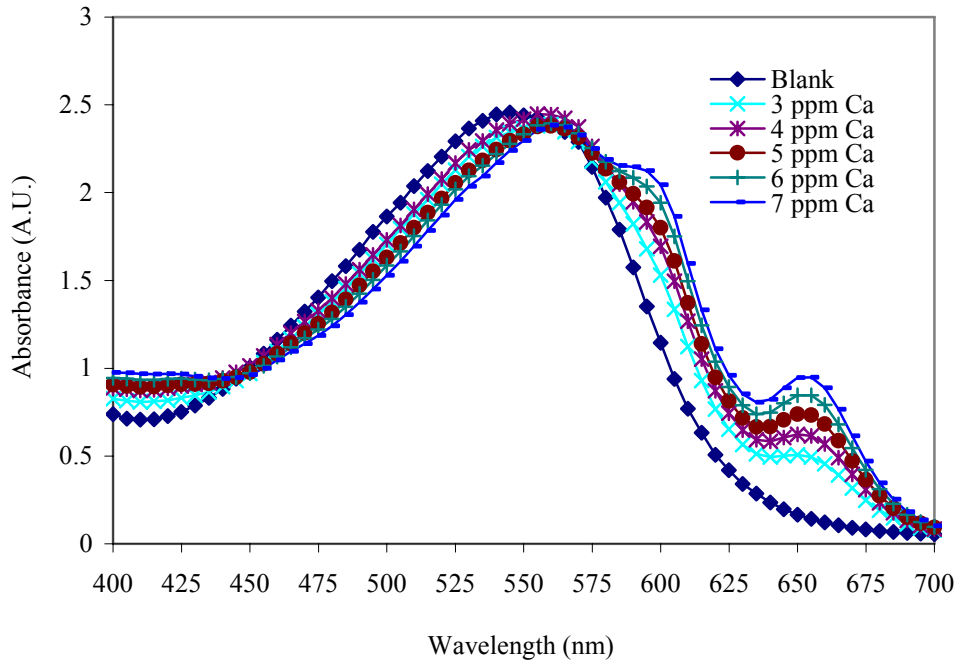


Figure 6.59. Spectra of calcium standards prepared in ultrapure water.

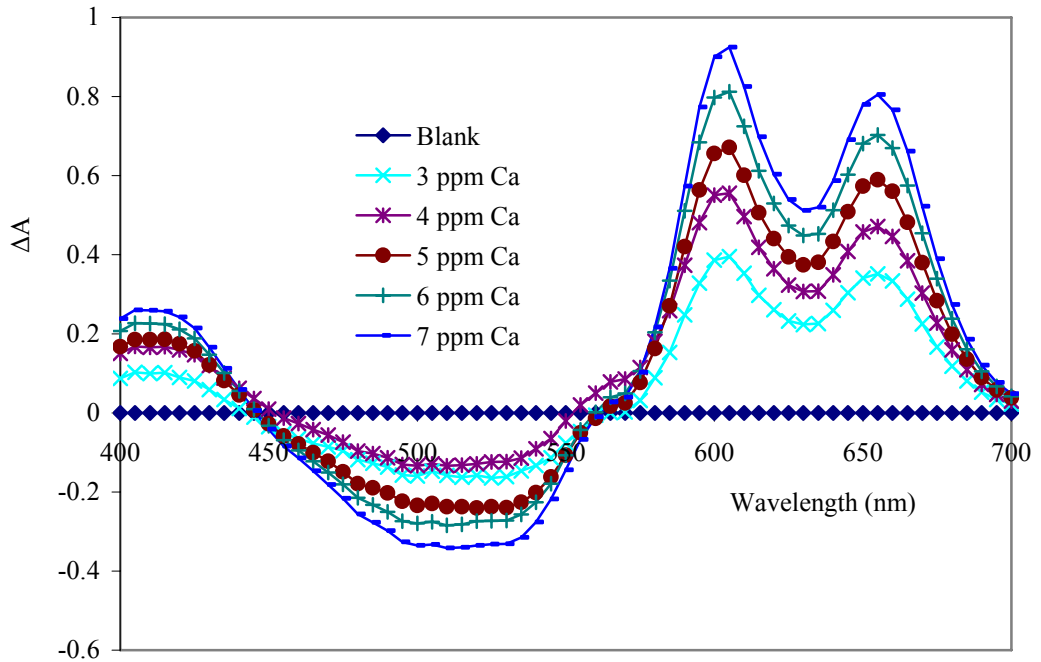


Figure 6.60. Spectra of calcium standards prepared in ultrapure water obtained by subtracting blank values.

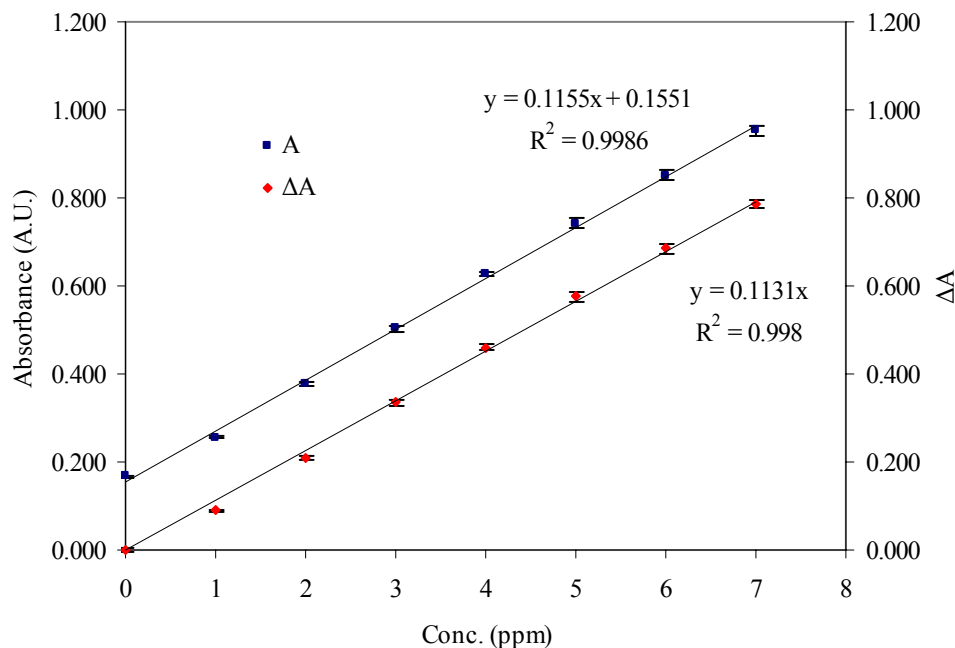


Figure 6.61. Calibration curve obtained by measuring absorbances of calcium standards prepared in ultrapure water at 650 nm.

Absorbances of solutions were also recorded at 655 nm. Those were closer to the absorbances measured at 650 nm as expected. Both absorbances and ΔA values were found to be linearly correlated at 655 nm (Figure 6.63).

Observations of the reductions of the absorbances between 460 and 545 nm with increasing calcium concentrations in spectra obtained by subtracting average value of the blank solution from averages of the absorbances of calcium-Arsenazo III complexes let us to measure absorbances at 500 nm. Absorbances decreased with increasing calcium concentrations in the solutions (Figure 6.64). This decrease in absorbances was linearly correlated with calcium concentrations in standard solutions. When ΔA values were calculated negative absorbances were obtained (Figure 6.64). These negative absorbances were also linearly correlated with increasing calcium concentrations. In both cases, standard deviations were found much greater than obtained at other wavelengths. Additionally correlation coefficients were lower than those obtained at other wavelengths.

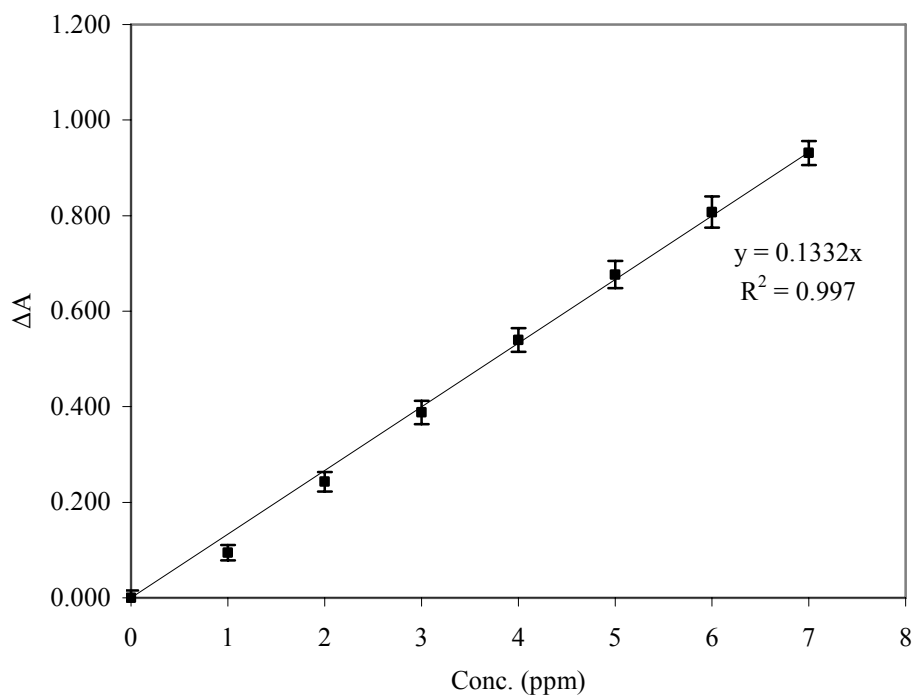
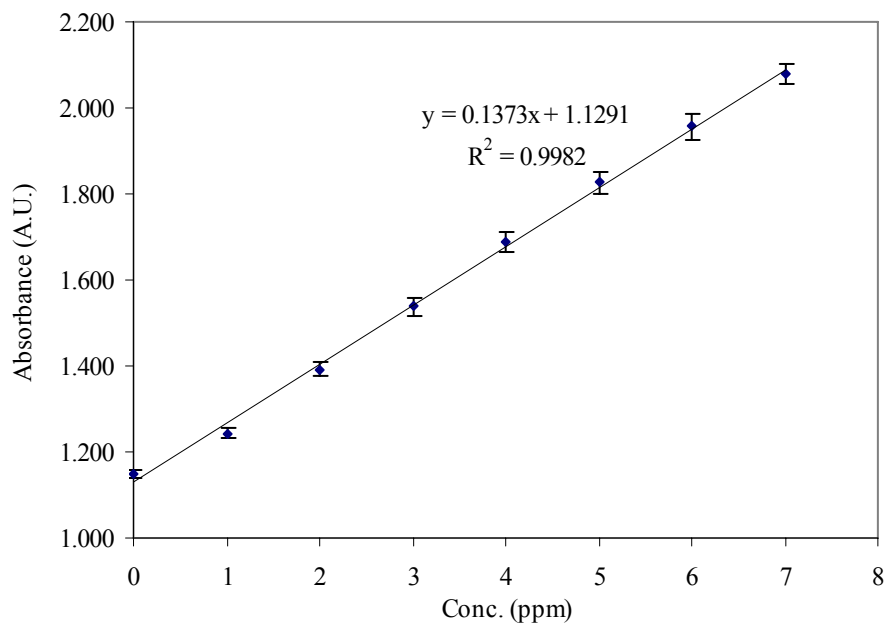


Figure 6.62. Calibration curve obtained by measuring absorbances of calcium standards prepared in ultrapure water at 600 nm.

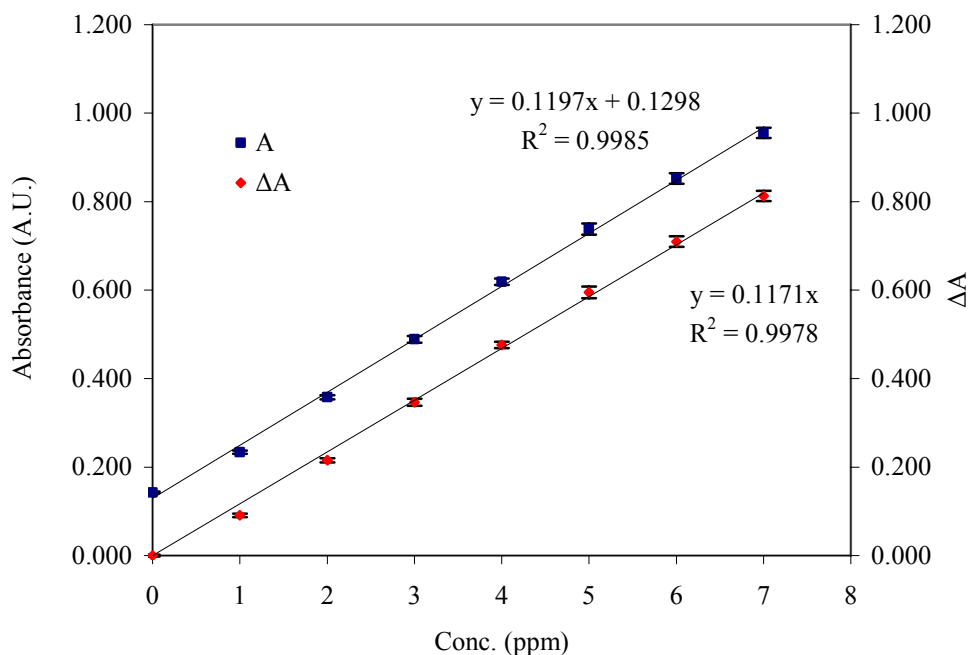


Figure 6.63. Calibration curve obtained by measuring absorbances of calcium standards prepared in ultrapure water at 655 nm.

Since absorbances obtained at 600 nm was greater than unity, absorbance values obtained at 655 nm were closer to those at 650 nm and lower correlation coefficients and greater standard deviations obtained at 500 nm, absorbance values of calcium-Arsenazo III complexes obtained in the presence of background electrolytes at 600, 655 and 500 nm were measured but results are not given in this thesis. Only calibrations obtained at 650 nm are reported.

For the all calcium standards prepared in electrolytical solutions, absorption spectra of calcium-Arsenazo III complexes and calibration curves constructed by absorbances measured at 650 nm are shown in Appendix G.

Absorption spectra of calcium-Arsenazo III complexes obtained in the presence of all electrolytes showed that dye itself exhibits absorption maximum at 545-550 nm. In all cases this peak shifted through 560 nm upon the formation of calcium-Arsenazo III complexes. Calcium-Arsenazo III complexes showed maximum absorption peak at 650 nm. When the spectra were obtained by subtracting absorbances of the blank solution from absorbances of calcium standard solutions, two maximum peaks were observed at 605 and 650 nm. Between 460 and 545 nm, negative values were observed when ΔA was used to construct spectra of the complexes.

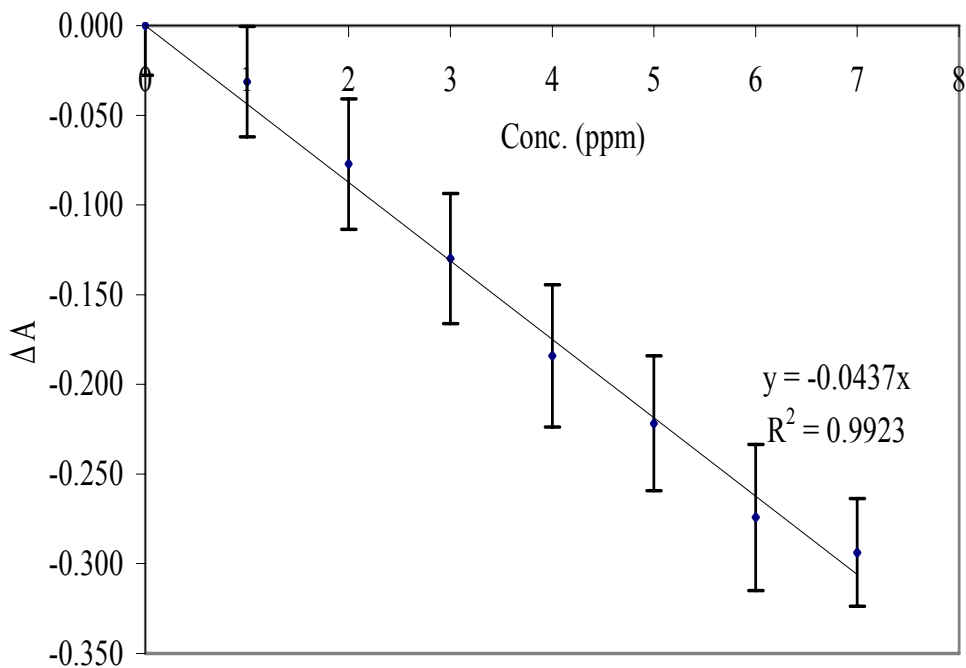
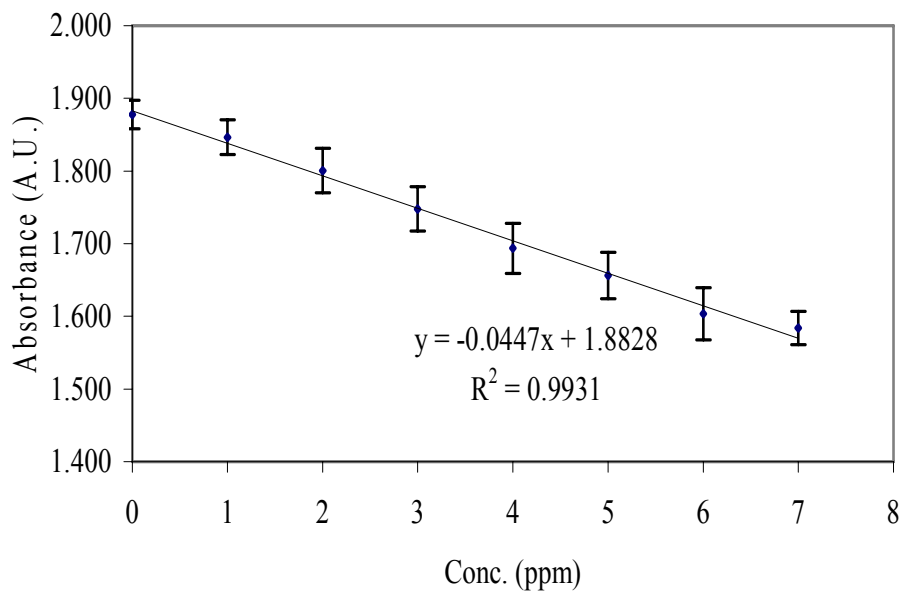


Figure 6.64. Calibration curve obtained by measuring absorbances of calcium standards prepared in ultrapure water at 500 nm.

Interferences of background ions in the calcium determination by Arsenazo III method were evaluated by statistical analysis. Absorbance values of the calcium standards prepared in ultrapure water at 650 nm were compared with the absorbances of the calcium standards in electrolytical solutions measured at 650 nm. Differences in mean values of the absorbances obtained for each calcium concentrations were determined by hypothesis testing with two-sided t -test for unpaired data. When the population variances are unknown, two different t statistics are used depending on the validity of assumption of the equality of variances of two populations. Assumption of the equality of population variance is therefore should first be validated. This can be preformed by comparing the ratios of the variance by two-sided F -test.

A methodology for the comparison of the mean absorbance values in this study is as follows (Baskan, 1993; Montgomery, 1996; Montgomery, 2001).

When samples are taken from two normally distributed populations and the variance of these populations are unknown, if the assumption of equality of variances of the both population can be made, test statistics, null and two-sided alternate hypotheses calculated are shown below.

$$\text{If } \sigma_1^2 = \sigma_2^2,$$

$$\text{Test statistics: } t_0 = \frac{\bar{x}_1 - \bar{x}_2}{S_p \sqrt{\frac{1}{n_1} + \frac{1}{n_2}}}, \quad v = n_1 + n_2 - 2 \quad (6.33)$$

$$S_p^2 = \frac{(n_1 - 1)S_1^2 + (n_2 - 1)S_2^2}{n_1 + n_2 - 2} \quad (6.34)$$

$$\text{Null hypothesis: } H_0 : \mu_1 = \mu_2 \quad (6.35)$$

$$\text{Alternate hypothesis } H_1 : \mu_1 \neq \mu_2 \quad (6.36)$$

$$\text{Criteria for rejection of null hypothesis } |t_0| > t_{\alpha/2, v} \quad (6.37)$$

If $\sigma_1^2 \neq \sigma_2^2$

$$\text{Test statistics} \quad t_0 = \frac{\bar{x}_1 - \bar{x}_2}{\sqrt{\frac{S_1^2}{n_1} + \frac{S_2^2}{n_2}}} \quad (6.38)$$

$$v = \frac{\left(\frac{S_1^2}{n_1} + \frac{S_2^2}{n_2}\right)^2}{\frac{\left(\frac{S_1^2}{n_1}\right)^2}{n_1 - 1} + \frac{\left(\frac{S_2^2}{n_2}\right)^2}{n_2 - 1}} \quad (6.39)$$

$$\text{Null hypothesis:} \quad H_0 : \mu_1 = \mu_2 \quad (6.40)$$

$$\text{Alternate hypothesis} \quad H_1 : \mu_1 \neq \mu_2 \quad (6.41)$$

$$\text{Criteria for rejection of null hypothesis} \quad |t_0| > t_{\alpha/2, v} \quad (6.42)$$

When the population variances are unknown and assumption of $\sigma_1^2 = \sigma_2^2$ can not be made, before using t statistics the validity of assumption $\sigma_1^2 = \sigma_2^2$ should be checked (Baskan, 1993). For this reason, validity of the assumption of $\sigma_1^2 = \sigma_2^2$ was checked by comparing the ratios of the variances by two sided F -test by assuming the populations normally distributed.

$$\text{Test statistics} \quad F_0 = \frac{S_1^2}{S_2^2} : v_1 = n_1 - 1, v_2 = n_2 - 1 \quad (6.43)$$

$$\text{Null hypothesis} \quad H_0 : \sigma_1^2 = \sigma_2^2 \quad (6.44)$$

$$\text{Alternate hypothesis} \quad H_1 : \sigma_1^2 \neq \sigma_2^2 \quad (6.45)$$

$$\text{Criteria for the rejection of null hypothesis} \quad F_0 > F_{\alpha/2, v_1, v_2} \text{ or } F_0 < F_{1-\alpha/2, v_1, v_2} \quad (6.46)$$

$$F_{v_1, v_2, 1-\alpha/2} = 1 / F_{v_2, v_1, \alpha/2} \quad (6.47)$$

In order to verify the validity of assumption of $\sigma_1^2 = \sigma_2^2$, two-sided F -test was performed to determine whether population variances are equal or not. Variances of absorbances of calcium standards prepared in ultrapure water were selected as reference and variances of absorbances of calcium standards prepared in electrolytical solutions were compared with absorbances of calcium standards in ultrapure water. Rejection or acceptance of null hypothesis, $H_0 : \sigma_1^2 = \sigma_2^2$ was decided by comparing calculated t_0 values with t values found. Confidence level in the comparison of variances was assumed 95 % ($\alpha=0.05$). F_0 values calculated from Equation 6.43 and compared with F values read from table for percentage points for F distribution table (Montgomery, 2001). When corresponding F value for ν_1 and ν_2 values can not be found in the table, F number for the closest degrees of freedom was selected. Table 6.6 shows calculated F_0 values and upper and lower confidence limits whereas Table 6.7 shows the results of rejection or acceptance of the assumption of equality of the variances.

When the null hypothesis is accepted, two-sided t -test methodology for $\sigma_1^2 = \sigma_2^2$ is used (Equations 6.33-6.37). However, in the case of rejection of null hypothesis, two-sided t -test for $\sigma_1^2 \neq \sigma_2^2$ is used (Equations 6.38-6.42). Confidence level in both tests was assumed as 99 % ($\alpha=0.01$). Since the null hypothesis in both methodologies is $H_0 : \mu_1 = \mu_2$, acceptance of the null hypothesis states that there is no interference coming from the presence of background electrolytes at 99 % confidence level. If the null hypothesis is rejected background electrolytes interferes in the Arsenazo III calcium analysis.

If the assumption of $\sigma_1^2 = \sigma_2^2$ is validated, t_0 values for the each calcium concentration was calculated by Equations 6.33 and 6.34. Results were compared with t values obtained from the table of percentage points for the t distribution (Montgomery, 2001). Criteria shown in Equation 6.37 were used to reject or accept the null hypothesis of $H_0 : \mu_1 = \mu_2$. If the assumption of $\sigma_1^2 = \sigma_2^2$ can not be made ($\sigma_1^2 \neq \sigma_2^2$), Equations 6.38 and 6.39 were used to calculate t_0 values and degrees of freedom, respectively. Criterion for the acceptance or the rejection of the null hypothesis in this case is shown in Equation 6.42. Calculated t_0 were compared with t values obtained from the table for percentage points for the t distribution (Montgomery, 2001).

In both methodologies, when t values for calculated degrees of freedom can not be found in the table t value for the closest degrees of freedom was selected.

Calculated t_0 values and t values for corresponding degrees of freedom and confidence limits are shown in Table 6.8 whereas results of the rejection and acceptance of null hypothesis ($H_0 : \mu_1 = \mu_2$) are summarized in Table 6.9.

Calcium standards in 142 mM NaCl

pK_{ca} of Arsenazo III for calcium was found to be strongly dependent on pH, presence of other cations and the buffer type and concentration (Bauer, 1981). In this study, imidazole buffer at a fixed concentration was used. The use of the imidazole buffer made it possible to buffer the solutions strongly at pH 6.5. Therefore, only the presence of background ions in considerably higher concentrations when compared to calcium may cause interferences during calcium analysis. Bauer (1981) found that the presence of KCl and NaCl showed identical effects on pK_{ca} . At pH 8.0, increase of KCl concentration from 0 to 100 mM, reduced 0.75 pK units. However, at pH 7.0, reduction was only 0.35. The effects of KCl and NaCl on the reduction of pK_{Ca} were mainly due to the effects of these salts on the ionic strength. Competitive binding of potassium was also effective on the reduction of pK_{Ca} .

When calcium standard solutions prepared in 142 mM NaCl were mixed with Arsenazo III dye reagents, absorbances were linearly correlated with calcium concentrations (Figure G.3). Correlation coefficients were found as 0.9988 and 0.998 for absorbances and ΔA values, respectively. If regression coefficient obtained by ΔA values ($y=0.1044x$) was compared to that found when calcium standard solutions prepared in ultrapure water ($y=0.1131x$), absorbance response with respect to calcium concentration was reduced in the presence of 142 mM NaCl.

According to statistical analysis, the presence of 142 mM NaCl was found to interfere at all calcium concentration levels except 2 ppm calcium concentration.

Table 6.6. Calculated F_0 values and confidence limits for rejection of null hypothesis in two-sided F -test for Arsenazo III-calcium analysis

Conc. (ppm)	142 mM NaCl $F_{19, 9, 0.025}$	27 mM NaHCO₃ $F_{19, 9, 0.025}$	115 mM NaCl 27 mM NaHCO₃ $F_{19, 9, 0.025}$	1.5 mM MgCl₂ $F_{19, 9, 0.025}$	1 mM Na₂HPO₄ $F_{19, 4, 0.025}$	1 mM H₃PO₄ $F_{19, 4, 0.025}$	10 mM H₃PO₄ $F_{19, 4, 0.025}$	5 mM KCl $F_{19, 4, 0.025}$	0.5 mM Na₂SO₄ $F_{19, 4, 0.025}$
0	0.971	0.434	2.679	0.243	4.799	0.436	0.619	1.745	12.798
1	4.655	0.160	0.593	0.112	4.702	0.808	6.085	2.796	6.085
2	10.397	0.774	0.784	0.538	1.365	3.684	3.366	11.485	2.219
3	1.242	3.329	4.968	0.859	34.858	64.737	90.632	16.184	37.763
4	5.638	2.875	3.084	5.537	12.122	2.116	5.825	34.502	2.894
5	4.392	6.294	3.775	6.856	21.967	82.988	1.399	13.337	82.988
6	11.896	10.949	2.721	16.954	21.079	174.658	7.641	10.450	7.501
7	6.323	2.253	25.641	3.830	5.205	5.495	3.966	2.707	2.686
Criteria for rejection	0.347 < F_0 < 3.670				0.281 < F_0 < 8.560				

Table 6.7. Results of *F*-test for the validation of the assumption of the equality of variances by two-sided *F*-test for Arsenazo III-calcium analysis

Conc. (ppm)	142 mM NaCl $F_{19, 9, 0.025}$	27 mM NaHCO₃ $F_{19, 9, 0.025}$	115 mM NaCl 27 mM NaHCO₃ $F_{19, 9, 0.025}$	1.5 mM MgCl₂ $F_{19, 9, 0.025}$	1 mM Na₂HPO₄ $F_{19, 4, 0.025}$	1 mM H₃PO₄ $F_{19, 4, 0.025}$	10 mM H₃PO₄ $F_{19, 4, 0.025}$	5 mM KCl $F_{19, 4, 0.025}$	0.5 mM Na₂SO₄ $F_{19, 4, 0.025}$
0	A	A	A	R	A	A	A	A	R
1	R	R	A	R	A	A	A	A	A
2	R	A	A	A	A	A	A	R	A
3	A	A	R	A	R	R	R	R	R
4	R	A	A	R	R	A	A	R	A
5	R	R	R	R	R	R	A	R	R
6	R	R	A	R	R	R	A	R	A
7	R	A	R	R	A	A	A	A	A

A: Acceptation of null hypothesis
R: Rejection of null hypothesis.

Table 6.8. Calculated t_0 values and t values for the rejection of null hypothesis in two-sided t-tests for Arsenazo III-calcium analysis

Conc. (ppm)	142 mM NaCl		27 mM NaHCO ₃		115 mM NaCl 27 mM NaHCO ₃		1.5 mM MgCl ₂		1 mM Na ₂ HPO ₄		1 mM H ₃ PO ₄		10 mM H ₃ PO ₄		5 mM KCl		0.5 mM Na ₂ SO ₄	
	$ t_0 $	t	$ t_0 $	t	$ t_0 $	t	$ t_0 $	t	$ t_0 $	t	$ t_0 $	t	$ t_0 $	t	$ t_0 $	t	$ t_0 $	t
0	18.556	2.763	20.077	2.763	50.209	2.763	27.541	3.106	0.605	2.807	0.507	2.807	2.765	2.807	5.039	2.807	3.088	2.819
1	8.315	2.763	13.127	3.169	32.884	2.763	11.154	3.169	5.388	2.807	0.945	2.807	10.527	2.807	3.266	2.807	4.002	2.807
2	1.900	2.787	24.558	2.763	24.114	2.763	12.387	2.763	2.480	2.807	1.623	2.807	18.045	2.807	3.705	2.819	4.498	2.807
3	5.110	2.763	20.476	2.763	21.428	2.763	6.504	2.763	10.005	2.819	7.285	2.831	33.483	2.831	0.535	2.807	4.612	2.819
4	14.400	2.763	19.558	2.763	14.205	2.763	2.747	2.763	4.690	2.819	3.603	2.807	24.370	2.807	0.442	2.819	1.491	2.807
5	10.009	2.763	17.882	2.771	9.171	2.763	3.219	2.771	0.707	2.807	6.183	2.831	14.486	2.807	0.160	2.819	0.822	2.831
6	13.079	2.797	20.846	2.787	6.318	2.763	0.555	2.807	9.214	2.807	8.898	2.845	17.168	2.807	1.978	2.831	1.600	2.807
7	16.727	2.771	13.568	2.763	8.714	2.819	0.819	2.763	3.639	2.807	6.880	2.807	21.134	2.807	0.418	2.807	0.743	2.807

Table 6.9. Results of *t*-tests for the validation of the equality of the means and interferences for Arsenazo III-calcium analysis

Conc. (ppm)	142 mM NaCl	27 mM NaHCO ₃	115 mM NaCl 27 mM NaHCO ₃	1.5 mM MgCl ₂	1 mM Na ₂ HPO ₄	1 mM H ₃ PO ₄	10 mM H ₃ PO ₄	5 mM KCl	0.5 mM Na ₂ SO ₄
0	R (I)	R (I)	R (I)	R (I)	A (NI)	A (NI)	A (NI)	R (I)	R (I)
1	R (I)	R (I)	R (I)	R (I)	R (I)	A (NI)	R (I)	R (I)	R (I)
2	A (NI)	R (I)	R (I)	R (I)	A (NI)	A (NI)	R (I)	R (I)	R (I)
3	R (I)	R (I)	R (I)	R (I)	R (I)	R (I)	R (I)	A (NI)	R (I)
4	R (I)	R (I)	R (I)	A (NI)	R (I)	R (I)	R (I)	A (NI)	A (NI)
5	R (I)	R (I)	R (I)	R (I)	A (NI)	R (I)	R (I)	A (NI)	A (NI)
6	R (I)	R (I)	R (I)	A (NI)	R (I)	R (I)	R (I)	A (NI)	A (NI)
7	R (I)	R (I)	R (I)	A (NI)	R (I)	R (I)	R (I)	A (NI)	A (NI)

A: Acception of null hypthesis

R: Rejection of null hypothesis

I: Interferes

NI: Not interferences.

Calcium standards in 27 mM NaHCO₃

In the presence of 27 mM NaHCO₃, absorbances and concentrations yielded linear calibration responses with a regression function of $y=0.1198x+0.1839$ (Figure G.6). Correlation coefficient was 0.9984. Regression function was found as $y=0.1196x$ when ΔA values were used. In this case correlation coefficient was also equal to 0.9984. Statistical analysis showed that 27 mM NaHCO₃ causes interferences at all calcium concentration levels.

Calcium standards in 115 mM NaCl & 27 mM NaHCO₃

The effects of the presence of 115 mM NaCl together with 27 mM NaHCO₃ in the standard solutions on the complexation of calcium with Arsenazo III dye are tested by checking linearity of the calibration curve. When calibration curves were constructed both by plotting absorbance and ΔA values with respect to calcium concentrations in the standard solutions linear calibration curves were obtained (Figure G.9). By using absorbances, regression function of $y=0.1127x+0.1987$ with a correlation coefficient of 0.9989 was found. Regression function and correlation function were $y=0.1122x$ and 0.9989, respectively when ΔA values were used to construct calibration curves.

Interferences due to the presence of 115 mM NaCl together with 27 mM NaHCO₃ were also tested by *t*-statistics. The presence of 115 mM NaCl together with 27 mM NaHCO₃ in the standard solutions interfered at all calcium concentration levels.

Calcium standards in 1.5 mM MgCl₂·6H₂O

Magnesium is the divalent cation which generally causes interferences in the calcium analysis with Arsenazo III (Lamkin and Williams, 1965, Michaylova and Ilkova, 1971). Masking agent, 8-hydroxyquinoline are used to avoid interferences of magnesium in calcium analyses (Morgan et al., 1993). Bauer (1981) found that pK_{ca} of Arsenazo III decreased when 0.1 mM magnesium was present at pH 8.0. However, the presence of magnesium up to 2 mM did not affect pK_{ca} of Arsenazo III for calcium at pH 7.0 (Bauer, 1981). It was possible to analyze low levels of calcium even concentration of magnesium was 100 fold higher than calcium when pH was 5.5 (Michaylova and Ilkova, 1971).

When magnesium was present in the standards solutions, linearity of correlation between absorbances and calcium concentrations was conserved (Figure G.12). When ΔA values were used correlation function of $y=0.1072x$ with a correlation coefficient of 0.998. Average absorbance of blank solution obtained when magnesium was present in the solutions was measured as 0.204. When this is compared to that found in ultrapure water (0.167), it seems that the presence of magnesium increases the absorbances. All absorbance values of the standard solutions except 7 ppm when magnesium was present were found to be higher than those of standard solutions prepared in ultrapure water. Absorbances of standards prepared in magnesium chloride and absorbances of standards prepared in ultrapure water become closer with increasing calcium concentrations. The effect of the presence of 1.5 mM $MgCl_2$ in standard solutions was also tested by comparing the absorbances obtained in the presence of 1.5 mM $MgCl_2$ with absorbances of calcium standards in ultrapure water by t -statistic. According to statistical analysis absorbances of blank solution, 1, 2, 3 and 5 ppm calcium standards were affected by the presence of magnesium chloride. However, interferences coming from the presence of magnesium chloride were insignificant at higher calcium levels.

Calcium standards in 1 mM Na_2HPO_4

Zyryanov and Baykov (2002) showed that in the presence of phosphate in solutions, absorbances of the Mn^{2+} -Arsenazo III and Co^{2+} -Arsenazo III complexes were reduced due to the associations of metal ions with phosphate anion. Absorbance of Mn^{2+} -Arsenazo III complex was severely reduced within the phosphate concentration range of 0-10 mM. Reduction of absorbance of Co^{2+} -Arsenazo III complex was however slight when phosphate was present in the solution up to 40 mM. Therefore linearity of calibration response was determined when calcium standard solutions were prepared in the presence of 1 mM PO_4^{3-} .

Calibration curves for calcium standards prepared in 1 mM Na_2HPO_4 are shown in Figure G.15. Calibration function obtained by plotting ΔA values against calcium concentrations in the standard solutions is $y=0.1103x$. Correlation coefficient was 0.9964.

Calcium standards in 1 mM H₃PO₄

The effects of the presence of 1 mM PO₄³⁻ on the absorbances of calcium-Arsenazo III complexes were also tested by preparing calcium standards in 1 mM H₃PO₄. In the presence of 1 mM H₃PO₄, absorbances of calcium-Arsenazo III complexes did not deviate from linearity. Calibration equation (Figure G.18) was $y=0.1092x$. The results of statistical analysis showed that 1 mM H₃PO₄ did not interfere up to 2 ppm calcium concentration. However absorbances were significantly affected by the presence of 1mM H₃PO₄ when calcium concentration level was 3 ppm and over.

Calcium standards in 10 mM H₃PO₄

Validity of calcium analysis by Arsenazo III reagent was also tested when standard solutions contained 10 mM H₃PO₄. Figure G.21 shows calibration curve obtained by reacting dye reagent and calcium standards containing 10 mM H₃PO₄. Calibration curve was linear also in this case. Correlation coefficient was higher than 0.99 as well. Average absorbance of blank value was measured as 0.164. This was similar to absorbance value obtained when calcium standards were prepared in ultrapure water (0.168). This suggests that phosphate in solution do not affect absorption of the dye at 650 nm. It should be noted that the presence of 10 mM H₃PO₄ is equal to 5 mM H₃PO₄ in the dye and standard reaction mixtures. Absorbances of the complexes obtained when 5 mM H₃PO₄ was present showed reduction when compared to those of complexes in ultrapure water. Reduction was greater when calcium concentration was higher. This suggests that presence of 10 mM H₃PO₄ interferes in the calcium analysis. However, 10 mM H₃PO₄ in the calcium solutions equals to 950 mg/L PO₄³⁻ which is almost 135 fold higher than 7 ppm calcium. When statistical analysis was used to determine the effect of 10 mM H₃PO₄ on the absorbances, the presence of 10 mM H₃PO₄ caused interference at all calcium concentration levels used.

Calcium standards in 5 mM KCl

As previously stated, 100 mM KCl only cause a 0.35 unit reduction in pK_{ca} of Arsenazo III at pH 7.0 (Bauer, 1971). It can be expected that the presence of 5 mM KCl in the standard solution do not affect apparent pK_{Ca} of Arsenazo III.

By using ΔA values, regression equation found in the presence of 5 mM (y=0.1126) (Figure G.24) was similar to that found when standards were prepared in ultrapure water y=0.1131x). This shows that presence of 5 mM KCl do not effect absorbance responses with respect to calcium concentrations of standard solutions. However *t*-statistics showed that 5 mM KCl interferes at 1 and 2 ppm calcium concentration but interferences were insignificant at higher calcium concentration levels.

Calcium standards in 0.5 mM Na₂SO₄

When calcium standards were prepared in 0.5 mM Na₂SO₄ solution, linear regression function found was y=0.1138x with a correlation coefficient of 0.9986 when ΔA values were used (Figure G.27). This was very close to that obtained in ultrapure water. However 0.5 mM Na₂SO₄ was found to interfere at 1, 2 and 3 ppm calcium concentrations according to statistical analysis. Interference of 0.5 mM KCl was insignificant when calcium concentration in standard solution was higher than 3 ppm.

Regression constants obtained from absorbance and ΔA values in the presence of different electrolytes at 650 nm are shown in Tables 6.10 and 6.11 respectively. When calcium concentration in any of these electrolytical solutions will be determined corresponding calibration equation obtained by ΔA values is used. By using calibration curves constructed in the presence of several electrolytes, interferences due these matrices could be corrected in the calcium determination.

Table 6.10. Calibration equations for calcium standards prepared in different electrolytes constructed by absorbance values at 650 nm in Arsenazo III-calcium analysis

Electrolyte	y=mx+n		
	m	n	R ²
Ultrapure Water	0.1155	0.1551	0.9986
142 mM NaCl	0.1069	0.1690	0.9988
27 mM NaHCO ₃	0.1198	0.1839	0.9984
115 mM NaCl & 27 mM NaHCO ₃	0.1127	0.1987	0.9989
1.5 mM MgCl ₂	0.1096	0.1916	0.9987
1 mM Na ₂ HPO ₄	0.1132	0.1530	0.9973
1 mM H ₃ PO ₄	0.1108	0.1596	0.9983
10 mM H ₃ PO ₄	0.1009	0.1489	0.9986
5 mM KCl	0.1152	0.1588	0.9987
0.5 mM Na ₂ SO ₄	0.1154	0.1604	0.9989

Table 6.11. Calibration equations for calcium standards prepared in different electrolytes constructed at ΔA values at 650 nm in Arsenazo III-calcium analysis

Electrolyte	$y = mx$	
	m	R^2
Ultrapure Water	0.1131	0.9980
142 mM NaCl	0.1044	0.9980
27 mM NaHCO ₃	0.1196	0.9984
115 mM NaCl & 27 mM NaHCO ₃	0.1122	0.9989
1.5 mM MgCl ₂	0.1072	0.9980
1 mM Na ₂ HPO ₄	0.1103	0.9964
1 mM H ₃ PO ₄	0.1092	0.9980
10 mM H ₃ PO ₄	0.0978	0.9973
5 mM KCl	0.1126	0.9980
0.5 mM Na ₂ SO ₄	0.1138	0.9986

6.1.3. Microplate Based Malachite Green Phosphate Assay

Spectrophotometric measurements in the malachite green assay for the phosphate determinations have been performed at different wavelengths: 610 nm (Van Veldhoven and Mannaerts, 1987; Cogan et al., 1999), 625 nm (Linge and Oldham, 2001), 640 nm (Szydłowska-Czerniak and Szyłk, 2003), 600 nm (Jeanotte et al., 2004), 650 nm (Attin et al., 2005a; Attin et al., 2005b). By Linge and Oldham (2001), broad peak between 600 nm and 635 nm and smaller peak at 435 nm were observed in spectrum scanning. Most of the wavelengths used in all above stated studies fell between 600 nm and 635 nm. However, only Attin et al. (2005a, 2005b) used 650 nm. This was probably due the use of HCl instead of H₂SO₄ in the assay.

When different electrolytical solutions were used as dissolution medium in the hydroxyapatite dissolution testing, any component in the dissolution medium should not interfere during phosphate analysis. Hydroxyapatite is the most stable calcium phosphate phase over physiological pH, thus its solubility is very low in such solutions. Generally, dilutions are needed to reduce the amount of interfering substances below the limit that they do not interfere. However, these dilutions make calcium and phosphate concentration to fall under the detection limit. A method which makes the analysis of the compound of interest possible when the high amounts of electrolytes present in the solution will be superior for the dissolution testing of hydroxyapatite. For this reason, possible interferences which may result from the presence of electrolyte in the solution were tested by preparing phosphate standards in various electrolyte solutions. All phosphate standards were prepared in electrolyte solutions instead of testing one or two standard concentrations prepared in the electrolyte solutions. Absorption spectra of solutions were scanned for all different electrolytes used to prepare phosphate standards in order to determine any alterations in light absorption spectra. Calibration curves obtained by this way will be used to determine phosphate concentration when the electrolytes are present as a matrix in the solutions.

When phosphate standards were prepared in ultrapure water or in electrolytical solutions, absorption spectra of the blank reagent showed two absorption peaks. One was at around 440-445 nm whereas the other was a wide peak between wavelengths of 600 and 640 nm with closer absorbance. This explains why different wavelengths between 610 and 650 were used in the literature. Spectra of the standard solutions with

respect to blank reagent were constructed by subtracting the absorbances of the blank solution from the absorbances of the standard solutions. Standard solutions again had a wide absorption peak between 600 and 645 nm. Absorption spectra for phosphate standards prepared in different electrolytical solutions are given in Appendix H. Absorbances measured at 650, 640, 630, 620 and 610 nm were used to construct calibration curves for all matrix matched solutions. Additionally ΔA values obtained by subtracting absorbances of blank values from absorbances of standard solutions were also used to construct calibrations curves. All calibration curves for phosphate analysis are given in Appendix H.

Regression coefficients of the all calibration equations and their correlation coefficients obtained by using absorbances values are shown in Table 6.12. Table 6.13 shows calibration equations by using ΔA values obtained by subtracting absorbance of blank solution from absorbances of standard solutions.

It is obvious that 0.25-2 ppm level of phosphate in the solution can be analyzed by using malachite green based method by measuring the absorbance at either at 650, 640, 630, 620 or 610 nm. Linear calibration curves for phosphate solutions prepared in different electrolyte solutions show that it is possible to determine the phosphate concentrations in these solutions when they individually exist in the dissolution medium as background electrolytes.

Interferences of background ions in the phosphate determination by malachite green method was also evaluated by statistical analysis methods stated previously in Section 6.1.2 Absorbance values of the phosphate standards prepared in ultrapure water measured at 650 nm were compared with the absorbances of the phosphate standards in electrolytical solutions measured at 650 nm. Assumption of the equality of population variances was tested by two-sided F -test. According to the results of F -statistics, two different two-sided t -tests (for unpaired data) were used to determine whether background electrolytes cause interferences or not at each phosphate concentration. Table 6.14 shows calculated F_0 values and upper and lower confidence limits whereas Table 6.15 shows the results of rejection or acceptance of the assumption of equality of the variances.

Table 6.12. Calibration equations obtained by using absorbances in malachite green phosphate assay

λ (nm)	$y=mx+n$	Ultrapure Water	142 mM NaCl	5 mM KCl	2.5 mM CaCl ₂	1.5 mM MgCl ₂
650	m	0.4348	0.4279	0.4549	0.4476	0.4392
	n	0.0390	0.0244	0.0344	0.0323	0.0298
	R²	0.9971	0.9934	0.9965	0.996	0.9946
640	m	0.4547	0.4496	0.4793	0.4699	0.4611
	n	0.0536	0.0378	0.0496	0.04699	0.0442
	R²	0.9966	0.9935	0.9965	0.9959	0.9947
630	m	0.4553	0.4506	0.4818	0.4706	0.4615
	n	0.0701	0.0529	0.0670	0.0642	0.0610
	R²	0.9968	0.9935	0.9966	0.9960	0.9948
620	m	0.4489	0.4438	0.4769	0.4641	0.4556
	n	0.0803	0.0620	0.0775	0.0747	0.0704
	R²	0.9968	0.9935	0.9965	0.9961	0.9947
610	m	0.4483	0.4425	0.4775	0.4645	0.4555
	n	0.0766	0.0586	0.0734	0.0709	0.0660
	R²	0.9969	0.9935	0.9966	0.9960	0.9946

(Cont. on next page)

Table 6.12. (cont.)

λ (nm)	$y=mx+n$	27 mM NaHCO ₃	115 mM NaCl / 27 mM NaHCO ₃	0.5 mM Na ₂ SO ₄	SBFA	SBFB
650	m	0.4300	0.4238	0.4453	0.4299	0.4135
	n	0.0172	0.0184	0.0353	0.0138	0.0147
	R²	0.9896	0.9904	0.9966	0.9876	0.9892
640	m	0.4557	0.4492	0.4697	0.4527	0.4391
	n	0.0317	0.0320	0.0501	0.0290	0.0265
	R²	0.9898	0.9909	0.9965	0.9884	0.9891
630	m	0.4579	0.4515	0.4717	0.4548	0.4425
	n	0.0501	0.0488	0.0675	0.0444	0.0411
	R²	0.9897	0.9909	0.9964	0.9885	0.9889
620	m	0.4533	0.4462	0.4665	0.4494	0.4376
	n	0.0606	0.0585	0.0779	0.05444	0.0499
	R²	0.9897	0.9910	0.9965	0.9889	0.9887
610	m	0.4543	0.4470	0.4696	0.4504	0.4388
	n	0.0566	0.0548	0.0716	0.0501	0.0458
	R²	0.9896	0.9910	0.9960	0.9889	0.9886

Table 6.13. Calibration equations obtained by using ΔA values in malachite green phosphate assay

λ (nm)	y=mx	Ultrapure Water	142 mM NaCl	5 mM KCl	2.5 mM CaCl ₂	1.5 mM MgCl ₂
650	m	0.4127	0.3960	0.4293	0.4213	0.4102
	R²	0.9934	0.9855	0.9920	0.9910	0.9884
640	m	0.4302	0.4162	0.4522	0.4423	0.4304
	R²	0.9925	0.9857	0.9919	0.9910	0.9884
630	m	0.4313	0.4172	0.4547	0.4429	0.4306
	R²	0.9928	0.9857	0.9921	0.9911	0.9884
620	m	0.4252	0.4107	0.4500	0.4373	0.4247
	R²	0.9928	0.9856	0.9920	0.9913	0.9881
610	m	0.4246	0.4094	0.4508	0.4374	0.4245
	R²	0.9929	0.9855	0.9921	0.9912	0.9880

(Cont. on next page)

Table 6.13. (cont.)

λ (nm)	$y=mx+n$	27 mM NaHCO ₃	115 mM NaCl / 27 mM NaHCO ₃	0.5 mM Na ₂ SO ₄	SBFA	SBFB
650	m	0.3900	0.3859	0.4209	0.3878	0.3746
	R²	0.9773	0.9791	0.9923	0.9741	0.9767
640	m	0.4136	0.4099	0.4439	0.4097	0.3981
	R²	0.9777	0.9800	0.9922	0.9757	0.9768
630	m	0.4155	0.4120	0.4456	0.4114	0.4008
	R²	0.9776	0.9801	0.9921	0.9757	0.9763
620	m	0.4111	0.4073	0.4407	0.4070	0.3961
	R²	0.9774	0.9802	0.9921	0.9763	0.9760
610	m	0.4119	0.4079	0.4417	0.4078	0.3969
	R²	0.9773	0.9802	0.9910	0.9762	0.9757

Calculated t_0 values and t values for corresponding degrees of freedom and confidence limits are shown in Table 6.16 whereas results of the rejection and acceptance of null hypothesis ($H_0 : \mu_1 = \mu_2$) are summarized in Table 6.17. According to the results of the hypothesis testing used for the determination of interferences caused by background electrolytes, all electrolytical solutions do not have significant effects on the absorbance value of the blank solution. The presence of 142 mM NaCl was found to interfere at all phosphate concentration levels except 1.25 mg/L. However t_0 value calculated at 1.25 mg/L phosphate level was closer to t values estimated by degrees of freedom and confidence interval. Although $\sigma_1^2 = \sigma_2^2$ assumption is validated, sodium chloride is found to interfere if σ_1^2 is not assumed equal to σ_2^2 .

Twenty seven millimolar NaHCO₃, solution containing 115 mM NaCl and 27 mM NaHCO₃, and SBFB solution interferes whereas 0.5 mM Na₂SO₄ do not interfere at the all phosphate concentration levels. Two point five millimolar calcium chloride solution causes interference for the analysis of the lowest phosphate concentration (0.25 mg/L). At all the other levels, the presence of calcium chloride does not cause interferences.

It was found that 1.5 mM MgCl₂ solution do not interfere at 0.5, 1.5 and 1.75 mg/L phosphate concentrations but interferes at all the other phosphate concentrations. Magnesium chloride possibly interferes at the low phosphate concentration level but when phosphate concentration is increased to 1.5 mg/L and over, interference of magnesium chloride becomes insignificant.

Five millimolar potassium chloride solution was found not to interfere at 0.5 and 1.25 mg/L phosphate level and to interfere at other levels. It is not reasonable that 5 mM KCl do not interfere at 0.5 and 1.25 mg/L phosphate levels while it is interfering at all other phosphate levels. It is therefore concluded that five millimolar potassium chloride interferes in phosphate analysis within selected confidence level (99 %).

SBFA solution interferes at all phosphate levels except 1.75 mg/L. This shows that when phosphate level increases the interference of potassium chloride becomes insignificant.

Table 6.14. Calculated F_0 values and confidence limits for rejection of null hypothesis in two-sided F -test for malachite green phosphate assay

Conc. (ppm)	142 mM NaCl $F_{19, 19, 0.025}$	27 mM NaHCO ₃ $F_{19, 14, 0.025}$	115 mM NaCl 27 mM NaHCO ₃ $F_{19, 14, 0.025}$	5 mM KCl $F_{19, 14, 0.025}$	2.5 mM CaCl ₂ $F_{19, 14, 0.025}$	1.5 mM MgCl ₂ $F_{19, 14, 0.025}$	0.5 mM Na ₂ SO ₄ $F_{19, 14, 0.025}$	SBFA $F_{19, 9, 0.025}$	SBFB $F_{19, 4, 0.025}$
0	9.277	3.702	8.150	14.559	7.690	2.928	18.250	2.167	14.519
0.25	0.863	2.248	1.649	2.679	1.557	0.477	2.081	2.437	4.770
0.5	3.327	1.406	4.097	3.384	3.474	0.568	1.649	2.960	4.086
0.75	1.543	0.751	1.105	6.863	5.901	0.849	3.827	1.894	3.340
1	0.800	1.135	0.984	4.480	3.407	0.618	2.916	3.214	10.291
1.25	1.444	1.171	1.219	8.255	10.263	1.547	7.667	2.762	4.901
1.5	1.854	0.723	2.215	3.201	4.666	2.224	13.320	4.473	7.669
1.75	0.977	1.083	0.663	2.478	4.523	1.283	9.423	2.371	3.118
Criteria for rejection	0.407 < F_0 < 2.51	0.339 < F_0 < 2.84						0.347 < F_0 < 3.67	0.281 < F_0 < 8.56

Table 6.15. Results of *F*-test for the validation of the assumption of the equality of variances by two-sided *F*-test for malachite green phosphate assay

Conc. (ppm)	142 mM NaCl	27 mM NaHCO ₃	115 mM NaCl 27 mM NaHCO ₃	5 mM KCl	2.5 mM CaCl ₂	1.5 mM MgCl ₂	0.5 mM Na ₂ SO ₄	SBFA	SBFB
0	R	R	R	R	R	R	R	A	R
0.25	A	A	A	A	A	A	A	A	A
0.5	R	A	R	R	R	A	A	A	A
0.75	A	A	A	R	R	A	R	A	A
1	A	A	A	R	R	A	R	A	R
1.25	A	A	A	R	R	A	R	A	A
1.5	A	A	A	R	R	A	R	R	A
1.75	A	A	A	A	R	A	R	A	A

A: Acceptance of null hypothesis

R: Rejection of null hypothesis.

Table 6.16. Calculated t_0 values and t values for the rejection of null hypothesis in two-sided t -tests for malachite green phosphate assay

Conc. (ppm)	142 mM NaCl		27 mM NaHCO ₃		115 mM NaCl 27 mM NaHCO ₃		5 mM KCl		2.5 mM CaCl ₂		1.5 mM MgCl ₂		0.5 mM Na ₂ SO ₄		SBFA		SBFB	
	$ t_0 $	t	$ t_0 $	t	$ t_0 $	t	$ t_0 $	t	$ t_0 $	t	$ t_0 $	t	$ t_0 $	t	$ t_0 $	t	$ t_0 $	t
0	1.882	2.807	0.605	2.750	0.626	2.787	0.072	2.819	1.066	2.787	0.410	2.704	0.710	2.819	0.074	2.763	2.670	2.807
0.25	3.973	2.704	20.866	2.704	19.084	2.704	3.090	2.704	3.719	2.704	6.119	2.704	0.743	2.704	18.637	2.763	13.806	2.807
0.5	5.734	2.756	14.726	2.704	6.893	2.756	0.264	2.750	1.001	2.750	2.068	2.704	1.590	2.704	12.222	2.763	7.714	2.807
0.75	3.618	2.704	14.026	2.704	15.814	2.704	2.861	2.779	0.172	2.771	4.679	2.704	0.573	2.750	13.560	2.763	8.992	2.807
1	2.919	2.704	12.805	2.704	13.439	2.704	3.302	2.756	2.586	2.750	4.101	2.704	1.350	2.704	13.950	2.763	8.164	2.831
1.25	2.651	2.704	10.010	2.704	11.689	2.704	1.981	2.787	0.688	2.797	2.928	2.704	1.532	2.787	9.736	2.763	9.949	2.807
1.5	2.782	2.704	6.696	2.704	10.481	2.704	3.043	2.75	1.700	2.763	1.322	2.704	2.163	2.807	5.045	2.763	7.863	2.807
1.75	2.713	2.704	5.345	2.704	8.887	2.704	13.351	2.704	2.720	2.763	1.298	2.704	1.956	2.797	1.877	2.763	7.193	2.807

Table 6.17. Results of *t*-tests for the validation of the equality of the means and interferences for malachite green phosphate assay

Conc. (ppm)	142 mM NaCl	27 mM NaHCO₃	115 mM NaCl 27 mM NaHCO₃	5 mM KCl	2.5 mM CaCl₂	1.5 mM MgCl₂	0.5 mM Na₂SO₄	SBFA	SBFB
0	A (NI)	A (NI)	A (NI)	A (NI)	A (NI)	A (NI)	A (NI)	A (NI)	A (NI)
0.25	R (I)	R (I)	R (I)	R (I)	R (I)	R (I)	A (NI)	R (I)	R (I)
0.5	R (I)	R (I)	R (I)	A (NI)	A (NI)	A (NI)	A (NI)	R (I)	R (I)
0.75	R (I)	R (I)	R (I)	R (I)	A (NI)	R (I)	A (NI)	R (I)	R (I)
1	R (I)	R (I)	R (I)	R (I)	A (NI)	R (I)	A (NI)	R (I)	R (I)
1.25	A (NI)	R (I)	R (I)	A (NI)	A (NI)	R (I)	A (NI)	R (I)	R (I)
1.5	R (I)	R (I)	R (I)	R (I)	A (NI)	A (NI)	A (NI)	R (I)	R (I)
1.75	R (I)	R (I)	R (I)	R (I)	A (NI)	A (NI)	A (NI)	A (NI)	R (I)

A: Acception of null hypothesis

R: Rejection of null hypothesis

I: Interferes

NI: Not interferences.

6.2. Characterization of Powders

Crystalline structures, specific surface areas, thermal behaviors, particle size and morphologies, calcium and phosphate molar ratios of hydroxyapatite powder synthesized in this study and commercial hydroxyapatite powder were characterized.

6.2.1. XRD Analysis of Powders

X-ray diffraction profiles of DHA and HA samples are shown in Figure 6.65. The presence of sharp diffraction peaks and splitting of major hydroxyapatite diffraction peak at 31 °C showed that commercial powder were highly crystalline. In contrast, DHA sample showed wide diffraction peaks indicative of nanocrystalline structure of the powder.

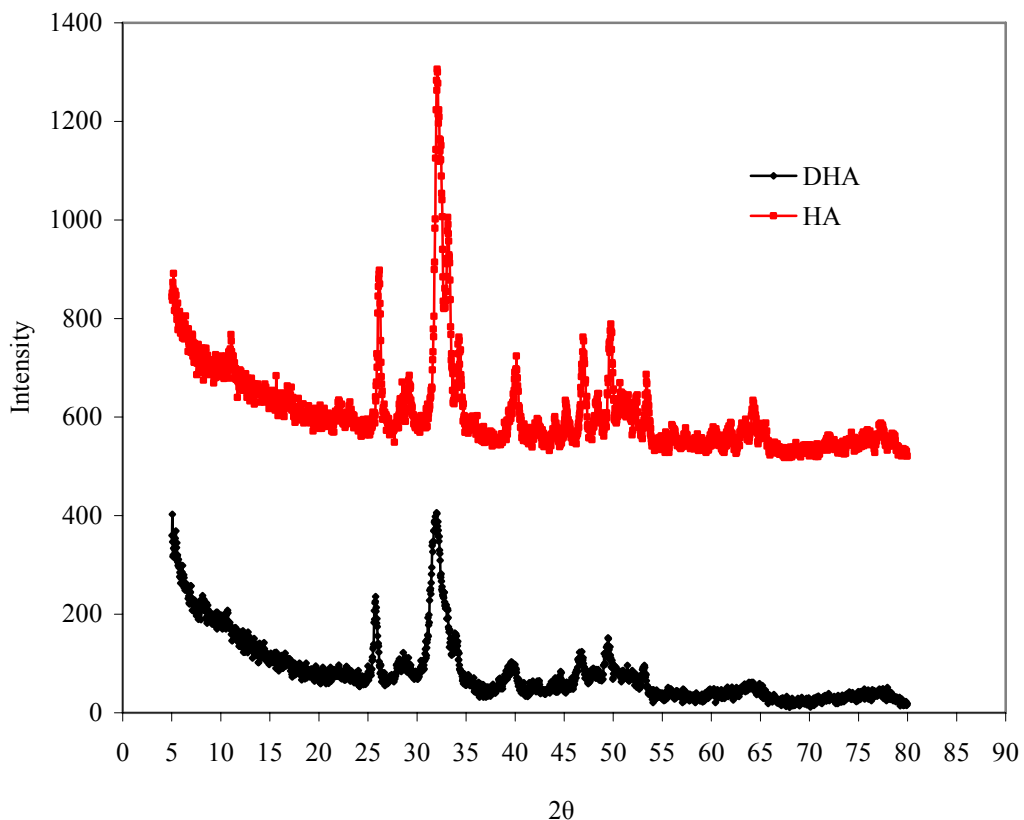


Figure 6.65. XRD profiles of DHA and HA powders.

6.2.2. Thermogravimetric Analyses

Thermogravimetric analysis and differential thermal analysis were used to determine water contents and thermal behavior of the hydroxyapatite samples. Thermogravimetric analysis results of the commercial hydroxyapatite sample (HA) are shown in Figure 6.66. HA sample showed continuous weight loss up to 300 °C. Weight loss still continued between 300 and 500 °C but with a different rate. After 500 °C, weight stays almost constant. Between 500 and 825 °C, only 0.2 wt. % reduction is observed. In total, up to 825 °C sample lost 5.67 % of its weight.

Similar to thermal behavior of HA powder, major fraction of weight loss from DHA powder was observed until 300 °C (Figure 6.67). Weight loss continued up to 950 °C. Weight loss observed between 300 and 950 °C was found to be approximately 2.5 %. Total weight loss was calculated as 10.58 wt. % when sample was heated to 950 °C.

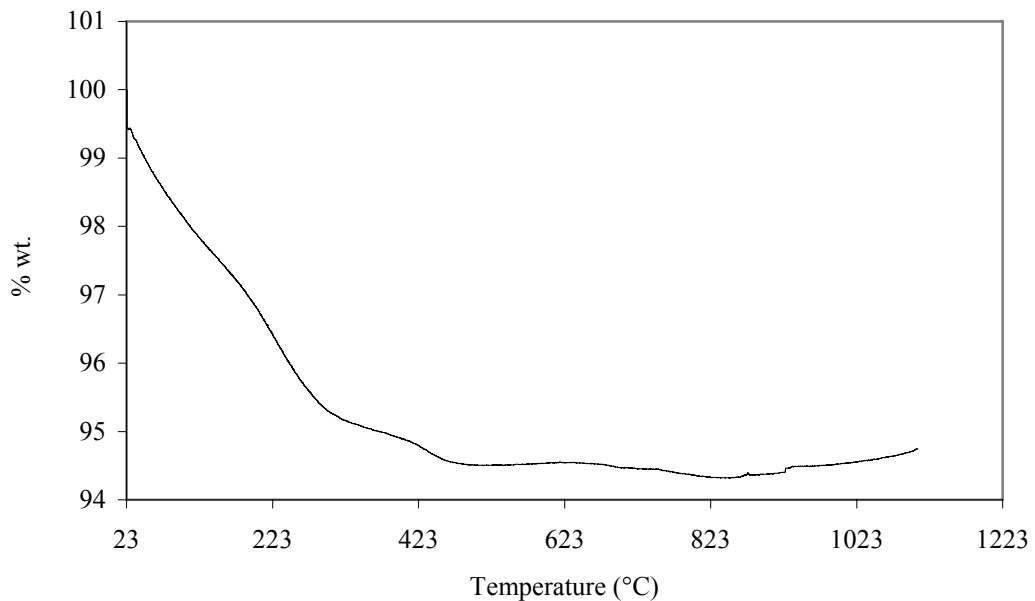


Figure 6.66. TG analysis profile of the sample HA.

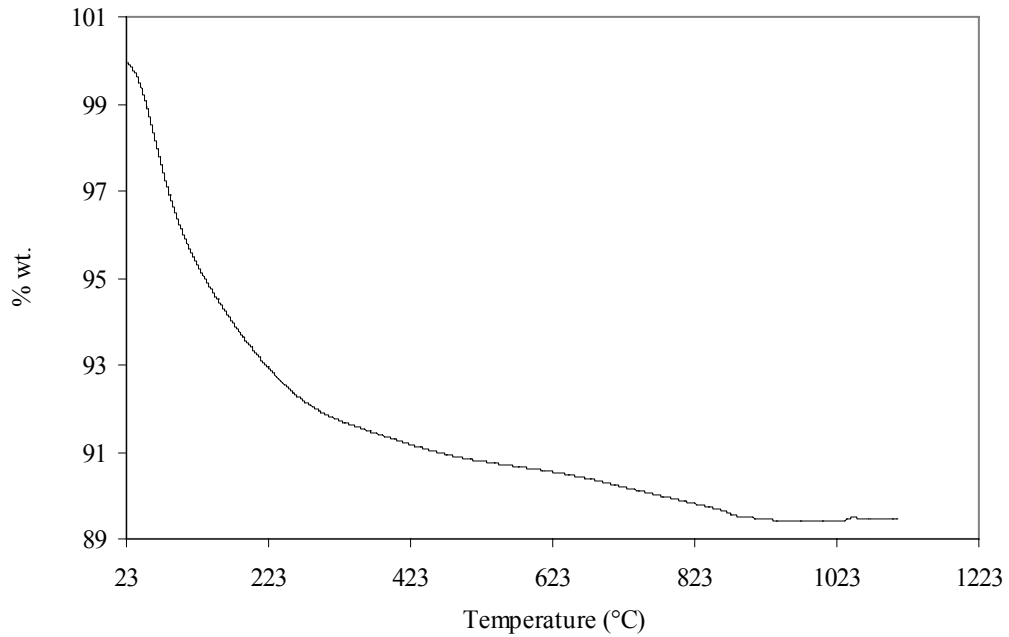


Figure 6.67. TG profile of the sample DHA.

6.2.3. BET Surface Area

Surface area and pore size measurements of hydroxyapatite powder were performed by nitrogen adsorption and desorption studies. Volumes of nitrogen adsorbed or desorbed plotted against relative pressures are shown in Figure 6.68.

As it can be seen from the graph, nitrogen adsorption and desorption behavior of hydroxyapatite almost exhibited Type II gas physisorption behavior according to IUPAC 1985 classification (Rouquerol et al., 1999). BET adsorption model was therefore used to calculate surface area. BET surface area of hydroxyapatite was found as 74.59 m²/g. Nitrogen adsorption and desorption profiles of DHA powder is shown in Figure 6.69. This sample also exhibited Type II physisorption behavior (Rouquerol et al., 1999). BET surface area was calculated to be 172.73 m²/g.

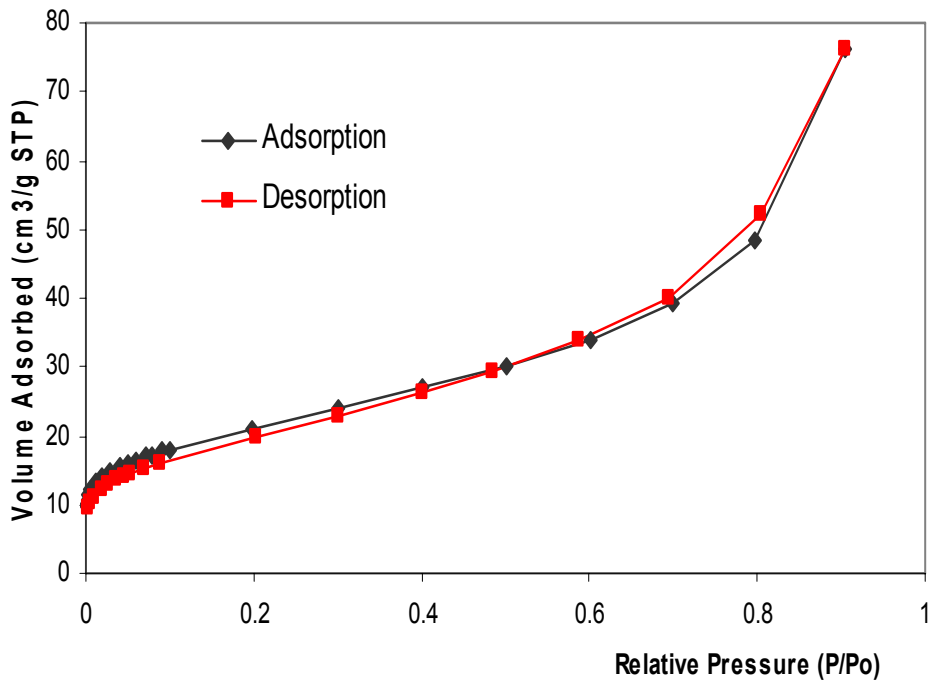


Figure 6.68. Adsorption and desorption of N₂ on HA powder.

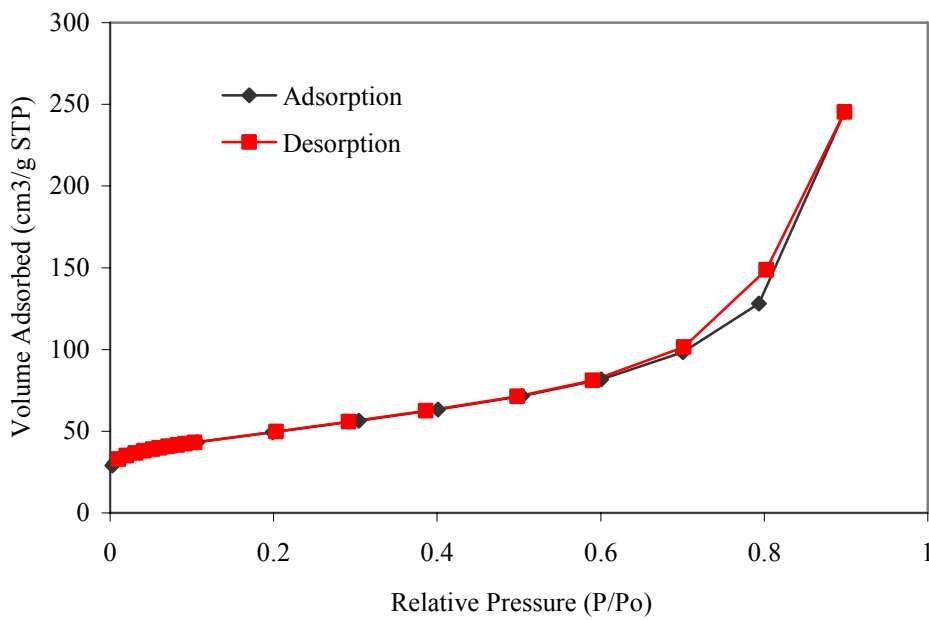


Figure 6.69. Adsorption and desorption of N₂ on DHA powder.

6.2.4. Scanning Electron Microscopy

Scanning electron microscopy was used to analyze morphology and particle size of commercial hydroxyapatite (HA) and hydroxyapatite powder synthesized in this study (DHA). SEM micrographs of commercial hydroxyapatite powder are shown in Figure 6.70. Sample was composed of rod-like particles. Major fraction of the particles was almost 200 nm in length and 30 nm in width. Smaller particles were also present in the sample.

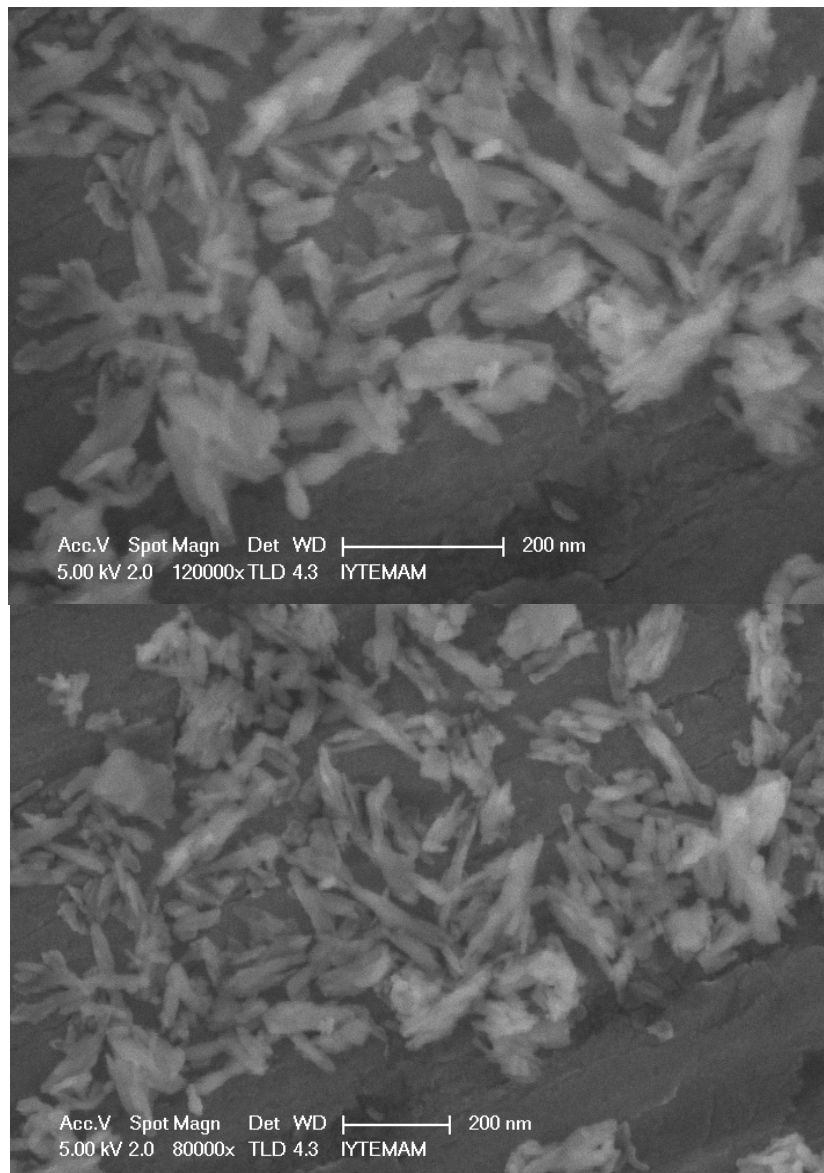


Figure 6.70. SEM micrographs of HA powder.

Particles of DHA sample were smaller than those of HA sample (Figure 6.71). They were as small as 10-20 nm in sizes. It should be noted that particles were mainly agglomerated. Because of small particle sizes, SEM analysis was performed at its limits of resolution. In order to reveal exact particle morphology, transmission electron microscopy (TEM) analysis should be used. However, small particle sizes of DHA obtained from SEM analysis was in accord with XRD results. XRD profile of DHA powder showed broad peaks indicative of either amorphous or nanocrystalline structure. Line broadening in XRD analysis was possibly the result of nanocrystals of the powder.

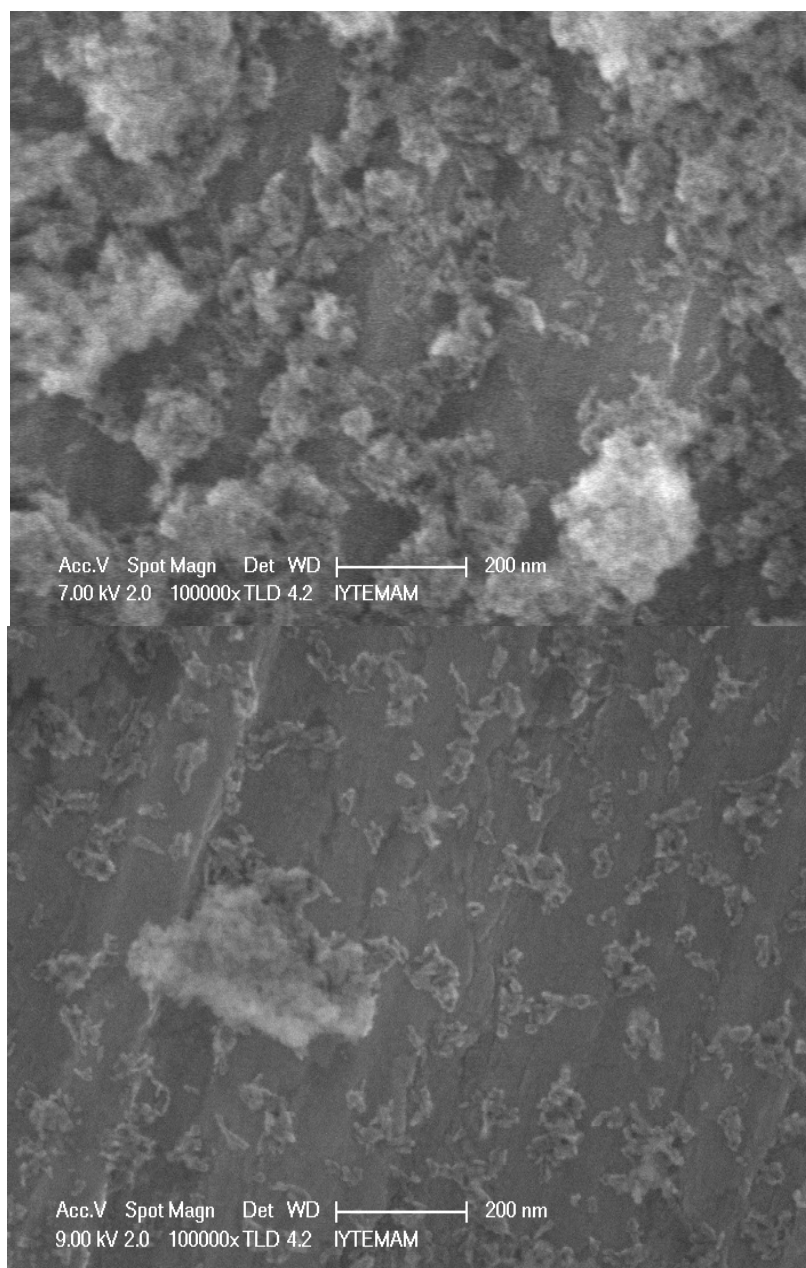


Figure 6.71. SEM micrographs of DHA powder.

6.2.5. FTIR Analysis

Fourier transform infrared radiation analysis was used to characterize the structures of hydroxyapatite powders. FTIR spectrum of the nano-sized hydroxyapatite powder prepared in this study is shown in Figure 6.72.

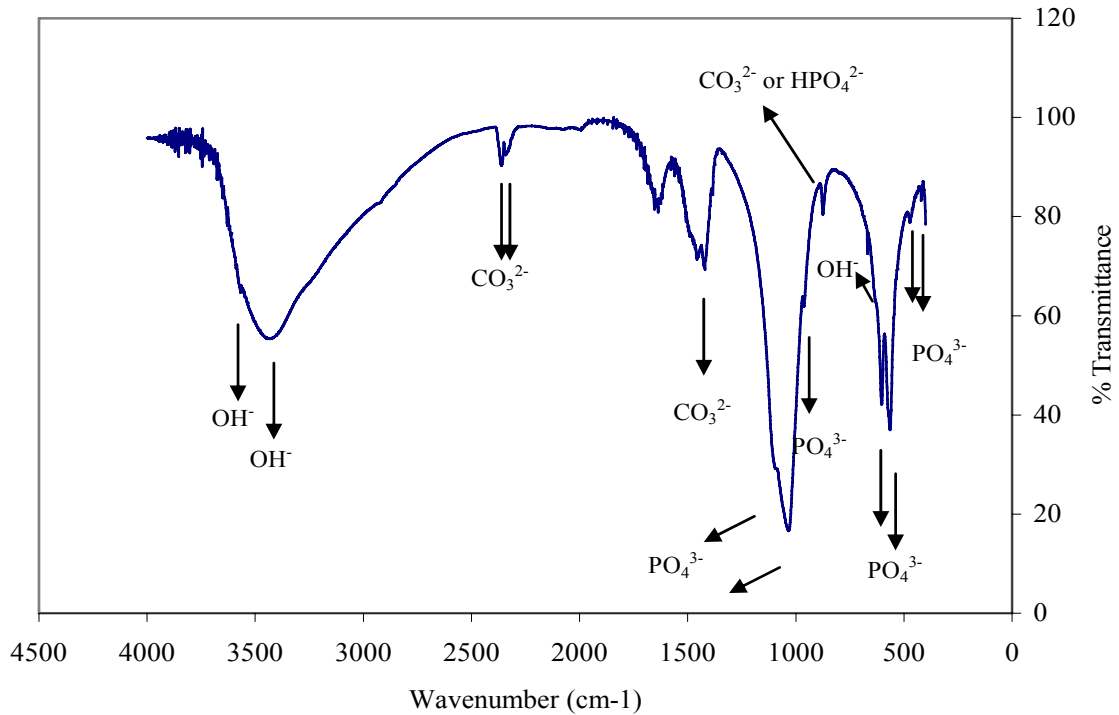


Figure 6.72. FTIR spectrum of DHA powder.

Hydroxyapatite synthesized in this study (DHA) showed characteristic peaks due to the presence of PO_4^{3-} ion (962 cm^{-1} for ν_1 , 473 cm^{-1} for ν_2 , 1033 and 1087 cm^{-1} for ν_3 and 563 and 603 cm^{-1} for ν_4) (Gibson and Bonfield, 2002; Padilla et al., 2008). The peaks observed at *ca.* 962 cm^{-1} and 473 cm^{-1} were due to ν_1 -non degenerate P-O symmetric stretching mode and doubly degenerate ν_2 O-P-O bending mode, respectively (Liou et al., 2004). Peaks at *ca.* 1033 and 1087 cm^{-1} were attributed to triply degenerate ν_3 antisymmetric P-O stretching mode whereas the peaks at approximately 563 and 603 cm^{-1} were the result of triply degenerate ν_4 O-P-O bending mode (Liou et al., 2004). Broad band observed at *ca.* 3432 cm^{-1} were assigned to the presence of absorbed water (Ye et al., 2009). Peaks observed nearly at 3571 and 632 cm^{-1} are reported to be the OH

stretching and liberation bands, respectively which are characteristic for hydroxyapatite (Ye et al., 2009). In our sample, these peaks observed at wavelengths of ca. 3568 cm^{-1} and 634 cm^{-1} . The band at 634 cm^{-1} was a shoulder instead of a peak.

FTIR analysis not only gives information on the presence of carbonate substitution but also provides the nature of carbonate substitution in hydroxyapatite lattice. Carbonate substitution in hydroxyapatite occurs in two sites, PO_4^{3-} (B-type) and OH^- sites (A type) (Gibson and Bonfield, 2002). Simultaneous substitution of phosphate and hydroxyl groups with carbonate yields AB-type carbonate substituted hydroxyapatite (Gibson and Bonfield, 2002). Substitution of carbonate into the lattice as well as the type of substitution has been determined by the presence and the positions of the carbonate bands in the FTIR spectra (Gibson and Bonfield, 2002; Padilla et al., 2008; Li et al., 2008; Lafon et al., 2008). Peaks found at 1450 , 1410 and 873 cm^{-1} are assigned to the peaks resulting from the B-type carbonate substitution (Landi et al., 2004). Peaks at 1450 , 1430 and 870 cm^{-1} were also reported for B-type carbonate substitution (Landi et al., 2003). On the other hand A-type substitution results in the generation of peaks at 1540 , 1450 and 880 cm^{-1} (Landi et al., 2003). It should be noted that the peak observed at 1450 cm^{-1} is reported for both A- and B-type carbonate substitution. Additionally peak found at 866 cm^{-1} was assigned to the labile or absorbed carbonate (Padilla et al., 2008; Lafon et al., 2008).

DHA sample showed peaks around 1420 and 1457 cm^{-1} which indicate the presence of B-type substitution. Additionally FTIR spectrum of the sample DHA showed noises between wavelengths of 1515 and 1578 cm^{-1} . One of the A-type carbonate peaks which is observed at 1540 cm^{-1} lies within this region. However, our sample did not show any peaks at 1540 cm^{-1} . Ratio of the intensities of the peaks observed at 880 and 873 cm^{-1} can be used to determine the ratio of A-type to B-type substitution (Gibson and Bonefield, 2002). Our sample had a single peak at 874 cm^{-1} which can be assigned to B-type substitution. The presence of any peak at 880 cm^{-1} was not observed in the sample DHA. However wavelength of 880 cm^{-1} is present within the tail of the peak observed at 874 cm^{-1} . There might be an overlap of these two peaks only if the absorbance at 880 cm^{-1} was very low when compared to that found at 874 cm^{-1} . According to the carbonate bands observed, our sample was found to be B-type carbonate substituted apatite. This finding coincides with Ca/P ratio of the sample. Calcium to phosphate molar ratio of the sample was found to be the value greater than stoichiometric ratio of 1.67. This is possible only if carbonate substitutes the phosphate

groups in the sample. In FTIR spectrum of the sample DHA, double peaks were also observed at 2343 and 2359 cm^{-1} . Bayraktar and Tas (2001) reported two peaks observed at 2368-2361 cm^{-1} as a combination of ν_2 and ν_3 CO_3^{2-} bands. In the light of their study, peaks observed at 2343 and 2359 cm^{-1} in the FTIR spectrum of DHA were assigned to the presence of carbonate in the sample. The peak present at 420 cm^{-1} could not be assigned to any functional group. One study however assigns the peak at 470-420 cm^{-1} to the presence of PO_4^{3-} ion (Pramanik et al., 2005).

Although the presence of the peak at 873 cm^{-1} is attributed to the carbonate present in the sample, there are studies in which the peak observed at around 868, 874 or 875 cm^{-1} was used as an indication of the presence of HPO_4^{2-} in hydroxyapatite (Furuzono et al., 2000; Zhang et al., 2002; Kuriakose et al., 2004; Siddharthan et al., 2004; Hutchens et al., 2006). The band observed at ca. 874 cm^{-1} is not only evidence for the presence of HPO_4^{2-} ion. The peaks observed at 1421, 1458 cm^{-1} (Zhang et al., 2002), 1094 cm^{-1} (Siddharthan et al., 2004), 530 cm^{-1} (Furuzono et al., 2000), and 1130 cm^{-1} (Lin et al., 2001). Vibration peaks for HPO_4^{2-} were also reported at 2900 cm^{-1} (ν_1), 988 cm^{-1} (ν_2), 872 cm^{-1} (ν_3), 524 cm^{-1} (ν_4), 1212 cm^{-1} (ν_5) and 1054 cm^{-1} (ν_6) by Prabakaran and Rajeswari (2006). None of these peaks except those at 874 cm^{-1} , 1420 cm^{-1} and 1457 cm^{-1} were detected in FTIR spectra of the sample DHA. The presence of the peaks observed at 874 cm^{-1} , 1420 cm^{-1} and 1457 cm^{-1} are used for the indication of B-type carbonate substitution of carbonate into hydroxyapatite structure.

Two more peaks were also observed for the sample DHA at 668 and 1385 cm^{-1} . The peak found at 668 cm^{-1} was assigned to OH group (Nayak et al., 2010). van der Houwen et al. (2003) relates the bands observed in the range of 1300-1500 cm^{-1} to the presence of carbonate and/or hydrogen phosphate ion. They also report that the peak observed at 1385 cm^{-1} may be due to the presence of sodium or chloride ions in the sample. Similarly, Lafon et al. (2003) assigns the peak at 1384 cm^{-1} to the presence of nitrates coming from precursors used in the synthesis of the powders. The peak found at 1385 cm^{-1} in FTIR profile of the sample DHA had a very low intensity suggesting that nitrate in the sample, if any, was in insignificant amount.

FTIR spectrum of commercial hydroxyapatite powder (HA) is shown in Figure 6.73. Peaks generated due to the presence of phosphate ion were observed at 473, 565, 602, 963 and 1065 cm^{-1} . The peak observed at 1065 cm^{-1} was in fact a wide broad band observed between 1018 and 1122 cm^{-1} which includes two bands (ca. 1033 and 1087 cm^{-1}) assigned to triply degenerate ν_3 antisymmetric P-O stretching mode (Liou et al.,

2004). Like the sample DHA, HA also exhibited a peak at 419 cm^{-1} and this peak was also attributed to the presence of PO_4^{3-} ion (Pramanik et al., 2005). The broad band observed at 3446 cm^{-1} was assigned to the adsorbed water on the sample HA whereas bands observed at 3568 and 631 cm^{-1} were attributed to the structural hydroxyl groups found in the sample.

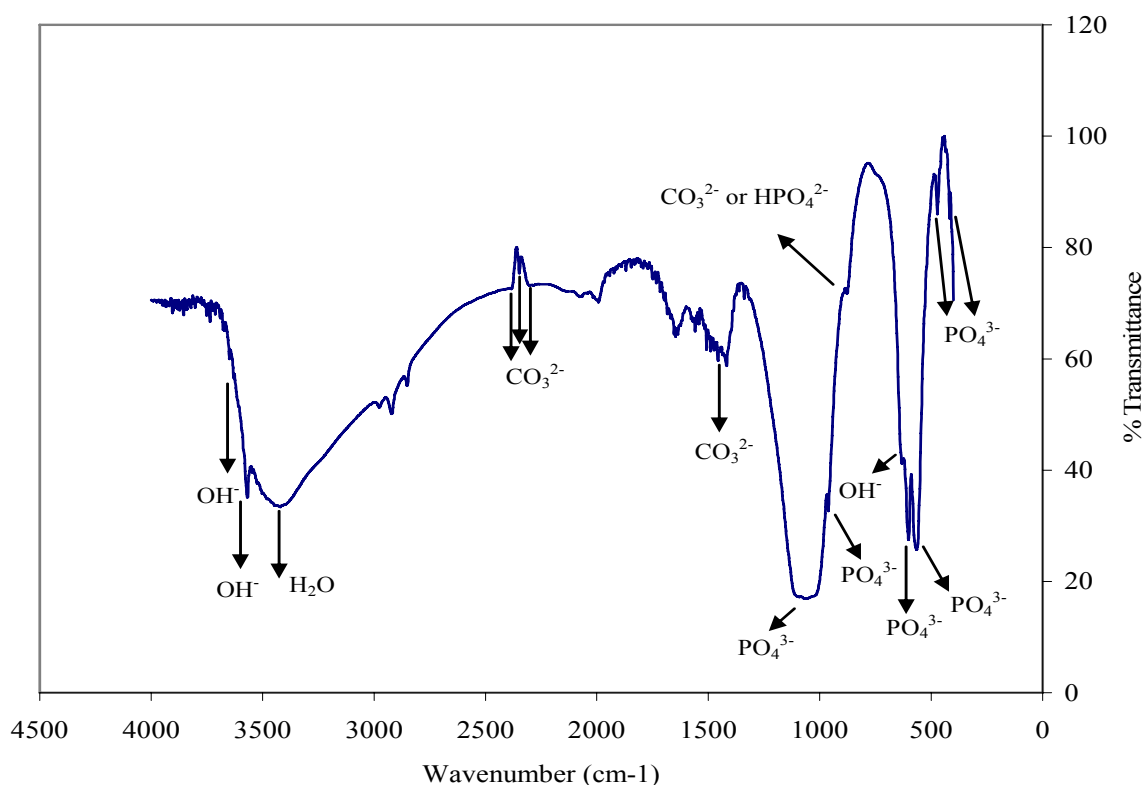
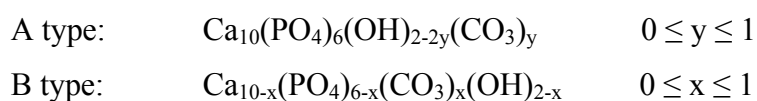


Figure 6.73 FTIR spectra of HA powder.

Carbonate bands in the spectrum of HA were observed at 878 , 1418 , 1456 and 2347 cm^{-1} . Peaks observed at 1418 and 1456 cm^{-1} together with Ca/P ratio of the HA sample which was greater than stoichiometric ratio of 1.67 suggested that this powder is possibly B-type carbonated apatite. Two shoulders at ca. 2384 and 2306 cm^{-1} were also observed for this sample. These peaks were also assigned to a combination of ν_2 and ν_3 CO_3^{2-} bands (Bayraktar and Tas, 2001).

However, the small peak observed at 878 cm^{-1} was between 880 and 870 cm^{-1} which are generally used to discriminate between A- and B-type carbonate substitutions, respectively (Gibson and Bonefield, 2002).

A and B apatites are generally expressed as following formulas (Lafon et al., 2008).



Here it should be stated that B-type carbonated apatite formula is given in a way that no other ion substitute calcium vacancies generated upon carbonate substitution into the lattice. When carbonate substitution is A-type where carbonate substitutes into hydroxyl groups Ca/P molar ratio does not deviate from the stoichiometric value (1.67). Since B-type carbonate substitution is the substitution of PO_4^{3-} ion with carbonate, Ca/P ratio becomes $(10-x)/(6-x)$ where x ranges between 0 and 1. Ca/P molar ratio therefore ranges between 1.67 and 1.8.

In FTIR spectrum of the sample HA, series of peaks with low intensities appearing as noises were also observed in the ranges of $1418\text{-}1578\text{ cm}^{-1}$ and $1627\text{-}1973\text{ cm}^{-1}$. These peaks might be related to the presence of carbonate in the sample or to the absorbed carbondioxide on the sample. Another interesting feature was the occurrence of the weak peak at 3649 cm^{-1} with a very low intensity. This peak was assigned to stretching vibrations OH groups of $\text{Ca}(\text{OH})_2$ by Ślósarczyk et al. (2005). In their study this sample was treated at $1250\text{ }^\circ\text{C}$ and contained calcium oxide.

Additionally it was not possible to assign the peaks observed at 1339 , 1647 , 1993 , 2851 , 2920 and 2970 cm^{-1} to the presence of any other groups. Summary of the FTIR peaks and their assignments according to the above stated literature are shown in Table 6.18.

Table 6.18. FTIR peaks of hydroxyapatite powders and their assignments

Hydroxyapatite IR Peak Assignments and Wavenumbers (cm ⁻¹)	
DHA	HA
420 PO ₄ ³⁻	419 PO ₄ ³⁻
473 PO ₄ ³⁻ v2	473 PO ₄ ³⁻
563 PO ₄ ³⁻ v4	565 PO ₄ ³⁻
603 PO ₄ ³⁻ v4	602 PO ₄ ³⁻
634 OH ⁻	631 OH ⁻
668	
874 CO ₃ ²⁻ (B type) or HPO ₄ ²⁻	878 CO ₃ ²⁻ (B type) or HPO ₄ ²⁻
962 PO ₄ ³⁻	963 PO ₄ ³⁻
1033 PO ₄ ³⁻	1065 (1018-1122 wide peak) PO ₄ ³⁻
1087 PO ₄ ³⁻	1339
1385 (nitrates or CO ₃ ²⁻ or HPO ₄ ⁻)	1418 CO ₃ ²⁻ B type
1420 CO ₃ ²⁻ B type	1456 CO ₃ ²⁻ B type
1457 CO ₃ ²⁻ B type	1647
1534-1576	1993
1636	2384 CO ₃ ²⁻
1992	2306 CO ₃ ²⁻
2343 CO ₃ ²⁻	2347 CO ₃ ²⁻
2359 CO ₃ ²⁻	2851
3432 OH ⁻	2920
3568 OH ⁻	2976
	3446 H ₂ O
	3568 OH ⁻
	3649 OH ⁻

6.2.6. Calcium/ Phosphate Molar Ratios

Calcium phosphate molar ratios of the powders were calculated after dissolving powders in hydrochloric acid and diluting to analysis ranges with ultrapure water. Calcium and phosphate concentrations were determined by Arsenazo III calcium analysis and malachite green phosphate assay. Along with the hydroxyapatite powders, commercial CaHPO_4 powder was used as reference.

Ca/P ratios of hydroxyapatite powders were found as 1.70 and 1.78 for HA and DHA powders respectively. Ca/P ratio of CaHPO_4 was found as 1.01 which was exactly equal to the theoretical value of calcium to phosphorous molar ratio of CaHPO_4 .

6.3. Dissolution Tests of Cold Isostatically Pressed Hydroxyapatite Pellets

Preliminary dissolution experiments performed by equilibrating uniaxially pressed hydroxyapatite pellets showed that monitoring of low level calcium concentrations in dissolution media is somewhat problematic. We were able to analyze calcium concentrations during equilibrations in ultrapure water by ICP-MS. However, for the determination of low levels of calcium in solutions containing 142 mM NaCl by ICP-MS was avoided due to the possibilities of interferences since carrier gas was argon and argon chloride formation in the presence of higher concentrations of chloride. It is well known that solutions with high solid contents are subject to spectroscopic and non-spectroscopic interferences and orifice clogging (Chen and Jiang, 2002). Ar^+ causes interferences for $^{40}\text{Ca}^+$ in ICP-MS analysis (Chen and Jiang, 2002). ICP-AES was therefore used for analysis of calcium in 142 mM NaCl. However, dilution of sodium in the solutions is required to reduce sodium content to 20 ppm in the solutions. After 200 times diluting the solutions in which sodium content was reduced to 15 ppm, calcium concentrations fell below the detection limit. After 50 times diluting the samples we were unable to detect calcium in the solutions.

Due to the problems associated with the calcium determination in 142 mM NaCl solution, hydroxyapatite pellets were immersed in 142 mM NaCl for 2 days. Calcium contents of the pellets before and after dissolutions were determined by ICP-AES analysis. Only 2 % hydroxyapatite was dissolved in this solution. Since the

hydroxyapatite is stable in physiological and alkaline pH values, difference in calcium contents of the powders before and after dissolution will be low.

In order to determine dissolution behavior of hydroxyapatite in solutions which contain ions found in the blood plasma, a method which makes it possible to determine ppm levels of calcium in the presence of high concentrations of other ions was needed. After the modification of Arsenazo III method for 1 to 8 ppm calcium containing solutions and testing the interference of several ions on the calcium analysis, calcium concentrations in dissolution media were analyzed by Arsenazo III-calcium analysis.

Malachite green phosphate suitable for ppm levels of phosphate determination were also tested for the interferences of background ions in the phosphate determination. Phosphate contents of the dissolution media are then determined by malachite green phosphate assay.

In order to test the dissolution of hydroxyapatite powders, hydroxyapatite discs were produced by cold isostatic press. Table 6.19 shows properties of hydroxyapatite discs after cold isostatic pressing. Pellets were found to be 51 ± 2 % dense after isostatic pressing. Percent densification of DHA pellet upon isostatic pressing was calculated as 53 ± 1 % (Table 6.20).

Two different hydroxyapatite powders, commercial hydroxyapatite (HA) and nano-sized hydroxyapatite synthesized in this study (DHA) were used in dissolution tests. Isostatically pressed HA and DHA pellets were immersed in different electrolytes. Advantage of the use of isostatically pressed discs is that they keep their integrities upon equilibration in dissolution media. All pellets prepared from commercial powder were kept intact during equilibration for 1 month. However, nano-sized hydroxyapatite powder was disintegrated into smaller parts but not into powdered form.

Dissolution of commercial hydroxyapatite pellet were tested in carbon dioxide free ultrapure water, 142 mM NaCl, 27 mM NaHCO₃, 115 mM NaCl & 27mM NaHCO₃ and 1.5 mM MgCl₂ solutions. Discs were also tested in ultrapure water and 142 mM NaCl solutions in which dissolved carbon dioxide were not removed. Dissolution of nano-sized hydroxyapatite powder which was synthesized in this thesis was tested in ultrapure water, 142 mM NaCl, 27 mM NaHCO₃ solutions.

Throughout the dissolution, pH, conductivity, calcium and phosphate concentrations of dissolution media were measured.

Table 6.19. Properties of HA pellets obtained by cold isostatic pressing

No	Weight (g)	D (mm)	h (mm)	Volume (cm ³)	Density (g/cm ³)	Densification (%)	Porosity (%)
1	0.2173	9.08	1.82	0.12	1.84	58	42
2	0.2381	9.08	2.40	0.16	1.53	48	52
3	0.2244	9.07	2.09	0.14	1.66	53	47
4	0.2284	9.09	2.16	0.14	1.63	52	48
5	0.2388	9.06	2.30	0.15	1.61	51	49
6	0.2148	9.15	2.05	0.13	1.59	50	50
7	0.2269	9.13	2.11	0.14	1.64	52	48
8	0.2343	9.02	2.21	0.14	1.66	53	47
9	0.2199	9.11	2.11	0.14	1.60	51	49
10	0.2331	9.10	2.19	0.14	1.64	52	48
11	0.2407	8.98	2.30	0.15	1.65	52	48
12	0.2203	9.16	2.15	0.14	1.55	49	51
13	0.2360	9.07	2.24	0.14	1.63	52	48
14	0.2234	9.11	2.11	0.14	1.62	51	49
15	0.2378	9.04	2.24	0.14	1.65	52	48
16	0.2207	9.10	2.18	0.14	1.56	49	51
17	0.2279	9.13	2.19	0.14	1.59	50	50
18	0.2278	9.13	2.21	0.14	1.57	50	50

(Cont. on next page)

Table 6.19. (cont.)

No	Weight (g)	D (mm)	h (mm)	Volume (cm³)	Density (g/cm³)	Densification (%)	Porosity (%)
19	0.2313	9.08	2.25	0.15	1.59	50	50
20	0.2271	9.13	2.22	0.15	1.56	49	51
21	0.2366	9.01	2.29	0.15	1.62	51	49
22	0.2394	9.07	2.30	0.15	1.61	51	49
23	0.2270	9.04	2.16	0.14	1.64	52	48
24	0.2352	9.07	2.28	0.15	1.60	51	49
25	0.2357	9.08	2.25	0.15	1.62	51	49
26	0.2247	9.12	2.26	0.15	1.52	48	52
27	0.2421	9.05	2.30	0.15	1.64	52	48
28	0.2349	9.02	2.29	0.15	1.61	51	49
29	0.2390	9.02	2.31	0.15	1.62	51	49
30	0.2339	9.05	2.24	0.14	1.62	51	49
Average	0.2306	9.08	2.21	0.14	1.62	51	49
Std.Dev.	0.0075	0.04	0.11	0.01	0.06	2	2

Table 6.20. Properties of DHA pellets obtained by cold isostatic pressing

No	Weight (g)	D (mm)	h (mm)	Volume (cm³)	Density (g/cm³)	Densification (%)	Porosity (%)
1	0.2397	8.55	2.50	0.1435	1.67	53	47
2	0.2398	8.49	2.45	0.1387	1.73	55	45
3	0.2456	8.70	2.52	0.1498	1.64	52	48
4	0.2416	8.61	2.50	0.1456	1.66	53	47
5	0.2392	8.63	2.49	0.1457	1.64	53	48
6	0.2432	8.52	2.48	0.1414	1.72	54	46
7	0.2430	8.59	2.51	0.1455	1.67	53	47
8	0.2444	8.58	2.44	0.1411	1.73	55	45
9	0.2396	8.60	2.51	0.1458	1.64	52	48
10	0.2441	8.65	2.44	0.1434	1.70	54	46
11	0.2364	8.68	2.38	0.1408	1.68	53	47
12	0.2402	8.55	2.46	0.1412	1.70	54	46
13	0.2421	8.62	2.54	0.1482	1.63	52	48
14	0.2363	8.63	2.46	0.1439	1.64	52	48
15	0.2461	8.63	2.51	0.1468	1.68	53	47
16	0.2401	8.63	2.46	0.1439	1.67	53	47
17	0.2418	8.51	2.48	0.1411	1.71	54	46
18	0.2394	8.63	2.47	0.1445	1.66	52	48

(Cont. on next page)

Table 6.20. (cont.)

No	Weight (g)	D (mm)	h (mm)	Volume (cm³)	Density (g/cm³)	Densification (%)	Porosity (%)
19	0.2397	8.68	2.48	0.1468	1.63	52	48
20	0.2399	8.54	2.54	0.1455	1.65	52	48
21	0.2434	8.59	2.57	0.1489	1.63	52	48
22	0.2386	8.55	2.47	0.1418	1.68	53	47
23	0.2405	8.56	2.55	0.1467	1.64	52	48
24	0.2398	8.55	2.48	0.1424	1.68	53	47
25	0.2430	8.70	2.46	0.1462	1.66	53	47
26	0.2401	8.62	2.49	0.1453	1.65	52	48
27	0.2400	8.57	2.40	0.1384	1.73	55	45
28	0.2403	8.58	2.43	0.1405	1.71	54	46
29	0.2398	8.64	2.46	0.1442	1.66	53	47
30	0.2423	8.53	2.52	0.1440	1.68	53	47
31	0.2409	8.53	2.50	0.1429	1.69	53	47
32	0.2462	8.51	2.55	0.1450	1.70	54	46
33	0.2386	8.55	2.48	0.1424	1.68	53	47
34	0.2429	8.51	2.50	0.1422	1.71	54	46
Average	0.2411	8.59	2.48	0.1439	1.6757	53	47
Std.Dev.	0.0024	0.0577	0.0417	0.0027	0.0306	1	1

Conductivity and pH changes during dissolution:

Changes in pH values of the dissolution media together with calcium and phosphate release were monitored in order to predict their dissolution behavior of hydroxyapatite pellets. Due to the problem of stabilization of pH during measurements, pH values of the dissolution media were measured at 25 °C after the removal of hydroxyapatite pellets from the dissolution media. Figure 6.74 shows variation of pH with time during immersion of hydroxyapatite pellets in ultrapure water and 142 mM NaCl which were not exposed to dissolved carbon dioxide removal together with 27 mM NaHCO₃ solution. Because of the difficulties associated with pH measurement of ultrapure water, initial pH values could not be measured. However at the end of 3 hours equilibration pH was found to be 6.37. During incubation pH reaches to 7.27 and stays constant thereafter. Initial pH value of 142 mM NaCl was 6.09 however after 24 hour it reaches to 7.08. pH was measured as 7.27 after 336 hours incubation. Initial pH of the bicarbonate solution was 8.72. Slight decrease was observed after 1 hour equilibration. At the end of 336 hours pH was measured as 8.63.

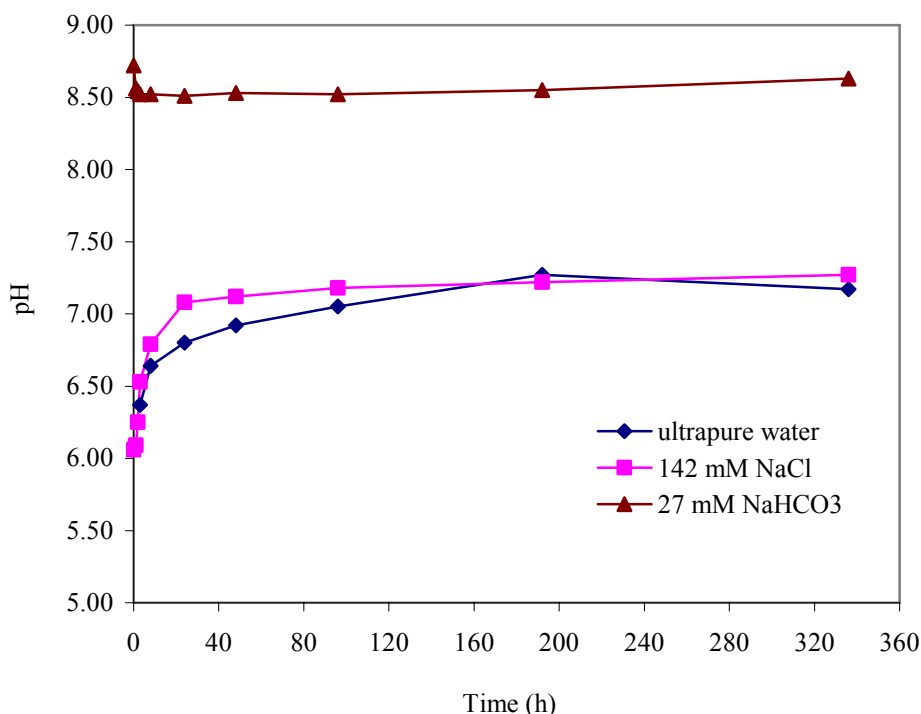


Figure 6.74. Time dependent pH changes during dissolution of HA pellets in ultrapure water, 142 mM NaCl and 27 mM NaHCO₃.

When hydroxyapatite pellets were immersed in CO₂ free ultrapure water, pH reached to 7.01 at the end of 720 hours (Figure 6.75). During equilibration in CO₂ free 142 mM NaCl, pH increases from 5.86 to 7.25. Similar behavior was also observed for DHA pellets immersed in CO₂ free ultrapure water and CO₂ free 142 mM NaCl. pH values was 7.31 and 7.27 for 142 mM NaCl and ultrapure water, respectively after 720 hours. During the dissolution of DHA in 27 mM NaHCO₃, initial pH increased slightly during hours of incubation then stayed almost constant (Figure 6.76).

Since conductivities of the solutions is directly related to total dissolved solids in dissolution media, conductivity measurements may be useful for the determination of dissolution behaviors of the powders. However, conductivities measured during dissolution were only useful for the monitoring dissolution in ultrapure water. According to the conductivity measurements, solution ionic strength reaches maximum after 96 hours during incubation of HA pellets in ultrapure water (Figure 6.77). However it was not possible to determine conductivity changes in 142 mM NaCl and 27 mM NaHCO₃ since these solutions already had considerably higher amounts of background ions (Figure 6.78).

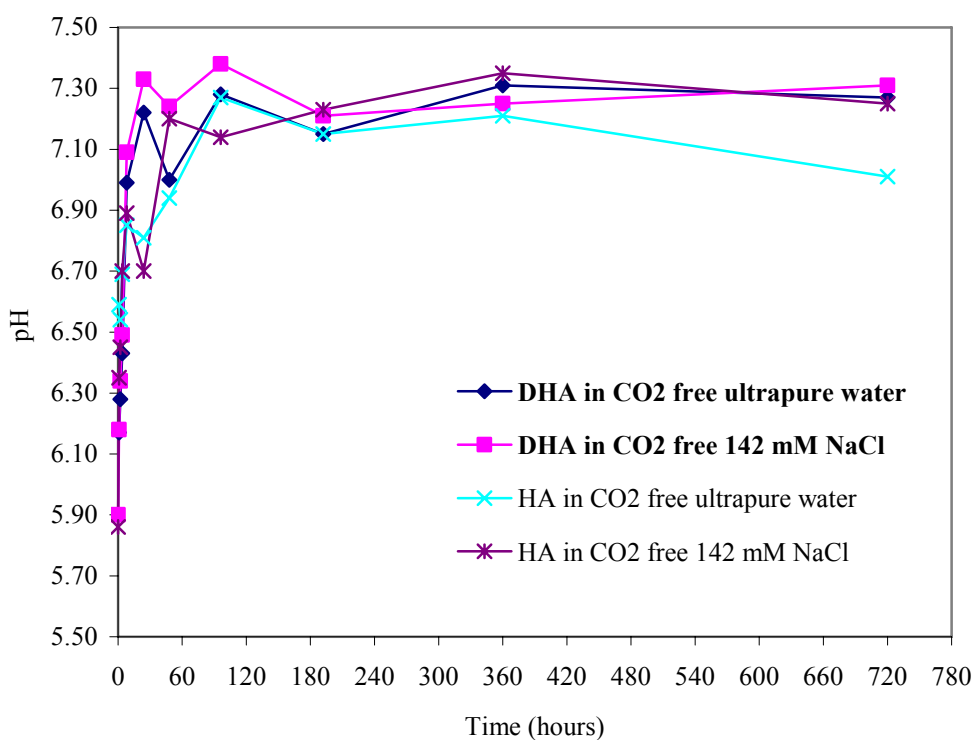


Figure 6.75. Time dependent pH changes during dissolution of HA and DHA pellets in CO₂ free ultrapure water, CO₂ free 142 mM NaCl and 27 mM NaHCO₃.

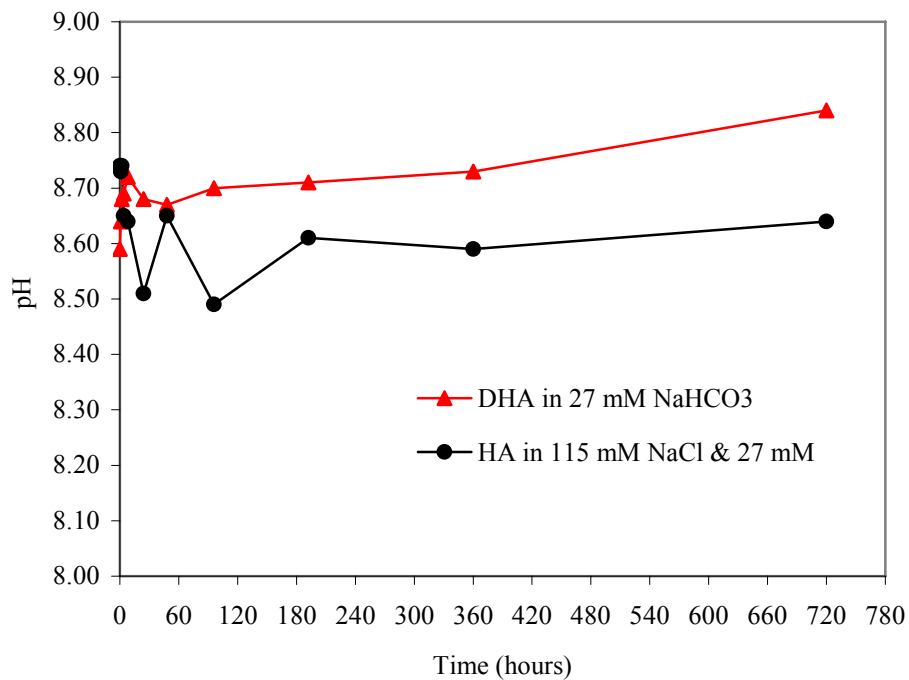


Figure 6.76. Time dependent pH changes during dissolution of DHA pellets in 27 mM NaHCO₃ and HA pellets in 115 mM NaCl and 27 mM NaHCO₃ containing solution.

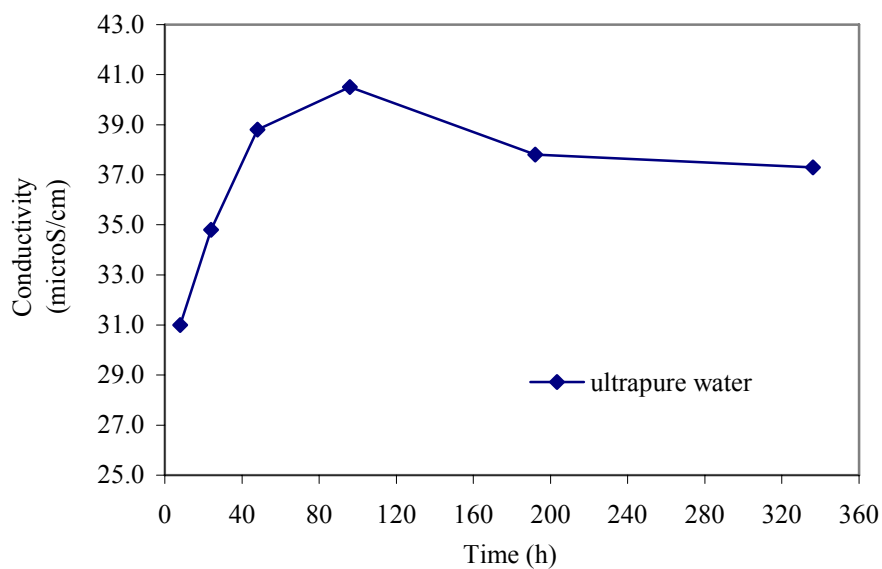


Figure 6.77. Conductivities of the solutions during HA dissolution in ultrapure water.

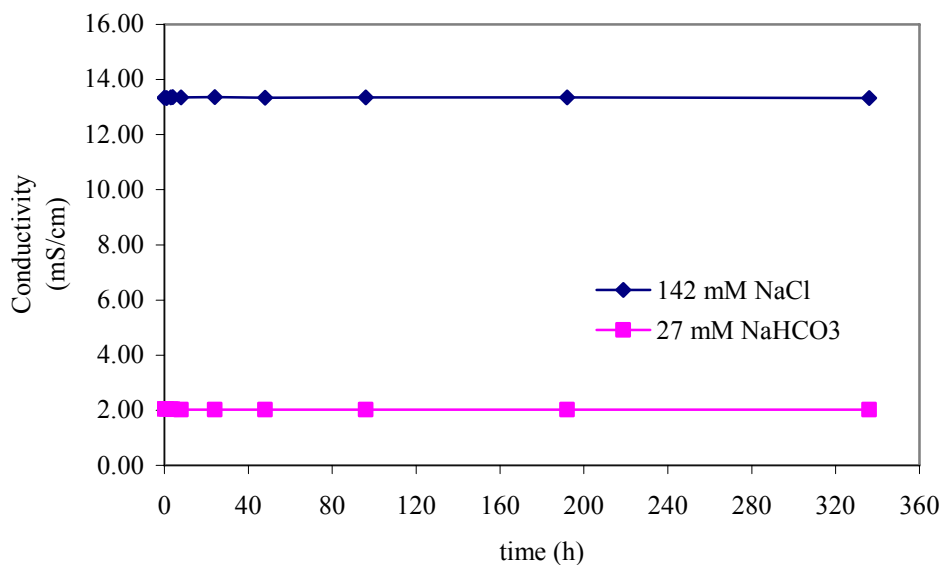


Figure 6.78. Conductivities of the solutions during HA dissolution in 142 mM NaCl and 27 mM NaHCO₃.

When dissolution of HA and DHA pellets were immersed in CO₂ free ultrapure water, conductivities showed that HA and DHA reaches equilibrium after 192 and 96 hours, respectively (Figure 6.79). Conductivities of the CO₂ free 142 mM NaCl during DHA and HA dissolution and conductivities of 27 mM NaHCO₃ during DHA dissolution stayed constant (Figure 6.80).

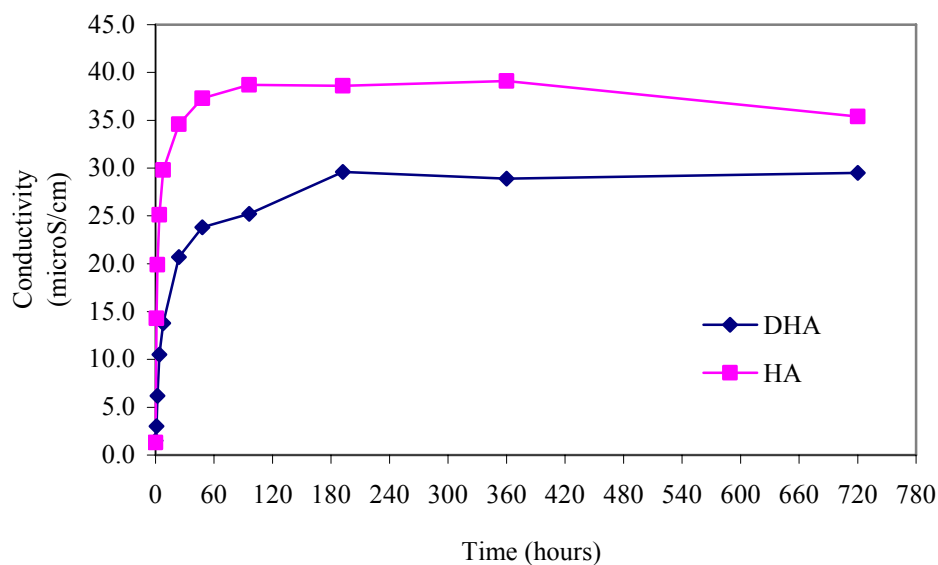


Figure 6.79. Conductivities of the solutions during HA and DHA dissolution in CO₂ free ultrapure water.

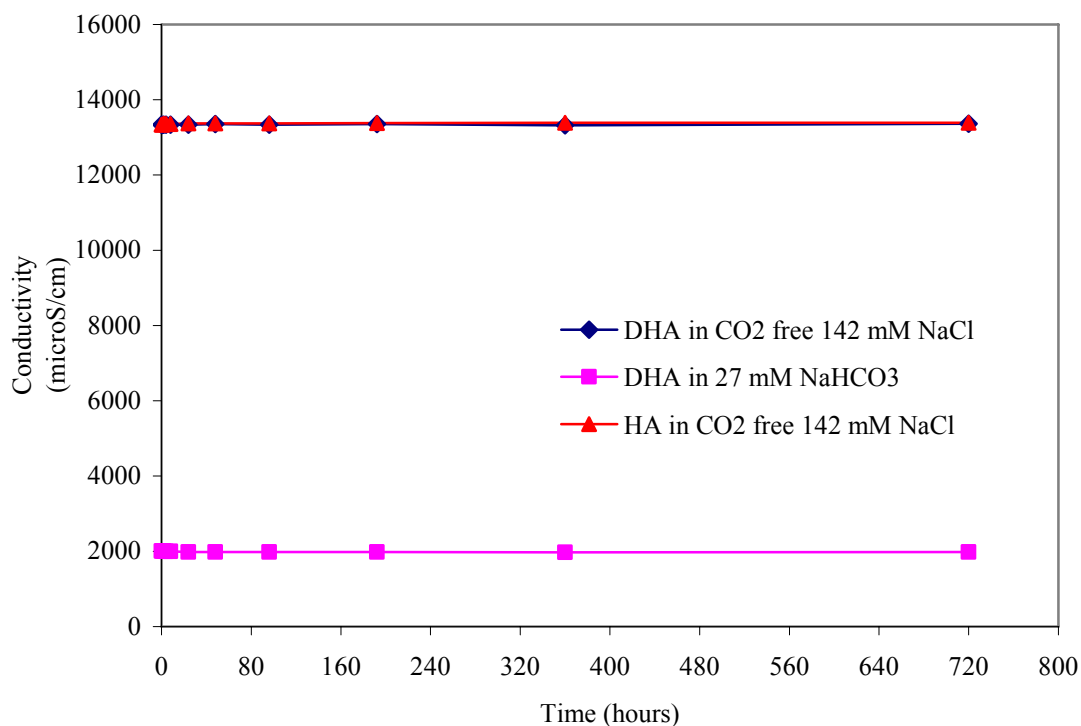


Figure 6.80. Conductivities of solutions during dissolution of HA and DHA pellets in CO₂ free 142 mM NaCl and 27 mM NaHCO₃ solutions.

Conductivity values of equilibration solutions during HA dissolution in CO₂ free 1.5 mM MgCl₂ showed that it is possible to monitor dissolution of HA although 1.5 mM MgCl₂ solution itself had a conductivity of 324 μS/cm (Figure 6.81). Equilibrium was reached faster 48 hours during dissolution of HA in 1.5 mM MgCl₂.

Dissolution in ultrapure water:

Calcium release from hydroxyapatite pellets immersed in ultrapure water in which dissolved carbon dioxide was not removed is shown in Figure 6.82. Calcium release was rapid in 8 hours dissolution. The highest concentration obtained after 48 hours dissolution was possibly due to the contamination of the sample taken. This point was therefore excluded in discussions. Calcium concentration in ultrapure water reaches saturation almost at 5.73 mg/L.

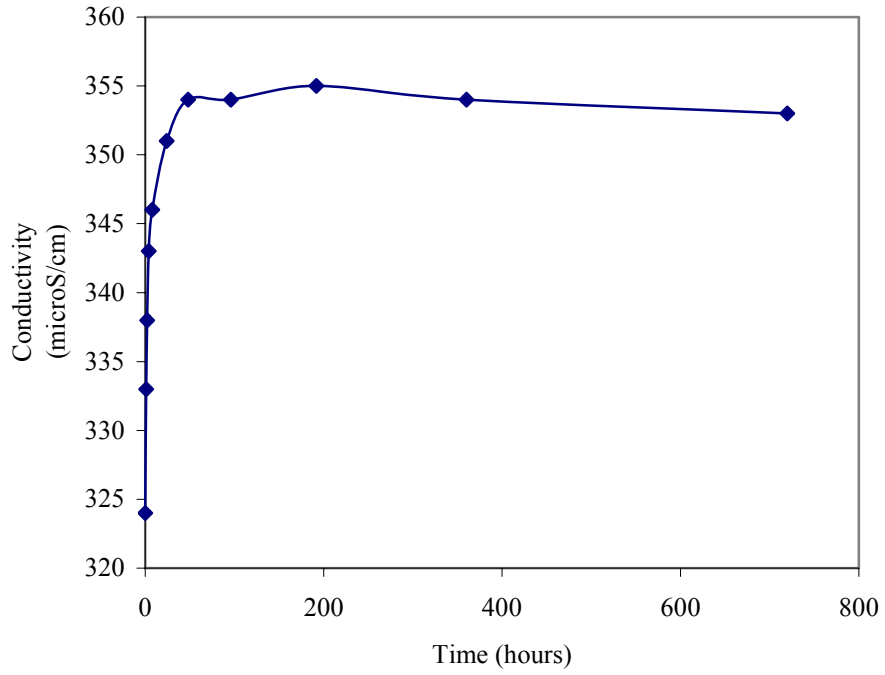


Figure 6.81. Conductivities of solutions during dissolution of HA in CO₂ free 1.5 mM MgCl₂.

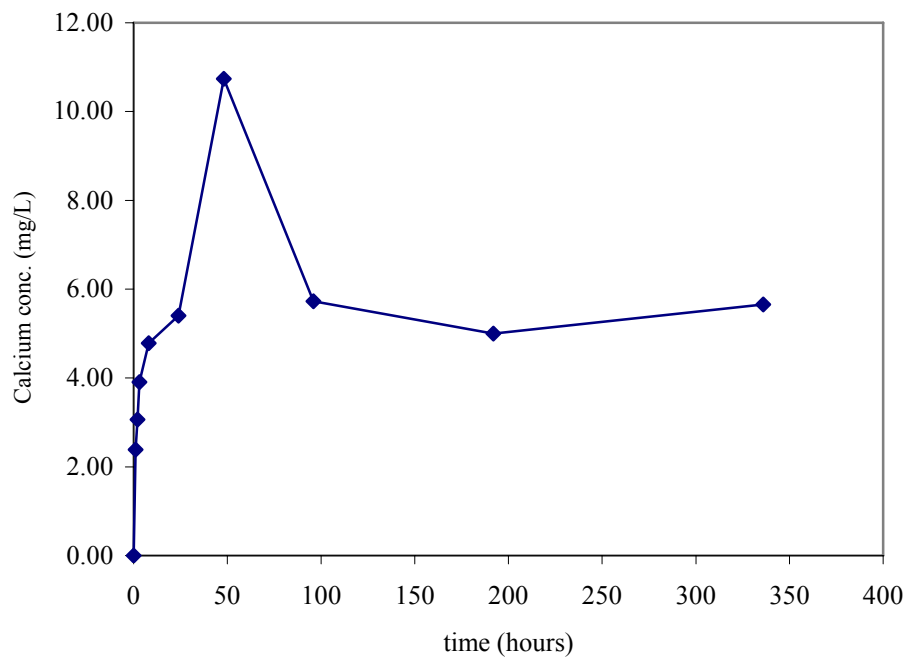


Figure 6.82. Calcium release profile upon dissolution of HA pellets in ultrapure water in which dissolved carbon dioxide was not removed.

Hydroxyapatite pellets immersed in carbon dioxide free ultrapure water exhibited similar dissolution trend obtained in ultrapure water whose dissolved carbon dioxide was not removed (Figure 6.83). Dissolution was faster until the end of 48 hours. Maximum calcium concentration was found at the end of 96 h as 6.35 mg/L. Calcium concentration was decreased gradually after 96 hours. At the end of 30 days, calcium concentration was found as 5.35 mg/L.

When nano-sized hydroxyapatite powder was equilibrated in CO₂ free ultrapure water, similar to HA in ultrapure water, calcium release rate was higher at the initial stages of dissolution (Figure 6.84). Highest calcium concentration, 6.08 mg/L, in the solutions was found after 192 hours. However, calcium concentration found after 96 hour incubation was 5.90 mg/L, almost similar to that found after 192 hours. This shows that calcium in the solution reaches equilibrium after 96 hours.

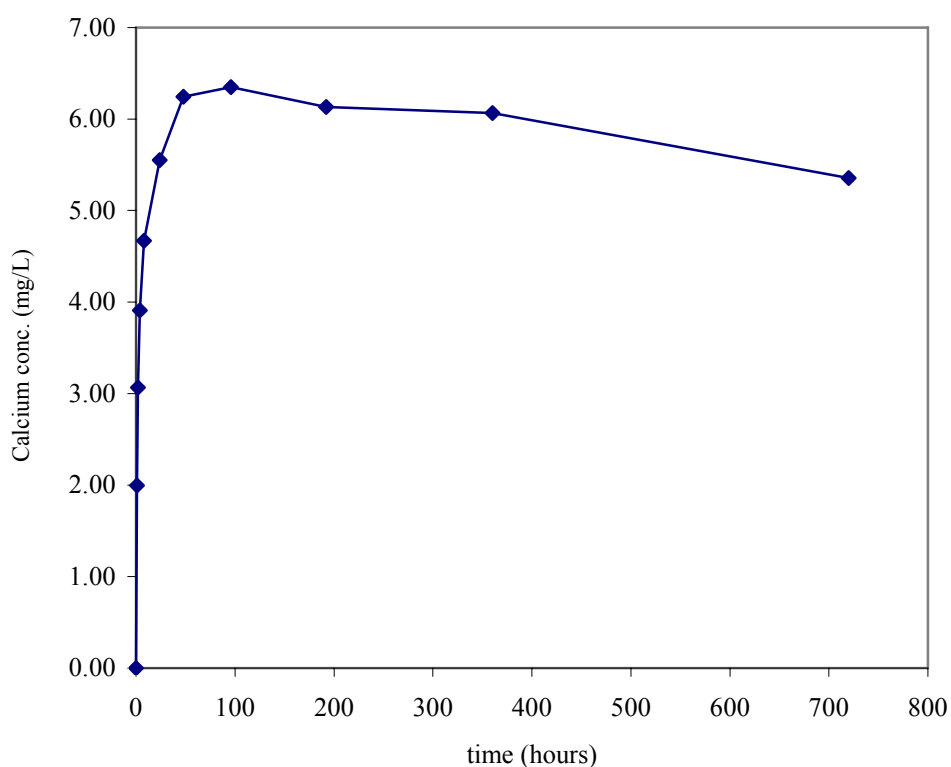


Figure 6.83. Calcium release profile upon dissolution of HA pellets in carbon dioxide free ultrapure water.

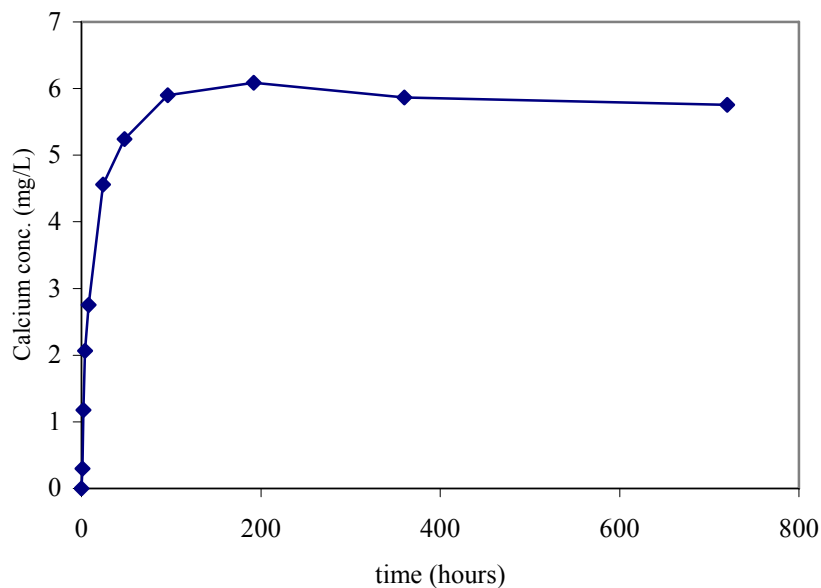


Figure 6.84. Calcium release profile upon dissolution of DHA pellets in carbon dioxide free ultrapure water.

When phosphate concentrations of the dissolution media were monitored during the dissolution of HA in ultrapure water whose dissolved carbon dioxide had not removed, maximum phosphate concentration was obtained at the end of 48 hours incubation (Figure 6.85). It was found as 5.34 mg/L. After 48 hours, reduction in phosphate concentration was observed. At the end of 14 days, phosphate concentration was reduced to 3.12 mg/L. If CO₂ free ultrapure water was used, maximum phosphate concentration was found at the end of 96 hours (Figure 6.86). Maximum phosphate concentration found in CO₂ free ultrapure water (3.90 mg/L) was lower than that found in ultrapure water which did not expose to degassing to remove carbon dioxide. Reduction of phosphate concentration was observed in further dissolution in CO₂ free ultrapure water. Phosphate concentrations after 360 hours and 720 hours were 3.07 and 2.17 mg/L, respectively.

Like HA dissolution in ultrapure water, DHA dissolution in CO₂ free ultrapure water showed the highest phosphate concentration after 96 hours equilibration (Figure 6.87). However, maximum phosphate concentration obtained was found as 2.27 mg/L during DHA dissolution. This was lower than that obtained in HA dissolution in CO₂ free ultrapure water. Upon further dissolution in ultrapure water, phosphate concentrations in dissolution media were reduced. At the end of 1 month phosphate concentration was measured as 0.74 mg/L.

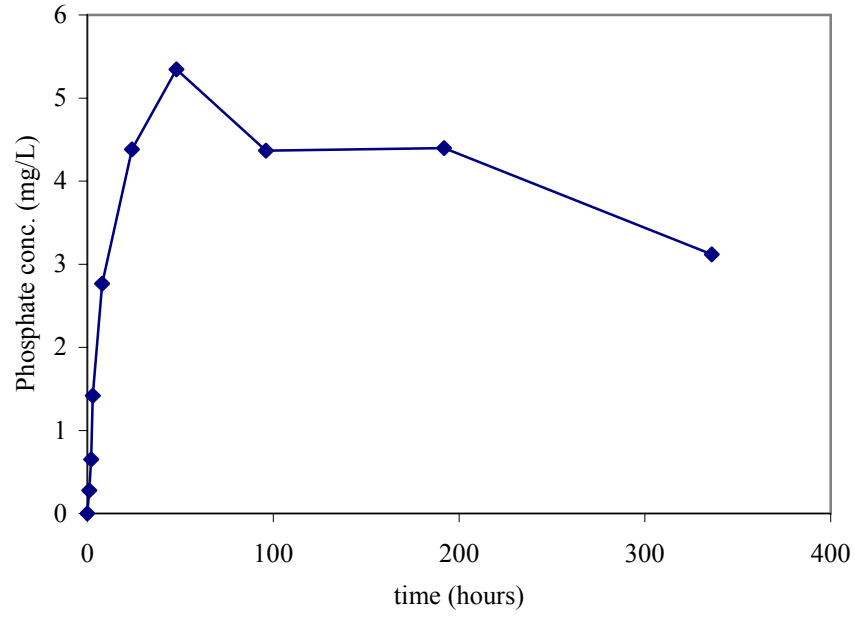


Figure 6.85. Phosphate concentrations in solutions upon dissolution of HA pellets in ultrapure water in which dissolved carbon dioxide was not removed.

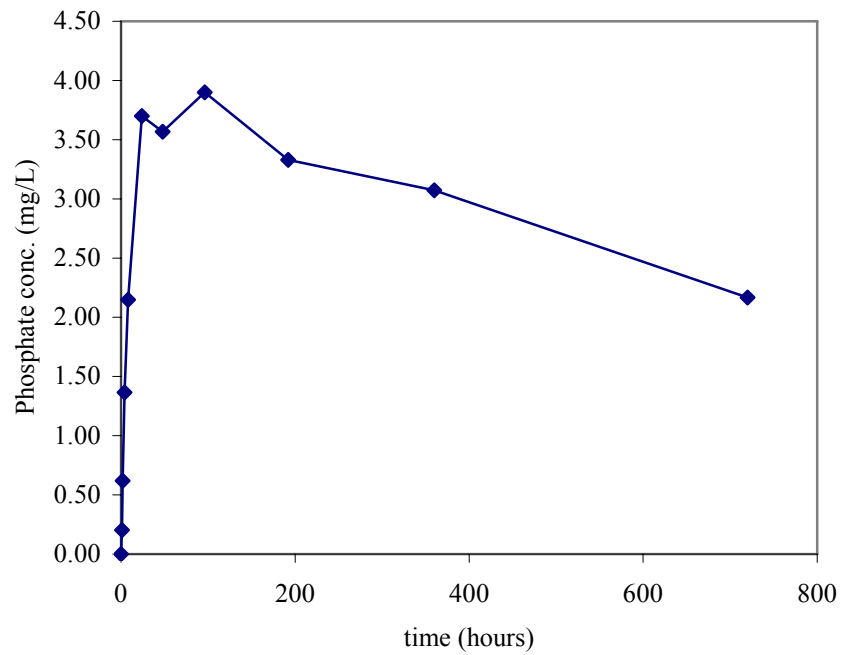


Figure 6.86. Phosphate concentrations in solutions upon dissolution of HA pellets in CO₂ free ultrapure water.

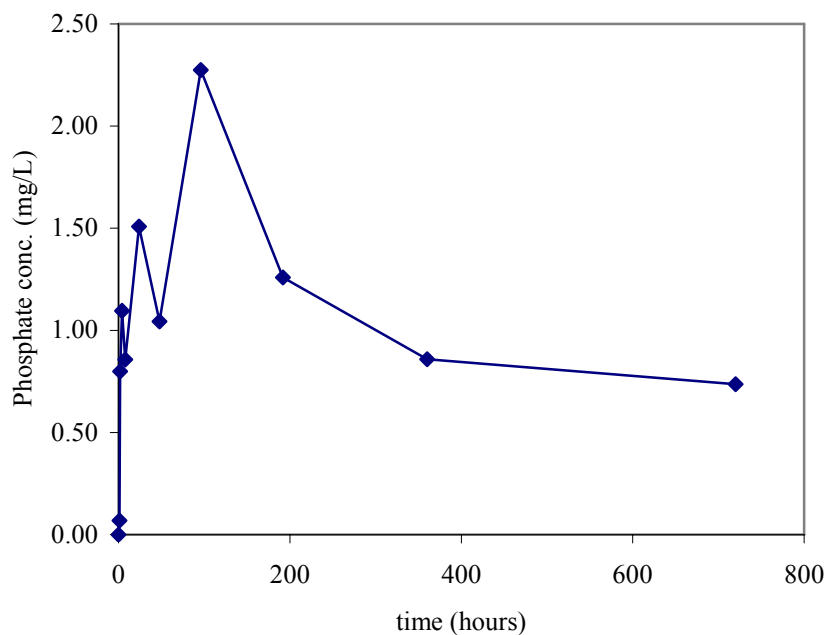


Figure 6.87. Phosphate concentrations in solutions upon dissolution of DHA pellets in CO₂ free ultrapure water.

During dissolution of HA and DHA powders, maximum concentrations obtained were taken as equilibrium concentrations since reductions in concentrations is either be linked to precipitation of new phases or adsorption of ions on the surfaces of powders.

When HA dissolution in both ultrapure water and CO₂ free ultrapure water was compared, equilibrium calcium concentrations were 5.83 and 6.35 mg/L for ultrapure water and CO₂ free ultrapure water, respectively. During DHA dissolution in CO₂ free ultrapure water equilibrium calcium concentration was found as 5.90 mg/L. These values were almost closer to each other. According to equilibrium calcium concentrations, HA dissolution in ultrapure water and CO₂ free ultrapure water and HA dissolution and DHA dissolution in CO₂ free ultrapure water were similar.

In contrast to equilibrium calcium concentrations, phosphate release from powders was different. Equilibrium phosphate concentration in HA dissolution in ultrapure water was attained after 48 hours and found to be 5.34 mg/L. This was reduced to 4.37 mg/L after 96 hours. In both HA and DHA dissolution in CO₂ free ultrapure water, equilibrium was attained after 96 hours and equilibrium phosphate concentrations were 3.90 mg/L and 2.27 mg/L, respectively. Equilibrium phosphate concentration was the lowest in DHA dissolution.

Dissolution in 142 mM NaCl

Calcium release kinetics from HA pellets in 142 mM NaCl solution which was not subjected to CO₂ removal procedure showed that equilibrium was reached after 96 hours (Figure 6.88). Equilibrium calcium concentration was 10.52 mg/L. Calcium concentration in solutions were almost kept constant after 96 hours. When HA pellets were immersed in CO₂ free 142 mM NaCl solution, equilibrium was again attained after 96 hours (Figure 6.89). Equilibrium calcium concentration found as 10.82 mg/L was almost the same found in 142 mM NaCl in which dissolved carbon dioxide was not removed. However, by further dissolution in CO₂ free media, calcium concentration was slightly reduced to 9.48 mg/L at the end of 1 month incubation period.

In contrast to HA equilibrated in 142 mM NaCl solutions, DHA pellets incubated in CO₂ free 142 mM NaCl released more calcium into the solutions. Equilibrium was obtained after 15 days but values found after 96, 192 hours and 15 days were closer to each other (Figure 6.90). Equilibrium calcium concentration was found as 14.32 mg/L in this case. This shows that DHA release more calcium in 142 mM NaCl solution when compared to HA. Contrary to HA equilibrated in CO₂ free 142 mM NaCl solution, calcium concentration almost stayed constant until the end of equilibration.

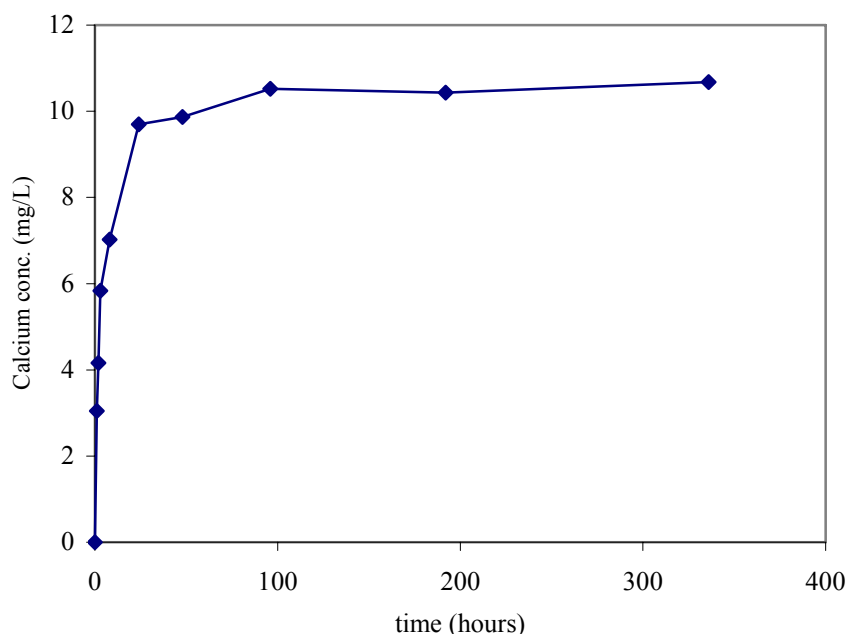


Figure 6.88. Calcium release from HA pellets in 142 mM NaCl in which dissolved carbon dioxide was not removed.

Phosphate release from HA pellets immersed in 142 mM NaCl in which dissolved carbon dioxide was not removed showed that phosphate release was faster until 24 hours. Release rate was reduced thereafter and highest phosphate concentration in solutions was found as 8.52 mg/L at the end of 96 hours incubation period. It seems that equilibrium was reached after 96 hours (Figure 6.91). However, phosphate concentration found at 48 hours (8.35 mg/L) was almost closer to 8.52 mg/L which was obtained at the end of 96 hours. When dissolved carbon dioxide was removed from the solution before incubation, equilibrium is attained after 48 hours (6.92). The equilibrium phosphate concentration was found to be 8.08 mg/L in this case. Phosphate was released rapidly in 24 hours, the release rate was reduced. After 48 hours, phosphate concentration started to decrease. At the end of 1 month, phosphate concentration was found as 5.49 mg/L.

Phosphate release from DHA pellets in CO₂ free 142 mM NaCl solution was different than HA immersed in CO₂ free 142 mM NaCl. Release was faster in 8 hours dissolution (Figure 6.93). It slows down thereafter and phosphate concentration reaches the maximum at the end of 24 hours (3.21 mg/L). However after 24 hour incubation, phosphate concentration begins to decrease. By the end of 96 hours, concentration almost stays constant. Phosphate concentration at the end of 360 hours was measured to be 2.38 mg/L. After 360 hours, slight increase was observed and concentration was increased to 2.89 mg/L.

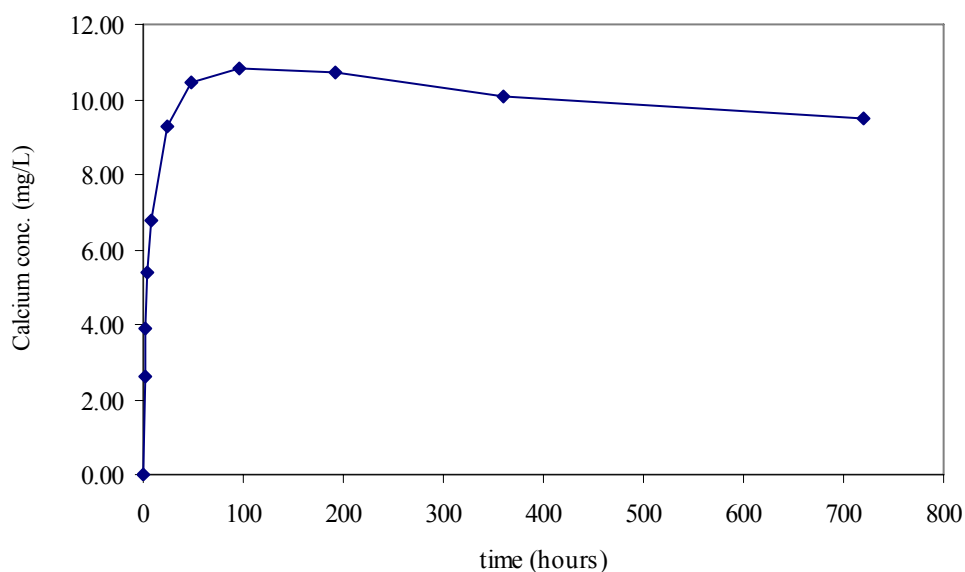


Figure 6.89. Calcium release from HA pellets in CO₂ free 142 mM NaCl.

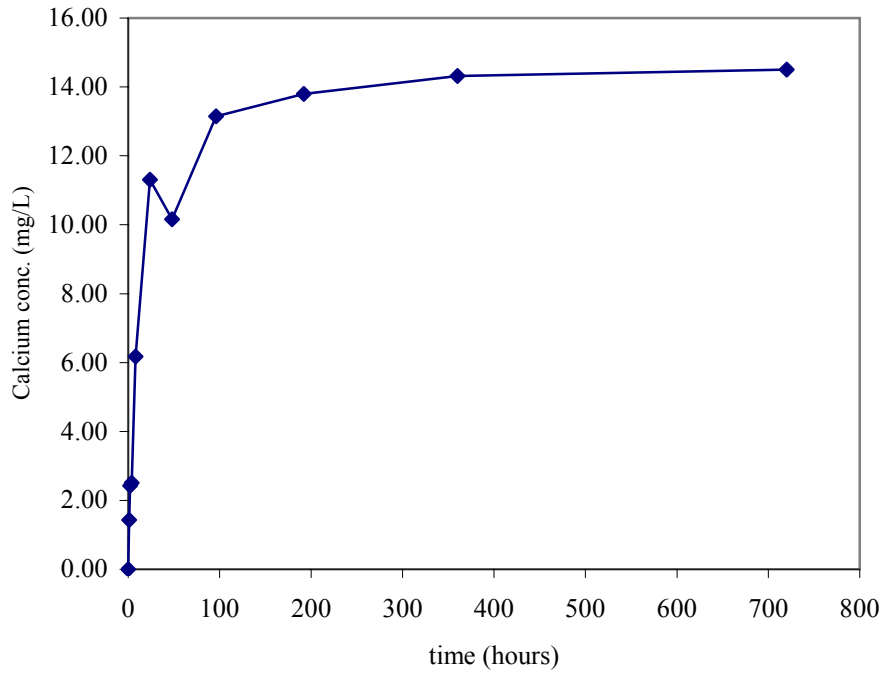


Figure 6.90. Calcium release from DHA pellets in CO₂ free 142 mM NaCl.

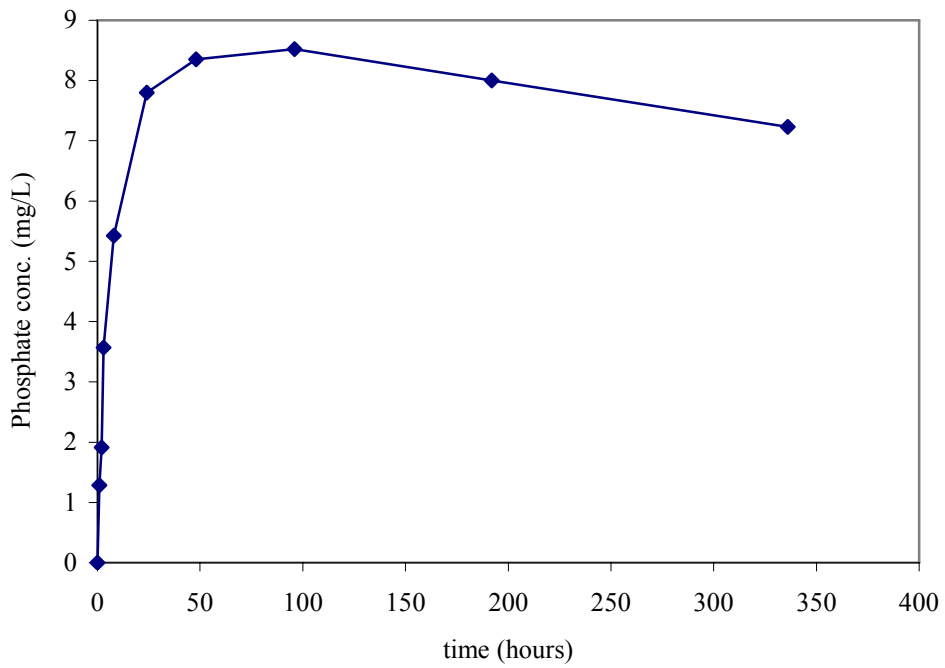


Figure 6.91. Phosphate release from HA pellets in 142 mM NaCl in which dissolved carbon dioxide was not removed.

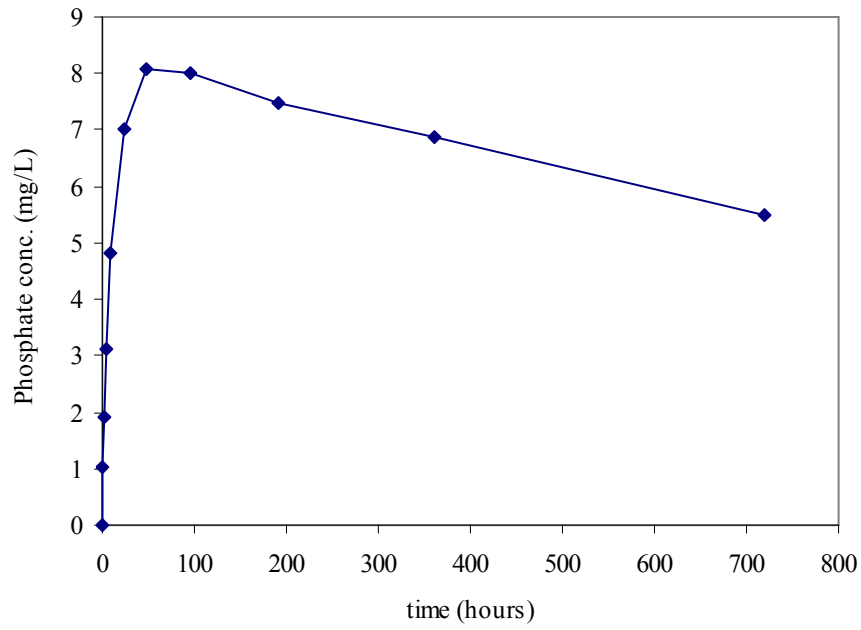


Figure 6.92. Phosphate release from HA pellets in CO₂ free 142 mM NaCl.

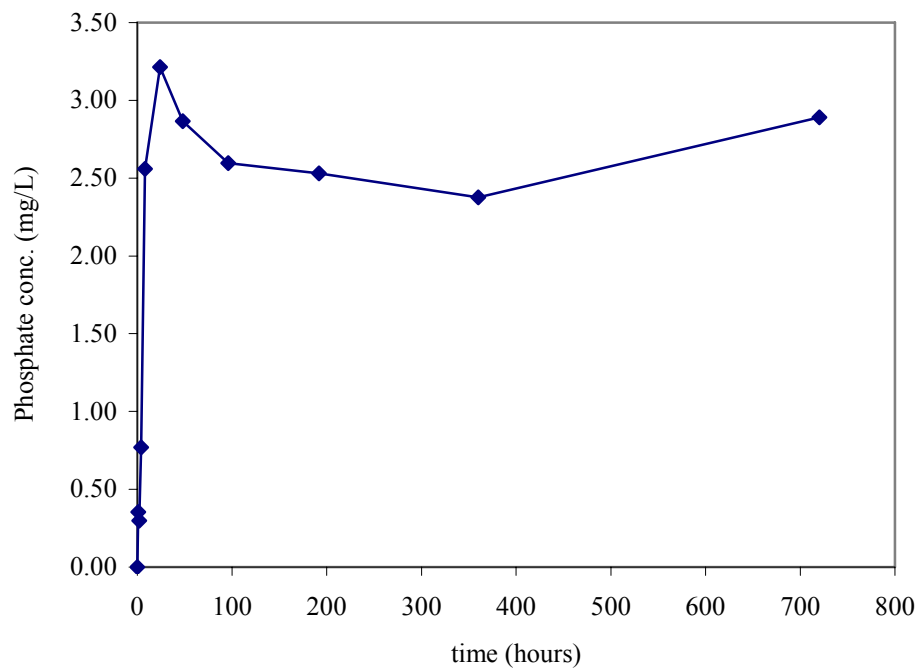


Figure 6.93. Phosphate release from DHA pellets in CO₂ free 142 mM NaCl.

Dissolution in 27 mM NaHCO₃

When HA pellets were immersed in 27 mM NaHCO₃, calcium concentrations were lower than 1 ppm (Figure 6.94). Calcium release from HA in bicarbonate solution was very low in comparison with pellets immersed in both ultrapure water and 142 mM NaCl solutions.

Lower calcium concentrations found in 27 mM NaHCO₃ solutions are in good agreement with the fact lower solubility of hydroxyapatite in alkaline pH values. Although lower calcium release, gradual reduction in calcium concentrations after 24 hour was observed. At the end of 336 hours, calcium concentration was found to be 0.23 mg/L.

Calcium release profile from DHA pellets in bicarbonate solution was almost similar to HA. Calcium concentrations in the solutions were lower than 1 ppm also in this case (Figure 6.95). However maximum calcium concentration was found after 48 hours. Highest calcium concentration was found to be 0.53 mg/L almost equal to that found when HA pellets were immersed in bicarbonate solution (0.57 mg/L). After 48 hours, calcium concentration started to decrease. This decrease was continued until 360 hours and stayed constant after 360 hours.

The use of equilibrium calcium concentration as a measure of the solubility of hydroxyapatite results in misinterpretations. When phosphate release from hydroxyapatite pellets immersed in 27 mM NaHCO₃ was determined (Figure 6.96), phosphate concentration in solutions showed continuous increase. Even at the end of 336 hours, solutions did not reach equilibrium. At the end of 336 hours, phosphate concentration was found to be 32.45 mg/L. Phosphate release from DHA pellets in bicarbonate solution showed similar trend like HA pellets (Figure 6.97). At the end of 360 hours phosphate concentration was found to be 42.03 mg/L whereas it was found 50.65 mg/L after 720 hours.

Lower calcium concentrations and reduction of calcium after a certain time in bicarbonate solution which have alkaline pH is reasonable because calcium carbonate precipitation is highly probable in calcium and carbonate containing solutions at high pH values. Calcium adsorption may occur on negative charged surface. High phosphate release when calcium release was low in fact suggests ion exchange between phosphate ions of hydroxyapatite and carbonate in the solution.

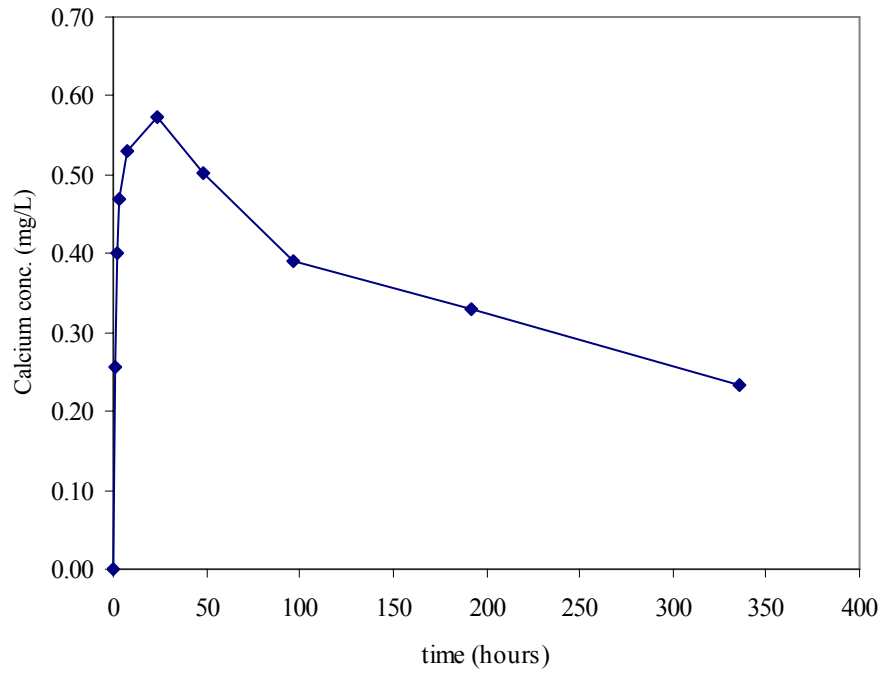


Figure 6.94. Calcium release from HA pellets in 27 mM NaHCO₃.

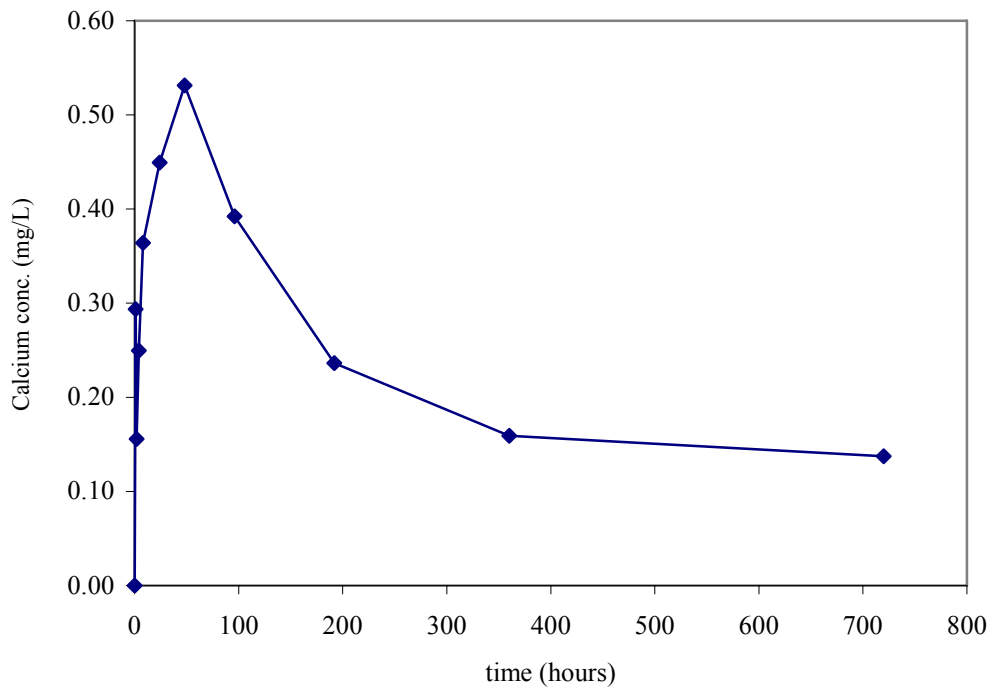


Figure 6.95. Calcium release from DHA pellets in 27 mM NaHCO₃.

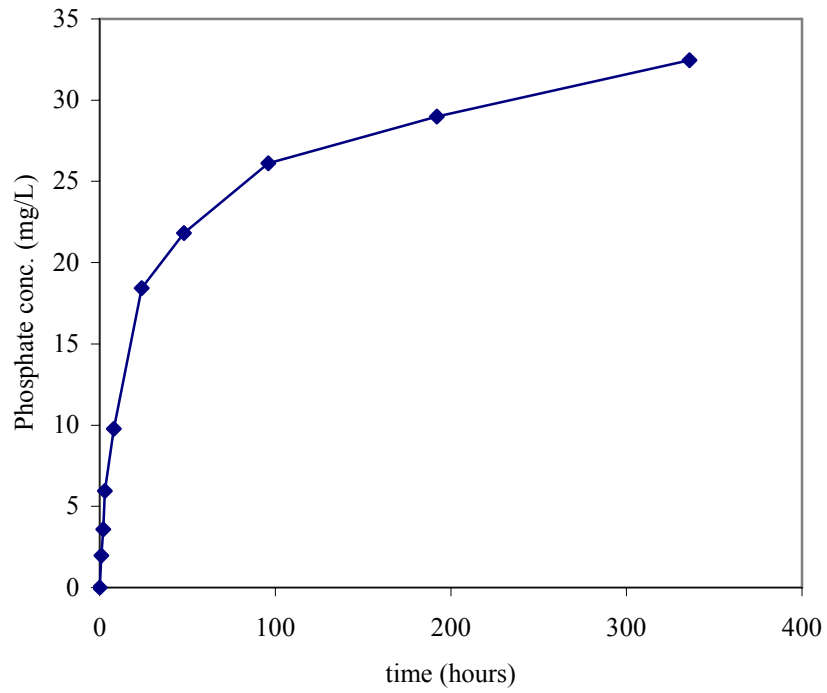


Figure 6.96. Phosphate release from HA pellets in 27 mM NaHCO₃.

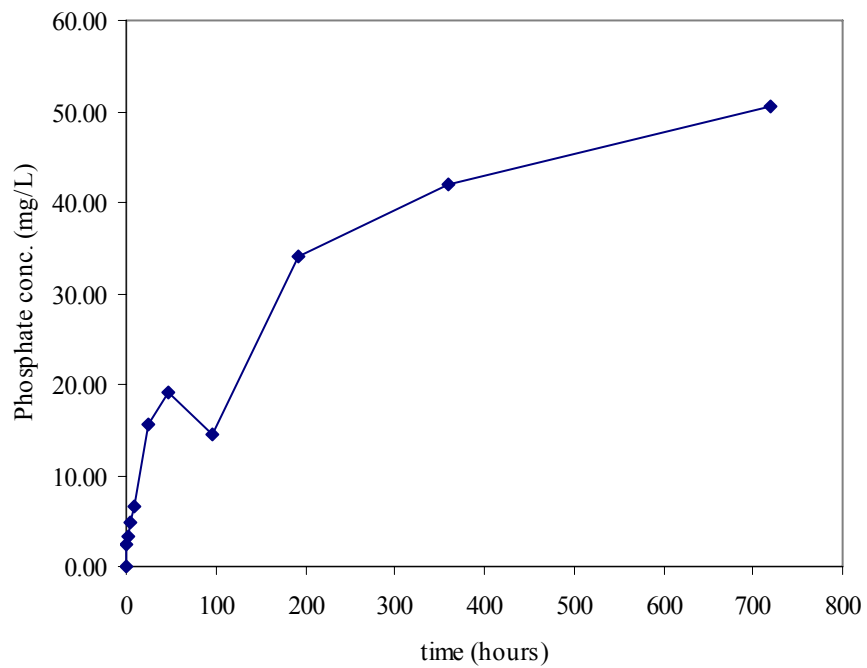


Figure 6.97. Phosphate release from DHA pellets in 27 mM NaHCO₃.

Dissolution in 115 mM NaCl and 27 mM NaHCO₃

Dissolution of HA in 115 mM NaCl and 27 mM NaHCO₃ containing solution exhibited similar behavior observed in 27 mM NaHCO₃ (Figure 6.98). Calcium concentrations in the solutions were very low when compared to dissolution in ultrapure water and 142 mM NaCl. Maximum concentration in the solutions was measured as 1.10 mg/L at the end of 24 hours. Decrease in calcium in the solutions was observed thereafter. It suggests that either calcium carbonate precipitation or calcium adsorption onto the surface hydroxyapatite occurs in 115 mM NaCl and 27 mM NaHCO₃ containing solution.

In contrast to calcium release, phosphate release was higher and phosphate concentration in the solution did not reach equilibrium in 115 mM NaCl and 27 mM NaHCO₃ containing electrolyte (Figure 6.99) although phosphate concentration at the end of 720 hours was 29.83 mg/L. This showed that ion exchange between phosphate groups of hydroxyapatite and carbonate in the solution were also observed 115 mM NaCl and 27 mM NaHCO₃ solution. The highest phosphate concentration in 115 mM NaCl and 27 mM NaHCO₃ containing solution was obtained after 720 hours. However this value was lower than phosphate concentration in 27 mM NaHCO₃ measured after 336 hours. This suggests that the presence of sodium chloride slows down the phosphate carbonate exchange kinetics.

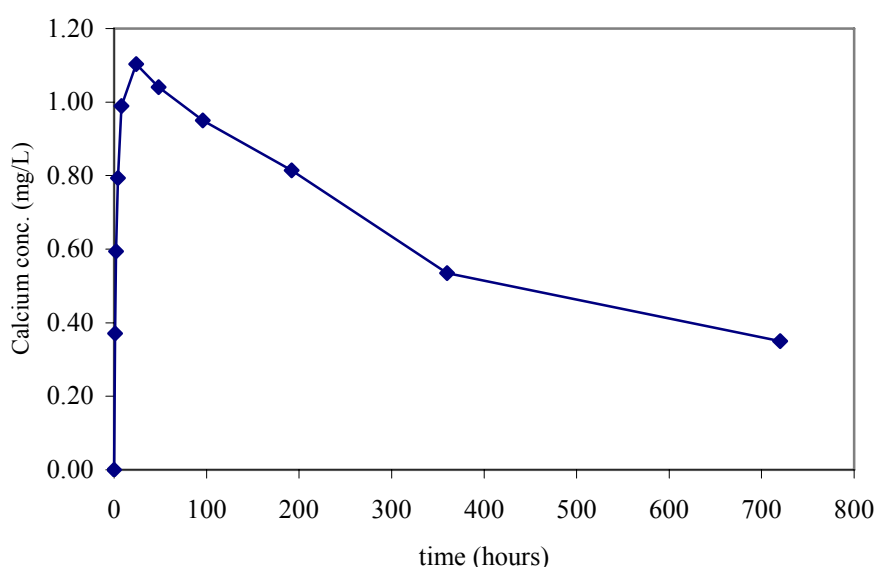


Figure 6.98. Calcium release from HA pellets in 115 mM NaCl and 27 mM NaHCO₃ containing solution.

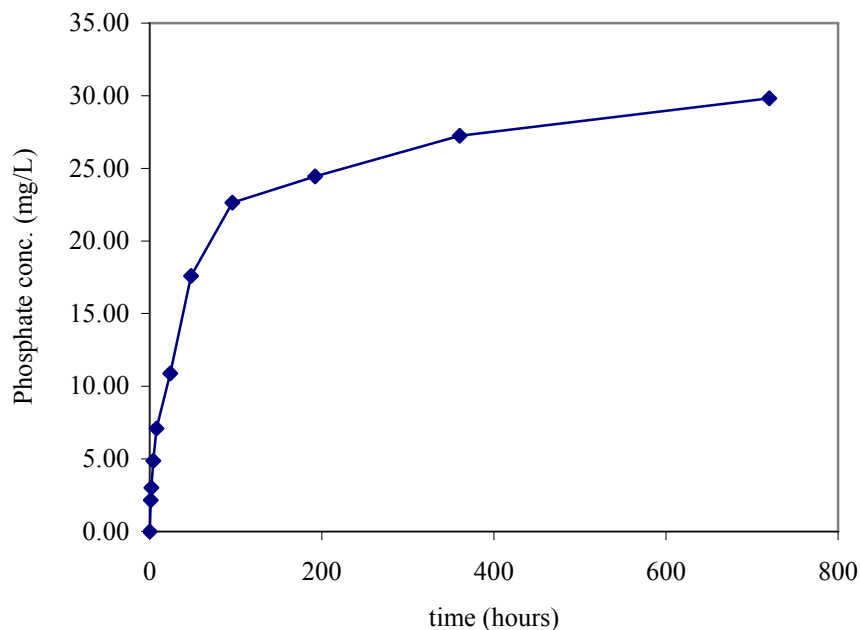


Figure 6.99. Phosphate release from HA pellets in 115 mM NaCl and 27 mM NaHCO₃ containing solution.

Dissolution in 1.5 mM MgCl₂·6H₂O

Magnesium is a well known inhibitor of hydroxyapatite crystallization. When only magnesium was present in physiological concentrations in unbuffered solutions, HA pellets released calcium into solutions continuously and equilibrium was not reached even after 720 hours (Figure 6.100). Calcium concentration found at the end of 720 hours was 14.65 mg/L.

Although calcium concentration in the solutions increased with an increase in time, phosphate release was different than that calcium release (Figure 6.101). Phosphate concentration in the solutions reached its maximum value at the end of 96 hours. Phosphate concentration at this point was found to be 4.05 mg/L. After this point, decrease in the phosphate concentrations was observed. Phosphate concentration at the end of 720 hours was found to be 2.24 mg/L. Higher calcium levels in the solutions suggested that ion exchange between calcium and magnesium occurs during equilibration in magnesium containing solution. However reduction in phosphate concentration after 96 hours suggested that phosphate adsorption on hydroxyapatite may likely to occur.

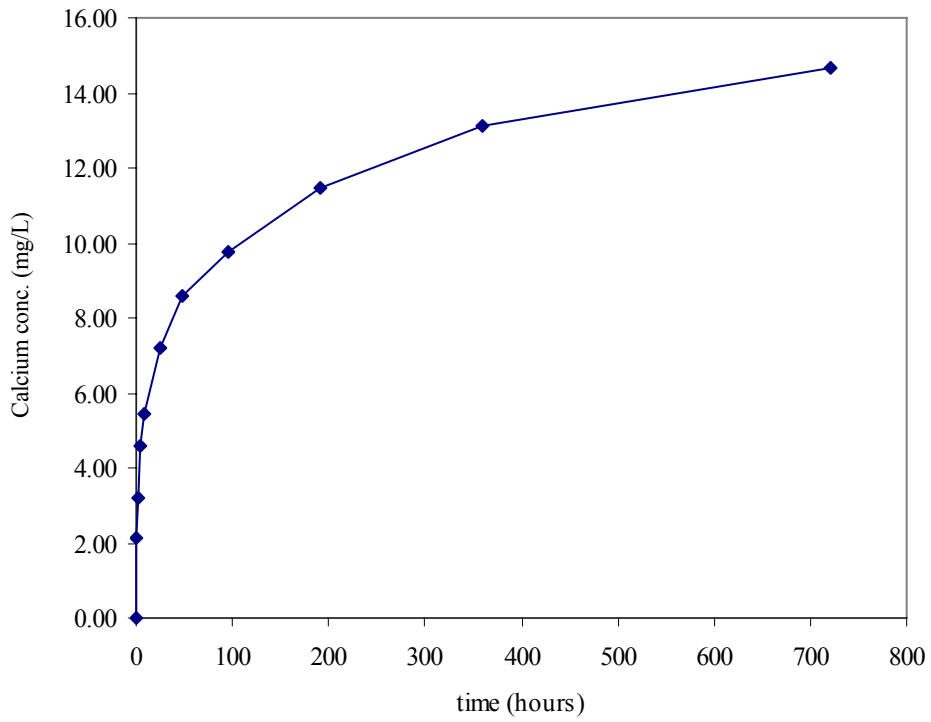


Figure 6.100. Calcium release from HA pellets in CO₂ free 1.5 mM MgCl₂.

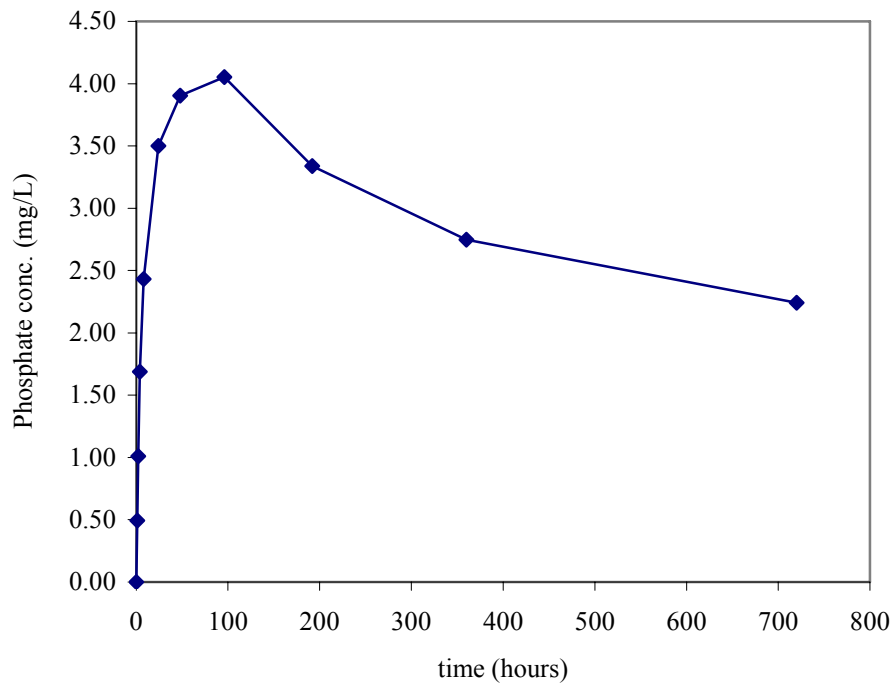


Figure 6.101. Phosphate release from HA pellets in CO₂ free 1.5 mM MgCl₂.

CHAPTER 7

CONCLUSION

The aim of this study was to determine the dissolution behavior of hydroxyapatite in different electrolytical solutions. Hydroxyapatite is the most stable calcium phosphate compound in solutions with neutral and alkaline pH values because its solubility at or above physiological pH is very low. Monitoring the calcium and phosphate release from the hydroxyapatite is important in order to understand time dependent changes in the solutions upon dissolution of hydroxyapatite. However, the low solubility of the hydroxyapatite makes it difficult to analyse calcium and phosphate concentrations in the solutions since they are in ppm level. In preliminary experiments, ICP analysis was chosen for the determination of calcium in dissolution media. The presence of 142 mM Na in the dissolution media required the dilutions to reduce sodium to acceptable levels. This caused calcium to fall below the detection limit. Presence of counter ion (Cl) made the use of ICP-MS impossible due to the possible interferences arising from high chloride concentration in the system.

A method suitable for the low level calcium determination especially in the presence of high concentrations of background matrix components is therefore needed. Arsenazo III dye based calcium assay was chosen for the calcium analysis in this study. This method has been widely used in serum and plasma calcium determinations. In these determinations, samples are diluted with dye reagents in 1:100 sample to dye volumetric ratios. Since the calcium concentration in plasma equals to 100 mg/L, dilution reduces the calcium concentration to 1 mg/L level. By this method, 100 mg/L calcium in the solutions can be analyzed. Since dilution is performed, concentration of other ions found in plasma reduces 100 folds. For these reason it was essential to modify Arsenazo III calcium analysis methods for 0.25-2 ppm and 1-8 ppm solution calcium levels.

Among all Arsenazo III and buffer concentrations and pH values tested 200 μ M Arsenazo III in 200 mM imidazole-Cl buffer pH 6.5 reagent was found suitable for the determination of 1 to 8 mg/L calcium in the solutions. By using this reagent the effects of the presence of 142 mM NaCl, 27 mM NaHCO₃, 115 mM NaCl and 27 mM

NaHCO₃, 1.5 mM MgCl₂, 1 mM Na₂HPO₄, 1 and 10 mM H₃PO₄, 5 mM KCl and 0.5 mM Na₂SO₄ on the calcium determination were then evaluated.

Determination of phosphate released from hydroxyapatite was performed by using malachite green phosphate assay. It was possible to analyze phosphate in solutions when phosphate concentration was in the range of 0.25-1.75 ppm. Phosphate standard solutions in this concentration range was prepared in different electrolyte solutions (142 mM NaCl, 115 mM NaCl and 27 mM NaHCO₃ containing solution, 27 mM NaHCO₃, 2.5 mM CaCl₂, 1.5 mM MgCl₂, 0.5 mM Na₂SO₄, 5 mM KCl, SBFA and SBFB solutions). The interferences due the presence of higher amounts of background electrolytes on phosphate determination were evaluated.

Dissolution of hydroxyapatite pellets produced from powder synthesized in this study and commercial hydroxyapatite powder were determined by measuring calcium and phosphate concentrations in the solutions. Calibration curves obtained in the presence of background ions were used to correct interferences due the background matrices. Dissolution behaviors of powders in ultrapure water and 142 mM NaCl were different with respect to calcium and phosphate concentrations indicating the presence of more than one mechanism in the system. Adsorption of ions onto the surfaces, precipitation of several phases or ion exchanges may simultaneously occur during dissolution in different electrolytical solutions. During equilibration of powders in bicarbonate containing solutions, calcium concentrations lower than 1 mg/L and high phosphate concentrations indicated that ion exchange between solution bicarbonate ions and hydroxyapatite phosphate ions. Equilibration of commercial hydroxyapatite powder in 1.5 mM MgCl₂ showed continuous calcium release. Since magnesium is a well-known crystallization inhibitor, precipitation of calcium phosphates was possibly avoided. However, low phosphate levels and higher calcium concentration showed that phosphate ions adsorb on the surface of hydroxyapatite and solution magnesium ions exchanges with calcium ions in hydroxyapatite.

Because great efforts were spent for the modification of calcium analysis method and for testing the interferences due to the presence of higher amounts of electrolytes, dissolution testing was restricted to major electrolyte solutions. Further studies can be the dissolution testing of the powders in 2.5 mM CaCl₂, 1.5 mM, 0.5 mM Na₂SO₄, 5 mM KCl, SBFA and SBFB solutions and in acidic solutions. Different simulated body fluids can also be used to determine the dissolution behavior of hydroxyapatite powders. Solutions containing higher amounts of phosphate and calcium

can be selected to determine the effects of undersaturation on the dissolution testing of the powders. Additionally, the effects of proteins found in blood and of the proteins involved in bone metabolism on the dissolution of hydroxyapatite can be determined by the addition of such proteins in dissolution media. Along with batch dissolution tests, surface potential measurements and potentiometric titrations can provide useful data for understanding the mechanisms responsible for bone turnover in normal and disease states. Such data will also be useful for the synthesis of calcium phosphate phases by wet chemical methods.

REFERENCES

- Ahmed, Z.; Kragie, L.; Connor, J. A. Stoichiometry and Apparent Dissociation Constant of the Calcium-Arsenazo III Reaction Under Physiological Conditions. *Biophysics Journal* **1980**, *32*, 907-920.
- Alimarin, I. P.; Savvin, S., B. Application of Arsenazo III and Other Azo-Compounds in the Photometric Determination of Certain Elements. *Pure and Applied Chemistry* **1966**, *13*, 445-456.
- AMS Diagnostics. www.amsdiagnostics.com/PDF20%Download./DI/L%2080133%20Calcium.02.pdf (accessed March 03, 2010).
- Analyticon® Biotechnologies AG. www.analyticon-diagnostics.com/download/aal/CaAIII-01_2003_IL3402.pdf (accessed March 03, 2010).
- Asai, S.; Koumoto, K.; Matsushita, Y.; Yashima, E.; Morinaga M.; Takeda, K. Iritani, E. Tagawa, T.; Tanahashi, M.; Miyazawa K. Advances in Nature Guided Materials Processing. *Science and Technology of Advanced Materials* **2003** *4*, 421-433.
- Attin, T.; Weiss, K.; Becker, K.; Buchalla, W.; Weigand A. Impact of Modified Acidic Soft Drinks on Enamel Erosion. *Oral Disease* **2005a**, *11*, 7-12.
- Attin, T.; Becker, K.; Hannig, C.; Buchalla, W.; Weigand, A. Suitability of Malachite Green Procedure to Detect Minimal Amounts of Phosphate Dissolved in Acidic Solutions. *Clinical Oral Investigations* **2005b**, *9*, 203-207.
- Babini, G., N.; Tampieri, A. Towards Biologically Inspired Materials. *British Ceramic Transactions* **2004**, *103*, 101-109.
- Baig, A. A.; Fox, J. L.; Young, R. A.; Wang, Z.; Hsu, J.; Higuchi, W. I.; Chhettry, A.; Zhuang, H.; Otsuka M. Relationships Among Carbonated Apatite Solubility, Crystallite Size and Microstrain Parameters. *Calcified Tissue International* **1999**, *64*, 437-449.
- Basargin, N. N.; Ivanov, V., M.; Kuznetsov, V. V.; Mikhailova, A. V. 40 Years since the Discovery of the Arsenazo III Reagent. *Journal of Analytical Chemistry* **2000**, *55*, 204-210.
- Baskan, S. *Uygulamalı İstatistik*; Ege Üniversitesi Fen Fakültesi Yayınları No: 150; Ege Üniversitesi Basımevi: İzmir, 1999.
- Bayraktar, D.; Tas, A. C. Formation of Hydroxyapatite Precursors at 37°C in Urea- and Enzyme Urease-Containing Body Fluids. *Journal of Materials Science Letters* **2001**, *20*, 401-403.

- Bauer, P. J. Affinity and Stoichiometry of Calcium Binding by Arsenazo III. *Analytical Biochemistry* **1981**, *110*, 61-72.
- Bengtsson, Å.; Shchukarev, A.; Persson, P.; Sjöberg, S. A Solubility and Surface Complexation Study of a Non-Stoichiometric Hydroxyapatite. *Geochimica et Cosmochimica Acta* **2009**, *73*, 257-267.
- Biolabo S. A. <http://www.biolabo.fr/pdfs/noticesE/biochimieE/AT%2090004.pdf> (accessed March 03, 2010).
- Bloebaum, R. D.; Lundeen, G. A.; Bachus, K. N.; Ison, I.; Hofmann A. A. Dissolution of particulate hydroxyapatite in a macrophage organelle model. *Journal of Biomedical Materials Research* **1998**, *40*, 104-114.
- Bohner, M.; Gbureck, U.; and Barralet, J. E. Technological Issues for the Development of More Efficient Calcium Phosphate Bone Cements: A Critical Assessment. *Biomaterials* **2005**, *26*, 6423-6429.
- Bohner, M. Calcium Orthophosphates in Medicine: From Ceramics to Calcium Phosphate Cements. *Injury, International Journal of the Care of the Injured* **2000**, *31*, S-D37-47.
- Boskey, A. L. Biomineralization: Conflicts, Challenges, and Opportunities. *Journal of Cellular Biochemistry* **1998**, *Supplements 30/31*, 83-91.
- Bow, J. S.; Liou S. C.; Chen S., J. Structural Characterization of Room Temperature Synthesized Nano-Sized β -Tricalcium Phosphate. *Biomaterials* **2004**, *25*, 3155-3161.
- Brown, H., M.; Rydqvist, B. Arsenazo III- Ca^{2+} Effect of pH, ionic strength, and Arsenazo III Concentration on Equilibrium Binding Evaluated with Ca^{2+} Ion-Sensitive Electrodes and Absorbance Measurements. *Biophysics Journal* **1981**, *36*, 117-137.
- Brown P. W. Phase Relationships in the Ternary System $\text{CaO-P}_2\text{O}_5\text{-H}_2\text{O}$ at 25 °C. *Journal of American Ceramic Society* **1992**, *75*, 17-22.
- BT Products. www.btproducts.com.tr/Admin/photos/urunpdf/633833484260312500.pdf (accessed March 03, 2010).
- Chaïrat, C.; Oelkers, E. H.; Schott, J.; Lartique, J. E. Fluorapatite Surface Composition in Aqueous Solution Deduced from Potentiometric, Electrokinetic, and Solubility Measurements. *Geochimica et Cosmochimica Acta* **2007**, *71*, 5888-5900.
- Chen, K.-L.; Jiang, S.-J. Determination of Calcium, Iron and Zinc in Milk Powder by Reaction Cell Inductively Coupled Plasma Mass Spectrometry. *Analytica Chimica Acta* **2002**, *470*, 223-228.

- Chema Diagnostica. www.chema.com/SITO2001.data/Elementi%20fissi/datasheetsUk/CalciumASX.pdf (accessed March 03, 2010).
- Chhetry, A.; Wang, Z.; Hsu J.; Fox, J. L.; Baig, A.; Barry, A. M.; Zhuang, H.; Otsuka, M.; Higuchi, W. I. Metastable Equilibrium Solubility Distribution of Carbonated Apatite as a Function of Solution Composition. *Journal of Colloids and Interface Science* **1999**, *218*, 57-67.
- Chin, K. O. A.; Nancollas, G. H. Dissolution of Fluorapatite. A Constant-Composition Kinetics Study. *Langmuir* **1991**, *7*, 2175-2179.
- Chiu, V., C., K.; Haynes, D. The pH Dependence and the Binding Equilibria of the Calcium Indicator-Arsenazo III, *Membrane Biochemistry* **1980**, *3*, 169-183.
- Chow, L. C.; Markovic M; Takagi S. A Dual Constant-Composition Titration System as an *in vitro* Resorption Model for Comparing Dissolution Rates of Calcium Phosphate Biomaterials. *Journal of Biomedical Materials Research Part B: Applied Biomaterials* **2003**, *65B*, 245-251.
- Chow, L. C.; Sun, L.; Hockey, B. Properties of Nanostructured Hydroxyapatite Prepared by a Spray Drying Technique. *Journal of Research of the National Institute of Standards and Technology* **2004**, *109*, 543-551.
- Chow, L. C. Next Generation Calcium Phosphate-Based Biomaterials. *Dental Materials Journal* **2009**, *28*, 1-10.
- Christian, G. D. *Analytical Chemistry*; John Wiley and Sons: New York; 1994.
- Cima Scientific. <http://www.cimascientific.com/2410.htm> (accessed April 06, 2010).
- Combes, C.; Rey, C. Amorphous calcium phosphates: synthesis, properties and uses in biomaterials, *Acta Biomaterialia* **2010**, in press.
- Cogan, E. B.; Birrel, G. B.; Griffith, O. H. A Robotics-Based Automated Assay for Inorganic and Organic Phosphates. *Analytical Biochemistry* **1999**, *271*, 29-35.
- D' Angelo, E.; Crutchfield, J.; Vandiviere, M. Rapid, Sensitive, Microscale Determination Phosphate in Water and Soil, *Journal of Environmental Quality* **2001**, *30*, 2206-2209.
- Dee, K. C.; Puleo, D. A.; Bizios, R. *An Introduction to Tissue- Biomaterial Interactions*; John Wiley & Sons, Inc.: New Jersey; 2002; pp 1-15.
- Department of Biochemistry, Faculty of Medicine, University of Szeged, Hungary. <http://biochem.szote.u-szeged.hu/edu/actual/en/pdf/05Catestangol.pdf> (accessed March 03, 2010).
- Dorozhkin, S. V.; Epple M. Biological and Medical Significance of Calcium Phosphates, *Angewandte Chemie International Edition* **2002**, *41*, 3130-3146.

- Dorozhkin, S. V. Calcium Orthophosphates. *Journal of Materials Science* **2007**, *42*, 1061-1095.
- Dorozhkin S.V. Calcium Orthophosphate Cements and Concretes. *Materials* **2009**, *2*: 221-291.
- Djošić, M. S.; Mišković-Stanković, V. B.; Kaćarević-Popović, Z. M.; Jokić, B. M.; Bibić, N.; Mitrić, M.; Milonjić, S. K.; Jančić-Heinemann, R.; Stojanović, J. Electrochemical Synthesis of Nanosized Monetite Powder and Its Electrophoretic Deposition on Titanium. *Colloids and Surfaces A: Physicochemical and Engineering Aspect* **2009**, *341*, 110-117.
- Ducheyne, P.; Radin, S.; King, L. The Effect of Calcium Phosphate Ceramic Composition and Structure on *in vitro* Behavior I. Dissolution. *Journal of Biomedical Materials Research* **1993**, *27*, 25-34.
- Elmore, K. L.; Farr, T. D. Equilibrium in the System Calcium Oxide-Phosphorous Pentoxide-Water. *Industrial and Engineering Chemistry* **1940**, *32*, 580-586.
- Eisenberger, S.; Lehrman, A.; Turner W.D. The Basic Calcium Phosphates and Related Systems. Some Theoretical and Practical Aspects. *Chemical Reviews* **1940**, *26*, 257-296.
- Fernández, E.; Gil, F. J.; Ginebra, M. P.; Driessens, F. C. M.; Planell, J. A.; Best, S. M. Calcium Phosphate Bone Cements for Clinical Applications Part I: Solution Chemistry. *Journal of Materials Science: Materials in Medicine* **1999**, *10*, 169-176.
- Ferraz, M. P.; Monteiro, F. J.; Manuel, C. M. Hydroxyapatite nanoparticles: A Review of Preparation Methodologie. *Journal of Applied Biomaterials and Biomechanics* **2004**, *2*, 74-80.
- Furuzono, T.; Taguchi, T.; Kishida, A.; Akashi, M.; Tamada, Y. Preparation and Characterization of Apatite Deposited on Silk Fabric Using an Alternate Soaking Process. *Journal of Biomedical Materials Research* **2000**, *50*, 344-352.
- Fulmer, M. T.; Ison, I. C.; Hankermayer, C. R.; Constantz, B. R.; Ross J. Measurements of the Solubilities and Dissolution Rates of Several Hydroxyapatites. *Biomaterials* **2002**, *23*, 751-755.
- Gawoski, J. M.; Walsh, D. Citrate Interference in Assays of Total Calcium in Serum. *Clinical Chemistry* **1989**, *35*, 2140-2141.
- Gbureck, U.; Barralet, J. E.; Hofmann, M.; Thull, R. Mechanical Activation of Tetracalcium Phosphate. *Journal of American Ceramic Society* **2004**, *87*, 311-313.

- Gibson, I. R.; Bonfield, W. Novel Synthesis and Characterization of an AB- type Carbonate-Substituted Hydroxyapatite. *Journal of Biomedical Materials Research* **2002**, *59*, 697-708.
- Greenwald, I. The Solubility of Calcium Phosphate II. The Solubility Product. *The Journal of Biological Chemistry* **1942**, *143*, 711-714.
- Gupta, S. K.; Rao, P. V. R., George, G.; Narasaraju T. S. B. Determination of Solubility Products of Phosphate and Vanadate Apatites of Calcium and Their Solid Solutions. *Journal of Materials Science* **1987**, *22*, 1286-1290.
- Hankermeyer, C. R.; Ohashi, K. L.; Delaney, D. C.; Ross, J.; Constantz B. R. Dissolution Rates of Carbonated Hydroxyapatite in Hydrochloric acid. *Biomaterials* **2002**, *23*, 743-750.
- Hannig, C.; Hamkens, A.; Becker, K.; Attin, R.; Attin T. Erosive Effects of Different Acids on Bovine Enamel: Release of Calcium and Phosphate *in vitro*. *Archives of Oral Biology* **2005**, *50*, 541-552.
- Hench, L. L. Bioceramics. *Journal of American Ceramic Society* **1998**, *81*, 1705-1728.
- Heslop, D. D.; Bi, Y., Baig, A. A.; Otsuka, M., Higuchi, W. I. A Comparative Study of the Metastable Equilibrium Solubility Behavior of High-Crystallinity and Low-Crystallinity Carbonated apatites Using pH and Solution Strontium as Independent Variable. *Journal of Colloids and Interface Science* **2005**, *289*, 14-25.
- Heughebaert, J. C.; Nancollas G. H. Solubility of Octacalcium Phosphate at 25 and 45 °C in the System $\text{Ca}(\text{OH})_2\text{-H}_3\text{PO}_4\text{-KNO}_3\text{-H}_2\text{O}$. *Journal of Chemical Engineering Data* **1985**, *30*, 279-281.
- Hosten, E.; Rohwer, H. Interaction of Anions with Arsenazo III-Lanthanide (III) Complexes. *Analytica Chimica Acta* **1997**, *345*, 227-233.
- Huang, J.; Best S. Ceramic Biomaterials. In *Tissue Engineering using Ceramics and Polymers*; Boccaccini A. R., Gough J. E., Eds.; Woodhead Publishing, Cambridge, 2007; p 7.
- Holt, L. E.; La Mer, V. K.; Chown, H. B. Studies in Calcification I. The Solubility Product of Secondary and Tertiary Calcium Phosphate Under Various Conditions. *The Journal of Biochemical Chemistry* **1925**, *LXVI*, 509-565.
- Hutchens, S. A.; Benson, R. S.; Evans, B. R.; O'Neil, H. M.; Rawn, C. J. Biomimetic Synthesis of Calcium-Deficient Hydroxyapatite in a Natural gel. *Biomaterials* **2006**, *27*, 4661-4670.
- Ishikawa, K. Calcium Phosphate Cement. In *Bioceramics and Their Clinical Applications*; Kokubo, T., Eds. Woodhead Publishing: Cambridge, 2008; pp 442-443.

- Ito, A.; Maekawa, K.; Tsutsumi, S.; Ikazaki, F.; Tateishi, T. Solubility product of OH-Carbonated Hydroxyapatite. *Journal of Biomedical Materials Research* **1997**, *36*, 522-528.
- Ito, A.; Onuma, K. Growth of Hydroxyapatite Crystals. In *Crystal Growth Technologies*; Byrappa, K.; Ohachi, T., Eds. William Andrew, Inc.: 2003; pp 438-462.
- Jeanotte, R.; Sommerville, D. W.; Hamel, C.; Whalen J. K. A Microplate Assay to Measure Soil Microbial Biomass Phosphorous. *Biology and Fertility of Soils* **2004**, *40*, 201-205.
- Johnsson, M. S. A.; Nancollas, G. H. The Role of Brushite and Octacalcium Phosphate in Apatite Formation. *Critical reviews in Oral Biology and Medicine* **1992**, *3*, 61-82.
- Kendrick, N. C.; Ratzlaff, R. W.; Blaustein, M. P. Arsenazo III as an Indicator for Ionized Calcium in Physiological Salt Solutions: Its Use for Determination of the CaATP Dissociation Constant. *Analytical Biochemistry* **1977**, *83*, 433-450.
- Koerten, H. K.; van der Meulen J. Degradation of Calcium Phosphate Ceramics. *Journal of Biomedical Materials Research* **1999**, *44*, 78-86.
- Kokubo, T. Apatite Formation on Surfaces of Ceramics, Metals and Polymers in Body Environment. *Acta Materialia* **1998**, *7*, 2519-2527.
- Kokubo, T.; Kushitani, H.; Sakka, S.; Kitsugi, T.; Yamamuro T. Solutions Able to Reproduce *in vivo* Surface-Structure Changes in Bioactive Glass-Ceramic A-W. *Journal of Biomedical Materials Research* **1990**, *24*, 721-734.
- Kokubo, T.; Takadama, H. How Useful is SBF in Predicting *in vivo* Bone Bioactivity ?. *Biomaterials* **2006**, *27*, 2907-2915.
- Königsberger, E.; Königsberger, L. C. Solubility and Body Fluids. In *Thermodynamics, Solubility and Environmental Issues*; Letcher T. M. Eds. Elsevier B. V.: Amsterdam, 2007; pp 445-461.
- Kurata, S.; Sato, K.; Kanri, Y.; Aoba T. Solubility Properties of Carbonatoapatites with Discrete Stoichiometric Compositions. *Journal of Oral Biosciences* **2006**, *48*, 114-125.
- Kuriakose, T. A.; Kalkura, S. N.; Palanichamy, M.; Arivuoli, D.; Dierks, K.; Bocelli, G.; Betzel, C. Synthesis of Stoichiometric Nanocrystalline Hydroxyapatite by Ethanol-Based Sol-Gel Technique at Low Temperature. *Journal of Crystal Growth* **2004**, *263*, 517-523.
- Kratochvil, B.; He, X.-W. A Study of the Ca²⁺-Arsenazo III System and Its Application to the Spectrophotometric Determination of Free Calcium in Solution. *Canadian Journal of Chemistry* **1990**, *68*, 1932-1936.

- Lafon, J. P.; Champion, E.; Barnache-Assollant, D. Processing of AB-type Carbonated Hydroxyapatite $\text{Ca}_{10-x}(\text{PO}_4)_6-x(\text{CO}_3)_x(\text{OH})_{2-x-2y}(\text{CO}_3)_y$ Ceramics with Controlled Composition. *Journal of the European Ceramic Society* **2008**, *28*, 139-147.
- Lafon, J. P.; Champion, E.; Barnache-Assollant, D.; Gibert, R.; Danna, A. M. Thermal Decomposition of Carbonated Calcium Phosphate Apatite. *Journal of Thermal Analysis and Calorimetry* **2003**, *72*, 1127-1134.
- Lamkin, E. G.; Williams, M. B. Spectrophotometric Determination of Calcium and Magnesium in Blood Serum with Arsenazo III and EGTA. *Analytical Chemistry* **1965**, *37*, 1029-1031.
- Landi, E.; Tampieri, A.; Celotti, G.; Vichi, L.; Sandri, M. Influence of Synthesis and Sintering Parameters on the Characteristics of Carbonate Apatite. *Biomaterials* **2004**, *25*, 1763-1770.
- Landi, E.; Celotti, G.; Logroscino, G.; Tampieri, A. Carbonated Hydroxyapatite as Bone Substitute. *Journal of the European Ceramic Society* **2003**, *23*, 2931-2937.
- Leary, N. O.; Pembroke, A.; Duggan, P. F. Single Stable Reagent (arsenazo III) for Optically Robust Measurement of Calcium in Serum and Plasma. *Clinical Chemistry* **1992a**, *38*, 904-907.
- Leary, N. O.; Pembroke, A.; Duggan, P. F. Measuring Albumin and Calcium in Serum in a Dual Test with the Hitachi 704. *Clinical Chemistry* **1992b**, *38*, 1342-1345.
- Levinkas, G. J.; Neuman, W. F. The Solubility of Bone Mineral. I. Solubility Studies of Synthetic Hydroxylapatite. *Journal of Physical Chemistry* **1955**, *59*, 164-168.
- Li, J.; Li, Y.; Zhang, L.; Zuo, Y. Composition of Calcium Deficient Na-Containing Carbonate Hydroxyapatite Modified with Cu (II) and Zn (II) Ions. *Applied Surface Science* **2008**, *254*, 2844-2850.
- Lin, J. H. C.; Kuo, K. H.; Ding, S. J.; Ju, C. P. Surface Reaction of Stoichiometric and Calcium Deficient Hydroxyapatite in Simulated Body Fluid. *Journal of Materials Science: Materials in Medicine* **2001**, *12*, 731-741.
- Linge, K. L.; Oldham, C. E. Interference from Arsenate When Determining Phosphate by the Malachite Green Spectrophotometric Method. *Analytica Chimica Acta* **2001**, *450*, 247-252.
- Liou, S.-C.; Chen, S.-Y.; Lee, H.-Y.; Bow, J.-S. Structural Characterization of Nano-Sized Calcium Deficient Apatite Powders. *Biomaterials* **2004**, *25*, 189-196.
- Logan, M. A.; Taylor, H. L. Solubility of Bone Salt, *The Journal of Biological Chemistry* **1937**, *119*, 293-307.

- Lorimer, J. W., Cohen-Adad, R. Thermodynamics of Solubility. In *The Experimental Determination of Solubilities*; Hefter G. T., Tomkins, R. P. T. Eds.; Wiley Series in Solution Chemistry; John Wiley and Sons Ltd.: West Sussex, 2003; Volume 6, p 21.
- Lu, X.; Leng Y. Theoretical Analysis of Calcium Phosphate Precipitation in Simulated Body Fluid. *Biomaterials* **2005**, *26*, 1097-1108.
- Lynn, A. K.; Bonfield, W. A Novel Method for the Simultaneous, Titrant-Free Control of pH and Calcium Phosphate Mass Yield. *Accounts of Chemical Research*. **2005**, *38*, 202-207.
- Magalhães, M. C. F. and Williams, P. A. Apatite Group Minerals: Solubility and Environmental Remediation. In *Thermodynamics, Solubility and Environmental Issues*; Letcher T. M. Eds. Elsevier B. V.: Amsterdam, 2007; pp 327-340.
- Marczenko, Z.; Balcerzak, M., Eds. *Separation, Preconcentration and Spectrophotometry in Inorganic Analysis. Analytical Spectroscopy Library Series*; Elsevier Science B. V.: Amsterdam, 2000; Volume 10.
- Markovic, M.; Fowler, B. O.; Tung, M. S. Preparation and Comprehensive Characterization of a Calcium Hydroxyapatite Reference Material. *Journal of Research of the National Institute of Standards and Technology* **2004**, *109*, 553-568.
- Martin, R. I.; Brown, P. W. Phase Equilibria Among Acid Calcium Phosphates. *Journal of American Ceramic Society* **1997**, *80*, 1263-1266.
- McDowell, H.; Gregory, T. M.; Brown W. E. Solubility of $\text{Ca}_5(\text{PO}_4)_3\text{OH}$ in the System $\text{Ca}(\text{OH})_2\text{-H}_3\text{PO}_4\text{-H}_2\text{O}$ at 5, 15, 25, and 37 °C. *Journal of Research of the National Bureau of Standards, A. Physics and Chemistry* **1977**, *81A*, 273-281.
- Michaylova, V.; Ilkova P. Photometric Determination of Micro Amounts of Calcium with Arsenazo III. *Analytica Chimica Acta* **1971**, *53*, 194-198.
- Mickiewicz, R. A. Polymer-Calcium Phosphate Composites For Use as An Injectable Bone Substitute. Master of Science Thesis, Massachusetts Institute of Technology, Cambridge, MA, June, 2001.
- Mindray Medical International Limited. www.mindray.com/main/images/2009/05/27/983151253841.pdf (accessed March 03, 2010).
- Minganti, C.; Gisin, B. F.; Gokel G., W. Chloride Anion Interference in the Spectrophotometric Determination of Arsenazo III. *Analytical Chemistry* **1983**, *55*, 383-385.
- Monteiro, M. M.; da Rocha, N. C. C.; Rossi, A. M.; Soares G. A. Dissolution Properties of Calcium Phosphate Granules with Different Composition in Simulated body Fluid. *Journal of Biomedical Materials Research* **2003**, *65A*, 299-305.

- Montgomery, D., C. *Introduction to Statistical Quality Control*, Third Edition; John Wiley and Sons, Inc.: New York, 1996.
- Montgomery, D., C. *Design and Analysis of Experiments*, Fifth Edition; John Wiley and Sons, Inc.: New York, 2001.
- Moreno, E. C.; Gregory, T. M.; Brown W. E. Preparation and Solubility of Hydroxyapatite, *Journal of Research of the National Bureau of Standards, A. Physics and Chemistry* **1968**, 72A, 773-782.
- Morgan, B. R.; Artiss, J. D.; Zak B. Calcium Determination in Serum with Stable Alkaline Arsenazo III and Triglyceride Clearing. *Clinical Chemistry* **1993**, 39, 1606-1612.
- mti diagnostics. http://www.mti-diagnostics.de/downloads/Bulkware_AV/B-AV-Calciumarsenazo-III.pdf (accessed April 06, 2010).
- Mullin, J. W. *Crystallization*, Third Edition; Butterworth-Heinemann Ltd.: Oxford, 1993.
- Murugan, R.; Ramakrishna, S. Development of Nanocomposites for Bone Grafting. *Composites Science and Technology* **2005**, 65, 2385-2406.
- Nancollas, G. H. The Involvement of Calcium Phosphates in Biological Mineralization and Demineralization Processes. *Pure and Applied Chemistry*, **1992**, 64, 1673-1678.
- National Biochemicals Corp. <http://www.nationalbiochem.com/pdf/TK%201143%20PS.Pdf> (accessed March 03, 2010.)
- Nayak, A. K.; Bhattacharya, A.; Sen, K. K. Hydroxyapatite-Antibiotic Minipellets for Bacterial Bone Infections Using Precipitation Technique: Preparation, Characterization and *in-vitro* Antibiotic Release Studies. *Journal of Pharmacy Research* **2010**, 3, 53-59.
- Němcová, I.; Metal, B. Dissociation Constants of Arsenazo III. *Talanta* **1986**, 33, 841-842.
- Neira, I. S.; Kolen'ko Y. V.; Lebedev O., I.; Tendeloo, G. V.; Gupta H. S.; Matsushita, N.; Yoshimura, M.; Guitián, F. Rational Synthesis of a Nanocrystalline Calcium Phosphate Cement Exhibiting Rapid Conversion to Hydroxyapatite. *Materials Science and Engineering C* **2009**, 29, 2124-2132.
- Oyane, A.; Kim, H-M.; Furuya, T.; Kokubo, T.; Miyazaki, T.; Nakamura, T. Preparation and Assessment of Revised Simulated Body Fluids. *Journal of Biomedical Materials Research* **2003a**, 65A, 188-195.
- Oyane, A.; Onuma, K.; Ito, A.; Kim, H-M.; Kokubo, T.; Nakamura, T. Formation and Growth of Clusters in Conventional and New Kinds of Simulated Body Fluids. *Journal of Biomedical Materials Research* **2003b**, 64A, 339-348.

- Padilla, S.; Izquierdo-Barba, I.; Vallet-Regi, M. High Specific Surface Area in Nanometric Carbonated Hydroxyapatite. *Chemistry of Materials* **2008**, *20*, 5942-5944.
- Pointe Scientific, Inc. www.pointescientific.com/products/PI/C7529.pdf (accessed March 03, 2010).
- Porter, A. E.; Botelho, C. M.; Lopes, M. A.; Santos, J. D.; Best, S.; Bonfield, W. Ultrastructural Comparison of Dissolution and Apatite Precipitation on Hydroxyapatite and Silicon-Substituted Hydroxyapatite *in vitro* and *in vivo*. *Journal of Biomedical Materials Research* **2004**, *69A*, 670-679.
- Prabakaran, K.; Rajeswari, S. Development of Hydroxyapatite from Natural Fish Bone through Heat Treatment. *Trends in Biomaterials and Artificial Organs* **2006**, *20*, 20-23.
- Pramanik, S.; Agarwal, A. K.; Rai, K. N. Development of High Strength Hydroxyapatite for Hard Tissue Replacement. *Trends in Biomaterials and Artificial Organs* **2005**, *19*, 46-51.
- Rohwer, H.; Rheeder, E.; Hosten, E. Interactions of Uranium and Thorium with Arsenazo III in an Aqueous Medium. *Analytica Chimica Acta* **1997**, *341*, 263-268.
- Rootare, H. M.; Deitz, V. R.; Carpenter F. G. Solubility Product Phenomena in Hydroxyapatite-Water Systems. *Journal of Colloid Science* **1962**, *17*, 179-206.
- Rouquerol, F.; Rouquerol, J.; Sing, K. *Adsorption by Powders and Porous Solids: Principles, Methodology and Applications*; Academic Press: San Diego, 1999.
- Rowatt, E.; Williams, R., J., P. The Interaction of Cations with the Dye Arsenazo III. *Biochemical Journal* **1989**, *259*, 295-298.
- Siddharthan, A.; Seshadri, S. K.; Sampath Kumar, T. S. Microwave Accelerated Synthesis of Nanosized Calcium Deficient Hydroxyapatite. *Journal of Materials Science: Materials in Medicine* **2004**, *15*, 1279-1284.
- Sikavitsas, I. V.; Temenoff, J. S.; Mikos, A. S. Biomaterials and Bone Mechanotransduction. *Biomaterials* **2001**, *22*, 2581-2593.
- Skartsila K.; Spanos N. Surface Characterization of Hydroxyapatite: Potentiometric Titrations Coupled with Solubility Measurements. *Journal of Colloid and Interface Science* **2007**, *308*, 405-412.
- Ślósarczyk, A.; Paszkiewicz, Z.; Paluszkiewicz, C. FTIR and XRD Evaluation of Carbonated Hydroxyapatite Powders Synthesized by Wet Methods. *Journal of Molecular Structure* **2005**, *744-747*, 657-661.

- Smith, A. N.; Posner, A. M.; Quirk, J. P. Incongruent Dissolution and Surface Complexes of Hydroxyapatite. *Journal of Colloid and Interface Science* **1974**, *48*, 442-449.
- Song, J.; Malathong, V.; Bertozzi, C. R. Mineralization of Synthetic Polymer Scaffolds: A Bottom-Up Approach for the Development of Artificial Bone. *Journal of American Chemical Society* **2005**, *127*, 3366-3372.
- Sprio, S.; Tampieri, A.; Landi, E.; Sandri, M.; Martorana, S.; Celotti, G.; Logroscino, G. Physico-chemical Properties and Solubility Behaviour of Multi-substituted Hydroxyapatite Powders Containing Silicon. *Materials Science and Engineering C* **2008**, *28*, 179-187.
- Strates, B. S.; Neuman, W. F.; Levinkas, G. The Solubility of Bone Mineral. II. Precipitation of Near-neutral Solutions of Calcium and Phosphate. *Journal of Physical Chemistry* **1957**, *61*, 279-282.
- Suchanek, W.; Yoshimura, M. Processing and Properties of Hydroxyapatite Based Biomaterials for Use as Hard Tissue Replacement Implants. *Journal of Materials Research* **1998**, *13*, 94-117.
- Sutter, J. R.; McDowell, H.; Brown W. E. Solubility Study of Calcium Hydrogen Phosphate. Ion-Pair Formation. *Inorganic Chemistry* **1971**, *10*, 1639-1643.
- Szydłowska-Czerniak, A.; Szyłk E. Spectrophotometric Determination of Total Phosphorus in Rape Seeds and Oils at Various Stages of Technological Process: Calculation of Phospholipids and Non-hydratable Phospholipids Contents in Rapeseed Oil. *Food Chemistry* **2003**, *81*, 613-619.
- Eaton, A. D.; Clesceri, L. S.; Greenberg, A. E., Eds. *Standard Methods for the Examination of Water and Wastewater*; 19th Edition, American Public Health Association, American Water Works Association, Water Environment Federation; United Book Press, Inc.: Maryland, 1995; pp 4-106-4-115.
- Takadama, H.; Hashimoto, M. T.; Takigawa, Y.; Mizuno, M.; Kokubo T. New and Conventional Simulated Body Fluids. *American Ceramic Society, Ceramic Engineering and Science Proceedings* **2004**, *25*, 571-576.
- Tampieri, A., Celotti, G.; Landi E. From Biomimetic Apatites to Biologically Inspired Composites. *Analytical and Bioanalytical Chemistry* **2005**, *381*, 568-576.
- Tang, R.; Wenju, W.; Haas, M.; Nancollas G. H. Kinetics of Dissolution of β -Tricalcium Phosphate. *Langmuir* **2001**, *17*, 3480-3485.
- Tang, R.; Henneman, Z. J.; Nancollas G. H. Constant Composition Kinetics Study of Carbonated Apatite Dissolution. *Journal of Crystal Growth* **2003a**, *249*, 614-624.
- Tang, R.; Hass, M.; Wu, W.; Gulde, S.; Nancollas, G. H. Constant Composition Dissolution of Mixed Phases II. Selective Dissolution of Calcium Phosphates. *Journal of Colloid and Interface Science* **2003b**, *260*, 379-384.

- Tas, A. C. Synthesis of Biomimetic Ca-Hydroxyapatite Powders at 37 °C in Synthetic Body Fluids. *Biomaterials* **2000**, *21*, 1429-1438.
- ThermoScientific. http://www.barnstead.com/eThermo/CMA/PDFs/Product/productPDF_51035.pdf (accessed March 03, 2010).
- Tung, M. S.; Eidelman, N.; Sieck, B.; Brown, W. E. Octacalcium Phosphate Solubility Product from 4 to 37 °C. *Journal of Research of the National Bureau of Standards* **1988**, *93*, 613-624.
- Valsami-Jones, E.; Ragnarsdottir, K. V.; Putnis, A.; Bosbach, A.; Kemp, A. J.; Cressey, G. The Dissolution of Apatite in the Presence of Aqueous Metal Cations at pH 2-7, *Chemical Geology* **1998**, *151*, 215-253.
- User Manual, SkanIt® Software for Multiskan® Spectrum version 2.2, Rev. 2.0 Thermo Electron Corporation.
- Van Veldhoven, P. P.; Mannaerts, G. P. Inorganic and Organic Phosphate Measurements in the Nanomolar Range. *Analytical Biochemistry* **1987**, *161*, 45-48.
- Vallet-Regi, M.; Gonzales-Calbet, M. Calcium Phosphates as Substitution of Bone Tissues. *Progress in Solid State Chemistry* **2004**, *32*, 1-31.
- van der Houwen, J. A. M.; Cressey, G.; Cressey, B. A.; Valsami-Jones, E. The Effect of Organic Ligands on the Crystallinity of Calcium Phosphate. *Journal of Crystal Growth* **2003**, *249*, 572-583.
- Vogel, G. L.; Chow, L. C.; Brown, W. E. A Microanalytical Procedure for the Determination of Calcium, Phosphate and Fluoride in Enamel Biopsy Samples. *Caries Research* **1983**, *17*, 23-31.
- Vogel, G. L. American Dental Association Foundation, Paffenbarger Research Center, National Institute of Standards and Technology, Gaithersburg, Maryland. Personal Communication, 2007.
- Wang, L.; Nancollas, G.H. Calcium Orthophosphates: Crystallization and Dissolution. *Chem. Rev.* **2008**, *108*, 4628-4669.
- Wopenka, B.; Pasteris, J. D. A Mineralogical Perspective on the Apatite in Bone. *Materials Science and Engineering* **2005**, *C25*, 131-143.
- Wu, W.; Tang, R.; Haas, M.; Nancollas G. H. Constant Composition Dissolution of Mixed Phases I. Synthetic Calcium Phosphates. *Journal of Colloid and Interface Science* **2001**, *244*, 347-352.
- Ye, H.; Liu, X. Y.; Hong, H. Characterization of Sintered Titanium / Hydroxyapatite Biocomposite using FTIR Spectroscopy. *Journal of Materials Science: Materials in Medicine* **2009**, *20*, 843-850.

- Zhang J.; Nancollas G. H. Kinetics and Mechanism of Octacalcium Phosphate Dissolution at 37 °C. *Journal of Physical Chemistry* **1992**, *96*, 5478-5483.
- Zhang, H.; Yan, Y.; Wang, Y.; Li, S. Thermal Stability of Hydroxyapatite Whiskers Prepared by Homogeneous Precipitation. *Advanced Engineering Materials* **2002**, *4*, 916-919.
- Zyryanov, A. B.; Baykov, A. A. Determination of Mn (II) and Co (II) with Arsenazo III. *Biochemistry* **2002**, *67*, 766-771.

APPENDIX A

CALCIUM REMOVAL FROM ARSENAZO III DYE SOLUTIONS

Throughout this study two 1 mM Arsenazo III stock solutions were used. Each solution was subjected to calcium removal before use. They are referred as solution 1 and solution 2. Calcium removal from Arsenazo III stock solutions is as follows:

Arsenazo III dye solution was prepared by weighing 0.7762 g Arsenazo III and dissolving in ultrapure water by stirring on a magnetic stirrer in a 1 liter polypropylene bottle. The volume of the solution was adjusted to 1 liter and mixed thoroughly. Dye solution was then filtered through Filtrak filter paper grade 288 into a new 1 liter capacity polypropylene bottle.

Calcium initially present in Arsenazo III dye was purified as suggested by Vogel et al. (1983) with some modifications. Approximately 15 g Dowex® 50Wx4-100 was equilibrated in nearly 40 mL ultrapure water for 3 days. A polypropylene column ($D_i \approx 16$ mm, $D_o \approx 20$ mm and $L \approx 200$ mm) was used to purify Arsenazo III solution. Glass wool was placed at the bottom of the column. Ion exchange resin was then packed into the column by the help of ultrapure water. Glass wool was also placed above the resin. Height of the resin packed into the column was approximately 10.4 cm. A peristaltic pump (Perista Pump SJ1211, BioInstrument ATTO) with a piping was connected to the entrance of the column. A pipe was also connected to the exit of the column and a clamp was attached to the exiting pipe to stop the flow. Prior the feeding of Arsenazo III dye into the column, 1 liter of 0.1 M HCl was used to regenerate the ion exchange resin. Initial and exit flow rate of the solutions was determined by measuring the time necessary to pump 10 mL of the solutions. Initial and exit volumetric flow rates were therefore found as 0.26 mL/s and 0.25 mL/s, respectively during the purification of solution 1. When solution 2 was purified, initial and exit volumetric flow rates were 0.18 mL/s and 0.16 mL/s, respectively.

After passing the HCl solution through the column, column was washed with 500 mL ultrapure water. Ultrapure water was removed from the column by passing air through the column. At this step, special care was taken to avoid the resin to get dry.

The ion exchange system used in the removal of calcium from the Arsenazo III dye solution is shown in Figure A.1.

After regeneration and washing of the resin, Arsenazo III dye solution was fed into the column and purified dye was collected at the bottom of the column into a 1 liter polypropylene bottle. At five minutes intervals, flow of the solution was stopped and samples for pH measurement were taken into 15 mL plastic centrifuge tubes by starting the flow of the solution again. After taking the samples for pH measurements, flow of the solution was started to collect the purified dye solution. At the end of purification of the dye solution, pH values of the samples were measured by pH meter (Metrohm 744). Samples for the pH measurements were added into the purified dye solutions. Finally, pH value of the purified reagent was also measured. Purified solution was transferred into a 1 liter polypropylene volumetric flask by polypropylene beaker and volume was adjusted into 1 liter by ultrapure water. After mixing well, solution was transferred into 1 liter polypropylene bottle. In order to avoid the contamination to the whole purified solution, aliquot from the purified reagent was taken into 100 mL polypropylene bottle and used as working solution. Solutions was protected from the light by wrapping aluminum foil around the bottle and kept at 4 °C.



Figure A.1. Cation exchange column chromatography system used to purify Arsenazo III dye a. front view, b. side view.

APPENDIX B

DETERMINATION OF ARSENAZO III CONCENTRATION IN PURIFIED SOLUTIONS

Concentration of Arsenazo III in the purified solution was determined according to Minganti et al. (1983). Concentration of the Arsenazo III in the purified reagent was determined from the molar extinction coefficient by recording the absorbencies of the dye solutions prepared in concentrated sulfuric acid at 675 nm. For this reason, five different solutions of Arsenazo III dye were prepared in concentrated sulfuric acid in triplicate except for the solutions one (six parallels) (Table B.1).

Five hundred, 250 and 125 μL of Arsenazo III dye were transferred into 25 mL glass capacity glass volumetric flasks. Concentrated sulfuric acid was then added into the flasks. Solutions were left to cool down to room temperature. Finally, volumes of the solutions were adjusted to 25 mL by concentrated sulfuric acid and all the solutions were mixed well.

Additionally, 500, 250, 125 μL of purified Arsenazo III solution were added into 25 mL capacity glass volumetric flasks. 250 μL and 125 μL of ultrapure water were added into 250 μL and 125 μL Arsenazo III containing flasks, respectively. Concentrated sulfuric acid was then added in the flasks and solutions were left to cool down to room temperature. Volumes were then brought to 25 mL by the addition of concentrated sulfuric acids. After volume adjustments, solutions were mixed well.

Table B.1 Solutions prepared for the determination of Arsenazo III concentration in solution 1

No	Volume of Arsenazo III (μL)	Volume of Ultrapure Water (μL)	Final Volume Adjusted by concentrated sulfuric acid (mL)	Replicate
1	500	-	25	6
2	250	-	25	3
3	125	-	25	3
5	250	250	25	3
6	125	375	25	3

Absorbances of the solutions at 675 nm were measured in a UV-Visible spectrophotometer (Perkin Elmer, Precisely, Lambda 25) vs. ultrapure water by using quartz cuvettes having 1 cm pathlength at 25 °C. First of all, instrument was autozeroed by ultrapure water both in reference and sample cells by using quartz cuvettes. One cuvette containing ultrapure water was then blanked against the other cuvette containing ultrapure water. Absorbencies of the samples (three samples from each 25 mL solution) were recorded against ultrapure water. Specifications of the absorbance analysis of Arsenazo III in sulfuric acid solutions are given as follows.

Specifications of absorbance measurements:

Wavelength (λ): 675 nm

Slit: 1 nm

Response: 2s

Peltier: 25 °C

Cuvettes: Quartz cuvettes with 1 cm pathlength

Additionally, spectra of the representative solutions were measured against ultrapure water in UV-Visible spectrophotometer (Perkin Elmer, Precisely, Lambda 25) quartz cuvettes having 1 cm pathlength at 25 °C. Instrument was autozeroed by ultrapure water both in reference and sample cells. Ultrapure water in reference cell was then blanked by ultrapure water in sample cell. Spectra of the solutions were recorded vs. ultrapure water.

Specifications of the spectrum scanning:

Start Wavelength (λ): 700 nm

End Wavelength (λ): 400 nm

Data Interval: 5 nm

Slit: 1 nm

Scan Speed: 240 nm/min

Peltier: 25 °C

When solution 2 was purified, determination of Arsenazo III concentration in was performed by transferring 500 microliters of Arsenazo III into 25 mL glass volumetric flasks (6 replicates). Concentrated sulfuric acid was then added into the flasks and solutions were left to cool down to room temperature. After the solutions were cooled, volumes were adjusted to 25 mL by concentrated sulfuric acid. Solutions were mixed thoroughly.

Absorbances of the solutions were measured in Multiskan® Spectrum microplate and cuvette reader (Thermo Electron Corp., Finland) in 1 cm quartz cells at 25 °C. Instruments was zeroed first by two empty quartz cuvettes and then by ultrapure water both in reference and sample quartz cuvetes. Absorbances of three samples from each replicate were recorded against ultrapure water at 675 nm.

APPENDIX C

PREPARATION OF ARSENAZO III REAGENTS TO BE USED IN CALCIUM ANALYSIS

Different buffers, different pH values, various Arsenazo III concentrations were tested for the construction of linear calibration curves for three different ranges of calcium concentrations (0.25-2 ppm, 1-8 ppm and 10-80 ppm calcium). Three different buffers, imidazole-Cl, acetate and formate buffers were used in the calcium analysis by Arsenazo III method.

Arsenazo III in Acetate Buffer

Two different solutions Arsenazo III solutions; one having 60 μM and the other containing 120 μM Arsenazo III, in 100 mM acetate buffer were prepared.

60 μM Arsenazo III & 100 mM Acetate Buffer pH 5.4:

Forty two point three milliliters 0.2 M sodium acetate was added into a 100 mL polypropylene bottle. To this solution, 5 mL 0.2 M acetic acid solution was added. Seven point five milliliters from purified Arsenazo III solution was transferred into the solution and 25 mL ultrapure water then added. Solution was mixed and kept at 25 °C without shaking in a shaking incubator. After keeping the solution at 25 °C, it was mixed by stirring on a magnetic stirrer and pH of the solution was recorded by stopping the stirring. 2.7 mL 0.2 M acetic acid was then added into the solution to adjust pH to 5.4. Solution was then transferred into a 100 mL polypropylene volumetric flask. Residue left on the pH meter probe and in the bottle was taken by ultrapure water and combined with the solution. Volume of the solution was brought to 100 mL by ultrapure water. Solution mixed well and transferred into 100 mL polypropylene bottle. Solution was again kept at 25 °C and final pH of the solution was recorded as 5.4. Bottles were wrapped with aluminum foil in order to protect solution from the light during the preparation as well as storing for further uses. Solution was stored at 4 °C until use.

120 μ M Arsenazo III & 100 mM Acetate Buffer pH 5.4:

For the preparation 120 μ M Arsenazo III in 100 mM acetate buffer, 49.1 mL 0.2 M sodium acetate was transferred into 100 mL capacity polypropylene bottle. To this solution, 0.9 mL 0.1 M acetic acid solution was added. Solution was mixed gently. Fifteen milliliters of purified Arsenazo III solution was transferred into the solution. Solution was kept at 25 °C without shaking in a thermoshake incubator. Solution was stirred on a magnetic stirrer. pH of the solution was measured while the stirring was stopped. Solution was transferred into 100 mL polypropylene bottle. Residue left on the pH meter probe and in the bottle was taken with ultrapure water and combined with the solution. Volume of the solution was then adjusted to 100 mL with ultrapure water and solution was mixed well. After that, solution was transferred into 100 mL polypropylene bottle. Final pH of the solution was measured and found as 5.4. Solution was kept at 4 °C when not in use. During the preparation of the reagent and storage at 4 °C, protection from the light was done by wrapping an aluminum foil around the bottles.

Arsenazo III in Formate Buffer

Solutions with two different Arsenazo concentrations (60 and 120 μ M) were prepared in formate buffer.

60 μ M Arsenazo III & Formate Buffer pH 3.8:

Seventy milliliters ultrapure water was transferred into a 100 mL polypropylene bottle. 0.84 mL of formic acid was then added and solution mixed gently. Seven point five milliliters of purified Arsenazo III solution was transferred into the bottle. Solution was incubated at 25 °C without shaking in a shaking incubator. It was then stirred on a magnetic stirrer. Solution was titrated with 1 M KOH to pH 3.8. Solution pH was monitored during the titration. However when the pH would be recorded, stirring was stopped. Total amount of 1 M KOH used to adjust pH 3.8 was approximately 12.8 mL. pH of the solution at the end of the titration was recorded as 3.80. Solution was then transferred into 100 mL polypropylene volumetric flask. Residue left on the pH probe

and in the bottle was removed with ultrapure water and combined with the solution. Volume of the solution was adjusted to 100 mL by ultrapure water and mixed well. Solution was then transferred into 100 mL polypropylene bottle and kept at 25 °C. Final pH of the solution was measured as 3.8. Solution was stored at 4 °C until its use. During the preparation bottles were protected from the light by wrapping aluminum foil.

120 μM Arsenazo III & Formate Buffer pH 3.8:

A hundred twenty μM Arsenazo III in formate buffer was prepared by similar way like in the preparation of 60 μM Arsenazo III in formate buffer. Sixty milliliters ultrapure water was added into a 100 mL polypropylene bottle and 0.84 mL formic acid was then transferred into the bottle. After gentle mixing the solution, 15 mL purified Arsenazo III solution was added to the solution. Solution was incubated at 25 °C for a while. Solution was then titrated with 1 M KOH to the pH of 3.80. During titration, solution pH was monitored; however stirring was stopped when the pH value was recorded. Approximately 16 mL 1 M KOH was used for the titration of the solution. pH of the solution at the end of titration was recorded as 3.80. The solution was then transferred into 100 mL capacity polypropylene bottle. Residue from the solution left on pH probe and in the bottle was removed by ultrapure water and added to the solution. Finally, volume of the solution was adjusted to 100 mL by ultrapure water and solution was mixed well. After transferring the solution into 100 mL polypropylene bottle, solution was again kept at 25 °C for a while. Final pH of the solution was measured and recorded as 3.8. Solution was stored at 4 °C until its use. During the preparation and storage of the solution, aluminum foil wrapped around the bottles was used to protect solution from the light.

Arsenazo III in Imidazole-Cl Buffer

Four different Arsenazo III solutions in imidazole buffer were prepared and tested for the calcium analysis.

60 μ M Arsenazo III & 100 mM Imidazole-Cl pH 6.5:

0.6875 gram imidazole was dissolved in approximately 60 mL ultrapure water and transferred into 100 mL polypropylene bottle. 7.5 mL purified Arsenazo III solution was added into the bottle. Solution was incubated at 25 °C statically in a thermoshake incubator. Solution was then titrated with 1 M HCl solution to the pH of 6.5. During the addition of 1M HCl, solution was stirred on the magnetic stirrer. When the solution's pH values would be recorded, stirring was stopped. Approximately 7.9 mL 0.1 M HCl was used to adjust the solution pH to 6.5. Solution was transferred into 100 mL polypropylene volumetric flask. Dye left on the pH probe and in the bottle was washed with ultrapure water and combined with the solution. Volume of the solution was adjusted to 100 mL by the addition of ultrapure water. Solution in volumetric flask was mixed well and transferred into 100 mL polypropylene bottle. Final pH of the solution was measured as 6.5. This solution was stored at 4 °C. Bottles during the preparation and storage were wrapped by aluminum foil in order to avoid light induced changes in the reagent.

60 μ M Arsenazo III & 200 mM Imidazole-Cl pH 6.5:

1.3764 gram imidazole was weighed and dissolved in approximately 70 mL ultrapure water. Solution was transferred into 100 mL capacity polypropylene bottle and 7.5 mL purified Arsenazo III solution was then added into this solution. After mixing the solution by stirring on a magnetic stirrer, it was incubated at 25 °C. Solution pH was then adjusted by 1 M HCl solution to pH 6.5. While adjustment of pH solution was stirred on the magnetic stirrer, but when the pH values would be recorded stirring was stopped. Approximately 16 mL 1 M HCl was used to adjust the pH value to pH 6.5. Solution was transferred into 100 mL polypropylene volumetric flask. Residue left on the pH probe and bottle was washed with ultrapure water and added into the solution.

Volume of the solution was brought to 100 mL by ultrapure water. After mixing the solution, it was transferred into 100 mL capacity polypropylene bottle. Solution was incubated at 25 °C for a while. Final pH of the solution was measured as 6.5. Solution was kept at 4 °C until its use. During the preparation and storage, bottles were wrapped with aluminum foil.

200 μM Arsenazo III & 200 mM Imidazole-Cl pH 6.5:

Imidazole, 1.3744 g, was dissolved in 50 mL ultrapure water and transferred into 100 mL polypropylene bottle. Twenty five milliliters of purified Arsenazo III solution was then added into the solution. This solution was then statically incubated at 25 °C in the thermoshake incubator. pH of solution was then adjusted to 6.5 by titrating the solution with 1 M HCl. While addition of 1 M HCl into the solution, solution was stirred on a magnetic stirrer but stirring was stopped during the pH measurements. Titration of the solution was completed when the pH was measured as 6.5. Approximately 15.8 mL 1 M HCl was spent for the titration of the solution to the desired pH value. After the adjustment of pH, solution was transferred into 100 mL polypropylene volumetric flask. Residual dye removed from the pH probe and bottle was taken by ultrapure water and combined with the solution. Volume was adjusted to 100 mL by ultrapure water. After thorough mixing of the solution in volumetric flask, it was transferred into a 100 mL polypropylene bottle. Final pH of the solution was checked and found as 6.5. Like all solutions prepared, this solution was also kept at 4 °C in a refrigerator for further uses. Solutions were protected from the light induced changes by wrapping aluminum foil around the bottles.

500 μM Arsenazo III & 200 mM Imidazole-Cl pH 6.5:

For the preapartion of 500 μM Arsenazo III in imidazole buffer, 1.3747 grams of imidazole was weighed. Since the volume of purified Arsenazo III solution to be added was high, imidazole was directly dissolved in 62.5 mL purified Arsenazo III solution. Solution was transferred into 100 mL capacity polypropylene bottle. Ten milliliters of ultrapure water was added into the solution. This solution was then statically incubated at 28 °C in the thermoshake incubator until pH adjustment. Titration of the solution

was performed while solution was stirred on a magnetic stirrer. One molar HCl was used for the titration of the solution pH to 6.5. During the pH measurements, stirring was stopped. Titration was performed until the solution pH was measured as 6.5. Fifteen point four milliliters of 1 M HCl was spent for the pH adjustment. After the titration, the solution was transferred into 100 mL polypropylene volumetric flask. Dye left on the pH probe was removed with ultrapure water. This ultrapure water was then used to recover dye left in the bottle and it was added into the solution. Solution volume was finally adjusted to 100 mL by ultrapure water. Solution was mixed well and transferred into a 100 mL polypropylene bottle. Final pH of the solution was measured and found as 6.5.

APPENDIX D

RESULTS OF CALCIUM REMOVAL FROM ARSENZO III SOLUTIONS

Commercial Arsenazo III dye may initially have large amounts of calcium (Vogel et al. 1983). For this reason, the first attempt was to purify calcium initially present in the dye. This was performed using the method suggested by Vogel et al. (1983). Calcium was removed from Arsenazo III by passing the dye through a cation exchange resin in H⁺ form. Throughout this study, two 1 mM Arsenazo III solutions were used. These are referred as solution 1 and solution 2. Each solution was subjected to calcium removal by cation exchange before use. In order to follow the efficiency of the purification process, pH values of the samples taken at definite intervals were measured. Figure D.1 shows the pH values of the samples taken in 5 minute intervals.

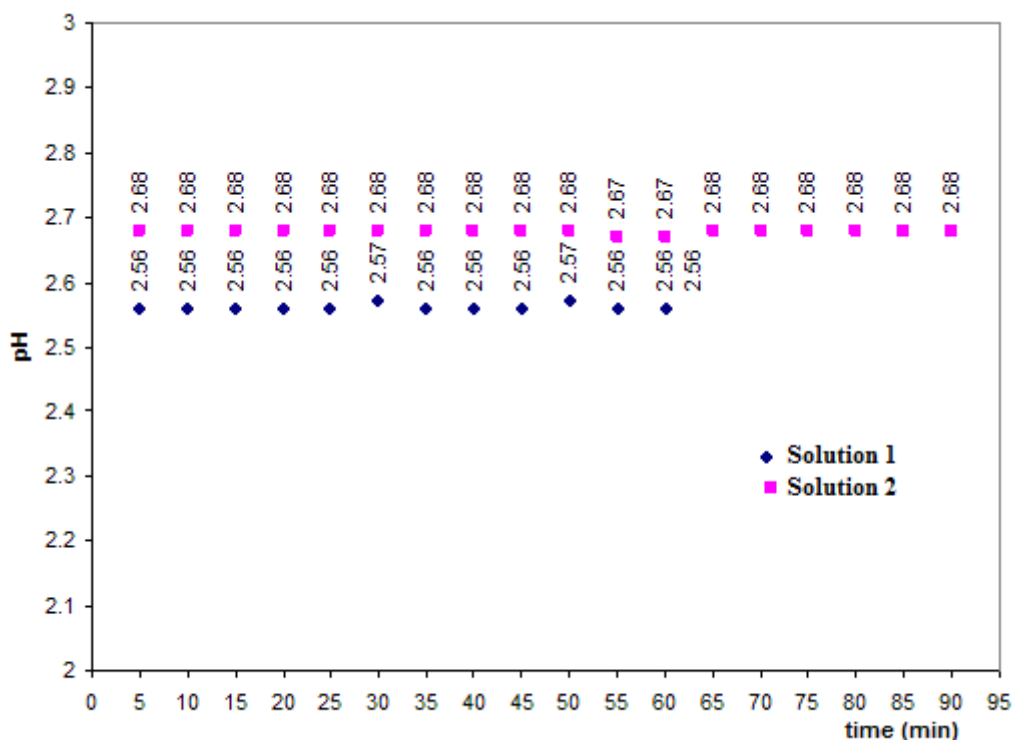


Figure D.1. pH values of the samples taken during the purification of Arsenazo III dye.

Space velocities during purification of solution 1 and solution 2 were 45 and 28.8 BV/h, respectively.

In the purification of solution 1, pH of the feed prior to purification was measured as 2.68. pH of the sample taken from the column at 5 min was found as 2.56. pH values of all the other samples were found as 2.56 or 2.57. Similarly for the solution 2, initial pH of the dye solution was measured as 2.81. pH of the sample taken after 5 min during the calcium removal was 2.68. pH values of the all samples were found to be constant during the purification. These show that pH of the purified solutions stayed constant throughout the purification process. Equality of pH values of all the samples to pH of the sample taken at 5 min means that cation exchanger kept its capacity for the removal of cations throughout the purification of the dye. Besides pH values of the dyes, pH value of the whole solutions (samples were also combined into the solution) were measured and found as 2.55 and 2.67 for purified solution 1 and solution 2, respectively. When solution 1 was purified, total H^+ concentration exchanged was found to be 0.66 mM from pH measurements. This equals to 0.66 milliequivalents of H^+ . Calcium exchanged was therefore equal to 0.66 milliequivalents. Calculated calcium concentration was therefore found as 13.2 mg/L. When solution 2 was purified 0.59 mM hydrogen was exchanged. This equals to 0.59 equivalents of calcium. Calcium in the dye solutions before cation exchange was found to be 11.8 mg/L. Total exchange capacity of the Dowex 50Wx4 was reported to be 1.1 meq/mL. Since approximately 10 mL resin was used for each dye solution, capacity of the column can be found as 11 meq Ca. This corresponds to 220 mg calcium. Since one liter dye solution was purified in the column at the each purification process, total calcium retained on the column was lower than 15 mg during the purification of dye.

APPENDIX E

ARSENAZO III CONCENTRATION IN PURIFIED SOLUTIONS

It is essential to know Arsenazo III concentration in the reagent used in calcium determinations for the accurate and precise calcium analysis. During the preparation of Arsenazo III solution, filtration caused a loss of some amount of dye solution. Additionally some amount of dye was also left in the column at the end of the calcium removal by ion exchange chromatography. After chromatography, volume of the solution was brought to 1 liter by ultrapure water. All these reasons necessitated the determination of Arsenazo III concentration in the purified solution.

In this study, Nemodruk's method (in Minganti et al., 1983) for the determination of Arsenazo III concentration was followed. This method was stated as the most convenient and widely used one (Minganti et al., 1983). It is based on the spectrophotometric analysis of the absorbance of the Arsenazo III solution prepared in concentrated H_2SO_4 . According to Nemodruk (in Minganti et al. 1983), extinction coefficient of Arsenazo III in concentrated sulfuric acid only changes with the changes in acid concentration and it is constant when the acid concentration is over 78 % (w/v).

Molar extinction coefficient of Arsenazo III prepared in concentrated sulfuric acid was reported as $52,800 \text{ M}^{-1}\text{cm}^{-1}$ by Nemodruk (Minganti et al. 1983, Zyryanov and Baykov, 2002). By using absorbance values read in 1 cm path length cuvettes and reported extinction coefficient, Arsenazo III concentration in the purified dye was calculated. Calculated concentration values of the Arsenazo III in the solutions prepared in concentrated sulfuric acid and calculated Arsenazo III concentrations of purified dye were shown in Table E.1.

Only the concentration calculated from the absorbance of the solution prepared by taking 500 μl from solution1 and diluting to 25 ml with H_2SO_4 was used as the concentration of solution 1. It was found as 800.57 ± 8.71 and taken as 800 μM for simplicity. For solution 2, Arsenazo concentration was found to be $797.19 \pm 5.17 \mu\text{M}$. For the simplicity, it was taken approximately as 797 μM for the preparation of Arsenazo III dye reagents.

Table E.1 Solutions used to determine Arsenazo III concentration in the purified solutions, their absorbance values and calculated concentrations

Solution	No	Volume of Arsenazo III (μL)	Volume of Ultrapure Water (μL)	Final Volume Adjusted by concentrated sulfuric acid (mL)	Absorbance	Molar Extinction Coefficient	Concentration of Arsenazo III in 25 mL (μM)	Concentration of Arsenazo III in the Purified Reagent (μM)	Number of Replicate Solutions	Number of Replicates of Samples Measured
1	1	500	-	25	0.8454 ± 0.0092	52,800	16.01 ± 0.17	800.57 ± 8.71	6	18
	2	250	-	25	0.4269 ± 0.0038	52,800	8.09 ± 0.07	808.52 ± 7.20	3	9
	3	125	-	25	0.2149 ± 0.0038	52,800	4.07 ± 0.07	814.02 ± 14.39	3	9
	4	250	250	25	0.4311 ± 0.0026	52,800	8.16 ± 0.05	816.48 ± 4.92	3	9
	5	125	375	25	0.2138 ± 0.0042	52,800	4.05 ± 0.08	809.85 ± 15.91	3	9
2	6	500	-	25	0.842 ± 0.005	52,800	15.94 ± 0.10	797.19 ± 5.17	6	18

APPENDIX F

ABSORBANCE VALUES OF MEASURED AT 600 nm IN THE OPTIMIZATION OF MICROPLATE BASED ARSENAZO III-CALCIUM ANALYSIS

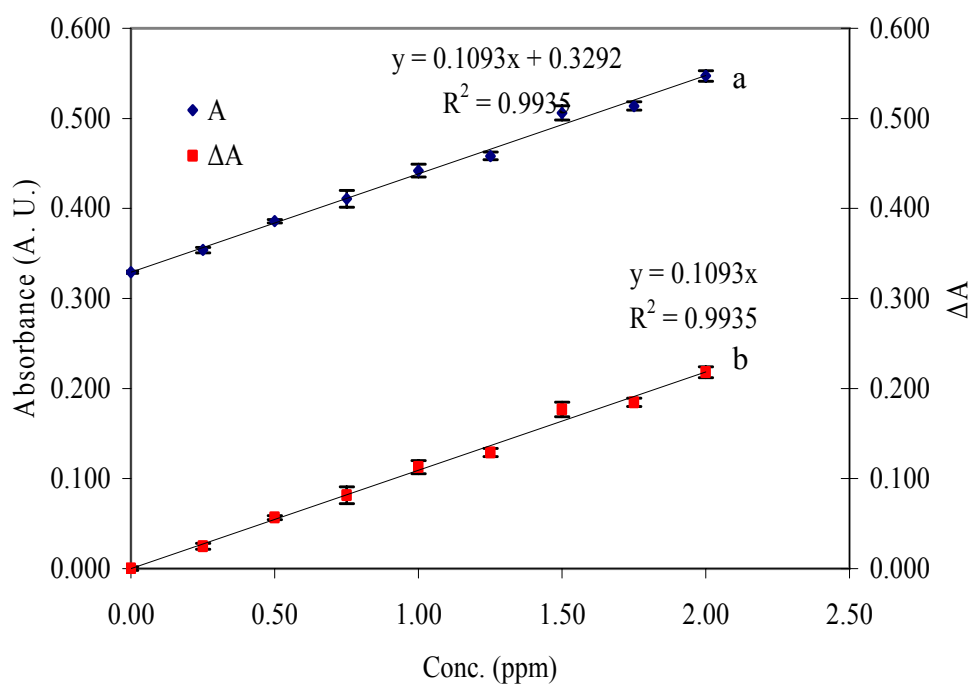


Figure F.1. Absorbance values of calcium standards (0.25-2 ppm) - 60 μ M AIII in 100 mM acetate buffer pH 5.4 (150 μ L standard-150 μ L dye reagent) at 600 nm a. without subtracting blank values, b. with subtracting blank values.

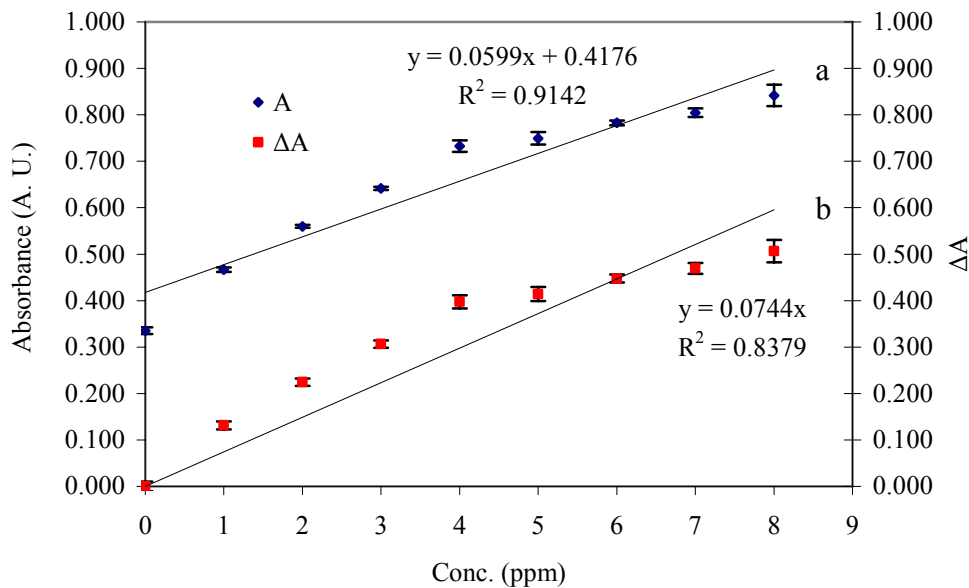


Figure F.2. Absorbance values of calcium standards (1-8 ppm) - 60 μ M AIII in 100 mM acetate buffer pH 5.4 (150 μ L standard-150 μ L dye reagent) at 600 nm a. without subtracting blank values, b. with subtracting blank values.

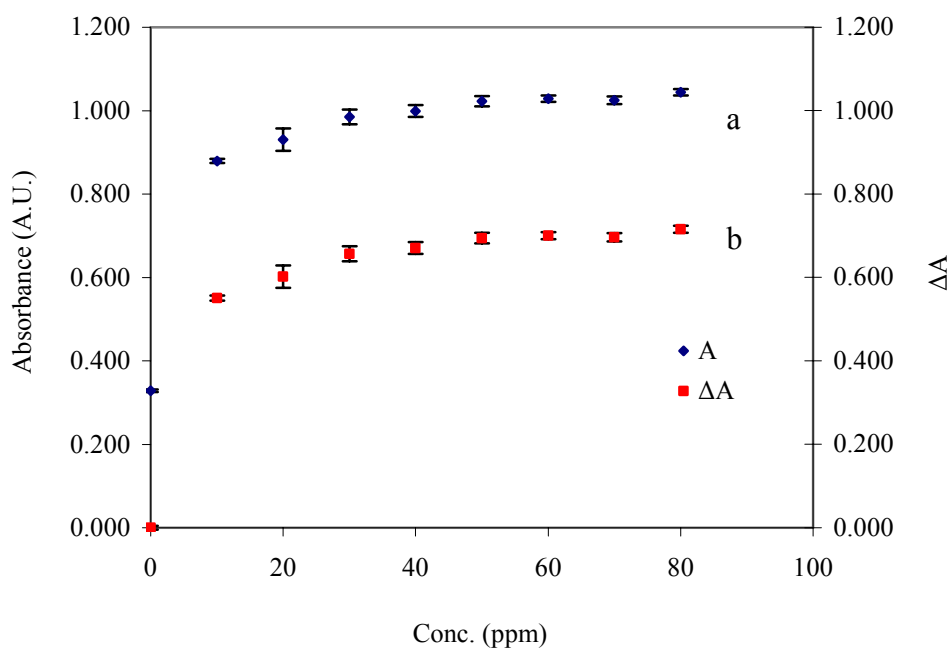


Figure F.3. Absorbance values of calcium standards (10-80 ppm) - 60 μ M AIII in 100 mM acetate buffer pH 5.4 (150 μ L standard-150 μ L dye reagent) at 600 nm a. without subtracting blank values, b. with subtracting blank values.

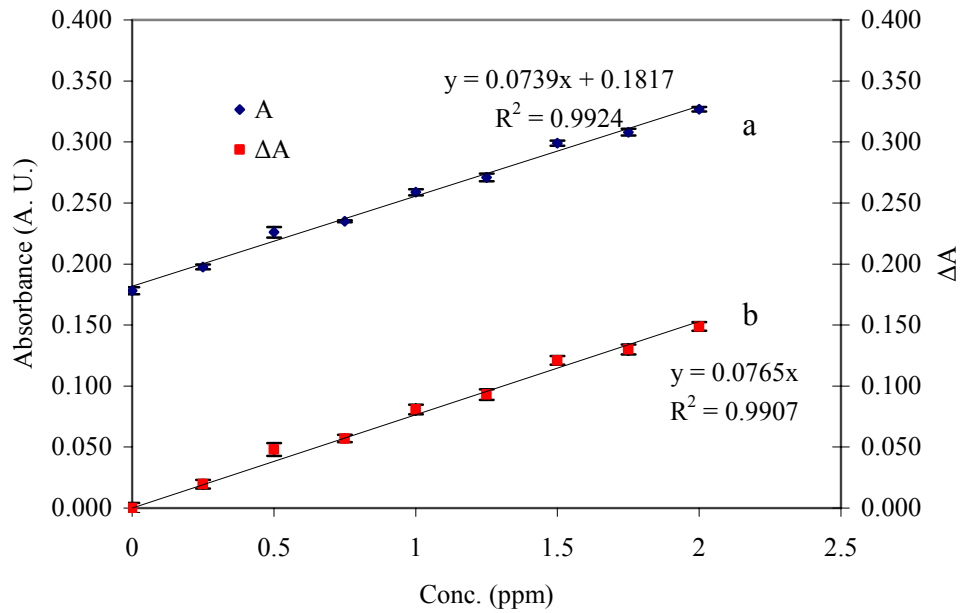


Figure F.4. Absorbance values of calcium standards (0.25-2 ppm) - $\frac{1}{2}$ (60 μ M AIII in 100 mM acetate buffer pH 5.4) (150 μ L standard-150 μ L dye reagent) at 600 nm a. without subtracting blank values, b. with subtracting blank values.

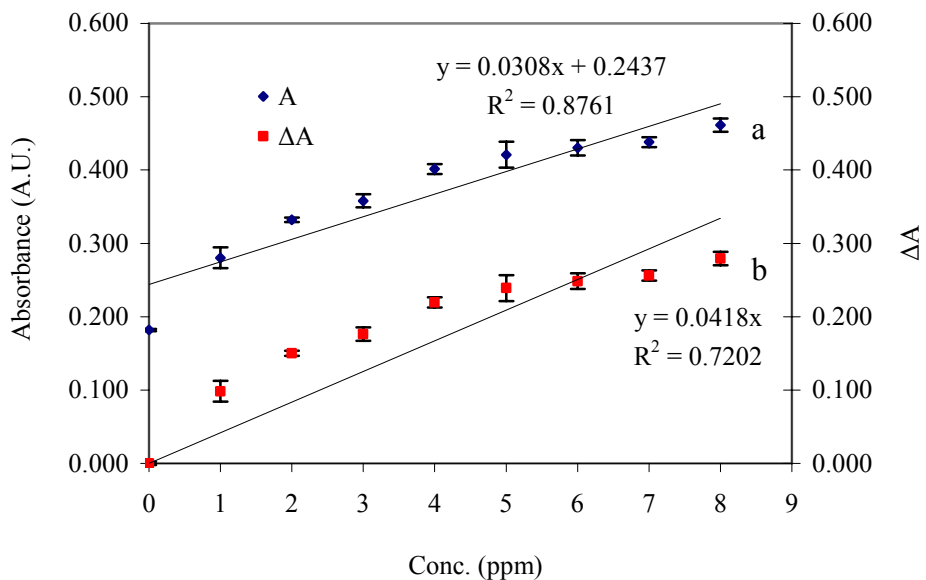


Figure F.5. Absorbance values of calcium standards (1-8 ppm) - $\frac{1}{2}$ (60 μ M AIII in 100 mM acetate buffer pH 5.4) (150 μ L standard-150 μ L dye reagent) at 600 nm a. without subtracting blank values, b. with subtracting blank values.

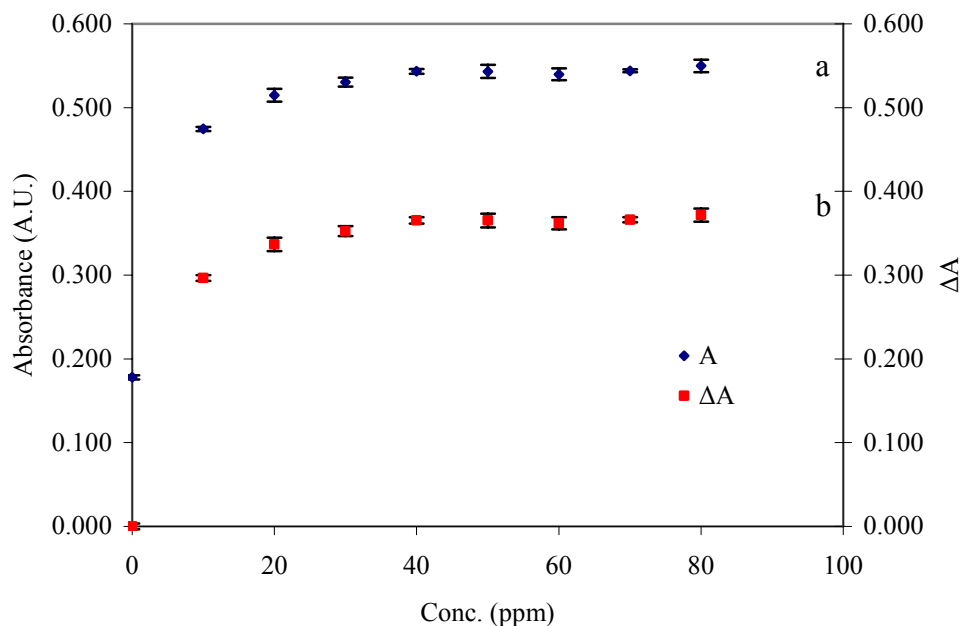


Figure F.6. Absorbance values of calcium standards (10-80 ppm) - $\frac{1}{2}$ (60 μ M AIII in 100 mM acetate buffer pH 5.4) (150 μ L standard-150 μ L dye reagent) at 600 nm a. without subtracting blank values, b. with subtracting blank values.

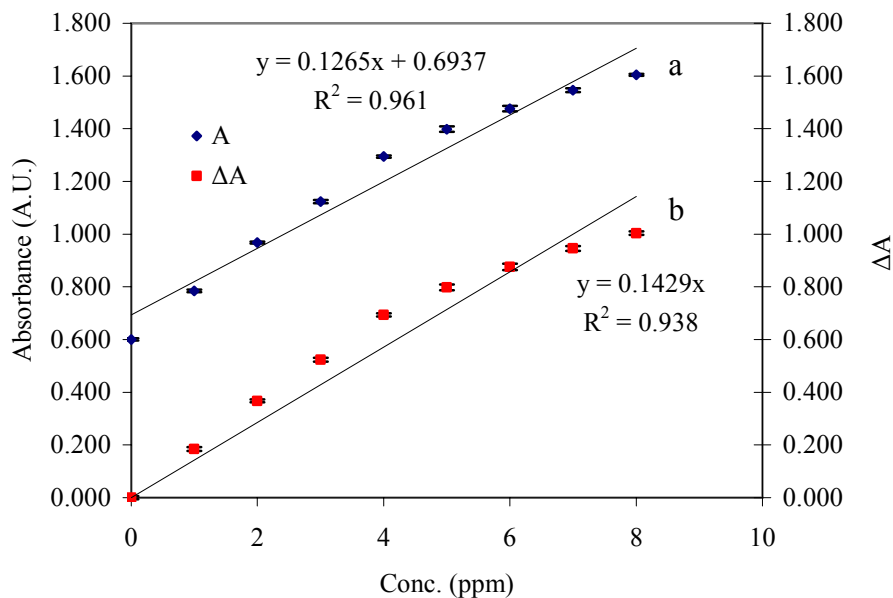


Figure F.7. Absorbance values of calcium standards (1-8 ppm) - 120 μ M AIII in 100 mM acetate buffer pH 5.4 (150 μ L standard-150 μ L dye reagent) at 600 nm a. without subtracting blank values, b. with subtracting blank values.

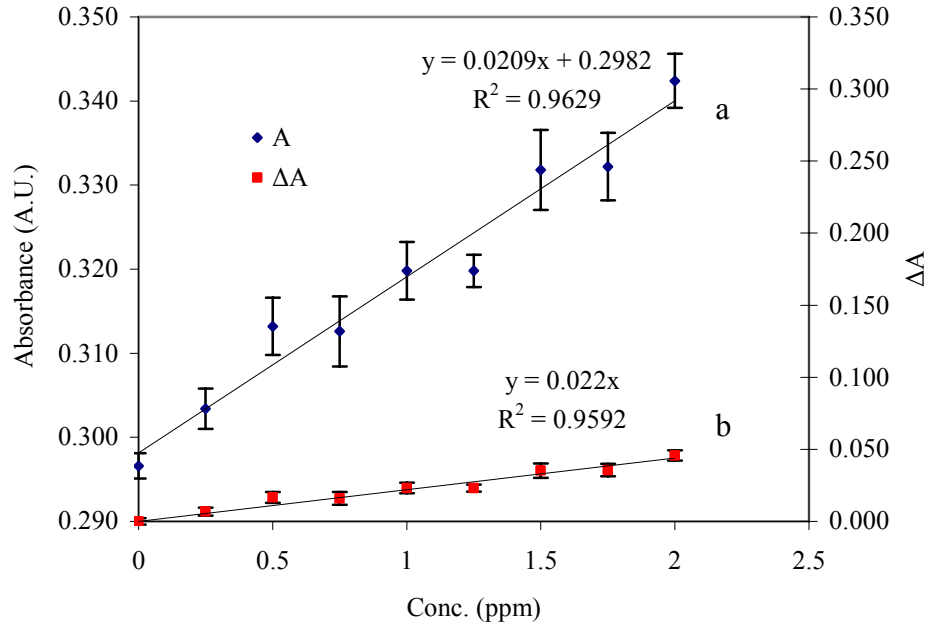


Figure F.8. Absorbance values of calcium standards (0.25-2 ppm) - 60 μ M AIII in formate buffer pH 3.8 (150 μ L standard-150 μ L dye reagent) at 600 nm a. without subtracting blank values, b. with subtracting blank values.

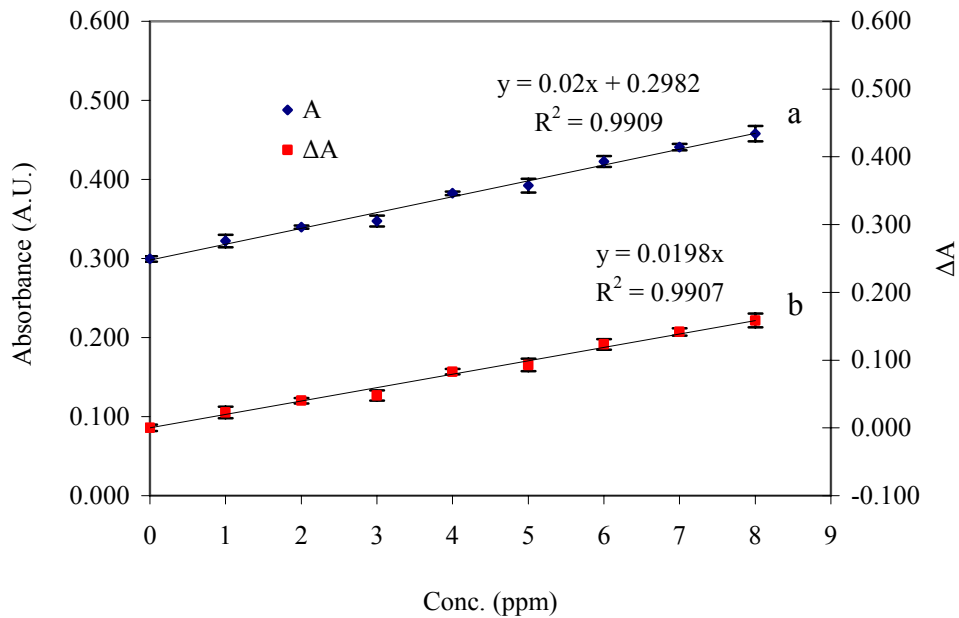


Figure F.9. Absorbance values of calcium standards (1-8 ppm) - 60 μ M AIII in formate buffer pH 3.8 (150 μ L standard-150 μ L dye reagent) at 600 nm a. without subtracting blank values, b. with subtracting blank values.

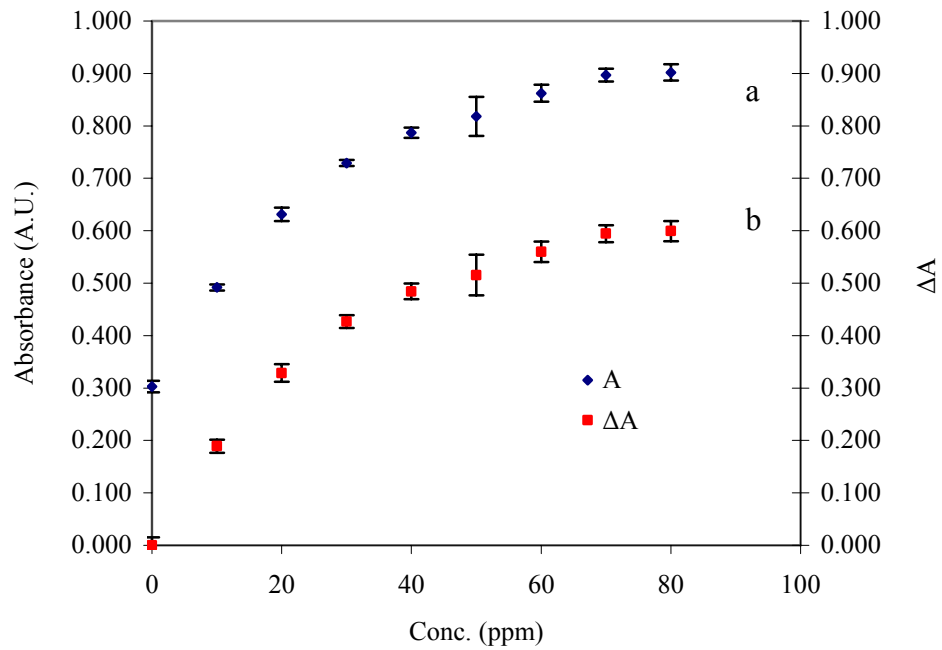


Figure F.10. Absorbance values of calcium standards (10-80 ppm) - 60 μM AIII in formate buffer pH 3.8 (150 μL standard-150 μL dye reagent) at 600 nm a. without subtracting blank values, b. with subtracting blank values.

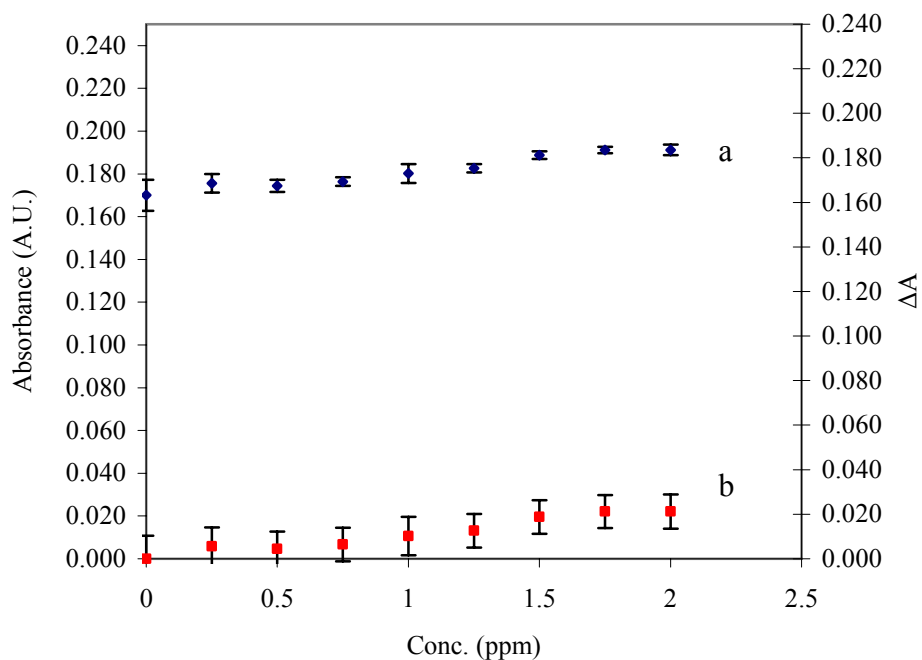


Figure F.11. Absorbance values of calcium standards (0.25-2 ppm) - $\frac{1}{2}$ (60 μM AIII in formate buffer pH 3.8) (150 μL standard-150 μL dye reagent) at 600 nm a. without subtracting blank values, b. with subtracting blank values.

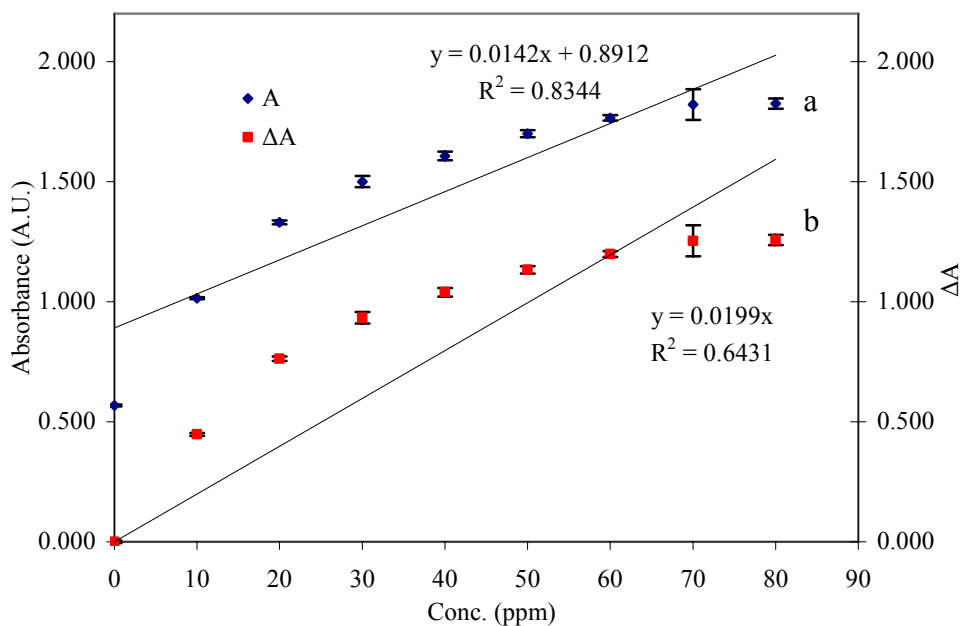


Figure F.12. Absorbance values of calcium standards (10-80 ppm) - 120 μM AIII in formate buffer pH 3.8 (150 μL standard-150 μL dye reagent) at 600 nm a. without subtracting blank values, b. with subtracting blank values.

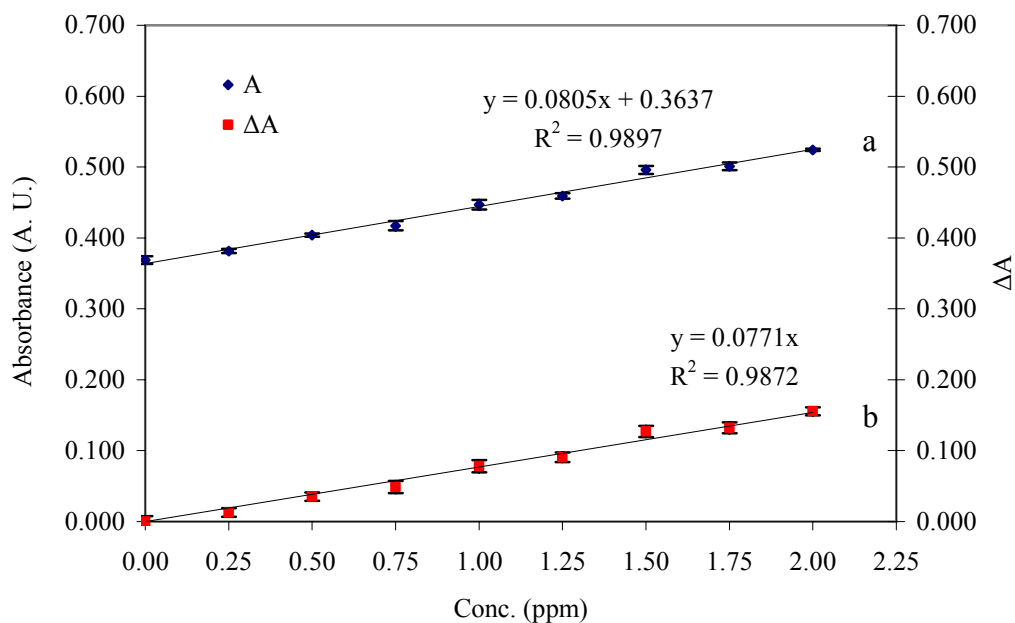


Figure F.13. Absorbance values of calcium standards (0.25-2 ppm) - 60 μM AIII in 100 mM Imidazole-Cl buffer pH 6.5 (150 μL standard-150 μL dye reagent) at 600 nm a. without subtracting blank values, b. with subtracting blank values.

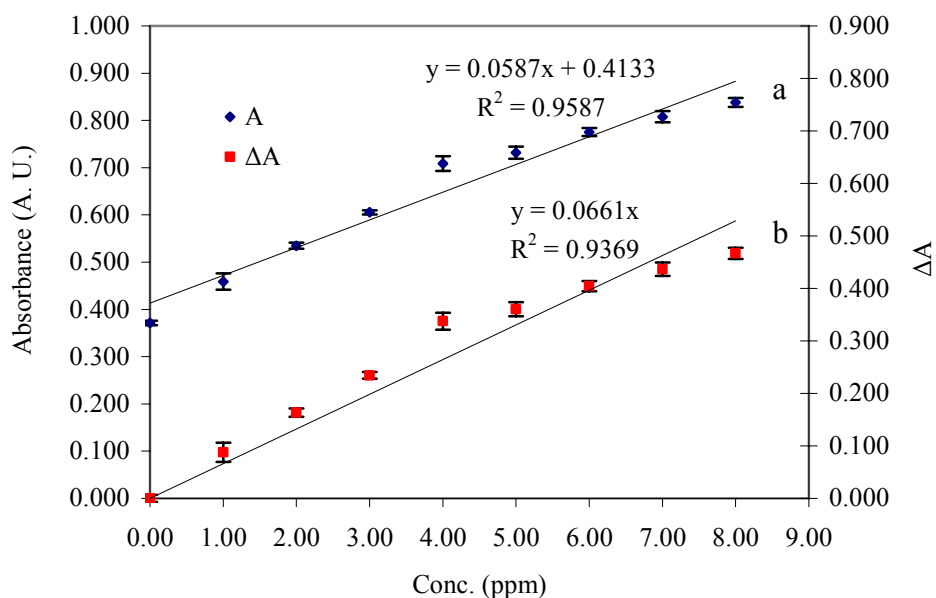


Figure F.14. Absorbance values of calcium standards (1-8 ppm) - 60 μ M AIII in 100 mM Imidazole-Cl buffer pH 6.5 (150 μ L standard-150 μ L dye reagent) at 600 nm a. without subtracting blank values, b. with subtracting blank values.

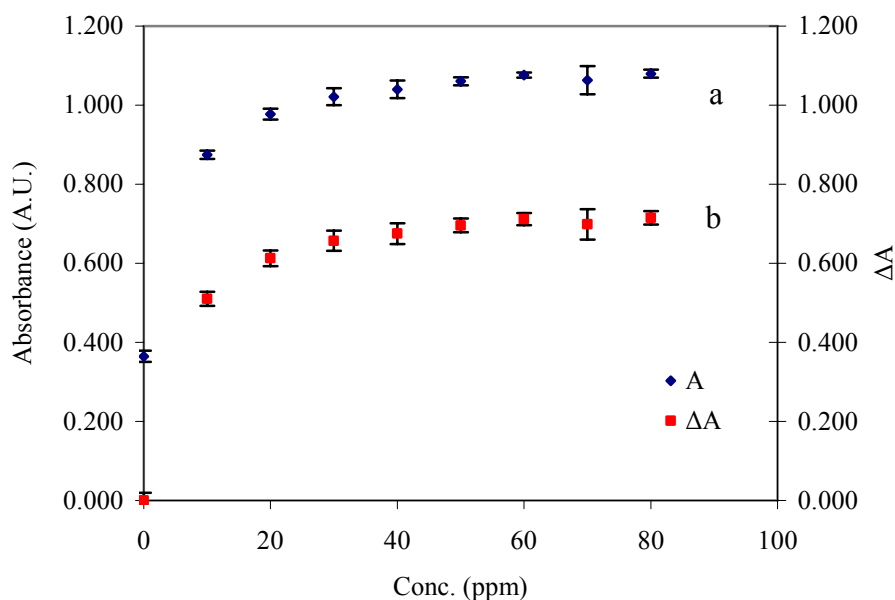


Figure F.15. Absorbance values of calcium standards (10-80 ppm) - 60 μ M AIII in 100 mM Imidazole-Cl buffer pH 6.5 (150 μ L standard-150 μ L dye reagent) at 600 nm a. without subtracting blank values, b. with subtracting blank values.

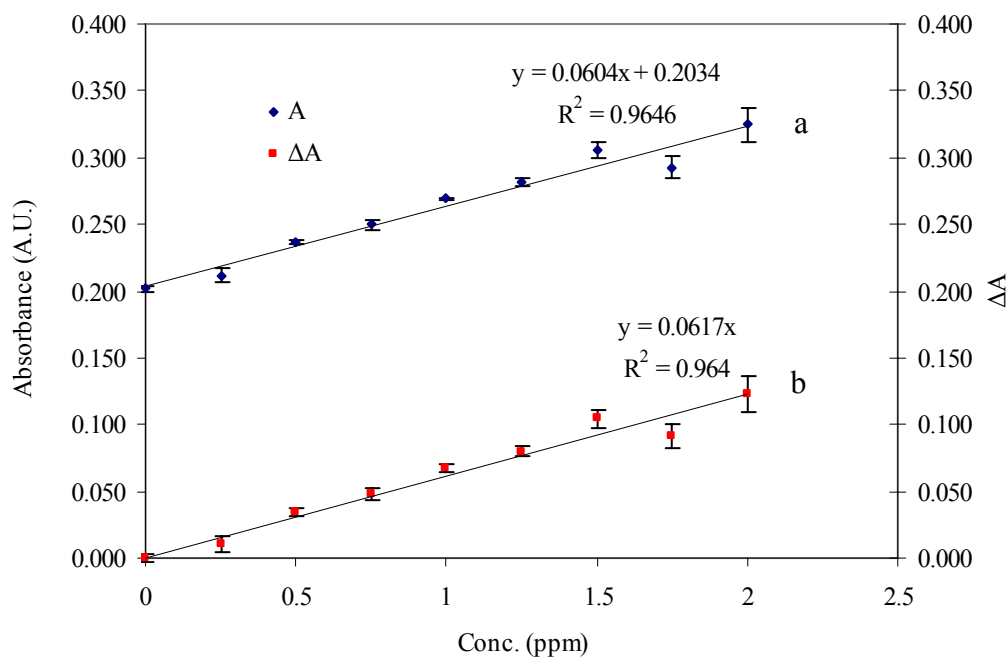


Figure F.16. Absorbance values of calcium standards (0.25-2 ppm) - $\frac{1}{2}$ (60 μ M AIII in 100 mM Imidazole-Cl buffer pH 6.5) (150 μ L standard-150 μ L dye reagent) at 600 nm a. without subtracting blank values, b. with subtracting blank values.

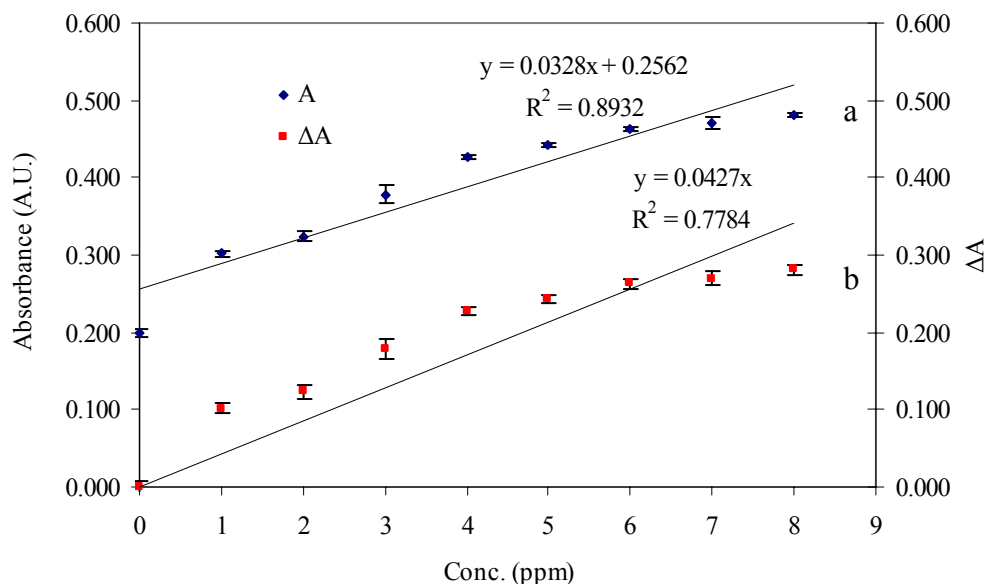


Figure F.17. Absorbance values of calcium standards (1-8 ppm) - $\frac{1}{2}$ (60 μ M AIII in 100 mM Imidazole-Cl buffer pH 6.5) (150 μ L standard-150 μ L dye reagent) at 600 nm a. without subtracting blank values, b. with subtracting blank values.

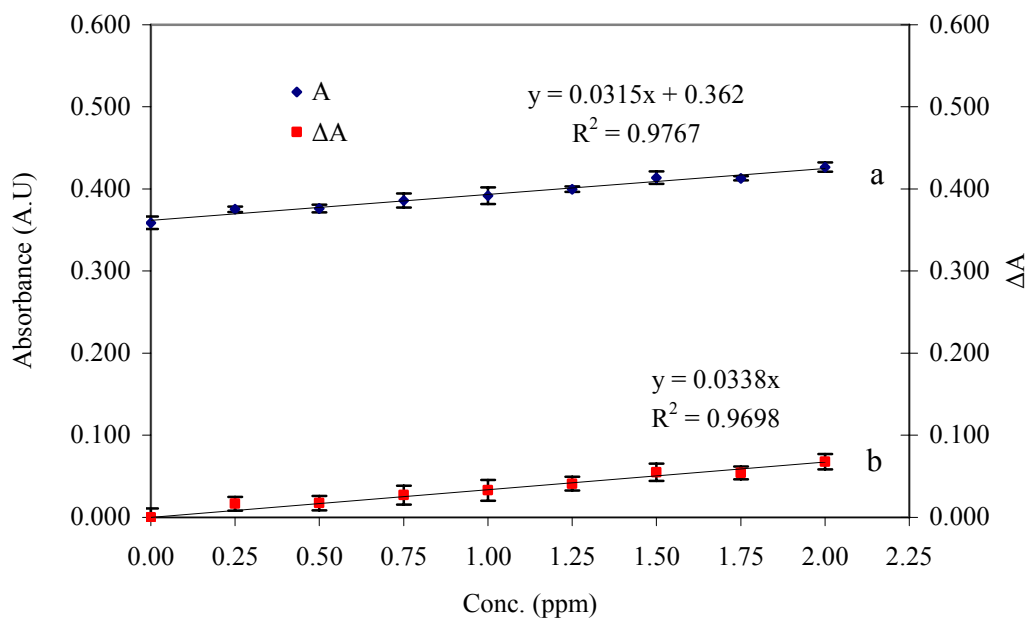


Figure F.18. Absorbance values of calcium standards (0.25-2 ppm) - 60 μ M AIII in 200 mM Imidazole-Cl buffer pH 6.5 (150 μ L standard-150 μ L dye reagent) at 600 nm a. without subtracting blank values, b. with subtracting blank values.

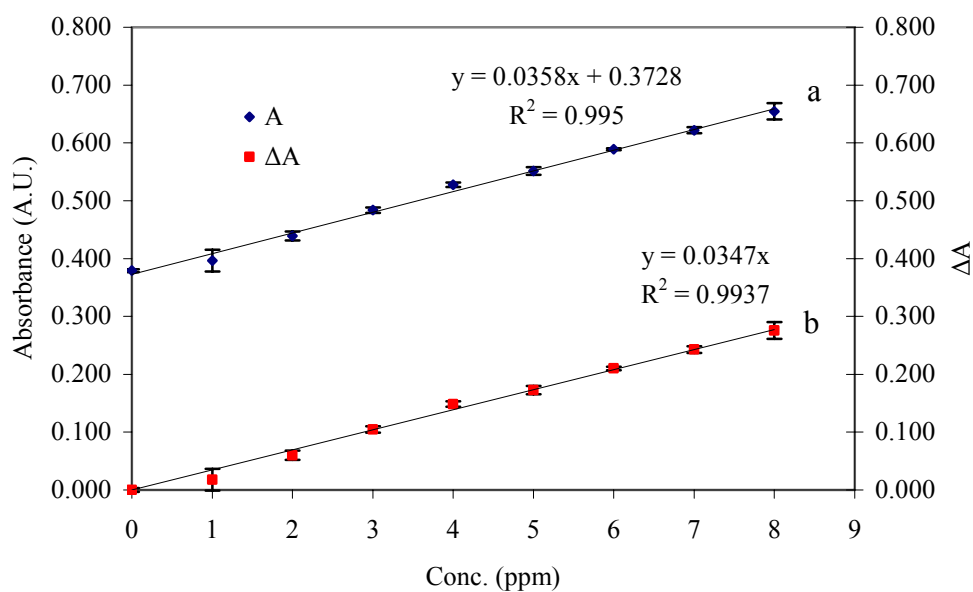


Figure F.19. Absorbance values of calcium standards (1-8 ppm) - 60 μ M AIII in 200 mM Imidazole-Cl buffer pH 6.5 (150 μ L standard-150 μ L dye reagent) at 600 nm a. without subtracting blank values, b. with subtracting blank values.

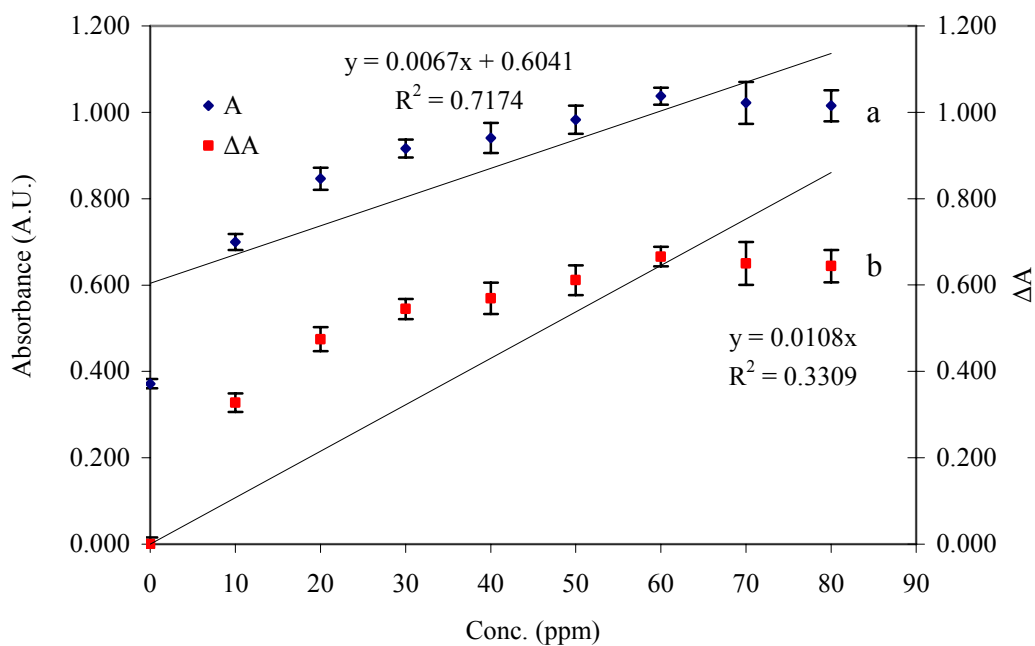


Figure F.20. Absorbance values of calcium standards (10-80 ppm) - 60 μ M AIII in 200 mM Imidazole-Cl buffer pH 6.5 (150 μ L standard-150 μ L dye reagent) at 600 nm a. without subtracting blank values, b. with subtracting blank values.

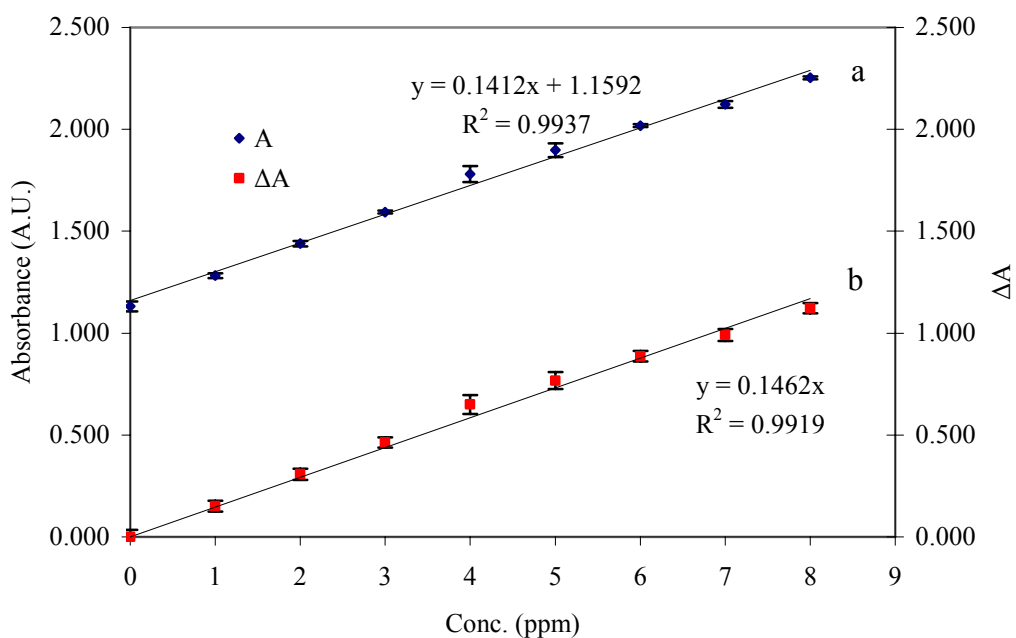


Figure F.21. Absorbance values of calcium standards (1-8 ppm) – 200 μ M AIII in 200 mM Imidazole-Cl buffer pH 6.5 (150 μ L standard-150 μ L dye reagent) at 600 nm a. without subtracting blank values, b. with subtracting blank values.

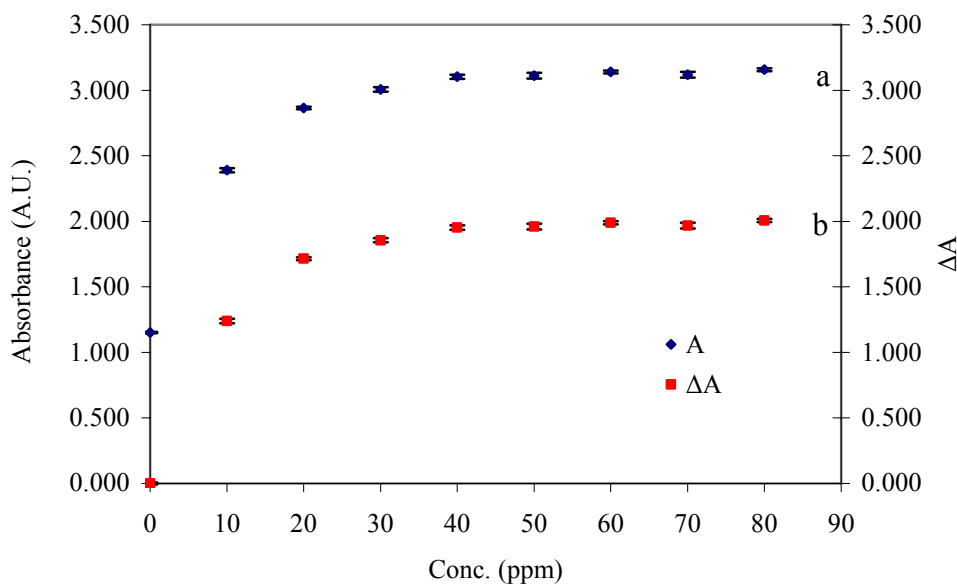


Figure F.22. Absorbance values of calcium standards (10-80 ppm) – 200 μM AIII in 200 mM Imidazole-Cl buffer pH 6.5 (150 μL standard-150 μL dye reagent) at 600 nm a. without subtracting blank values, b. with subtracting blank values.

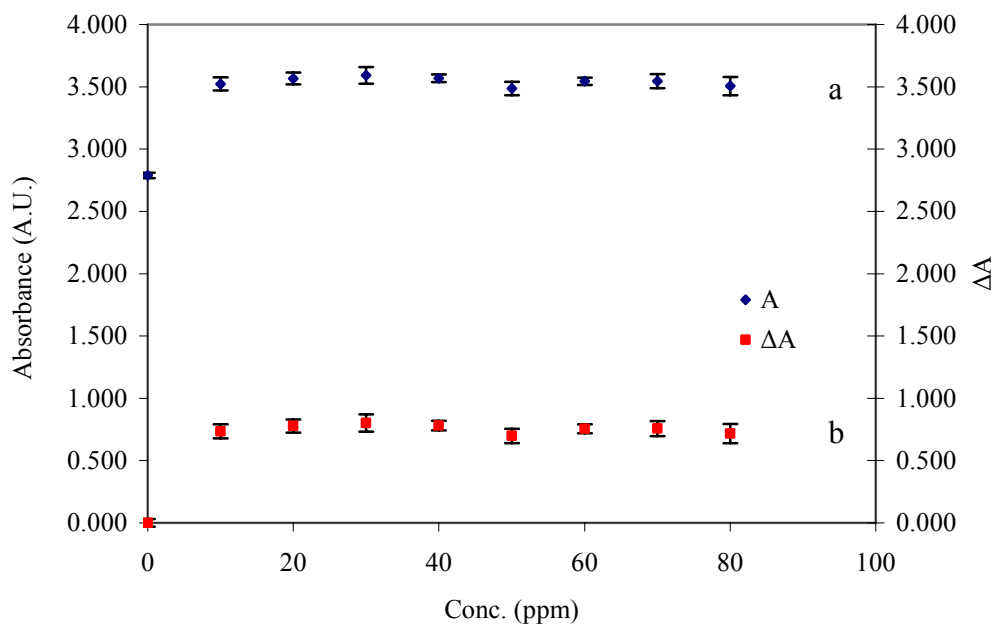


Figure F.23. Absorbance values of calcium standards (10-80 ppm) – 500 μM AIII in 200 mM Imidazole-Cl buffer pH 6.5 (150 μL standard-150 μL dye reagent) at 600 nm a. without subtracting blank values, b. with subtracting blank values.

APPENDIX G

CALCIUM DETERMINATION IN DIFFERENT ELECTROLYTE SOLUTIONS BY MICROPLATE BASED ARSENazo III-CALCIUM ANALYSIS

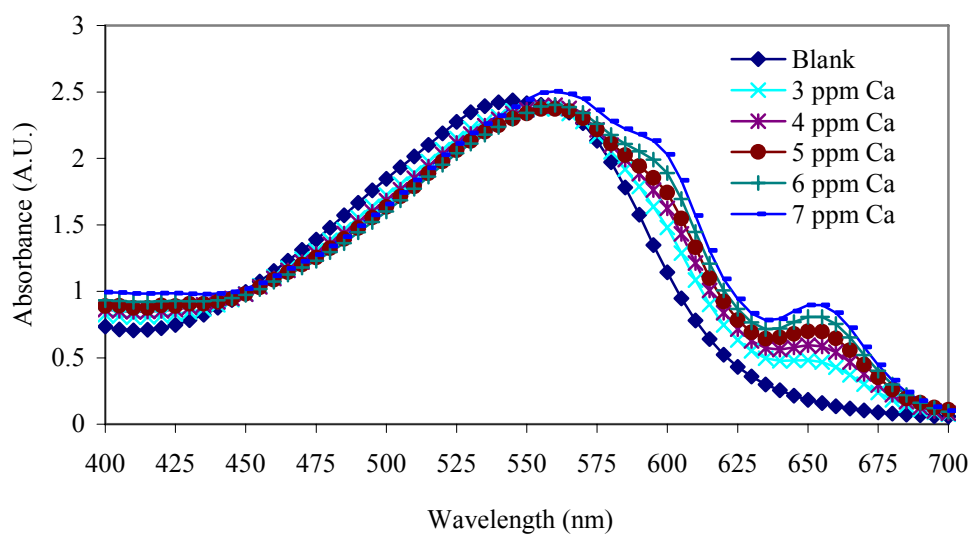


Figure G.1. Spectra of calcium standards prepared in 142 mM NaCl.

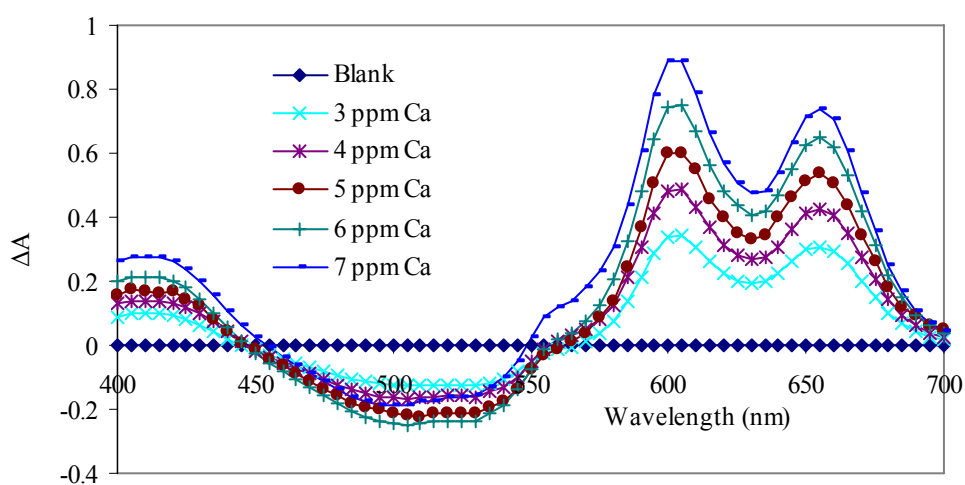


Figure G.2. Spectra of calcium standards prepared in 142 mM NaCl obtained by subtracting blank values.

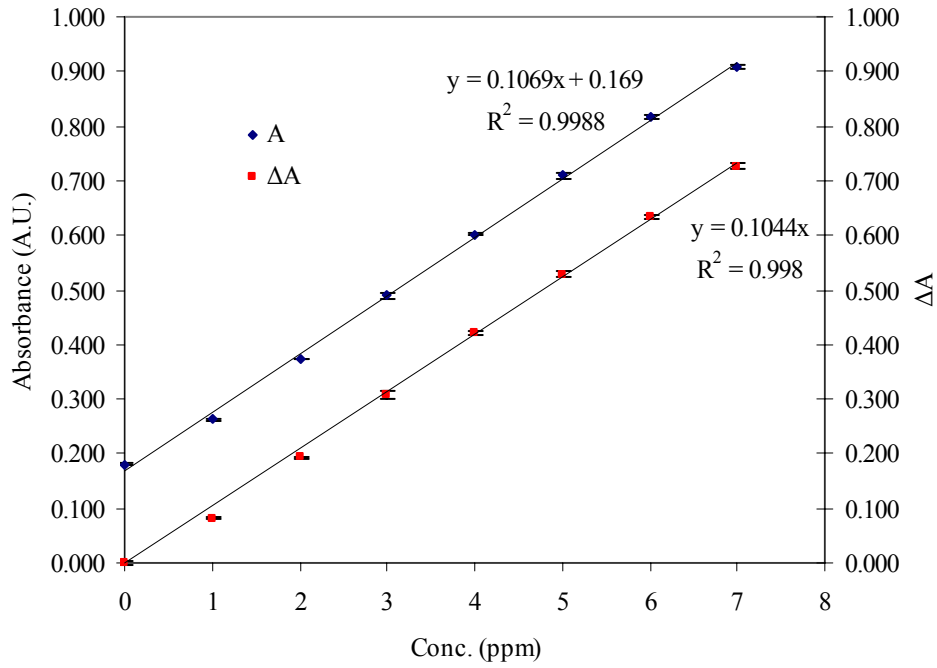


Figure G.3. Calibration curve obtained by measuring absorbances of calcium standards prepared in 142 mM NaCl at 650 nm.

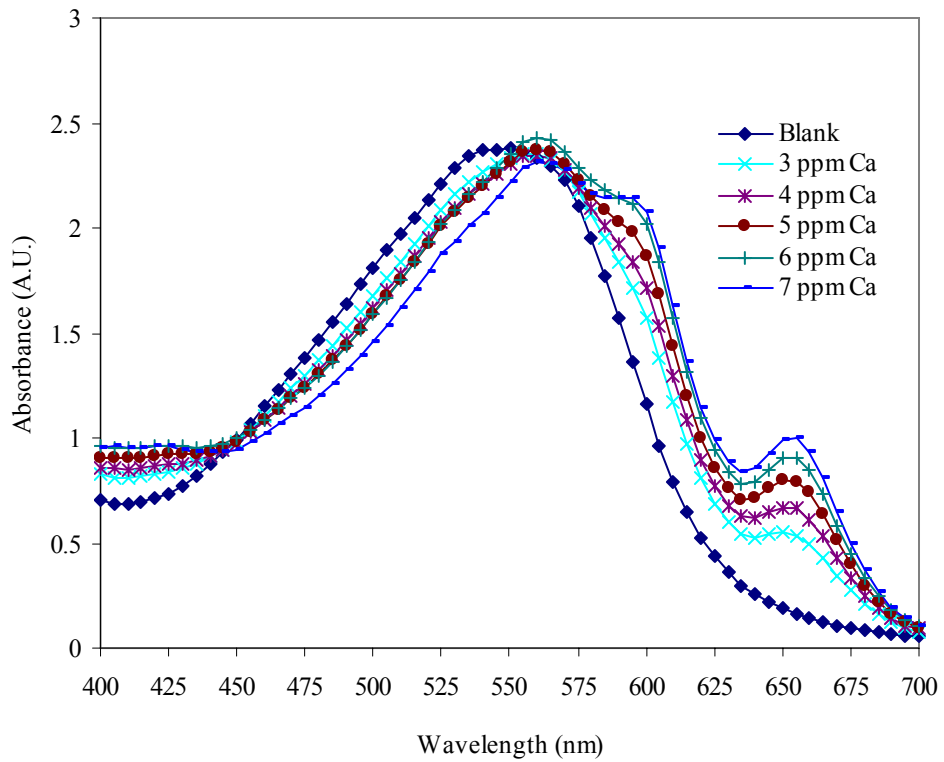


Figure G.4. Spectra of calcium standards prepared in 27 mM NaHCO₃.

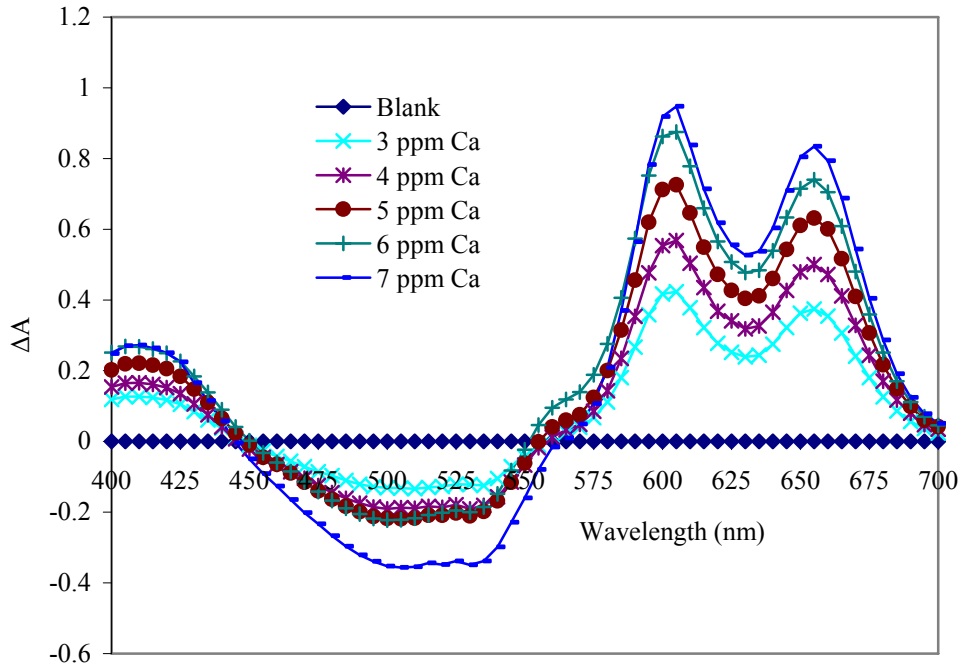


Figure G.5. Spectra of calcium standards prepared in 27 mM NaHCO₃ obtained by subtracting blank values.

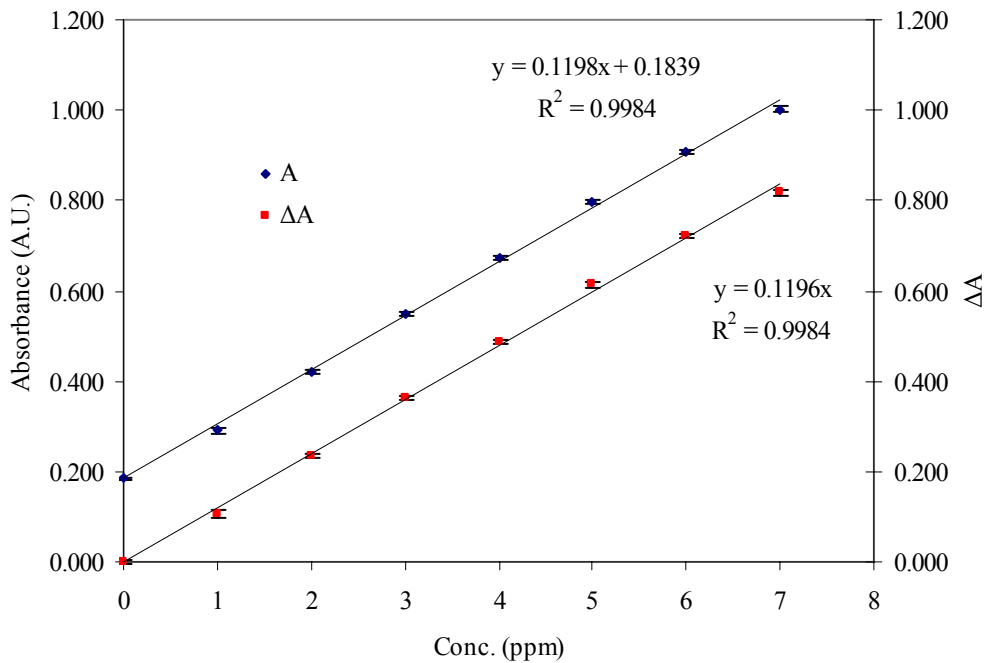


Figure G.6. Calibration curve obtained by measuring absorbances of calcium standards prepared in 27 mM NaHCO₃ at 650 nm.

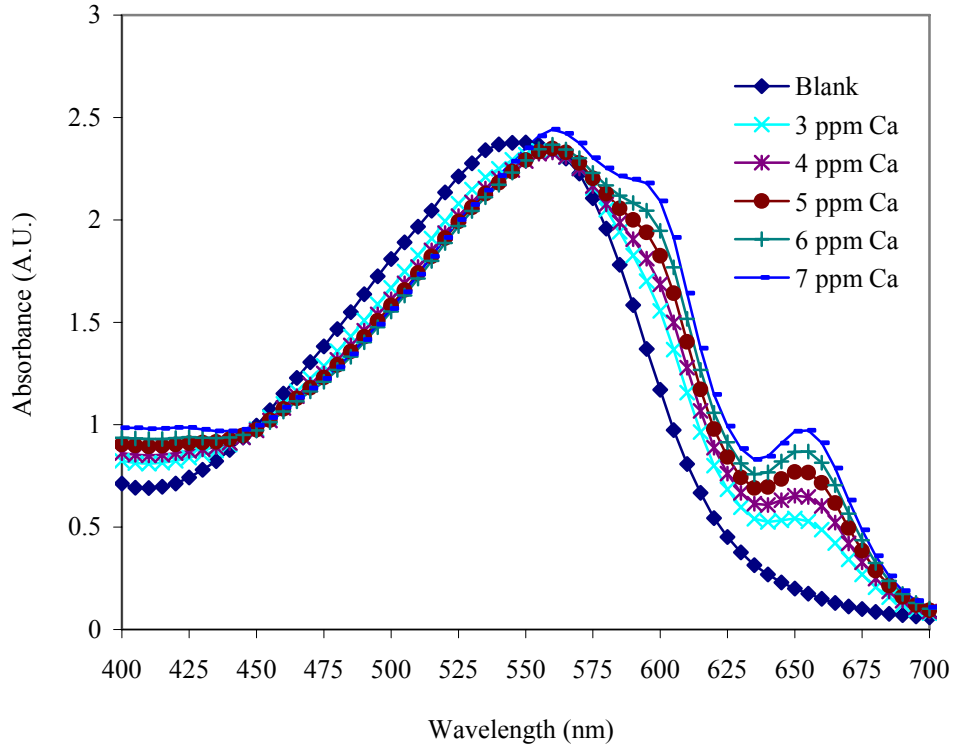


Figure G.7. Spectra of calcium standards prepared in 115 mM NaCl & 27 mM NaHCO₃.

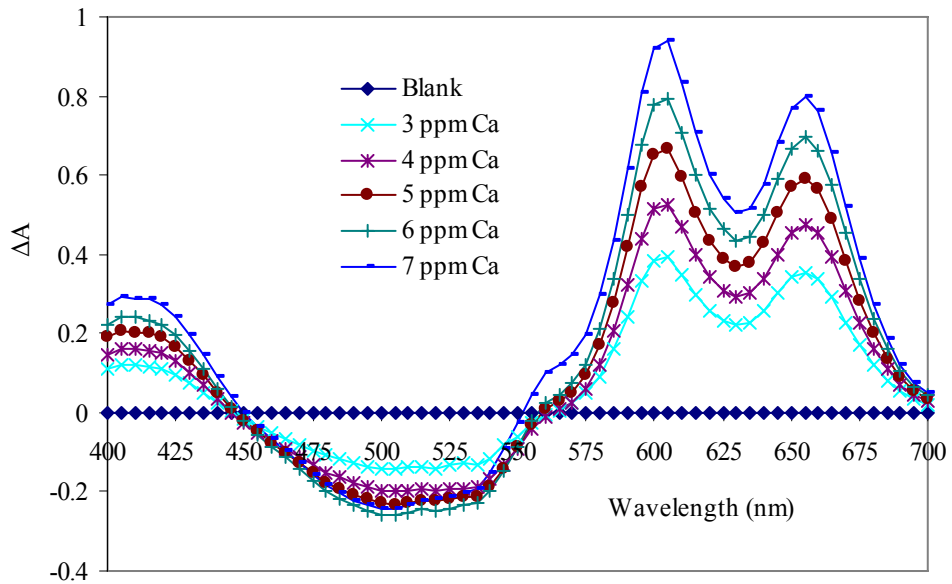


Figure G.8. Spectra of calcium standards prepared in 115 mM NaCl & 27 mM NaHCO₃ obtained by subtracting blank values.

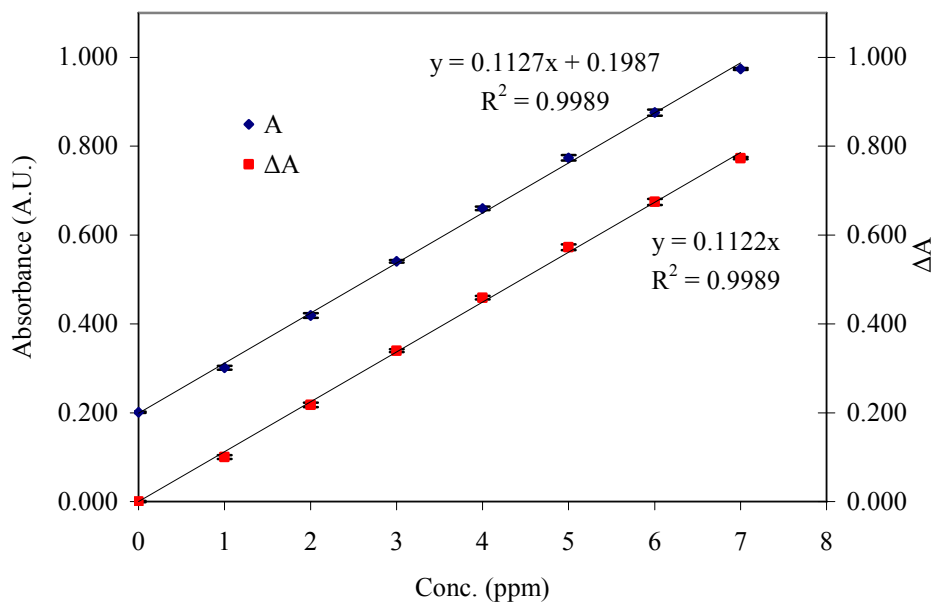


Figure G.9. Calibration curve obtained by measuring absorbances of calcium standards prepared in 115 mM NaCl & 27 mM NaHCO₃ at 650 nm.

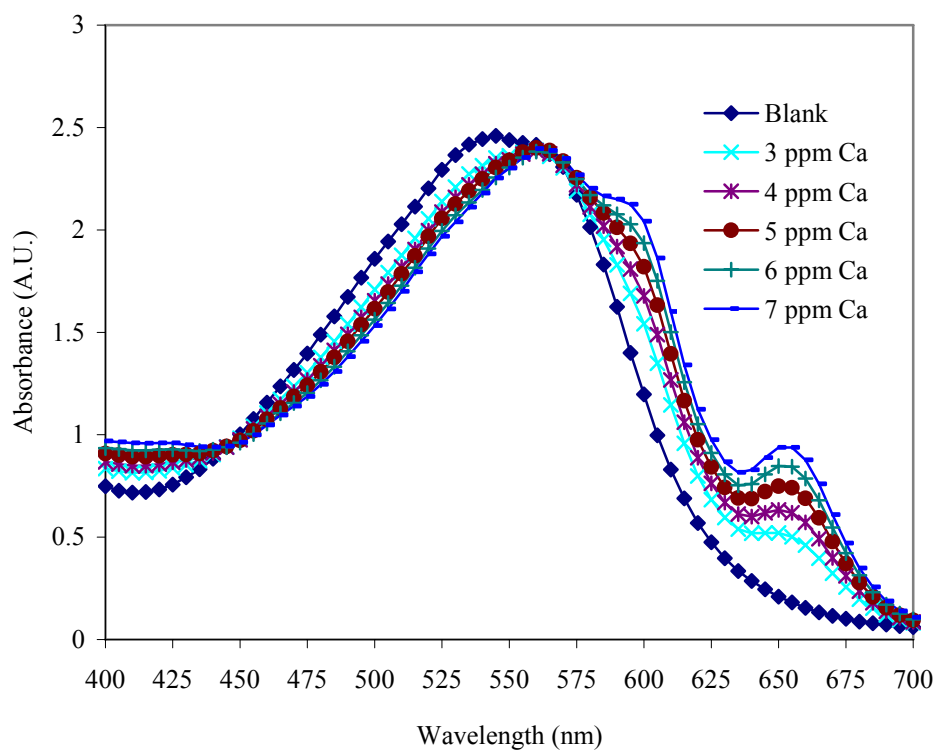


Figure G.10. Spectra of calcium standards prepared in 1.5 mM MgCl₂·6H₂O.

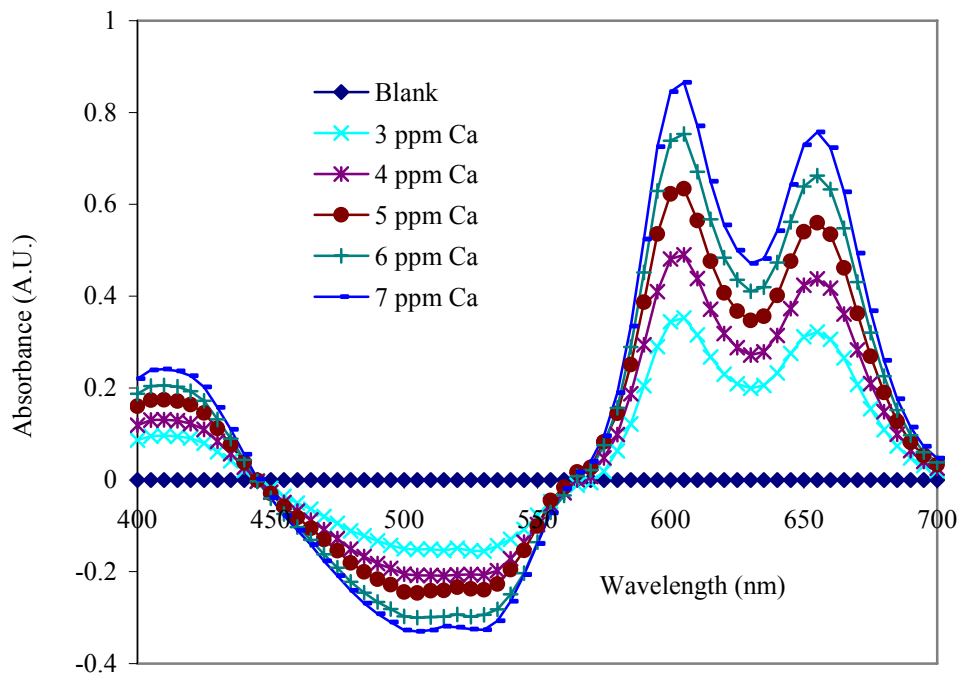


Figure G.11. Spectra of calcium standards prepared in 1.5 mM $\text{MgCl}_2 \cdot 6\text{H}_2\text{O}$ obtained by subtracting blank values.

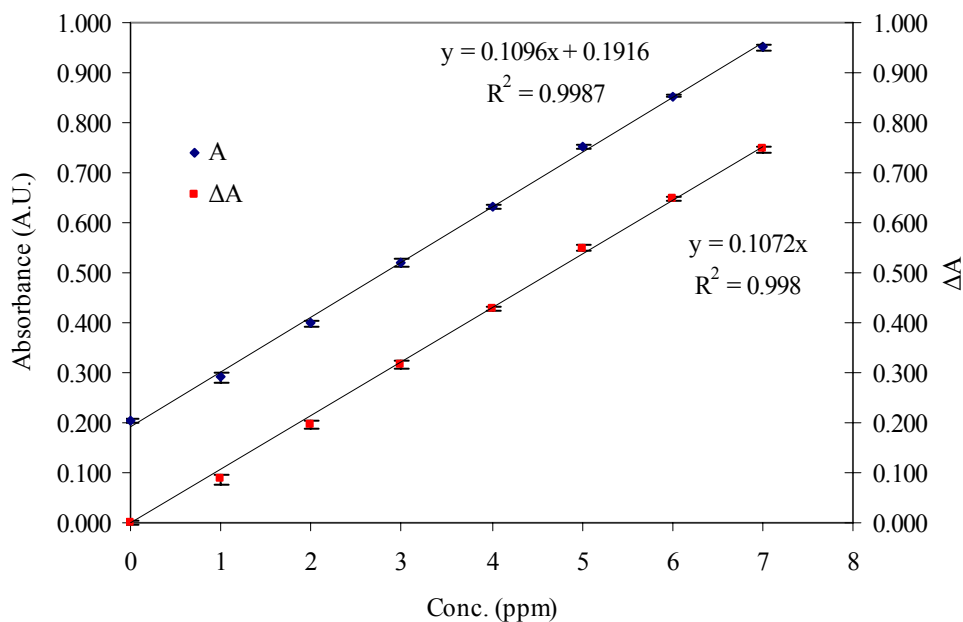


Figure G.12. Calibration curve obtained by measuring absorbances of calcium standards prepared in 1.5 mM $\text{MgCl}_2 \cdot 6\text{H}_2\text{O}$ at 650 nm.

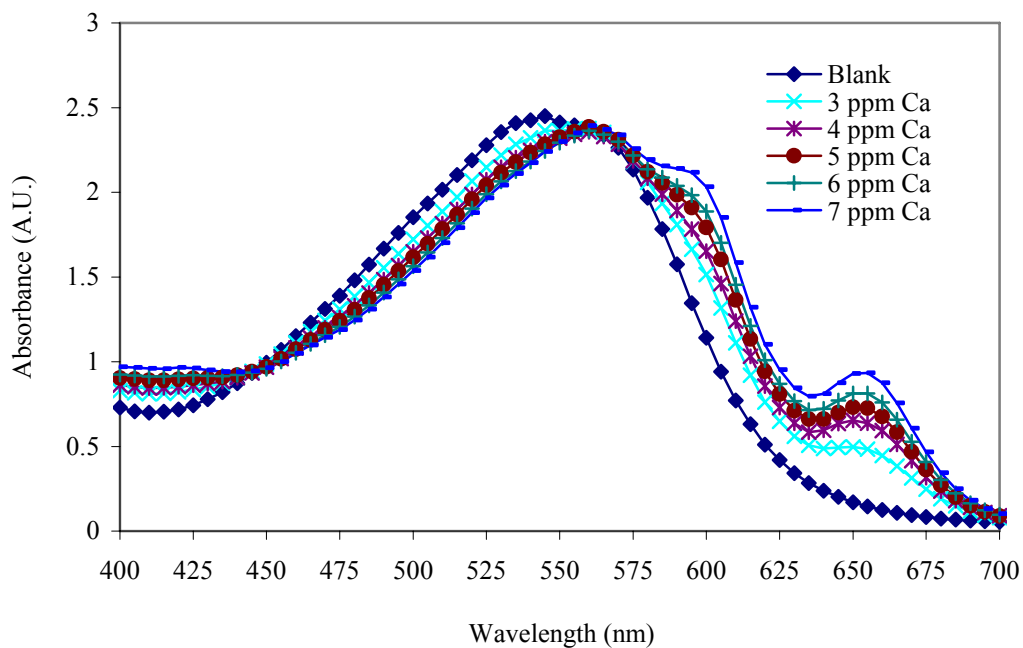


Figure G.13. Spectra of calcium standards prepared in 1 mM Na_2HPO_4 .

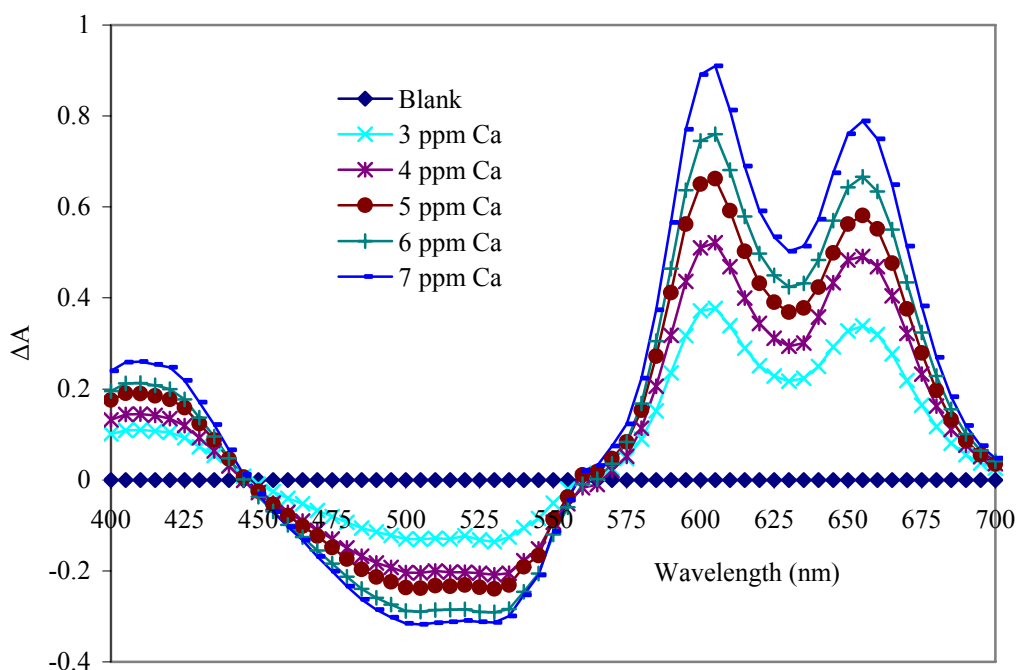


Figure G.14. Spectra of calcium standards prepared in 1 mM Na_2HPO_4 obtained by subtracting blank values.

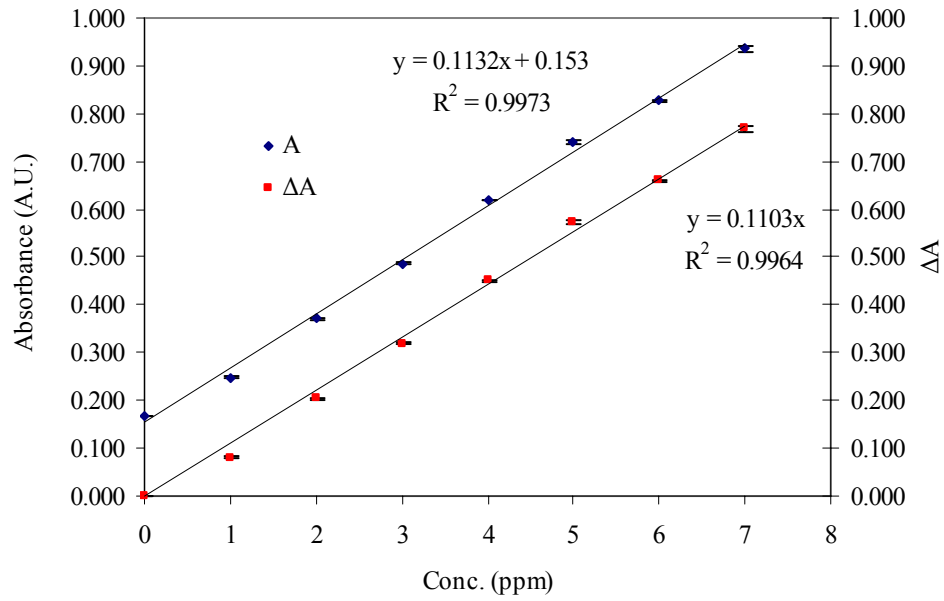


Figure G.15. Calibration curve obtained by measuring absorbances of calcium standards prepared in 1 mM Na_2HPO_4 at 650 nm.

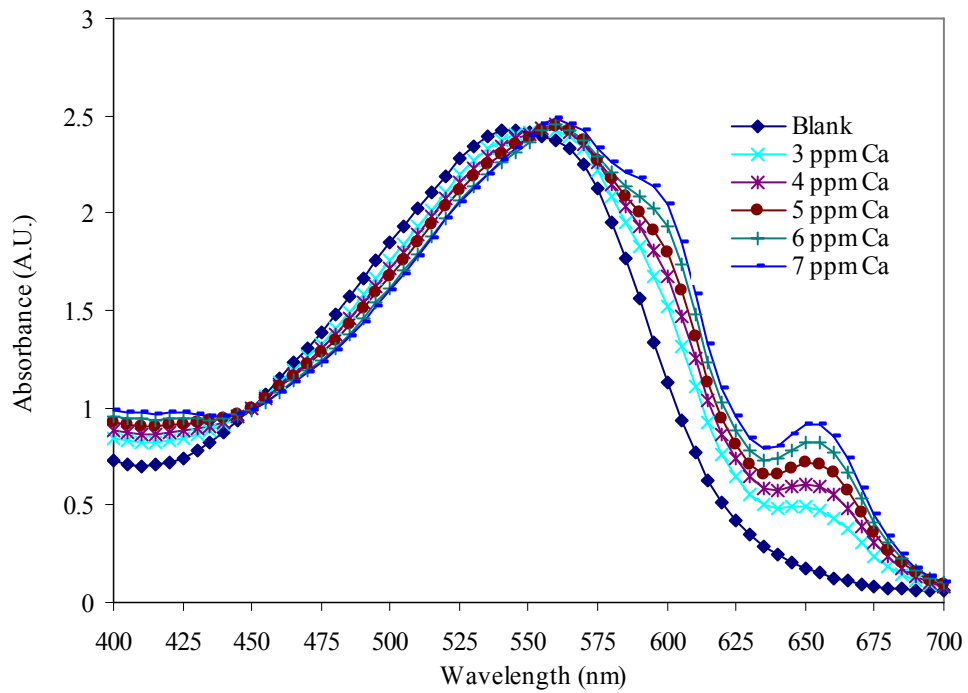


Figure G.16. Spectra of calcium standards prepared in 1 mM H_3PO_4 .

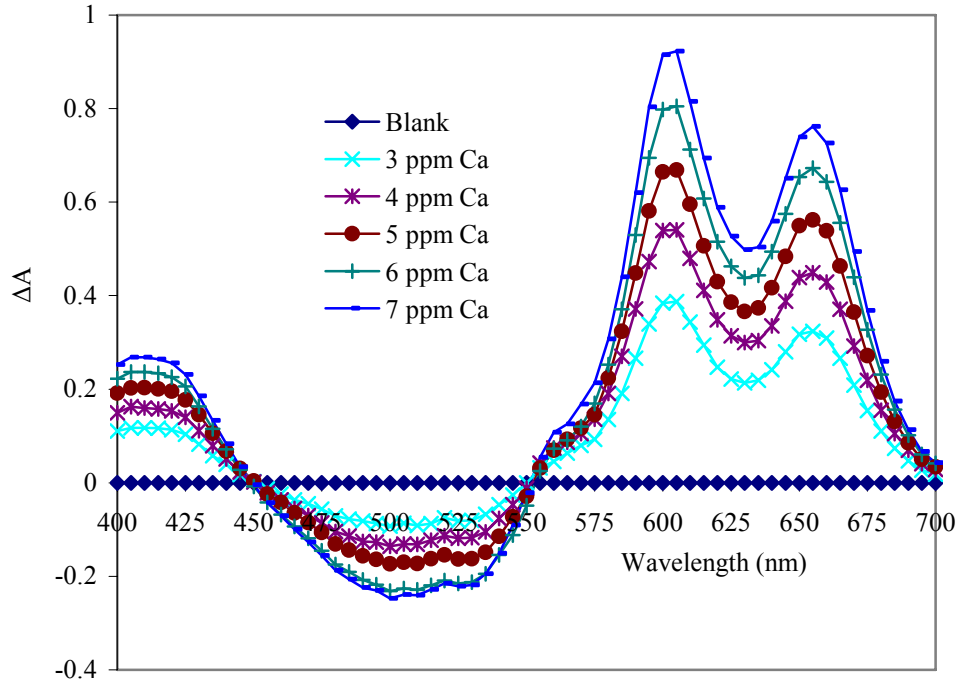


Figure G.17. Spectra of calcium standards prepared in 1 mM H_3PO_4 obtained by subtracting blank values.

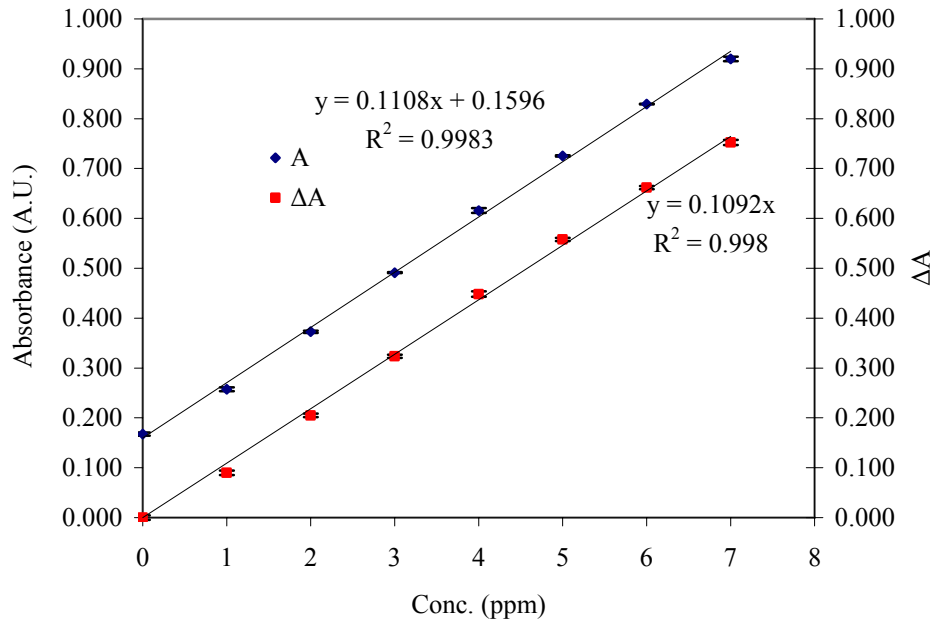


Figure G.18. Calibration curve obtained by measuring absorbances of calcium standards prepared in 1 mM H_3PO_4 at 650 nm.

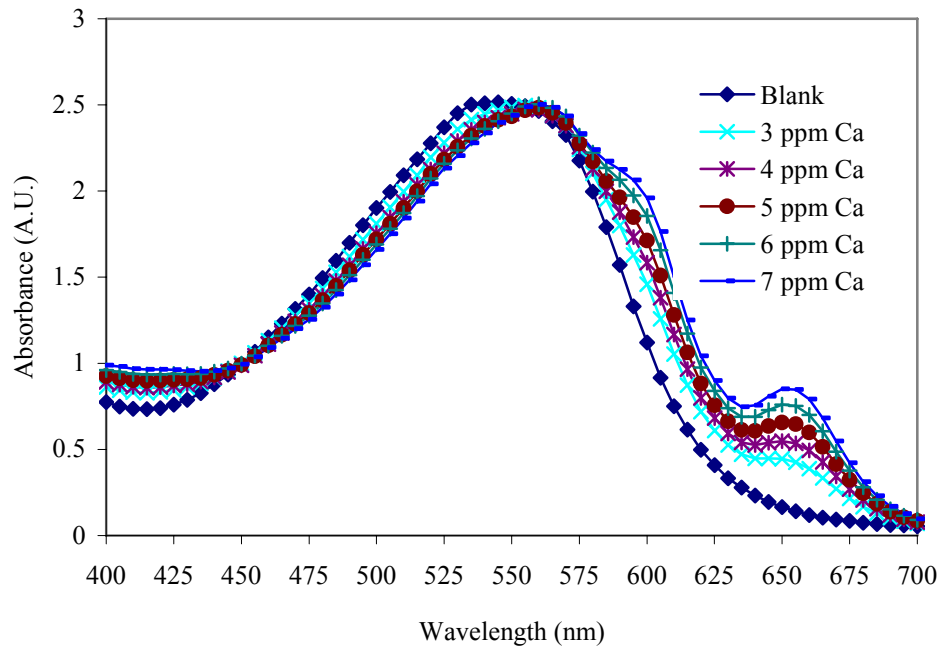


Figure G.19. Spectra of calcium standards prepared in 10 mM H_3PO_4 .

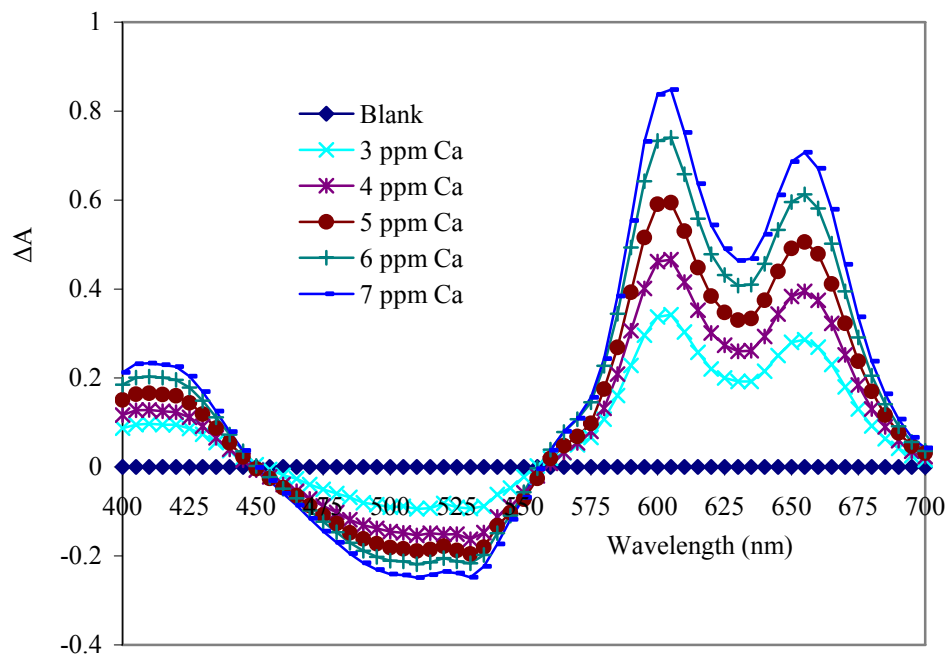


Figure G.20. Spectra of calcium standards prepared in 10 mM H_3PO_4 obtained by subtracting blank values.

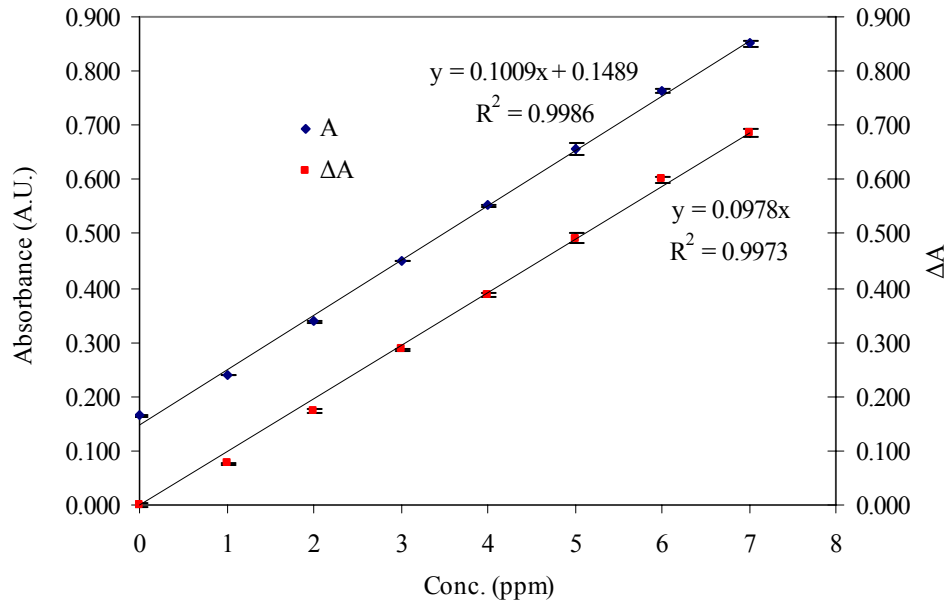


Figure G.21. Calibration curve obtained by measuring absorbances of calcium standards prepared in 10 mM H_3PO_4 at 650 nm.

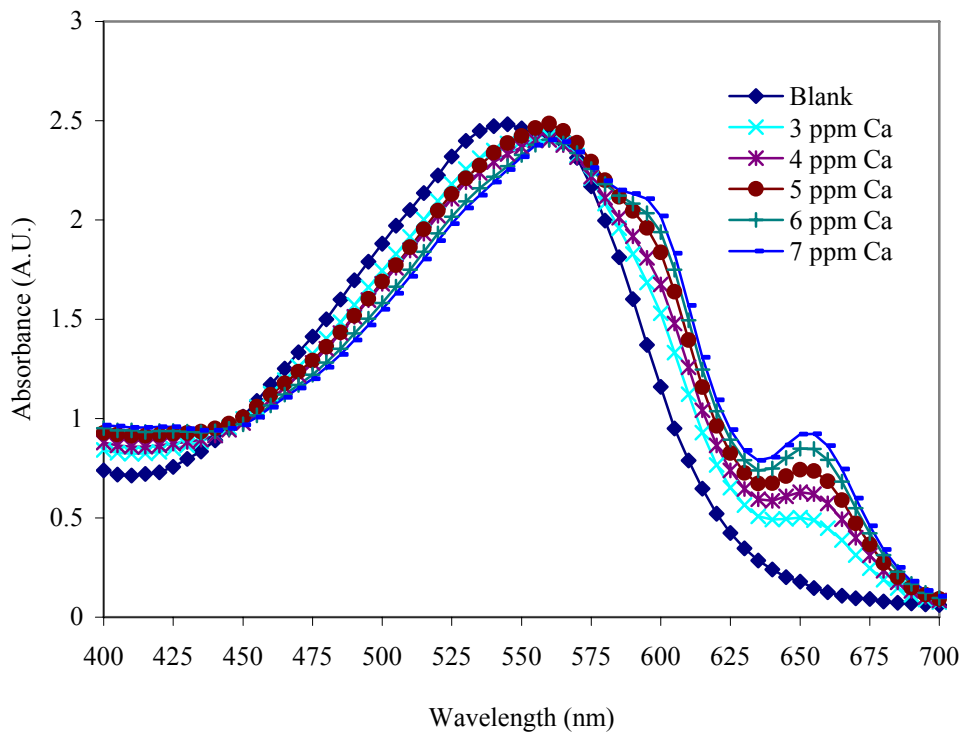


Figure G.22. Spectra of calcium standards prepared in 5 mM KCl.

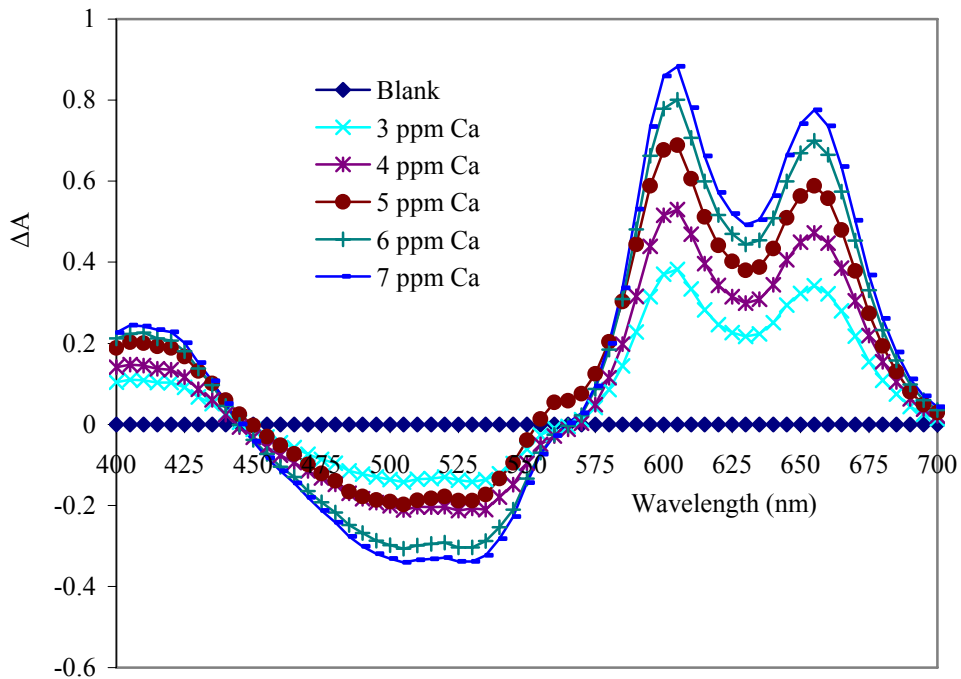


Figure G.23. Spectra of calcium standards prepared in 5 mM KCl obtained by subtracting blank values.

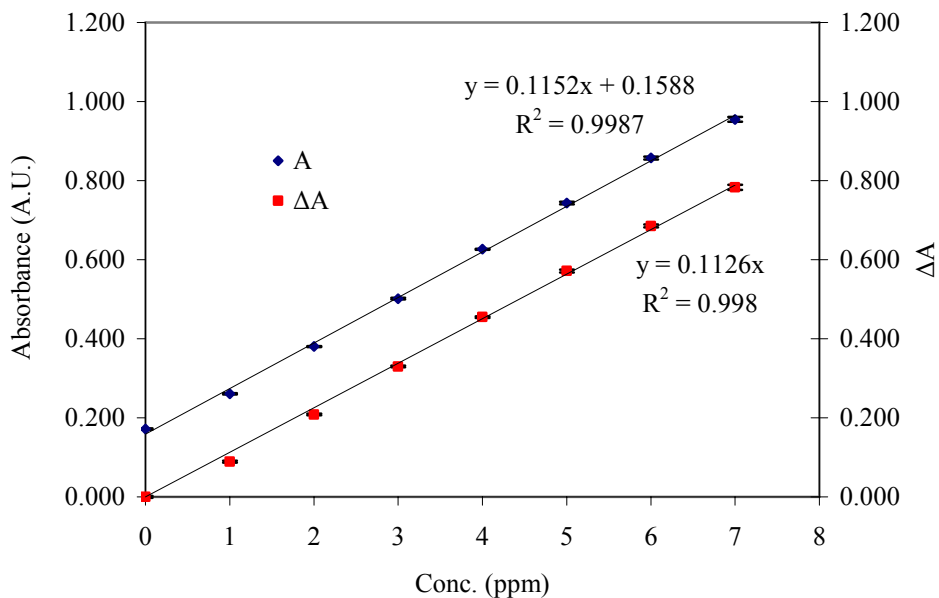


Figure G.24. Calibration curve obtained by measuring absorbances of calcium standards prepared in 5 mM KCl at 650 nm.

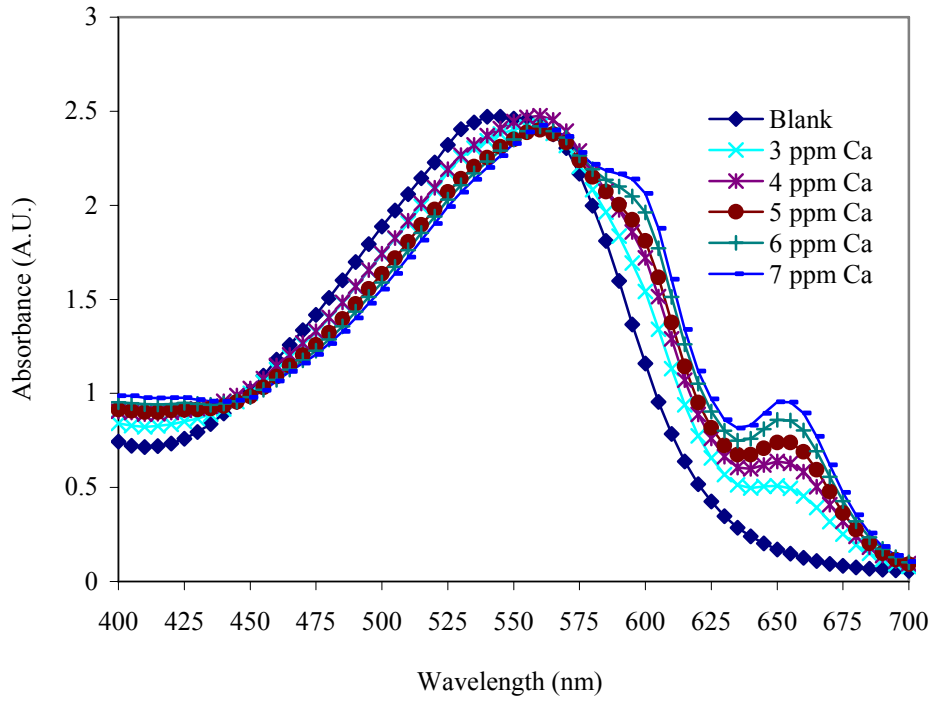


Figure G.25. Spectra of calcium standards prepared in 0.5 mM Na₂SO₄.

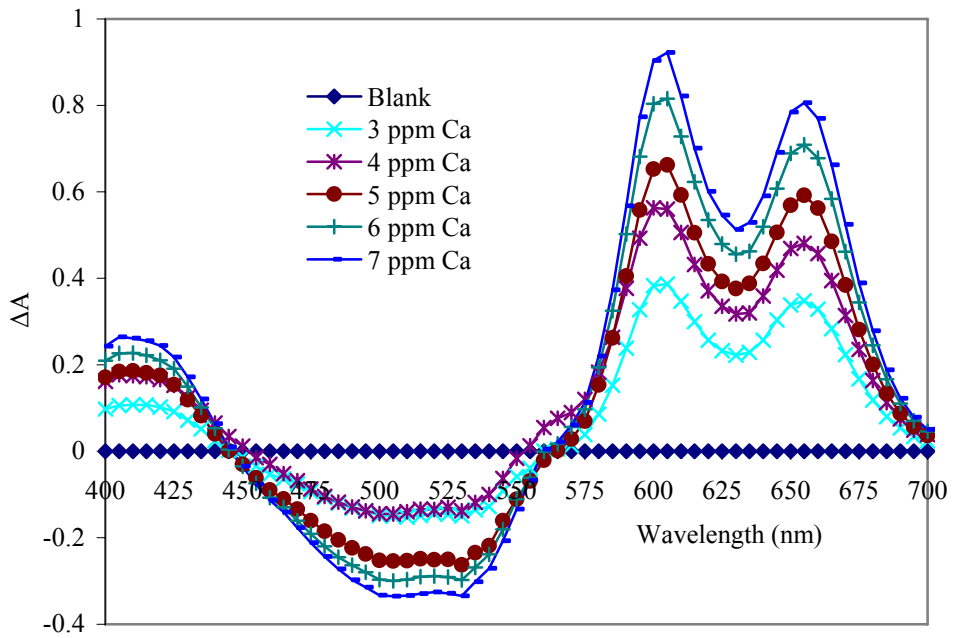


Figure G.26. Spectra of calcium standards prepared in 0.5 mM Na₂SO₄ obtained by subtracting blank values.

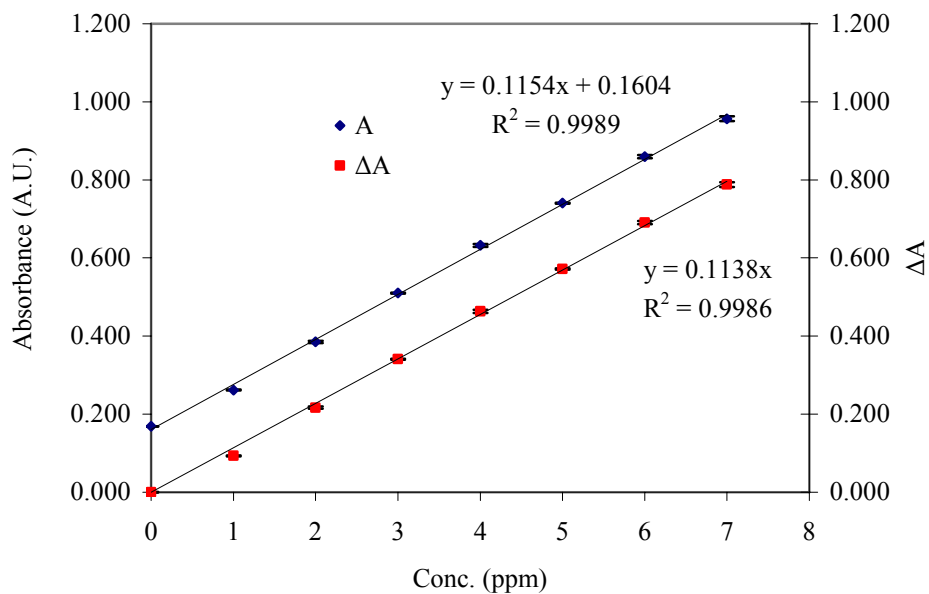


Figure G.27. Calibration curve obtained by measuring absorbances of calcium standards prepared in 0.5 mM Na₂SO₄ at 650 nm.

APPENDIX H

SPECTRA AND CALIBRATION CURVES FOR MALACHITE GREEN PHOSPHATE ASSAY

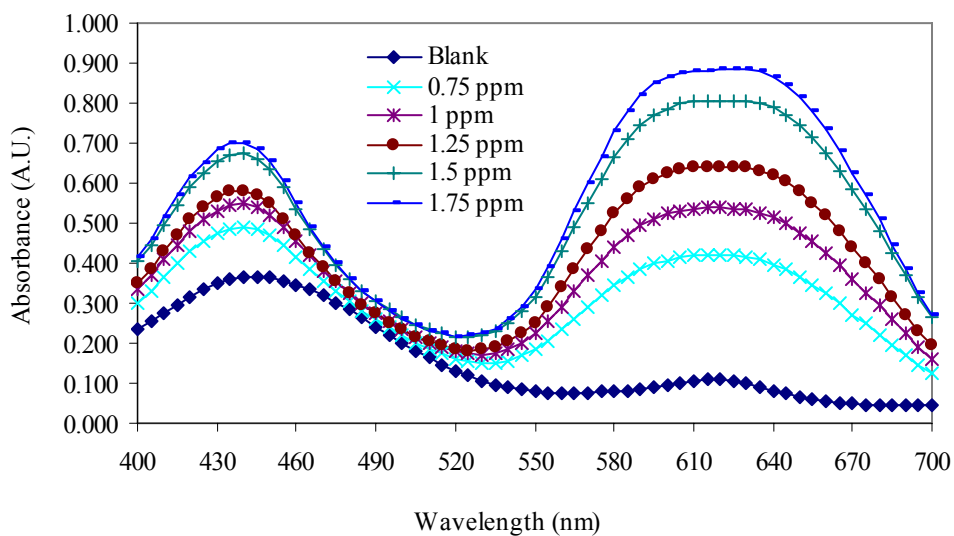


Figure H.1. Absorption spectra of phosphate standard solutions prepared in ultrapure water.

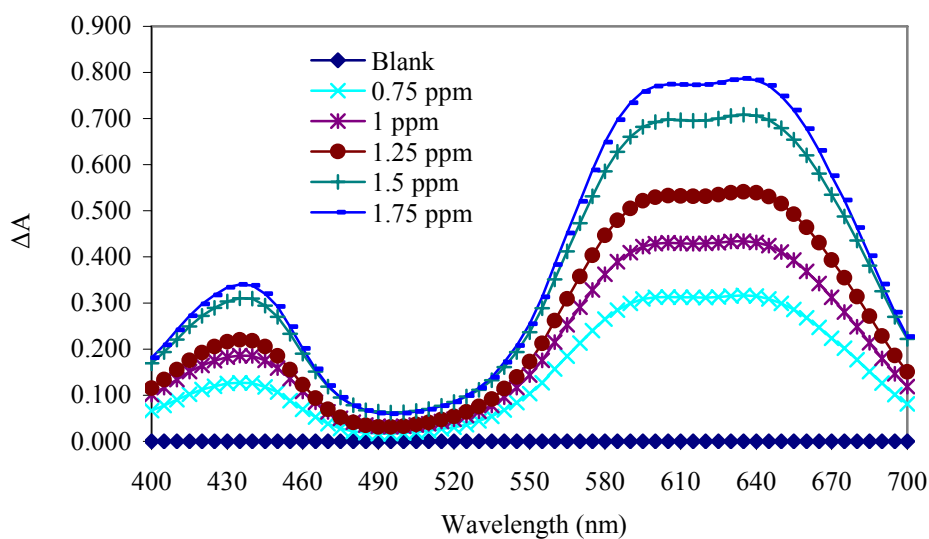


Figure H.2. Absorption spectra of phosphate standard solutions prepared in ultrapure water obtained by subtracting blank values.

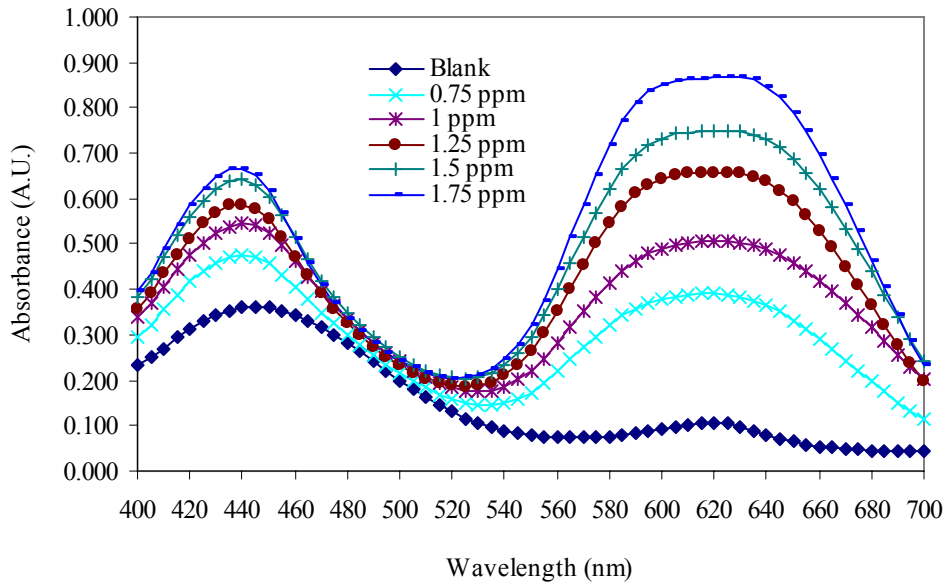


Figure H.3. Absorption spectra of phosphate standard solutions prepared in 142 mM NaCl.

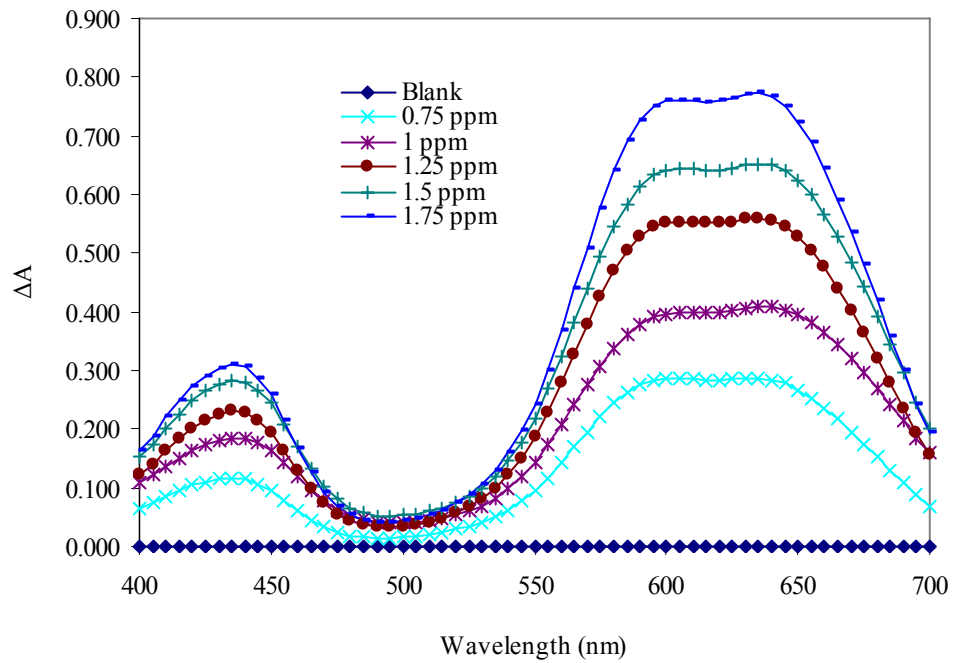


Figure H.4. Absorption spectra of phosphate standard solutions prepared in 142 mM NaCl obtained by subtracting blank values.

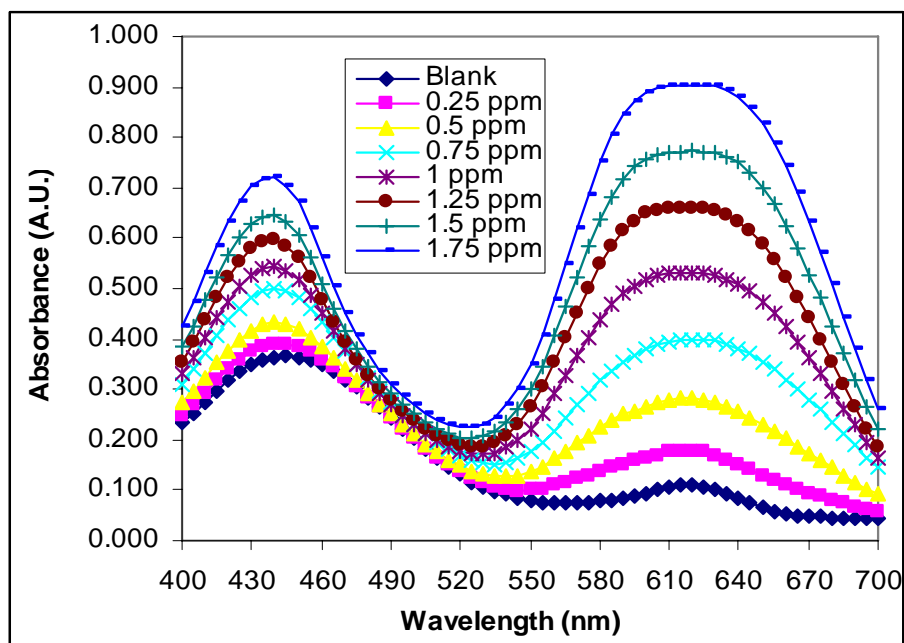


Figure H.5. Absorption spectra of phosphate standard solutions prepared in 5 mM KCl.

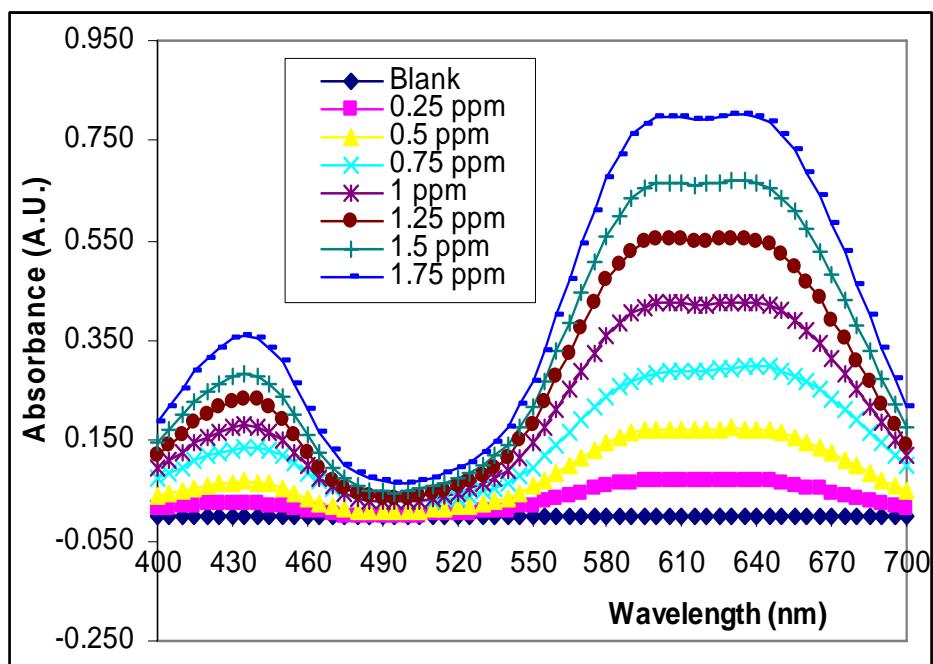


Figure H.6. Absorption spectra of phosphate standard solutions prepared in 5 mM KCl obtained by subtracting blank values.

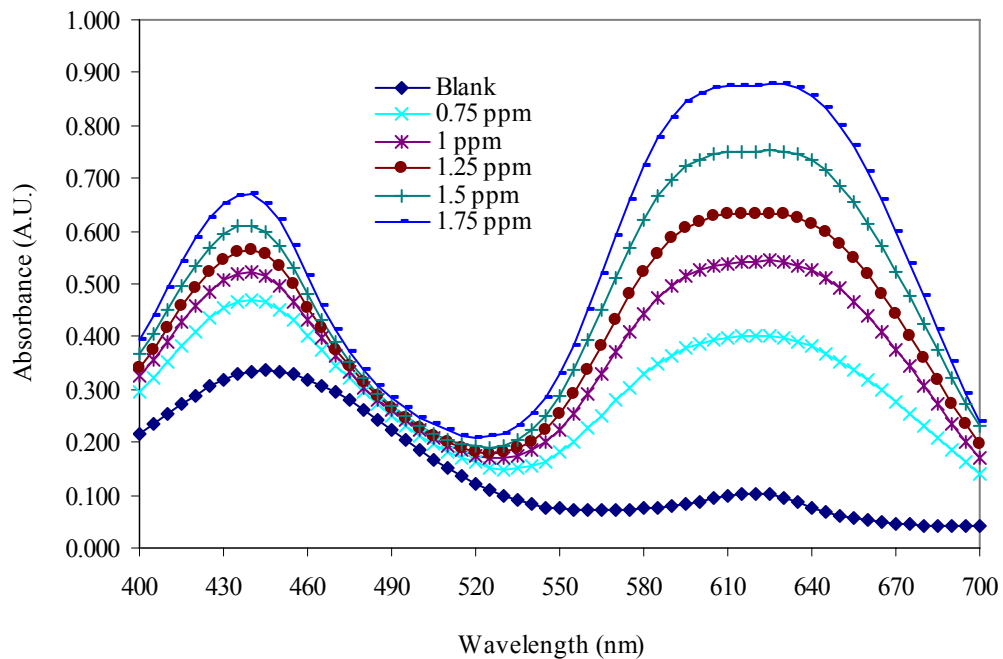


Figure H.7. Absorption spectra of the phosphate standards prepared in 2.5 mM CaCl_2 .

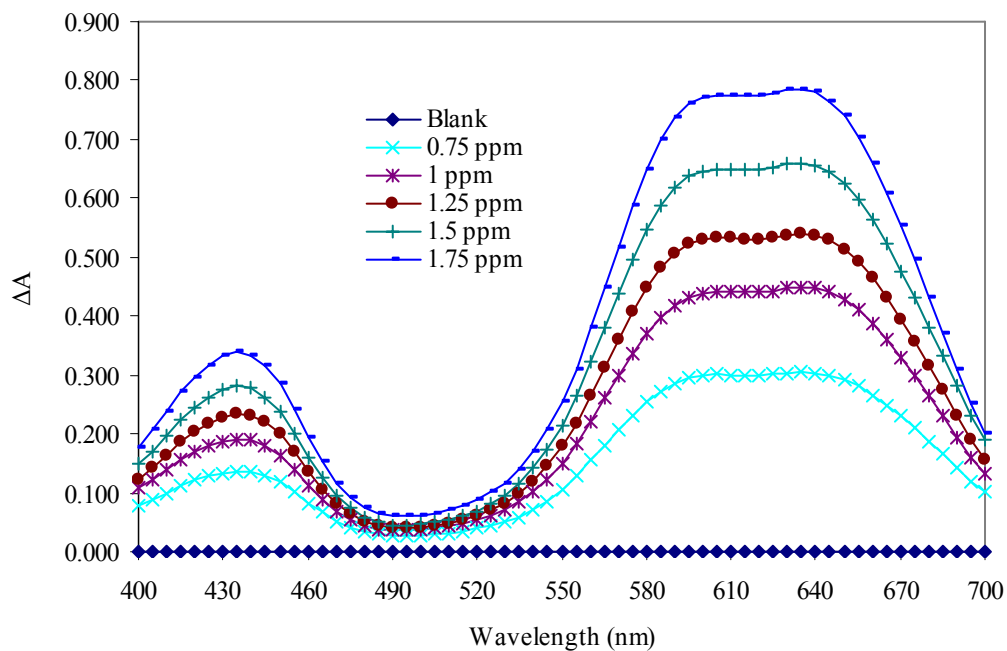


Figure H.8. Absorption spectra of the phosphate standards prepared in 2.5 mM CaCl_2 obtained by subtracting blank values.

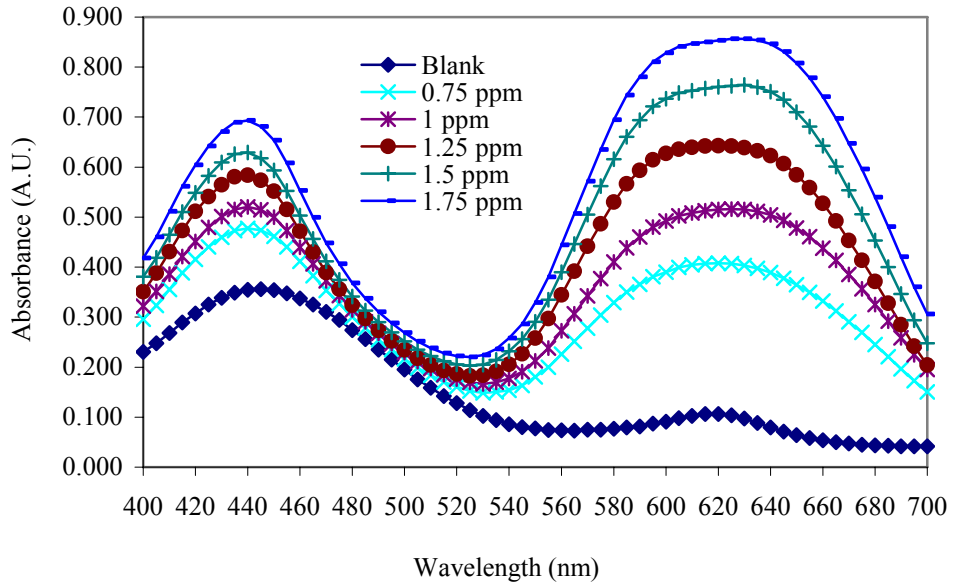


Figure H.9. Absorption spectra of the phosphate standards prepared in 1.5 mM MgCl₂.

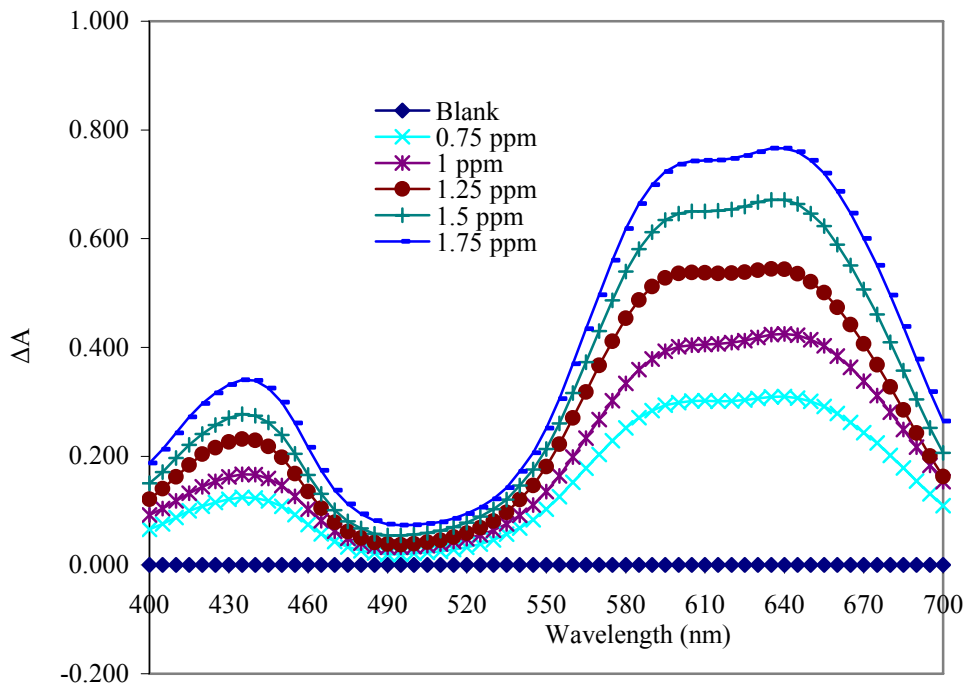


Figure H.10. Absorption spectra of the phosphate standards prepared in 1.5 mM MgCl₂ obtained by subtracting blank values.

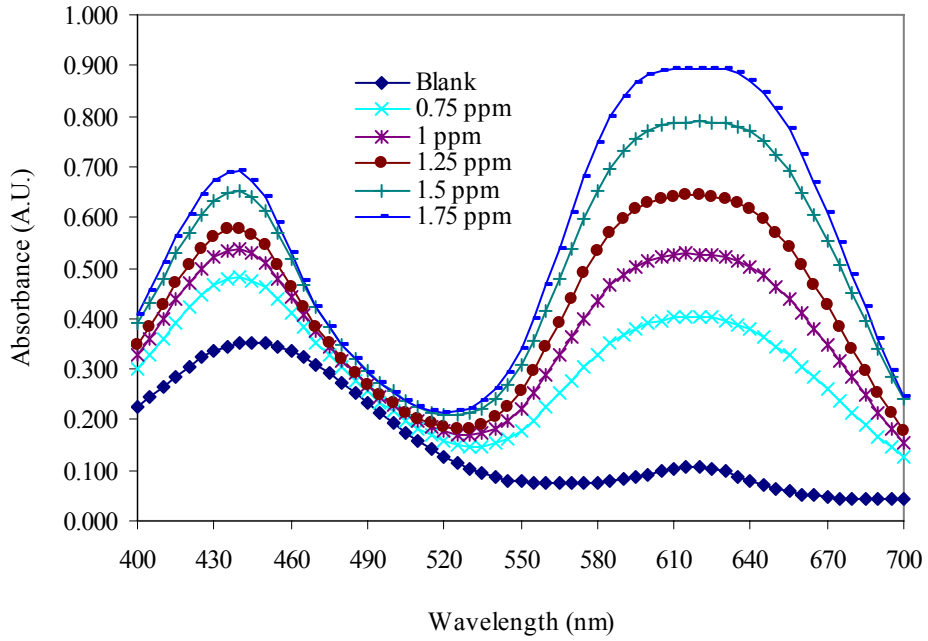


Figure H.11. Absorption spectra of the phosphate standards prepared in 0.5 mM Na_2SO_4 .

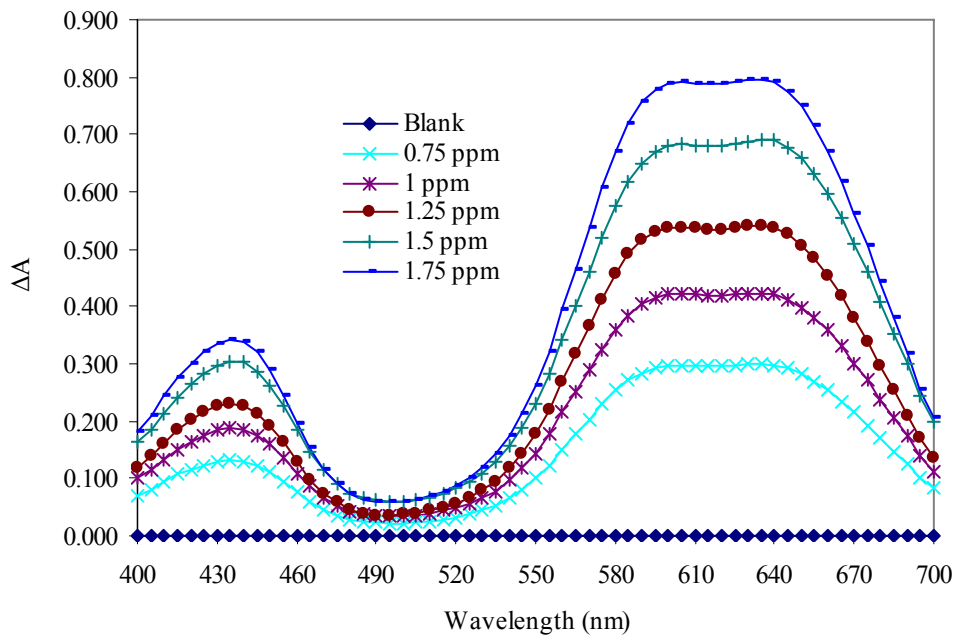


Figure H.12. Absorption spectra of the phosphate standards prepared in 0.5 mM Na_2SO_4 obtained by subtracting blank values.

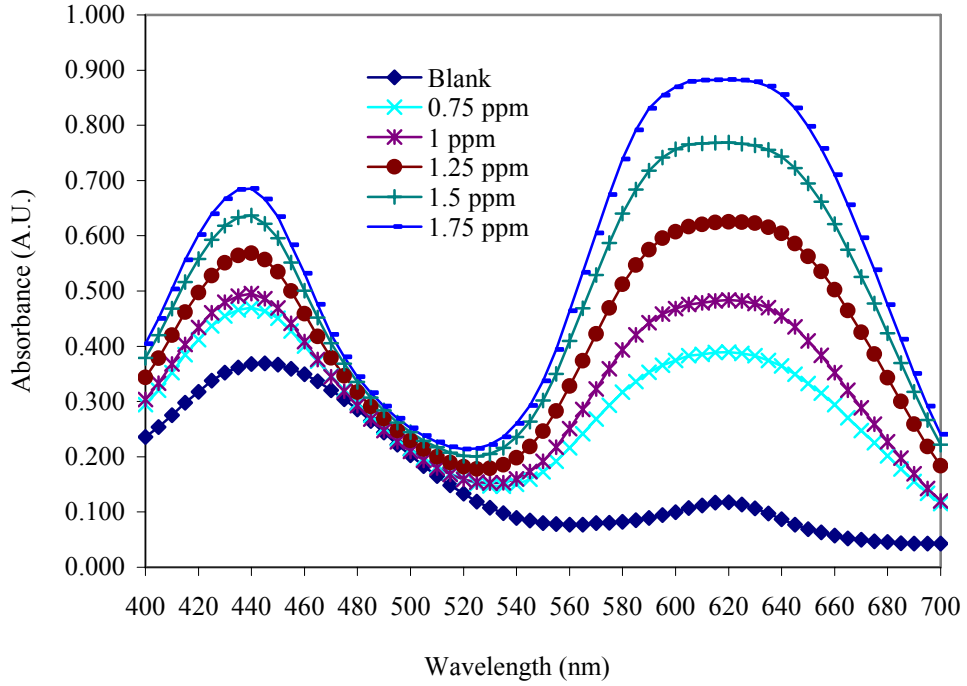


Figure H.13. Absorption spectra of the phosphate standards prepared in 27 mM NaHCO_3 .

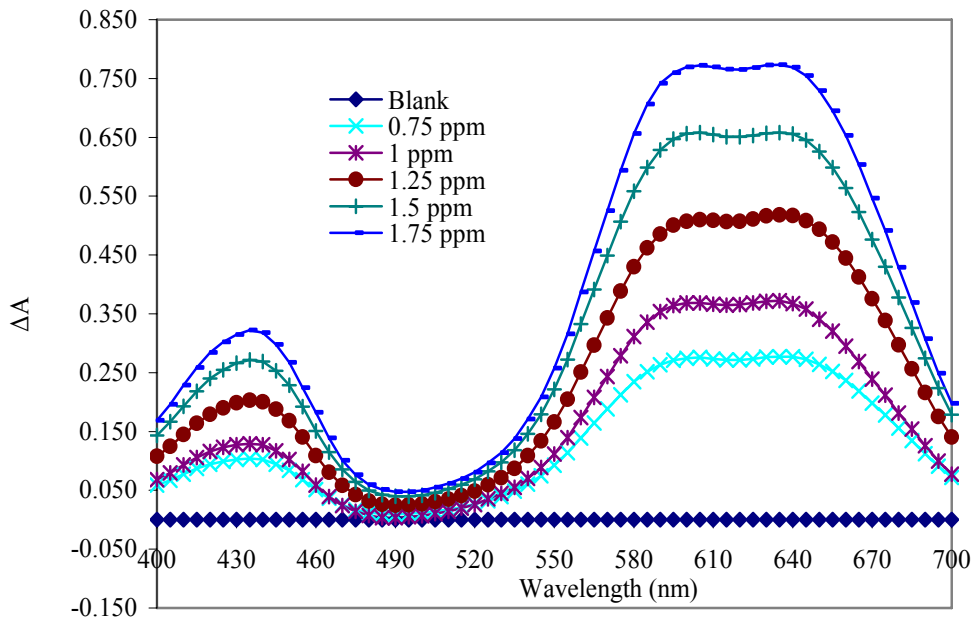


Figure H.14. Absorption spectra of the phosphate standards prepared in 27 mM NaHCO_3 obtained by subtracting blank values.

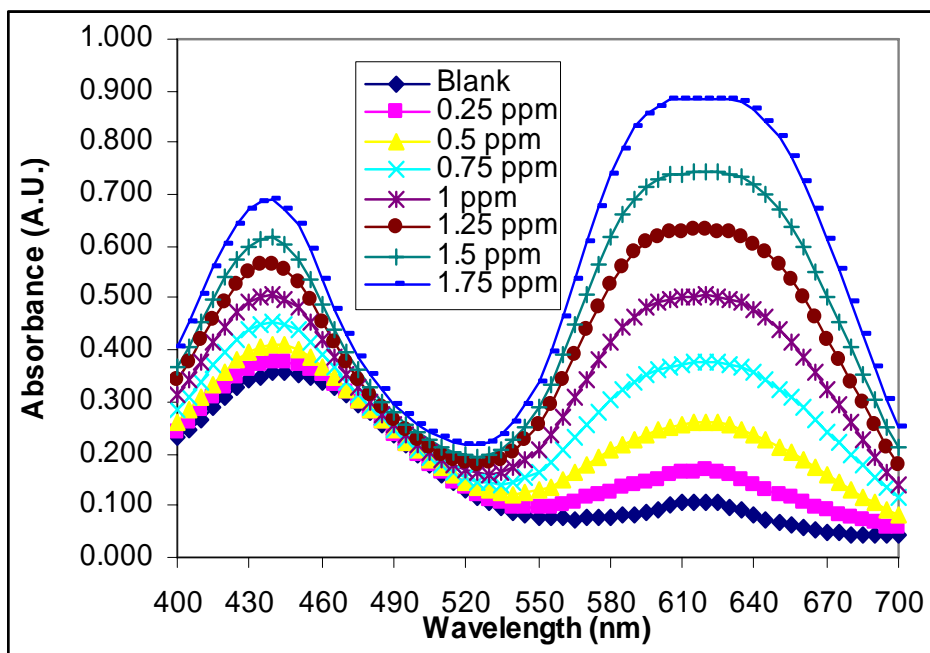


Figure H.15. Absorption spectra of the phosphate standards prepared in 115 mM NaCl and 27 mM NaHCO₃ containing solution.

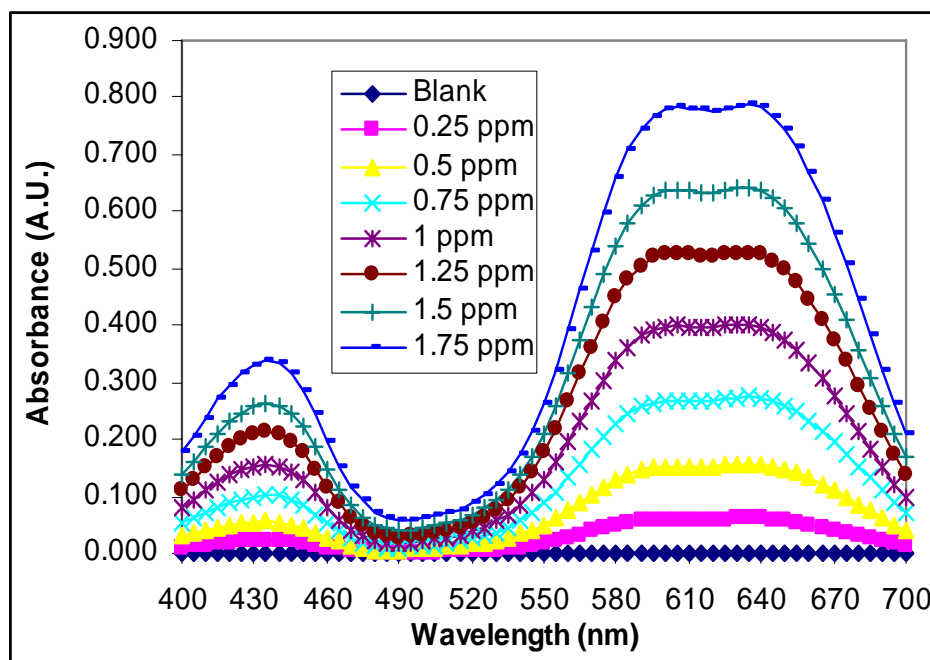


Figure H.16. Absorption spectra of the phosphate standards prepared in 115 mM NaCl and 27 mM NaHCO₃ containing solution obtained by subtracting blank values.

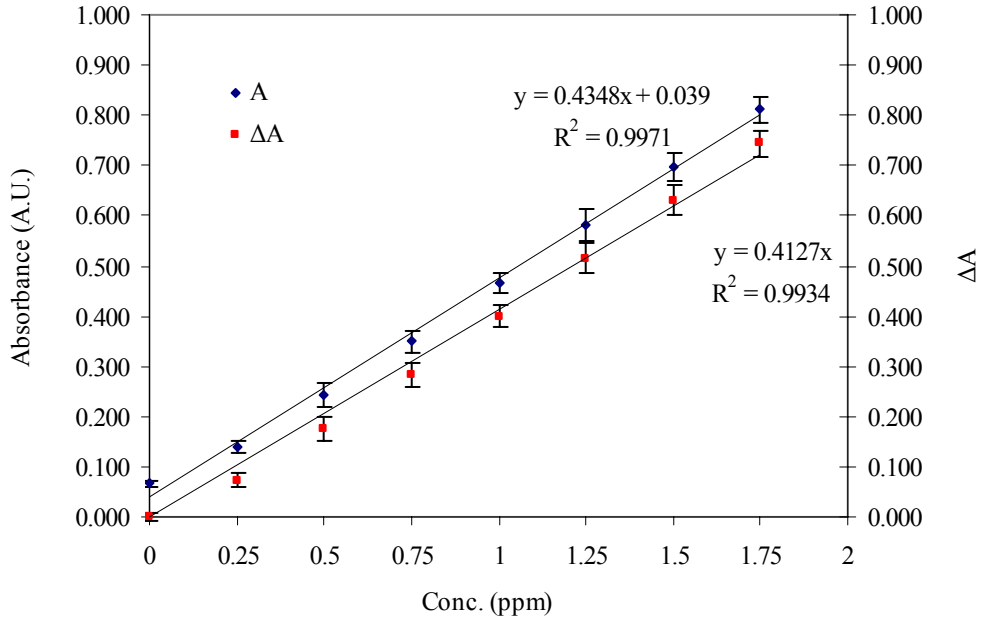


Figure H.17. Calibration curves for the phosphate standards prepared in ultrapure water at 650 nm.

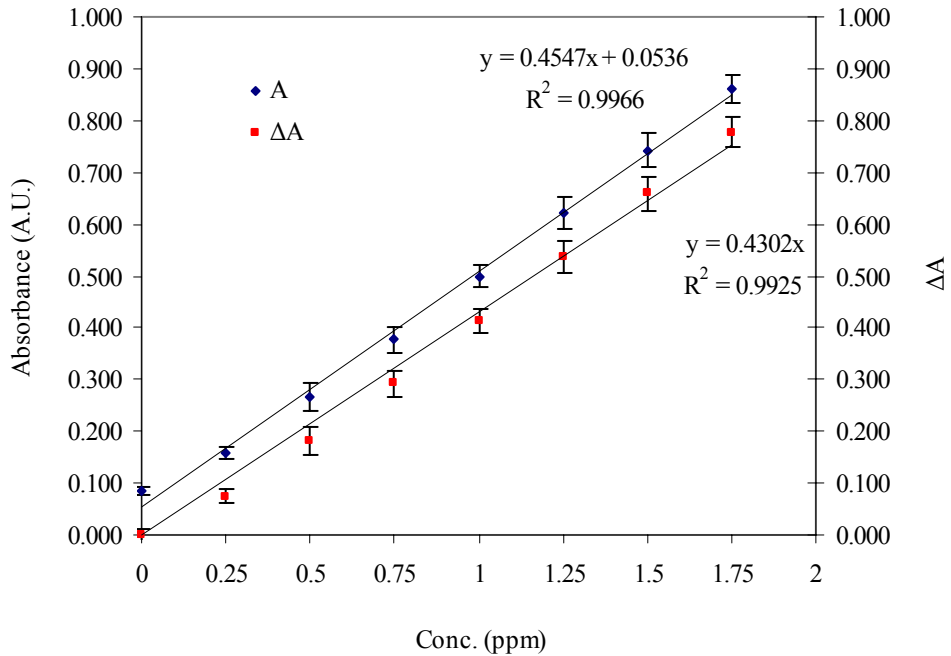


Figure H.18. Calibration curves for the phosphate standards prepared in ultrapure water at 640 nm.

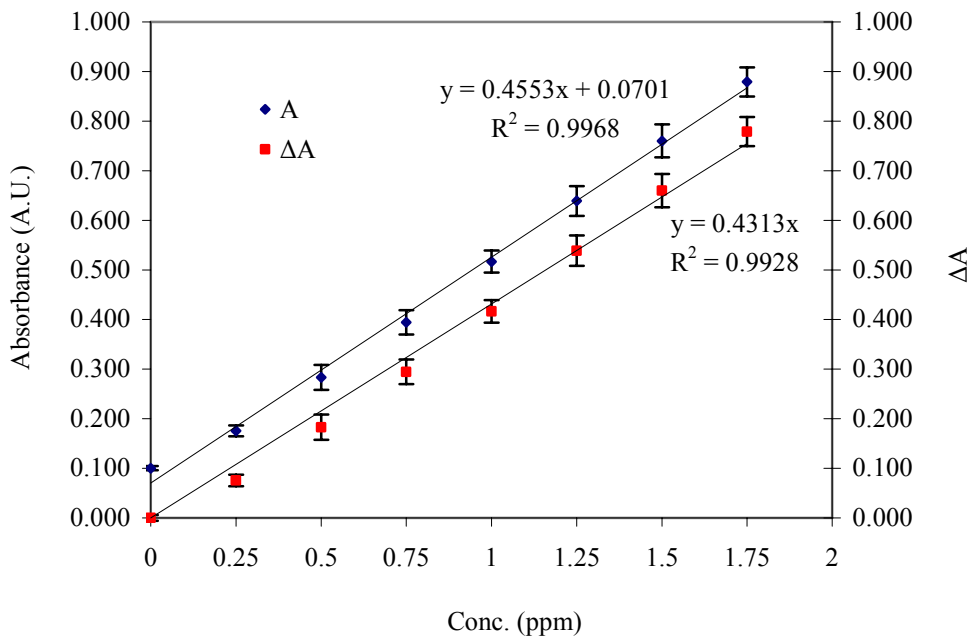


Figure H.19. Calibration curves for the phosphate standards prepared in ultrapure water at 630 nm.

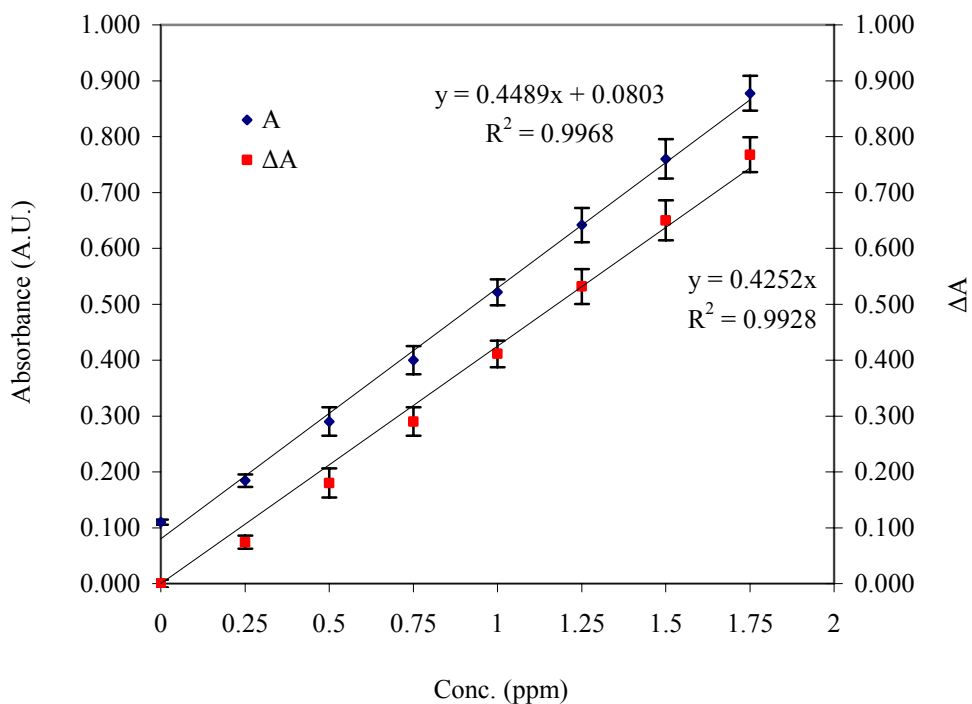


Figure H.20. Calibration curves for the phosphate standards prepared in ultrapure water at 620 nm.

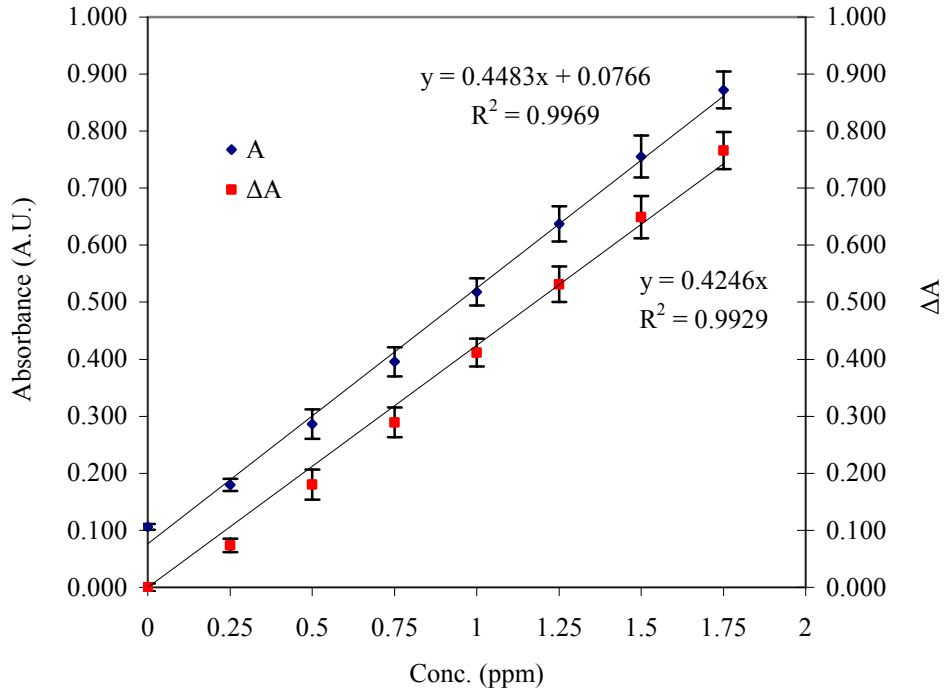


Figure H.21. Calibration curves for the phosphate standards prepared in ultrapure water at 610 nm.

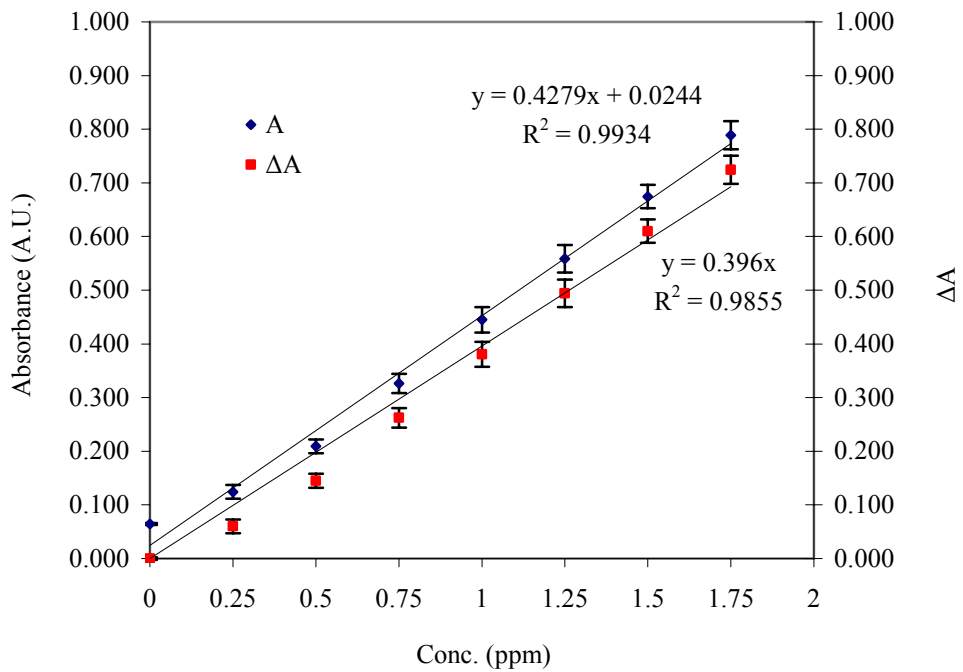


Figure H.22. Calibration curves for the phosphate standards prepared in 142 mM NaCl at 650 nm.

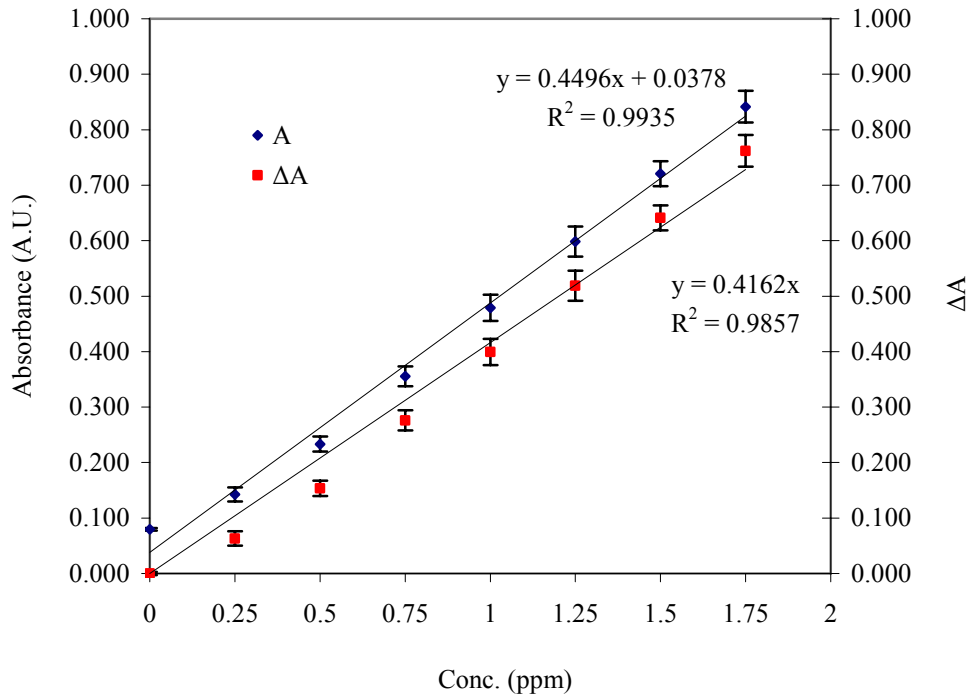


Figure H.23. Calibration curve for the phosphate standards prepared in 142 mM NaCl at 640 nm.

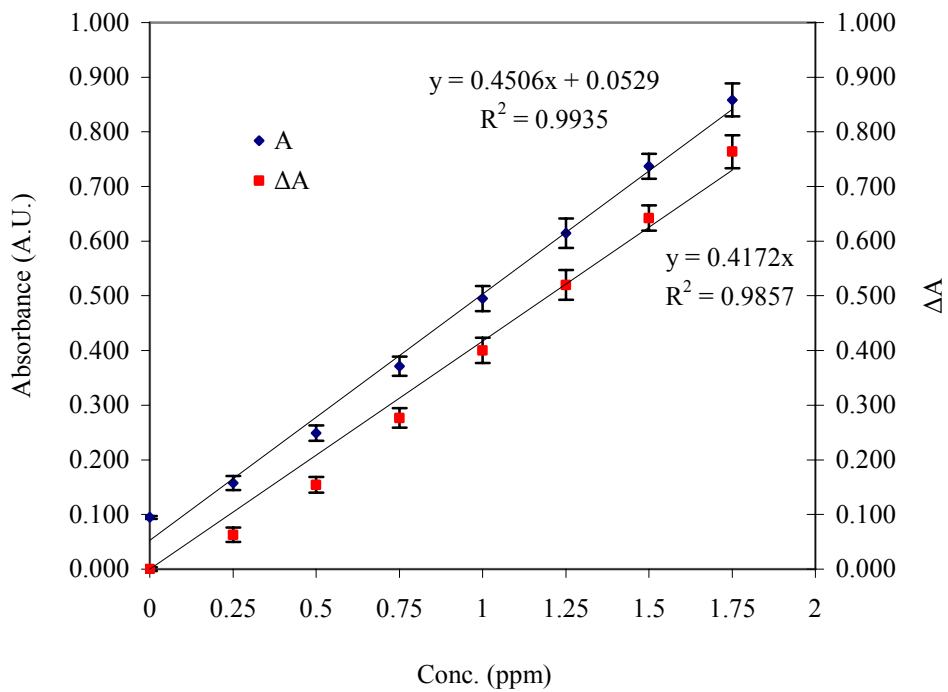


Figure H.24. Calibration curve for the phosphate standards prepared in 142 mM NaCl at 630 nm.

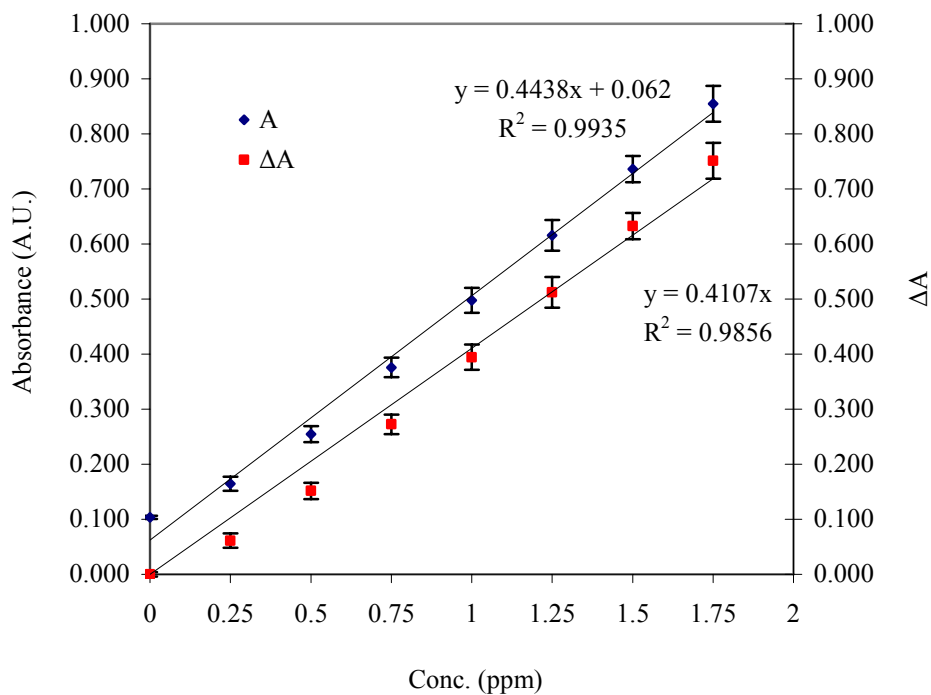


Figure H.25. Calibration curve for the phosphate standards prepared in 142 mM NaCl at 620 nm.

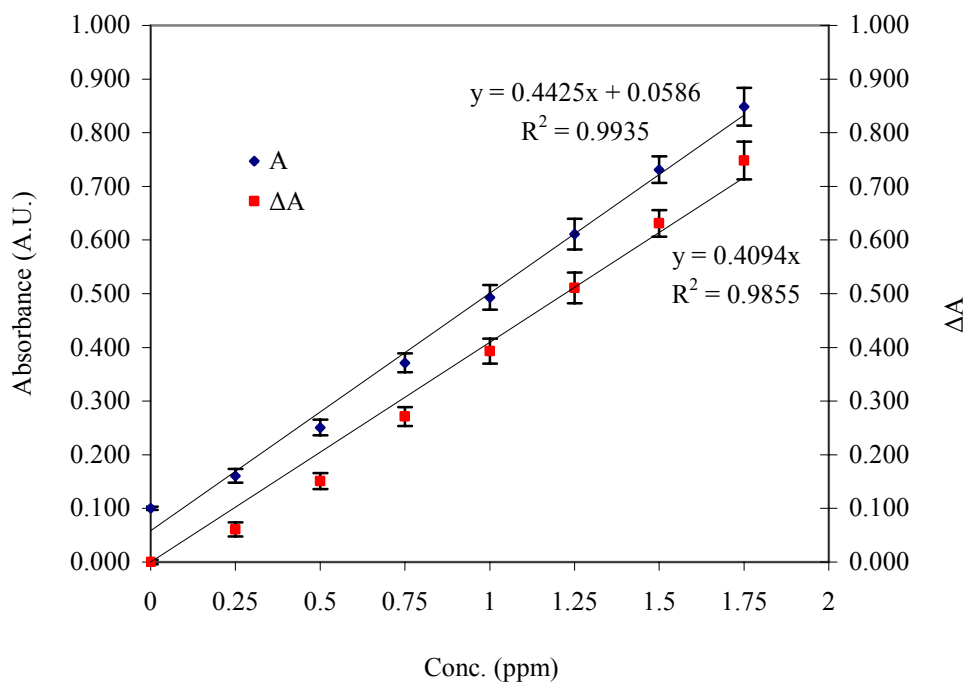


Figure H.26. Calibration curve for the phosphate standards prepared in 142 mM NaCl at 610 nm.

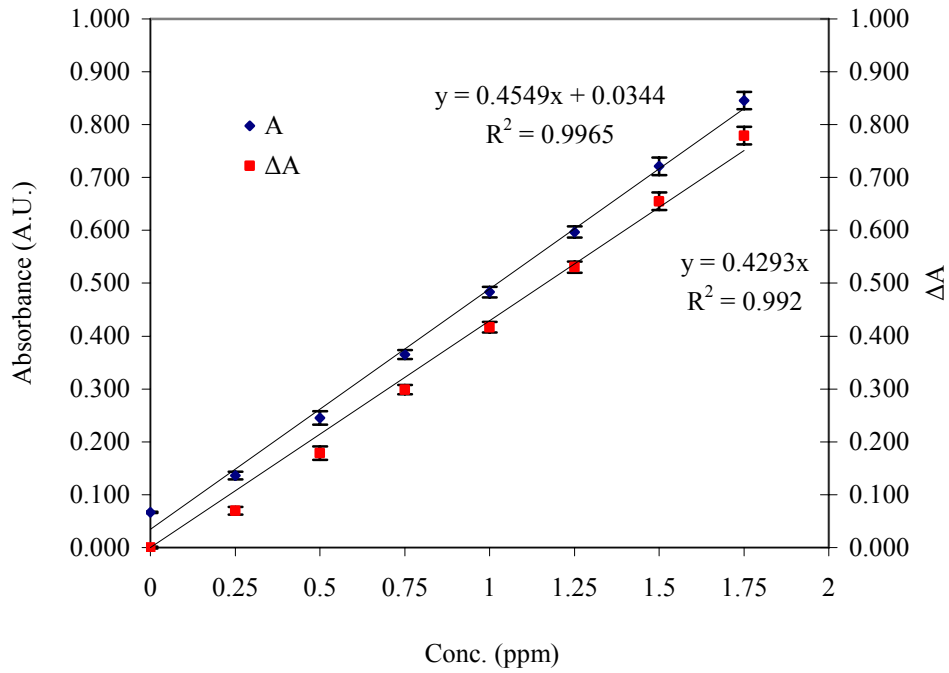


Figure H.27. Calibration curve for the phosphate standards prepared in 5 mM KCl at 650 nm.

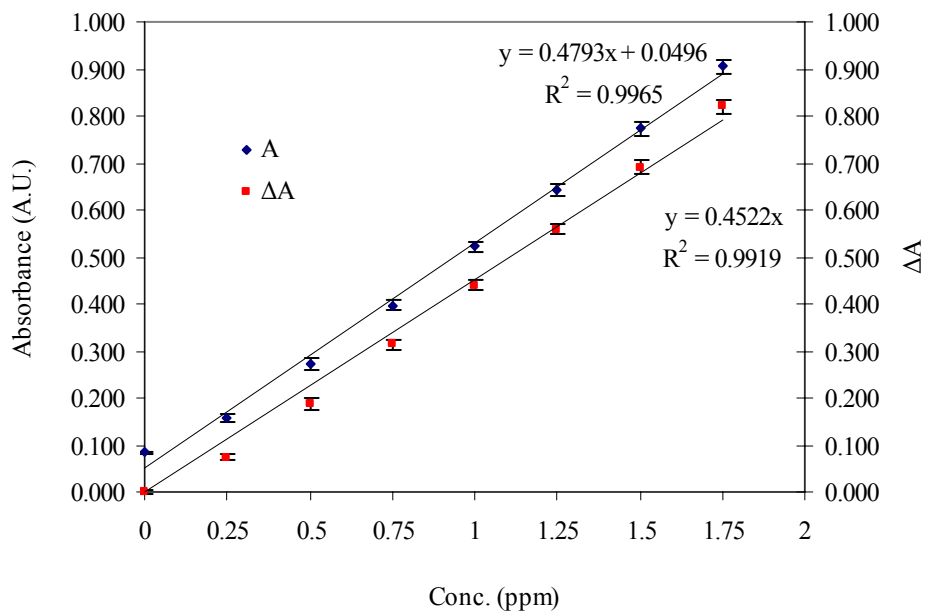


Figure H.28. Calibration curve for the phosphate standards prepared in 5 mM KCl at 640 nm.

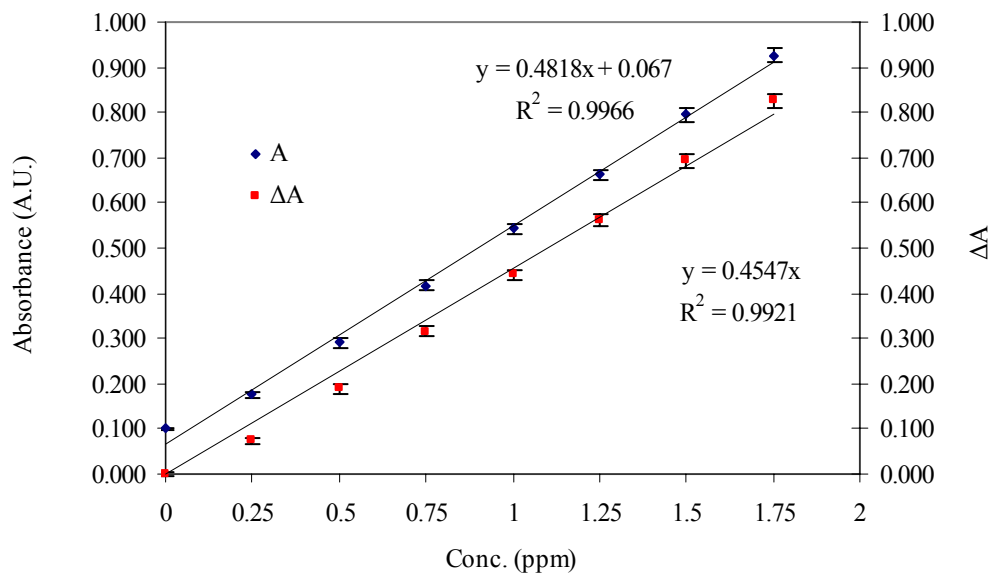


Figure H.29. Calibration curve for the phosphate standards prepared in 5 mM KCl at 630 nm.

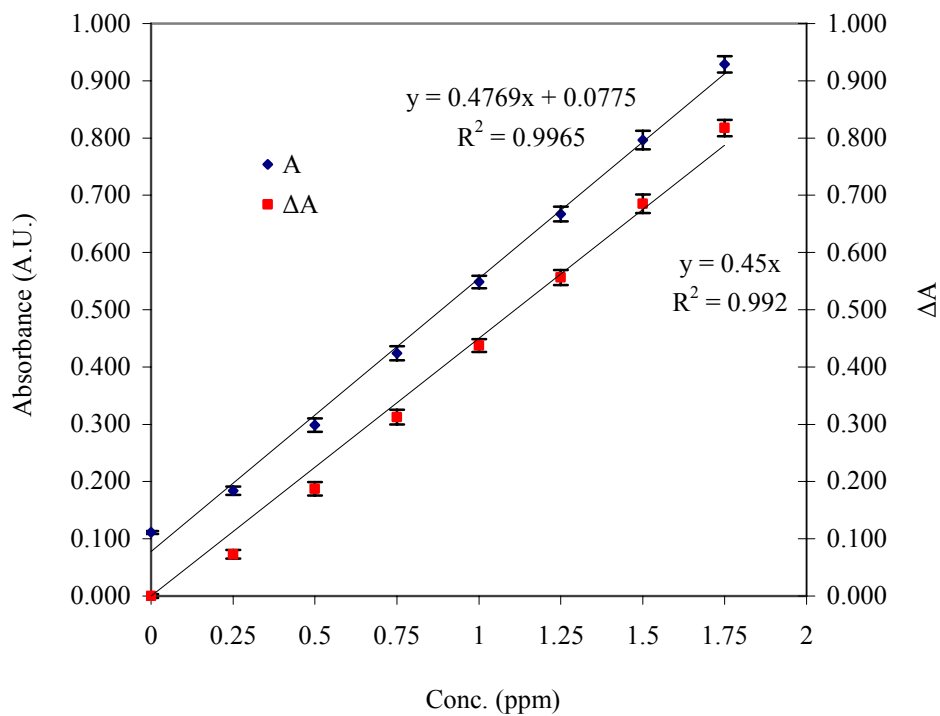


Figure H.30. Calibration curve for the phosphate standards prepared in 5 mM KCl at 620 nm.

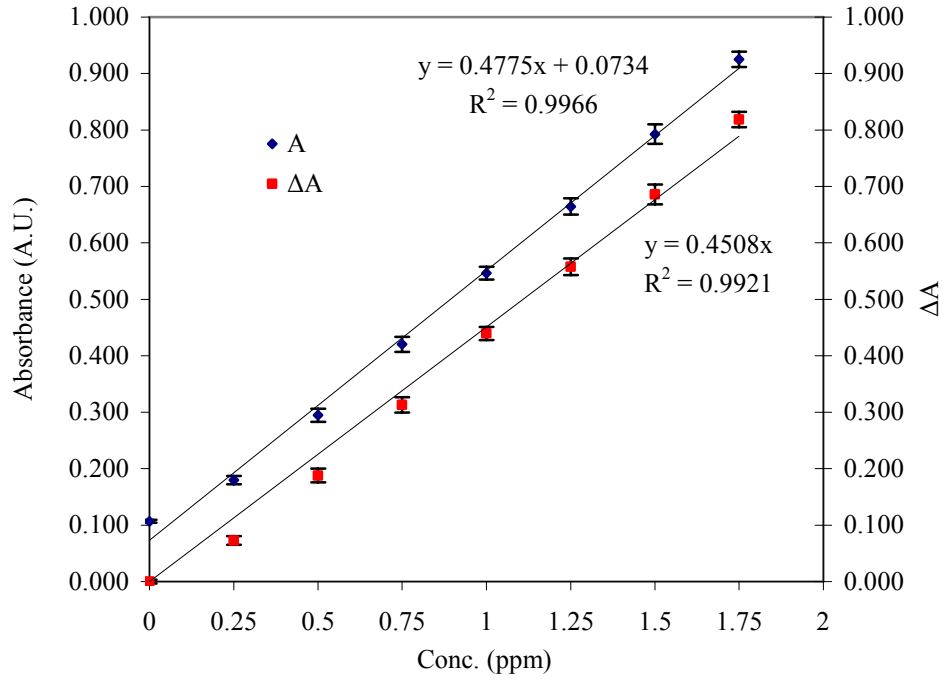


Figure H.31. Calibration curve for the phosphate standards prepared in 5 mM KCl at 610 nm.

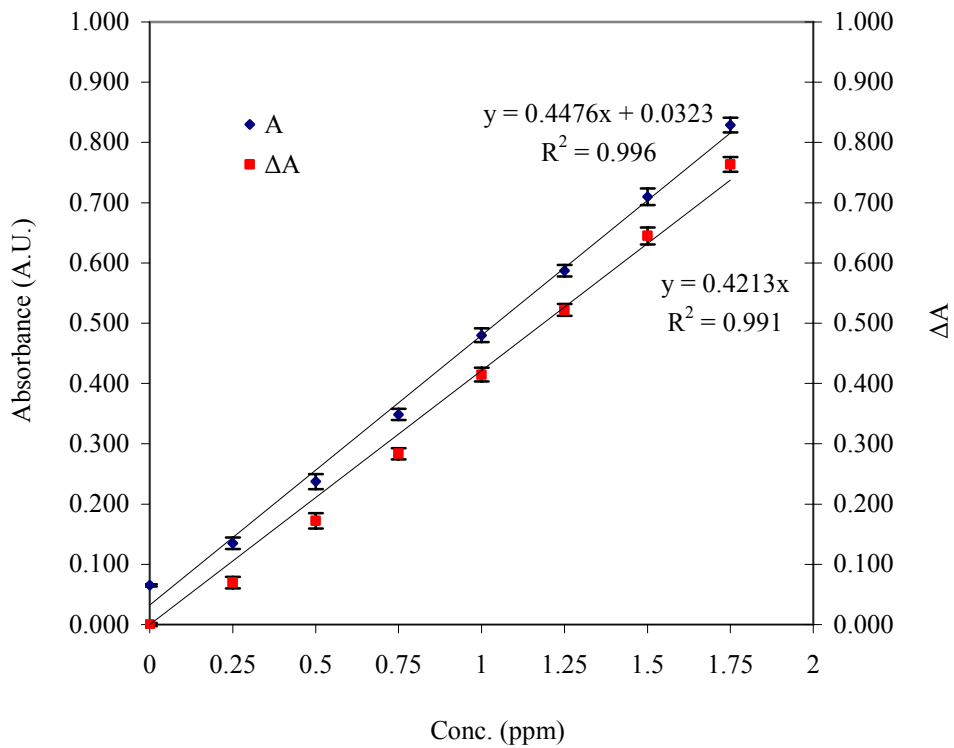


Figure H.32. Calibration curve for the phosphate standards prepared in 2.5 mM CaCl₂ at 650 nm.

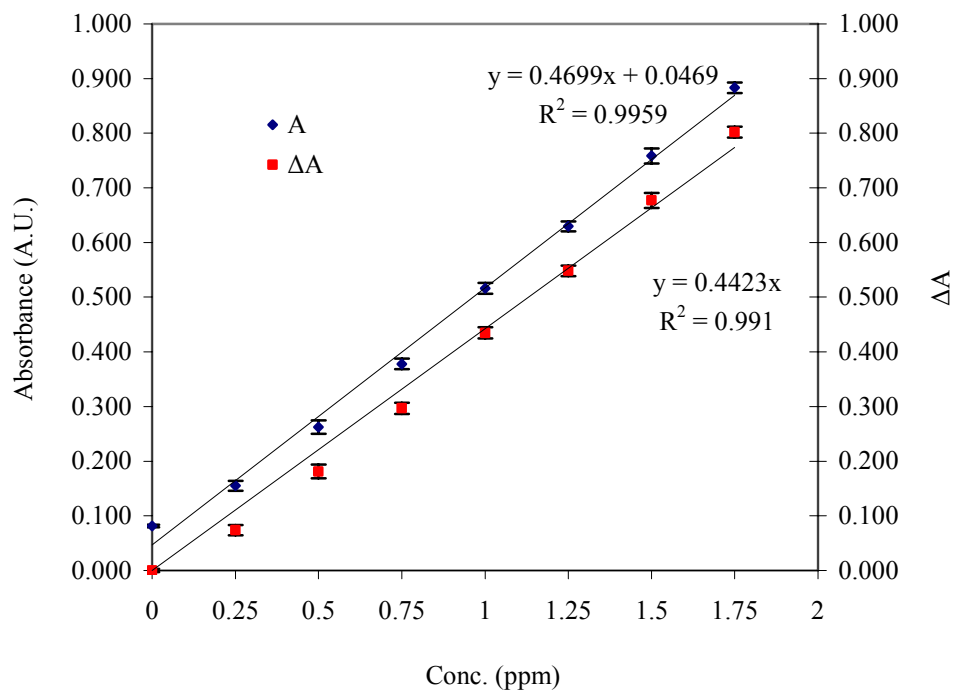


Figure H.33. Calibration curve for the phosphate standards prepared in 2.5 mM CaCl₂ at 640 nm.

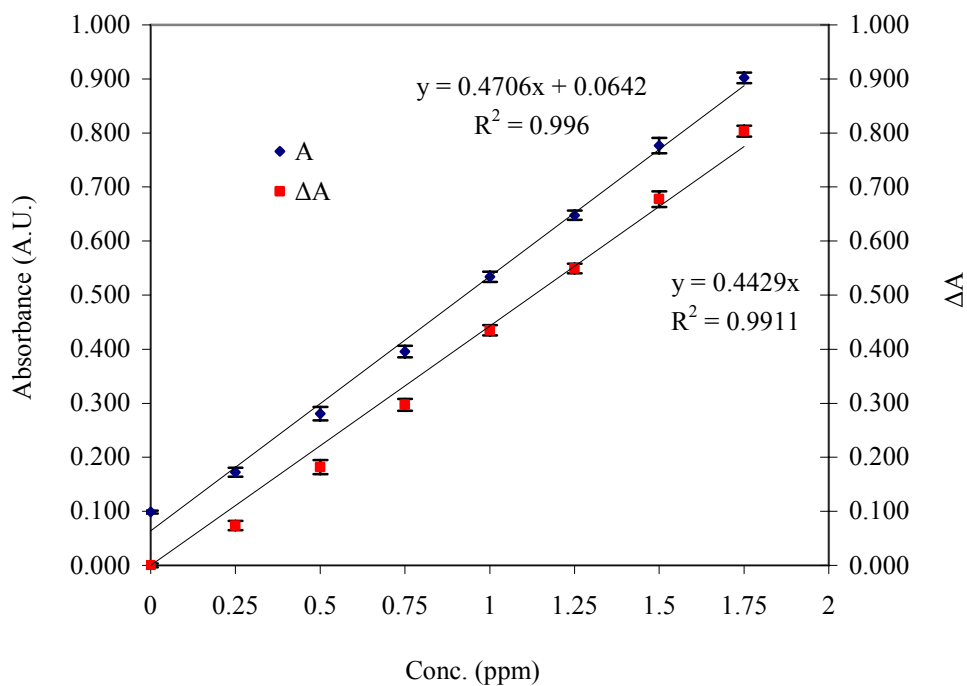


Figure H.34. Calibration curve for the phosphate standards prepared in 2.5 mM CaCl₂ at 630 nm.

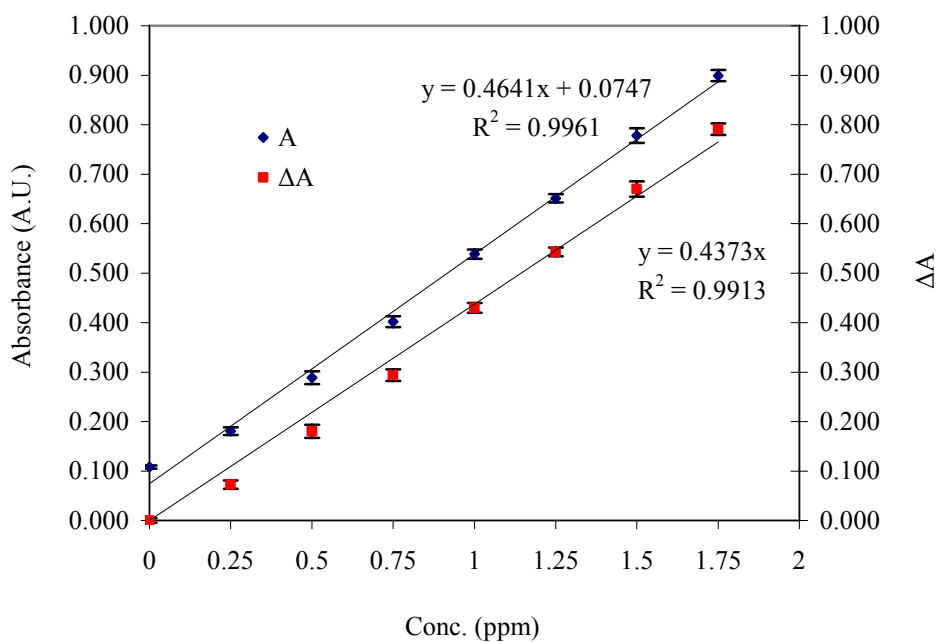


Figure H.35. Calibration curve for the phosphate standards prepared in 2.5 mM CaCl₂ at 620 nm.

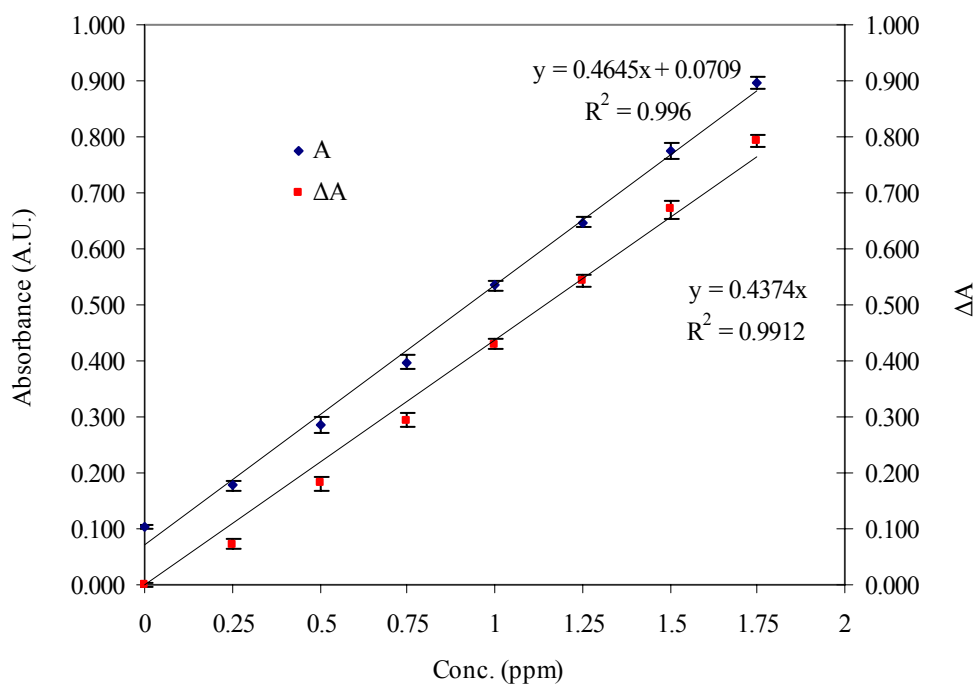


Figure H.36. Calibration curve for the phosphate standards prepared in 2.5 mM CaCl₂ at 610 nm.

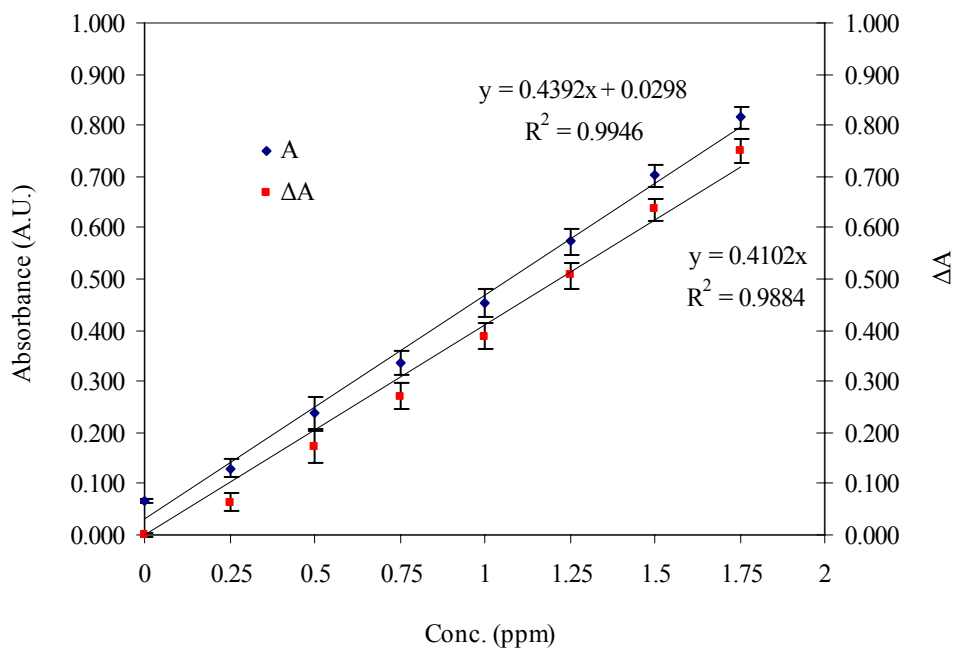


Figure H.37. Calibration curve for the phosphate standards prepared in 1.5 mM MgCl₂ at 650 nm.

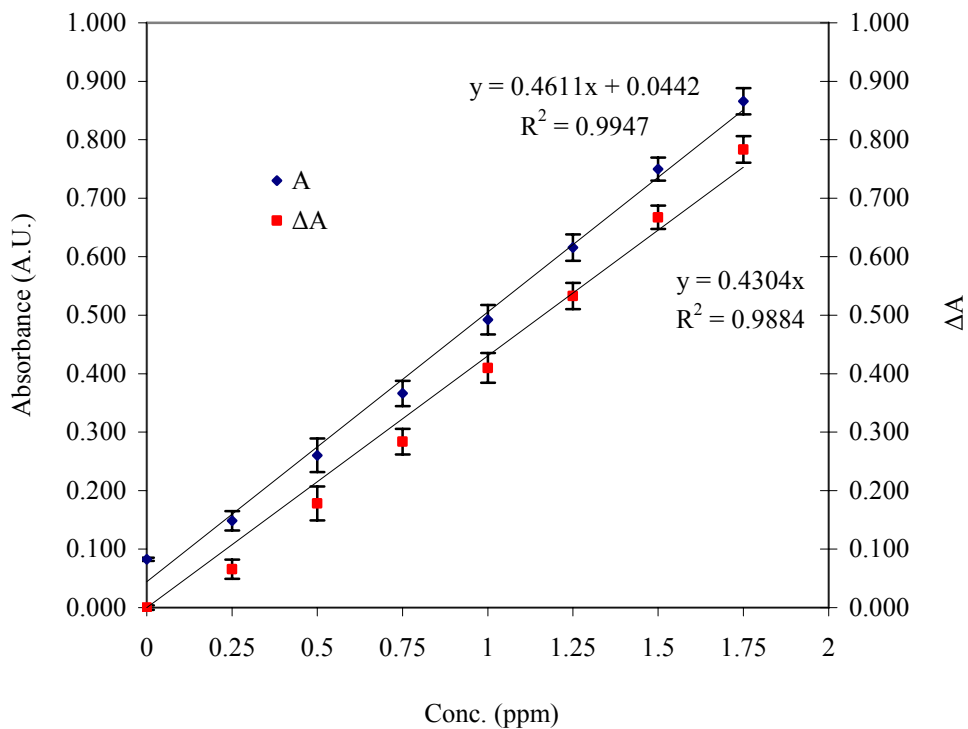


Figure H.38. Calibration curve for the phosphate standards prepared in 1.5 mM MgCl₂ at 640 nm.

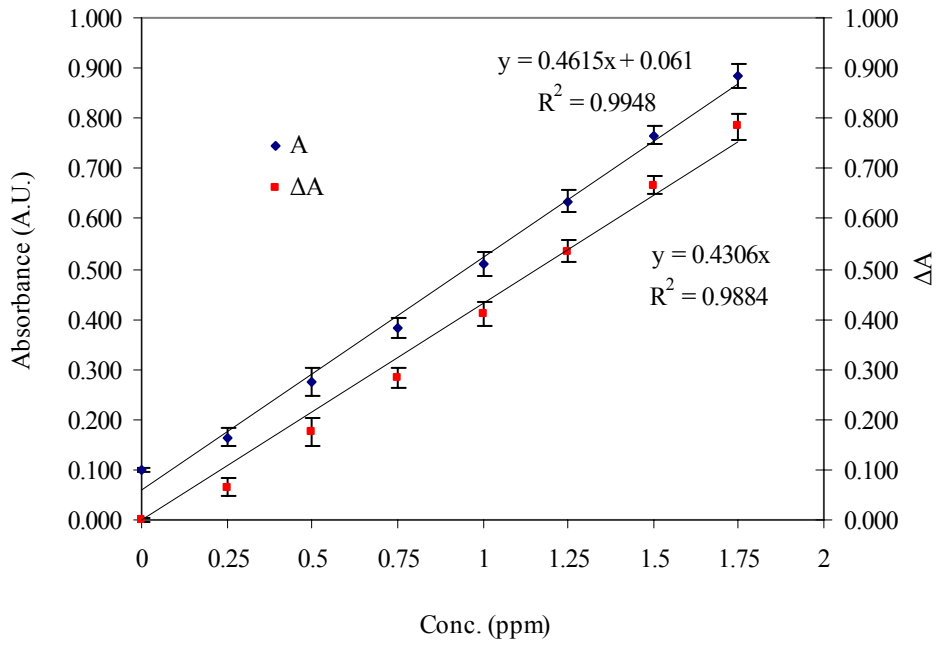


Figure H.39. Calibration curve for the phosphate standards prepared in 1.5 mM MgCl₂ at 630 nm.

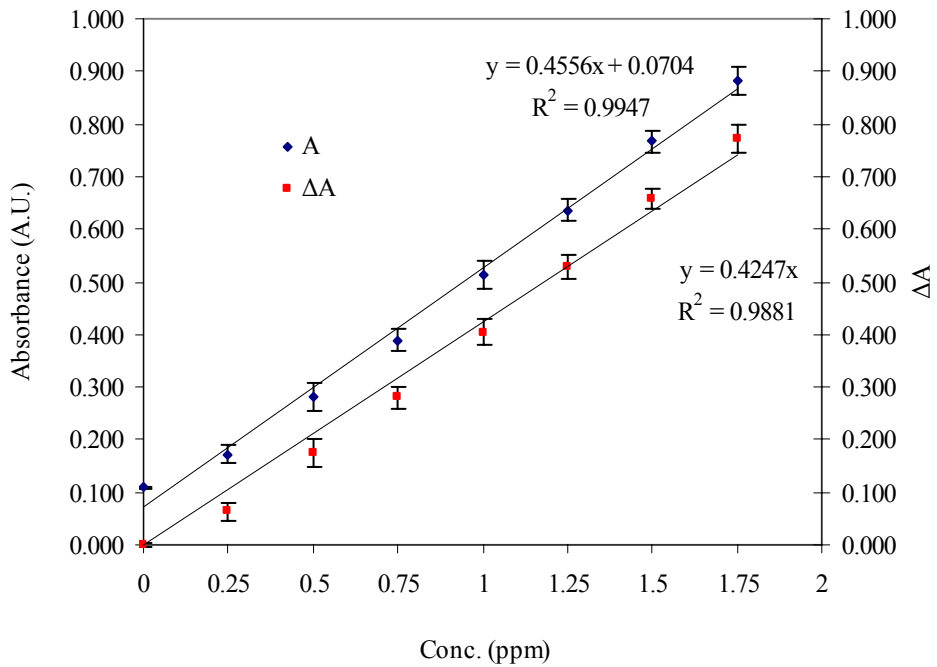


Figure H.40. Calibration curve for the phosphate standards prepared in 1.5 mM MgCl₂ at 620 nm.

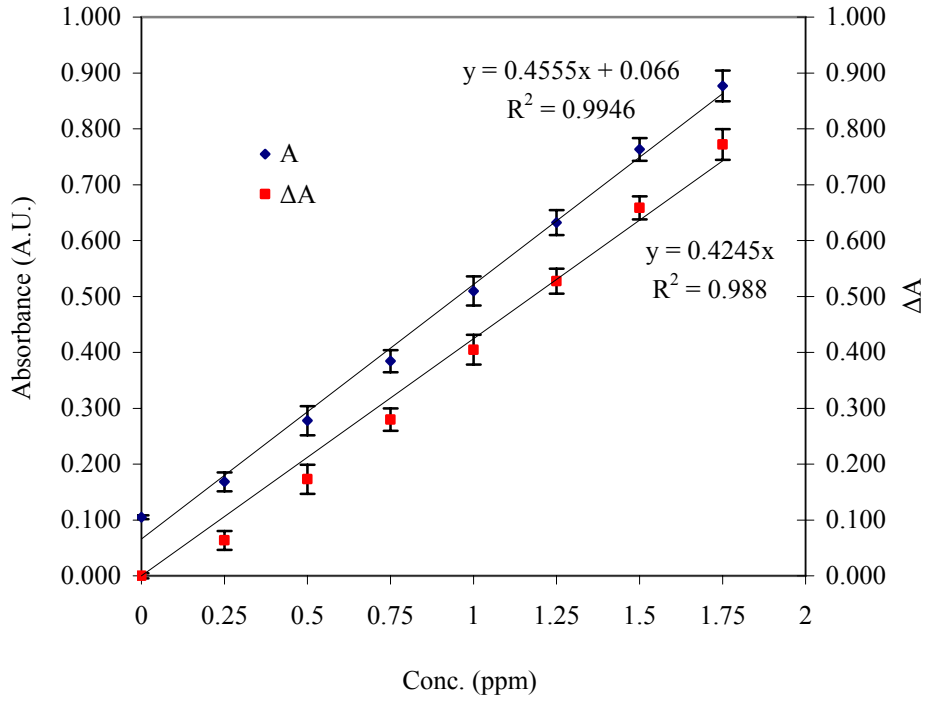


Figure H.41. Calibration curve for the phosphate standards prepared in 1.5 mM MgCl₂ at 610 nm.

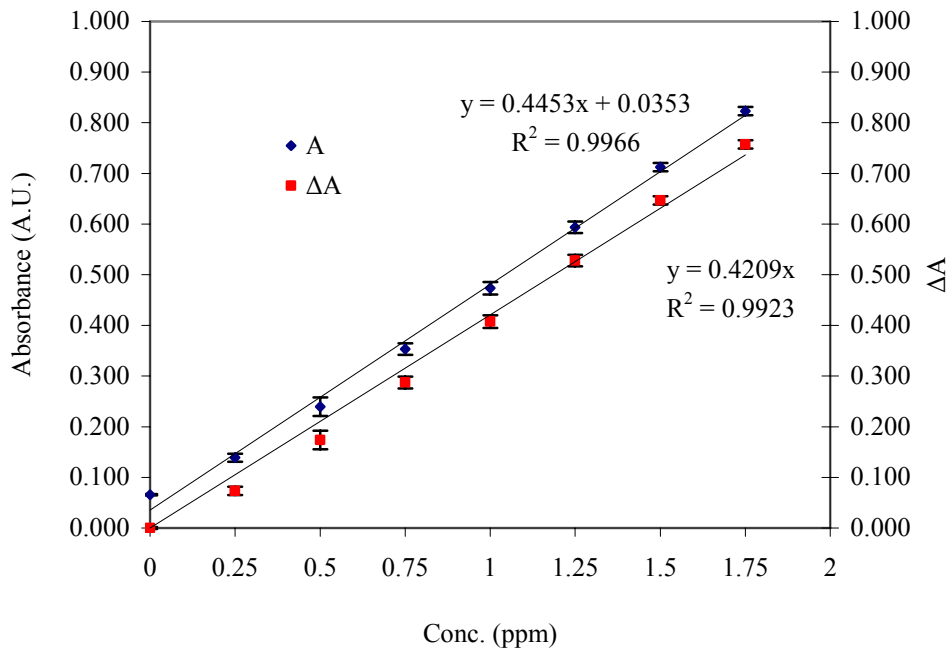


Figure H.42. Calibration curves for the phosphate standards prepared in 0.5 mM Na₂SO₄ at 650 nm.

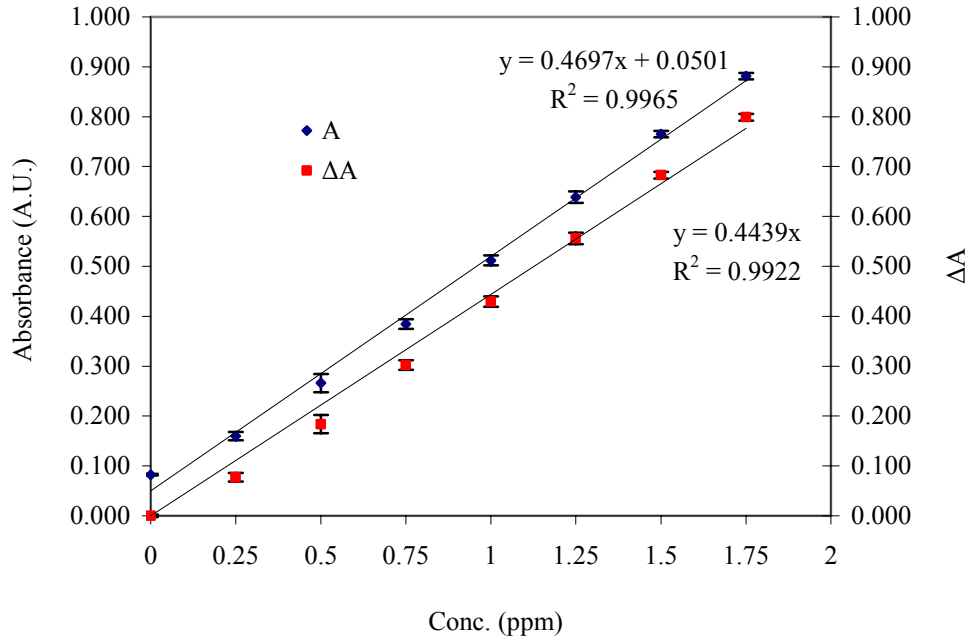


Figure H.43. Calibration curves for the phosphate standards prepared in 0.5 mM Na_2SO_4 at 640 nm.

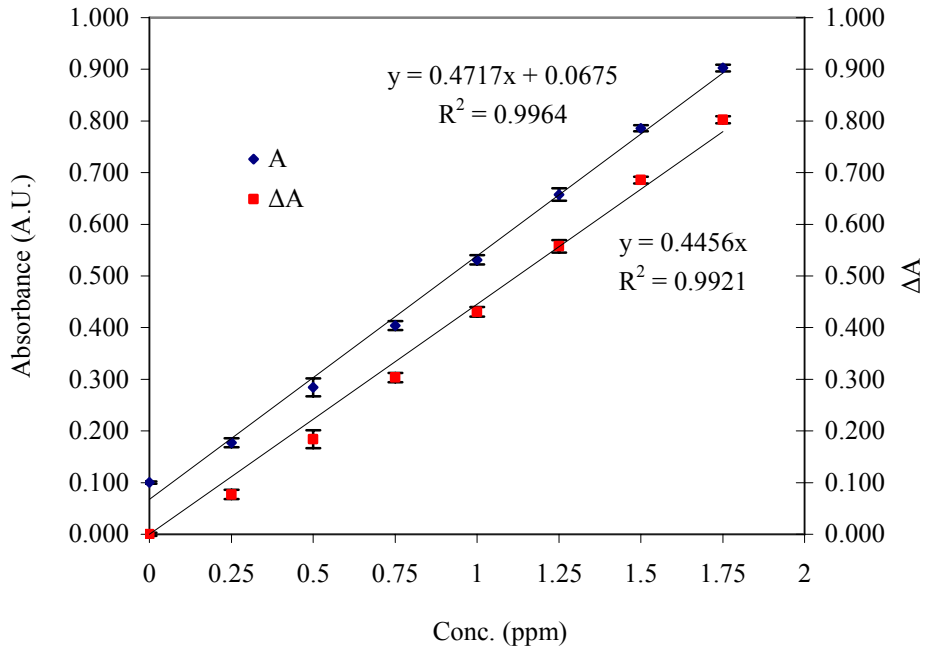


Figure H.44. Calibration curves for the phosphate standards prepared in 0.5 mM Na_2SO_4 at 630 nm.

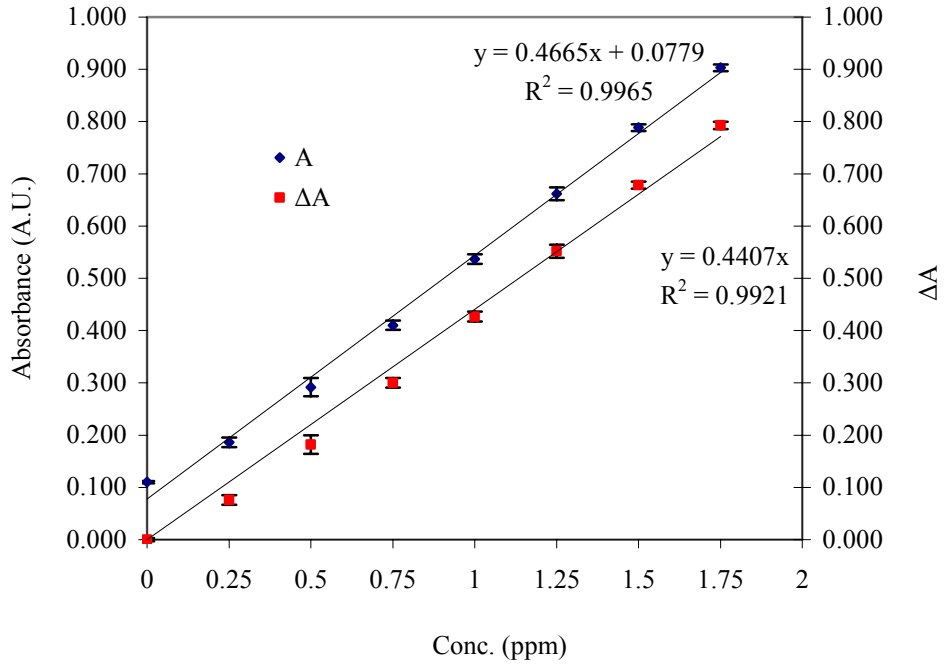


Figure H.45. Calibration curves for the phosphate standards prepared in 0.5 mM Na_2SO_4 at 620 nm.

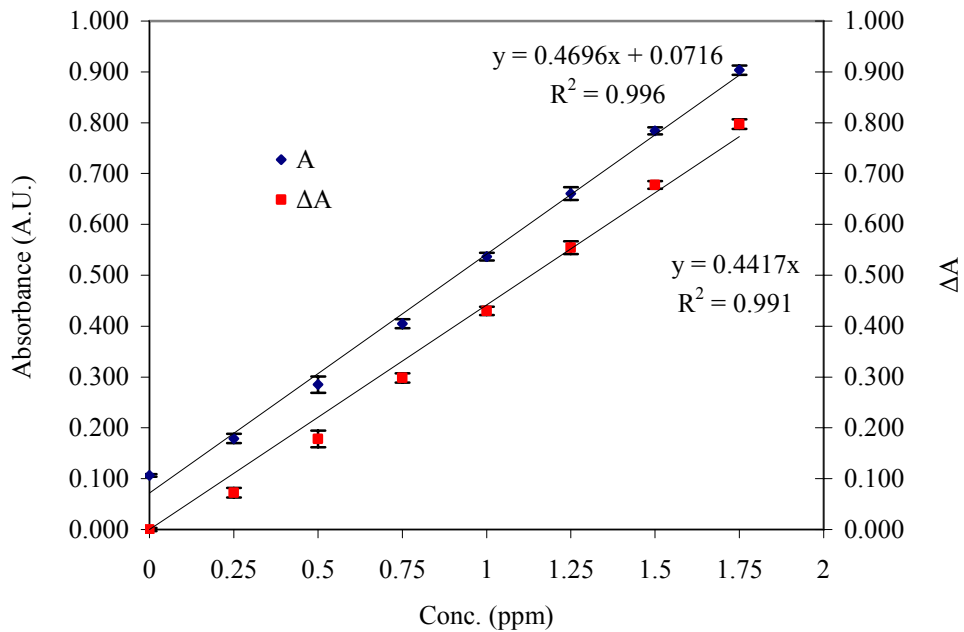


Figure H.46. Calibration curves for the phosphate standards prepared in 0.5 mM Na_2SO_4 at 610 nm.

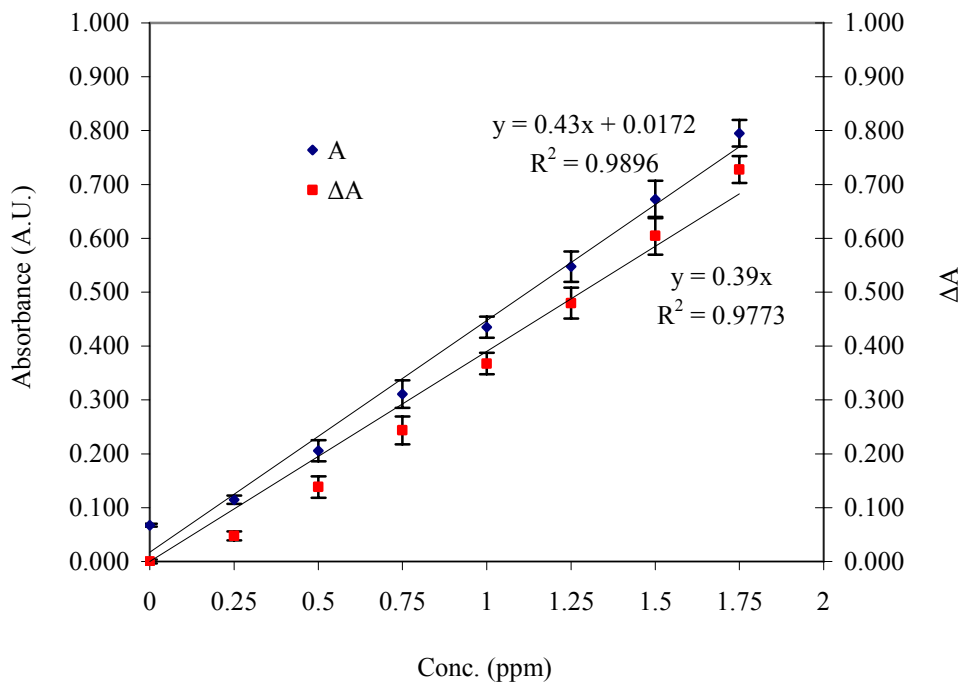


Figure H.47. Calibration curves for the phosphate standards prepared in 27 mM NaHCO_3 at 650 nm.

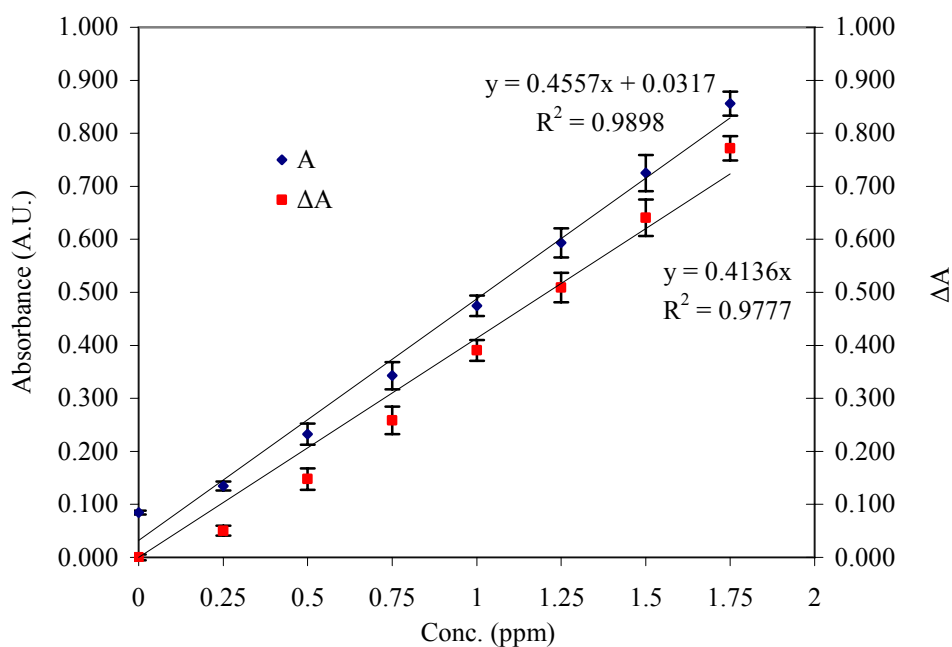


Figure H.48. Calibration curves for the phosphate standards prepared in 27 mM NaHCO_3 at 640 nm.

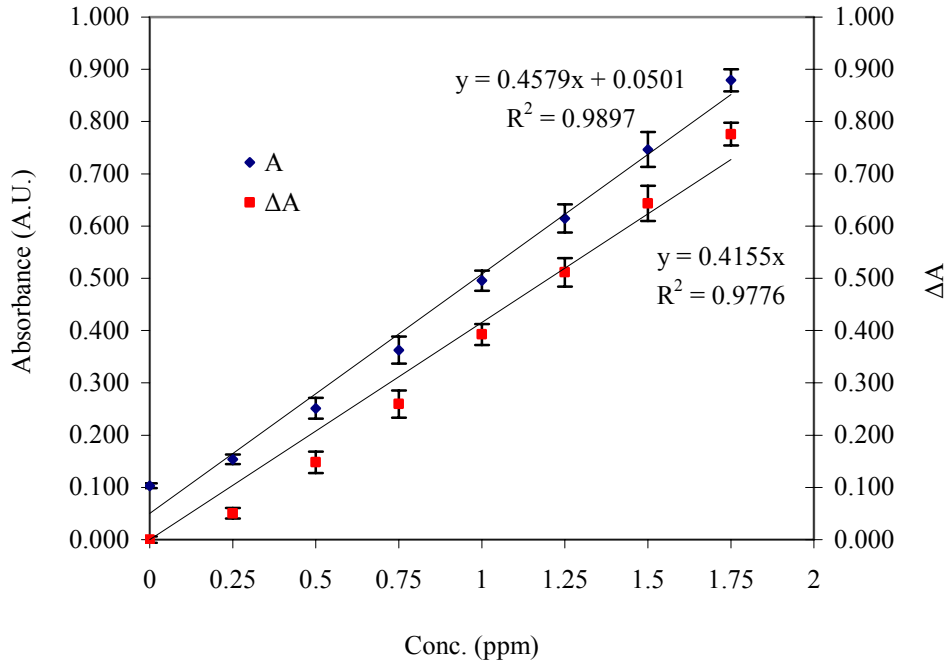


Figure H.49. Calibration curves for the phosphate standards prepared in 27 mM NaHCO_3 at 630 nm.

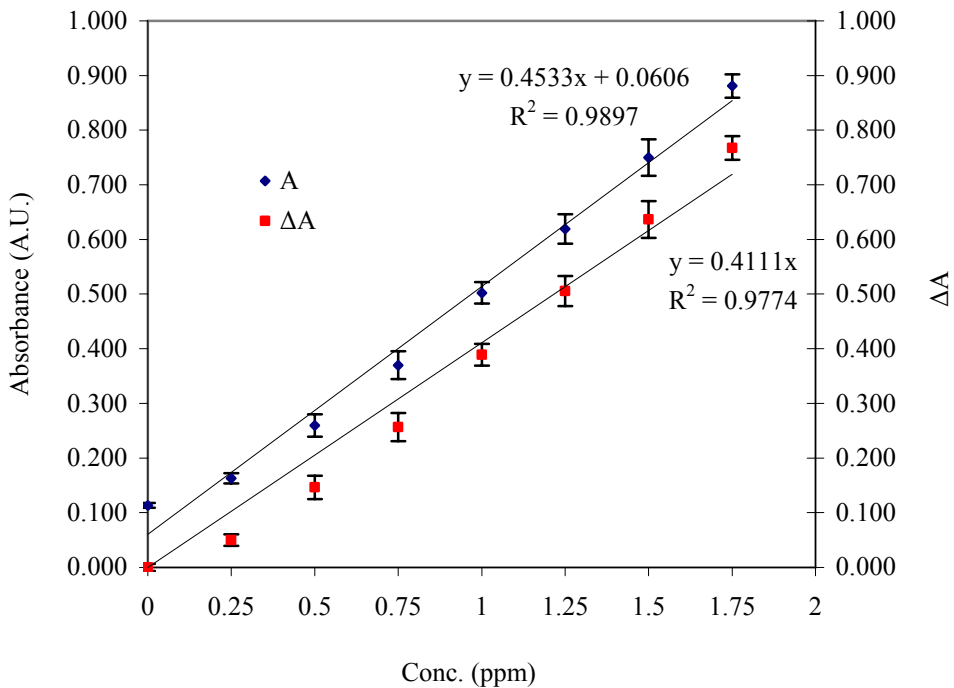


Figure H.50. Calibration curves for the phosphate standards prepared in 27 mM NaHCO_3 at 620 nm.

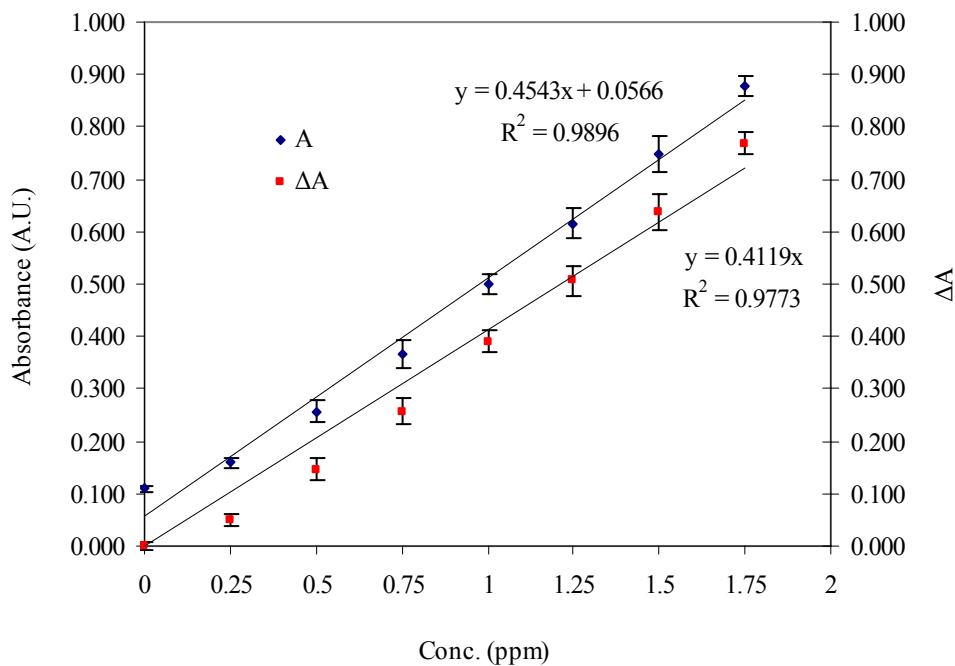


Figure H.51. Calibration curves for the phosphate standards prepared in 27 mM NaHCO_3 at 610 nm.

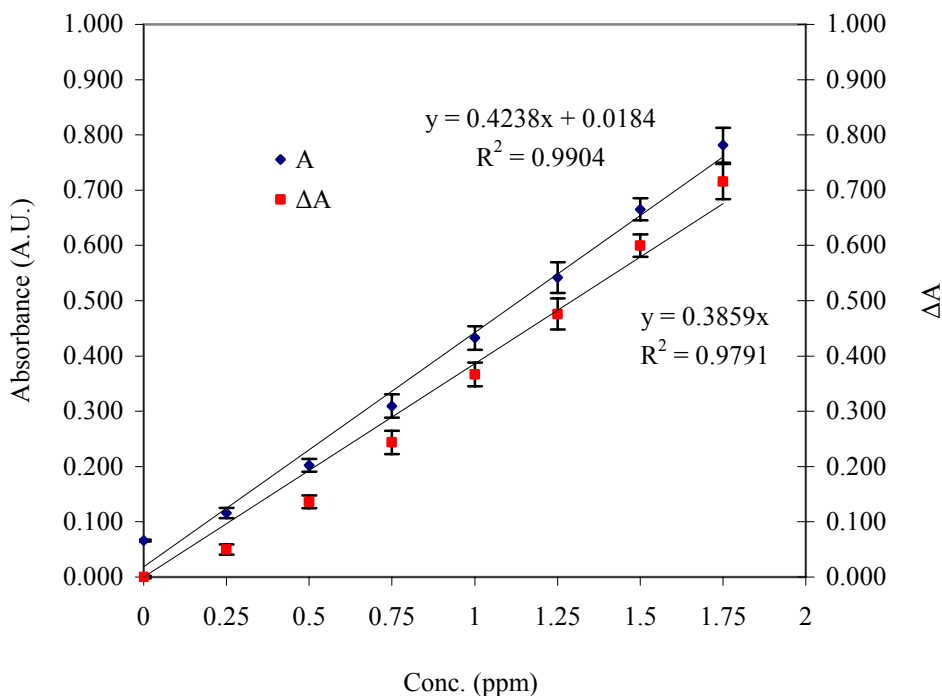


Figure H.52. Calibration curve for the phosphate standards prepared in 115 mM NaCl and 27 mM NaHCO_3 containing solution at 650 nm.

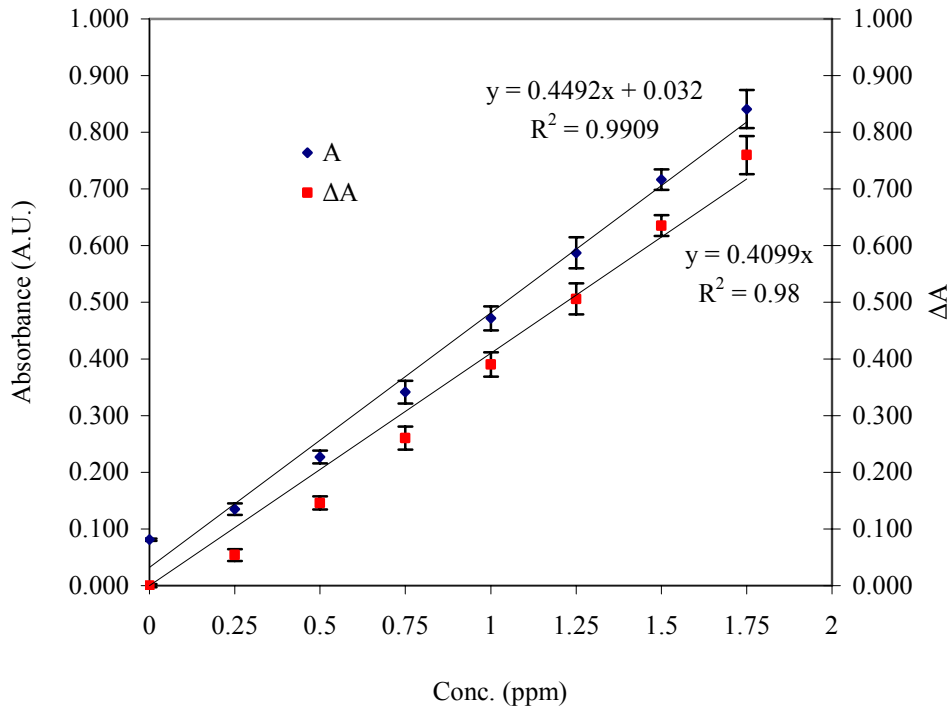


Figure H.53. Calibration curves for the phosphate standards prepared in 115 mM NaCl and 27 mM NaHCO₃ containing solution at 640 nm.

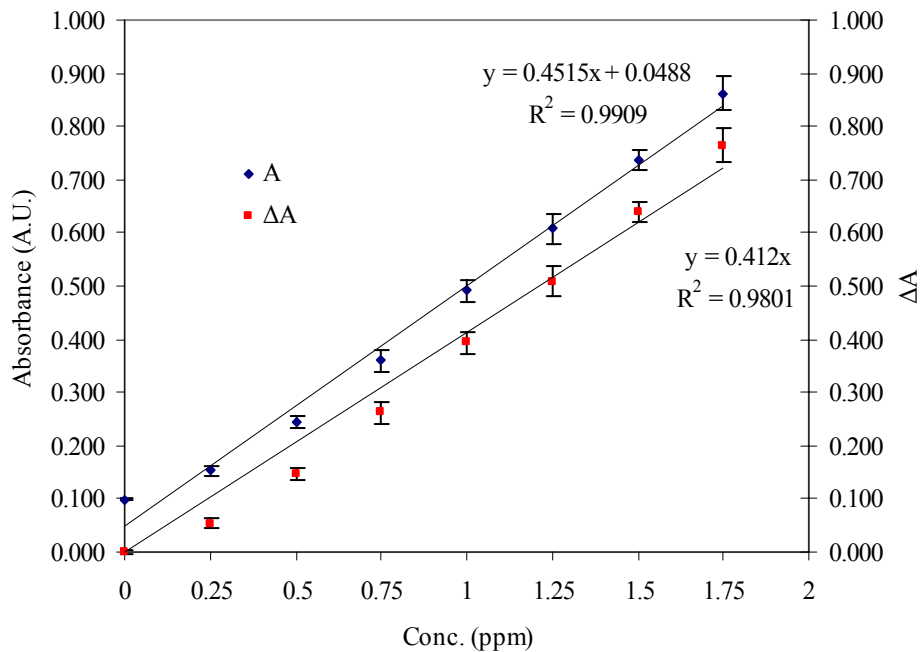


Figure H.54. Calibration curves for the phosphate standards prepared in 115 mM NaCl and 27 mM NaHCO₃ containing solution at 630 nm.

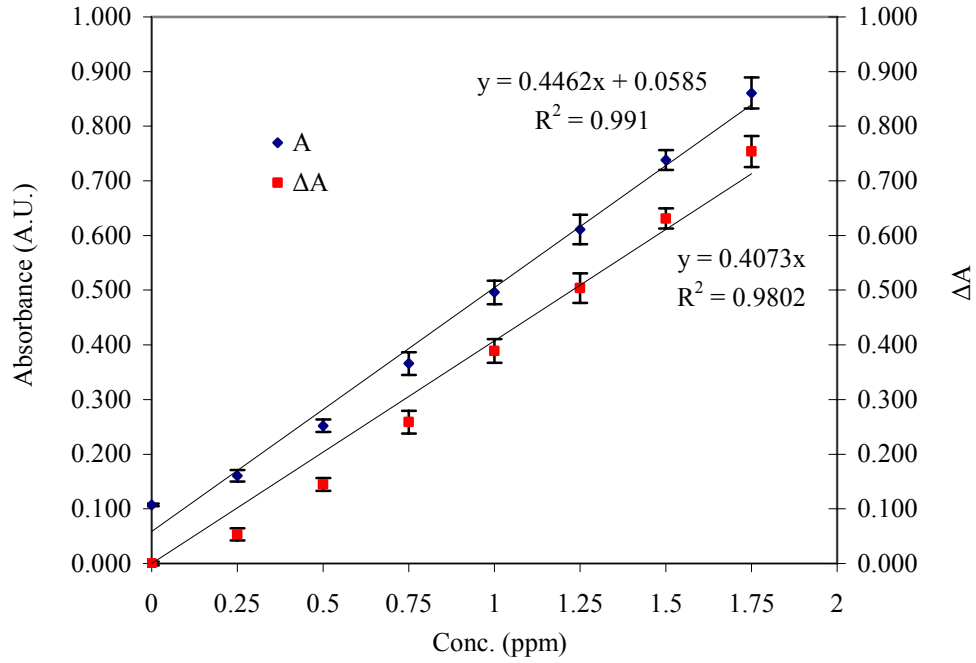


Figure H.55. Calibration curves for the phosphate standards prepared in 115 mM NaCl and 27 mM NaHCO₃ containing solution at 620 nm.

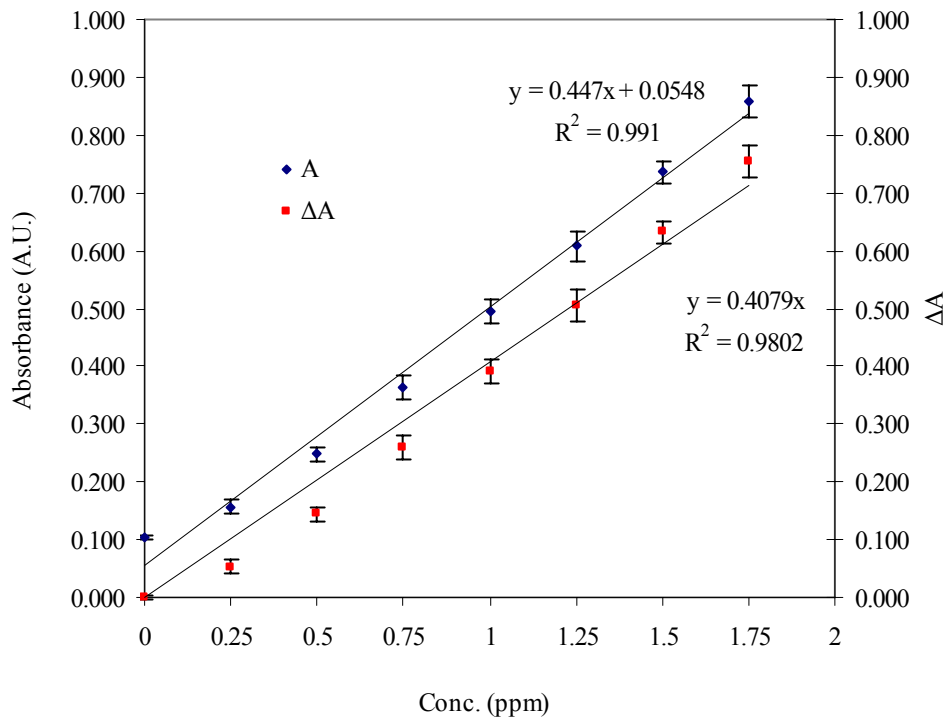


Figure H.56. Calibration curves for the phosphate standards prepared in 115 mM NaCl and 27 mM NaHCO₃ containing solution at 610 nm.

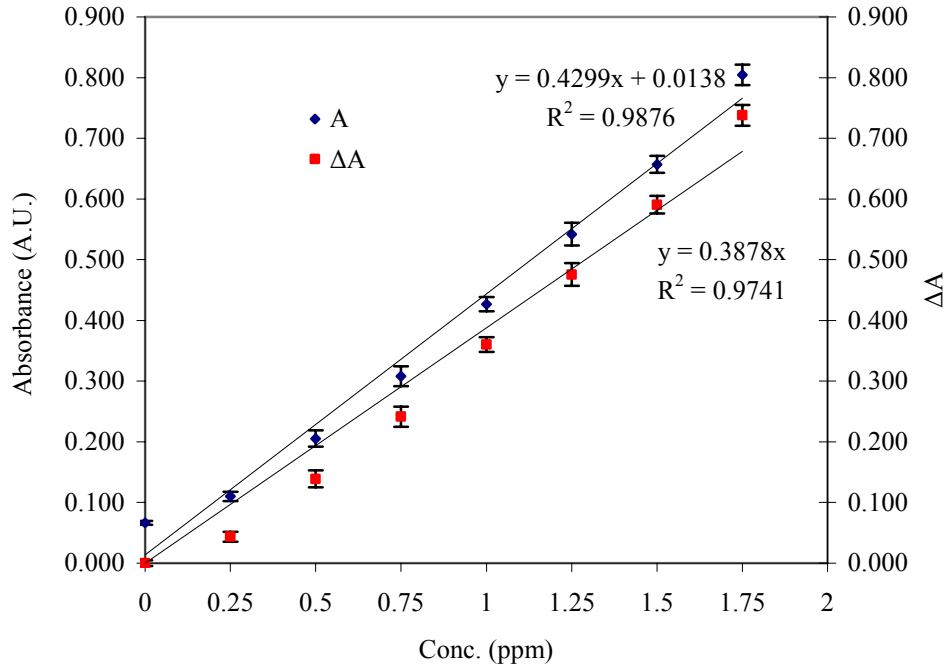


Figure H.57. Calibration curve for the phosphate standards prepared in SBFA solution at 650 nm.

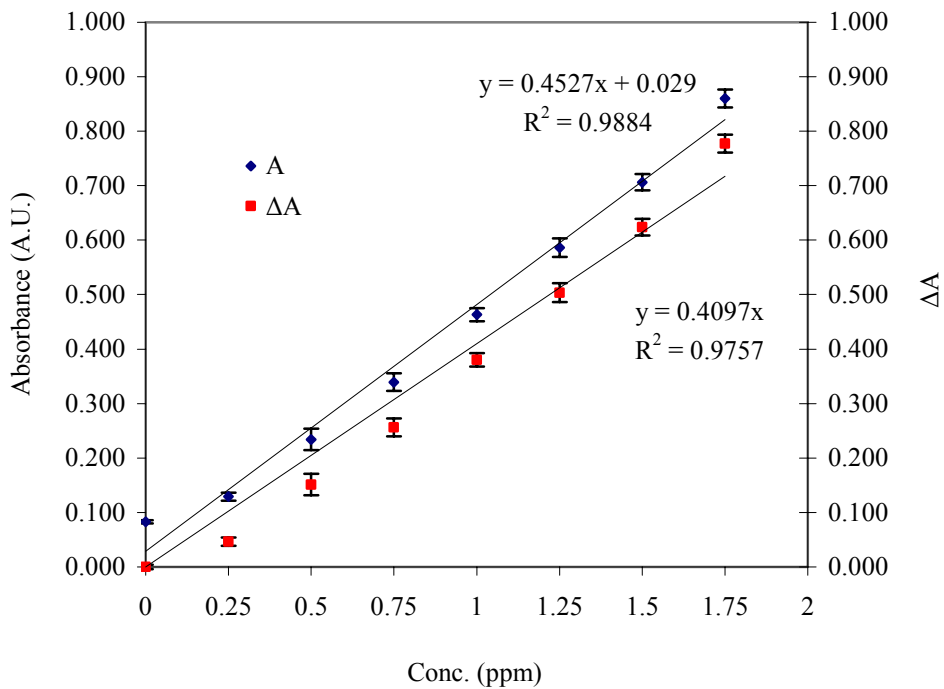


Figure H.58. Calibration curves for the phosphate standards prepared in SBFA solution at 640 nm.

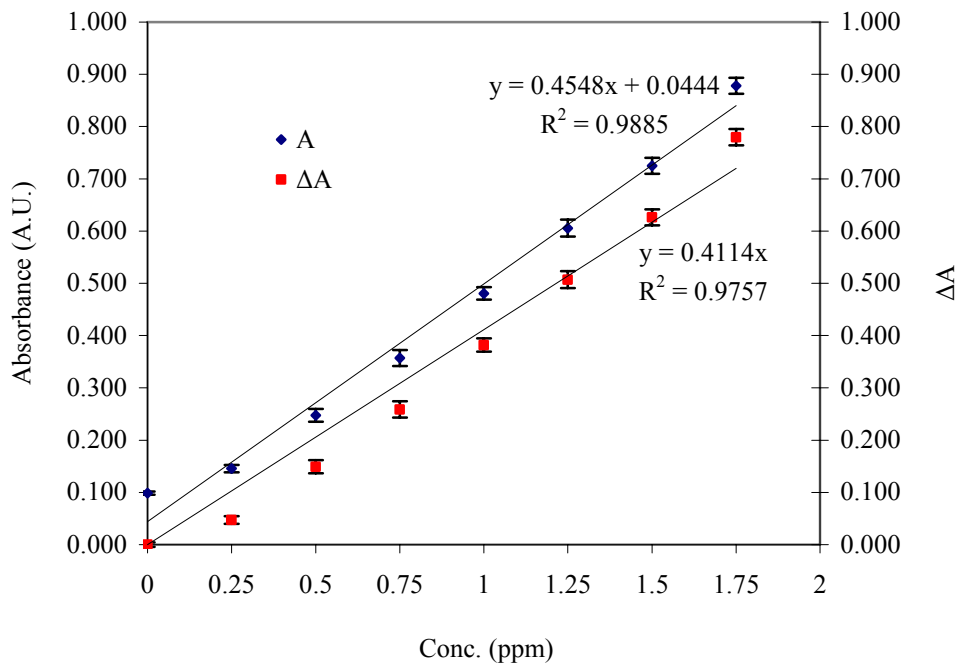


Figure H.59. Calibration curves for the phosphate standards prepared in SBFA solution at 630 nm.

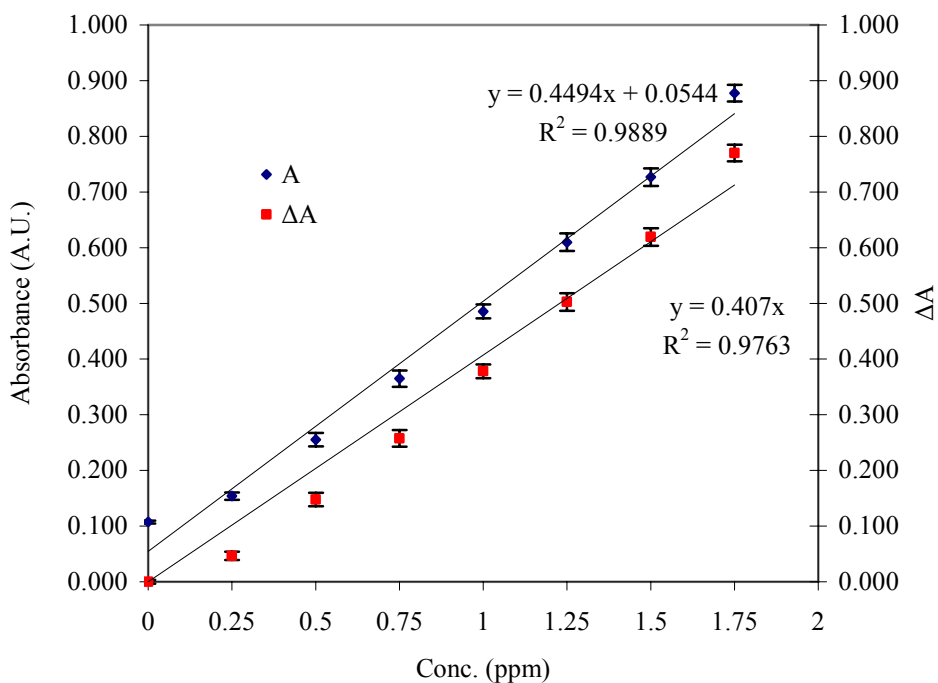


Figure H.60. Calibration curves for the phosphate standards prepared in SBFA solution at 620 nm.

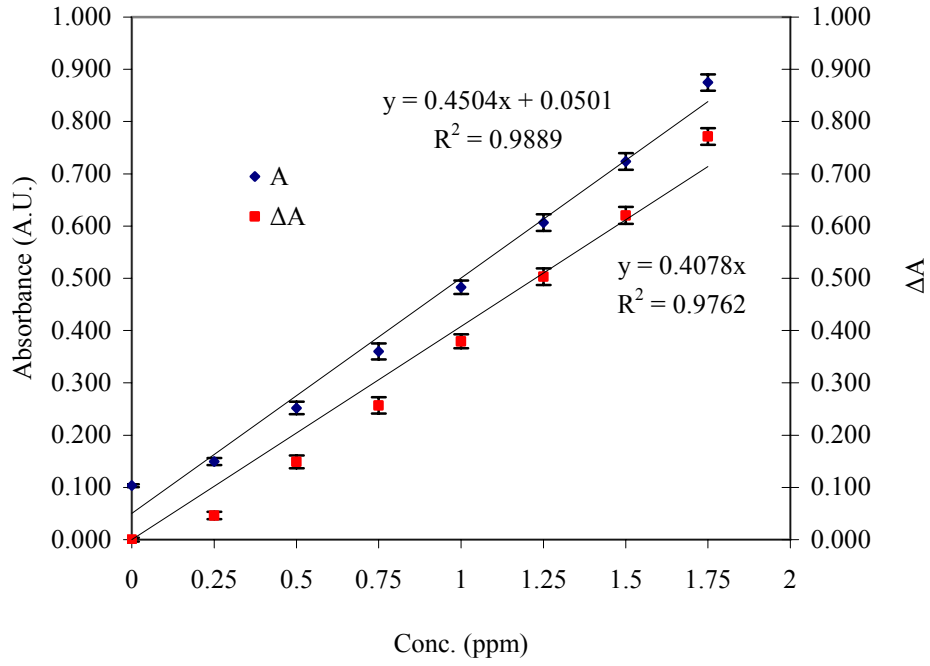


Figure H.61. Calibration curves for the phosphate standards prepared in SBFA solution at 610 nm.

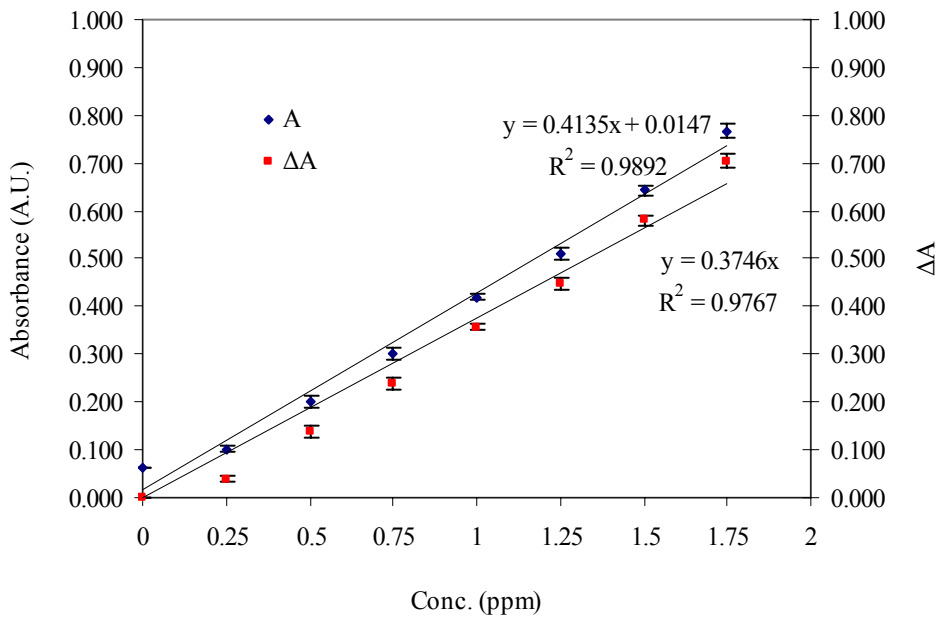


Figure H.62. Calibration curve for the phosphate standards prepared in SBFB solution at 650 nm.

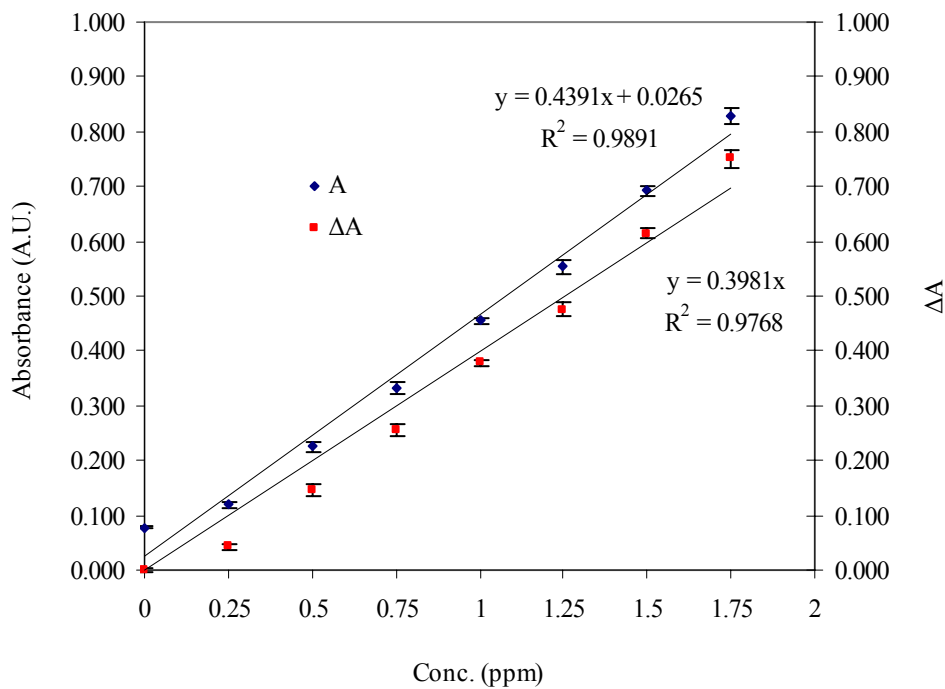


Figure H.63. Calibration curves for the phosphate standards prepared in SBF solution at 640 nm.

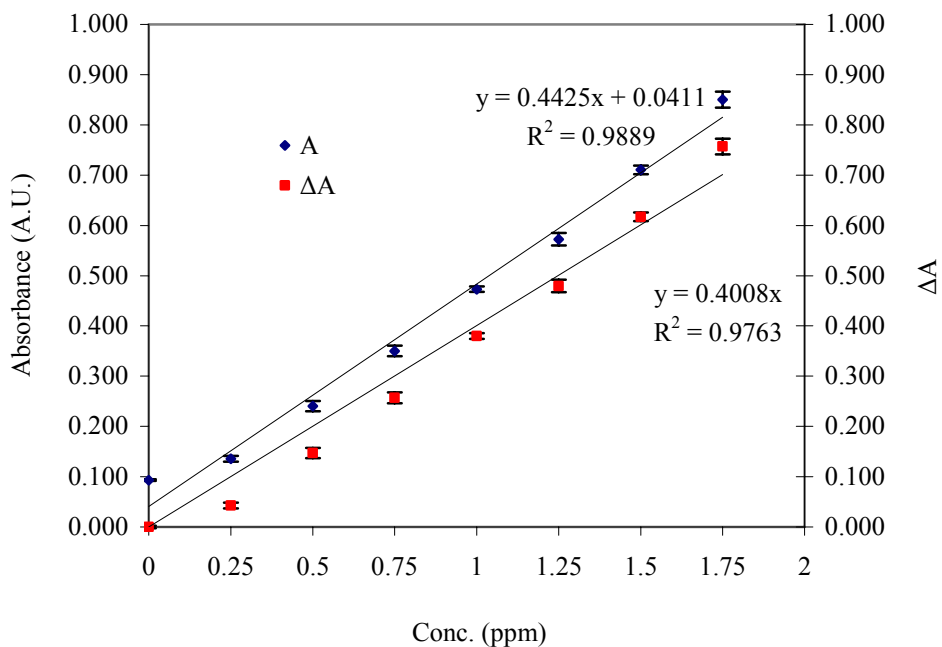


Figure H.64. Calibration curves for the phosphate standards prepared in SBF solution at 630 nm.

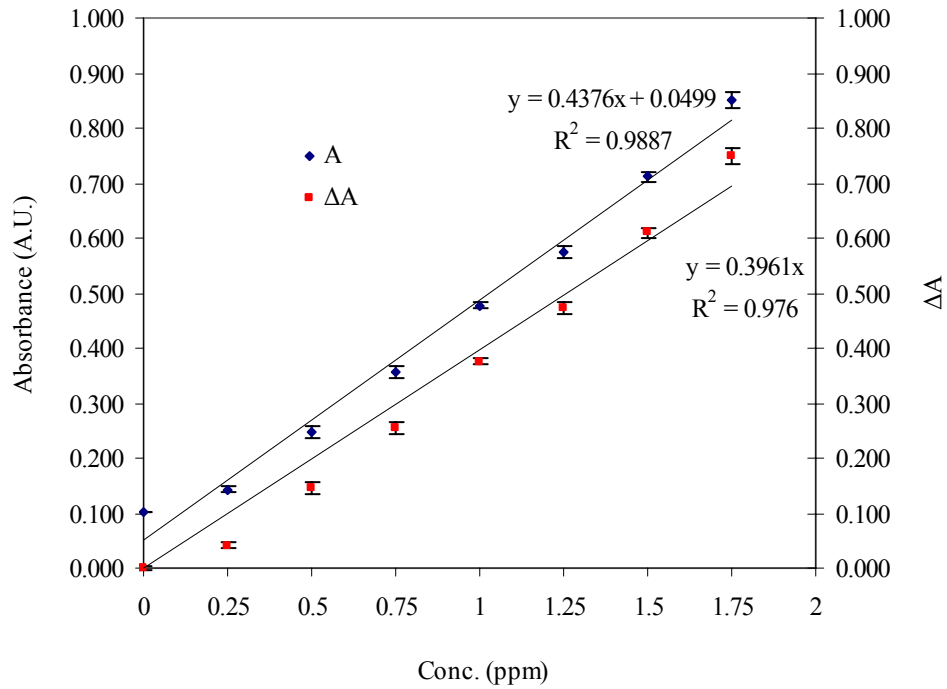


Figure H.65. Calibration curves for the phosphate standards prepared in SBF solution at 620 nm.

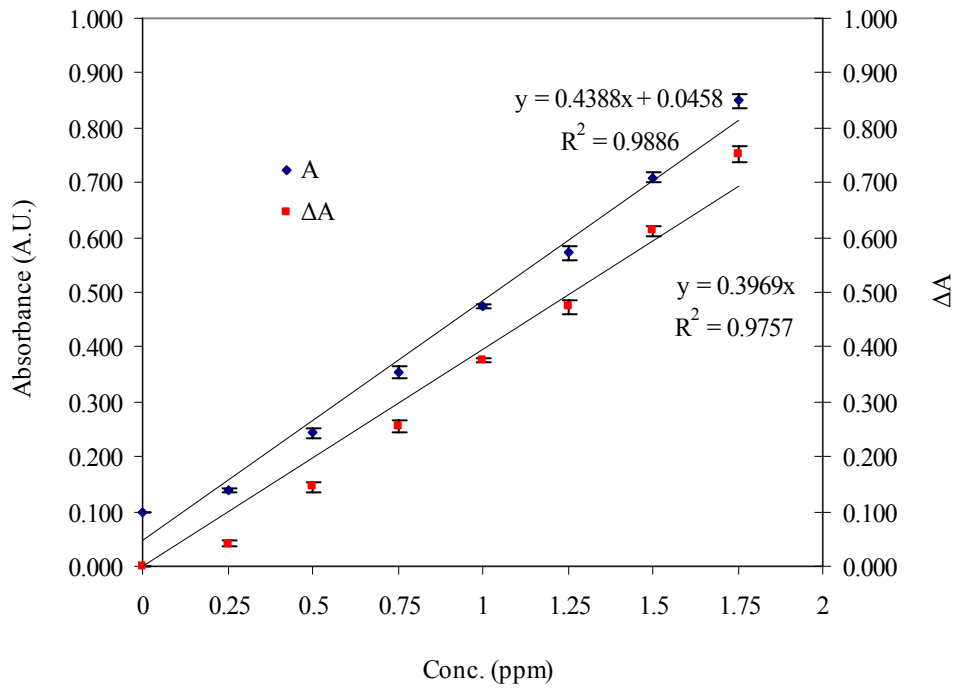


Figure H.66. Calibration curves for the phosphate standards prepared in SBF solution at 610 nm.

VITA

Name Surname : Ali Emrah Çetin
Date of Birth : 09.11.1975
Place of Birth : Van
Addresses : 65/15 Sok. No: 18/1 D:2 Üçkuyular İZMİR TURKEY, 35350
Phone: : +90 232 2791727 **GSM:** +90 537 6694682
Emails : aliemrahcetin@iyte.edu.tr, aliemrahcetin@hotmail.com

EDUCATION

- Ph.D.** Izmir Institute of Technology, Faculty of Engineering, Department of Chemical Engineering, 2010.
- M.Sc.** Izmir Institute of Technology, Faculty of Engineering, Department of Biotechnology and Bioengineering, Biotechnology Program, 2002.
- B.Sc.** Ege University, Faculty of Engineering, Department of Food Engineering, 1999.

EXPERIENCE

- 1999-2002 Research Assistant at Department of Biotechnology, İzmir Institute of Technology
- 2002-2010 Research Assistant at Department of Chemical Engineering, İzmir Institute of Technology

PUBLICATIONS

- PhD. Thesis** : Preparation and Characterization of Resorbable Calcium Phosphate Based Bioceramics
- MSc. Thesis** : Isolation and Molecular Characterization of Lactic Acid Bacteria from Raw Milk
- BSc. Thesis** : Determination of Drying Characteristics of Some Vegetables by using Microwave and Infrared Dryers
- 1) Erten Y., Güneş-Yerkesikli A., **Çetin A. E.** and Çakıcıoğlu –Özkan, F. 2008. CO₂ Adsorption and Dehydration Behavior of LiNaX, KNaX, CaNaX and CeNaX zeolites, Journal of Thermal Analysis and Calorimetry, 94 (3), 715–718 (Article).
- 2) Mecitoglu C., Yemenicioglu A., Arslanoglu A, Elmacı Z. S., Korel F. and **Cetin A. E.** 2006. “Incorporation of partially purified hen egg white lysozyme into zein films for antimicrobial food packaging”, Food Research International, 39, (1), p.12-21 (Article).
- 3) Erdem, İ., **Çetin A.E.**, Büyükkileci A.O. ve H. Ertürk, 2003. Cholesterol analysis by HPLC in egg yolks from Turkish market. 1st International Symposium on Recent Advances in Food Analysis, Prague Czech Republic. Abstract Book p52. (Poster Presentation).